December 2025

THREE-DIMENSIONAL HYDRODYNAMIC AND SALINITY MODEL FOR THE DELAWARE RIVER ESTUARY CALIBRATION REPORT

Technical Report No. 2025 - 5

Managing, Protecting and Improving
the Water Resources of the
Delaware River Basin since 1961

Delaware River Basin Commission
DELAWARE • NEW JERSEY
PENNSYLVANIA • NEW YORK
UNITED STATES OF AMERICA

This page is intentionally left blank.

Three-Dimensional Hydrodynamic and Salinity Model for the Delaware Estuary, Model Calibration Report

DRBC Report No: 2025-5

Prepared by Dr. Fanghui Chen, PE, Amy Shallcross, PE, and Dr. Joseph Fogarty

DELAWARE RIVER BASIN COMMISSION
25 COSEY ROAD, WEST TRENTON, NEW JERSEY, 08628

KRISTEN BOWMAN KAVANAGH, EXECUTIVE DIRECTOR

Suggested Citation

Chen, F., Shallcross, A., and Fogarty, J. (2025). *Three-Dimensional Hydrodynamic and Salinity Model for the Delaware Estuary, Model Calibration Report*: DRBC Report No: 2025-5. West Trenton, New Jersey. Delaware River Basin Commission.
url: https://www.nj.gov/drbc/library/documents/SalinityModelCalibrationDec2025.pdf.

Acknowledgements

The Delaware River Basin Commission (DRBC) staff are grateful to the following nationally renowned experts for their valuable guidance, advice, and insightful technical review of this project: Dr. Carl Cerco from USACE (retired); Dr. Bob Chant, Department of Marine and Coastal Sciences from Rutgers University; Dr. Hugo Rodriguez formerly from GHD[1], and Dr. Gaurav Savant from Rivers and Estuarine Engineering Branch at USACE-ERDC-CHL[2]. All four have extensive experience in the fields of oceanography and estuary environmental hydrodynamics modeling.

The project was developed and documented by Dr. Fanghui Chen, Amy Shallcross of the Water Resource Operations Branch, and Dr. Joseph Fogarty from the Science and Water Quality Management Branch of the Delaware River Basin Commission. The draft report was reviewed by former DRBC Executive Director Steven J. Tambini. Development of this scientific modeling study would not have been possible without the contributions of DRBC staff, including Dr. Namsoo Suk, Dr. Li Zheng, and others, who provided guidance and comments.

Disclaimers

The model described herein was developed as a tool for evaluating the effects of sea level rise on salinity. Model results are presented for information purposes only. Nothing herein represents a rule, regulation, or guidance.

[1] GHD is a maritime and coastal engineering consulting firm.
[2] [2] USACE-ERDC-CHL: US Army Corps of Engineers, Engineer Research and Development Center (ERDC), Coastal and Hydraulics Laboratory (CHL).

Executive Summary

In 2018, the Delaware River Basin Commission (DRBC) initiated a project to evaluate the effects of sea level rise on salinity intrusion from the ocean into the Delaware River Estuary. With sea level rise, salinity transport farther into the Estuary is anticipated due to the increasing force of the ocean and associated hydrodynamics. While higher and more widespread storm surge and an increased frequency of high-tide flooding are of significant concern for the basin's water resources and stakeholders, many other studies exist that describe the magnitude and probability of those impacts.

Under normal and drought conditions, ocean-based salinity is managed by maintaining freshwater inflows to the Estuary through reservoir releases to meet a flow objective at Trenton, New Jersey. The current flow and drought management plans were developed more than 40 years ago, and their effectiveness must be re-evaluated considering climate change, sea level rise, and other factors.

The movement of salinity in the Delaware Estuary is a highly dynamic, spatially variable phenomenon, requiring a complex three-dimensional (3D) hydrodynamic salinity model. The model developed by the DRBC, SM3D or salinity model, documented herein, simulates hydrodynamic phenomena, including transport mechanisms (e.g., water depth, current velocity, salinity, water temperature, and mixing coefficients) over a range of hydrologic conditions with a degree of accuracy and confidence necessary to study salinity intrusion, with consideration of projected sea level rise (SLR). The software used for the model is the Environmental Fluid Dynamics Code (EFDC), originally developed by Dr. John Hamrick (Hamrick, 1992) and supported by the U.S. Environmental Protection Agency (USEPA). The EFDC model code has been applied to a wide range of water bodies and has been used extensively in the United States and worldwide for many environmental studies. EFDC was selected because it provides the capability to simulate the important physical processes affecting salinity transport. With SM3D, salinity intrusion events can be simulated and compared for current and future conditions, such as sea level rise and climate change.

The model domain for SM3D includes the tidal Delaware River from Trenton, New Jersey, to the mouth of the bay and a large portion of the coastal area, which extends 46 mi from the bay mouth out to the continental shelf in the Atlantic Ocean. The Chesapeake and Delaware (C&D) Canal, an important source of both fresh and saline water to the Delaware Estuary, is also incorporated. The model was calibrated for 2017 and 2018, for which a robust record of data needed for the model was available. The model calibration was also tested and adjusted with 2016, a drier year. Then, the period of 2016 to 2020 was simulated and the model performed similarly. The model was then used to simulate additional years of data, including 2011–2013 and 2001–2003, during a drought period, to test its ability under multiple hydrologic conditions (flow).[3] Collectively, the

[3] For some years assumptions were required to create input data if they were not available.

11 years simulated include a range of flow and tidal conditions representative of low, average, and high flows with several severe storm events. The sensitivity of the model results to several inputs, estimated due to missing or unavailable information, was also evaluated (e.g., salinity distribution at the ocean open boundary of the model; the net flow moving through the Chesapeake-Delaware Canal; etc.). Input required included bathymetry, grid resolution, water surface elevations at the western end of C&D Canal that affect the net flow in C&D Canal, water surface elevations at the ocean open boundary, water temperature and salinity at the open ocean and C&D Canal boundaries, water temperature and salinity and inflows from the non-tidal river, including flow on the Delaware River at Trenton, NJ, 32 tributaries downstream of Trenton, 71point source discharges[4], as well as 8 major surface water withdrawals from the Delaware River mainstem. Meteorological data such as air temperature, pressure, wind speed and directions from 5 weather stations are also part of the model inputs.

An analysis of the SM3D model's ability to reproduce observed conditions indicates salinity intrusion is adequately simulated, and the model can be used to evaluate the effects on salinity from sea level rise and freshwater inflows. SM3D will be used to provide science-based information for current and future studies, and, thus, will be periodically updated and refined with new information as it becomes available. The application of SM3D for evaluating the potential impacts of sea level rise on climate change is documented separately (Chen, et. al., 2025).

The work documented herein is focused on the development and calibration of a three-dimensional hydrodynamic salinity model (SM3D or salinity model). SM3D is different than another three-dimensional eutrophication model developed by DRBC to study dissolved oxygen and nutrient-related water quality issues. In the eutrophication model, linked 3D hydrodynamic and water quality models were developed. Originally, the intent was to develop a single three-dimensional model to evaluate both salinity intrusion and eutrophication. However, the different focus and needs of each study could not be met with a single model. Therefore, two dedicated models were developed. Differences between the eutrophication model and SM3D include the resolution of the model domain, framework (grid), extent, time step, and the specification of boundary conditions. All references to the hydrodynamic model in this report refer to SM3D.

[4] A point source discharge is any pollution release at a specific point, as opposed to nonpoint sources where pollution enters waters from diffuse locations such as stormwater runoff from farms. In this study, 71 major point source discharges are included, including industrial facilities (factories, power plants), municipal sewage treatment plants, landfills, and mines. Details are provided in Section 3.3.

Table of Contents

List of Figures

List of Tables

List of Acronyms/Abbreviations

1D	one-dimensional
3D	three-dimensional
32-hr-LPF	32-hour Low-pass Filter or Low-pass Filtered Results
ADCIRC	Advanced Circulation Model and related Database
ADCP	Acoustic Doppler Current Profiler
APHA	American Public Health Association
ASC	Average Seasonal Cycle
Bay	The Delaware Bay or “the Bay”
°C	degrees Celsius
C&D Canal	Chesapeake and Delaware Canal
CEAM	USEPA Center for Exposure Assessment Modeling
cfs	cubic feet per second
cm	centimeter
cm/s	centimeters per second
CSO	Combined Sewer Overflow
DE	Delaware
DEM	Digital Elevation Model
DRBC	Delaware River Basin Commission
ECOM	Estuarine and Coastal Ocean Model
EFDC	Environmental Fluid Dynamics Code
EPA	U.S. Environmental Protection Agency
Estuary	The Delaware Estuary, or “the Estuary”
ETM	Estuarine Turbidity Maximum
FEMA	Federal Emergency Management Agency
FNC	Federal Navigation Channel
GVC	Generalized Vertical Coordinate (Grid)
LCL	Laterally Constrained and Localized (sigma region)

m	meters
m/s	meters per second
m^2/s	meters squared per second
m^3/s	meters cubed per second
mg/L	milligram per liter
µS/cm	microsiemens per centimeter
MAE	Mean Absolute Error
MHHW	Mean Higher High Water
MLLW	Mean Lower Low Water
MS4	Municipal Separate Storm Sewer System
MUA	Municipal Utility Authority
NCDC	National Climatic Data Center (NOAA)
NJ	New Jersey
NOAA	National Oceanic and Atmospheric Administration
NPS	non-point source
NSE	Nash–Sutcliffe Efficiency
NY	New York
NYHOPS	New York Harbor Observing and Prediction System
ppt	parts per thousand
PA	Pennsylvania
POM	Princeton Ocean Model
PS	point source
PWD	Philadelphia Water Department
psu	Practical Salinity Unit
QA/QC	quality assurance/quality control
RM	River Mile
RMSE	Root mean square error
RMSD	Root mean square deviation. In many contexts, RMSE and RMSD are often used interchangeably
ROMS	Regional Ocean Modeling System

SC	Specific conductance
SF	Salt Front
SJRWMD	St. Johns River Water Management District
SLR	Sea level rise
SM3D	Three-dimensional salinity model
SM3D+M	Three-dimensional salinity model, with additional marshes
STP	Sewage Treatment Plant
Stdv	Standard Deviation
TWP	Township
USGS	U.S. Geological Survey
USACE	U.S. Army Corps of Engineers
ubRMSD	Unbiased root mean square difference
WASP	USEPA Water Quality Analysis Simulation Program
WHG	Woods Hole Group, Inc.
WOA13	NOAA Ocean Climate Lab's Product World Ocean Atlas Database 2013
WPCF	Water Pollution Control Facility
WSE	Water Surface Elevation
WWTP	Wastewater Treatment Plant
xyz	A coordinate system in three-dimensions
#-dma	#-day moving average

1. INTRODUCTION

The Delaware River Basin Commission (DRBC) developed a three-dimensional hydrodynamic salinity model (SM3D) for the Delaware Estuary using the U.S. Environmental Protection Agency (USEPA) supported Environmental Fluid Dynamics Code (EFDC). SM3D simulates hydrodynamic and transport phenomena (e.g., tides, water depth, current velocity, salinity, and water temperature) over a range of hydrologic and meteorologic conditions with the accuracy needed to support the evaluation of salinity intrusion under various flow conditions, including future sea level rise (SLR). The objectives of this study are to:

- Develop a model for future studies to evaluate the impact of sea level rise on salinity.
- Determine the major mechanisms that drive salinity transport in the Delaware Estuary.
- Define the spatial distribution and vertical structure of salinity in the Delaware Estuary.
- Evaluate the impacts of freshwater inflows on salinity intrusion.
- Identify additional tools and research to improve the understanding of salinity intrusion.

1.1 DELAWARE RIVER BASIN AND STUDY AREA

The Delaware River Basin is located on the eastern coast of the United States, considered part of both the Northeast and Middle Atlantic regions. The Delaware River forms multiple interstate boundaries, separating New York, Pennsylvania, New Jersey, and Delaware, and covering an area of 13,539 square miles (sq. mi.). The main stem is approximately 330 mi long from its headwaters in the Catskill Mountains in New York to the mouth of the Delaware Bay at the Atlantic Ocean between Cape May, NJ, and Cape Henlopen, DE (Figure 1.1-1). It is the longest undammed river east of the Mississippi river, and more than 150 miles of the main stem are classified as "Wild and Scenic". Although the river only drains four-tenths of a percent (0.4 percent or 4/1000) of the continental U.S., approximately five percent of the nation's population (14.2 million people) rely on the waters of the Delaware River Basin for drinking water. The mainstem river is both tidal and non-tidal. Locations along the Delaware River are referenced by river mile (RM). The non-tidal Delaware River flows from Hancock, NY, (RM 330) to Trenton, NJ, (RM 133). The tidal river, or Delaware River Estuary, is where freshwater from the watershed mixes with salt water from the ocean, and is located between Trenton, NJ (RM 133) and the mouth of the Delaware Bay (RM 0). The study area for this project is the Delaware River Estuary.[5]

[5] The study area is different than the model domain. The model domain extends into the ocean to better specify boundary conditions as described in Section 3.

1.1.1 Delaware Estuary

The tidal portion of the Delaware River is a coastal plain estuary with a relatively homogeneous shallow depth (8 to 10 m, or 26 to 33 ft). Approximately 80 percent of the Estuary is less than 9 m (30 ft) deep, except for the 102 miles long Federal Navigation Channel (FNC), which was dredged to 13.7 m (45 ft) below Mean Lower Low Water (MLLW) through a U.S. Army Corps of Engineers (USACE) channel deepening project that began in 2010 and was mostly completed in 2016[6]. The width at the bay mouth is 11 mi, and the widest part of the bay is 27 mi across. The width decreases exponentially upstream of the bay: 2.4 mi wide near RM 60, 0.5 mi wide at RM 100 in Philadelphia, PA, approximately 0.25 mi wide at RM 117.5 in Burlington, NJ, and less than 1,000 ft wide at RM 133 in Trenton, NJ. The shoreline convergence and narrowing of the river affect the amplitude and shape of the tidal wave as it propagates upstream. According to the National Oceanographic and Atmospheric Administration (NOAA), the observed M2 (Principal lunar semidiurnal constituent, and the dominant tidal harmonic constituent) tide amplitude increases from 0.62 m (2.02 ft) at Lewes, DE, to 0.84 m (2.75 ft) at Philadelphia, PA, and to 1.07 m (3.51 ft) at Newbold, PA, which is 1.7 times larger than the mouth of the bay. The range of the water surface elevation defined by the tidal range between Mean Higher High Water (MHHW) and MLLW is 1.42 m (4.65 ft) at the bay mouth, 2.04 m (6.69 ft) at Philadelphia, and 2.56 m (8.39 ft) at Newbold.

Near the mouth of the Delaware Bay, relatively stable winter northern winds may cause downwelling (i.e., ocean water sinks on the continental shelf), while southern and southwestern winds in the summer may cause upwelling (i.e., rise of ocean water with higher salinity). The seasonal and interannual variability in wind and tides near the mouth of Delaware Bay has significant influence on salinity transport in the estuary. A consistent seasonality known as the Average Seasonal Cycle (ASC) in the observed tides is reported at several NOAA tide gauge stations (Lewes, Cape May, and Atlantic City). The monthly mean sea level tends to be lower during wintertime (from December to March) and relatively higher during summertime (from July to October), as shown in Figure 1.1-2. According to NOAA, ASC is caused by regular fluctuations in coastal temperatures, salinities, winds, atmospheric pressures, and ocean currents. The ASC pattern is consistent with observations that wind-induced downwelling occurs more often in the winter and upwelling is a more dominant phenomenon in the summer. Persistent downwelling results in weaker salinity intrusion and relatively stronger vertical stratification. Conversely, upwelling intensifies vertical mixing and strengthens the salinity intrusion into the Estuary. Seawater temperature and density also affect water surface elevation. Near the mouth of the bay,

[6] The timeline of the channel deepening project is reported by the Port of Philadelphia: https://www.philaport.com/channel-deepening/ A small portion of the dredging was done in 2018-2019. The project was finally completed in 2020.

a difference of 10°C in water temperature may result in a 20 cm difference in water surface elevation[7].

The temperate Delaware Bay is categorized as a weakly stratified or as partially mixed estuary resulting from moderate tidal forcing and weak to moderate river discharge (Valle-Levinson 2009). The tidally-averaged mean salinity profile has either weak or no stratification from surface to bottom, which indicates vigorous vertical mixing between river and ocean water. The vertical salinity structure in the water column results from differences between river flow forcing, pushing saltwater seaward, and tidal forcing, pushing saltwater into the Delaware Estuary. A clear tidally-averaged longitudinal salinity structure exists in the Delaware Estuary. Using long-term averaged information of salinity, *S* (*S* = the long-term averaged and depth-averaged salinity with unit in parts per thousand [ppt][8]), Dolgopolova (2014) characterized the river into four zones: (1) the 53 mi from Scudders Falls north of Trenton, NJ, to Marcus Hook, PA, gage (RM 79), where S is less than 0.25 ppt; (2) the 58 mi of the upper Delaware Bay estuary from the Marcus Hook gage to the line from Port Mahon, DE, to Egg Island, NJ, (RM 21), where *S* ranges from 0.25 to 25 ppt; (3) the 25 mi of the lower Delaware Bay estuary from the line between Port Mahon to Egg Island to the mouth of the bay (RM 0), with S greater than 25 ppt; and (4) the coastal zone of the ocean.

1.1.2 Chesapeake and Delaware (C&D) Canal

The Delaware Estuary is hydraulically connected with the northern Chesapeake Bay through the C&D Canal . The C&D Canal is a ship channel 18 mi in length that connects the Delaware Estuary with the Chesapeake Bay in the states of Delaware and Maryland. The canal is 450 ft (137.2 m) wide (bottom width) and 35 ft (10.7 m) deep. It is an electronically controlled commercial waterway, carrying 40 percent of all ship traffic in and out of the Port of Baltimore, MD (Ward et al., 2009).

The Susquehanna River, west of the Basin, the longest river (444-mi) on the East Coast of the United States, is the largest tributary to the Chesapeake Bay. Its watershed drains almost half of Pennsylvania and provides 90 percent of the freshwater flow to the upper Chesapeake Bay, where the eastern end of the C&D Canal is located, and approximately half of the total freshwater flow to the entire bay. Water from the Susquehanna River, combined with a much weaker tidal influence, makes the northern Chesapeake Bay at the western end of the C&D Canal fresher than the Delaware Estuary at the eastern end of the C&D Canal.

The flow magnitude, flow direction, and net flow from the C&D Canal are controlled by the water density and the tidal amplitude and phase at each end of the C&D Canal. According to NOAA[9],

[7] Personal discussion with Robert Chant in December 2019.
[8] In this report, salinity unit is Practical Salinity Unity [psu]. The numeric difference between psu and ppt is small; both indicate salinity. The difference has been discussed by scientists, e.g. https://blog.seabird.com/ufaqs/what-are-the-differences-between-salinity-expressions-in-ppt-psu-practical-salinity-and-absolute-salinity/
[9] NOAA tide station at Chesapeake City, DE: https://tidesandcurrents.noaa.gov/stationhome.html?id=8573927 and station at Reedy Point, DE: https://tidesandcurrents.noaa.gov/stationhome.html?id=8551910

the MLLW level at Chesapeake City, MD, near the western end of the C&D Canal is more than 16 inches higher than at Reedy Point, DE, near the eastern end of the canal. An approximately 10-hr tidal phase difference is observed between the ends of the C&D Canal. The salinity at the eastern (Delaware) end of the C&D Canal is higher than the western (Chesapeake) end by 2 to 3 ppt. A series of studies have revealed that long-term net flow within the C&D Canal moves eastward (toward Delaware) at rates ranging from 1,060 to 9,152 cfs (30 to 259 m^3/s) (Pritchard and Gardner, 1974; Thatcher and Najarian, 1981; Johnson et. al., 1999). Ward et al. (2009) used data collected from 1992–1993 to develop a one-dimensional (1D) flow model of the C&D Canal based on the dynamic form of the Saint-Venant equations (Saint-Venant, 1871, Beven and Wood 1992), and used the model to identify non-tidal residual net flow in the canal and to evaluate the effects of regional-scale meteorological events, such as the Nor'easter of December 1992. These meteorological events can cause significant perturbations to the ordinary astronomic tides at each end of the model, in turn affecting salinity and water quality in both the upper Chesapeake and middle Delaware estuaries. They concluded that the average net flow in the C&D Canal is eastward (toward Delaware), ranging from 3,000 to 4,000 cfs (85 to 113 m^3/s) during 1992–1993. However, the flow direction was reversed during November and December 1992, when a notable northeaster event increased water level in the Delaware Bay and diverted the water to move westward through the canal for about 60 hours. The 4,000 cfs value is approximately 10 percent of the long-term average discharge of the Susquehanna River at Conowingo, MD, (40,000 cfs).

In the hydrodynamic and water quality modeling work conducted for the Chesapeake Bay by the U.S. Army Corps of Engineers (USACE) (Wang and Johnson, 2002), the C&D Canal was treated as a river boundary with a constant outflow of 750 cfs specified at the eastern end of the C&D Canal. This assumption was also used for DRBC's 1D hydrodynamic model DYNHYD5 (DRBC, 2003). However, flows are dynamic and can exceed 100,000 cfs through the canal. Normally, the flow reverses direction every 6 hr or so as the tide changes. During episodic events, large flows may continue in the same direction for two to three days. Thus, the treatment of the C&D Canal as a river with a constant outflow in the three-dimensional (3D) Chesapeake Bay hydrodynamic model is an over-simplification, and the estimated long-term average net flow from the canal differed from USACE's study significantly. A more thorough study may be needed over a longer time span, considering the large net flow from Chesapeake Bay to the Delaware Estuary through the C&D Canal.

1.2 Salinity

Salinity is the mass of dissolved salts in water. Salinity, expressed as psu (practical salinity units), is calculated as a function of measured conductivity (or specific conductance [SC]) and temperature (Method 2520B from American Public Health Association [APHA], 1995). One psu is approximately equivalent to 1 mg of salt per gram of water (mg/g) or 1 ppt (part per thousand).

On average, the salinity of seawater is 35 psu[10]. The salinity of freshwater is considered to be approximately 0.45 psu.

The Delaware Estuary has a spatially variable longitudinal salinity profile, from seawater (~35 psu) in the Atlantic Ocean[11] to freshwater inflows at Trenton, NJ (lower than 0.45 psu). This salinity profile is a unique characteristic that differentiates tidal rivers and estuaries from other types of surface waters. The salinity structure is maintained mainly by two competing forces: 1) river flow, which tends to drive saltwater seaward; and 2) tidal forcing and gravitational circulation, which tends to drive saltwater upstream. Turbulent shear and meteorological forcing (precipitation, evaporation, and wind) also impact salinity distribution.

Although most of the tidal river upstream of RM 70 is typically vertically well-mixed, vertical stratification exists in the lower estuary, especially near the mouth of the bay. Downstream of RM 70, an estuary exchange flow and tidally-averaged salinity structure are evident. The tidally-averaged circulation shows that deep and salty water near the bottom flows landward, and fresher shallow water moves seaward. This two-layer bi-directional circulation pattern is also known as estuary exchange circulation. Near the mouth of the bay, the magnitude of the volumetric flux of the tidally-averaged estuary exchange flow is often many times greater than that of the river alone (MacCready and Geyer, 2010). The deep incoming ocean saltwater is continually diluted by shallower, fresher water via turbulent mixing driven by tides. During the neap tide, a stronger exchange flow and relatively stronger salinity stratification are observed compared to the spring tide. During high-flow periods, stronger vertical stratification is observed and during low-flow periods, stratification is weaker due to a relatively stronger tidal forcing.

The salt front location (salt front)[12] is used to monitor salinity intrusion into the upper Estuary. It is defined as the 7-day moving average chloride concentration of 250 mg/L (isochlor). The value of 250 mg/L (salinity of approximately 0.5 psu) is based on a secondary drinking water standard, which is used to assess the suitability of water for conventional drinking water treatment. The "normal" salt front is located between RM 68, near the Delaware Memorial Bridge (RM 69), and RM 74. The salt front is not measured but calculated with specific conductance (SC) data from U.S. Geological Survey (USGS) stations at Reedy Island (RM 54.1), Chester (RM 83.6), Fort Mifflin (RM 91.9), and Ben Franklin Bridge (RM 100.1) using a log–linear interpolation technique. The log-linear interpolation is used because SC at Reedy Island can be 3 orders of magnitude larger than SC at Ben Franklin. The interpolated location can differ by up to 5 miles when different station pairs are used to calculate the salt front.

[10] Prior to 1978, oceanographers referred to the physical quantity ppt (g salt per kg water). In 1978, the Practical Salinity Scale (with numeric units of psu) was adopted to ensure consistency across different oceans.
[11] At the mouth of the Bay, salinity fluctuates from 22 to 31 psu (median is 27.5 psu) based on data collected at NOAA station at Lewes DE from 2017 to 2022. Around the model ocean boundary, it is around 33 to 35 psu. The maximum salinity in the ocean generally may reach to 37 in the Atlantic Ocean. Average ocean salinity is about 35 ppt, with variations due to evaporation (increasing salt) and precipitation/river runoff (decreasing salt).
[12] https://www.nj.gov/drbc/programs/flow/salt-front.html and https://drbc.net/Sky/hydro/saltfront.html

1.3 Technical Approach

1.3.1 Previous Hydrodynamic Modeling in the Delaware Estuary

Many hydrodynamic models have been used to evaluate the Delaware Coast and Bay or the Delaware Estuary in the past, including the Princeton Ocean Model (POM), the Estuarine and Coastal Ocean Model (ECOM), the Regional Ocean Modeling System (ROMS), Curvilinear-grid Hydrodynamics model in 3D (CH3D and CH3D-Z), the Advanced Circulation model (ADCIRC), and EFDC. The models differ based on their representations of the physical characteristics of the estuary (bathymetry, extent, granularity, etc.), assumptions of the underlying equations for phenomena that affect hydrodynamics or salinity, and the numerical schemes used to solve the system of equations. Model selection depends on the purpose of the modeling effort or analysis. Applications of the different models have been reported in a variety of studies (e.g., Xu 2006; Kim and Johnson 2007; Castellano and Kirby 2011; Schmalz 2011).

Full three-dimensional numerical realization allows for the representation of more physical processes, including buoyancy forcing due to river discharges, tidal forcing, meteorological forcing and surface heat exchange, wind forcing (local and remote), wind–wave induced current, and other processes. As a result, three-dimensional models have been used to study vertical stratification and its variability during flood-tide, ebb-tide, and cross-channel momentum balance (Aristizábal and Chant 2014), salt fluxes (Aristizábal and Chant 2013), thermal circulation (Salehi 2017), the effect of wind waves on momentum budget and subtidal exchange (Pareja-Roman et al., 2019), wave energy and interactions between bathymetry and wave processes (Chen et al., 2018), and the processes responsible for coastal changes including sediment transport (Warner et al., 2010).

These detailed theoretical and modeling studies have focused primarily on short time scales from a few tidal cycles to a few months. Recently, the forcing mechanisms that drive salinity transport were investigated for longer time scales (seasonal to interannual) for the Chesapeake Bay (15-year simulation by Xu et al. [2012] and 7-year simulation by Kim [2013]). However, the impact of long-term variability in river flows, tidal surface elevation at the ocean boundary, and meteorological forcing on the salinity structure, and salinity intrusion has not been thoroughly studied for the Delaware Estuary.

1.3.2 Environmental Fluid Dynamics Code (EFDC)

EFDC, a three-dimensional hydrodynamic model, was selected as the model platform because it provides the capability to simulate changes in water level, velocity, water temperature, and salinity

in a tidally-dominated environment with complex bathymetry and geometry. The EFDC model was originally developed by John Hamrick from Tetra Tech Inc. (Hamrick, 1992) and is supported by U.S. Environmental Protection Agency (EPA) The physics of the EFDC model, and many aspects of its computational scheme, are equivalent to the widely used POM (Blumberg and Mellor, 1987) and its adaptation for shallow water environments named ECOM (Blumberg et al., 1999), as well as the CH3D model originally developed for the Chesapeake Bay (Johnson et al., 1993). EFDC has been applied in projects involving coastal and river-estuary environments nationwide (e.g., Wool et al., 2003; St. Johns River Water Management District [SJRWMD], 2012; Tetra Tech Inc., 2015). EFDC is also able to simulate the wetting and drying process and inundation of marsh areas on salinity transport, an important factor for future conditions such as SLR.

1.3.3 Three-Dimensional Salinity Model (SM3D)

DRBC intended to develop one three-dimensional hydrodynamic model for multiple purposes: a eutrophication study and a salinity study. However, the eutrophication study required the hydrodynamic model to link with a water quality model, EPA's Water Quality Analysis Simulation Program (WASP) for the simulation of dissolved oxygen and associated parameters. After testing multiple numerical model grid configurations, evaluating the requirements for linking EFDC to WASP, and selecting model options and assumptions, it was determined that two separate models were needed to adequately model salinity and eutrophication. Both hydrodynamic models were developed with EFDC, but the extent of the model domains differ. For the eutrophication study, the model domain extends from the head of tide on the Delaware River at Trenton (RM 133) to the mouth of Delaware Bay (RM 0). The open boundary was set at the bay mouth to utilize all the nutrient data collected there; thus, numerous parameters that govern bio-chemical processes can be calibrated in the linked EFDC–WASP model. In contrast, the domain for the salinity model (SM3D) extends into the ocean to minimize the uncertainty in the salinity boundary condition at the ocean open boundary. A summary of major differences between the two models is presented in Appendix A.

Multiple versions of the model grid were developed for the SM3D to determine the appropriate model domain for the SLR and salinity study. The grid for SM3D (Grid v2.2) is confined by the existing shoreline with limited marsh areas. Limiting the marsh area results in a more compact grid that is computationally efficient. A sensitivity test was performed with a modified grid (Grid v4.2, results specified as SM3D+M) with more peripheral low-lying marsh areas infrequently inundate under current conditions. Comparisons of results from SM3D and SM3D+M indicated the additional marsh area had minimal impact on the simulated salinity intrusion. Thus, SM3D with Grid v2.2 is sufficient for calibration using historic conditions. However, with SLR, more frequent inundation of peripheral low-lying marsh areas may have a more noticeable effect on salinity. In a separate report (Chen, et. al. 2025), SM3D and SM3D+M are used with sea level rise to further evaluate how the amount of marsh area affects simulated salinity. The effects of various vertical resolutions of the numerical grid on SM3D model predictions were also evaluated (Section 2.4).

SM3D was calibrated for the years 2018-2019 for which detailed information was available to specify boundary conditions. The calibration was refined with simulations of 2016. Then, all years between 2016-2020 were then simulated to verify that the model performs well for multiple years and conditions. For these simulations from 2016 onwards, the bathymetry reflects a 45 ft deep Federal Navigation Channel (FNC). For simulations of earlier years, 2001-2003 and 2011-2013, when sufficient data were available for comparison, the model was adjusted to reflect the pre-2016 FNC bathymetry with the 40 ft channel. These years were simulated, prior to channel dredging, and used to simulate 2001-2003 and 2011-2013 because data were available to check model performance. Collectively, these 11 years include a range of flow and tidal conditions representative of low, average, and high flows, including multiple severe storm events. Ranked annual median daily flow for the Delaware River at Trenton is shown in Figure 1.4-1. The years 2011 and 2018 are the two wettest years in the last 110 years. Normal years were represented by 2012, 2013, and 2017. Dry years were represented by 2001 and 2002, during the third-worst drought on record.

1.4 Conclusion

SM3D produces accurate results for the conditions simulated and information available to develop the model. Model performance was evaluated using model-to-data comparisons of tidal water surface elevations and harmonic constituents, current velocity, water temperature, net C&D flow, and salinity. Typical goodness-of-fit statistics are presented for the full calibration period and shorter periods with additional data or during conditions of critical concern, such as low flows and high salinity intrusion. Results are also presented graphically as appropriate (low-pass filtered, tidally-averaged, depth-averaged, etc.) for the specific parameter. These graphics include times-series, bar charts, box plots, longitudinal and vertical profiles, target diagrams, and scatter plots.

1.5 Report Organization

Section 1 provides a general overview of the Delaware Estuary and outlines the study objectives. Section 2 addresses the selection, capabilities, and limitations of the three-dimensional hydrodynamic model and selected components of EFDC for the SM3D model. Section 3 details model development, including specifications for boundary conditions. Calibration and validation results are presented in Section 4. The findings and potential refinement opportunities are summarized in Section 5.

Supplemental information is presented in three Appendices. Appendix A includes a summary of the differences between the salinity model SM3D, described herein, and the 3D-hydrodynamic model coupled with a water quality model used for the Eutrophication Study. Appendix B presents the sensitivity analysis of the vertical grid resolution. Appendix C includes the results of additional sensitivity analyses of the influence of the net flow through the C&D Canal, as well as the

uncertainty in salinity boundary conditions at both the ocean open boundary and the C&D Canal open boundary.

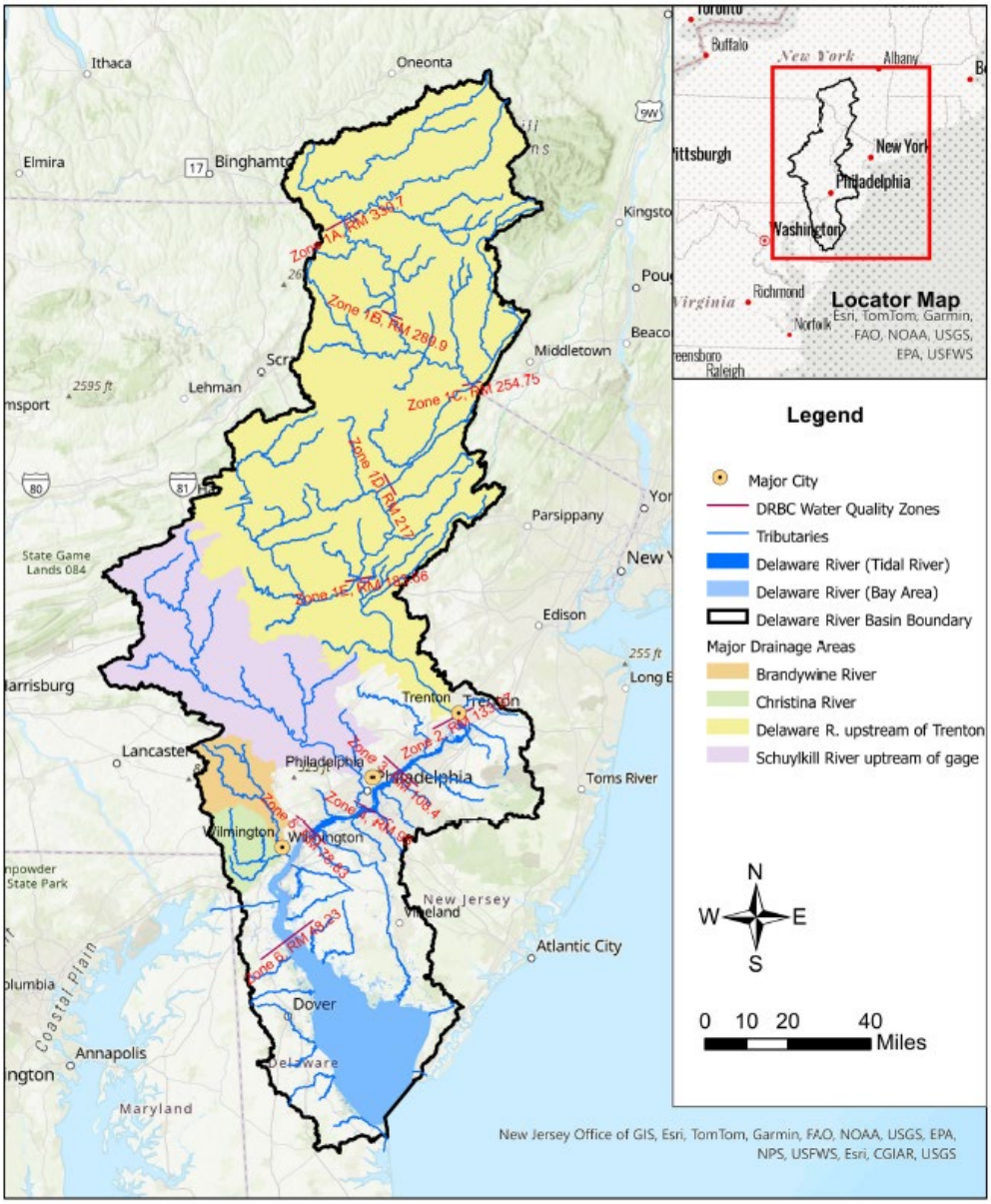

Figure 1.1-1 Delaware River and Bay

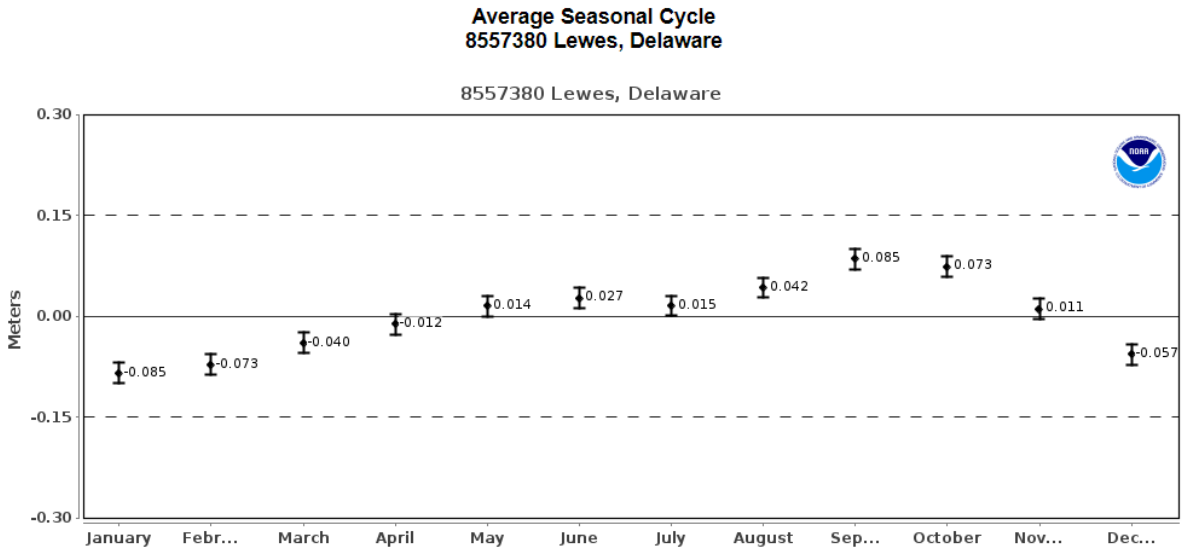

The average seasonal cycle of mean sea level, caused by regular fluctuations in coastal temperatures, salinities, winds, atmospheric pressures, and ocean currents, is shown along with each month's 95 percent confidence interval.

https://tidesandcurrents.noaa.gov/sltrends/sltrends_station.shtml?id=8557380

Figure 1.1-2 Average Seasonal Cycle at 8557380 Lewes, Delaware

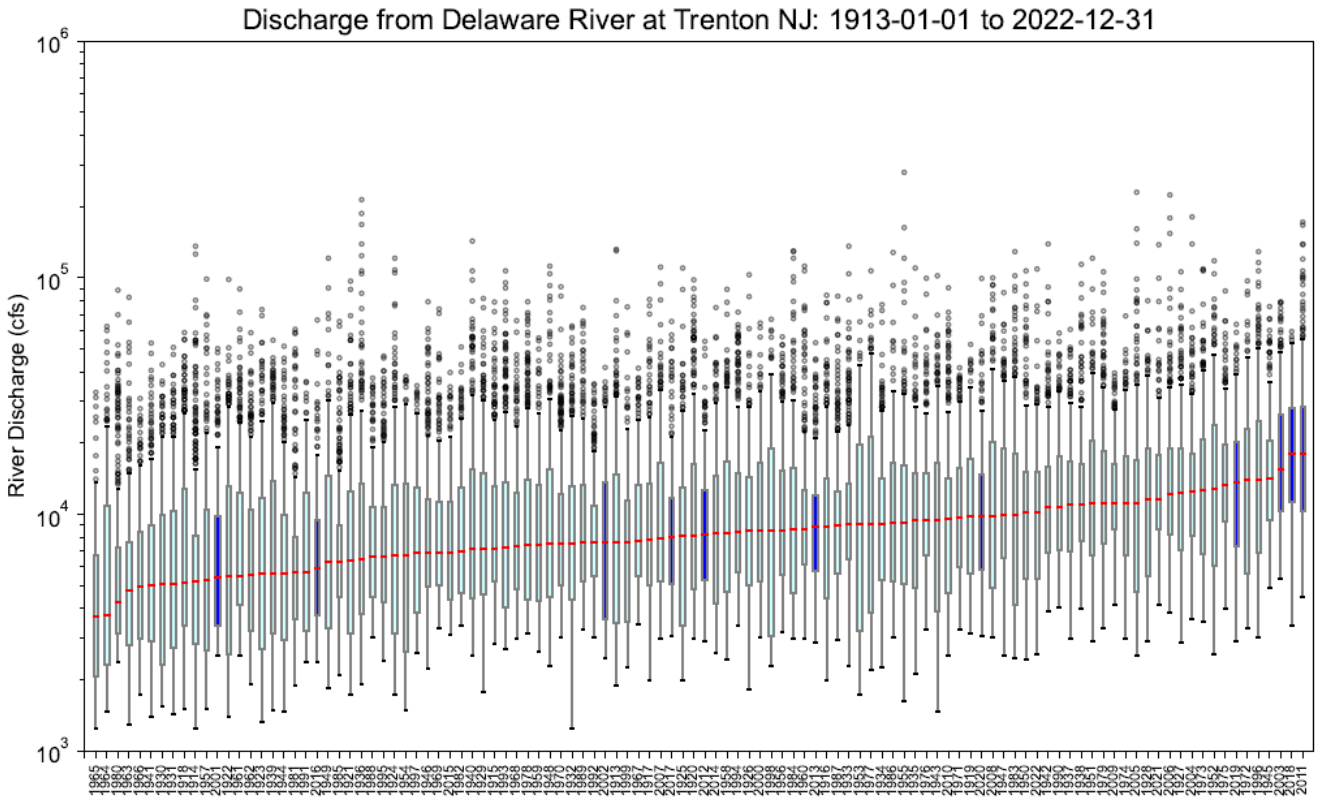

The box extends from the first quartile (Q1) to the third quartile (Q3) of the data, with a line at the median. The whiskers extend from the box to the farthest data point lying within 1.5x the inter-quartile range (IQR) from the box. Flier points are those past the end of the whiskers. Simulated years are highlighted in blue. They are 2001-2003, 2011-2013, and 2016-2020. Daily flow observations of the Delaware River at Trenton (USGS Gage 01468500) were used for the analysis.

Figure 1.4-1 Historical Flow in Delaware River at Trenton (1912 to 2022 Period) Ranked by Annual Median Flow

2. THREE-DIMENSIONAL HYDRODYNAMIC AND SALINITY MODEL

2.1 General Description

SM3D was developed with EFDC (Hamrick, 1992), which is supported by EPA. EFDC is a general-purpose hydrodynamic model code for the simulation of time-variable flow in rivers, lakes, reservoirs, estuaries, and coastal areas. The conservation of mass and momentum equations, as well as transport equations for temperature and salinity, are used to simulate the fundamental processes affecting the movement of water in an estuary. The state equation (Equation. 2.1-6) links water density to salinity and water temperature. EFDC has been applied to a wide range of environmental studies. A complete description of EFDC is given in Hamrick (1992) and Tetra Tech Inc. (2002). The model has been used extensively in the United States and worldwide (e.g., Wool et al., 2003; Sucsy and Morris, 2002; SJRWMD, 2012; and Ji et al., 2007).

The version of EFDC used in this study was obtained by DRBC in 2018 from the EPA Center for Exposure Assessment Modeling (CEAM) website. DRBC added one subroutine to the source code based on the algorithm from ADCIRC used to calculate the nodal factors and equilibrium arguments for more accurate specification of the tidal forcing at the ocean open boundary using the information extracted from ADCIRC.

The continuity and momentum equations used in EFDC are:

$$\frac{\partial u}{\partial x}+\frac{\partial v}{\partial y}+\frac{\partial w}{\partial z}=0 \tag{2.1-1}$$

$$\frac{\partial u}{\partial t}+\frac{\partial u^2}{\partial x}+\frac{\partial uv}{\partial y}+\frac{\partial uw}{\partial z}-fv+g\frac{\partial \eta}{\partial x}=\frac{\partial}{\partial z}\left(K_M\frac{\partial u}{\partial z}\right)-\frac{g}{\rho_0}\frac{\partial}{\partial x}\int_z^\eta \rho dz+F_x \tag{2.1-2}$$

$$\frac{\partial v}{\partial t}+\frac{\partial uv}{\partial x}+\frac{\partial v^2}{\partial y}+\frac{\partial vw}{\partial z}+fu+g\frac{\partial \eta}{\partial y}=\frac{\partial}{\partial z}\left(K_M\frac{\partial v}{\partial z}\right)-\frac{g}{\rho_0}\frac{\partial}{\partial y}\int_z^\eta \rho dz+F_y \tag{2.1-3}$$

$$\frac{\partial T}{\partial t}+\frac{\partial uT}{\partial x}+\frac{\partial vT}{\partial y}+\frac{\partial wT}{\partial z}=\frac{\partial}{\partial z}\left(K_H\frac{\partial T}{\partial z}\right)+\frac{1}{\rho_0 C_p}\frac{\partial I}{\partial z}+F_T \tag{2.1-4}$$

$$\frac{\partial S}{\partial t}+\frac{\partial uS}{\partial x}+\frac{\partial vS}{\partial y}+\frac{\partial wS}{\partial z}=\frac{\partial}{\partial z}\left(K_H\frac{\partial S}{\partial z}\right)+F_S \tag{2.1-5}$$

$$\rho=f(S,T) \tag{2.1-6}$$

where:

η = water surface elevation
u, v, and w = velocity components along the x, y, and z direction, respectively
ρ_0 and ρ = reference density and in situ density of water

g = gravitational acceleration
f = Coriolis parameter
K_M = vertical viscosity for momentum mixing
F_x and F_y = horizontal momentum diffusion in x and y direction, respectively
T = water temperature
S = salinity
K_H = vertical diffusivity for turbulent mixing of temperature and salinity
F_T and F_S = horizontal diffusion terms for temperature and salinity, respectively
$\partial I/\partial z$ = solar radiation forcing term
C_p = specific heat
t = time

Although the Delaware Estuary is commonly considered weakly stratified, vertical mixing and along-channel salinity structure vary in time depending on river discharge, tidal forcing, and meteorological forcing (Aristizábal and Chant, 2013 and 2015). These conditions make it necessary to use a three-dimensional mode in EFDC to simulate the salinity transport in the Delaware Estuary. EFDC implements the Mellor–Yamada level 2.5 turbulence closure scheme (Mellor and Yamada, 1982) as modified by Galperin et al. (1988) to parameterize vertical mixing. One of many characteristics of EFDC is the wetting–drying feature, which can be used to simulate the flooding and drying of intertidal areas caused by tidal actions (Ji et al., 2001).

2.2 Generalized Vertical Coordinate (GVC) Grid

According to Tetra Tech, Inc. (2006), EFDC was originally formulated to use a sigma stretched vertical coordinate. In the sigma coordinate formulation, the number of vertical layers is the same at all horizontal locations in the model domain. This formulation is widely accepted and adequate for a large range of applications. However, the bathymetry (primarily depth) of the Delaware River Estuary varies significantly in the lateral direction from a deep (relatively steep-sided) navigational channel to a much shallower flank, forming V or T-shaped cross-sections. A traditional Z or hybrid coordinate system (i.e., a generalized vertical coordinate [GVC] grid) is more desirable because it reduces the numerical error in the lateral direction, and model results are more consistent with the observations. Another reason for using a GVC grid over a sigma grid is to resolve numerical instability that might result from “razor-thin” vertical layers in very shallow areas near shorelines or in the low-lying marshes when a sigma grid is applied. A GVC grid was therefore chosen to represent the lateral bathymetric variation. This grid configuration allows for the horizontal model domain to be represented by laterally constrained and localized-sigma regions (LCL sigma). In the LCL region, the number of active vertical layers is variable, unlike the traditional sigma grid in which the number of vertical layers is constant. The number of vertical layers is fixed during a simulation at the location of any given cell (defined by the coordinates in the horizontal plane and identified by I and J indices), and the thickness of each vertical layer (identified by the k index of

the cell) increases or decreases with the rising or falling water level (i.e., it is a localized sigma for each individual cell). Theoretical and computational aspects of the generalized vertical coordinate are described in Tetra Tech, Inc. (2006). An upwind finite difference scheme is used to solve the system of equations for the grid.

2.3 Capabilities and Limitations

SM3D does not include the simulation of wave-induced currents, wave–current interactions, sediment transport, and groundwater (interactions with surface water and aquifer-estuary salinity exchange) even though EFDC can be customized to do so (e.g., Zhang et al, 2011; USACE, 2014; and Jones, et al. 2015). The wave–current interactions and sediment transport processes were not needed for the evaluation of seasonal salinity intrusion due to the following considerations:

- The impact of remote wind waves from offshore on significant wave height and wave energy inside the bay is limited to the area near the bay mouth. Waves are controlled by local winds and bathymetry for most of the estuary above the lower bay (Chen et al., 2018). Although wind–wave induced surface drag could increase by 30 percent for the short time scale of storm events, the net contribution of wave-related vortex forces to the momentum budget is an order of magnitude smaller than the other leading factors such as surface stress, bottom stress, and pressure gradient (Pareja-Roman, et al. 2019).

- Wave energy flux or wave power is proportional to the wave period and the square of the wave height. For instance, the period of a local wind wave is on the order of 10 seconds; the period of swell, generated by the wind far away from the local area, is on the order 10 to 30 seconds; the period of astronomical tides, like M2, are on the order of several hours; the period of meteorological subtidal components may be on the order of 34 hr or more. Thus, the subtidal and astronomical tidal waves dominate the long-term transport rather than the local wind waves.

- The simulation of sediment resuspension, transport, and deposition of sediment due to wind-wave action was not needed to evaluate salinity intrusion and outside the scope of this study.

- The role of waves on salinity transport may be more pronounced in shallow water areas near shorelines, which are affected by wind direction and wind fetch. Wave energy dissipates exponentially through the water column, and salinity transport primarily occurs at or near-the bottom of the Estuary. Thus, the impact of wind and waves on upstream salinity transport is constrained to the upper layer of the water column. The effect of waves on salinity transport is considered small. Similar studies have been conducted without coupling the hydrodynamic model with wave and sediment transport models with good results (Wool et al., 2003; SJRWMD, 2012).

- Wave-current interactions tend to produce short-term effects on salinity that do not persist, particularly in the upper Estuary. Salinity transport over relatively longer time scales is the result of stronger net-tidal forcing and less affected by relatively short-term meteorological processes, such as tropical storm events. The exclusion of wind–wave–current interaction did not improve a model's performance related to salinity intrusion (Cook et al., 2023).
- The effects of groundwater-surface water interactions and salinity transport into aquifers will have de minimis effect on salinity intrusion into the upper Estuary[13] Although salinity intrusion into aquifers is also of concern, it is outside the scope of the study and not needed for the purposes for which the model will be used.

The ability of a model to reproduce observed conditions is attributable to several factors including the representation and extent of the model domain, the choice of physical processes to be simulated and the assumptions required to do so, the accuracy of measured data, and irreducible uncertainties. Uncertainty is inherent in any measurement (sensors, surveys, samples) and in the accuracy of observed field data used to both develop boundary conditions and for assessing calibration. When data are missing, assumptions and estimates are needed to assign boundary conditions that may or may not reflect historical conditions. While the best information and professional judgement guide estimates for missing information, it must be recognized that model error and bias are in part due to the amount of information available to develop and calibrate the model.

[13] According to Vince DePaul (retired, USGS), the direct contribution of groundwater to surface water is less than 1% of the total Bay water volume. Personal Communication, January 12, 2021.

3. HYDRODYNAMIC MODEL DEVELOPMENT

3.1 MODEL DOMAIN AND NUMERICAL GRID

The geographical extent of the SM3D model domain includes: (1) the entire Delaware Estuary, from the head of tide at Trenton fall line (RM 133) to the mouth of the bay (RM 0); (2) a large portion of the ocean in the vicinity of the outside of the bay, which extends 68 km (or 42 mi) onto the continental shelf in the Atlantic Ocean; (3) the C&D Canal to the NOAA tide gage station at Chesapeake City, MD (8573927)[14]; and (4) short reaches of 31 major tributaries. The large portion of the offshore coastal area outside the Bay was included in SM3D for defining the salinity boundary condition and to evaluate the hydrodynamics of the estuary exchange flow with sea level rise.

It is common practice to establish model boundaries for tidal systems some distance away from the area of interest. Salinity in the Atlantic Ocean farther from Delaware Bay is relatively constant[15] and can be defined without observed data. Otherwise, salinity at the mouth of the Bay must be specified with observed data because it is highly variable and flow dependent. The same is true for the water surface elevation (WSE) and current velocity, because the boundary condition at the mouth can materially affect circulation patterns and tidal dynamics, and thus the exchange of water between the ocean and the Delaware Bay.

The salinity at the mouth of the bay (NOAA gauge station 8557380 at Lewes, DE)[16] is highly time-variable and flow dependent. During high spring flows, the salinity gradient is more severe due to the warmer freshwater plume discharging over colder, more dense salt water at the mouth of the bay, resulting in a steeper gradient from the surface to the bottom. In contrast the salinity of the ocean is relatively constant with a more consistent gradient. To minimize the uncertainty in specifying the model boundary conditions of ocean salinity among other factors, a large portion of the offshore coastal area is included in the numerical grid to provide a more realistic representation of hydrodynamics and transport processes in the vicinity of the bay mouth (e.g., fresher water transported into the Atlantic Ocean during ebb tide and saltwater transported into the Delaware Bay during a subsequent flood tide). Therefore, the downstream ocean open boundary is the Atlantic Ocean 68 km (or 42 mi) from shore on the continental shelf along the 60-m isobath. The northern and southern boundaries of the coastal zone are 96 and 100 km (60 and

[14]NOAA Tide station at Chesapeake City, MD: https://tidesandcurrents.noaa.gov/stationhome.html?id=8573927
[15] The ocean salinity at location far away (more than 40 to 100 miles) from the Delaware Bay near the Delaware and New Jersey coast is relatively stable with average value of 35 psu, and the difference from the surface to the bottom may range from 33 to 37 psu with deeper waters often saltier depending on location. At location farther north of the Atlantic Ocean, the surface water gradually becomes saltier and denser and sinks that drives the movement of the meridional overturning circulation (AMOC), forming North Atlantic Deep Water (NADW) that flows south at depth, influencing the vertical structure.
[16]NOAA Tide station at Lewes, DE: https://tidesandcurrents.noaa.gov/stationhome.html?id=8557380

62 mi) from the mouth of Delaware Bay, respectively. The numerical grid with the bathymetry as simulated is shown on Figure 3.1-1 (1-6). Bathymetry data are discussed in Section 3.2.

A curvilinear and orthogonal numerical grid was used to represent the geometry of the Delaware River and Bay study area. The extent of the model domain represented in the grid includes low-lying marsh areas, which add complexity and computational burden due to the simulation of the wetting and drying process that occur with inundation. To balance model skill at predicting salinity intrusion with computational efficiency, a sensitivity analysis was performed with different amounts of marsh area in the domain. Two versions of the grid were developed and tested during the model calibration. One version, Grid v2.2, does not include all low-lying marshes surrounding the bay area. Another version of the model, Grid v4.2, includes more peripheral low-lying marshes surrounding the bay.

Grid v2.2 contains a total of 2,510 grid cells with the upper portion (upstream of RM 70 near City of Wilmington, DE) of the tidal river being discretized with 1,260 grid cells in the horizontal plane. The average grid cell size in the river channel upstream of RM 70 was 540 m and 240 m in longitudinal and lateral directions, respectively. Grid cells in Zone 6 (downstream of RM 70) are much larger, and the average length in the longitudinal and lateral directions was 1,984 m and 1,962 m (or approximately 2x2 km), respectively.

Grid v4.2, contains 2,976 grid cells and more peripheral low-lying marshes, and has the same inflow and open boundaries configurations as Grid v2.2. Simulations were performed with both of the grids and inclusion of the additional peripheral marsh areas did not significantly change the model results, most likely because the inundation frequency of those area is low under historical and current conditions. Therefore, Grid v2.2 was used for SM3D. However, the intended use of SM3D is to evaluate the impacts of SLR on salinity intrusion because those peripheral areas will likely be inundated more frequently. Additional sensitivity testing with Grid v4.2 and SLR is documented in a separate report (Chen, et. al., 2025).

For SM3D, up to 20 vertical layers were assigned to cells at the ocean boundary. Eight vertical layers were used for most cells that represent the navigational channel. Model sensitivity tests to vertical layer resolution indicated that more than five but less than 10 layers inside the navigational channel are adequate for model performance (Appendix B).

3.2 Bathymetry

The bathymetry for the grid, a GIS raster surface, was developed using multiple sources. The primary source of information was a 2011 survey by the Federal Emergency Management Agency (FEMA). Other sources included detailed surveys of the navigation channel and the mouth of the C&D Canal, as well as NOAA Navigation charts.

The FEMA Region III Storm Surge Study (FEMA, 2011) is documented in the report titled *Coastal Storm Surge Analysis System Digital Elevation Model* (FEMA 2011). The report provides a detailed summary of the construction of the Digital Elevation Model (DEM). The FEMA 2011 DEM was produced by merging the latest coastal LIDAR and other topographic survey data sets with the most reliable bathymetric datasets of the region. The complete DEM includes the coastal areas for Delaware, Pennsylvania, New Jersey, Maryland, Virginia, West Virginia, and North Carolina, and offshore areas including the continental shelf and a portion of the deeper ocean. The horizontal datum is NAD83, and the vertical datum is NAVD88. The raster grid resolution is 1/3 arc-seconds (~10 m).

Since the 2011 FEMA survey, USACE dredged several locations along the Federal Navigation Channel (FNC) from 40 ft to 45 ft deep below Mean Lower Low Water (MLLW) and areas near the confluence of the C&D Canal and the Delaware River. The dredging involved the deepening of the existing 102-mile long 40-ft-deep FNC to a depth of 45 ft below MLLW including sections from Philadelphia Harbor, PA to Beckett Street Terminal, Camden, NJ. The USACE dredging project started in 2010 and was mostly completed in 2016 and finally finished in 2020[17]. NOAA Nautical charts were used to define the bathymetry of the C&D Canal, which was set to 35 feet below MLLW, as well as river bathymetry near the confluence of Schuylkill River with the Delaware River. Additional bathymetric information was available from NOAA nautical charts (12277 covers C&D Canal, 12304 covers Delaware Bay, 12311 to 12314 cover segments of the Delaware River)[18]. USACE surveyed the dredged areas of both the FNC and areas around the C&D Canal and Delaware Memorial Bridge after the Channel Deepening project was completed in 2022 and 2023. The additional post-dredge bathymetry was available from USACE Philadelphia District Survey Office, in March 2023. Post-dredge surveys were used to adjust the FEMA bathymetry to reflect most recent conditions in and around the channel. For the years simulated after the dredging, the bathymetry for the FNC was adjusted with the post-dredging bathymetry, reflecting the 45 ft channel. For years prior to 2016, the FEMA 2011 bathymetry was used with the channel depth adjusted to 40 ft channel bathymetry.

Information from surveys in November 2022 and February 2023 was used for the C&D Canal confluence with the Delaware River and the area of the Delaware River near Delaware Memorial Bridge. Those surveys were limited to the ship channel and the surrounding 20 feet. The USACE survey raw dataset (sounding data points) is in *xyz* text format with water depth in feet referenced to MLLW datum. The survey sounding depth was converted to NAVD88 datum using the NOAA conversion factor at tide gage 8551910 Reedy Point, DE, which is located in the middle of the surveyed area. The data was projected (summarized) to the model grid cell by taking the mean bathymetry of all the sounding points located inside a grid cell.

[17] The timeline about USACE channel deepening project is provided by the Port of Philadelphia: https://www.philaport.com/channel-deepening/

[18] NOAA chart can be found on the website: https://charts.noaa.gov/InteractiveCatalog/nrnc.shtml?rnc=12312

The overall model bathymetry projected on the numerical grid was shown in Figure 3.1-1(1). The horizontal datum is NAD83, and the vertical datum is NAVD88. The raster grid resolution is 1/3 arc-seconds (~10 m). The raw data (sounding data points) is in *xyz* text format with water depth in feet referenced to MLLW datum. The survey sounding depth was converted to NAVD88 datum using the conversion factor provided by NOAA at tide gage 8551910 Reedy Point, DE, located in the middle of the surveyed area. This data was projected (summarized) to the model grid cell by taking the mean bathymetry of all the sounding points that are located inside a grid cell. The survey data, used to refine the bathymetry, are presented in Figure 3.2-1, and the updated bathymetry in the area adjusted with USACE 2022-2023 survey data is presented in Figure 3.2-2.

3.3 Boundary Conditions

SM3D requires specification of the following boundary conditions:

- Water surface elevations at the ocean boundary.
- Water surface elevations at the western end of the C&D Canal.
- Freshwater inflow at the upstream boundary on the Delaware River mainstem.
- Freshwater inflows from tributaries, point source discharges, and net flow being removed through major water withdrawals.
- Water temperature and salinity for all inflows and point source discharges
- Water temperature and salinity for all open boundaries
- Climate/meteorological forcing data, including air temperature, pressure, dew point, precipitation, wind speed and direction, and solar radiation.

3.3.1 Water Surface Elevation Boundary Condition

Elevation boundary conditions consist of three components: 1) astronomical tide, 2) subtidal fluctuation (meteorological forcing), and 3) additional adjustments that account for the steric effect as well as long-term circulation (geostrophic currents). A geostrophic current is an oceanic current in which the pressure gradient force is balanced by the Coriolis effect. The concept was used in a modeling study for the New York harbor region by Blumberg et al. (1999) using ECOM. A detailed discussion about specification of the water surface elevation at the ocean boundary was given in Georgas (2010) as explained for the New York Harbor Observing and Prediction System (NYHOPS) hydrodynamic model. The water level at the ocean open boundary is prescribed as a

summation of the tidal, η_T, and non-tidal, η_{NT}, parts. In NYHOPS, the non-tidal part is further disaggregated to extra-tropical storm and cyclone surge, η_C , and the long-term steric effect, η_S, components.

$$\eta_{total} = \eta_T + \eta_{NT} \ = \eta_T + \eta_C + \eta_S \tag{3.3-1}$$

In the equation, the second term represents the "sub-tidal fluctuation due to meteorological forcing", and the third term represents long-term effect including the thermal expansion and contraction of the seawater associate with the long-term ocean circulation (geostrophic currents), which may cause a phenomenon as "cross-shelf climatological slope" or "cross-shelf elevation slope" at the United State northeast coast (Blumberg et al., 1999).

The long-term steric effect on the regional water level is caused by seasonal thermal expansion and contraction. Similar to the ECOM and NYHOPS models, EFDC uses the Boussinesq approximation, and the water is assumed incompressible and internal volume is conserved. Therefore, the steric effect can only be included as an open boundary water level adjustment.

The astronomical tide can be calculated by a series of harmonic functions. Tidal harmonic constituents at the EFDC model open boundary were extracted from ADCIRC (Szpilka et al., 2016). The dominant tidal constituent is the principal lunar semi-diurnal (M2). In addition to M2, eight other constituents (S2, N2, K2, K1, O1, Q1, M4 and M6) are included in the tidal boundary condition[19]. The amplitude and phase of each harmonic constituent vary with location, and corresponding values were determined by the coordinates of the 52 grid cells at the ocean boundary. The following equation is used by EFDC to combine all constituents and construct the time variable water surface elevation boundary conditions:

$$WSE_{ob}(t) = \sum_{n=1}^{k} \left(A_n(t) F_n(t_0) \, cos\left(\frac{2\pi}{T_n}(t - t_0) + V_n(t) - \emptyset_n \right) \right) \tag{3.3-2}$$

where $WSE_{ob}(t)$ is the tidal component of the total water surface elevation at time t; k is the number of relevant constituents; n is the index of a constituent; A_n, $\emptyset_n$ and T_n are the local tidal amplitude, phase, and period of a constituent; F_n is the nodal amplitude factor; and V_n is the astronomical argument. F_n and V_n are adjustments of the secular change in the astronomical tide at the beginning of the simulation period.

The period (or frequency) is an absolute constant for a given harmonic constituent. The amplitudes and phases are temporally constant but spatially variable. The nodal factors and equilibrium arguments are spatially constant but temporally variable. The nodal factor (F_n) in Equation (3.3-2) adjusts the amplitude of a given harmonic constituent to account for the fact that the orbit of the moon slowly changes and comes back to its original position in roughly 18.61 years, which is called precession or nodal cycle. The nodal factor varies slightly from year to year.

[19] Tidal database named as "*Western North Atlantic, Caribbean and Gulf of Mexico Tidal Databases*" are available from website: http://adcirc.org/products/adcirc-tidal-databases/

The equilibrium argument (V_n) adjusts the phases to allow for astronomical conditions to match the start time of a simulation (or the start time of a time series of data). For the purposes of comparisons with data for water surface elevation and current velocity, these two parameters must be calculated correctly such that the model results will be properly synchronized in time.

The sub-tidal signals η_C, (due to meteorological forcing), at the ocean boundary from the bay mouth were assumed to be equivalent to what was observed at NOAA Station (8557380) at Lewes, DE. This assumption can be justified by the fact that the time of travel of these long waves between these two locations is relatively short (e.g., with wave-length of a few hundreds of km and wave period greater than a couple of hours to more than 34 hr).[20] In this study, the sub-tidal fluctuations were calculated as the total tide (verified data) minus the astronomical tide at the station location with no amplitude and phase change. Other researchers have used this adjustment to reflect local impact from the coastal ocean circulation. For example, a shoaling factor ranged from 0.5 to 0.7 was used to further adjust the sub-tidal fluctuations in ECOM for New York harbor by Blumberg et al. (1999) and NYHOPS (Georgas, 2010). No shoaling factor was used for the SM3D model.

The long-term steric effect on the regional water level is closely related to and embedded in the Average Seasonal Cycle (ASC) reported by NOAA at Lewes station. Mellor and Ezer (1995) approximated the steric effect using two pairs of sinusoidal and cosinusoidal water level fluctuations. Each pair has two harmonics: one with an annual and one with a semiannual periodicity. The annual signal is generally considerably larger than the semiannual signal. In this study, the ASC analyzed by NOAA at Lewes, DE, was used to approximate the long-term steric effect at the model ocean open boundary. In this study, the ASC observed at Lewes was used to determine an adjustment to the overall non-tidal component to further improve the model performance. It is difficult to segregate the "non-tidal" signal into long-term steric effects and short-term effects caused by meteorological forcings (air temp and pressure, solar radiation, precipitation, and wind) and storm surge. Therefore, the third component used to describe the steric effect, η_S (Equation 3.1-1), was treated as a calibration parameter.

NOAA hourly verified data at Station (8573927) Chesapeake City, MD, were used at the western end of the C&D Canal open boundary. For time periods without data, the total tide was specified as the predicted tide at Chesapeake City (provided by NOAA) plus the observed sub-tidal fluctuations at the closest station, either Reedy Point, DE, at the eastern end of C&D Canal (8551910).[21]

The vertical datum used in the SM3D model is NAVD88. Tide data at NOAA stations were converted to NAVD88 for specification of the model boundary condition or for performing model-

[20] https://www.weather.gov/jetstream/tsuwind_max

[21] The sub-tidal signal from Tolchester Beach, MD, in Chesapeake Bay (8573364) was also evaluated, but Reedy Point produced slightly better results for salinity transport into the Delaware Estuary.

to-data comparisons. The datum conversion is provided in Table 3.3-1. Conversion factor values are based on NOAA's Vertical Datum Transformation, V.3.6.1[22].

Table 3.3-1. Vertical Datum Conversion for NOAA Stations in Delaware Estuary

No.	Station	Station ID	Vertical Datum	Conversion Factor to NAVD88 (m)
1	Lewes, DE	8557380	NAVD88	0.000
2	Cape May, NJ	8536110	NAVD88	0.000
3	Brandywine Shoal Light, DE	8555889	MLLW	-0.872
4	Ship John Shoal, NJ	8537121	MLLW	-0.963
5	Reedy Point, DE	8551910	NAVD88	0.000
6	Chesapeake City, MD	8573927[23]	MLLW	-0.474
7	Delaware City, DE	8551762	MLLW	-0.887
8	Marcus Hook, PA	8540433	MLLW	-0.890
9	Philadelphia, PA	8545240	NAVD88	0.000
10	Burlington, NJ	8539094	MLLW	-1.016
11	Newbold, PA	8548989	MLLW	-1.152

Note: NAVD88 meter = MLLW meter + Conversion Factor

3.3.2 Freshwater Inflows

Freshwater inflows into the Delaware River Estuary were incorporated as tributary boundaries to the model, including flow from the upstream boundary at Trenton, tributaries (gaged and ungaged tributary areas), point source discharges, and surface water withdrawals. Groundwater–surface water interaction was not considered because the contribution is not significant. Based on data from 2018 through 2019, the contributions of freshwater to the Delaware River Estuary from the Delaware River at Trenton, Schuylkill River, Christina–Brandywine River, and remaining tributaries were 51, 15, 4 and 11 percent, respectively. Point source (PS) discharges contributed approximately 4 percent, and non-point source (NPS) discharges, including municipal separate storm sewer systems (MS4) and combined sewer overflow (CSO) discharges, contributed 5

[22] NOAA Vdatum are constantly updated as indicated in the version log at NOAA/NOS's VDatum: Current Events. Additional information is available at https://vdatum.noaa.gov/contact.php

[23] See description in text. As of May 2020, the updated NOAA conversion factor to NAVD88 from MLLW at the Chesapeake City gage is -0.487 meter. https://tidesandcurrents.noaa.gov/datums.html?datum=MLLW&units=1&epoch=0&id=8573927&name=Chesapeake+City&state=MD

percent. Direct precipitation onto the Delaware Estuary waters contributes another 10 percent of the total freshwater budget.

Inflows from 32 major tributaries were specified using USGS gaging station data. Hourly flow data were utilized for the Delaware River at Trenton and the Schuylkill River because of their significant contributions to the total freshwater input, while daily flows were utilized for the remaining tributary inflows. Flow rates in the Delaware River at Trenton are presented in Figure 3.3-1. Inflow boundaries for tributaries were established at DRBC's 2017–2018 water quality monitoring locations (Zheng et al., 2024). Tributary flow rates were estimated using available USGS gage data. For tributaries without gages, the flow rate was estimated based on data from a similar watershed and prorated by the drainage-area ratio. Average inflows during 2017 from the 32 major tributaries are presented in Table 3.3-2.

A total of 71 major point source discharges (Table 3.3-3) and 8 water withdrawals (Table 3.3-4) were included in the model. The point source (PS) discharges are relatively small compared to flows from the major tributaries. However, these sources become more important for local hydrodynamics during the low-flow season. The point source discharges were classified as Tier 1 and Tier 2[24] based on the Point-Discharge Monitoring Programs from 2011–2015 and another monitoring program from 2018 to 2019 (Zheng et al., 2024). Flows for smaller discharges, known as Tier 3, were based on monthly National Pollutant Discharge Elimination System (NPDES) monitoring reports. The 2011-2015 discharges were 14 to 16 percent less than those of 2018-2019. For years prior to 2016, the discharge data from 2011-2015 were used. For periods after and including 2016, the 2018-2019 data were used.

Flows from non-point source (NPS), MS4, and CSO discharges are not explicitly addressed because the volumes only have limited local influence on hydrodynamics during higher flow periods, which is not the condition of concern for this study. In addition, much of the volume is likely captured in tributary flows or point source discharges.

[24] Tier 1, 2, 3 refer to the EPA Antidegradation Policy described in the NPDES Permit Writers' Manual (https://www3.ePAgov/npdes/pubs/chapt_06.pdf) and https://www.ePAgov/wqs-tech/key-concepts-module-4-antidegradation#tab-4. Tier 1 facilities comprise 95% of the cumulative point discharge load for ammonia, total Kjeldahl nitrogen (TKN), and 5-day biological oxygen demand (BOD-5) based on the data sets collected between 2011 and 2015. Tier 2 facilities include facilities contributing to the 95% cumulative load for phosphorus, soluble reactive phosphorus (SRP,), nitrate, and total nitrogen (TN) that were not already included in Tier 1. Tier 3 facilities were those facilities not included in Tiers 1 or 2. More information is available online at https://www.nj.gov/drbc/library/documents/WQAC/082417/yagecic_point-source-monitoring.pdf.

Table 3.3-2. Summary of River Flow (Mainstem and Tributaries) Boundaries in the Model

Count	Tributaries	RM	USGS Gauge	Annual average 2017 flow (cfs)
1	Delaware River at Trenton (mainstem)	134.3	01463500	10,310
2	Assunpink Creek	133.8	01464000	114
3	Crosswicks Creek	128.4	01464500	113
4	Neshaminy Creek	115.6	01465500	261
5	Rancocas Creek North Branch	111.1	01467000	141
6	Rancocas Creek South Branch	111.1	01465850	142
7	Poquessing Creek	111.7	01465798	23
8	Pennypack Creek	109.8	01467048	59
9	Pennsauken Creek South Branch	105.4	01467081	20
10	Pennsauken Creek North Branch	105.4	N/A	22
11	Frankford Creek	104.6	01467087	28
12	Cooper River	101.6	01467150	47
13	Big Timber Creek	95.5	N/A	59
14	Schuylkill River	92.5	01474500	2,500
15	Mantua Creek	89.7	N/A	51
16	Darby Creek	85.3	N/A	86
17	Crum Creek	84.9	01475850	31
18	Ridley Creek	84.2	01476480	30
19	Chester Creek	82.9	01477000	79
20	Raccoon Creek	80.7	01477120	38
21	Oldman Creek	77.0	N/A	45
22	Christina River	70.7	01478000	224
23	Brandywine Creek	70.7	01481500	314
24	Salem River	58.4	01482500	55
25	Alloway Creek	54.5	N/A	37
26	Appoquinimink River	51.2	N/A	78
27	Cohansey River	37.8	01412800	53
28	Leipsic River	35.0	01483500	41
29	St. Jones River	23.7	01483700	92
30	Murderkill River	23.1	01484000	54
31	Maurice River	20.0	01411500	241
32	Mispillion River	13.0	N/A	87

Table 3.3-3. Summary of Major Point Source Discharges

Count	Facility Name of Major Point Sources
1	Philadelphia Water Department (PWD) Northeast, PS Tier-1
2	PWD Southwest, PS Tier-1
3	City of Wilmington, PS Tier-1
4	PWD Southeast, PS Tier-1
5	Delaware #1 Water Pollution Control Facility (WPCF) (Camden), PS Tier-1
6	DELCORA, PS Tier-1
7	Gloucester County Utilities Authority, PS Tier-1
8	Hamilton Township (TWP) WPCF, PS Tier-1
9	Trenton Sewer Utility, PS Tier-1
10	Lower Bucks County Joint Municipal Authority, PS Tier-1
11	Morrisville Borough Municipal Authority, PS Tier-1
12	Willingboro Water Pollution Control Plant, PS Tier-1
13	Mount Holly WPCF, PS Tier-2
14	Chambers Works, PS Tier-2
15	Kent County Levy Court, PS Tier-2
16	Delaware City Refining, PS Tier-2
17	Cumberland County Utilities Authority, PS Tier-2
18	Hartford Road Water Pollution Control Facility, PS Tier-2
19	City of Millville Wastewater Treatment Plant (WWTP), PS Tier-2
20	Central Ave. Wastewater Treatment Plant (Burlington TWP), PS Tier-2
21	Bordentown Sewerage Authority Blacks Creek Sewage Treatment Plant (STP), PS Tier-2
22	Moorestown TWP WWTP, PS Tier-2
23	Burlington City STP, PS Tier-2
24	Delran TWP Sewer Utility Department, PS Tier-2
25	Florence Township STP, PS Tier-2
26	Polymer Additives Inc. (i.e., Valtris Specialty Chemicals), PS Tier-2
27	Bristol Borough Water & Sewer Authority, PS Tier-2
28	Riverside Sewerage Authority, PS Tier-2
29	Pennsville Sewerage Authority, PS Tier-2
30	GROWS Landfill, Waste Management, PS Tier-2
31	Paulsboro Refining Company, PS Tier-2
32	FPL Energy Marcus Hook, PS Tier-3
33	Evonik Degussa, PS Tier-3
34	Tinicum Township, PS Tier-3
35	Exelon Generating Company, Eddystone, PS Tier-3
36	U.S. Steel, Fairless-203, PS Tier-3

Count	Facility Name of Major Point Sources
37	U.S. Steel, Fairless-103, PS Tier-3
38	Boeing, PS Tier-3
39	Rohm & Haas Chemicals, Bristol, PS Tier-3
40	Monroe Energy, PS Tier-3
41	Canton Village STP, PS Tier-3
42	Menu Foods Inc., PS Tier-3
43	Logan Township Municipal Utility Authority (MUA), PS Tier-3
44	Beverly Sewerage Authority, PS Tier-3
45	Salem City Wastewater Treatment Facility, PS Tier-3
46	Palmyra STP, PS Tier-3
47	Penns Grove Sewerage Authority, PS Tier-3
48	Riverton STP, PS Tier-3
49	Carneys Point STP, PS Tier-3
50	PSEG Nuclear Salem Generating Station, PS Tier-3
51	Former BP Paulsboro Terminal NO 4555, PS Tier-3
52	Bridgeport Disposal LLC, PS Tier-3
53	PSEG Fossil – Burlington Generating Station, PS Tier-3
54	Surfside Products LLC, PS Tier-3
55	Hoeganaes Corporation, PS Tier-3
56	Mexichem Specialty Resins, PS Tier-3
57	Chemours Company Repauno, PS Tier-3
58	MAFCO Worldwide Corp, PS Tier-3
59	Occidental, PS Tier-3
60	Middletown–Odessa–Townsend, PS Tier-3
61	Delaware City STP, PS Tier-3
62	Port Penn STP, PS Tier-3
63	Milton STP, PS Tier-3
64	General Chemical, PS Tier-3
65	Formosa Plastics, PS Tier-3
66	Calpine Mid-Atlantic Generation, PS Tier-3
67	DuPont Edgemoor, PS Tier-3
68	Hope Creek Generating Station, PS Tier-3
69	Mercer Generating Station, PS Tier-3
70	City of Lewes, PS Tier-3
71	Cinnaminson Sewerage Authority, PS Tier-3

Table 3.3-4. Summary of Major Withdrawals

Count	Facility Name of Major Withdrawals
1	Burlington City Water Department (2 intakes)
2	Aqua Pennsylvania, Inc.
3	Kimberly-Clark Corporation
4	Lower Bucks County Joint Municipal Authority
5	Chemours Company, FC, LLC, Edgemoor
6	Chambers Dupont Chemours (combined intakes)
7	USX-US Steel Division
8	City of Philadelphia

3.3.3 Water Temperature and Salinity

Water temperature and salinity that are specified at all model open boundaries, at all freshwater inflow boundaries, and from PS discharges are described in the section.

Water Temperature and Salinity at Ocean Boundary

Salinity at the open ocean boundary was based on monthly statistics from the World Ocean Atlas 2013 (WOA13) database[25] (Locarnini, et. al., 2013; Zweng et al., 2013). The monthly mean salinity data from 2005–2012 are shown in Figure 3.3-3 (1-12) and values that were used for the model boundary are summarized for the near-surface and near-bottom ocean salinity in Table 3.3-5. Vertical variations of water temperature and salinity with depth (35 to 45 m at the boundary) were represented. Relatively weak vertical stratification of salinity was found from the bed up to 10 m below the surface at 42 mi (68 km) offshore. The annual average salinity at 5-m and 30-m depths are 31.8 and 33.1 psu, respectively, with an average difference of approximately 1.3 psu (0.6 to 1.9 psu, except 3.2 psu in April). Near-surface salinities (5 m) were assigned to the top three layers, and all layers below used a value reflective of salinity at deeper depths (30 m).

[25]Data access: https://www.nodc.noaa.gov/OC5/woa13/woa13data.html

Table 3.3-5. Monthly Statistical Mean of Ocean Salinity Near the Mouth of Delaware Bay

Month	Near-Surface Depth = 5m (psu)	Near-Bottom Depth = 30m (psu)	Difference: Bottom – Surface (psu)
January	32.6	33.2	0.6
February	32.7	33.3	0.6
March	32.5	33.3	0.8
April	32.1	35.3	3.2
May	31.4	32.5	1.1
June	30.9	32.8	1.9
July	30.5	32.3	1.8
August	31.1	32.6	1.5
September	31.9	32.5	0.6
October	32.0	32.8	0.8
November	32.3	32.9	0.6
December	31.8	33.4	1.6
Average	31.8	33.1	1.3

Data source: World Ocean Atlas 2013 (WOA13) database (Locarnini, et. al., 2013; Zweng et al., 2013) The monthly statistics are based on data collected from 2005 to 2012.

Water temperature varies significantly over the course of the year. The surface temperature at the ocean open boundary (top layer) was assumed to be the same as the observed near-surface water temperature at NOAA Station (8557380) at Lewes, DE. The water temperature below the surface at the model ocean boundary was adjusted from the surface value based on the WOA13 data near the mouth of the Delaware Bay (Table 3.3-6). The average difference in water temperature between near-surface and 10-m depth ranged from -0.3°C in February to 4.3°C in July. These monthly mean differences were deducted from the surface water temperature and uniformly assigned to layers 4 through 20 (ocean bottom). Water temperatures for the second and third layer were assigned based on linear interpolation between the top layer and fourth layer.

The water temperature and salinity boundary conditions at the C&D Canal were established based on water temperature and conductivity data from NOAA Station (8573927) Chesapeake City, MD. For 2001–2003 and 2011–2013, when salinity data were not available, a salinity rating curve was developed and used to specify the boundary conditions at the western end of the C&D Canal. Multiple linear regression (MLR) analysis was conducted using salinity data from NOAA Station Chesapeake City, MD, and USGS Station Reedy Island, DE, and flow data from USGS Station (01576000) Susquehanna River at Marietta, PA, from April 2, 2017, to May 31, 2019. The 30-day moving average salinity data were used in the analysis and resulted in a regression

correlation coefficient (R-squared) of 0.77. The observed and predicted salinity at Chesapeake City during the same period are presented in Figure 3.3-4. The salinity rating curve is given as:

$$S = 0.1832 + 0.40083\, S_r + 0.00885 \times 10^6 \times Q_m^{-1} \quad (3.3\text{-}3)$$

where S is salinity (psu) at Chesapeake City (western end of C&D canal); Sr is salinity at Reedy Island; and Q_m is the flow rate (in cfs) for Susquehanna River at Marietta, PA. Daily averaged salinity at Chesapeake City is approximately half of that observed at Reedy Island. As expected, salinity is low when flows were high in the Susquehanna River, indicating an inverse relationship between the Chesapeake City salinity and Susquehanna River flow at Marietta.

Table 3.3-6. Monthly Mean Water Temperature (°C) Near the Mouth of Delaware Bay

Month	Water Temp. (surface)	Water Temp. (Depth = 5 m)	Water Temp. (Depth = 10 m)	Difference (surface - D10 m)
1	7.11	7.15	7.19	-0.08
2	5.08	5.12	5.38	-0.3
3	5.63	5.58	5.5	0.13
4	10.42	9.19	8.68	1.74
5	14.76	14.24	12.79	1.97
6	20.45	19.76	17.21	3.24
7	23.93	23.09	19.67	4.26
8	24.35	23.94	21.74	2.61
9	21.9	21.81	21.67	0.23
10	16.29	16.42	16.44	-0.15
11	15.1	15.15	15.25	-0.15
12	10.14	10.39	10.39	-0.25

Data source: World Ocean Atlas 2013 (WOA13) database (Locarnini et al., 2013; Zweng et al., 2013) The monthly statistics are based on data collected from 2005 to 2012.

In November 2019, USGS established a gauge inside the C&D Canal near the eastern end of the Canal, located on the north shore of the canal, 2 mi southwest of Delaware City, 3 miles from the entrance to Delaware Bay. The data available include water level, water temperature, specific conductance, and tidally filtered and unfiltered discharge. The tidal flow data are available from mid-August 2021 to present. The information was used to verify the methodology to estimate the boundary condition for the C&D Canal (Section 4.3.4).

Water Temperature and Salinity at Freshwater Inflow at Trenton and Tributaries

Temperature in the Delaware River at Trenton varies seasonally, with minimum temperatures of 1–5°C during winter and maximum temperatures of approximately 25°C during summer.

Temporal variations in water temperature, specific conductance, and salinity at USGS Station (1463500) at Trenton, NJ, during the eight simulated years are shown in Figure 3.3-2 (1-13).

Water temperature and specific conductance data from USGS stations were used to specify the temperature and salinity boundary conditions for all tributary inflows using the standard method (American Public Health Association, 1995). For tributaries below Trenton and above the confluence of the Schuylkill River and the Delaware River, the grab sample data were used to scale the continuous salinity from Trenton to the tributary boundary (Section 3.3.5). For tributaries located downstream of the Schuylkill River, salinity was assigned values from the Schuylkill River. When specific conductance data were not available for the Schuylkill River, the salinity was set to 0.2 psu.

Continuous water temperature and specific conductance data from USGS stations and grab samples from the DRBC 2018-2019 Monitoring Program (Zheng, et al., 2024) were used to specify the temperature and salinity boundary conditions for tributary inflows. Continuous data were available for the Delaware River at Trenton and Schuylkill River at Philadelphia. For tributaries below the Schuylkill River, data from the Schuylkill River were used to specify salinity. An analysis of the grab sample data indicated that using the Delaware River salinity for tributaries between Trenton and the confluence of the Schuylkill River would underestimate the load from those tributaries. Average salinity from the Assunpink Creek at Mill Hill Park and Poquessing Creek was two and three times higher, respectively, than that of Delaware River. Therefore, the grab sample data were used to calculate a scale factor for the continuous salinity the tributaries. The scaling factors are summarized in Table 3.3-7.

Table 3.3-7. Scaling Factor Used in Specification of the Tributary Salinity based on the Salinity of the Delaware River at Trenton, NJ.

Site	Average Salinity	Scale Factor
Delaware River at Trenton	0.123	1
Assunpink Creek at Mill Hill Park	0.253	2.06
Crosswicks Creek at Groveville Park	0.117	0.96
Neshaminy Creek at Hulmeville Road	0.291	2.38
Poquessing Creek at Frankford Avenue	0.375	3.06
Rancocas Creek North Branch	0.062	0.51
Rancocas Creek South Branch	0.103	0.84
Pennypack Creek at Torresdale Avenue	0.345	2.82
Pennsauken Creek North Branch	0.246	2.01
Pennsauken Creek South Branch	0.311	2.54
Frankford Creek at Frankford Avenue	0.374	3.05
Cooper River at Chandler's Run	0.198	1.62
Big Timber Creek	0.158	1.29
Schuylkill River at Falls Bridge*	0.246	na

*Average salinity provided for reference only.

Point Source Salinity

Dischargers are not typically required to monitor salinity, and continuous data were not available for all point sources (PS). Under a DRBC program for the Eutrophication Study[26], dischargers were required to collect either monthly or weekly data, including specific conductance, chloride, total dissolved solids (TDS), and total suspended solids (TSS) (Zheng, et. al, 2024). which can be used to calculate salinity. Table 3.3-8 summarizes the salinity from the major facilities (Tier 1) based on DRBC PS data collected from 2011-2016 and 2018-2020 monitoring programs (Zheng, et al. 2024)[27] along with comparable values estimated by the Philadelphia Water Department (PWD) (2020).[28] Tier 1 discharges contribute approximately 80 percent of the total discharged water volume from all point sources.-Tier 2 and Tier 3 discharges were assigned salinities of 0.48

[26] https://www.nj.gov/drbc/library/documents/WQAC/082417/yagecic_point-source-monitoring.pdf

[27] Information is provided in Sections 2.1 and 2.2, and Appendix A in the DRBC Report, "Modeling Eutrophication Processes in the Delaware River Estuary: Three-Dimensional Water Quality Model". (DRBC Report No. 2024-5). Delaware River Basin Commission.

[28] PWD (May 2020): https://water.phila.gov/pool/files/salinity-model-validation-report-2020-05.pdf
Values based on PWD's 2014 discharge flow rates, and available information for TDS concentration, conductivity, or chloride from publicly available from DRBC, EPA-PCS database, NJDEP-OPRA database, Pennsylvania, and Delaware.

psu. PS salinity varies slightly from month to month with small fluctuations over the course of one year. Salinities from the 2011-2016[29] monitoring program were used for years prior to 2016. PWD values were used for simulations of 2016 and later, because the dataset is complete and incorporated values from DRBC's monitoring program.

Table 3.3-8. Salinity (psu) for Major Tier-1 Facilities.

Major Tier-1 Facility Name	2011-2013	2018-2020	PWD
Camden County Municipal Utilities Authority	0.47		0.39
City of Wilmington, Department of Public Works	0.56		0.46
DELCORA	0.43		0.55
Gloucester County Utilities Authority	0.85	0.73	0.67
Hamilton Township - Wastewater Utility	0.45	0.49	0.36
Lower Bucks County Joint Municipal Authority	0.41	0.42	0.31
Morrisville Borough Municipal Authority	0.63		0.51
Philadelphia Water Department Northeast	0.47		0.45
Philadelphia Water Department Southeast	0.43		0.43
Philadelphia Water Department Southwest	0.56		0.48
Trenton Sewer Utility	0.26	0.37	0.19
Willingboro Municipal Utilities Authority	0.32	0.30	0.25

Note: Columns 2011-2013 and 2018-2020 values were calculated with water temperature and specific conductance data with Standard Method (APHA, 1995). PWD (May 2020) values were calculated with a different methodology (conversion equations: S = CL*1.8e-03 + 0.046 and S = TDS*8.5e-04+0.052, where S is salinity [psu] and CL is Chloride concentration [mg/L], TDS is the total dissolved solids [mg/L]).

3.3.4 Meteorological Forcing

Meteorological forcing boundary conditions include air temperature and pressure, dew point, cloud conditions, wind speed, wind direction, precipitation, and net shortwave solar radiation. This information is used by the model to calculate the heat flux at the water surface, and it affects the vertical distribution of water temperature in the water column. Since surface heat flux is spatially variable over the large model domain, meteorological data collected at multiple NOAA National Climatic Data Center (NCDC) weather stations were used for the climate forcing boundary conditions. Five weather stations were used for the model as shown in Figure 3.3-5 and summarized in Table 3.3-9. Temporal variations in meteorological data for 2017 are shown in

[29] During the First-Round Monitoring program (2011-2016), sampling at Tier 1 facilities occurred between 2011-2013. Sampling at smaller facilities began afterwards and continued until2016.

Figure 3.3-6 (1-5). The shortwave solar radiation, which is required as model input and not reported at these stations, was calculated based on other parameters. The theoretically calculated net shortwave solar radiation values (not shown in the figures) were used to fill in the data gaps in the model input files, with assumptions made for dew point, relative humidity, and cloud cover.

The 2017 wind roses data depict temporal frequencies of wind speed and direction and are presented in Figure 3.3-7 (1-5) at NOAA-NCDC stations at Trenton, NJ, Philadelphia, PA, New Castle, DE, Dover, DE, and Cape May, NJ, respectively. In the open water area of the lower Delaware Bay, wind is typically from the north or northwest direction during the winter and from the south during the summer. In the open water area of the lower Delaware Bay, wind is typically from the north or northwest direction during the winter and from the south during the summer.

Table 3.3-9. NOAA-NCDC Weather Stations

Count	STATION	USAF	WBAN	Latitude	Longitude
1	Trenton Mercer Airport	724095	14792	40.277	-74.816
2	Philadelphia International Air	724080	13739	39.873	-75.227
3	New Castle County Airport	724180	13781	39.674	-75.606
4	Dover AFB Airport	724088	13707	39.133	-75.467
5	Cape May County Airport	745966	03726	39.008	-74.908

USAF = Air Force Datsav3 station number;
WBAN = NCDC Weather Bureau Army Navy station identifier number

Wind speed over the bay is relatively stronger compared to the wind observed at land-based stations. Based on limited wind data collected at Ship John Shoal station and Brandywine Shoal Light station during 2008, the wind speed in the middle of the bay area was 30-50 percent stronger than the measured wind speed at Dover or Cape May land-based stations. Wind rose data collected in 2008 from Brandywine Shoal Light and Ship John Shoal stations are presented in Figures 3.3-7 (6) and 3.3-7 (7), respectively. However, due to lack of continuous observed wind data from those two stations, wind data collected from the land-based weather stations were used in this modeling study to represent wind over the bay. The use of land-based observations without adjustment produces risk that the effect of wind on computed circulation is under-estimated. Surface heat exchange may also be under-estimated. Therefore, the wind speed over the bay area (based on data from Dover Airport and Cape May County Airport) was estimated by applying a factor of 1.5 to the land-based observations, representing a 50 percent increase in wind speed. In the future, further model improvement may be investigated with respect to specification of the wind boundary conditions.

3.4 Initial Conditions

Model simulations start on January 1, and the initial condition is specified with the results from a simulation of 31 days to “spin-up” the model (the values on the last day of the “spin-up” become the initial condition for January 1) The 31-day spin-up period is used to eliminate the transient effects on model predictions due to the specification of initial conditions. For consecutive years, the initial conditions are specified with the output from the previous year, rather than those of the “spin-up” simulation (initial conditions for continuous simulations are set from the previous simulation, also known as a “hot start”). For “spin-up” simulations, the initial conditions for temperature and salinity are set to January 1 of the year to be simulated, and flow boundary conditions are set as constants. Water surface elevation, water temperature, and salinity for the “spin-up” period were interpolated between the upstream boundary at Trenton and the ocean open boundary.

4. HYDRODYNAMIC MODEL CALIBRATION

4.1 MODEL CALIBRATION

Results used to assess the calibration, accuracy, and reliability of SM3D include: tidal fluctuations in water surface elevation, depth-averaged current velocity, and longitudinal and vertical distribution of temperature and salinity. The calibration period is from 2016 through 2020, including two years with low-flow periods: 2016 (the driest year in the past decade) and 2019, when the salt front reached RM 90 and RM 85, respectively. Since the critical season for salinity intrusion is from September through December, model performance was examined not only for 2016-2020, but also for subsets of the simulation during the dry periods in 2016 and 2019. Simulations other than these five years were used for model validation, in which all model parameters remain unchanged.

Data

Observed data for comparing model results are presented in Tables 4.1-1 and 4.1-2 and station locations are presented in Figures 4.1-1 to 4.1-3. Other datasets used for model calibration or validation include a 2011 Rutgers University survey of velocity and longitudinal salinity (Figure 4.1-4) and the DRBC Boat Run dataset[30] (Figure 4.1-5). The specific data used for model-to-data comparisons are:

- Hourly water surface elevation (astronomic tidal and sub-tidal fluctuations) at NOAA stations
- Depth-averaged current velocity (comparison with Rutgers survey data, 2011)
- Depth-averaged current velocity at NOAA stations (2012, 2018)
- Depth-averaged current velocity at PWD Buoy stations (2012, 2016)
- Tidal flow and net flow at USGS gage in the C&D Canal (2021-2022)
- Daily salinity at NOAA stations
- Daily salinity at USGS stations
- Grab sample salinity and chloride concentration at DRBC Boat Run sampling stations
- Water temperature at NOAA and USGS stations
- Longitudinal salinity profile (comparison with Boat Run data and Rutgers survey data, 2011)

[30] DRBC boat-run data can be downloaded from this website: https://www.nj.gov/drbc/programs/quality/wq-data.html

Calibration and Validation Periods

Periods with data for model development, calibration, and validation included 2001-2002, 2011-2013, 2016-2020, and 2021-2022. Different types of data were often not concurrently available, of short duration, or lacked spatial and/or temporal granularity. SM3D was developed over time and data from different periods were used to calibrate and validate the model. The evolution of SM3D with data from different time periods is summarized below.

1. Initial development and calibration occurred with available information for 2018-2019 (**Model_v1).**
2. Simulations were performed with **Model_v1** for 2001-2003, a dry period, and 2011-2013. For those years, the bathymetry was adjusted to reflect the channel depth at the time.[31] The model also performed well, and no adjustments were required. Velocity data from 2011 were used to assess performance.
3. Revisions were made to **Model_v1** with updated post-dredge bathymetry to reflect the 45 ft channel depth and adjust several boundary conditions. Then, the model was recalibrated, focusing on the dry years of 2016 and 2019 (**Model _v2).**
4. In 2023, data became available for the C&D Canal (2021-2022). The **Model_v2** was used to simulate 2021-2022 with the newly available data for the C&D Canal. Minor adjustments were made to the datum of the Canal and a turbulence parameter (Sections 3.3.1, 4.3.4) (**Model_v3** is the final calibrated version of **SM3D** was used in this study**)**
5. The calibration years (2016-2020) were then re-simulated with **SM3D,** and performance statistics were calculated. The model performed well.
6. Additional years (2001-2003 and 2011-2013) were simulated with **SM3D** and compared with observed data. The model was shown to perform well for a range of conditions reflected in all years simulated.

Results

Both graphical presentations and quantitative statistics were used to assess calibration of SM3D (Model_v3). Time-series plots of simulated and observed parameters were used to determine how well the model reproduces the trends and magnitudes of the observed conditions. The "goodness-of-fit" was evaluated for velocity, salinity, and water temperature, with a series of statistical measures typically used to assess model accuracy and reliability (MacWilliams et al.,

[31] Dredging of the federal navigation channel from 40 ft to 45 ft occurred between 2012-2017. For the initial model development, the bathymetry of the model was defined with FEMA 2011 data and then the depth of the channel was adjusted to 40 ft. Thus, the initial calibration (2018-2019) occurred with a 45 ft channel. For the 2001-2003 and 2011-2013 simulations, the channel depth was adjusted to 40 ft (Section 3.2).

2015). The statistics include: 1) model skill, 2) correlation coefficient (r), 3) bias and normalized bias by standard deviation of the observed data, 4) root mean square error (RMSE), 5) unbiased root mean square difference (ubRMSD) and 6) ubRMSD normalized by the standard deviation of the observed data. The formulas for calculating the commonly-used correlation coefficient (or coefficient of determination, R^2) and RMSE are not provided herein.

Table 4.1-1 Summary of NOAA Tide Stations for Comparing Model Results

Station	NOAA Station ID	Data Type	Data Availability [1]	RM
Lewes, DE	8557380	Verified Hourly Water Level	1975-02-26 to Present	0
		Conductivity	2017-04-05 to Present	
		Water Temperature	2000-04-10 to Present	
Cape May, NJ	8536110	Verified Hourly Water Level	1972-04-06 to 2002-12-10 2003-04-01 to Present	~ 2
		Conductivity	2017-04-26 to Present	
		Water Temperature	1997-05-22 to Present	
Brandywine Shoal Light, DE	8555889	Verified Hourly Water Level	2002-07-01 to 2012-10-29 2014-11-12 to 2016-06-23 2017-06-20 to Present	10.0
		Conductivity	2002-06-24 to 2002-09-09 2002-12-13 to 2012-10-29 2014-11-12 to 2016-01-23	
		Water Temperature	2002-11-06 to 2004-04-30 2004-08-26 to 2012-10-29 2014-11-21 to 2016-01-23	
Ship John Shoal, NJ	8537121	Verified Hourly Water Level	2002-08-14 to 2009-05-11 2009-11-07 to Present	37.0
		Conductivity	2002-07-17 to 2009-05-11 2009-11-09 to 2014-09-20 2015-12-16 to 2018-02-03 2018-07-27 to 2018-10-18	
		Water Temperature	2002-07-17 to 2002-07-24 2002-11-06 to 2003-10-02 2004-05-24 to 2004-05-25 2006-03-21 to 2009-05-11 2009-11-07 to 2018-02-03 2018-07-27 to Present	
Reedy Point, DE (East end C&D Canal)	8551910	Verified Hourly Water Level	1980-05-13 to Present	58.5
		Conductivity	N/A	
		Water Temperature	1994-06-22 to Present	
Chesapeake City, MD	8573927	Verified Hourly Water Level	2003-08-29 to Present	West end of C&D Canal
		Conductivity	2017-03-22 to Present	
		Water Temperature	2003-08-29 to Present	
Delaware City, DE	8551762	Verified Hourly Water Level	2001-10-16 to Present	60.5
		Conductivity	N/A	

Station	NOAA Station ID	Data Type	Data Availability [1]	RM
		Water Temperature	2001-10-16 to Present	
Marcus Hook, PA	8540433	Verified Hourly Water Level	2002-07-19 to 2015-07-07 2017-02-01 to Present	79.3
		Conductivity	2002-06-14 to 2004-03-25 2004-07-03 to 2009-9-16	
		Water Temperature	2002-09-23 to 2003-05-21 2004-05-24 to 2004-05-25 2006-03-21 to 2015-07-07 2017-02-01 to Present	
Philadelphia, PA	8545240	Verified Hourly Water Level	1989-03-01 to Present	98.5
		Conductivity	N/A	
		Water Temperature	1997-06-06 to Present	
Burlington, Delaware River, NJ	8539094	Verified Hourly Water Level	2002-06-10 to Present	117.5
		Conductivity	2002-08-15 to 2011-12-30	
		Water Temperature	2002-08-15 to 2004-04-01 2004-08-25 to Present	
Newbold, PA	8548989	Verified Hourly Water Level	2001-11-14 to Present	126.3
		Conductivity	N/A	
		Water Temperature	2001-11-14 to Present	

Model primary calibration period is 2016–2020, and validation years include 2011–2013 and 2001–2003.

Table 4.1-2. Summary of USGS Stations and Data for Comparing Model Results

Station	USGS Station ID	Data Type	Data Availability [1,2]	DRBC River Mile (RM)
Delaware River at Trenton, NJ	01463500	Discharge	1981-10-01 to Present	134.3
		Conductivity	2007-10-01 to Present	
		Water Temperature	2007-10-01 to Present	
Delaware River at Ben Franklin Bridge at Philadelphia, PA	01467200	Conductivity	2007-10-01 to Present	100.1
		Water Temperature	2007-10-01 to Present	
Delaware River at Fort Mifflin at Philadelphia, PA	01474703	Conductivity	2007-10-01 to Present	91.9
		Water Temperature	2007-10-01 to Present	
Delaware River at Chester, PA	01477050	Conductivity	2007-10-01 to Present	83.6
		Water Temperature	2007-10-01 to Present	
Delaware River at Reedy Island Jetty, DE	01482800	Conductivity	2007-10-01 to Present	54.1
		Water Temperature	2007-10-01 to Present	

1. There are data gaps within the time-period listed in the Data Availability column.

2. Model primary calibration period is 2018-2019, and validation years include 2011–2012 and 2001–2003.

Model skill is calculated as:

$$skill = 1 - \left[\sum_{n=1}^{N} |X_{Mi} - X_{Oi}|^2\right] / \left[\sum_{n=1}^{N} (|X_{Mi} - \overline{X}_O| + |X_{Oi} - \overline{X}_O|)^2\right] \quad (4.1\text{-}4)$$

where X is the variable being compared,$\overline{X}$ is the time average of X. M_i is model value at time i of N total times, and O_i is the observation at time i. Perfect agreement between model results and observations yields a skill of 1. Negative bias indicates that the model underpredicts relative to data, while positive bias indicates that the model overpredicts relative to data. The bias of model estimates is calculated as:

$$bias = \frac{1}{N}\sum_{n=1}^{N} X_{Mi} - \frac{1}{N}\sum_{n=1}^{N} X_{Oi} \quad (4.1\text{-}5)$$

Similar to RMSE, ubRMSD quantifies the model–data differences, but with the effects of bias removed from the calculation. As ubRMSD increases, the difference between oscillations in the predicted and observed variable becomes larger. The ubRMSD is calculated as

$$ubRMSD = \left[\frac{1}{N}\sum_{n=1}^{N} \left[\left(X_{Mi} - \overline{X}_M\right) - \left(X_{Oi} - \overline{X}_O\right)\right]^2\right]^{0.5} \quad (4.1\text{-}6)$$

Guidelines for determining model performance have been recommended by some researchers and agencies (e.g., Willmott, 1981; Hess et al., 2003; Zhang et al., 2006; Patchen, 2007; and Bever & MacWilliams, 2013). NOAA (Hess et al., 2003 and Zhang et al., 2006) proposed acceptable error bounds for predicting water level (15 cm), current velocity (26 cm/s), phase (0.5 hr), water temperature (7.7°C), and salinity (3.5 psu). Other criterion for acceptable water temperature error bounding is stricter at 3.0°C (Patchen 2007). These criteria were designed for operational nowcast and forecast models to support navigational applications.

MacWilliams et al. (2015) established a standardized set of cutoff values for both the skill scores and target diagram (see their Table 1) as a succinct method to evaluate and report the accuracy of a large number of comparisons. Model predictions are considered accurate when skill scores are greater than 0.975 for water surface elevation, greater than 0.85 for salinity (acceptable range is 0.7–0.85), and greater than 0.9 for current speed or velocity (acceptable range is 0.8–0.9) The thresholds for classifying model performance using the target statistics were based on the distance from the origin of target diagram plots, and threshold applied to classify the accuracy of model predictions based on the target statistics were the same for each variable. It is classified as acceptable if all predictions fall inside a radius of 1 and considered accurate if all predictions fall inside a radius of 0.5. In this study, statistical measures such as bias, RMSE, ubRMSD, R, R-squared, and target diagrams are used to quantitatively evaluate the model performance. In accordance with the established Quality Assurance Project Plan (DRBC, 2019) developed for DRBC's eutrophication model, a "weight of evidence" approach was used to assess the acceptability of the model for its intended purpose.

4.2 Calibration Parameters

The model was calibrated using the following steps and parameters:

(1) The spatial variable bottom roughness height and the adjustment of non-tidal signals in the ocean surface elevation boundary conditions were determined through the calibration of water surface elevation and current velocities at multiple locations within the Estuary.

(2) A parameter (E3) related to the turbulence model, which governs the vertical mixing process due to turbulent shear and buoyancy, was finalized through calibration of salinity at multiple locations in the Estuary.

The calibration process involved several iterations of simulations. Initial estimates of the tidal surface elevation adjustment at the C&D Canal boundary and the turbulence model parameter E3 were used during the first step to determine bottom roughness and adjust the non-tidal signals in the ocean's water surface boundary conditions. These parameters determined through step 1 remained unchanged during step 2, allowing for the finalization of both the datum conversion factor at the C&D Canal boundary and the turbulence model parameter E3. With newly collected flow data by USGS inside the C&D Canal since 2021, the adjustment of the tidal surface elevation at the C&D Canal boundary was verified based on model-to-data comparison of the flow in the C&D Canal.

In addition, horizontal eddy diffusivity coefficient (AHD), time step, and wetting/drying parameters were specified and adjusted to improve model stability.

4.2.1 Bottom Roughness Height (Z0)

The model was first calibrated with tidal water surface elevation using the data from nine NOAA tide stations along the Delaware River by adjusting the effective bed roughness, which accounts for friction from the bed. Bottom roughness affects the current circulation as well as the amplitude and phase of the progressive wave that propagates from the mouth of the bay upstream.

The composition of bottom sediments in the upper estuary includes fine sands, coarse sediment, and gravel with silt accumulation in spots. Muddy and fine sediments are found within the zone of estuarine turbidity maximum (ETM), from RM 50 to 75 (or 80 to 100 km upstream of the bay mouth) (Sharp et al., 2009). This spatial variability made it necessary to implement a spatially-variable effective bottom roughness height (Z0) throughout the model domain, ranging from 0.1 to 4.4 cm. The range of effective bed roughness typically used in estuarine hydrodynamic models is 0.1 to 10 cm (Blumberg and Mellor, 1987). Table 4.2-1 presents the Z0 values used in the model. Bottom roughness height was set to be small in Zone 5, where the ETM is located, to reflect the clay and silt sediment bed locally. The bottom roughness height was set to be slightly higher in the deeper navigation channel than the shallower area adjacent to it in Zones 4, 5 and

6 to reflect a relatively rougher sediment bed due to a higher current velocity and near-bed shear stress. DRBC-defined water quality zones can be found in Figure 3.1-1.

Table 4.2-1. Spatially Variable Bottom Roughness Height Used in Model

Region	Inside FNC (cm)	Outside FNC (cm)
2 (upstream RM 117.5)	1.1	1.1
2 (downstream RM 117.5)	0.7	0.7
3	0.37	0.36
4	0.37 to 1.0	0.36 to 0.5
5 (upstream RM 68)	0.8	0.36 to 0.5
Around DMB area	1.0	0.36 to 0.5
5 (downstream RM 68)	0.36 to 0.6	0.35 to 0.5
6	0.4	0.4
Ocean	0.1	
C&D Canal	4.4	
Tributaries	1.3	
River Floodplains	2.3	
Low-lying Marshes [1]	2.5	

1. SM3D was calibrated first without low-lying marshes; sensitivity simulations were conducted to investigate the impact from marshes (Chen, et al., 2025). Simulations with and without marshes produced similar results under current tidal and hydrologic conditions

4.2.2 Steric Effect at the Ocean Boundary

As discussed in Section 3.3.1, the long-term steric component in Equation (3.1-1) was treated as an adjustable calibration parameter in this modeling study. The long-term steric component was adjusted using the average seasonal cycle (ASC) of Lewes, DE, as a reference to improve the model performance during model calibration. The long-term steric effect on the regional water level is closely related to and embedded in the ASC at NOAA station at Lewes, DE, which was used to approximate the long-term steric effect at the model ocean boundary.

NOAA long-term tide (water surface elevation) data at Lewes and other nearby stations (such as Atlantic City, NJ) demonstrate the seasonality of the mean sea level. Figure 1.1-2 shows the ASC at NOAA Station at Lewes based on 50 years of observed tides. According to NOAA, the ASC is caused by regular fluctuations in coastal temperatures, salinities, winds, atmospheric pressures, and ocean currents. A sensitivity analysis showed that adjusting the long-term steric component in the specification of the water level boundary conditions improved the prediction of the seasonal variation in the tide and salinity.

4.2.3 Adjustment to Tidal Surface Elevation in C&D Canal

As discussed in Section 3.3.1, the vertical datum used in the model was NAVD88. NOAA tide data collected at Station (8573927) Chesapeake City, MD, were based on MLLW datum[32]. Thus, tidal water surface elevation was converted from MLLW to NAVD88 as follows: NAVD88 = MLLW – 0.474 m. This conversion factor (0.474 m) was calculated with the datum conversion software VDATUM, with an uncertainty range of +/- 10 cm for this location (VDATUM website[33]).

The adjustment to tidal water surface elevation at the C&D Canal western boundary was treated as an additional calibration parameter, due to the relatively large uncertainty range. The predicted net flow in the C&D Canal is sensitive to the tidal water surface elevation at both ends of the canal, and the flow of less saline water into Delaware Bay has a significant impact on salinity intrusion.

NOAA deploys an ADCP at the C&D Canal near Chesapeake City (station cb1301), mounted horizontally at a given depth. However, no analysis is available such that ADCP data can be used to calculate a mean velocity or flow rate through a relationship (rating). For its Next Generation Water Observing System, in late 2019 USGS installed additional equipment to measure the current velocity and flow rate in the C&D Canal.

For 2021 - 2022, discharge data for the C&D Canal near the Delaware City end of the canal were available from USGS[34] and were used to evaluate the methodology developed to specify the boundary condition at the Chesapeake City end. With this new data set, the calibrated model for 2016-2000 was used to simulate 2021-2022 and compare the model results for the flow through the C&D Canal with the measured flow rate. From those results, it was determined that the WSE boundary condition at the Chesapeake City end of the Canal could be adjusted by -7 cm to improve model performance. The resulting net flows are in general agreement with the published net flow range (see Section 4.3.4). The observed average monthly net flows from the C&D Canal into the Delaware River for 2021 and 2022 were 212 and -247 cfs (or 6 and -7 m^3/s), respectively. The simulated average monthly net flows were 1,942 cfs and -742 cfs (or 55 and -21 m^3/s), respectively.

[32]NOAA started providing WSE data in the vertical datum of NAVD88 in May 2020 in addition to MLLW at Station (8573927) Chesapeake City, MD. The NAVD88 datum is 0.487m above the MLLW datum reported on the website in 2020, but this information was not available at the time when the model was initially developed in 2019. This information can be used for future studies and the model can be revised based accordingly.
https://tidesandcurrents.noaa.gov/datums.html?datum=MLLW&units=1&epoch=0&id=8573927&name=Chesapeake+City&state=MD
[33] NOAA VDATUM website: https://vdatum.noaa.gov/vdatumweb/vdatumweb?a=101102420190304
VDATUM documentation for uncertainties: https://vdatum.noaa.gov/docs/est_uncertainties.html
[34] USGS C&D Canal station website: https://waterdata.usgs.gov/nwis/uv?site_no=01482695&legacy=1

4.2.4 Turbulent Model Parameter (*E3*)

EFDC utilizes the Mellor and Yamada (1982) turbulence model to calculate the eddy viscosity and eddy diffusivity, which govern the vertical mixing process due to turbulent shear and buoyancy from vertical stratification of water temperature and salinity. Mellor and Yamada (1982) considered the equal contribution of turbulent shear and buoyancy to the length scale equation. Burchard (2001) demonstrated that all empirical parameters in the original model of Mellor and Yamada (1982) were calibrated except *E3* (or here in EFDC named *CTE3*). *CTE3* was set to be equal to *E1* of 1.8 by Mellor and Yamada (1982) as the default value due to lack of information. In this study, *CTE3* was calibrated through model to data comparison of salinity. Varying the *CTE3* value had minimal impact on the simulated tidal water surface elevations but a significant impact on salinity. A sensitivity analysis demonstrated that increasing *CTE3* enhanced vertical stratification of salinity and resulted in salinity intrusion occurring farther upstream; salinity intrusion was best simulated with a *CTE3* of 2.2, which is within the range of 1 to 8 given in the literature (Burchard, 2001).

4.2.5 Parameters Affecting Model Stability

The parameters affecting model stability that are examined include: Smagorinsky horizontal eddy diffusivity coefficient (AHD) that is used to calculate the horizontal eddy diffusivity (AH), time step, and wetting/drying parameters (*Hdry* and *Hwet*).

The Smagorinsky coefficient, AHD, in calculating the horizontal eddy diffusivity (AH) in EFDC, was calculated using the Smagorinsky equation (Hamrick, 1992; Smagorinsky,1963), expressed in Cartesian coordinates as:

$$AH = AHD * \Delta x * \Delta y \sqrt{\left(\frac{\partial u}{\partial x}\right)^2 + \frac{1}{2}\left(\frac{\partial v}{\partial x} + \frac{\partial u}{\partial y}\right)^2 + \left(\frac{\partial v}{\partial y}\right)^2} \quad (4.2\text{-}1)$$

u, v = horizontal velocity in x and y directions
Δx, Δy = grid cell dimensions in x and y directions
AHD = Smagorinsky horizontal eddy diffusivity coefficient, an adjustable parameter in EFDC

The Smagorinsky coefficient (*AHD*), a spatially-constant adjustable parameter, is dependent on the spatial resolution of the numerical grid. Preliminary calibration simulations, with spatially-constant *AHD* values between 0.001 to 0.05 m^2/s, indicated that 0.005 and 0.02 m^2/s were the minimum and maximum values needed to ensure numerical stability. The Smagorinsky coefficient value was set to 0.01 m^2/s and was not adjusted for subsequent simulations. This value is in the range (0.01 to 0.1 m^2/s) suggested for the New York Harbor modeling study by Blumberg and Pritchard (1997). Model prediction of salinity transport is less sensitive to the Smagorinsky coefficient as compared with the turbulent parameter (*CTE3*) that affects vertical mixing.

Preliminary diagnostic simulations were conducted with SM3D to ensure that the numerical grid structure and resolution did not produce localized numerical instabilities or unrealistic results. The preliminary simulations were also used to determine the optimum time steps for numerical stability, which were determined to be 5 to 10 seconds for SM3D.

The threshold depths for when a cell becomes dry or wet, *Hdry* and *Hwet*, were set to 20 and 25 cm, respectively. The parameter *Hdry* specifies the water depth at which a cell becomes dry, while *Hwet* specifies the depth at which the cell becomes wet. Relatively high values for these two parameters were necessary to improve model stability.

4.3 Model Results

The parameters used to assess model calibration and validation include tidal water surface elevation, current velocity, water temperature, net flow in the C&D Canal, and salinity. Representative results and associated goodness of fit statistics are provided for the simulated periods. Although the calibration period is considered to be from 2016-2020, goodness of fit statistics are presented for shorter periods based on data availability or periods of high salinity intrusion (critical periods). Results are presented in chronological order and not necessarily referenced as calibration (2016-2020) or validation periods (2001-2003, 2011-2013, 2021-2022).

4.3.1 Tidal Water Surface Elevation

Evaluating performance for WSE was the first calibration step. The tidal wave enters the estuary at its mouth near Cape May, NJ, and progresses upstream to the head of tide at Trenton, NJ. The measured range in WSE (total tide) is the sum of astronomical tide and subtidal meteorological fluctuations at a given location. According to NOAA at each tide gage along the Delaware Estuary[35], the mean range of tide[36] observed at the mouth of the estuary (RM 0) is 4.1 ft (1.2 m) and increases to 5.6 ft (1.7 m) at Ship John Shoal (RM 37) and 7.8 ft (2.4 m) at Newbold (RM 126.3). The mean range of tide at Trenton, NJ (RM 133) is 8.2 ft (2.5 m)[37].

Tidal harmonic analyses were performed for 2019[38] with observed data and model predictions. The amplitude and phase of nine major harmonic constituents were compared (Table 4.3-1). The principal lunar semidiurnal (M2, 12.42-hr period) is the dominant harmonic constituent throughout the estuary. Figure 4.3-1 (1) – (8) shows a model-to-data comparison of the amplification of tidal amplitude for the dominant harmonic constituent M2 and eight major constituents. The observed

[35] https://tidesandcurrents.noaa.gov/map/index.html?region=Delaware
[36] Mean range of tide = The difference in height between mean high water and mean low water.
[37] NOAA TRENTON MARINE TERMINAL, NJ, Station ID: 8539993 (data available from 1979 to 1992, and discontinued after 11/2,1992) https://tidesandcurrents.noaa.gov/stationhome.html?id=8539993#:~:text=Mean%20Range%3A,8.18%20ft .
[38] Model results from one year were sufficient for conducting the tidal harmonic analysis. Analysis results from other years yielded similar good model performance.

tidal amplitude of M2 increased from 0.58 m at the mouth to 0.89 m at Ship John Shoal (RM 37), then decreased to 0.70 m at Marcus Hook (RM 79.3). The observed M2 amplitude is 1.08 m at Newbold (RM 126.3). The maximum positive error in predicted M2 tidal amplitude was 7.2 cm at Ship John Shoal and maximum negative error is -8.2 cm at Marcus Hook. The amplitude of shallow-water constituents M4 and M6, which reflect the influence of river inflows and bathymetry, are also presented in Figure 4.3-2. A complete model-to-data comparison of the nine major harmonic constituents at nine NOAA stations are summarized in Table 4.3-2.

The errors were within the acceptable bounds of 15 cm for water level and 0.5 hr for phase recommended by NOAA (Hess et al. 2003; Zhang et al. 2006), except for a few non-dominant constituents with small amplitude that showed a relatively larger difference in phase (most notably, K1 and Q1). The comparisons indicate that SM3D adequately reproduced the amplitude and phase of all astronomical tide components.

Table 4.3-1. Harmonic Constituents for Model Performance Evaluation

No.	Name	Description
1	M2	Principal lunar semidiurnal constituent
2	S2	Principal solar semidiurnal constituent
3	N2	Large lunar elliptic semidiurnal constituent
4	K1	Lunar diurnal constituent
5	M4	Shallow water overtides of principal lunar constituent
6	O1	Lunar diurnal constituent
7	M6	Shallow water overtides of principal lunar constituent
8	Q1	Large lunar elliptic diurnal constituent
9	K2	Lunisolar semidiurnal constituent

Table 4.3-2. Summary of Tidal Harmonic Analysis

Station	Station ID	River Mile	Tide	Amplitude (m)			Phase (degree)			Phase (hr)		
				SM3D	Data	Difference	SM3D	Data	Difference	SM3D	Data	Difference
LEWES	8557380	0	M2	0.577	0.584	-0.007	27.37	31.55	-4.18	0.94	1.09	-0.14
			S2	0.101	0.106	-0.005	54.46	57.19	-2.73	1.82	1.91	-0.09
			N2	0.133	0.136	-0.003	7.07	8.89	-1.82	0.25	0.31	-0.06
			K1	0.092	0.104	-0.012	188.60	201.42	-12.82	12.54	13.39	-0.85
			M4	0.009	0.011	-0.002	148.15	188.71	-40.56	2.56	3.26	-0.70
			O1	0.079	0.084	-0.005	195.88	189.99	5.89	14.05	13.63	0.42
			M6	0.006	0.005	0.001	418.08	350.01	68.07	4.81	4.03	0.78
			Q1	0.015	0.014	0.000	183.15	179.93	3.22	13.67	13.43	0.24
			K2	0.027	0.029	-0.003	51.64	57.95	-6.31	1.72	1.93	-0.21
CAPE MAY	8536110	2	M2	0.705	0.696	0.009	28.69	28.85	-0.16	0.99	1.00	-0.01
			S2	0.120	0.121	-0.001	59.08	55.86	3.22	1.97	1.86	0.11
			N2	0.154	0.155	-0.001	10.96	8.44	2.52	0.39	0.30	0.09
			K1	0.096	0.106	-0.010	188.03	199.30	-11.27	12.50	13.25	-0.75
			M4	0.010	0.012	-0.003	91.04	101.38	-10.34	1.57	1.75	-0.18
			O1	0.080	0.085	-0.004	195.62	186.93	8.69	14.03	13.41	0.62
			M6	0.007	0.008	-0.001	66.80	29.56	37.24	0.77	0.34	0.43
			Q1	0.014	0.014	0.001	184.86	180.06	4.80	13.80	13.44	0.36
			K2	0.032	0.034	-0.002	54.31	53.85	0.46	1.81	1.79	0.02
SHIP JOHN SHOAL	8537121	37	M2	0.894	0.822	0.072	62.03	71.76	-9.73	2.14	2.48	-0.34
			S2	0.143	0.122	0.021	98.48	104.35	-5.87	3.28	3.48	-0.20
			N2	0.180	0.162	0.018	47.19	53.69	-6.50	1.66	1.89	-0.23
			K1	0.100	0.114	-0.014	202.14	220.37	-18.23	13.44	14.65	-1.21
			M4	0.041	0.034	0.007	29.65	32.31	-2.66	0.51	0.56	-0.05
			O1	0.086	0.087	-0.002	211.55	207.76	3.79	15.17	14.90	0.27

Station	Station ID	River Mile	Tide	Amplitude (m)			Phase (degree)			Phase (hr)		
				SM3D	Data	Difference	SM3D	Data	Difference	SM3D	Data	Difference
			M6	0.026	0.020	0.006	250.78	274.79	-24.01	2.88	3.16	-0.28
			Q1	0.013	0.014	-0.001	212.99	199.27	13.72	15.90	14.87	1.02
			K2	0.039	0.037	0.002	90.69	103.65	-12.96	3.01	3.45	-0.43
REEDY POINT	8551910	58.5	M2	0.763	0.780	-0.017	96.42	107.96	-11.54	3.33	3.72	-0.40
			S2	0.114	0.102	0.011	134.44	142.10	-7.66	4.48	4.74	-0.26
			N2	0.144	0.144	0.000	81.45	90.23	-8.78	2.86	3.17	-0.31
			K1	0.069	0.096	-0.027	224.33	242.86	-18.53	14.91	16.15	-1.23
			M4	0.067	0.053	0.014	109.58	125.32	-15.74	1.89	2.16	-0.27
			O1	0.061	0.072	-0.011	231.80	228.54	3.26	16.62	16.39	0.23
			M6	0.035	0.031	0.004	23.78	51.65	-27.87	0.27	0.59	-0.32
			Q1	0.008	0.012	-0.004	246.69	228.43	18.26	18.41	17.05	1.36
			K2	0.034	0.034	0.000	122.40	139.29	-16.89	4.07	4.63	-0.56
DELAWARE CITY	8551762	60.5	M2	0.796	0.785	0.011	100.89	113.21	-12.32	3.48	3.91	-0.43
			S2	0.119	0.103	0.016	139.37	147.46	-8.09	4.65	4.92	-0.27
			N2	0.151	0.144	0.007	86.29	95.19	-8.90	3.03	3.35	-0.31
			K1	0.086	0.107	-0.022	226.98	244.58	-17.60	15.09	16.26	-1.17
			M4	0.075	0.065	0.010	119.88	139.34	-19.46	2.07	2.40	-0.34
			O1	0.077	0.085	-0.008	236.29	231.47	4.82	16.95	16.60	0.35
			M6	0.040	0.032	0.008	24.70	59.28	-34.58	0.28	0.68	-0.40
			Q1	0.010	0.013	-0.003	246.16	225.23	20.93	18.37	16.81	1.56
			K2	0.035	0.034	0.001	127.17	142.82	-15.65	4.23	4.75	-0.52
MARCUS HOOK	8540433	79.3	M2	0.696	0.781	-0.086	142.25	146.70	-4.45	4.91	5.06	-0.15
			S2	0.095	0.096	-0.001	180.68	181.89	-1.21	6.02	6.06	-0.04
			N2	0.125	0.140	-0.016	125.12	127.49	-2.37	4.40	4.48	-0.08
			K1	0.085	0.108	-0.023	249.87	262.24	-12.37	16.61	17.43	-0.82

Station	Station ID	River Mile	Tide	Amplitude (m)			Phase (degree)			Phase (hr)		
				SM3D	Data	Difference	SM3D	Data	Difference	SM3D	Data	Difference
			M4	0.100	0.091	0.009	178.03	194.84	-16.81	3.07	3.36	-0.29
			O1	0.078	0.086	-0.007	257.94	248.32	9.62	18.50	17.81	0.69
			M6	0.038	0.035	0.003	125.57	158.20	-32.63	1.44	1.82	-0.38
			Q1	0.009	0.013	-0.004	267.89	244.22	23.67	19.99	18.23	1.77
			K2	0.030	0.033	-0.003	164.94	176.84	-11.90	5.48	5.88	-0.40
PHILADELPHIA	8545240	98.5	M2	0.797	0.834	-0.037	184.62	183.76	0.86	6.37	6.34	0.03
			S2	0.100	0.094	0.006	228.73	222.67	6.06	7.62	7.42	0.20
			N2	0.131	0.143	-0.012	168.09	164.59	3.50	5.91	5.79	0.12
			K1	0.088	0.112	-0.023	268.82	281.31	-12.49	17.87	18.70	-0.83
			M4	0.053	0.084	-0.031	257.71	252.61	5.10	4.45	4.36	0.09
			O1	0.081	0.087	-0.006	274.80	265.85	8.95	19.71	19.07	0.64
			M6	0.050	0.049	0.001	215.32	246.24	-30.92	2.48	2.83	-0.36
			Q1	0.009	0.013	-0.004	288.34	263.63	24.71	21.52	19.68	1.84
			K2	0.031	0.033	-0.002	207.17	215.22	-8.05	6.89	7.15	-0.27
BURLINGTON	8539094	117.5	M2	1.016	1.001	0.015	202.27	213.46	-11.19	6.98	7.36	-0.39
			S2	0.129	0.117	0.013	250.44	258.39	-7.95	8.35	8.61	-0.27
			N2	0.164	0.166	-0.002	187.84	196.14	-8.30	6.60	6.90	-0.29
			K1	0.094	0.115	-0.021	277.12	296.20	-19.08	18.42	19.69	-1.27
			M4	0.156	0.123	0.034	334.17	338.14	-3.97	5.76	5.83	-0.07
			O1	0.085	0.089	-0.004	282.36	279.37	2.99	20.25	20.04	0.21
			M6	0.035	0.028	0.007	332.22	347.77	-15.55	3.82	4.00	-0.18
			Q1	0.009	0.014	-0.004	298.27	277.47	20.80	22.26	20.71	1.55
			K2	0.039	0.038	0.001	226.89	248.51	-21.62	7.54	8.26	-0.72
NEWBOLD	8548989	126.3	M2	1.076	1.080	-0.004	205.72	218.32	-12.60	7.10	7.53	-0.43
			S2	0.139	0.123	0.016	254.40	263.30	-8.90	8.48	8.78	-0.30

Station	Station ID	River Mile	Tide	Amplitude (m)			Phase (degree)			Phase (hr)		
				SM3D	Data	Difference	SM3D	Data	Difference	SM3D	Data	Difference
			N2	0.174	0.180	-0.006	191.98	201.63	-9.65	6.75	7.09	-0.34
			K1	0.096	0.117	-0.021	278.90	297.72	-18.82	18.54	19.79	-1.25
			M4	0.202	0.155	0.047	340.74	346.68	-5.94	5.88	5.98	-0.10
			O1	0.086	0.093	-0.007	284.26	281.93	2.33	20.39	20.22	0.17
			M6	0.067	0.062	0.005	6.09	31.73	-25.64	0.07	0.36	-0.29
			Q1	0.009	0.014	-0.005	298.14	280.55	17.59	22.25	20.94	1.31
			K2	0.041	0.039	0.001	232.52	254.09	-21.57	7.73	8.45	-0.72

Figure 4.3-3 (1)–(8) presents example time series of predicted and observed hourly and 32-hour-lowpass-filtered water surface elevation (WSE) (total tide, including both astronomical and meteorological fluctuations) at eight NOAA tide stations for July through September of 2019, for visualizing the model predictions qualitatively. A statistical analysis of 1-to-1 model to data comparisons of hourly and 32-hour-lowpass-filtered for 2016–2020 is shown in Figure 4.3-4 (1)–(8). Target diagrams for simulated hourly and 32-hour-lowpass-filtered WSE for 2016-2020 and the critical season of 2016 are presented in Figure 4.3-5 and 4.3-6, respectively. The statistics for the 2016-2020 period and for the critical period from September through December 2016 and 2019, used to quantify the model performance, are summarized in Table 4.3-3 (a), 4.3-3 (b), and 4.3-3 (c), respectively.

Hourly as well as the sub-tidal signals of the WSE (total tide) were simulated with adequate accuracy to meet the objectives of this study. The predicted hourly WSE had minimal bias (typically less than 0.12 m) and low ubRMSD (ranged from 0.07 to 0.24 m) either for the multi-year long-term or for the critical season. For example, the model bias and ubRMSE error at Philadelphia were -0.05 to -0.06 m and 0.11 to 0.13 m, respectively. The model skill score ranged from 0.977 to 0.995. These statistical measures demonstrate that the model accurately predicted the tidal water surface elevation throughout the system.

Table 4.3-3 (a). Model Performance Predicting Hourly Water Surface Elevation (2016–2020)

Station ID	NAME	State	NOBS	RMSE	ubRMSE	Bias	R2	Skill	MAE	NSE
8557380	LEWES	DE	43847	0.101	0.084	0.056	0.971	0.989	0.080	0.957
8536110	CAPE MAY	NJ	43842	0.091	0.084	0.036	0.979	0.994	0.070	0.974
8555889	BRANDYWINE	DE	34606	0.098	0.087	-0.046	0.977	0.993	0.079	0.970
8537121	SHIP JOHN SHOAL	NJ	43842	0.165	0.161	-0.034	0.952	0.985	0.135	0.936
8551910	REEDY POINT	DE	42465	0.163	0.156	-0.048	0.937	0.982	0.134	0.929
8551762	DELAWARE CITY	DE	43842	0.178	0.172	-0.047	0.929	0.980	0.148	0.919
8540433	MARCUS HOOK	PA	34297	0.148	0.136	-0.058	0.958	0.985	0.115	0.945
8545240	PHILADELPHIA	PA	43842	0.134	0.122	-0.054	0.967	0.989	0.103	0.960
8539094	BURLINGTON	NJ	43842	0.230	0.195	-0.123	0.941	0.979	0.189	0.916
8548989	NEWBOLD	PA	43842	0.234	0.227	-0.060	0.932	0.981	0.186	0.926

Table 4.3-3 (b) Model Performance Predicting Hourly Water Surface Elevation (September to December 2016)

Station ID	NAME	State	NOBS	RMSE	ubRMSE	Bias	R2	Skill	MAE	NSE
8557380	LEWES	DE	2927	0.092	0.076	0.052	0.977	0.991	0.074	0.966
8536110	CAPE MAY	NJ	2927	0.077	0.070	0.032	0.984	0.995	0.060	0.981
8537121	SHIP JOHN SHOAL	NJ	2927	0.164	0.164	-0.011	0.946	0.984	0.138	0.932
8551910	REEDY POINT	DE	2927	0.168	0.163	-0.044	0.928	0.980	0.141	0.919
8551762	DELAWARE CITY	DE	2927	0.181	0.180	-0.020	0.918	0.978	0.154	0.909
8545240	PHILADELPHIA	PA	2927	0.122	0.112	-0.048	0.971	0.991	0.096	0.965
8539094	BURLINGTON	NJ	2927	0.230	0.209	-0.097	0.932	0.979	0.189	0.914
8548989	NEWBOLD	PA	2927	0.242	0.239	-0.034	0.923	0.980	0.194	0.919

Table 4.3-3 (c) Model Performance Predicting Hourly Water Surface Elevation (September to December 2019)

Station ID	NAME	State	NOBS	RMSE	ubRMSE	Bias	R2	Skill	MAE	NSE
8557380	LEWES	DE	2927	0.099	0.083	0.054	0.972	0.990	0.078	0.961
8536110	CAPE MAY	NJ	2927	0.093	0.088	0.031	0.977	0.993	0.070	0.973
8555889	BRANDYWINE	DE	2922	0.099	0.088	-0.046	0.977	0.992	0.078	0.969
8537121	SHIP JOHN SHOAL	NJ	2927	0.173	0.171	-0.025	0.943	0.983	0.142	0.927
8551910	REEDY POINT	DE	2927	0.172	0.166	-0.048	0.928	0.980	0.141	0.920
8551762	DELAWARE CITY	DE	2927	0.190	0.183	-0.049	0.919	0.977	0.158	0.906
8540433	MARCUS HOOK	PA	2927	0.154	0.139	-0.066	0.953	0.983	0.118	0.939
8545240	PHILADELPHIA	PA	2927	0.145	0.130	-0.065	0.962	0.988	0.109	0.953
8539094	BURLINGTON	NJ	2927	0.249	0.218	-0.120	0.927	0.975	0.204	0.900
8548989	NEWBOLD	PA	2927	0.258	0.251	-0.058	0.916	0.977	0.207	0.908

4.3.2 Current Velocity

Comparison with NOAA ADCP Survey Data in Delaware Bay

Current velocity measurements during 2012 and 2018–2019 were available from NOAA stations db0201 at Reedy Point (RM 58.5, near the C&D canal) and db0501 and db0502 at Brown Shoal Light, NJ. A representative comparison of observed and predicted depth-averaged along-channel and cross-channel current velocity at Reedy Point is shown in Figure 4.3-7 for January 30 to February 5, 2012. A 1-to-1 comparison of observed versus predicted along-channel, depth-averaged velocity magnitude for a longer period (January 1 to May 5, 2012) is shown in Figure 4.3-8. The statistical measures for depth-averaged current velocity at db0201 for this 4-month period were ubRMSD = 16.8 cm/s, bias = 6.6 cm/s, and skill score = 0.955, indicating that the model adequately predicted depth-averaged current velocity at this location. Similarly, agreement

between predicted and observed depth-averaged current velocity at db0501 was reasonable. For example, Figure 4.3-9 shows the comparison of temporal variation of the depth-averaged current velocity at db0501 for June 25–30, 2012, and the 1-to-1 comparison is presented in Figure 4.3-10. The model showed good agreement for depth-averaged current velocity at db0501 for June 2012. Similar model-to-data comparisons of depth-averaged current velocity at station db0502 for the period of September 6, 2018, to February 25, 2019, are presented in Figures 4.3-11 (showing a short period as an example) and Figure 4.3-12.

From April 8 to June 27, 2011, Rutgers University deployed bottom-mounted ADCP mooring stations in the middle reach of Delaware Bay at RM 42 and RM 33 (Figure 4.1-4). Model-to-data comparisons of longitudinal and cross-sectional channel current velocity at Station C5 (RM 42) from April 18 through June 30, 2011, were performed. An example of this comparison for June 6–12, 2011 is shown in Figure 4.3-13 as an example, and the full data set is shown in Figure 4.3-14. An example of a predicted vertical profile of current velocity compared to the ADCP data is presented in Figure 4.3-15. The model was able to adequately capture the vertical structure of the current velocity at this location. The statistical measures for predicted along-channel depth-averaged current velocity at four ADCP station locations are summarized in Table 4.3-4, with a skill score of 0.938–0.991 and ubRMSD of 8.8 to 15.4 cm/s. These statistical measures indicate that SM3D simulated current velocity with sufficient accuracy to meet the objectives of this study.

Table 4.3-4. Model Performance Predicting Depth-Averaged Current Velocity

Station	Source	ID	Period of Record	N	R^2	Bias (cm/s)	RMSE (cm/s)	ubRMSD (cm/s)	Skill Score
Brown Shoal Light	NOAA	db0501	06-01-2012 to 06-30-2012	718	0.964	1.0	8.9	8.8	0.991
Delaware Bay Channel LB 10	NOAA	Db0502	09-06-2018 to 02-25-2019	4075	0.936	-1.3	11.5	11.5	0.983
Reedy Point	NOAA	db0201	01-01-2012 to 05-05-2012	2811	0.955	6.6	16.8	15.4	0.955
Station C5	2011 Survey	C5	04-18-2011 to 06-30-2011	1729	0.938	3.3	15.6	15.2	0.938

Comparison with PWD ADCP Survey Data in the Upper Tidal River

PWD installed three buoys equipped with ADCPs at Burlington (Buoy A, RM 117.4), Philadelphia Eagle Point (Buoy B, RM 93.7), and Marcus Hook (Buoy C, RM 77.1) in May 2012 (Figure 4.3-16). Each data collection system consists of a surface buoy-mounted, downward looking, 1-MHz Nortek Aquadopp acoustic Doppler profiler with Z-cell technology. After initial calibration issues, these ADCPs collected data starting in August 2012. Each buoy provides data in 0.5 m vertical bins covering the full water column depth. The data provides a near complete profile of current measurements, from approximately 1.2 m below the surface down to approximately 1 m above the bottom, averaged at a six-minute interval. Small gaps in the time series occur from instrument service visits, where the instrument was recovered, data downloaded, and redeployed; these gaps could introduce significant error in harmonic analysis. In this study, time periods with minimum gaps were used: August 21 to September 20, 2012, and April 4 to August 8, 2016.

- Harmonic Analysis for Depth-averaged Current Velocity

Similar to the tidal harmonic analysis for water surface elevation, this section examines the tidal component of current velocity at the three buoy stations. The harmonic analysis was performed for the along-channel depth-averaged current velocity using the program T-Tide. The results are summarized in Table 4.3-5 and 4.3-6. The analysis showed that, similar to WSE, M2 is the dominant tidal component. Since the tidal wave energy is proportional to the square of the amplitude, those harmonic constituents other than M2 carried much lower energy and presented less impact on hydrodynamics and salinity transport in this area. Comparisons with 2012 data set show that the maximum error in the amplitude between model predictions and observations was -14.8, 6.9, and -5.2 cm/s for Buoy A, B, and C, respectively. The absolute errors are all within the acceptable error bound of 26 cm/s for predicting current speed recommended by NOAA (Hess et al., 2003; Zhang et al., 2006). The maximum error in M2 component phase was 0.13, 0.60, and 0.40 hr at Buoy A, B, and C, respectively. At Buoys A and C, the error values are less than the acceptable error bound of 0.5 hr suggested by NOAA for a coastal model to evaluate model performance for predicted current velocity (Hess et al., 2003; Zhang et al., 2006). Generally, the phase mismatch at Buoy B by less than 0.6 hr is considered as less significant for predicting long-term salinity transport compared to the navigation application, which the NOAA standard is applied. Similar accuracy was obtained with the comparison of the 2016 dataset as well.

Table 4.3-5. Harmonic Analysis for Depth-averaged Current Velocity (SM3D), August 21 to September 20, 2012

Buoy	RM	Tidal Component	Amplitude (cm/s)			Phase (degree)			Phase (hr)		
			Predicted	Observed	Difference	Predicted	Observed	Difference	Predicted	Observed	Difference
A	117.4	M2	41.42	56.23	-14.81	120.42	116.7	3.72	4.15	4.03	0.13
		S2	6.94	7.84	-0.9	172.64	172.4	0.24	5.75	5.75	0.01
		N2	6.14	7.76	-1.62	121.13	119.13	2	4.26	4.19	0.07
		K1	2.07	3.14	-1.07	180.96	210	-29.04	12.03	13.96	-1.93
		M4	12.74	12.7	0.04	260.39	242.29	18.1	4.49	4.18	0.31
		O1	2.24	2.37	-0.13	169.96	178.71	-8.75	12.19	12.82	-0.63
		M6	7.34	7.91	-0.57	274.55	249.47	25.08	3.16	2.87	0.29
B	93.7	M2	69	62.13	6.87	110.85	93.48	17.37	3.82	3.23	0.60
		S2	11.17	8.28	2.89	161.66	149.25	12.41	5.39	4.98	0.41
		N2	10.28	7.51	2.77	109.58	98.77	10.81	3.85	3.47	0.38
		K1	3.72	4.6	-0.88	176.5	208.39	-31.89	11.73	13.85	-2.12
		M4	10.47	6.12	4.35	234.15	217.72	16.43	4.04	3.76	0.28
		O1	3.59	4.11	-0.52	166.38	142.32	24.06	11.93	10.21	1.73
		M6	5.6	5.48	0.12	194.24	139.39	54.85	2.23	1.60	0.63
C	77	M2	75.97	81.13	-5.16	96.9	85.37	11.53	3.34	2.95	0.40
		S2	11.94	10.38	1.56	142.95	133.82	9.13	4.77	4.46	0.30
		N2	11.23	10.51	0.72	92.76	87.23	5.53	3.26	3.07	0.19
		K1	4.78	5.52	-0.74	171.47	197.72	-26.25	11.40	13.15	-1.75
		M4	6.24	8.39	-2.15	169.73	143.1	26.63	2.93	2.47	0.46
		O1	4.67	5.51	-0.84	159.59	165.55	-5.96	11.45	11.87	-0.43
		M6	5.77	6.59	-0.82	123.73	101.42	22.31	1.42	1.17	0.26

Table 4.3-6. Harmonic Analysis for Depth-averaged Current Velocity (SM3D), April 4 to August 8, 2016

Buoy	RM	Tidal Component	Amplitude (cm/s)			Phase (degree)			Phase (hr)		
			Predicted	Observed	Difference	Predicted	Observed	Difference	Predicted	Observed	Difference
B	93.7	M2	72.01	70.53	1.48	108.67	86.74	21.93	3.75	2.99	0.76
		S2	7.99	6.48	1.51	148.10	131.37	16.73	4.94	4.38	0.56
		N2	10.2	11.29	-1.09	89.23	68.57	20.66	3.14	2.41	0.73
		K1	3.48	5.77	-2.29	196.97	172.76	24.21	13.10	11.49	1.61
		M4	11.61	5.83	5.78	227.16	164.11	63.05	3.92	2.83	1.09
		O1	2.74	4.07	-1.33	188.15	174.33	13.82	13.49	12.50	0.99
		M6	6.22	4.57	1.65	188.11	110.07	78.04	2.16	1.27	0.90
C	77	M2	81.77	85.02	-3.25	94.62	84.97	9.65	3.26	2.93	0.33
		S2	9.05	8.18	0.87	130.13	124.14	5.99	4.34	4.14	0.20
		N2	11.82	12.85	-1.03	73.22	57.76	15.46	2.57	2.03	0.54
		K1	4.59	6.4	-1.81	189.86	179.00	10.86	12.62	11.90	0.72
		M4	7.05	8.7	-1.65	161.44	137.75	23.69	2.78	2.38	0.41
		O1	3.73	4.35	-0.62	181.74	171.37	10.37	13.03	12.29	0.74
		M6	6.59	6.4	0.19	120.74	99.69	21.05	1.39	1.15	0.24

- Along-channel Depth-averaged Current Velocity

Model performance for predicted along-channel depth-averaged current velocity at three PWD buoy stations is summarized in Table 4.3-7 and 4.3-8 for 2012 and 2016, respectively. Model-to-data time-series comparisons, 1-to-1 plots, and target statistics are presented in Figure 4.3-17 through 4.3-26. RMSEs are all less than 20 cm/s; skill scores are all above 0.96, and target diagram results are within the 1-radius circle, which indicates good accuracy for predicted depth averaged current speeds at these buoy locations (MacWilliams et al., 2015).

The 1-to-1 comparison figures indicate that there are small phase shifts between the predictions and observations at all three buoys. These mismatches could be caused by the imperfect specification of spatially varying bottom roughness and simplified model geometry and bathymetry around the upper Estuary near Trenton. This relatively small phase shift in the current velocity does not significantly affect long-term salinity transport.

Table 4.3-7. Model Performance Predicting Hourly Depth-Averaged Current Velocity at PWD Buoy Locations, August 21 to September 20, 2012

Buoy	N	R^2	Bias (cm/s)	RMSE (cm/s)	ubRMSD (cm/s)	Skill Score
A	720	0.926	-2.7	14.7	14.4	0.966
B	721	0.883	0.6	18.5	18.5	0.965
C	721	0.947	-3.2	14.6	14.2	0.985

Table 4.3-8. Model Performance Predicting Hourly Depth-Averaged Current Velocity at PWD Buoy Locations, April 4 to August 8, 2016

Buoy	N	R^2	Bias (cm/s)	RMSE (cm/s)	ubRMSD (cm/s)	Skill Score
B	3024	0.941	8.0	15.9	13.7	0.980
C	3025	0.959	-2.3	13.6	13.4	0.989

- The tidally averaged circulation – estuary exchange flow structure

The tidally averaged circulation as shown schematically in Figure 4.3-27 (from MacCready and Geyer, 2010) shows that despite the net seaward flow through any cross-section due to the upland river freshwater flows, in lower portions of the cross-section, the water typically flows landward near the entrance of the bay. This near-bottom ocean inflow gradually rises and joins the river flowing seaward in the upper half of the water column, resulting in an overall pattern called the estuary exchange flow (depicted as Q1 and Q2). With continuous ADCP current velocity data (the 2011 Rutgers survey and 2012 data from NOAA station db0501), the estuary exchange flow pattern can be observed through a tidally averaged along-channel current velocity profile.

Figure 4.3-28 through 4.3-30 show tidally averaged currents versus depth at Station C5 (RM 42). The negative currents in deeper water represent net ocean inflow, and the positive currents near the surface represent the net outflow. Figure 4.3-28 shows the tidally averaged vertical profile of the residual current velocity during a four-day period in a spring tide from June 29 to July 3, 2011, and Figure 4.3-29 shows the tidally averaged vertical profile for a 4-day period in a neap tide from June 20 to 24, 2011. Figure 4.3-30 is the tidally averaged vertical profile for a one-month period of July 2011. The model overestimated net flow during July 2011 following some high-flow events in April and May. The monthly average flow at Trenton was 31,430, 25,420, and 13,540 cfs for April, May, and June 2011, respectively. Possible factors that could cause the velocity difference may be the vertical resolution of the grid, the size (volume) of the grid cell, the slope (vertical stability of the instrument), mismatch of position in cross-section, and overall representation of the bathymetry in the immediate and nearby vicinity. The numerical grid cell that contains the

ADCP site is large (530 x 1790 m), and the grid bathymetry represents the spatially averaged bathymetry covered by the grid cell. The ADCP instrument was installed on a slope in the navigation channel, and the model may not have sufficient detail to represent the depth of the site. Nonetheless, these figures show a reasonably good agreement between the observed and simulated results.

4.3.3 Water Temperature

Water density is a function of salinity and water temperature. As water temperature changes, so does the water density. Although the impact of water temperature on salinity transport is a secondary factor, accurate prediction of the water temperature is important for evaluating water quality of the river and habitat areas. Comparisons of near surface water temperature at various NOAA and USGS gaging stations during the 2016 to 2020 period are presented in Figures 4.3-31 and 4.3-32. A summary of the statistical measures for 2016 to 2020 is presented in Table 4.3-9. The model simulated the seasonal variation in temperature at all stations, with an average bias from –0.92 to 0.41 °C over the course of 5-year simulations from 2016 to 2020. The ubRMSE error for this period at all locations ranged from 0.47 to 2.14°C. The model skill for simulated near surface water temperature ranged from 0.985 to 0.999, and the maximum absolute error (MAE) ranged from 0.42 to 1.89 °C. The model performed reasonably well and the model errors were within the acceptable error of 3°C for water temperature (e.g., NOAA 2003 standard, Patchen 2007, Nickitas Georgas 2010). However, water surface temperature was over-predicted at a few locations during the summer months of July and August such as NOAA gage at Lewes, DE, (at the Bay Mouth) and NOAA gage at Delaware City, and under-predicted at Marcus Hook (RM 79.3) during summer. The model over-estimated water temperature in the down-bay area may be attributed to the lack of detailed spatial meteorological data over the huge area of the bay to specify wind and estimate other parameters for input. Wind is much stronger over the bay than observed at Dover airport. Stronger winds result in more heat loss through evaporation; hence a lower water temperature is predicted. Further improvement to predict water temperatures in the bay area near the mouth may be considered in the future.

Model performance for simulated near-surface water temperature at four locations (USGS gage at Reedy Island, USGS gage at Chester, NOAA Philadelphia tide gage, and USGS gage at Ben Franklin Bridge) was evaluated during a critical season from September through December in 2016 and 2019 when there were significant salinity intrusion events occurred, are presented in the 1-to-1 plots in Figure 4.3-33 and Figure 4.3-34, respectively, and the statistical measures are summarized in Table 4.3-10 and 4.3-11. Model skill scores for predicted water temperature for the critical season for salinity intrusion ranged from 0.971 to 0.999, all close to the value of 1 for a perfect model-data comparison. The comparison results in the target diagrams in Figure 4.3-35 and Figure 4.3-36 fall within the 0.5-radius, indicating that the model predicted well the water temperature throughout the Delaware River Estuary during the critical season of 2016 and 2019, respectively.

Table 4.3-9. Model Performance Predicting Near Surface Hourly Water Temperature (2016-2020 Period)

Station ID	NAME	NOBS	RMSE (°C)	ubRMSE (°C)	Bias (°C)	R2	Skill	MAE	NSE
8557380	NOAA LEWES	39129	1.65	1.62	0.33	0.976	0.989	1.295	0.951
8536110	NOAA CAPE MAY	40088	1.97	1.93	0.41	0.969	0.985	1.463	0.932
8537121	NOAA SHIP JOHN SHOAL	27180	1.65	1.65	0.04	0.978	0.992	1.349	0.964
1482800	USGS REEDY ISLAND	42735	1.28	1.23	-0.34	0.989	0.995	1.026	0.979
8551910	NOAA REEDY POINT	41895	1.17	1.14	-0.26	0.989	0.996	0.894	0.984
8551762	NOAA DELAWARE CITY	39673	2.28	2.14	0.79	0.958	0.984	1.892	0.926
8540433	NOAA MARCUS HOOK	31796	1.31	0.94	-0.92	0.991	0.994	1.073	0.976
1477050	USGS CHESTER	36247	1.11	1.06	-0.34	0.988	0.996	0.896	0.982
1467200	USGS BEN FRANKLIN BRIDGE	35809	0.92	0.89	-0.24	0.994	0.997	0.753	0.987
8545240	NOAA PHILADELPHIA	42005	1.05	1.03	-0.19	0.991	0.997	0.830	0.986
8539094	NOAA BURLINGTON	35468	0.62	0.60	-0.15	0.996	0.999	0.466	0.995
8548989	NOAA NEWBOLD	42185	0.54	0.47	-0.27	0.997	0.999	0.417	0.996

Table 4.3-10. Model Performance Predicting Near Surface Hourly Water Temperature (September to December 2016 Period)

Station ID	NAME	NOBS	RMSE (°C)	ubRMSE (°C)	Bias (°C)	R2	Skill	MAE	NSE
8557380	NOAA LEWES	2784	2.52	1.03	2.31	0.979	0.963	2.314	0.842
8536110	NOAA CAPE MAY	2783	2.34	1.35	1.92	0.977	0.972	2.002	0.873
8537121	NOAA SHIP JOHN SHOAL	2775	2.25	1.02	2.01	0.995	0.977	2.019	0.896
1482800	USGS REEDY ISLAND	2782	1.65	1.22	1.11	0.996	0.988	1.326	0.946
8551910	NOAA REEDY POINT	2771	1.44	1.00	1.03	0.992	0.991	1.122	0.962
8551762	NOAA DELAWARE CITY	2783	2.12	1.41	1.58	0.993	0.980	1.751	0.907
1477050	USGS CHESTER	2783	1.35	1.20	0.62	0.994	0.992	1.150	0.965
1467200	USGS BEN FRANKLIN BRIDGE	2244	1.27	1.13	0.58	0.994	0.990	1.125	0.952
8545240	NOAA PHILADELPHIA	2779	1.28	1.21	0.41	0.996	0.993	1.130	0.969
8539094	NOAA BURLINGTON	2780	0.76	0.75	0.10	0.995	0.998	0.639	0.991
8548989	NOAA NEWBOLD	2781	0.70	0.60	-0.36	0.995	0.998	0.556	0.992

Table 4.3-11. Model Performance Predicting Near Surface Hourly Water Temperature (September to December 2019 Period)

Station ID	NAME	NOBS	RMSE (°C)	ubRMSE (°C)	Bias (°C)	R2	Skill	MAE	NSE
8557380	NOAA LEWES	2333	1.07	1.06	-0.04	0.973	0.992	0.813	0.967
8536110	NOAA CAPE MAY	2330	1.09	0.90	-0.61	0.984	0.992	0.904	0.966
8537121	NOAA SHIP JOHN SHOAL	2779	1.76	0.45	-1.70	0.996	0.985	1.700	0.939
1482800	USGS REEDY ISLAND	2783	0.81	0.53	-0.61	0.996	0.997	0.649	0.988
8551910	NOAA REEDY POINT	2770	1.06	1.05	-0.14	0.980	0.995	0.755	0.980
8551762	NOAA DELAWARE CITY	2327	2.03	2.03	0.05	0.973	0.971	1.770	0.839
8540433	NOAA MARCUS HOOK	2758	1.50	0.77	-1.28	0.998	0.991	1.291	0.959
1477050	USGS CHESTER	2558	1.06	0.61	-0.87	0.997	0.995	0.893	0.980
1467200	USGS BEN FRANKLIN BRIDGE	2383	1.08	0.42	-0.99	0.997	0.995	1.000	0.978
8545240	NOAA PHILADELPHIA	2323	1.10	0.44	-1.01	0.997	0.994	1.014	0.975
8539094	NOAA BURLINGTON	2459	0.54	0.39	-0.37	0.997	0.999	0.437	0.995
8548989	NOAA NEWBOLD	2716	0.94	0.51	-0.78	0.996	0.996	0.790	0.985

4.3.4 Net Flow in the C&D Canal

The Delaware Estuary is hydraulically connected with the northern Chesapeake Bay through the C&D Canal. The flow magnitude, flow direction, and net flow from the canal are controlled by the water density and the tidal amplitude and phase at each end of the canal. The net flow from the C&D Canal influences the salinity in the Delaware Estuary. There were no or limited data reported in the past, and that led to modelers making significant simplifications in their models (see descriptions in Section 1.1.3). An earlier study by USACE (Ward et al., 1992) found that the average net flow in the C&D Canal is eastward (toward Delaware), ranging from 3,000 to 4,000 cfs (85 to 113 m^3/s) during 1992–1993. However, the flow direction was reversed during November and December 1992, when a notable northeaster event increased water level in the Delaware Bay and diverted the water to move westward through the canal for about 60 hours. The tidal flow in the C&D Canal usually switches direction every 6 hours, and the total tidal flow is order of magnitude larger than the tidally filtered flow; however, the absolute value of the net flow is significant, e.g., 4,000 cfs is approximately 10 percent of the long-term average discharge of the Susquehanna River at Conowingo, MD, (40,000 cfs), or roughly one third of the median of the annual average flow rate of the Delaware River at Trenton (11,950 cfs). In this study, the tidally filtered flow represents a "net" flow moving from Chesapeake Bay to the Delaware Estuary. During certain extreme weather conditions, the flow may be in one direction for a couple of days, such was observed during November and December 1992.

In late 2020 USGS installed additional equipment in the C&D Canal (USGS 01482695) to measure the current velocity and flow rate among other parameters (see location of this gage in Figure 4.3-37). It started reporting discharge data in August 2021 and is used as an additional calibration metric. The data help to constrain the model in simulated net flow through the C&D Canal. Simulated and observed hourly and tidally filtered flow[39] are presented in time series and compared in 1-to-1 plots in Figures 4.3-38 to 4.3-39 and in Figuress 4.3-41 to 4.3-42 for 2021 and 2022, respectively. The monthly residual flow for 2021 and 2022 are presented in Figures 4.3-40 and 4.3-43, respectively, to examine whether any discernable seasonal pattern exists in the net flow from the C&D Canal. The monthly residual flow is calculated as the monthly average of the 32-hr-LPF flow[40]. Error bar represent 2 times the standard error. The observed and simulated average of the monthly net flow are 6 m^3/s (212 cfs) and 55 m^3/s (1942 cfs) during March through December 2021, respectively, and those values are -7 m^3/s (-247 cfs) and -21 m^3/s (-742 cfs) during January through December 2022, respectively. The net flow observed in the 2021-2022 period is lower than what was observed in the 1992-1993 period, but they were the same order of magnitude. Data collected from 2021 to 2022 may not be sufficient to reveal seasonality for the C&D net flow. A future study may analyze data collected during more severe "dry" or "wet" years. Model performance predicting net flow in C&D Canal is presented in Table 4.3-12.

[39] USGS used different filter to calculate the filtered flow, while DRBC used a 32-hour-low-pass filter to get the filtered flow.
[40] 32-hr-LPF flow stands for the 32-hr-Low-Pass-Filtered flow.

Table 4.3-12. Model Performance Predicting Net Flow in C&D Canal

Year	NOBS	RMSE	ubRMSE	Bias	R2	Skill	MAE	NSE
2021	6962	221.3	216.5	46.2	0.832	0.944	172.7	0.742
2022	8507	280.5	280.2	-13.4	0.812	0.941	208.0	0.727

4.3.5 Salinity

Adequately predicting salinity intrusion and the longitudinal and vertical salinity structure is essential for SM3D. The model was calibrated (2016–2020)[41] and validated (2001–2003; 2011–2013) with data from 11 years representing a range of hydrological and meteorological conditions. The following three types of data were used to evaluate model performance:

1. Continuous near-surface salinity (conductivity or specific conductance) measurements at multiple NOAA and USGS gage locations.
2. Discrete sampling of along-channel salinity profiles (DRBC Boat Run survey and Rutgers University 2011 survey data). Boat-Run data were collected near the water surface. The survey data from Rutgers University contained both near-surface and near-bottom salinity.

Salinity varies widely and fluctuates over the time scale of a tidal cycle. In addition to hourly averages, data and output were compared using a 32-hr low-pass filter (32-HR-LPF) to remove tidal oscillations from the hourly datasets, allowing for a clearer comparison of model and data responses.

Model performance for simulated salinity for multi-year period

Predicted hourly-averaged and 32-HR-LPF salinity at nine locations in the Delaware Estuary are presented in Figures 4.3-44 (1) -(9), and a target diagram in Figure 4.3-45 for the calibration period (2016 to 2020). Model performance of simulated near-surface 32-HR-LPF salinity is summarized in Table 4.3-13. The results demonstrate that SM3D adequately predicts salinity. The simulated salinity for the validation period of 2001-2003 is also presented in Figures 4.3-46 (1-4), and the target diagram in Figure 4.3-47. Statistical measures for model performance for simulated near-surface 32-HR-LPF salinity are summarized in Table 4.3-14. Model performance for simulated salinity for the validation period of 2011-2013 is presented in Figures 4.3-48 and 4.4-49, and statistical measures for simulated near-surface 32-HR-LPF salinity are summarized in Table 4.3-15.

[41] The SM3D model was also used to simulate 2021 - 2022 conditions to utilize the flow data collected at the USGS gage in the C&D Canal to further improve the calibration of the canal datum and a turbulence parameter (Section 4.1).

Table 4.3-13. Model Performance Predicting Near-surface 32-hour-low-pass-filtered Salinity during 2016-2020

Station ID	NAME	NOBS	Data Stdv.	Model Stdv.	RMSE	ubRMSE	Bias	R2	Skill	MAE	NSE
8557380	Lewes DE	27286	1.66	1.53	1.38	1.17	0.73	0.536	0.792	1.103	0.305
8537121	Ship John Shoal	10467	3.12	3.71	2.14	2.12	0.26	0.673	0.894	1.756	0.530
1482800	Reedy Island	42775	3.01	2.78	1.41	1.32	-0.49	0.808	0.938	1.013	0.781
1477050	Chester	36338	0.19	0.19	0.07	0.07	0.00	0.882	0.968	0.031	0.876
1474703	Ft. Mifflin	17215	0.07	0.05	0.03	0.03	-0.02	0.820	0.914	0.023	0.736
1467200	Ben Franklin Bridge	39627	0.03	0.03	0.01	0.01	0.00	0.851	0.959	0.008	0.842
14670261	Pennypack Woods	19653	0.02	0.02	0.02	0.01	-0.01	0.718	0.888	0.011	0.573
1482695	USGS CD Canal	5195	1.80	1.26	1.39	1.00	-0.96	0.713	0.781	1.091	0.408
1482100	Delaware Memorial Bridge	2985	0.91	0.66	0.55	0.50	-0.23	0.713	0.868	0.396	0.633

Note: Stdv = standard deviation.

Table 4.3-14. Model Performance Predicting Near-surface 32-hour-low-pass-filtered Salinity during 2001-2003

Station ID	NAME	NOBS	Data Stdv	Model Stdv	RMSE	ubRMSE	Bias	R2	Skill	MAE	NSE
8537121	Ship John Shoal	6735	2.67	3.68	2.96	2.47	1.63	0.549	0.763	2.258	-0.228
1482800	Reedy Island	1078	2.90	3.15	1.14	1.00	-0.55	0.901	0.964	0.868	0.844
1477050	Chester	782	0.27	0.24	0.06	0.06	-0.02	0.957	0.985	0.030	0.947
1467200	Ben Franklin Bridge	836	0.03	0.03	0.01	0.01	0.00	0.932	0.982	0.006	0.927

Note: Stdv = standard deviation.

Table 4.3-15. Model Performance Predicting Near-surface 32-hour-low-pass-filtered Salinity during 2011-2013

Station ID	NAME	NOBS	Data Stdv	Model Stdv	RMSE	ubRMSE	Bias	R2	Skill	MAE	NSE
8537121	Ship John Shoal	20012	3.79	4.15	2.16	2.12	-0.43	0.742	0.922	1.745	0.676
1482800	Reedy Island	25303	2.82	2.71	1.72	1.55	-0.74	0.712	0.898	1.246	0.630
1477050	Chester	16728	0.08	0.08	0.04	0.04	0.00	0.801	0.944	0.020	0.793
1467200	Ben Franklin Bridge	18305	0.02	0.03	0.01	0.01	0.00	0.878	0.963	0.007	0.838

Note: Stdv = standard deviation.

The model accurately reflects observed salinity at two critical stations, Ship John Shoal (RM 37) and Reedy Island (RM 54.1), with RMSE of 2.14 and 1.41 psu, respectively, during 2016-2020. The long-term average salinity was reproduced at those stations with a small bias between -0.5 to 0.3 psu during 2016–2020, and the standard deviation of predicted salinity was similar to the standard deviation of the data.

Considering that no conductivity data were collected during 2001–2003 and 2011–2013 at Lewes, DE, and the western open boundary of the C&D Canal, uncertain model boundary conditions introduce additional uncertainty to predicted salinity during these periods. RMSE for simulated salinity at Ship John Shoal (RM 37) and Reedy Island (RM 54.1) is roughly 2-3 psu and 1-2 psu, respectively, during these periods. Overall model performance is reasonable, with skill scores of 0.87~0.97 (2016–2020), except at the USGS gage in the C&D Canal (skill = 0.78) and the NOAA gage at Lewes (skill = 0.79). Lewes is a less important location for evaluating salinity intrusion. The grid cell size is too large near Lewes to accurately reflect the complex geometry and bathymetry. Overall, the results demonstrate that the model adequately predicts salinity near Ship John Shoal and Reedy Island in Delaware Bay. Further improvements in simulating the salinity in the C&D Canal may be needed in the future.

Model performance for simulated salinity in 2016 and 2019

Higher salinity farther upstream was observed in 2016 and 2019, during the critical season from September to December. Model performance for simulated salinity during these periods is presented in this section. Observed and predicted near-surface hourly and 32-HR-LPF salinity during September–December 2016 at Ship John Shoal, Reedy Island, Chester, Ft. Mifflin, and Ben Franklin Bridge are presented in Figures 4.3-50 and in the target diagram in Figure 4.3-51.

Observed and predicted near-surface hourly and 32-HR-LPF salinity during September–December 2019 at Ship John Shoal, Reedy Island, Chester, Ft. Mifflin, and Ben Franklin Bridge are presented in Figures 4.3-52 and in the target diagram in Figure 4.3-53. Salinity data were not available at Lewes, DE. Model performance for simulated near-surface 32-hour-LPF salinity is summarized in Tables 4.3-16 and 4.3-17. Data points for Reedy Island, Chester, Ft Mifflin, and Ben Franklin Bridge are all within the 1-radius circle on the target diagram, while Ship John Shoal results are outside the 1.5-radius circle. Salinity at Ship John Shoal was overpredicted during October 2016. Skill scores greater than 0.85 have been used to show accurate modeling of salinity, while scores between 0.7 and 0.85 indicate "acceptable" performance (MacWilliams et al., 2015). The skill scores for predicted 32-hour-LPF salinity at Reedy Island, Chester, Ft. Mifflin, and Ben Franklin Bridge are 0.68, 0.92, 0.87, and 0.69, respectively. As discussed in Section 3.3, the salinity discrepancy at Ben Franklin Bridge is partly due to uncertainty in boundary conditions for tributary inflows as well as PS discharges, which also contribute to the background salinity level in the upper tidal river, especially for river reaches upstream of the Schuylkill River confluence with the Delaware River.

Table 4.3-16. Model Performance Predicting Near-surface 32-hour-low-pass-filtered Salinity during September through December 2016

Station ID	NAME	NOBS	Data Stdv	Model Stdv	RMSE	ubRMSE	Bias	R2	Skill	MAE	NSE
8537121	Ship John Shoal	1168	1.11	1.38	3.10	1.11	2.90	0.380	-0.782	2.896	-6.880
1482800	Reedy Island	2783	1.85	1.37	1.70	1.47	-0.85	0.383	0.678	1.320	0.158
1477050	Chester	2784	0.37	0.32	0.19	0.19	0.00	0.736	0.918	0.139	0.735
1474703	Ft. Mifflin	2016	0.09	0.07	0.06	0.04	-0.04	0.797	0.868	0.039	0.619
1467200	Ben Franklin Bridge	2246	0.03	0.02	0.03	0.02	-0.01	0.597	0.693	0.019	0.369

Table 4.3-17. Model Performance Predicting Near-surface 32-hour-low-pass-filtered Salinity during September through December 2019

Station ID	NAME	NOBS	Data Stdv	Model Stdv	RMSE	ubRMSE	Bias	R2	Skill	MAE	NSE
8557380	Lewes DE	2333	0.96	0.65	1.24	0.98	0.76	0.092	0.290	0.987	-0.681
1482800	Reedy Island	2784	2.37	2.08	1.33	1.28	-0.37	0.710	0.905	1.031	0.685
1477050	Chester	2579	0.15	0.18	0.08	0.07	0.04	0.846	0.936	0.054	0.703
1474703	Ft. Mifflin	2054	0.05	0.05	0.02	0.01	-0.01	0.919	0.965	0.014	0.869
1467200	Ben Franklin Bridge	2779	0.04	0.04	0.01	0.01	0.00	0.947	0.984	0.008	0.934

Model simulated salinity longitudinal profile compared with Boat Run data

Comparisons of 12 predicted and observed Boat Run longitudinal salinity profiles during 2017 are presented in Figure 4.3-54 (1-12). Comparisons from other years showed similar agreement between predictions and the data. The predicted tidally-averaged salinity longitudinal profile agreed with the Boat Run data over a wide range of flow and tidal conditions.

Comparisons of predicted and observed salinity and water temperature of along-channel longitudinal profiles during the 2011 Rutgers survey are presented in Figures 4.3-55 and 4.3-56, respectively. The data were collected over a 30-hr time span from September 16, 2011, at 15:00 to September 17, 2011, at 21:00. The survey was conducted one week after a high-flow event when the maximum flow at Trenton was over 177,000 cfs on September 9, 2011. This is greater than a 10-year flood at Trenton, which is 169,000 cfs (Schopp and Firda, 2008). The observed salt front was downstream of RM 54 during that period. The survey covered approximately two and half tidal cycles. The model successfully reproduced near-surface and near-bottom salinities as well as water temperature longitudinal profiles during this transient period that followed a very high influx of freshwater flow.

Model-to-data comparisons of salinity indicate that the model tended to underpredict salinity intrusion somewhat during wet weather and high flow events; however, this does not necessarily reflect a model calibration issue. The discrepancies between predicted and observed salinity during high flow periods are more likely due to uncertainty in the model boundary conditions. Other potential factors that may contribute to the discrepancies include model limitations due to numerical grid resolution in the horizontal and vertical planes and level of detail in the simulation of horizontal and vertical turbulent diffusion.

The results discussed above demonstrate that SM3D simulated salinity adequately for low flows, the condition of concern for this study. Further investigations to improve salinity predictions for higher flows may be performed as new data become available and resources allow.

4.4 Model Application Information

In the upper reaches of the Estuary, the concentration of chlorides and the salt front location are used to reference concerns about salinity intrusion. Although salinity is simulated with SM3D, both chloride concentrations and the salt front can be calculated with the results. For the comparison of model results with observed data, the simulated chlorides were calculated by converting the simulated salinity to chloride[42], and the salt front was then interpolated between the same locations as the observed data. Chloride concentrations of the observed data were calculated

[42] The conversion equations from salinity to chloride that were developed based on DRBC Boat Run data are:
*Chlorinity (mg/L) = 582.8 * Salinity (psu) – 63, for Salinity ≥ 0.2 psu; and*
*Chlorinity (mg/L) = 267.6 * Salinity (psu), for Salinity < 0.2 psu.*

using measured specific conductance and the relationship developed with the Boat Run data[43] from 2000 to 2022. The directly simulated salt front location, using 0.54 psu (approximately 250 mg/l chlorides), is also presented. Model performance for chlorides and the salt front is largely reflective of that for salinity. Therefore, goodness of fit statistics is not presented and only a few graphics are shown for reference.

4.4.1 Chloride Concentration

Comparisons of observed and predicted daily chlorinity[44] for Reedy Island (RM 54.1), Chester (RM 83.6), Fort Mifflin (RM 91.9), and Ben Franklin Bridge (RM 100.1) are presented in Figures 4.4-1, 4.4-2, and 4.4-3 for 2016-2020, 2001-2003, and 2011-2013, respectively. The model successfully reproduced chloride concentrations and behavior at all four locations throughout the calibration period (2016-2020). Differences can be attributed to the uncertainty in boundary conditions.[45] For 2001-2003, a dry period, chlorides were slightly underpredicted, but higher peaks were slightly overpredicted. For 2011-2013, a wetter period, chlorides at Reedy Island were under predicted at lower concentrations and overpredicted at higher concentrations. Chlorides were reproduced at Chester and Ben Franklin Bridge (data were not available at Fort Mifflin). For 2001-2003 and 2011-2013, some of the differences between observed and simulated results are likely due to the uncertainty in the bathymetry representing the FNC for the simulated years. The bathymetry is affected by the USACE channel deepening project that was started in 2010 and finished in 2020. It is impossible for the model to accurately represent the continuous and incremental changes of bathymetry over time during this dredging period. SM3D was developed for a 45 ft channel, but to simulate 2001-2003 and 2011-2013, the channel was adjusted to 40 ft depth during those periods.

[43] The relationship of specific conductance (SC) to chlorides was developed with the Boat Run data from 2000 and 2018. For SC > 320 [µS/m at 25ºC], CL = 0.297SC – 59.4. For SC <= 320 [µS/m at 25ºC], CL = 0.119SC – 1.55. CL denotes the Chloride concentration [mg/L].

[44] Chlorinity and Chlorides or Chloride concentrations are used interchangeably in this study.
Chlorinity measures chloride ions in water, while salinity is the total concentration of all dissolved salts (like sodium chloride, magnesium sulfate, etc.), with Chlorides represent approximately 55 percent of the total dissolved solids in sea water. Chlorinity and salinity are related by a constant ratio: Salinity (psu) = 0.03 + 0.00180655 (mg/l) and allowing scientists to calculate total saltiness from chloride measurement, which is crucial for understanding ocean chemistry, circulation, and ecosystem health. The empirical relationship is valid until salinity is below 2 psu.

[45] The overestimate of chlorides in September and October 2017 may be related to the boundary conditions, particularly salinity (Appendix C). Ten hurricanes were observed in 2017, including two Category 4 and two Category 5 hurricanes. Hurricanes Irma and Maria affected the DRB in September and October 2017. The ocean boundary salinity in the model may be too high for such an active hurricane season.

4.4.2 Salt Front

Comparisons of the simulated salt front location and the observed location are presented in Figures 4.4-4 through 4.4-6, for 2016-2020, 2001-2003, and 2011-2013, respectively. In addition to the salt front (7-dma of the 250 mg/l chloride concentration or 0.54 psu), the hourly location of the 0.54 psu salinity contour was included on the graph. The hourly model output is intended to show the range of the salt front during a day and the uncertainty of both the model and observed data. During the calibration period (Figure 4.4-4), the salt front movement was predicted reasonably well and the two most upstream locations, during the dry periods in 2016 and 2019, were also captured by the model. However, the salt front location was over-predicted by approximately three miles during September and October 2017, likely related to the salinity estimated for the ocean boundary condition. For 2001-2003, the model adequately predicts the most upstream salt front location and behavior, except in the spring of 2002, during a high flow period when the salt front was below RM 60. In part, the difference is due to the lack of observed data available for the log-linear interpolation and higher flows. The monthly mean flow for May 2002 (20,240 cfs) was higher than 20,000 cfs, similar to the monthly mean flow for April 2001 (24,960 cfs). Figures 4.4-7 and Figure 4.4-8 present the salt front during the two dry periods between September and December in 2016 and 2019. For both years, the salt front location is slightly over-predicted for much of the period, but the most upstream location is accurately captured.

5. SUMMARY

SM3D (Model_v3) was developed and calibrated using EFDC as a reliable tool to use for studies about the effects of flow management (reservoir operations, storage, and diversions) and climate change (hydrology and sea level rise) on salinity in the Delaware River Estuary. SM3D simulates hydrodynamic and transport information (e.g., tides, water depth, current velocity, salinity, and water temperature) over a range of hydrological and meteorological conditions with the degree of accuracy and confidence needed to support the objectives of those studies.

Model development, calibration, and validation results are summarized in this report. SM3D was able to adequately reproduce tidal water surface elevations, current velocity, water temperature, and salinity. Sensitivity simulations demonstrated that the specification of 8 vertical layers inside the FNC was adequate and efficient for simulating salinity transport in the Delaware Estuary.

SM3D is intended to be a “living model” and will be revised as new data become available. For example, only limited data were available to thoroughly evaluate the exchange of flow and salinity between the Chesapeake Bay and Delaware Bay through the C&D Canal. The net inflow contribution from Chesapeake Bay affects salinity transport and better quantification of flows may be possible with data from newly established monitoring stations within the C&D Canal. Long term records of the C&D Canal flow data that cover a variety of hydrological conditions will be more valuable to further improve model performance in simulating salinity intrusion in the Delaware Estuary. Additional information such as longitudinal and cross-sectional salinity profiles, or more detailed and updated bathymetric surveys, may be useful to refine the model to further improve the accuracy in the results.

Figures for Section 3.0

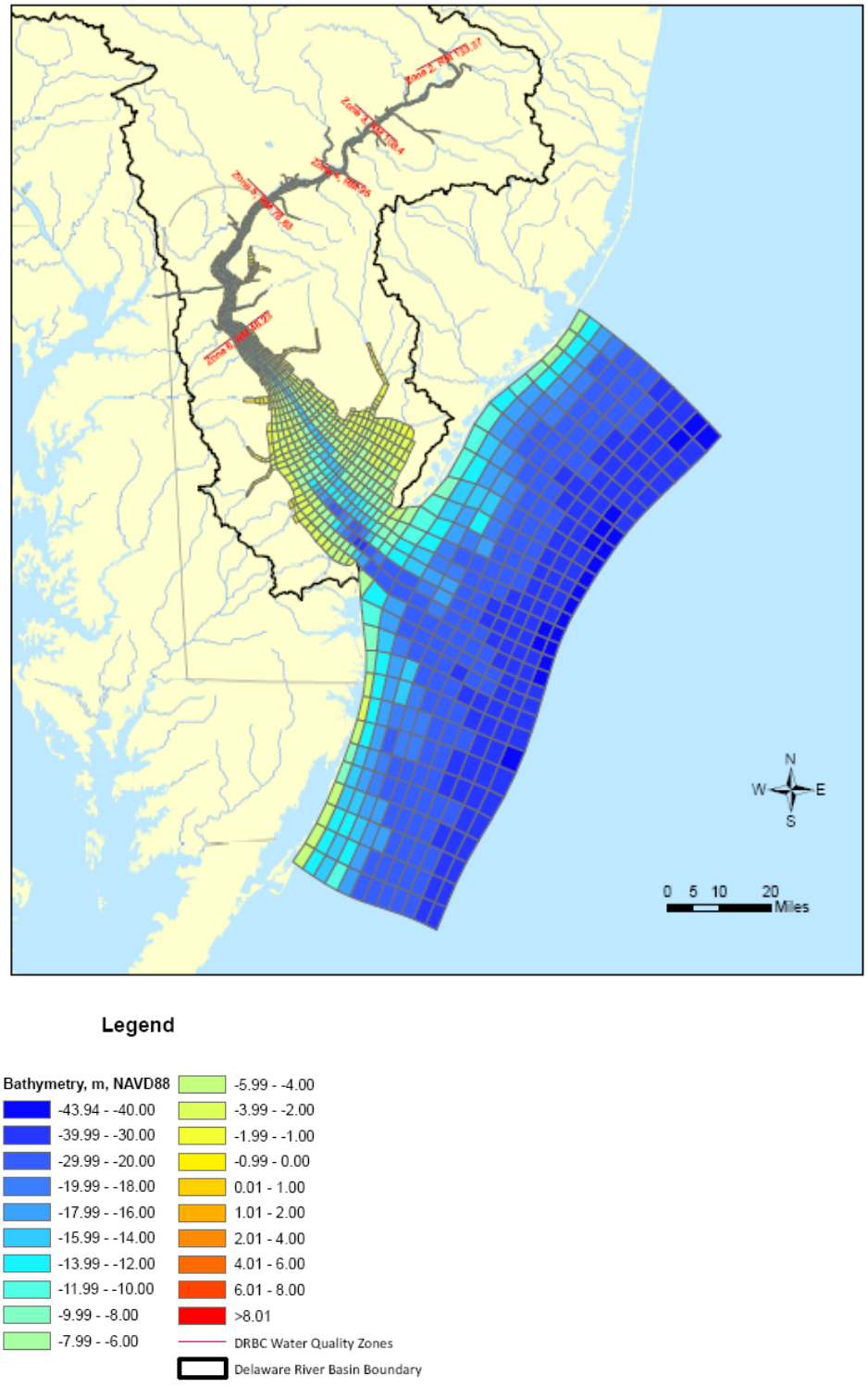

Figure 3.1-1 (1) Numerical Grid and Projected Bathymetry

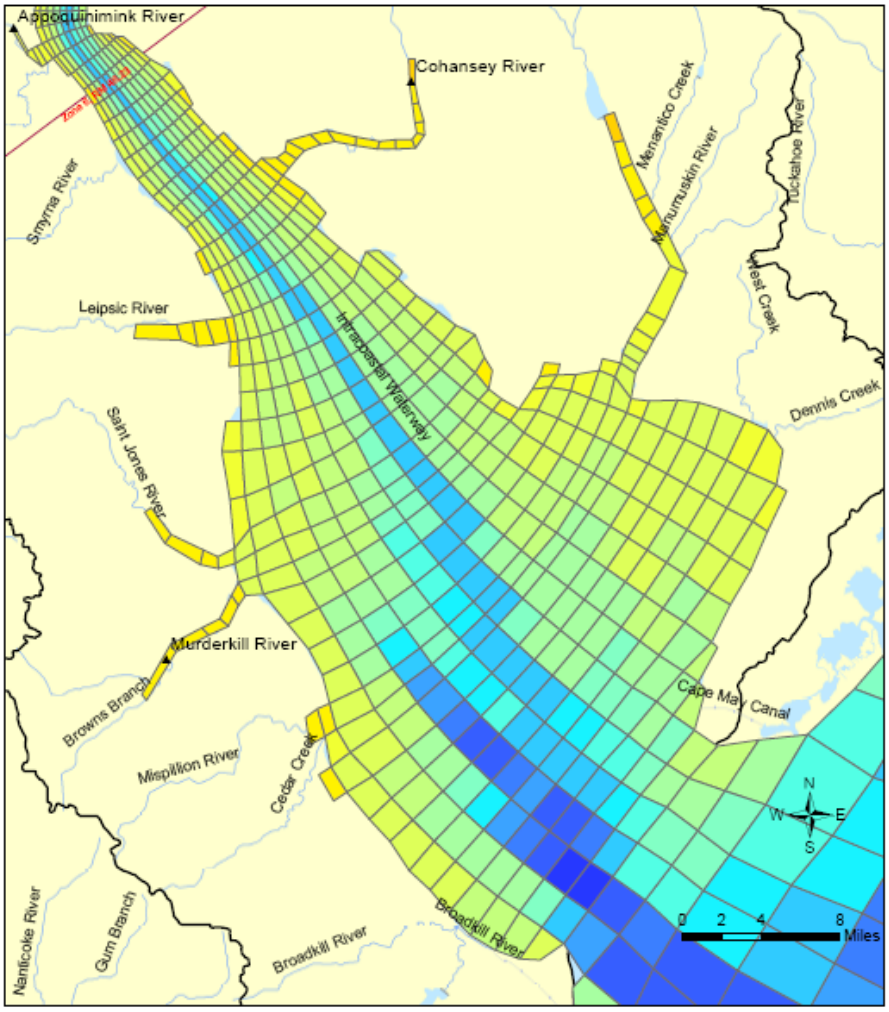

Legend

Bathymetry, m, NAVD88	
-43.94 - -40.00	-5.99 - -4.00
-39.99 - -30.00	-3.99 - -2.00
-29.99 - -20.00	-1.99 - -1.00
-19.99 - -18.00	-0.99 - 0.00
-17.99 - -16.00	0.01 - 1.00
-15.99 - -14.00	1.01 - 2.00
-13.99 - -12.00	2.01 - 4.00
-11.99 - -10.00	4.01 - 6.00
-9.99 - -8.00	6.01 - 8.00
-7.99 - -6.00	>8.01
	DRBC Water Quality Zones
	Delaware River Basin Boundary

Figure 3.1-1 (2) Numerical Grid and Projected Bathymetry (Zone 6)

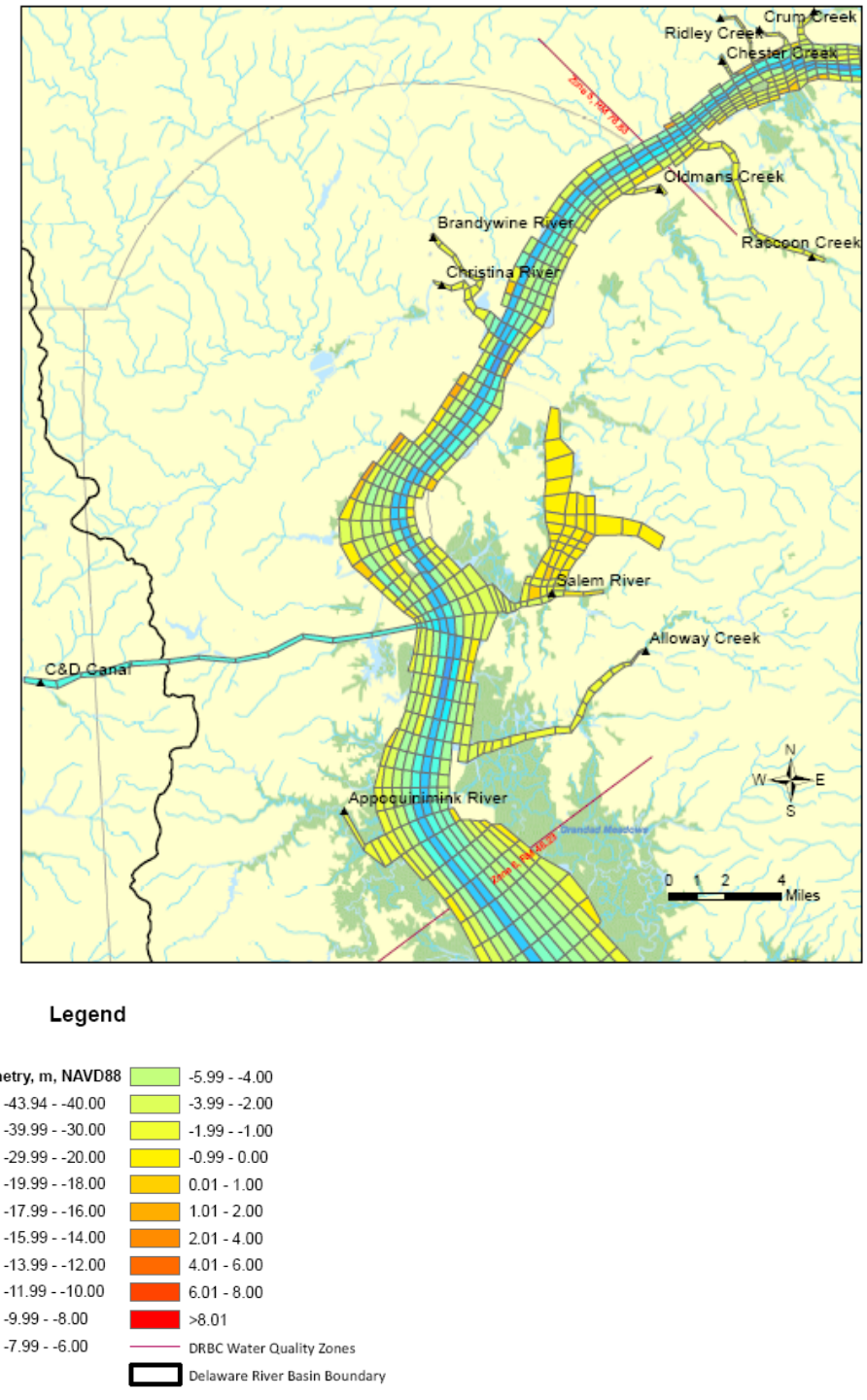

Figure 3.1-1 (3) Numerical Grid and Projected Bathymetry (Zone 5)

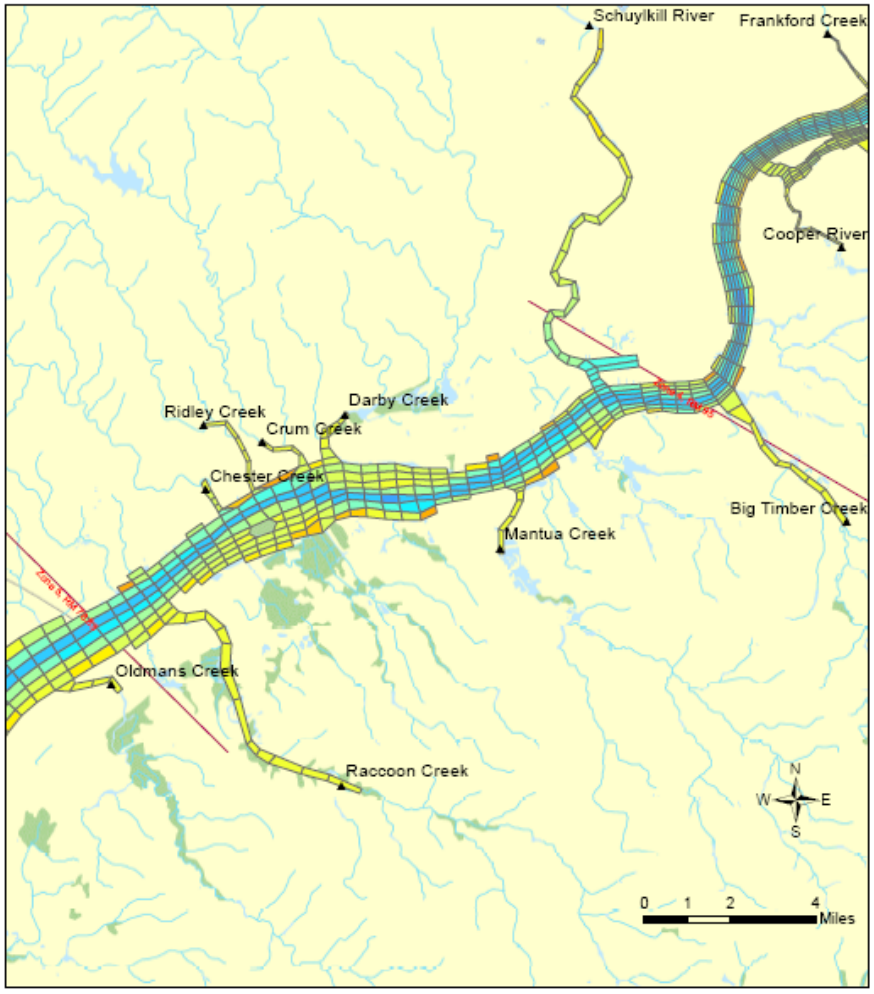

Figure 3.1-1 (4) Numerical Grid and Projected Bathymetry (Zone 4)

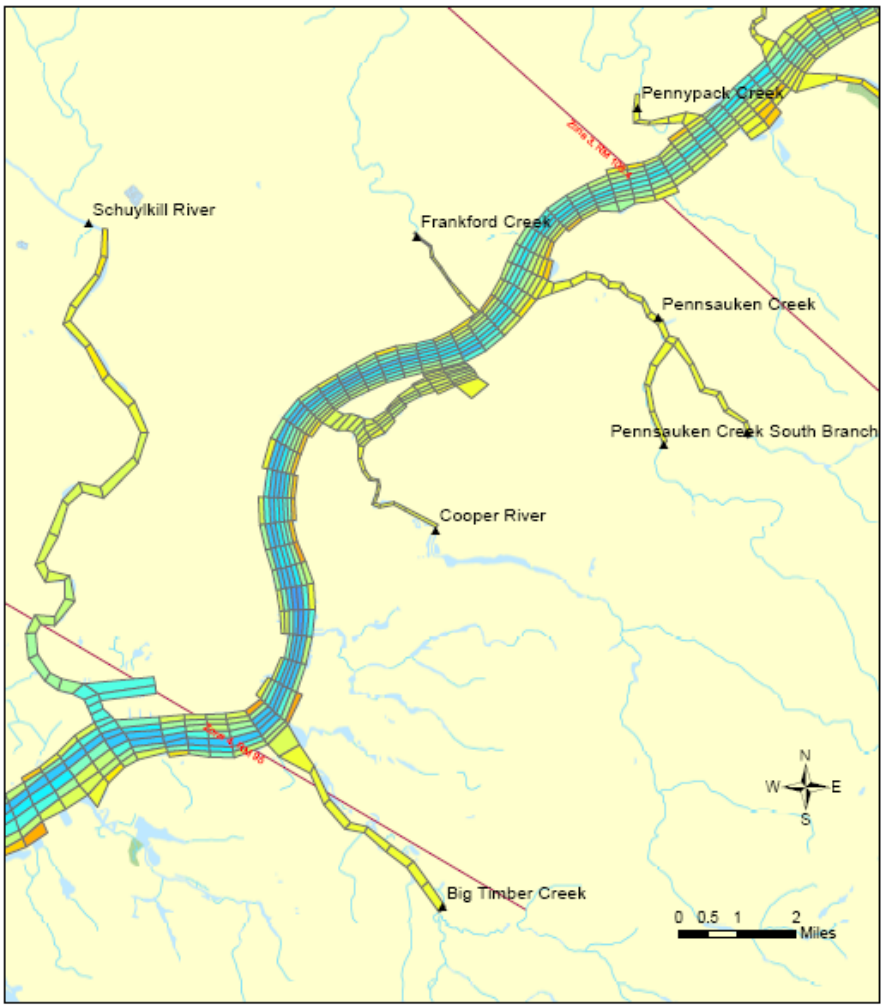

Legend

Bathymetry, m, NAVD88	-5.99 - -4.00
-43.94 - -40.00	-3.99 - -2.00
-39.99 - -30.00	-1.99 - -1.00
-29.99 - -20.00	-0.99 - 0.00
-19.99 - -18.00	0.01 - 1.00
-17.99 - -16.00	1.01 - 2.00
-15.99 - -14.00	2.01 - 4.00
-13.99 - -12.00	4.01 - 6.00
-11.99 - -10.00	6.01 - 8.00
-9.99 - -8.00	>8.01
-7.99 - -6.00	DRBC Water Quality Zones
	Delaware River Basin Boundary

Figure 3.1-1 (5) Numerical Grid and Projected Bathymetry (Zone 3)

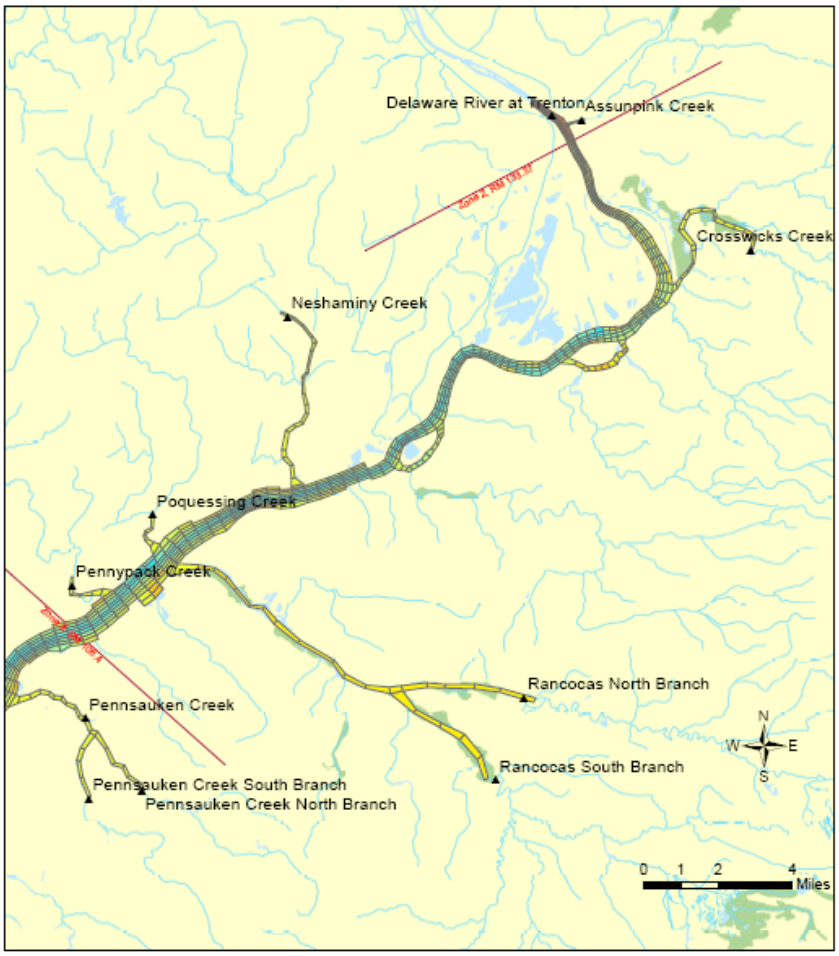

Legend

Bathymetry, m, NAVD88	
-43.94 - -40.00	-5.99 - -4.00
-39.99 - -30.00	-3.99 - -2.00
-29.99 - -20.00	-1.99 - -1.00
-19.99 - -18.00	-0.99 - 0.00
-17.99 - -16.00	0.01 - 1.00
-15.99 - -14.00	1.01 - 2.00
-13.99 - -12.00	2.01 - 4.00
-11.99 - -10.00	4.01 - 6.00
-9.99 - -8.00	6.01 - 8.00
-7.99 - -6.00	>8.01
	DRBC Water Quality Zones
	Delaware River Basin Boundary

Figure 3.1-1 (6) Numerical Grid and Projected Bathymetry (Zone 2)

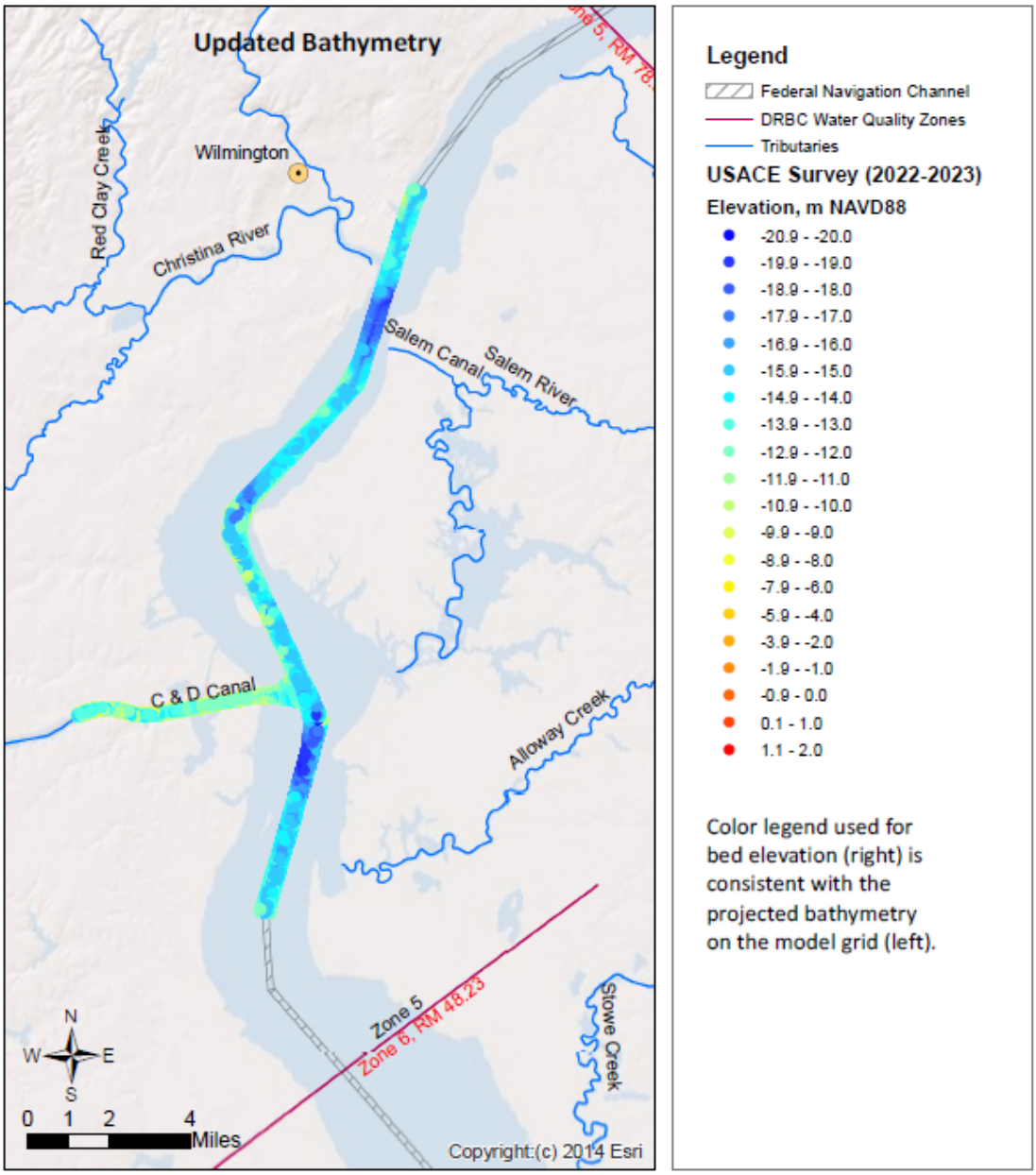

Figure 3.2-1 USACE 2022-2023 Bathymetry Survey Data. The area of C&D confluence with the Delware River and the area of the Delaware River near Delaware Memorial Bridge was surveyed by the in February 2023. The area south of the bridge leading to the C&D flare was surveyed in November 2022. The sounding water depth was converted to the bathymetry in meter NAVD88.

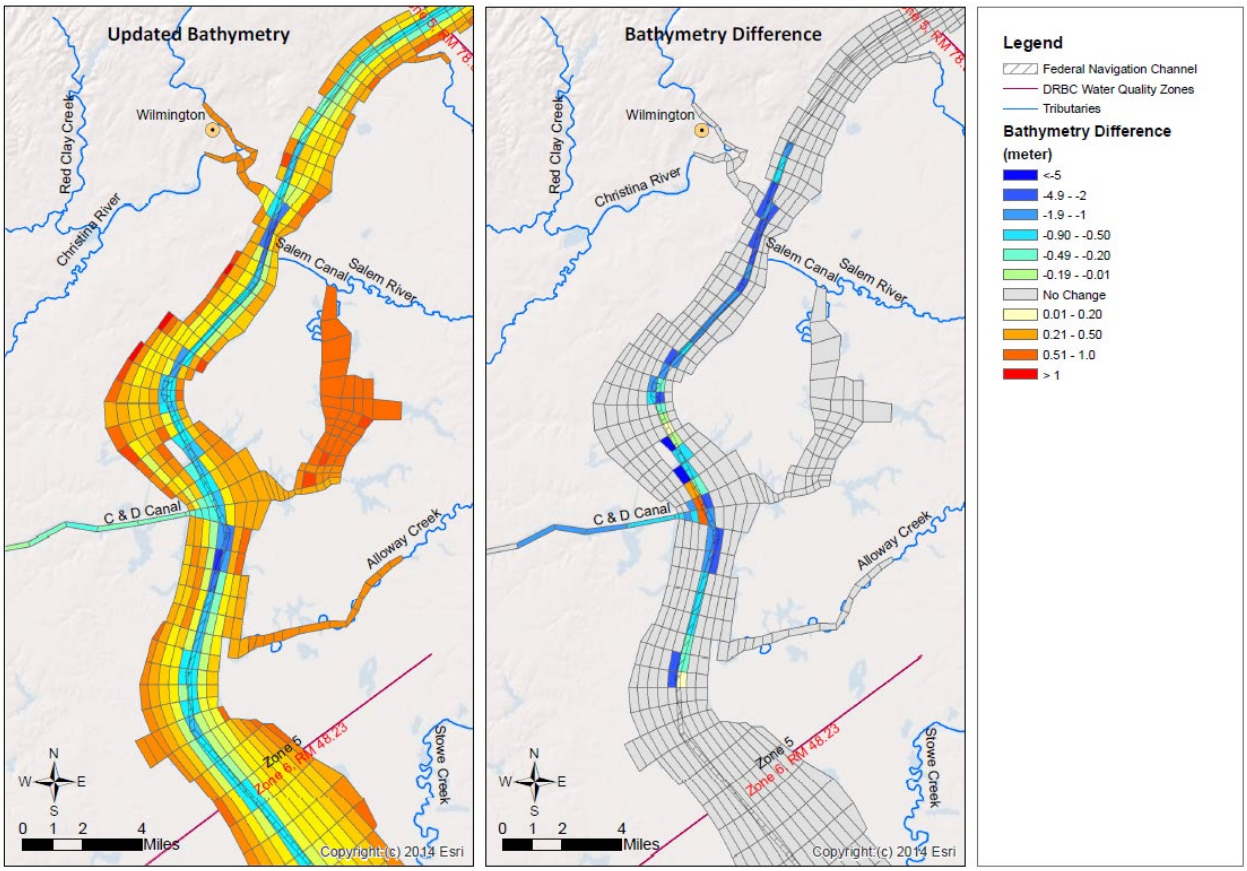

Figure 3.2-2 Updated Post-dredging Bathymetry using USACE 2022-2023 Survey Data

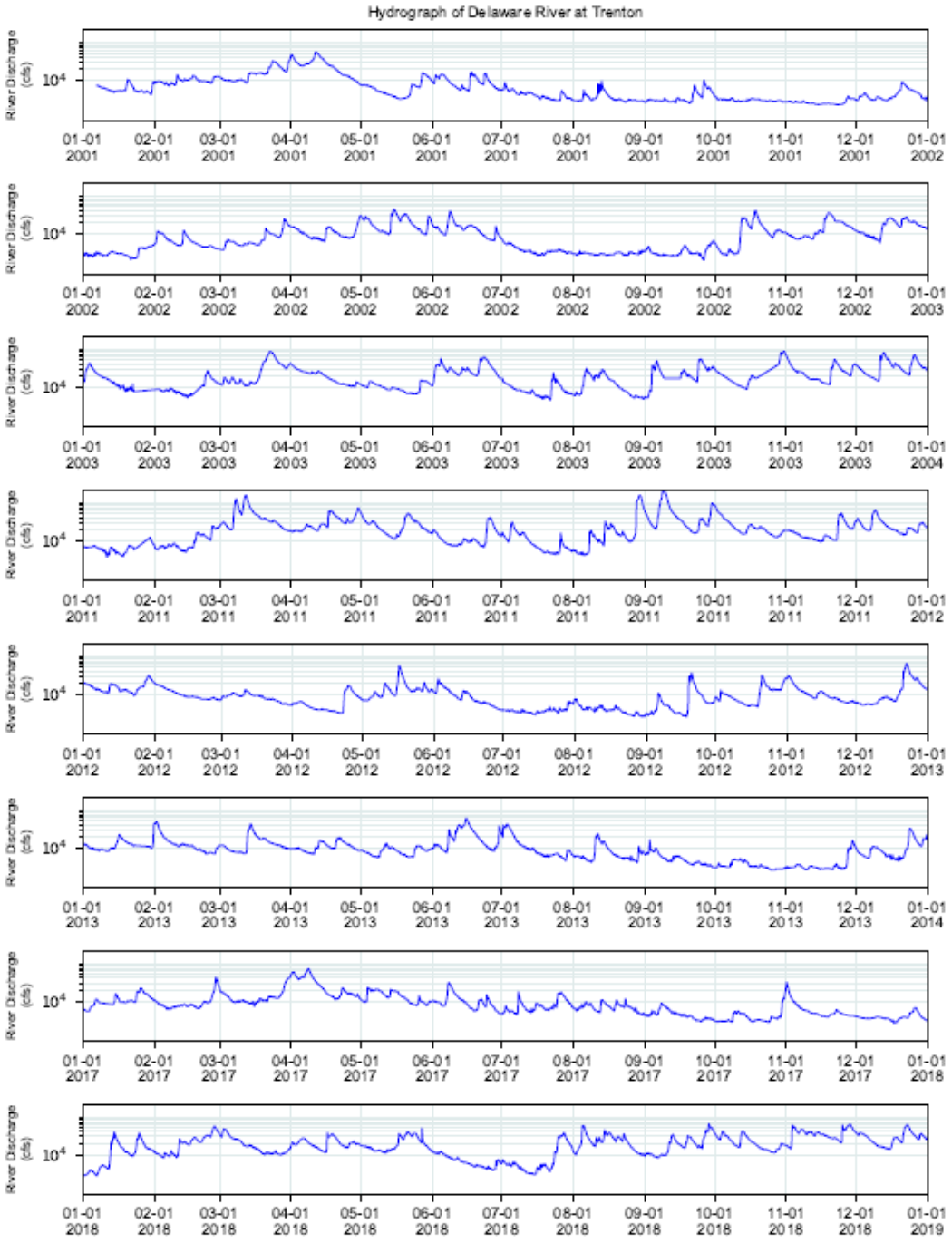

USGS gage #: 1463500

Figure 3.3-1 Hydrograph of Delaware River at Trenton for Selected Years

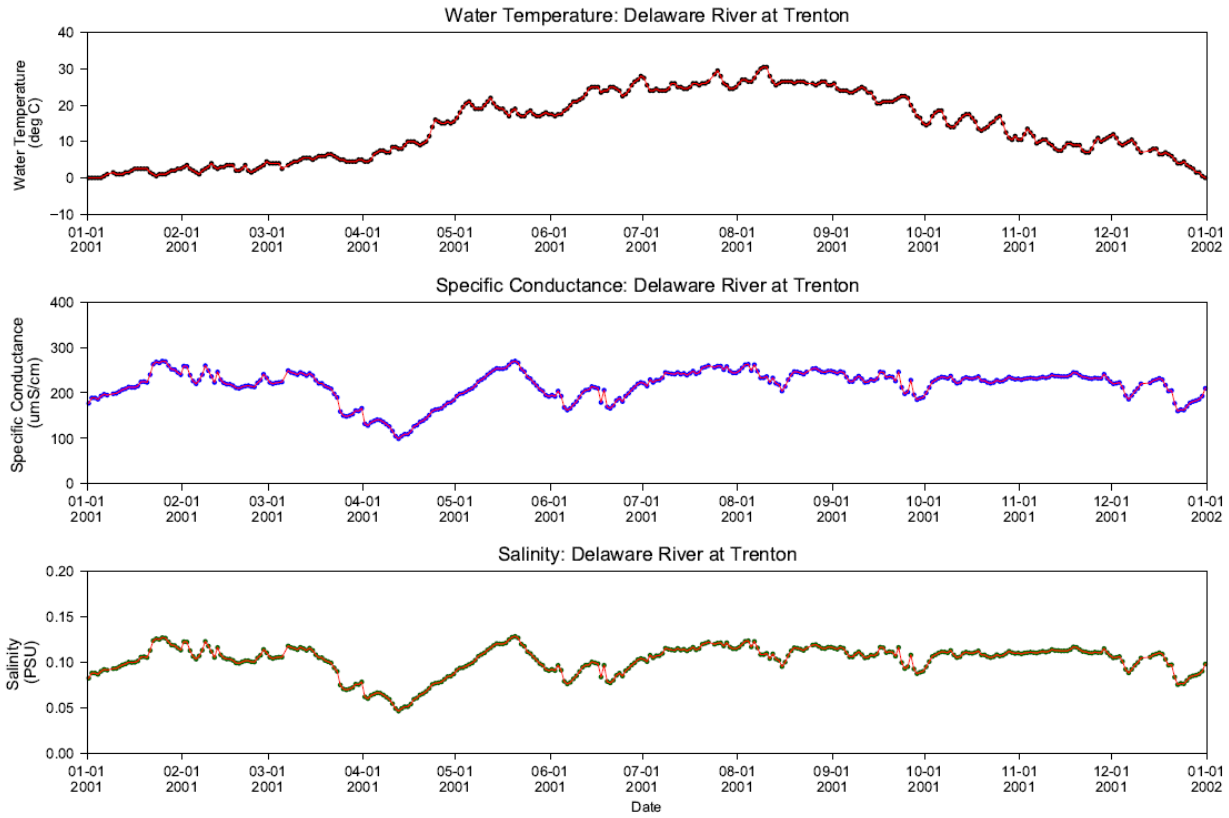

Historical USGS daily data were used and interpolated to hourly time interval for model input.

Figure 3.3-2 (1) Water Temperature and Specific Conductance Data Collected at USGS Station 01436500, Delaware River at Trenton During 2001

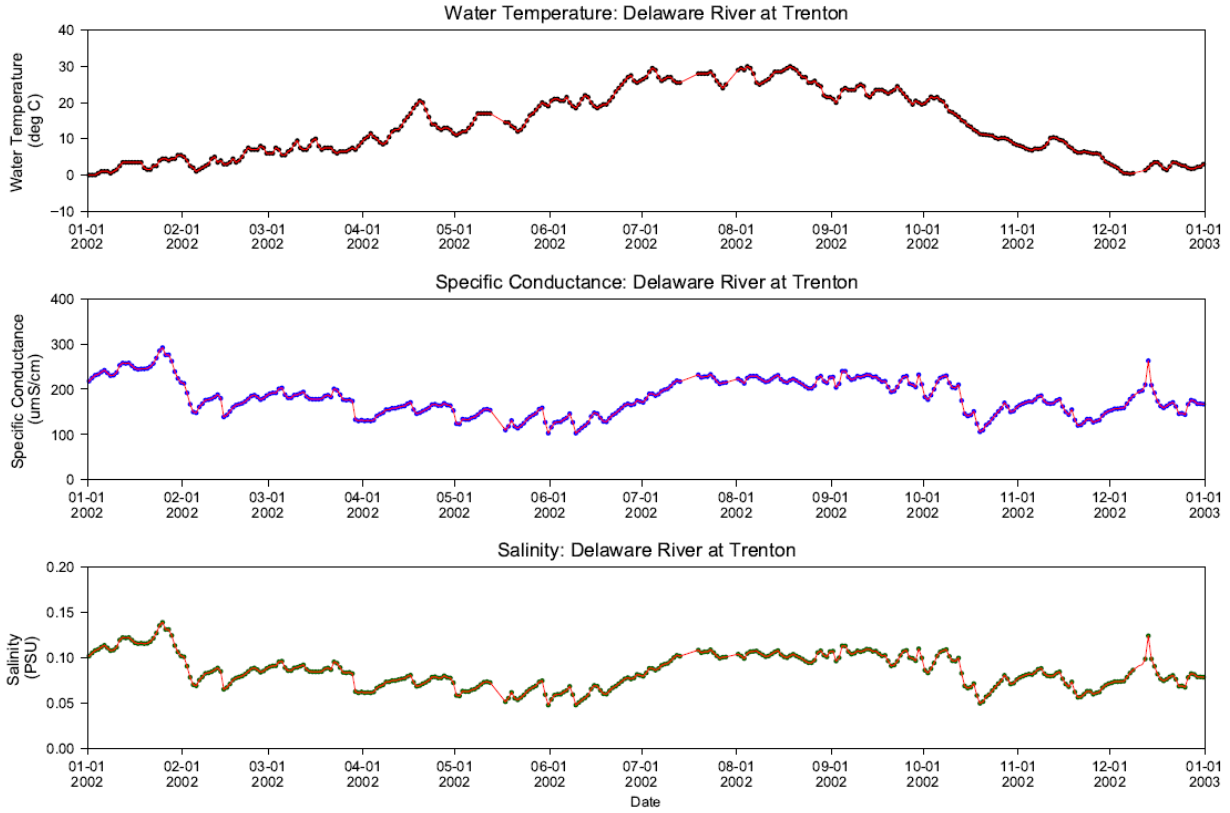

Historical USGS daily data were used and interpolated to hourly time interval for model input.

Figure 3.3-2 (2) Water Temperature and Specific Conductance Data Collected at USGS Station 01436500, Delaware River at Trenton During 2002

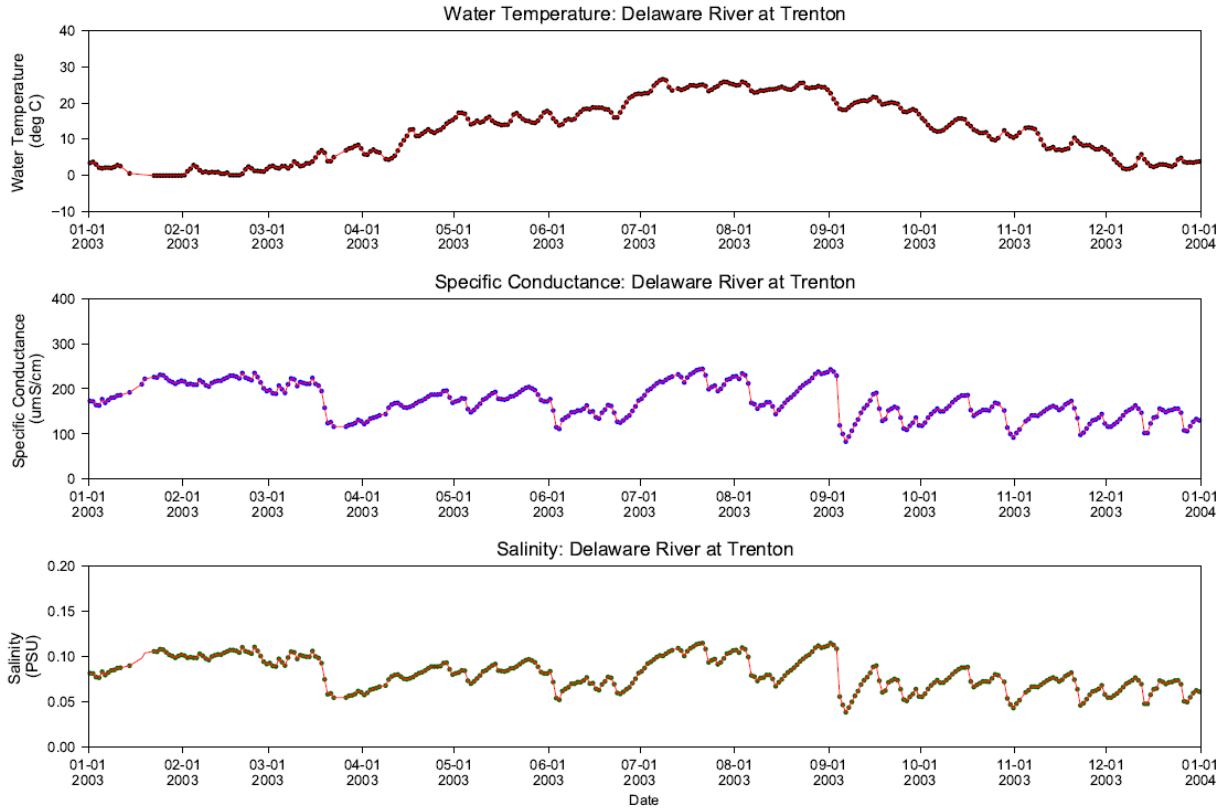

Historical USGS daily data were used and interpolated to hourly time interval for model input.

Figure 3.3-2 (3) Water Temperature and Specific Conductance Data Collected at USGS Station 01436500, Delaware River at Trenton During 2003

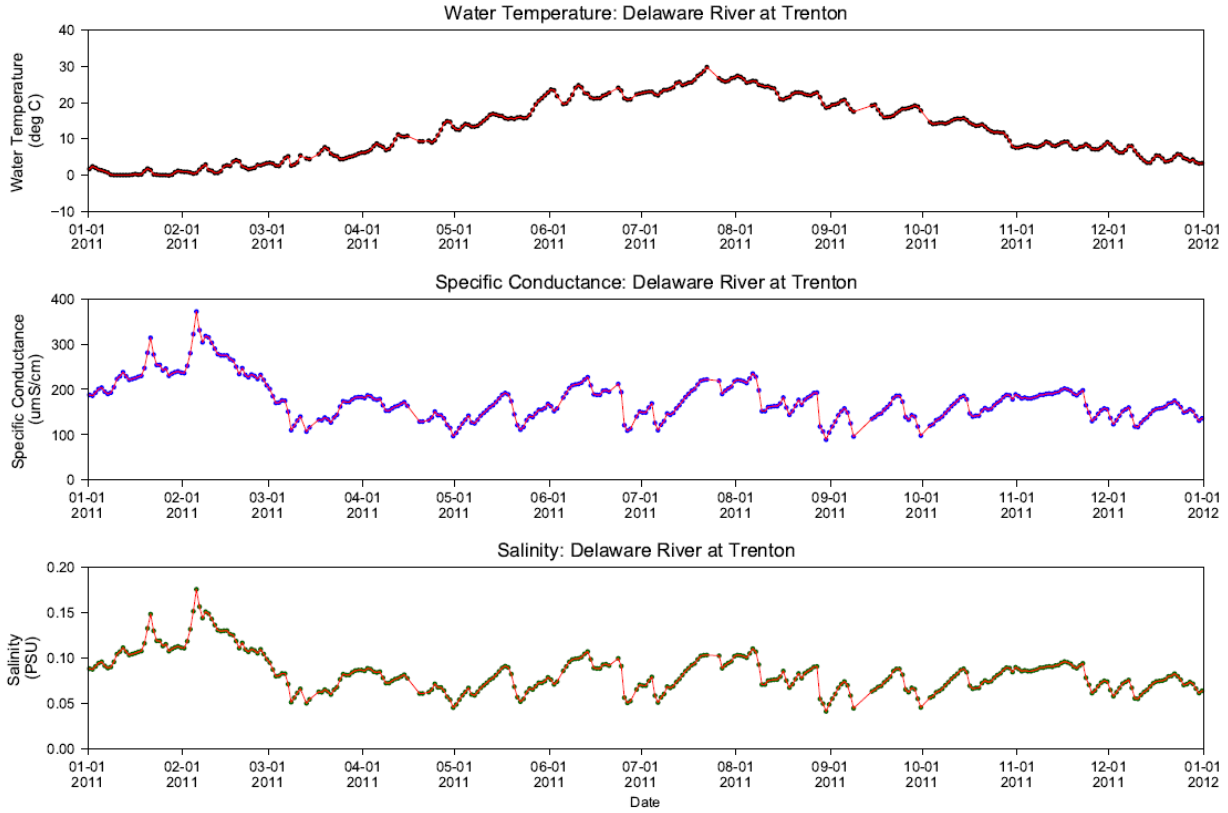

Historical USGS daily data were used and interpolated to hourly time interval for model input.

Figure 3.3-2 (4) Water Temperature and Specific Conductance Data Collected at USGS Station 01436500, Delaware River at Trenton During 2011

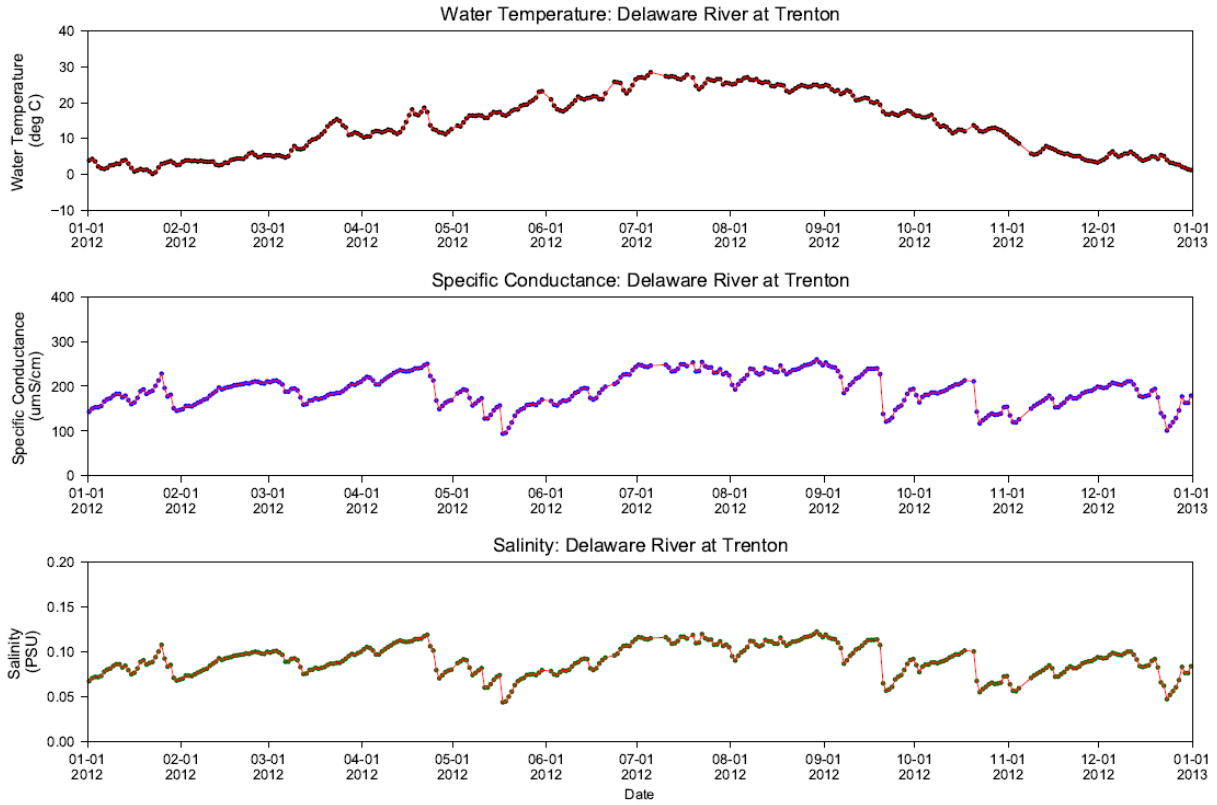

Historical USGS daily data were used and interpolated to hourly time interval for model input.

Figure 3.3-2 (5) Water Temperature and Specific Conductance Data Collected at USGS Station 01436500, Delaware River at Trenton During 2012

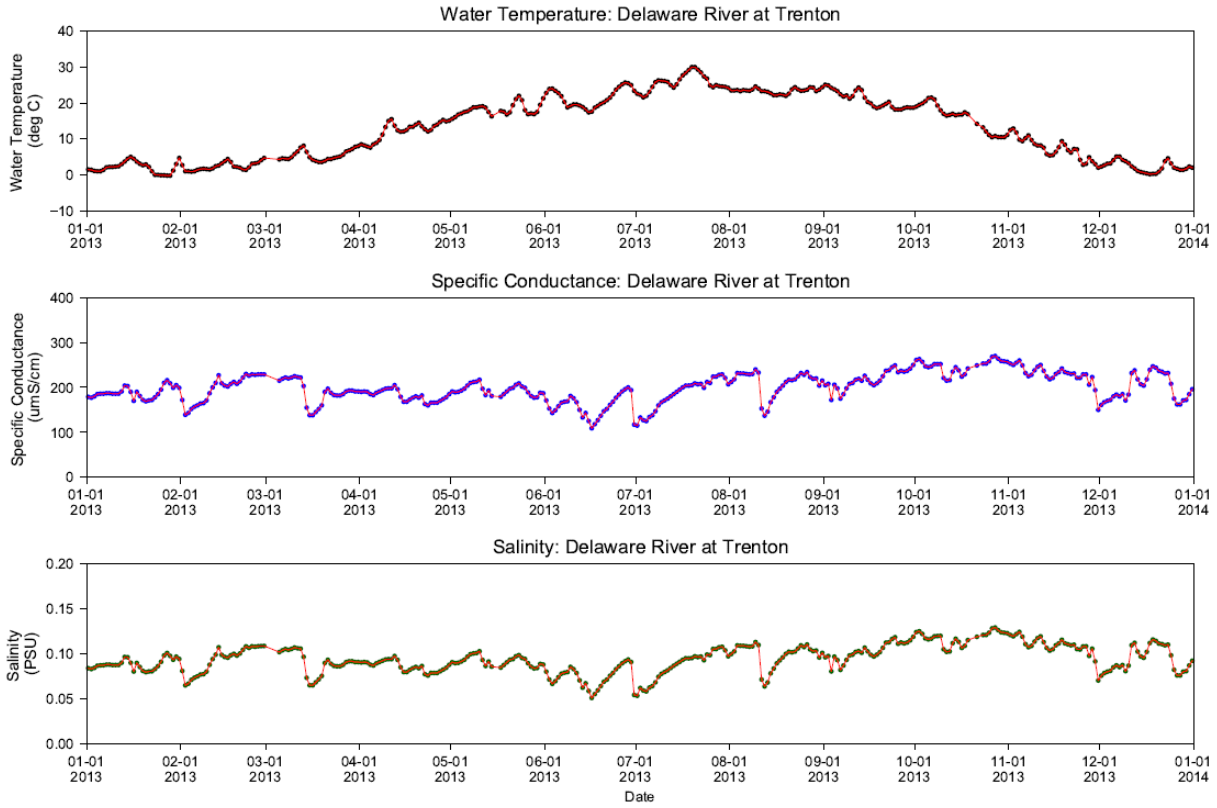

Historical USGS daily data were used and interpolated to hourly time interval for model input.

Figure 3.3-2 (6) Water Temperature and Specific Conductance Data Collected at USGS Station 01436500, Delaware River at Trenton During 2013

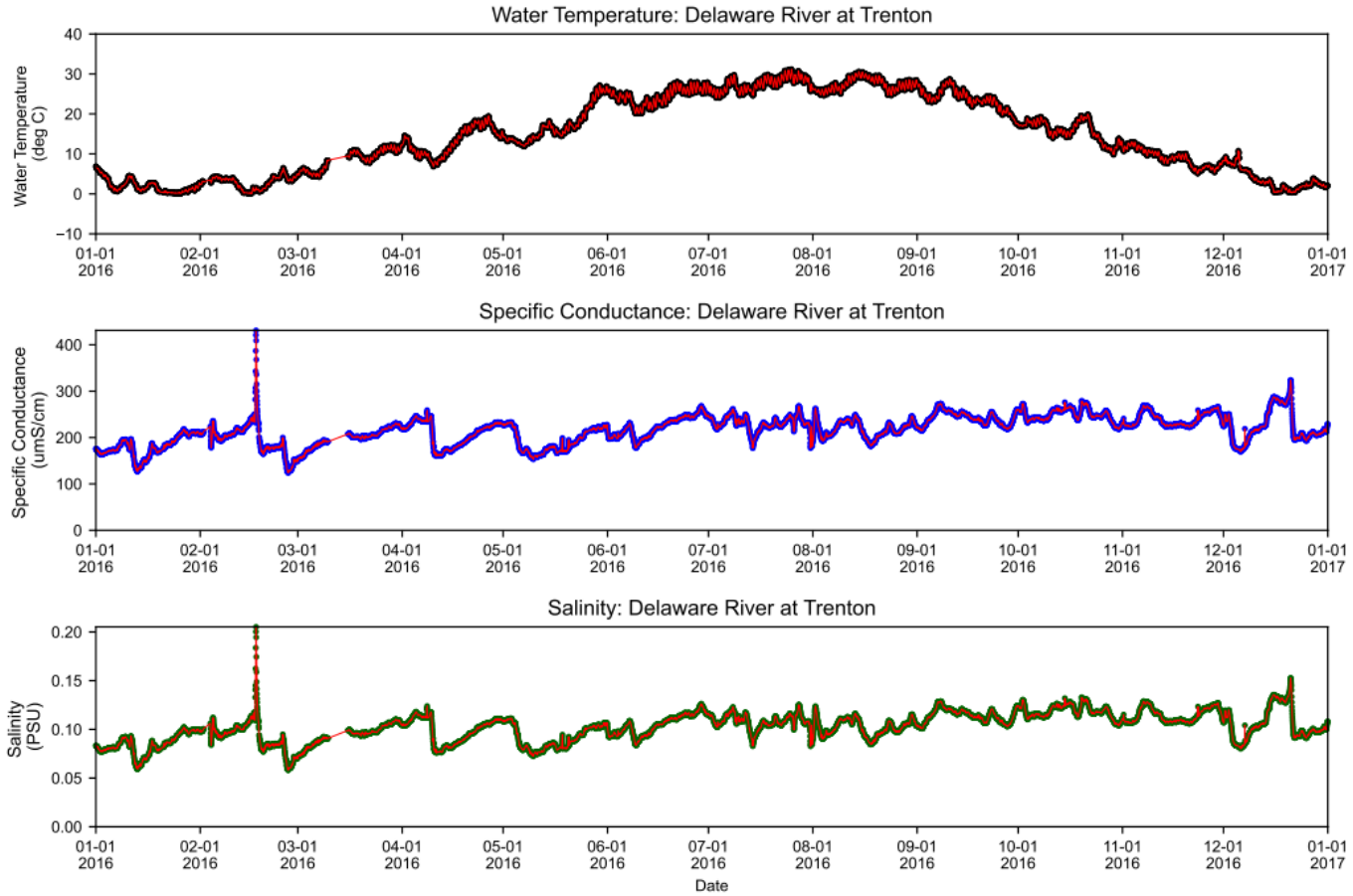

Historical USGS sub-hourly data were used and interpolated to hourly time interval for model input.

Figure 3.3-2 (7) Water Temperature and Specific Conductance Data Collected at USGS Station 01436500, Delaware River at Trenton During 2016

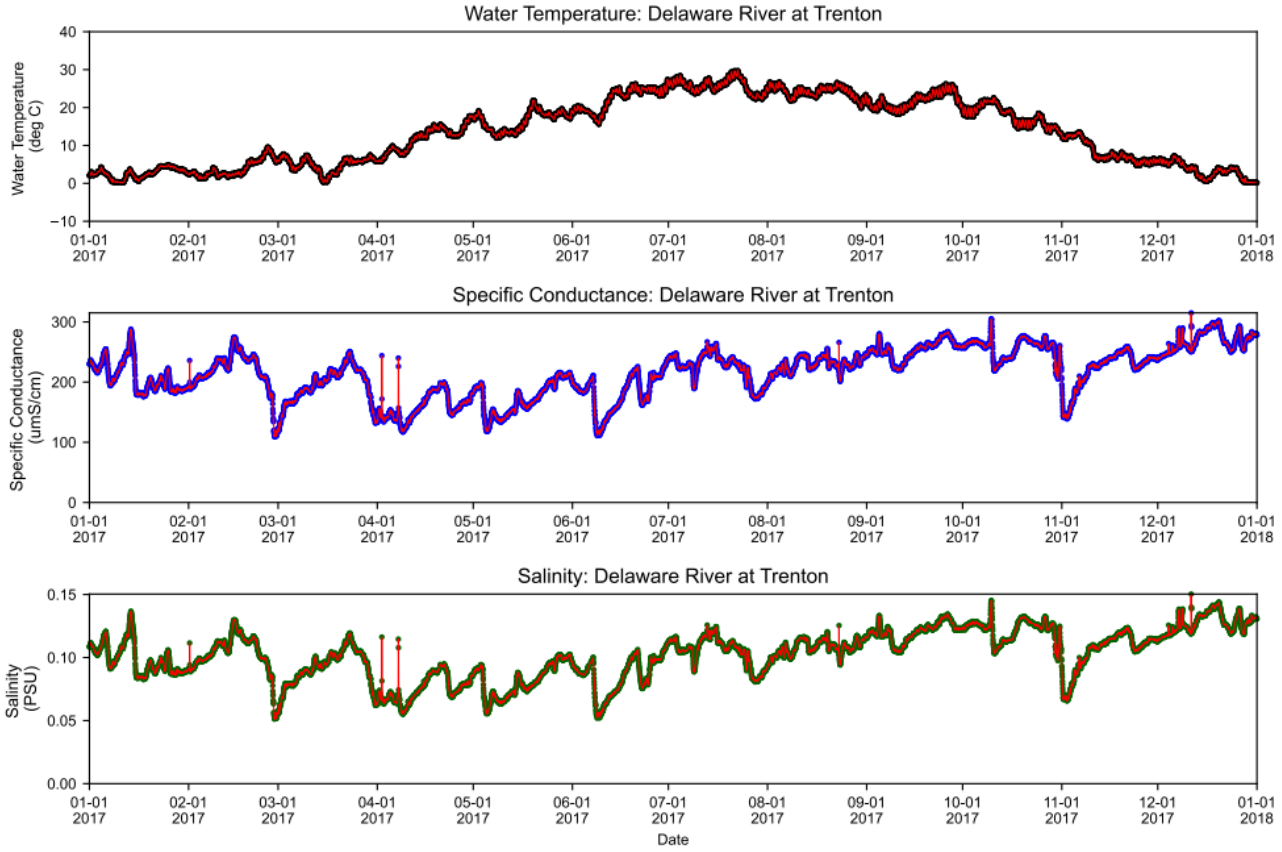

Historical USGS sub-hourly data were used and interpolated to hourly time interval for model input.

Figure 3.3-2 (8) Water Temperature and Specific Conductance Data Collected at USGS Station 01436500, Delaware River at Trenton During 2017

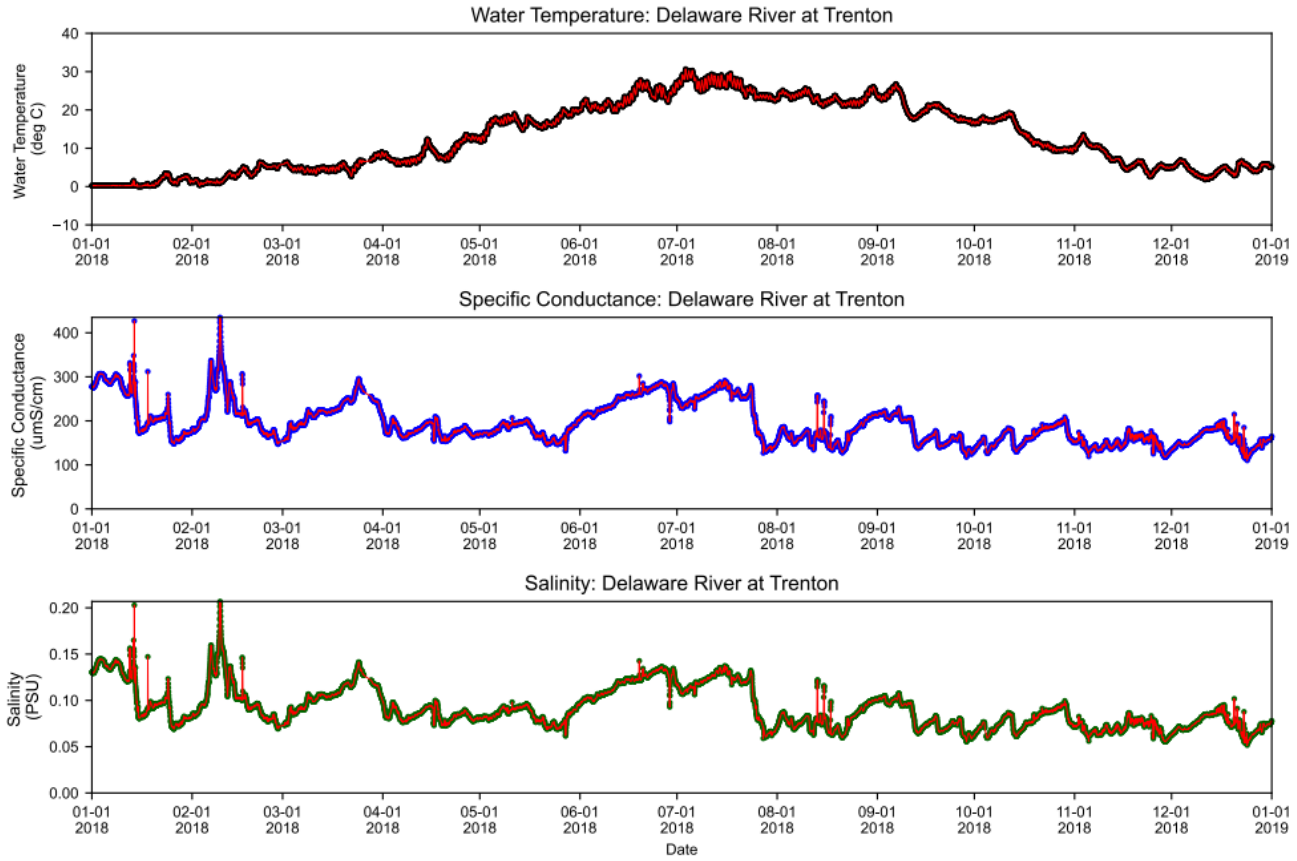

Historical USGS sub-hourly data were used and interpolated to hourly time interval for model input.

Figure 3.3-2 (9) Water Temperature and Specific Conductance Data Collected at USGS Station 01436500, Delaware River at Trenton During 2018

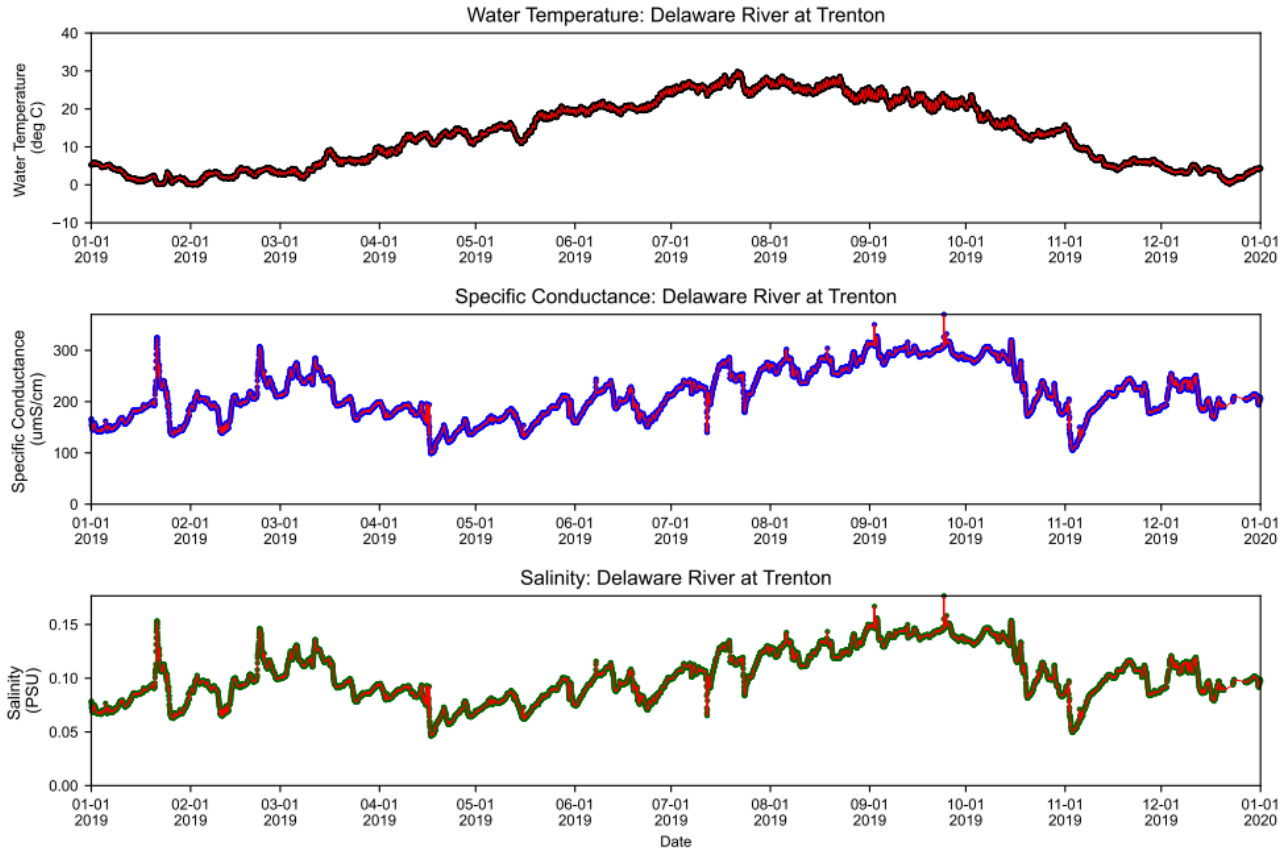

Historical USGS sub-hourly data were used and interpolated to hourly time interval for model input.

Figure 3.3-2 (10) Water Temperature and Specific Conductance Data Collected at USGS Station 01436500, Delaware River at Trenton During 2019

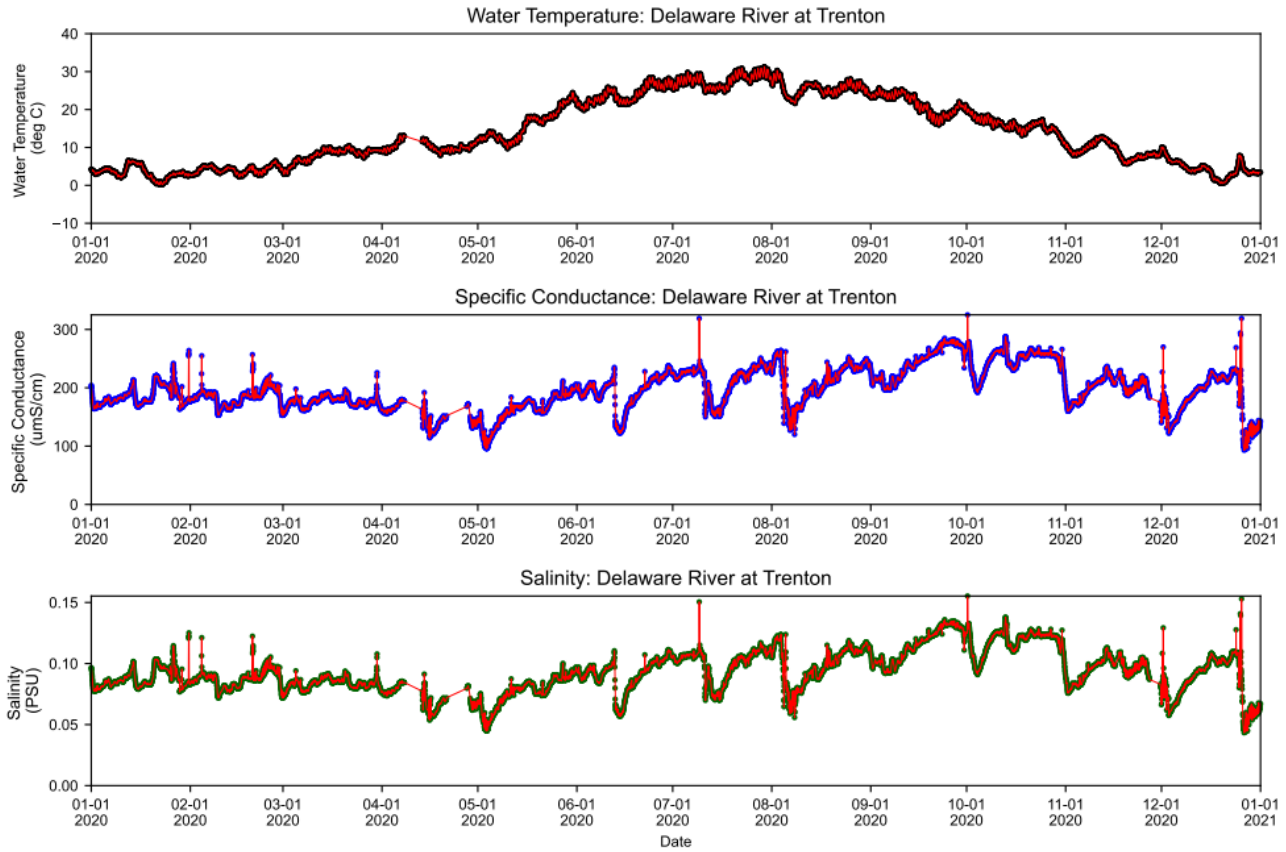

Historical USGS sub-hourly data were used and interpolated to hourly time interval for model input.

Figure 3.3-2 (11) Water Temperature and Specific Conductance Data Collected at USGS Station 01436500, Delaware River at Trenton During 2020

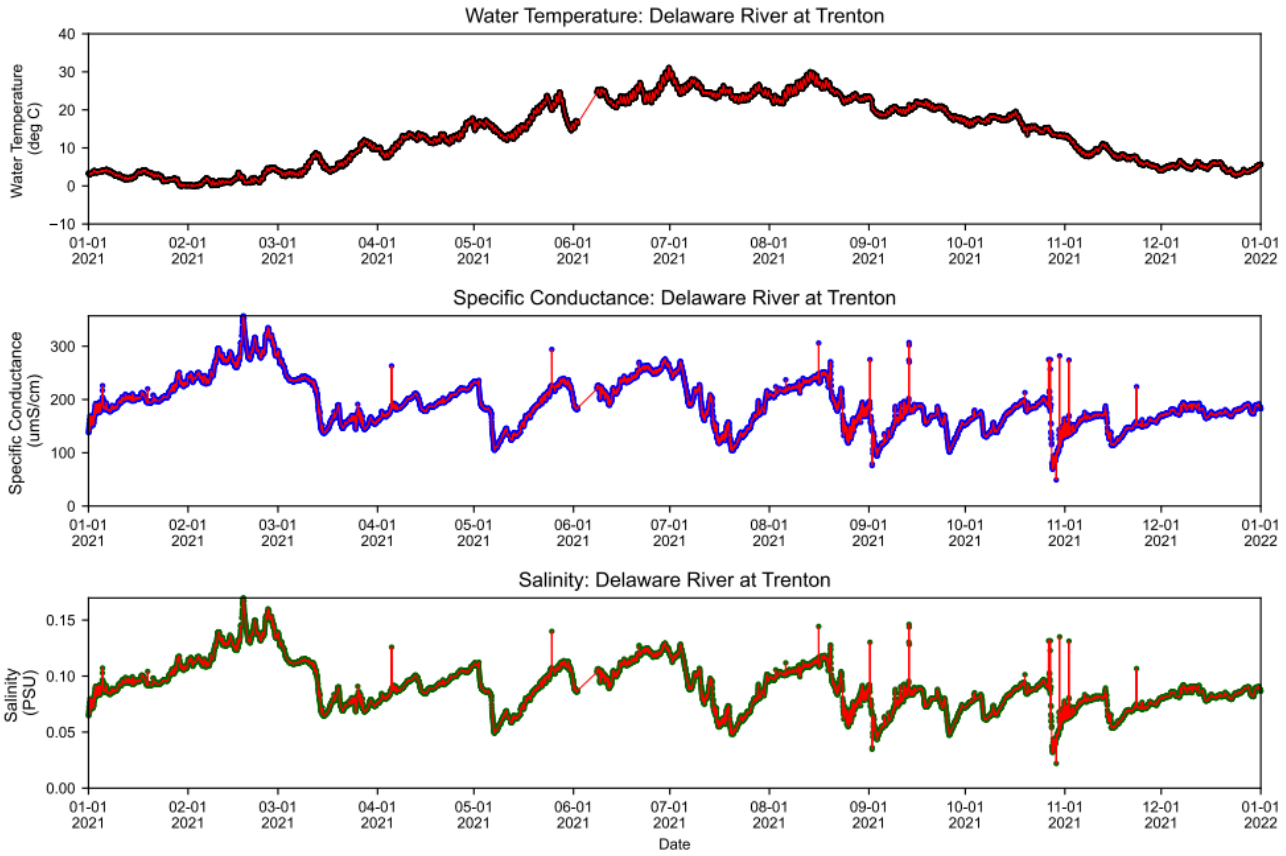

Historical USGS sub-hourly data were used and interpolated to hourly time interval for model input.

Figure 3.3-2 (12) Water Temperature and Specific Conductance Data Collected at USGS Station 01436500, Delaware River at Trenton During 2021

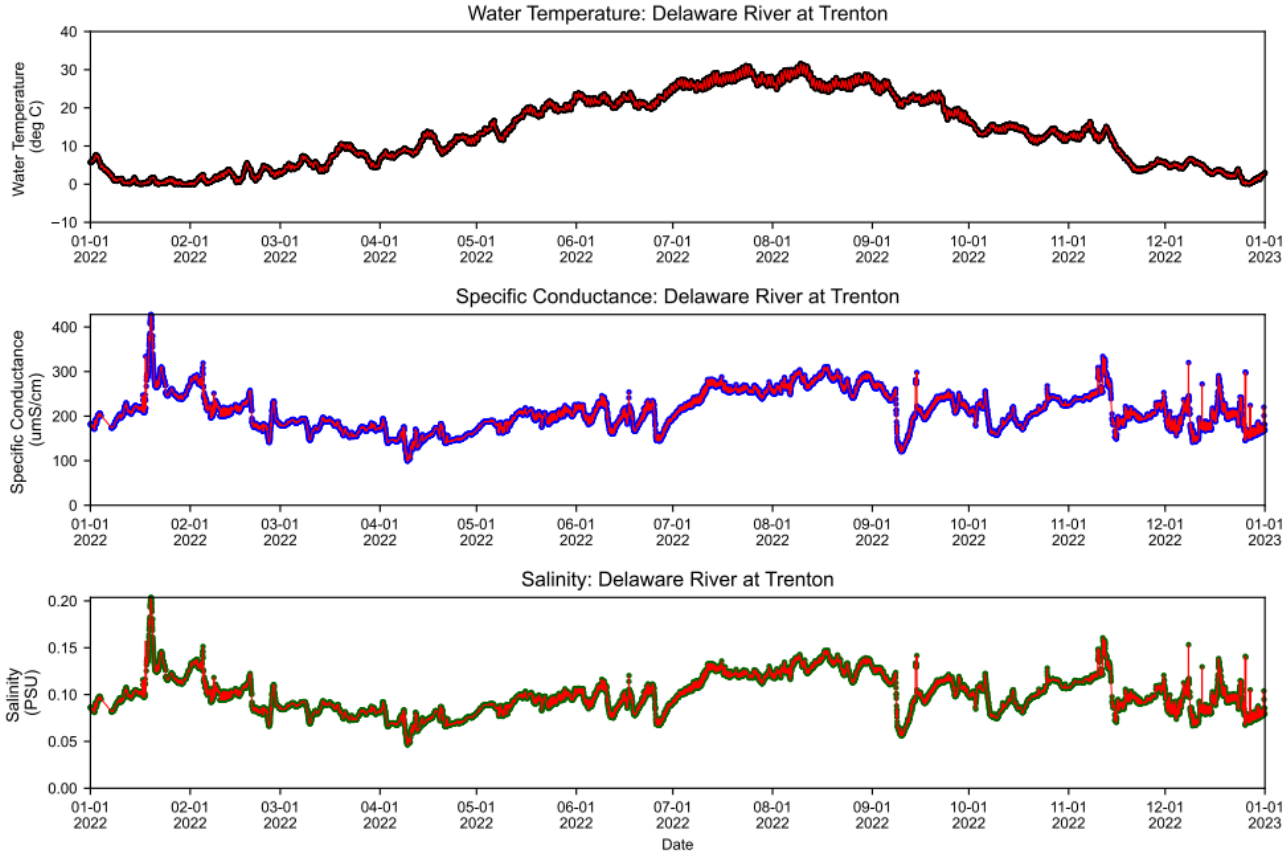

Historical USGS sub-hourly data were used and interpolated to hourly time interval for model input.

Figure 3.3-2 (13) Water Temperature and Specific Conductance Data Collected at USGS Station 01436500, Delaware River at Trenton During 2022

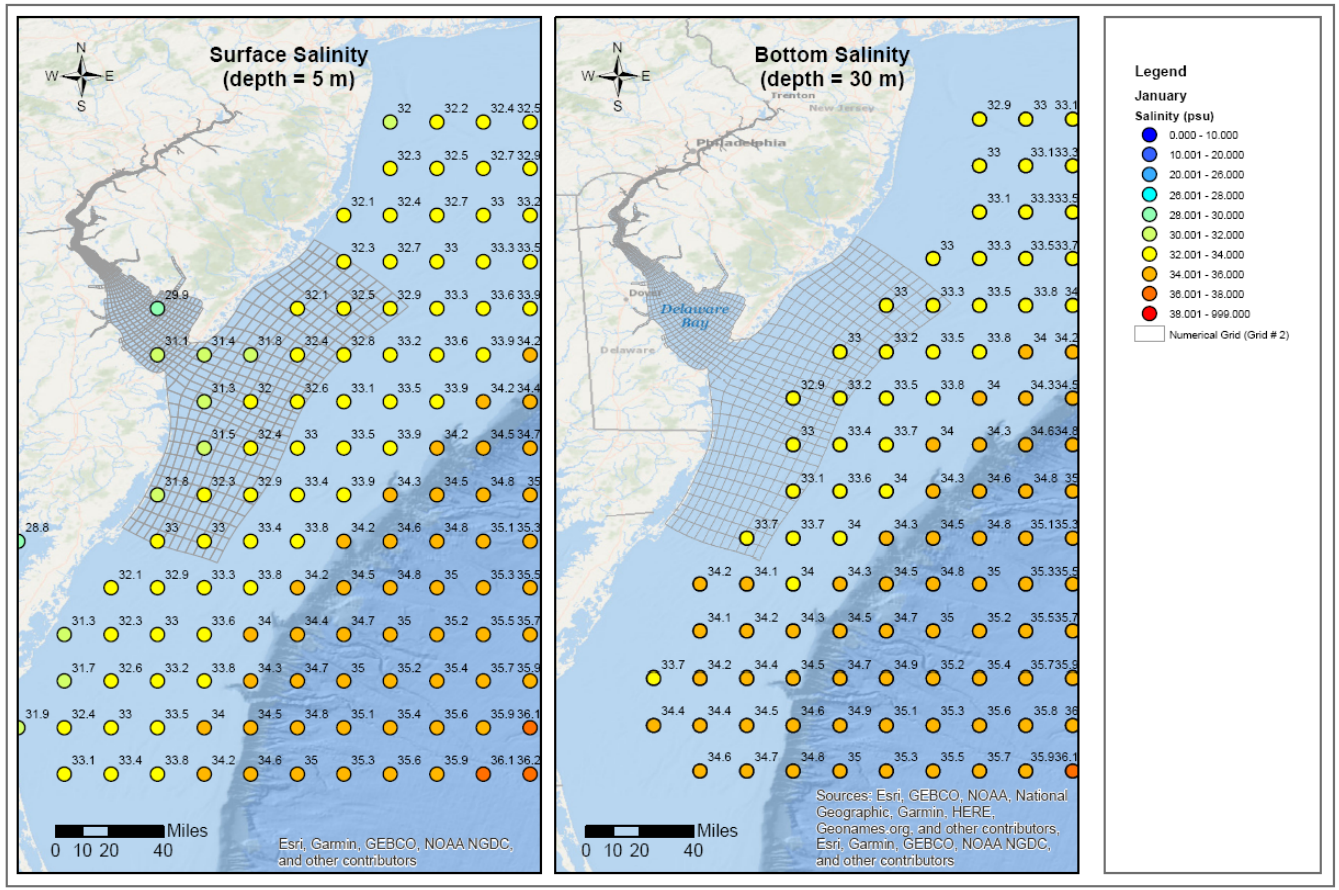

Analysis was based on World Ocean Atlas 2013 (WOA13) database (Locarnini et al., 2013; Zweng et al., 2013)

Figure 3.3-3 (1) Near-Surface and Near-Bottom Salinity near Ocean Boundary Based on WOA13 Database: January Statistical Mean (2005–2012)

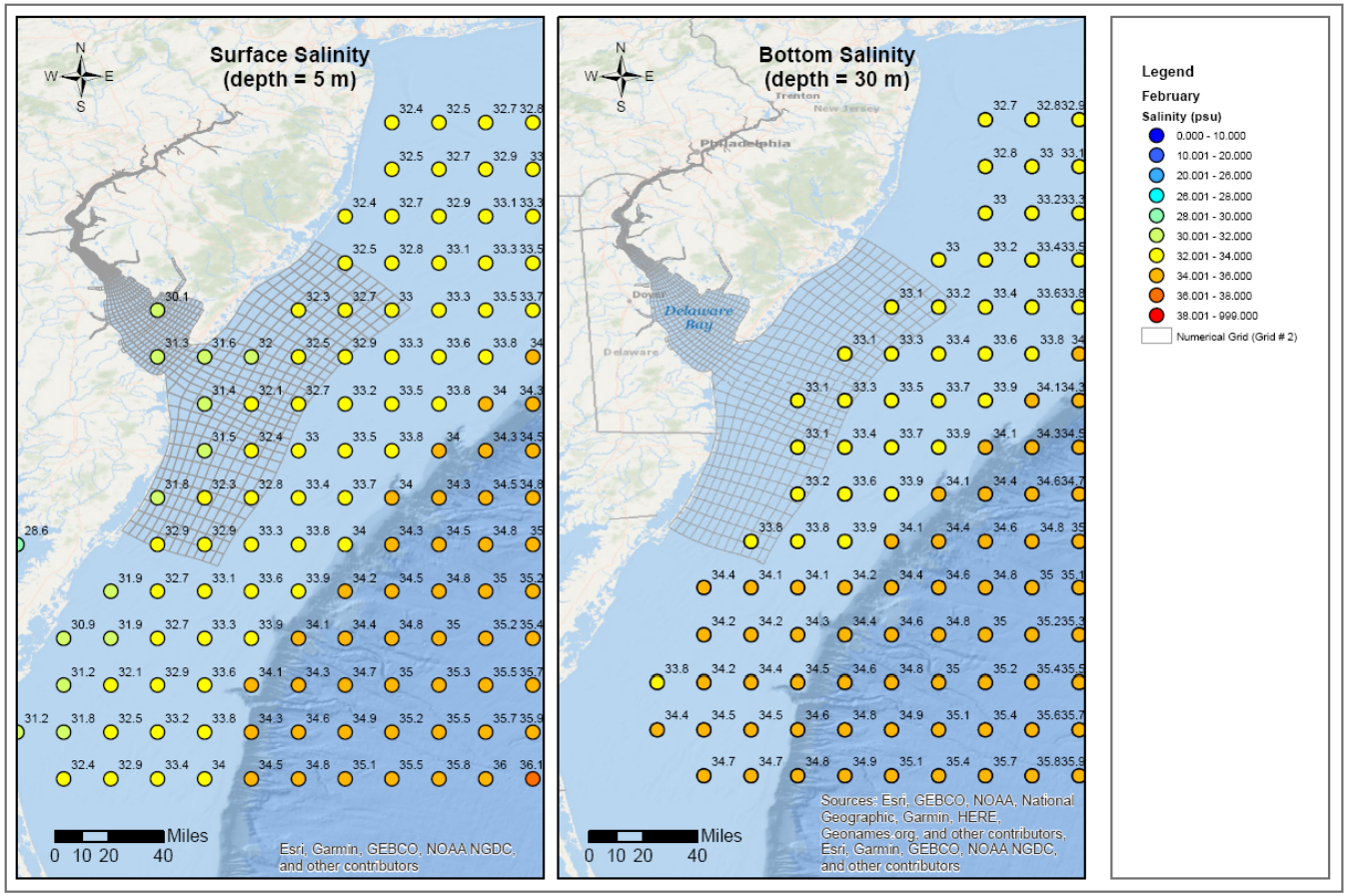

Analysis was based on World Ocean Atlas 2013 (WOA13) database (Locarnini et al., 2013; Zweng et al., 2013)

Figure 3.3-3 (2) Near-Surface and Near-Bottom Salinity near Ocean Boundary Based on WOA13 Database: February Statistical Mean (2005–2012)

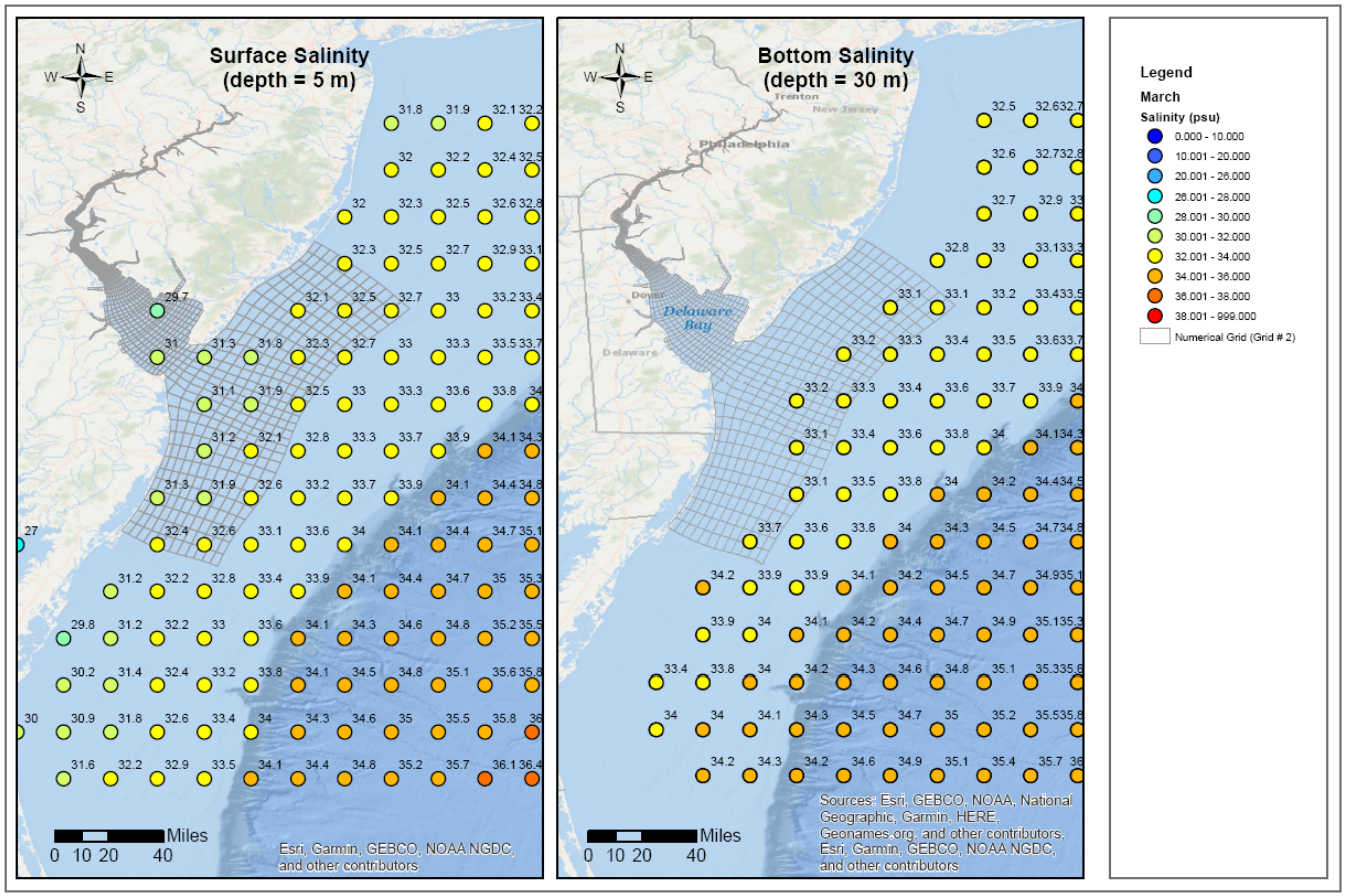

Analysis was based on World Ocean Atlas 2013 (WOA13) database (Locarnini et al., 2013; Zweng et al., 2013)

Figure 3.3-3 (3) Near-Surface and Near-Bottom Salinity near Ocean Boundary Based on WOA13 Database: March Statistical Mean (2005–2012)

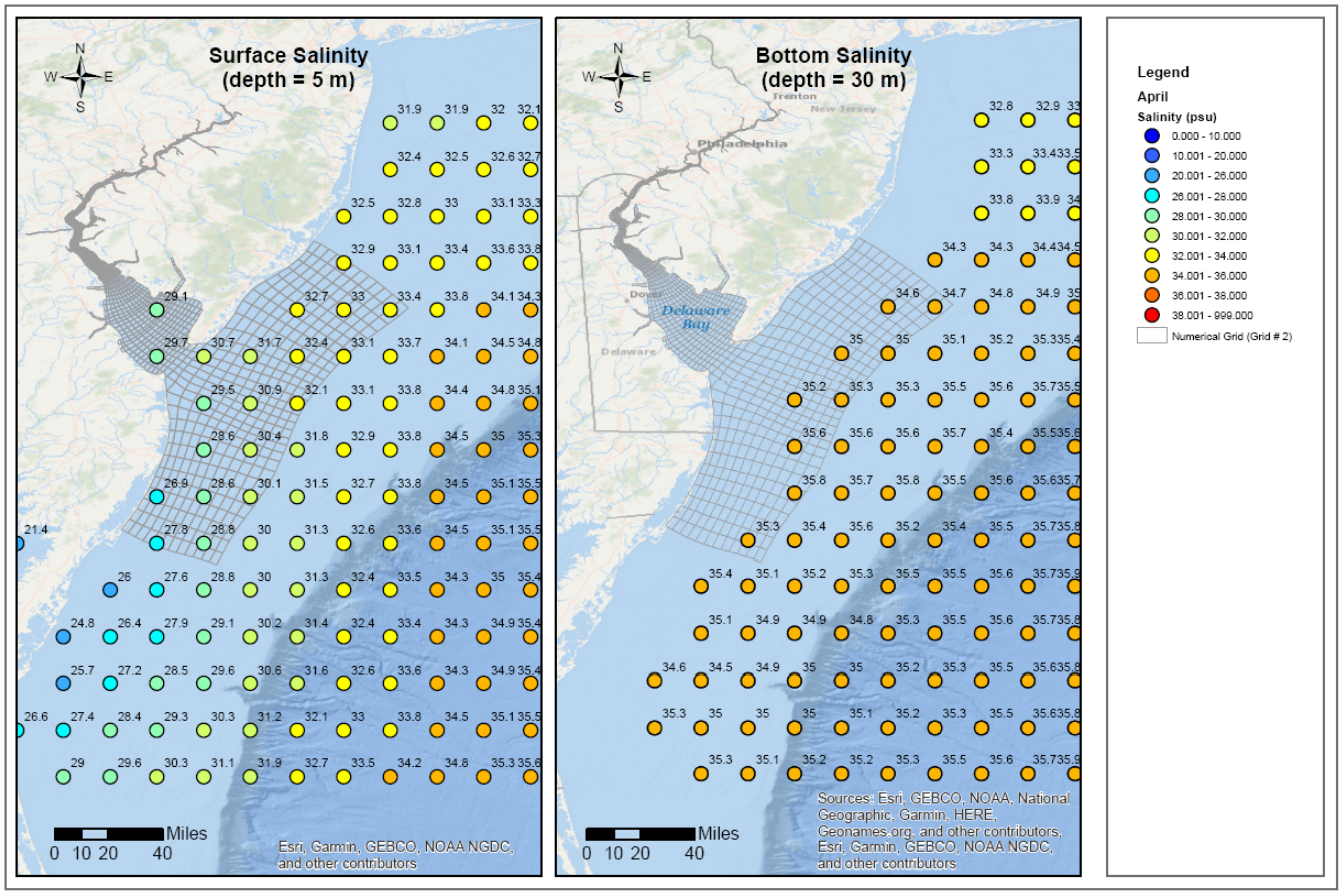

Analysis was based on World Ocean Atlas 2013 (WOA13) database (Locarnini et al., 2013; Zweng et al., 2013)

Figure 3.3-3 (4) Near-Surface and Near-Bottom Salinity near Ocean Boundary Based on WOA13 Database: April Statistical Mean (2005–2012)

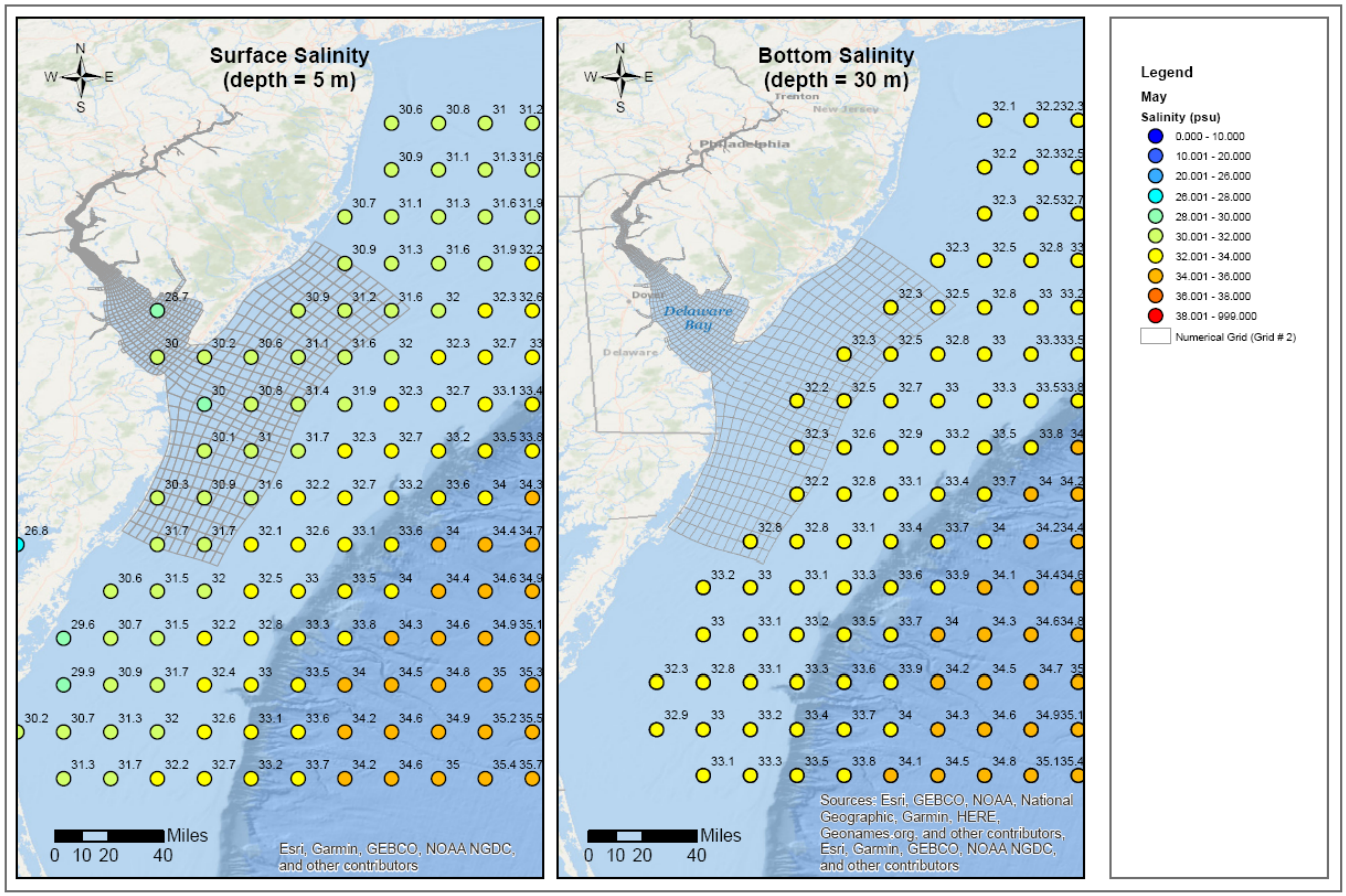

Analysis was based on World Ocean Atlas 2013 (WOA13) database (Locarnini et al., 2013; Zweng et al., 2013)

Figure 3.3-3 (5) Near-Surface and Near-Bottom Salinity near Ocean Boundary Based on WOA13 Database: May Statistical Mean (2005–2012)

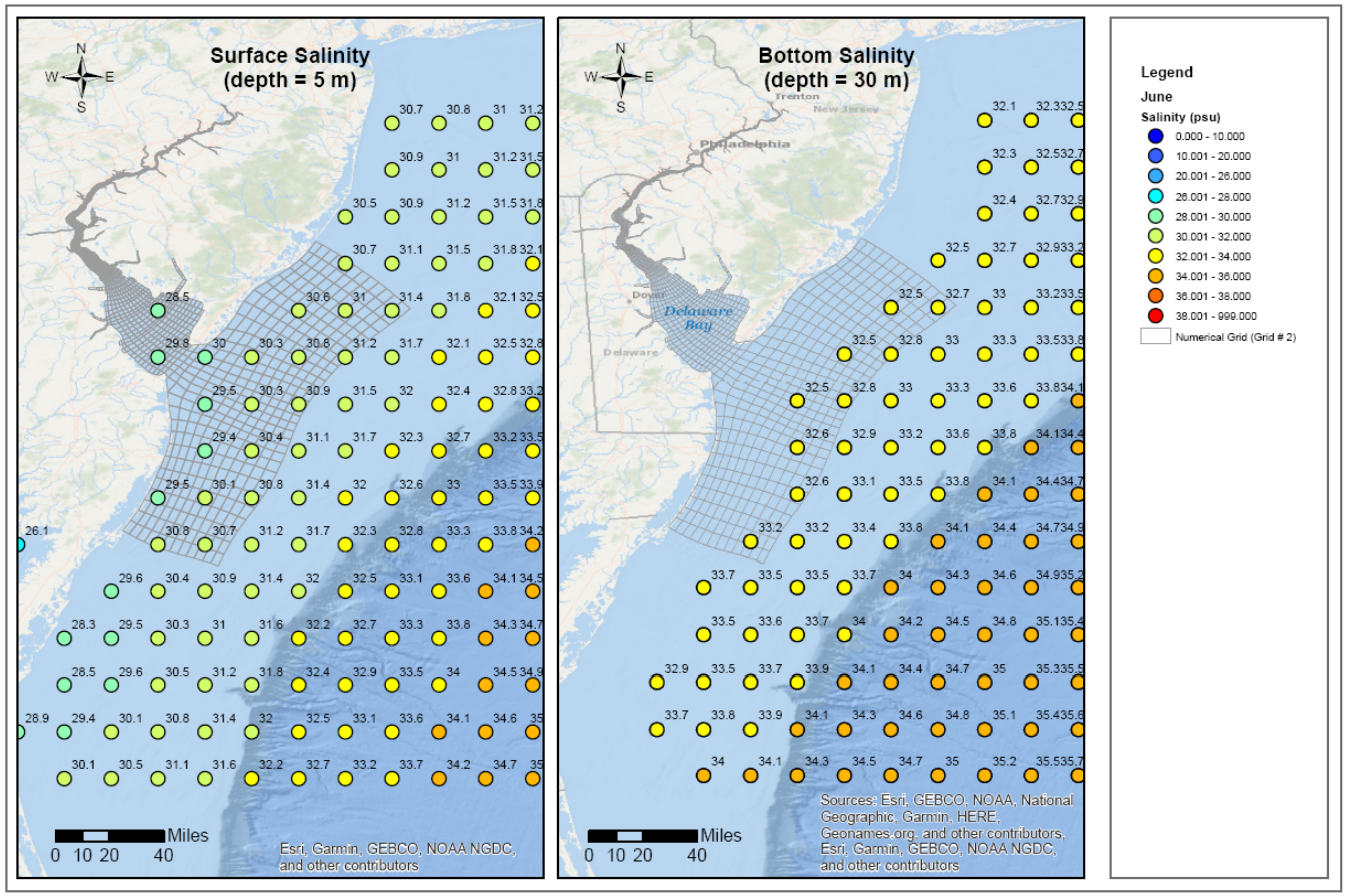

Analysis was based on World Ocean Atlas 2013 (WOA13) database (Locarnini et al., 2013; Zweng et al., 2013)

Figure 3.3-3 (6) Near-Surface and Near-Bottom Salinity near Ocean Boundary Based on WOA13 Database: June Statistical Mean (2005–2012)

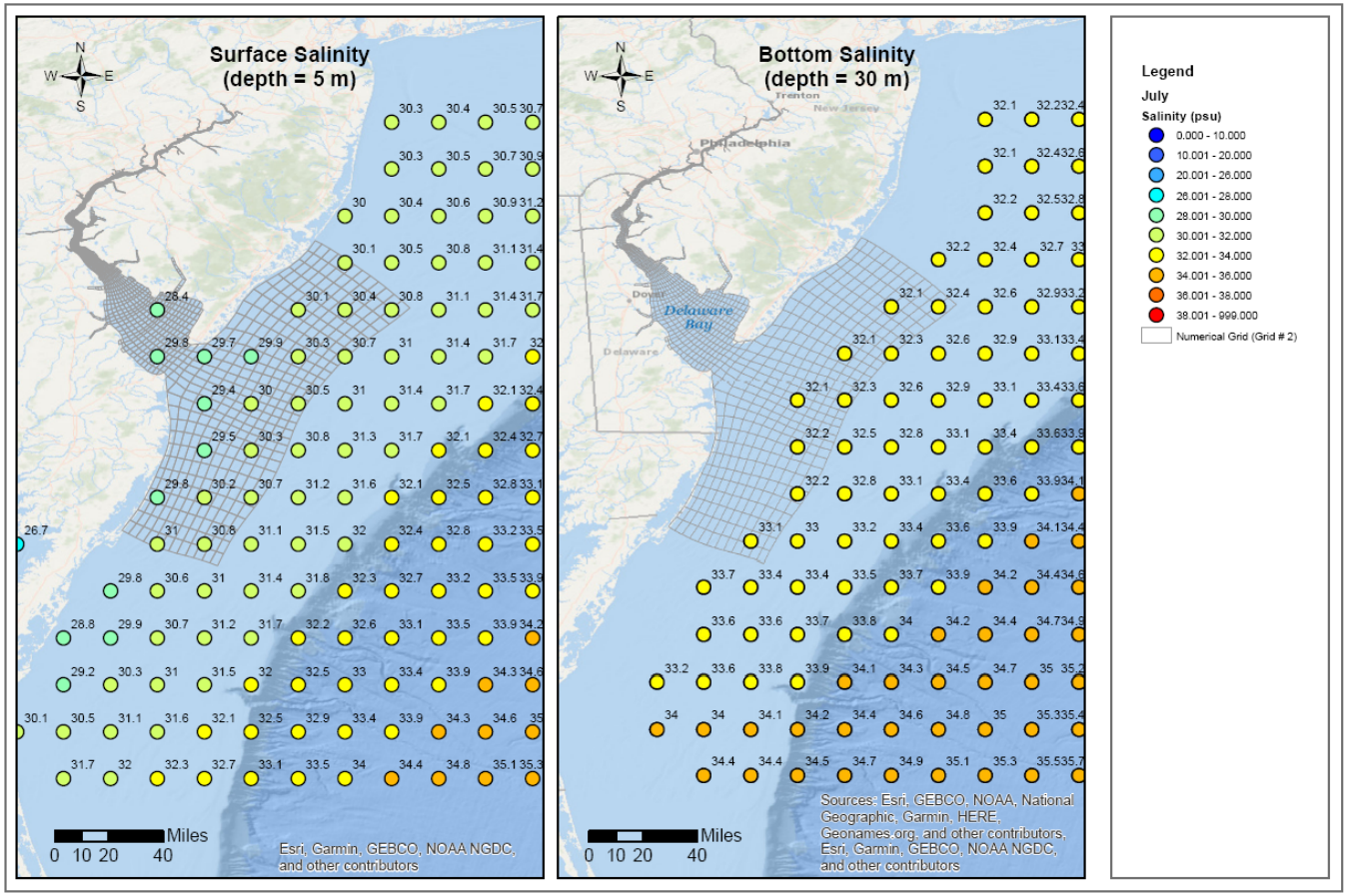

Analysis was based on World Ocean Atlas 2013 (WOA13) database (Locarnini et al., 2013; Zweng et al., 2013)

Figure 3.3-3 (7) Near-Surface and Near-Bottom Salinity near Ocean Boundary Based on WOA13 Database: July Statistical Mean (2005–2012)

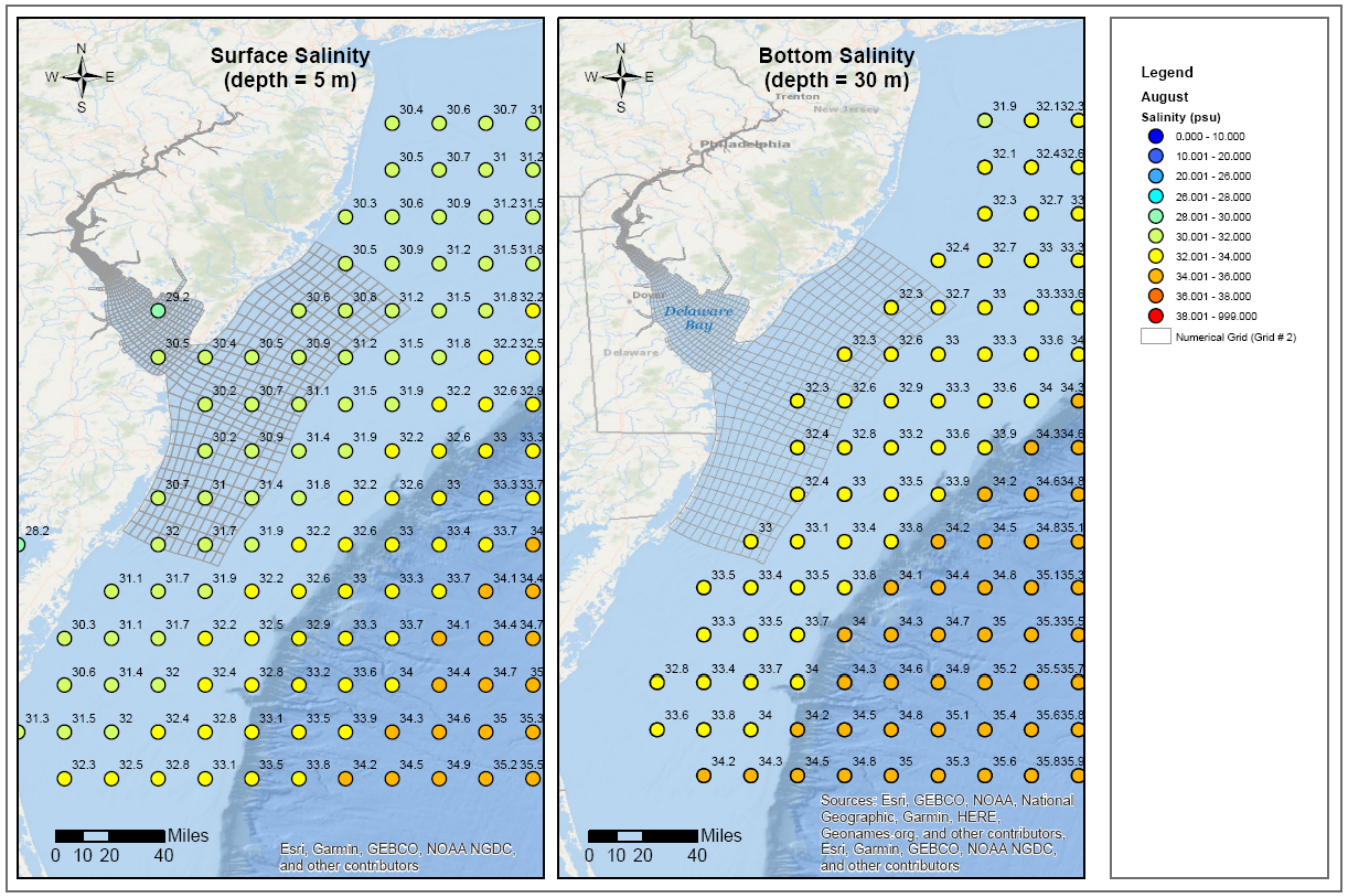

Analysis was based on World Ocean Atlas 2013 (WOA13) database (Locarnini et al., 2013; Zweng et al., 2013)

Figure 3.3-3 (8) Near-Surface and Near-Bottom Salinity near Ocean Boundary Based on WOA13 Database August Statistical Mean (2005–2012)

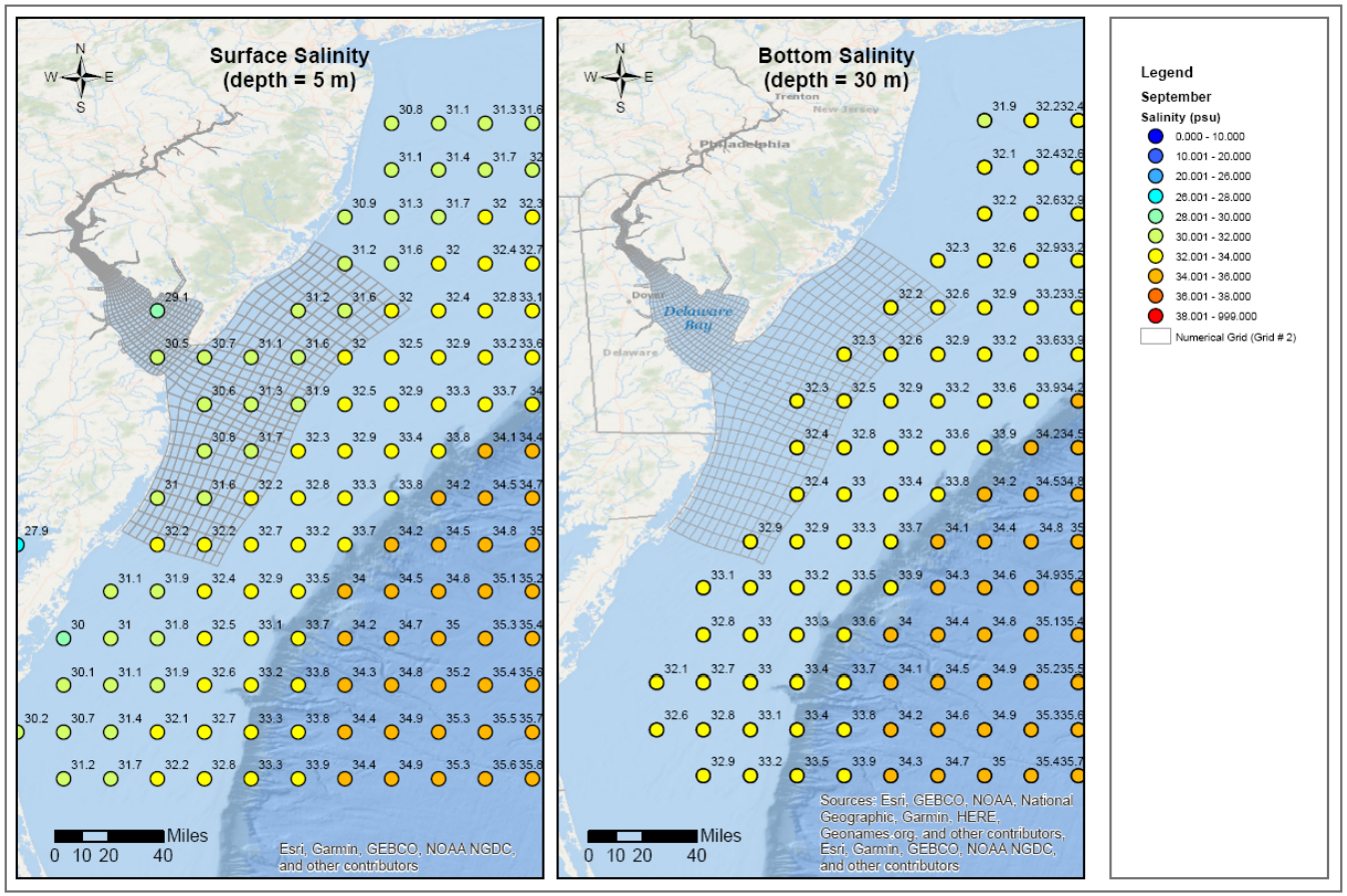

Analysis was based on World Ocean Atlas 2013 (WOA13) database (Locarnini et al., 2013; Zweng et al., 2013)

Figure 3.3-3 (9) Near-Surface and Near-Bottom Salinity near Ocean Boundary Based on WOA13 Database: September Statistical Mean (2005–2012)

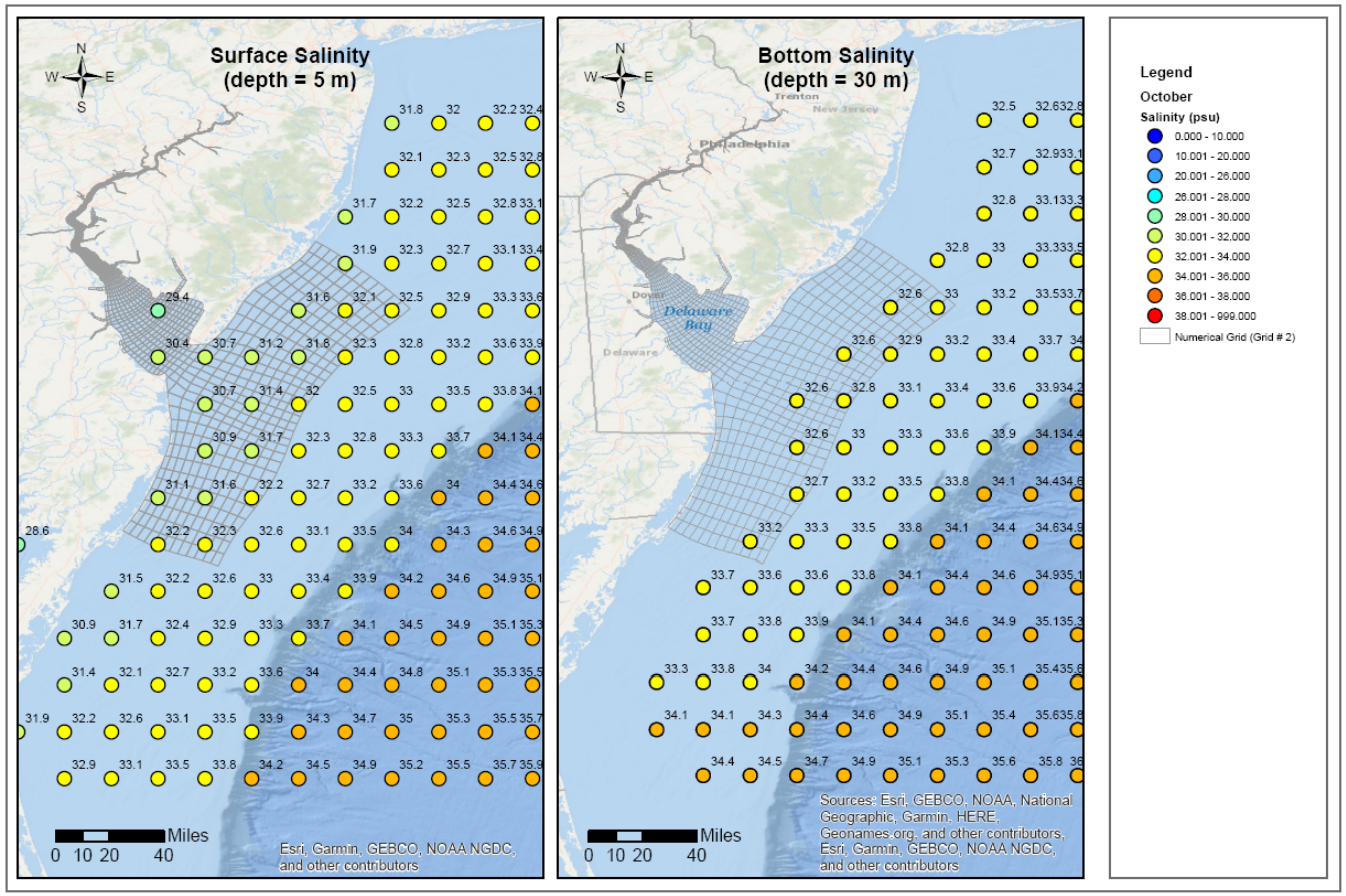

Analysis was based on World Ocean Atlas 2013 (WOA13) database (Locarnini et al., 2013; Zweng et al., 2013)

Figure 3.3-3 (10) Near-Surface and Near-Bottom Salinity near Ocean Boundary Based on WOA13 Database: October Statistical Mean (2005–2012)

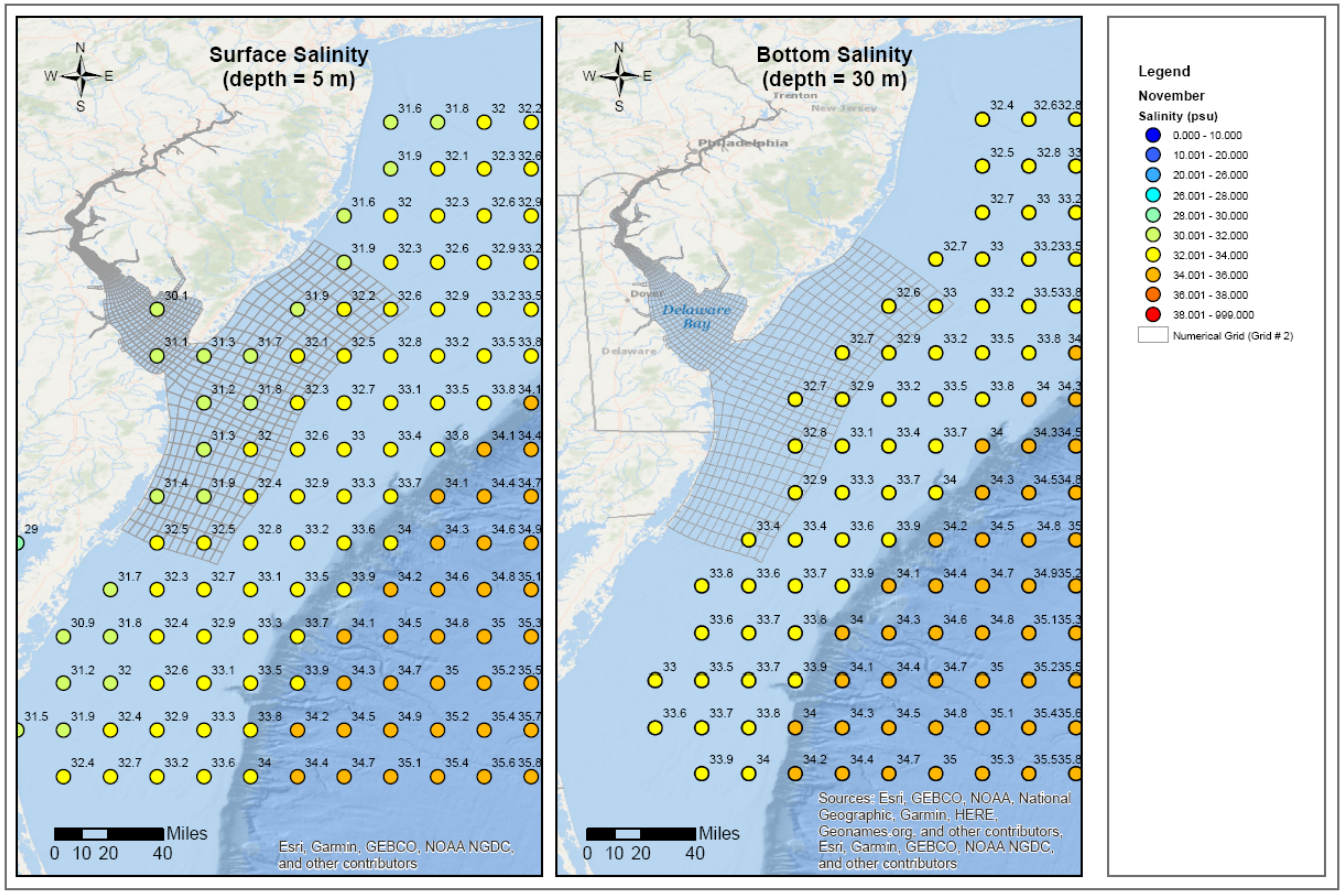

Analysis was based on World Ocean Atlas 2013 (WOA13) database (Locarnini et al., 2013; Zweng et al., 2013)

Figure 3.3-3 (11) Near-Surface and Near-Bottom Salinity near Ocean Boundary Based on WOA13 Database: November Statistical Mean (2005–2012)

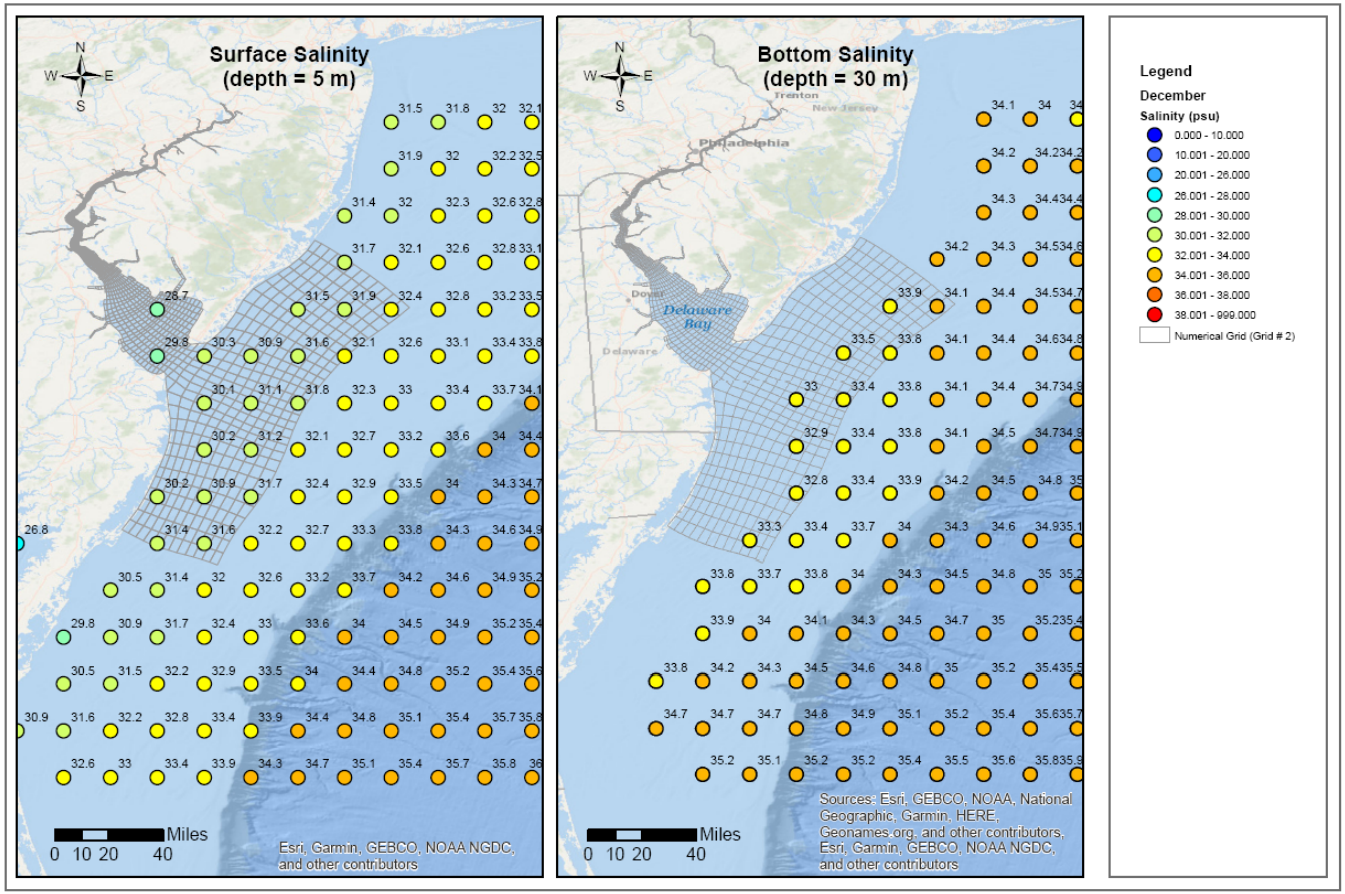

Analysis was based on World Ocean Atlas 2013 (WOA13) database (Locarnini et al., 2013; Zweng et al., 2013)

Figure 3.3-3 (12) Near-Surface and Near-Bottom Salinity near Ocean Boundary Based on WOA13 Database: December Statistical Mean (2005–2012)

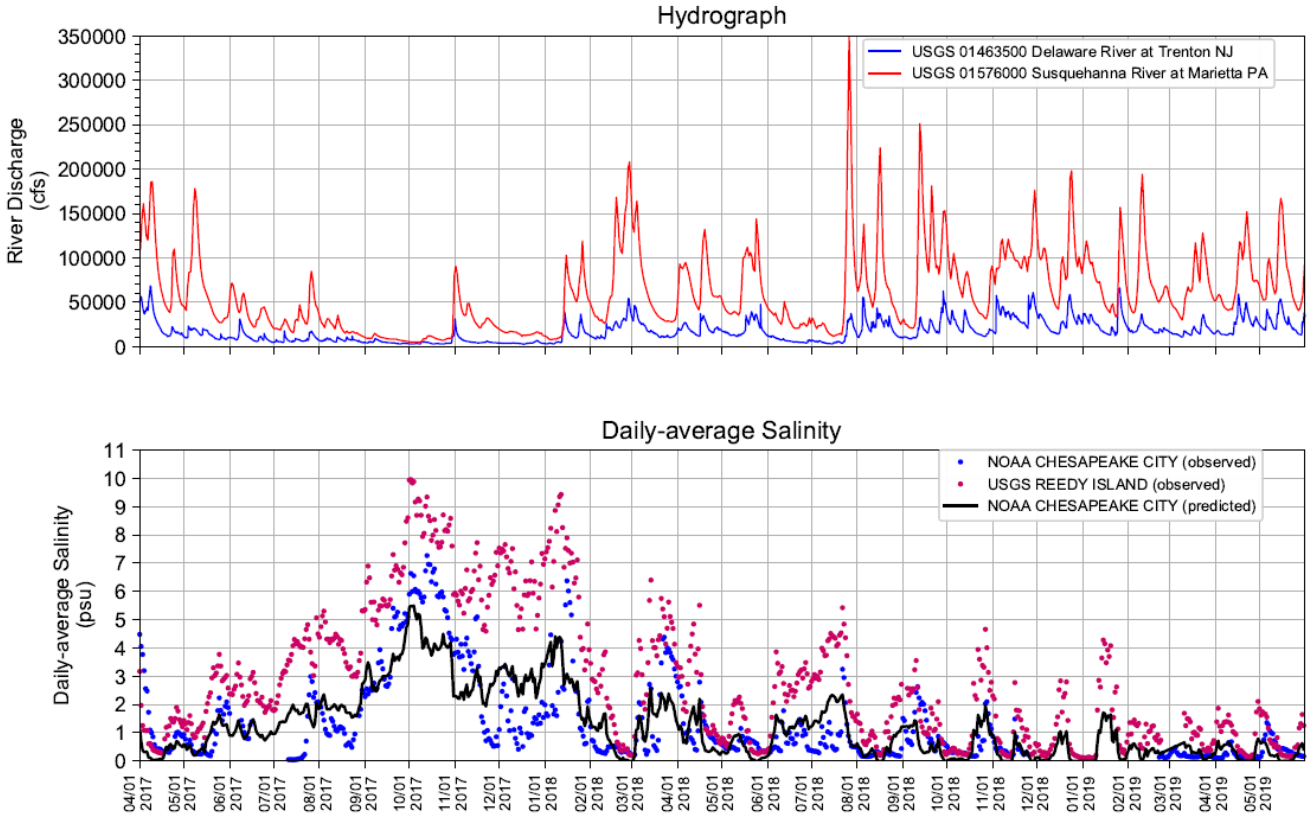

Predicted salinity at Chesapeake City (black line) was calculated using a rating curve that was developed using salinity data at Reedy Island and Susquehanna River flow at Marietta, PA

Figure 3.3-4 Predicted Daily-averaged Salinity at Chesapeake City using Rating Curve

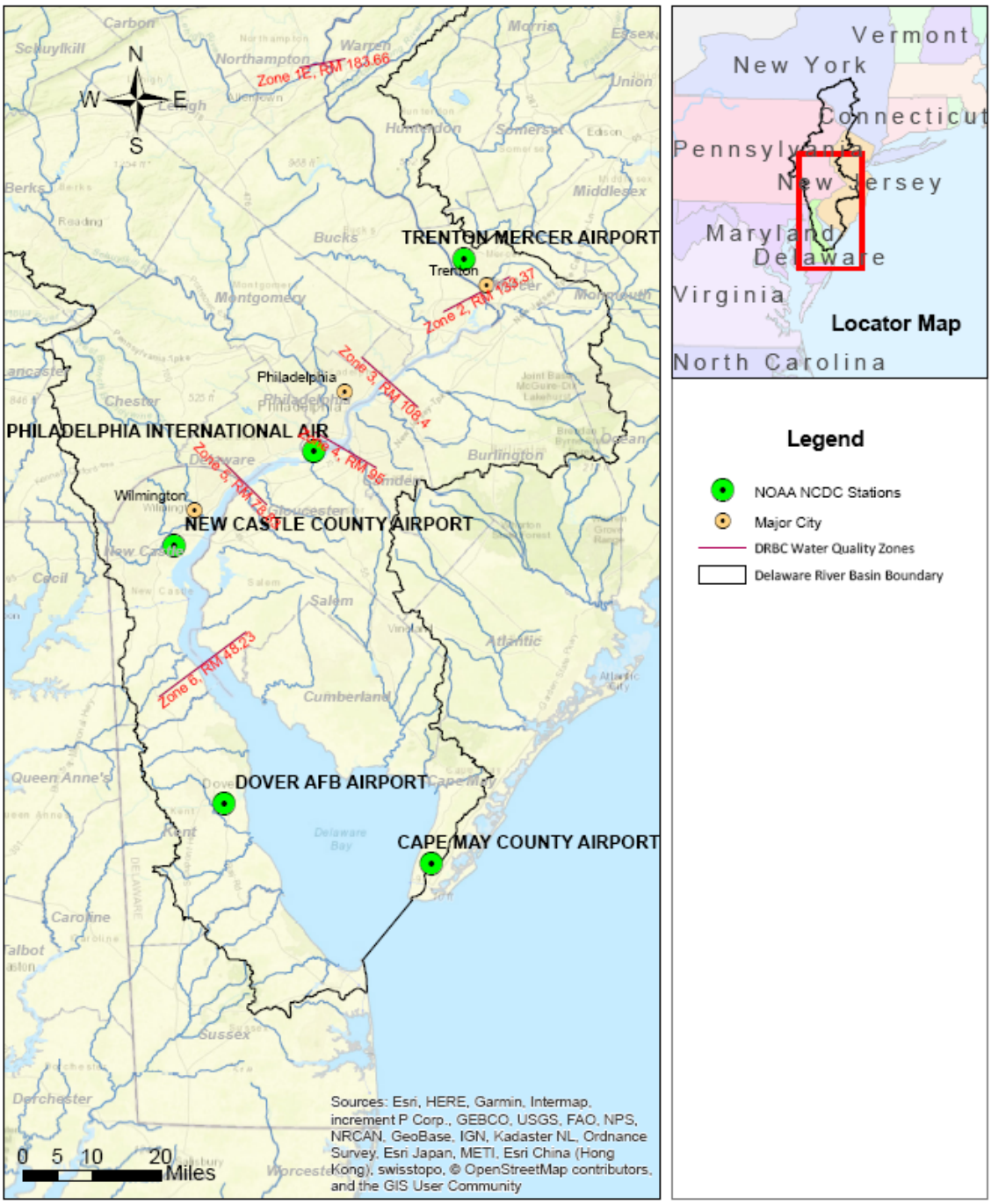

Figure 3.3-5 Location Map of Five Weather Stations

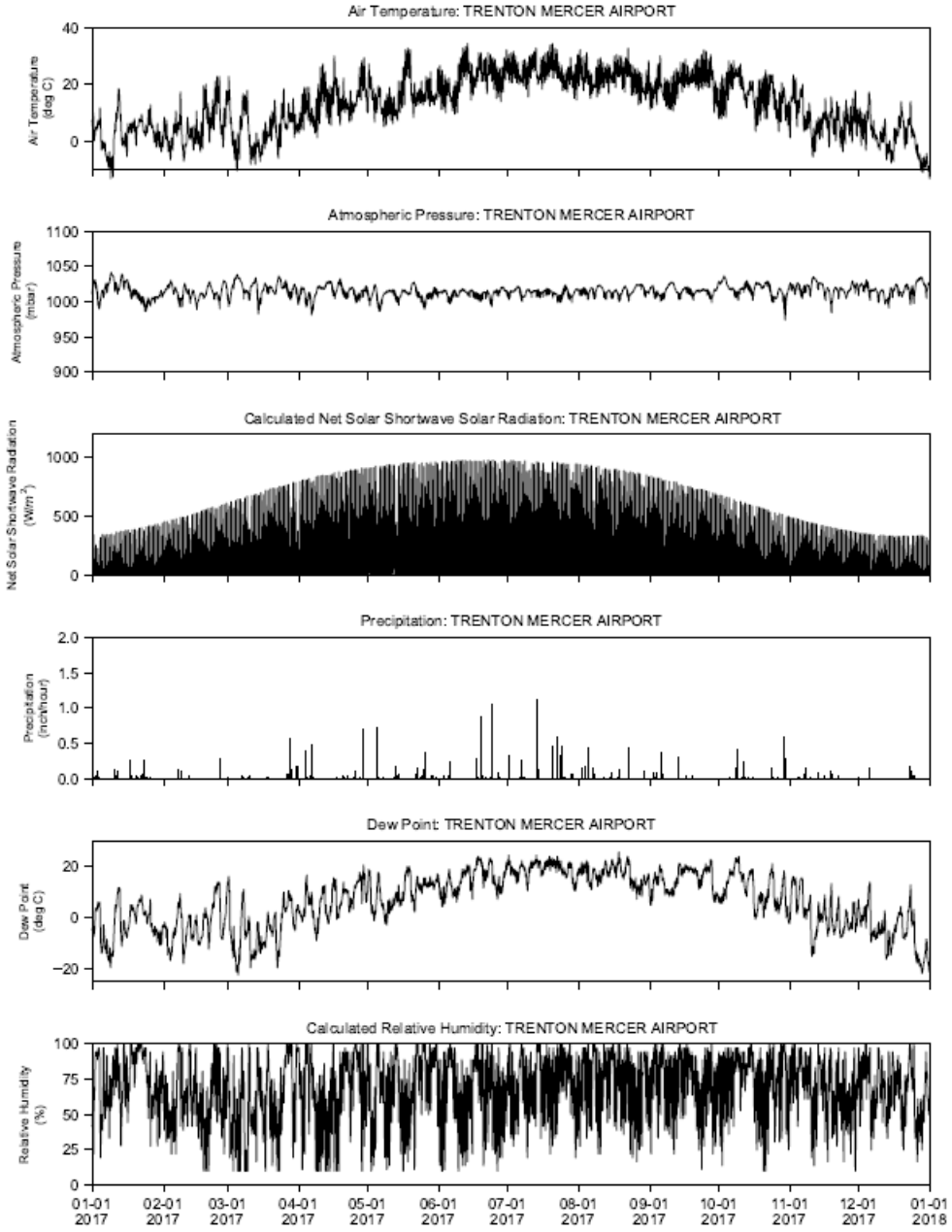

Figure 3.3-6 (1) Meteorological Data Collected at NOAA-NCDC Station at Trenton Mercer Airport during 2017

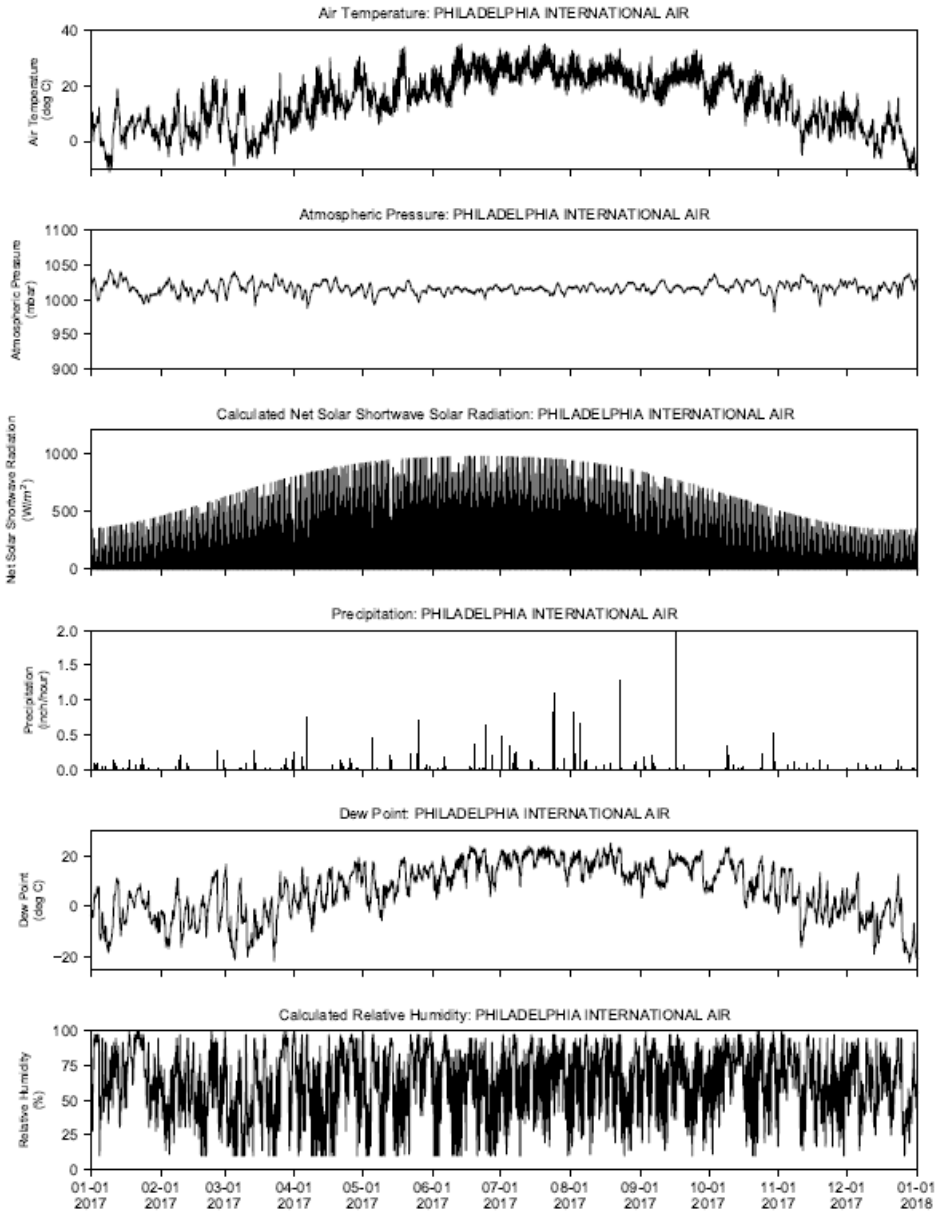

Figure 3.3-6 (2) Meteorological Data Collected at NOAA-NCDC Station at Philadelphia International Airport during 2017

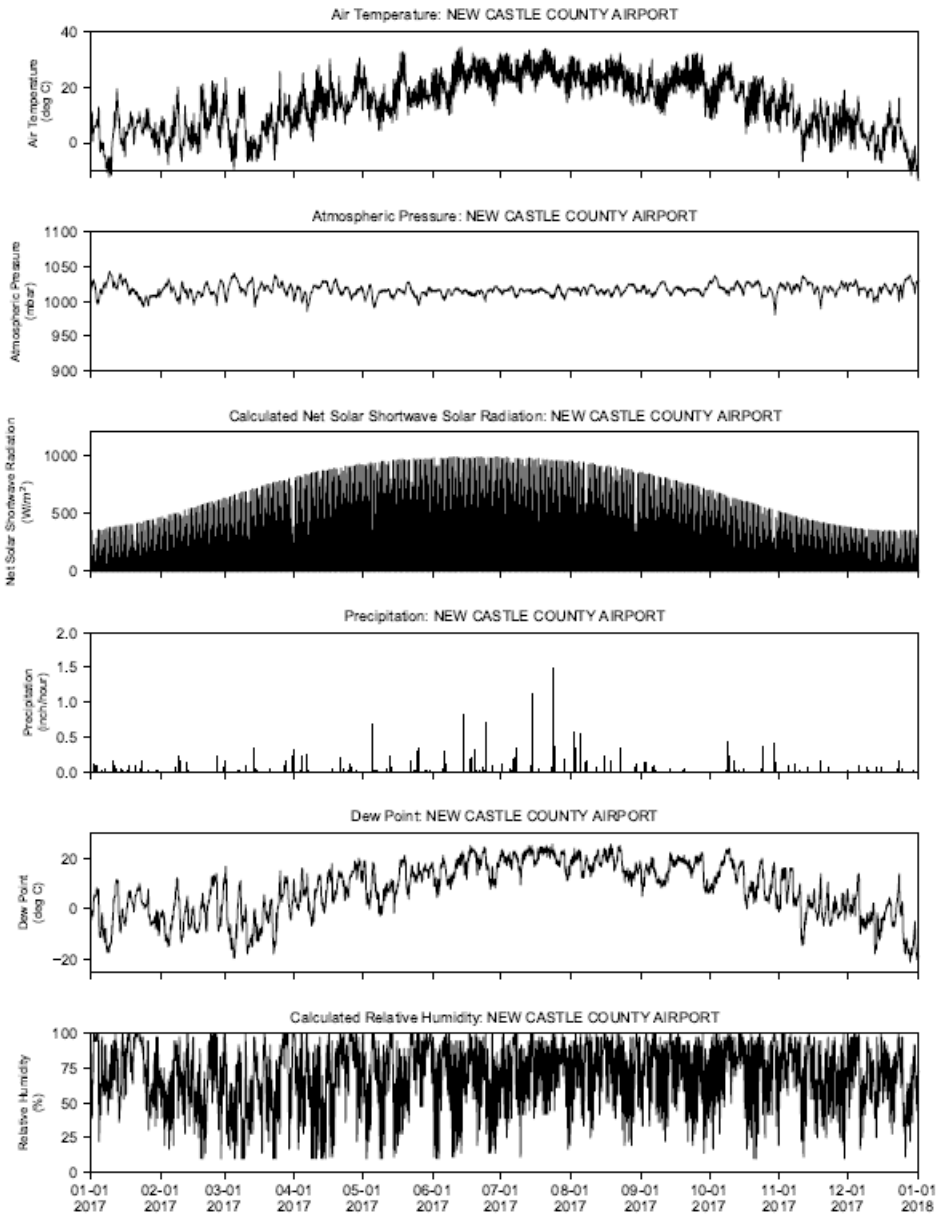

Figure 3.3-6 (3) Meteorological Data Collected at NOAA-NCDC Station at New Castle County Airport during 2017

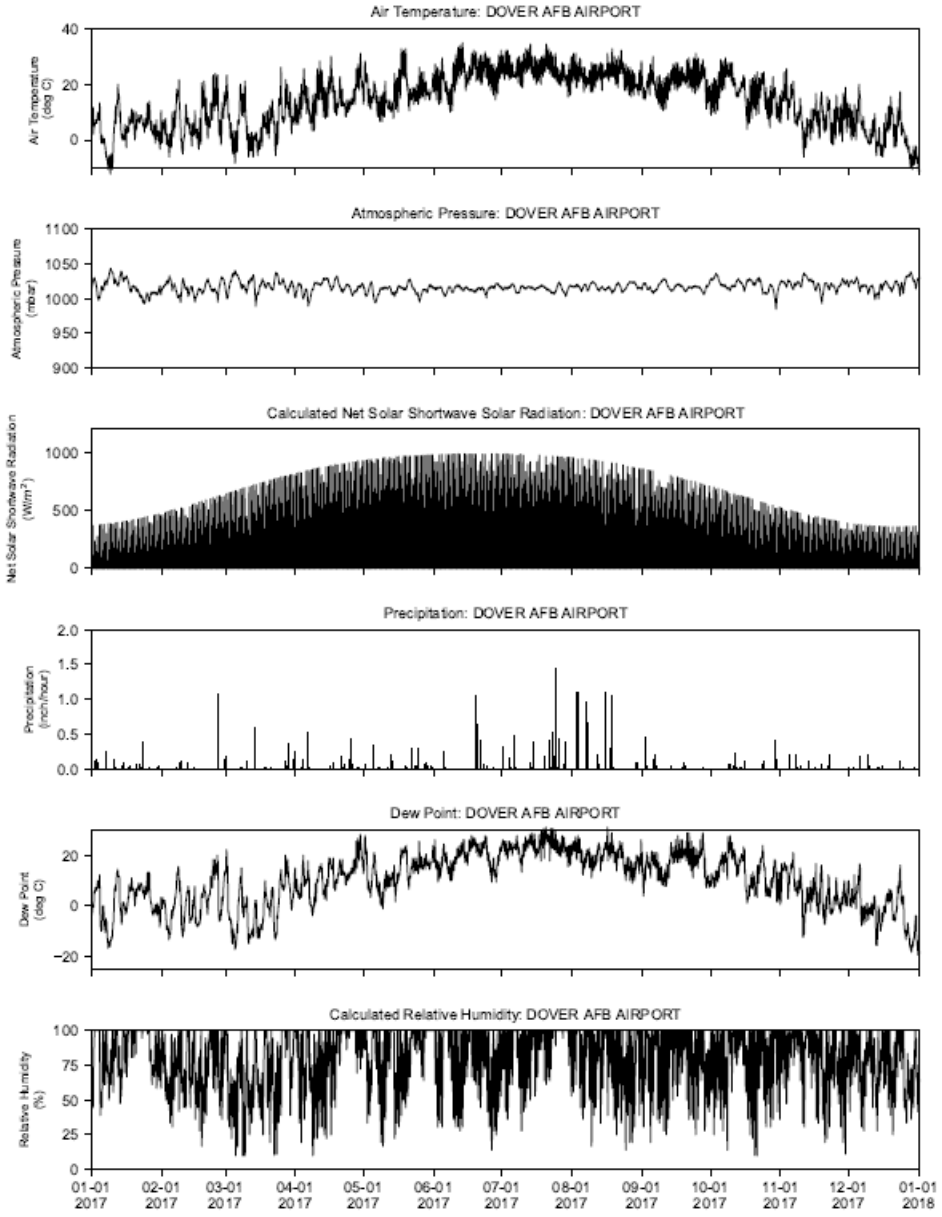

Figure 3.3-6 (4) Meteorological Data Collected at NOAA-NCDC Station at Dover AFB Airport during 2017

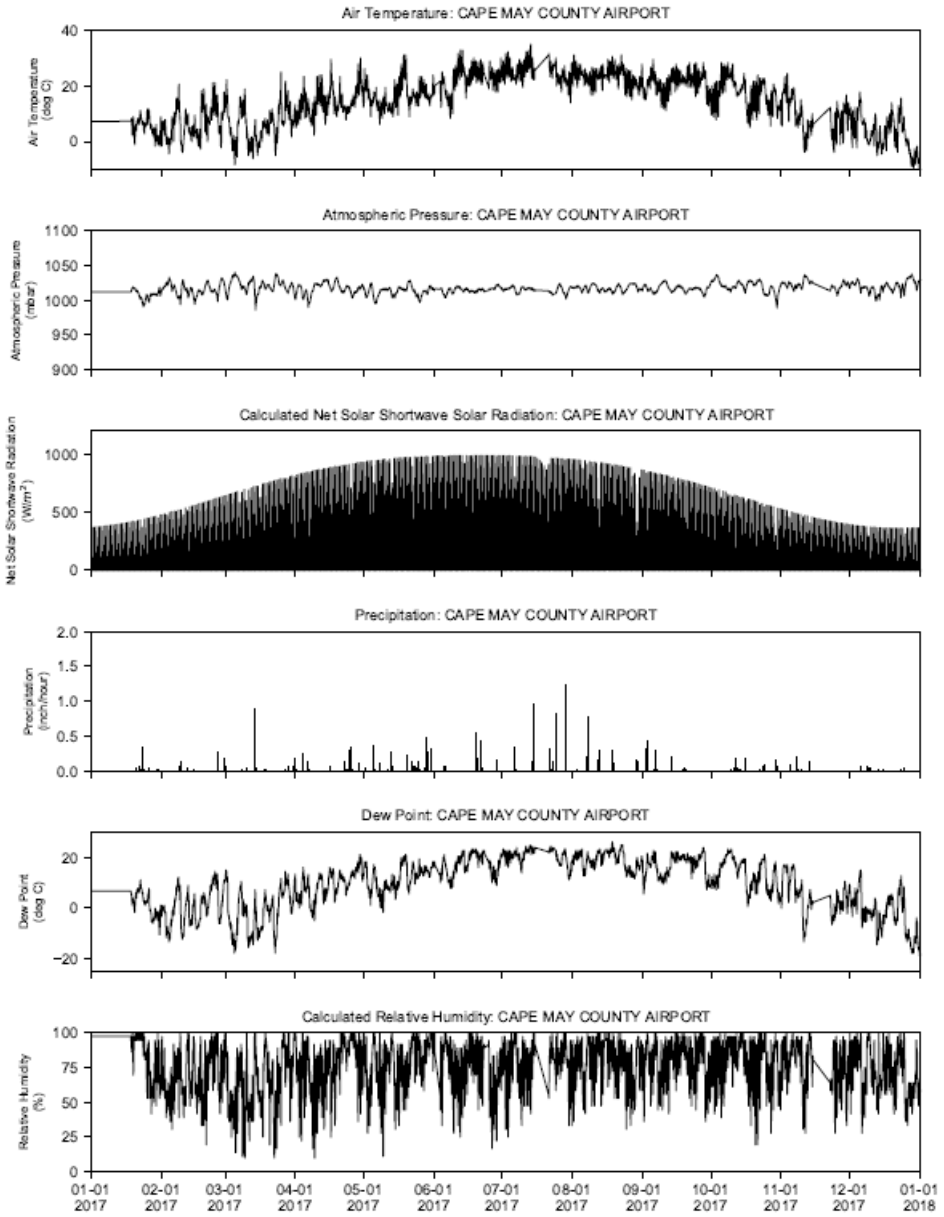

Figure 3.3-6 (5) Meteorological Data Collected at NOAA-NCDC Station at Cape May Airport during 2017

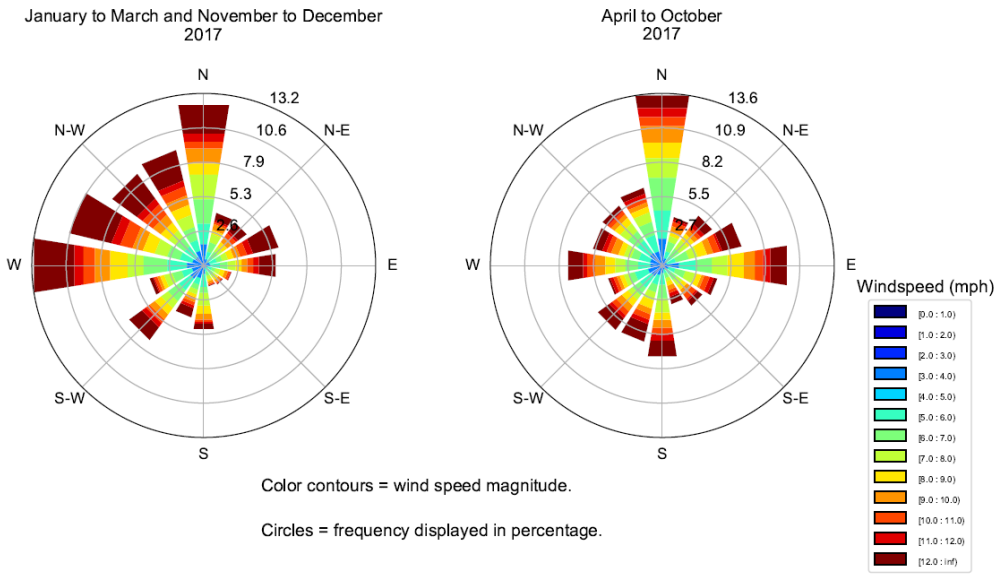

Figure 3.3-7 (1) Wind Data Collected at NOAA-NCDC Station at Trenton Mercer Airport during 2017

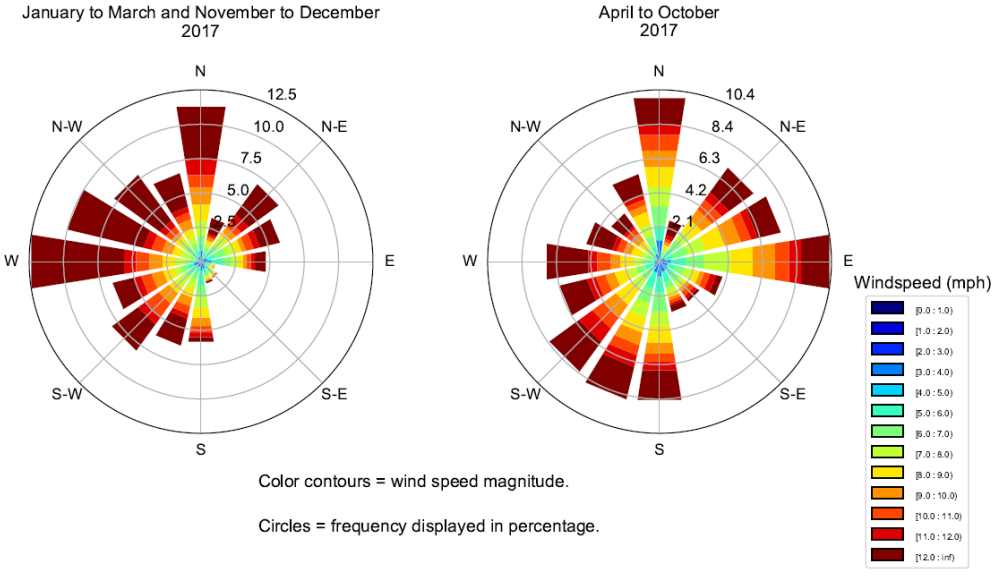

Figure 3.3-7 (2) Wind Data Collected at NOAA-NCDC Station at Philadelphia International Airport during 2017

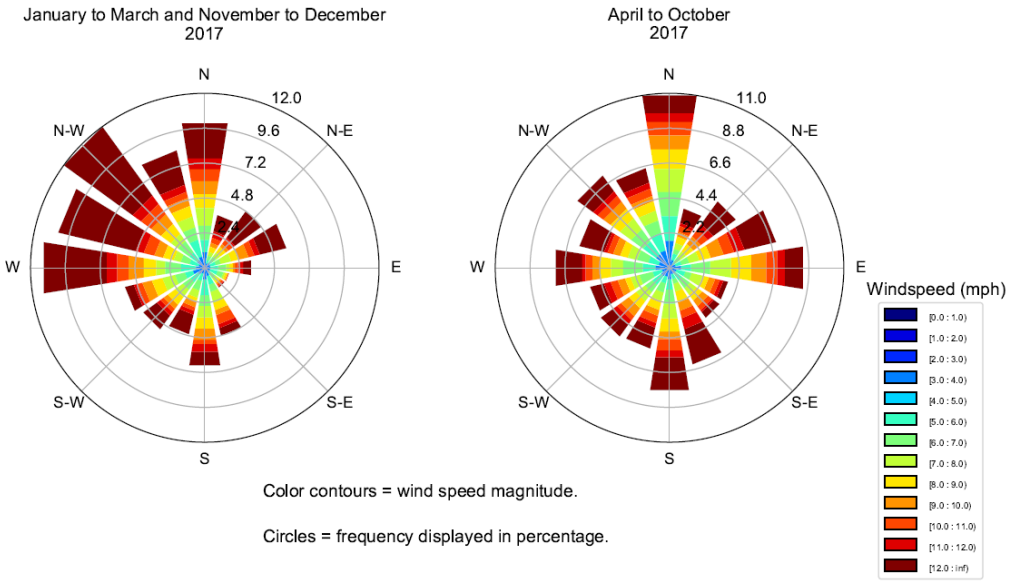

Figure 3.3-7 (3) Wind Data Collected at NOAA-NCDC Station at New Castle County Airport during 2017

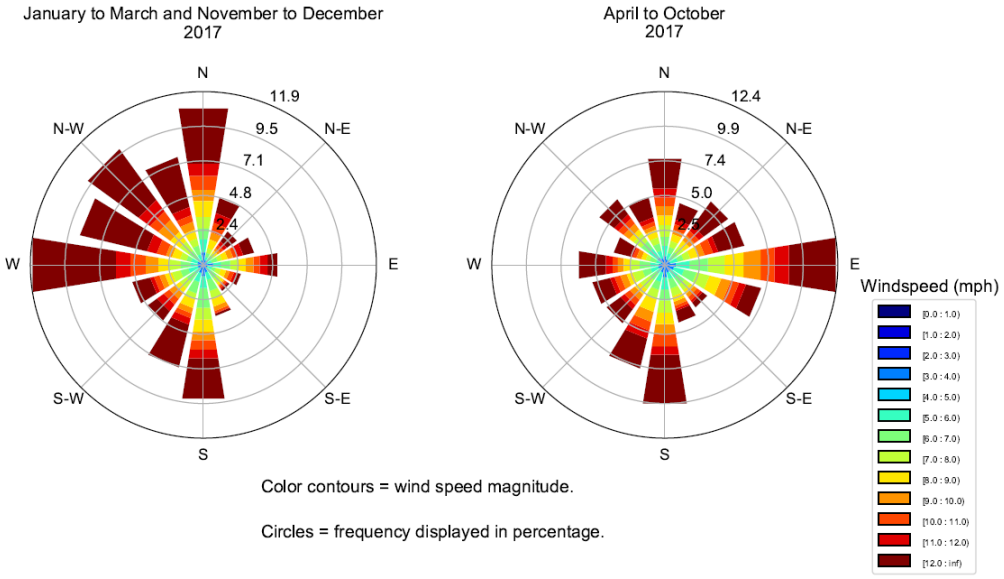

Figure 3.3-7 (4) Wind Data Collected at NOAA-NCDC Station at Dover AFB Airport during 2017

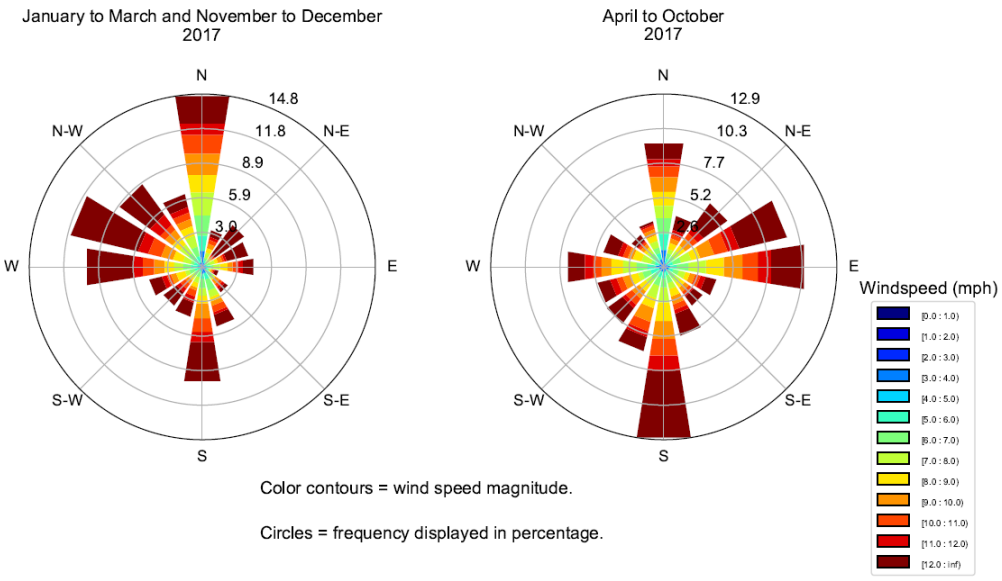

Figure 3.3-7 (5) Wind Data Collected at NOAA-NCDC Station at Cape May Airport during 2017

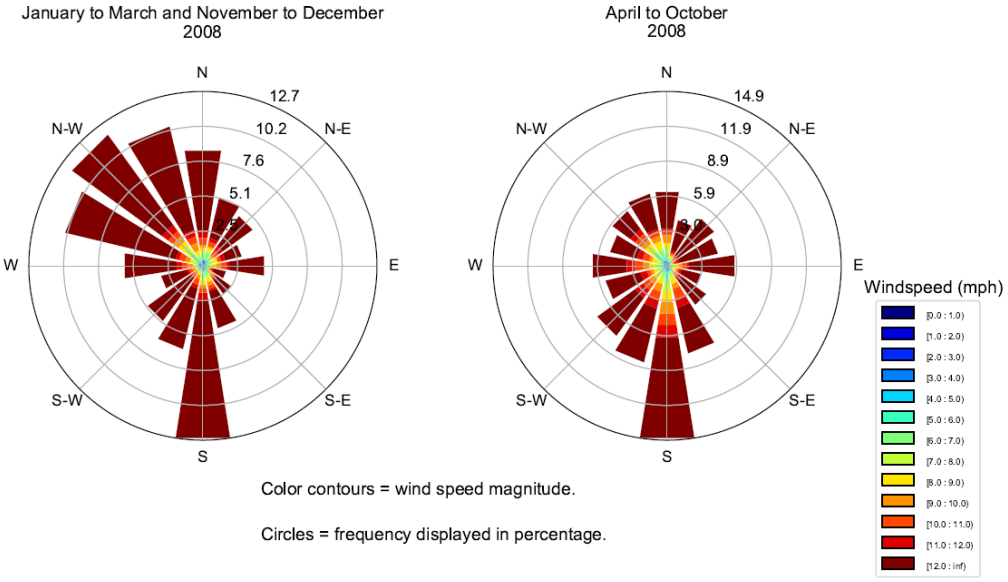

Figure 3.3-7 (6) Wind Data Collected at NOAA-NCDC Station at Brandywine Shoal Light during 2008

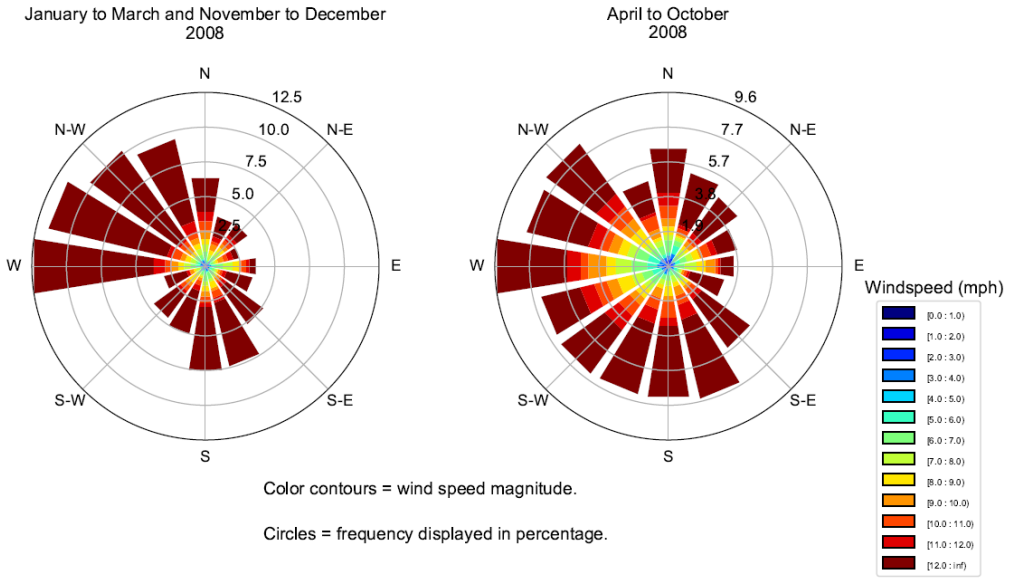

Figure 3.3-7 (7) Wind Data Collected at NOAA-NCDC Station at Ship John Shoal during 2008

Figures for Section 4.0

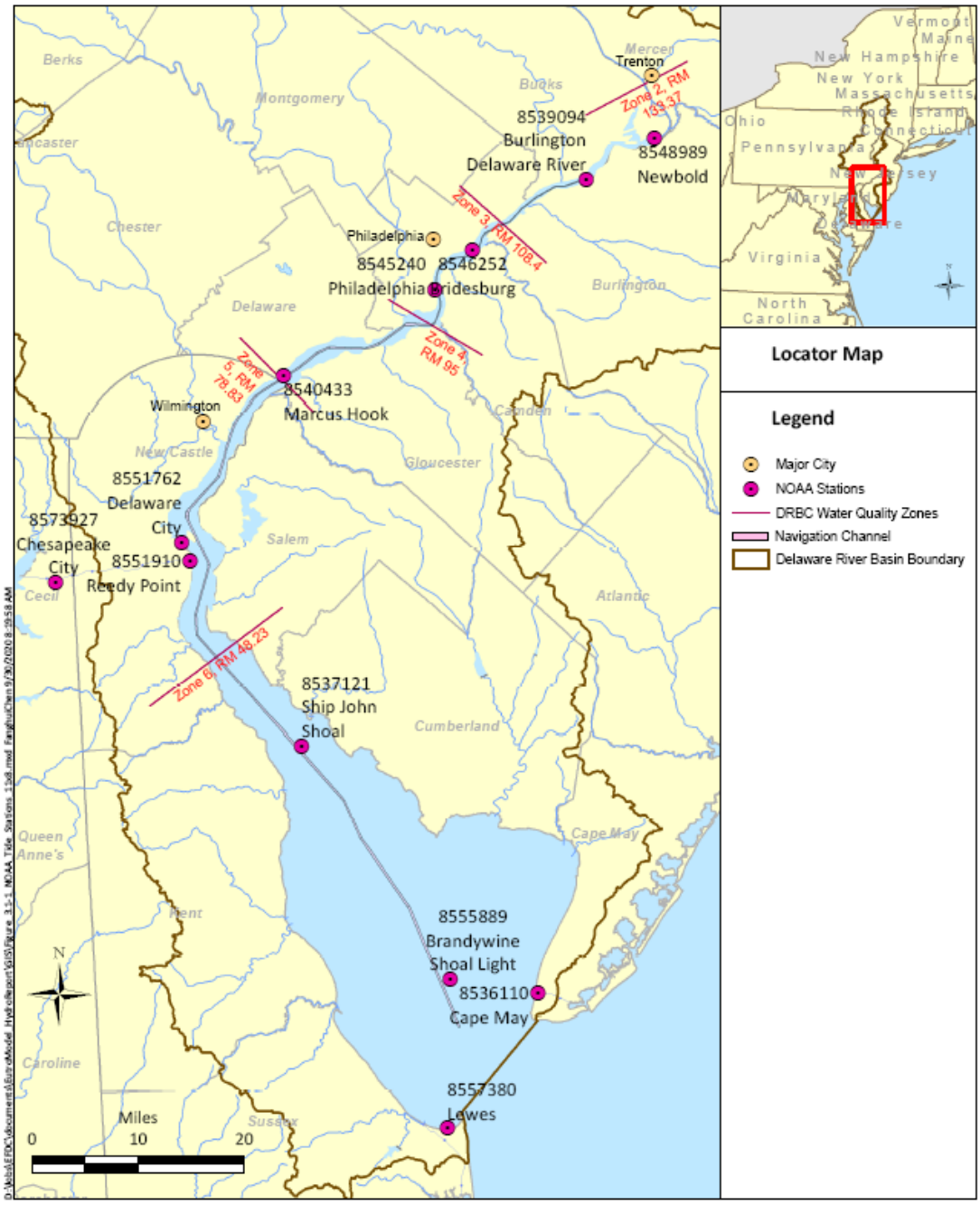

Figure 4.1-1 NOAA Tide Stations in Delaware Estuary

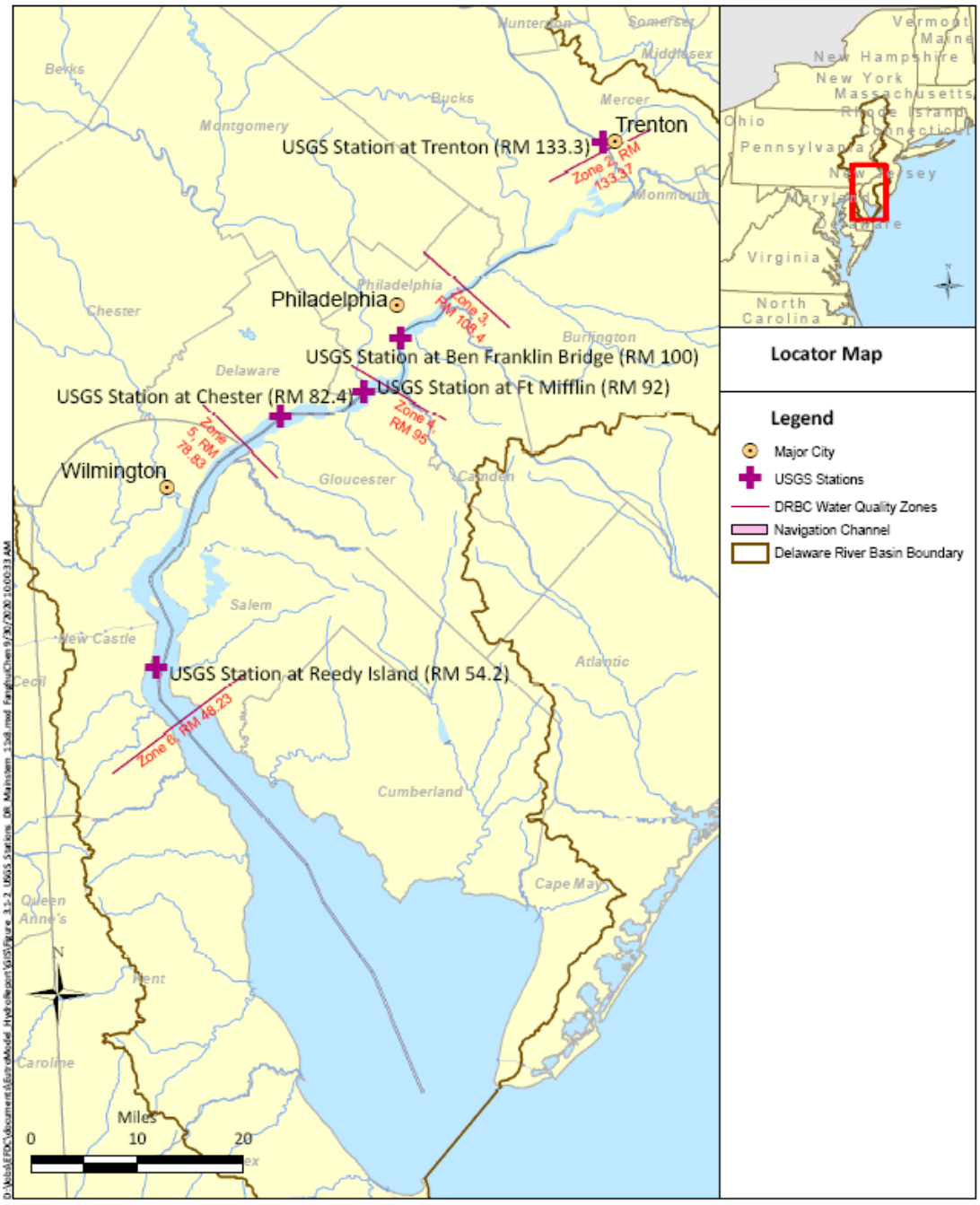

Figure 4.1-2 USGS Water Quality Monitoring Stations on Delaware River Mainstem

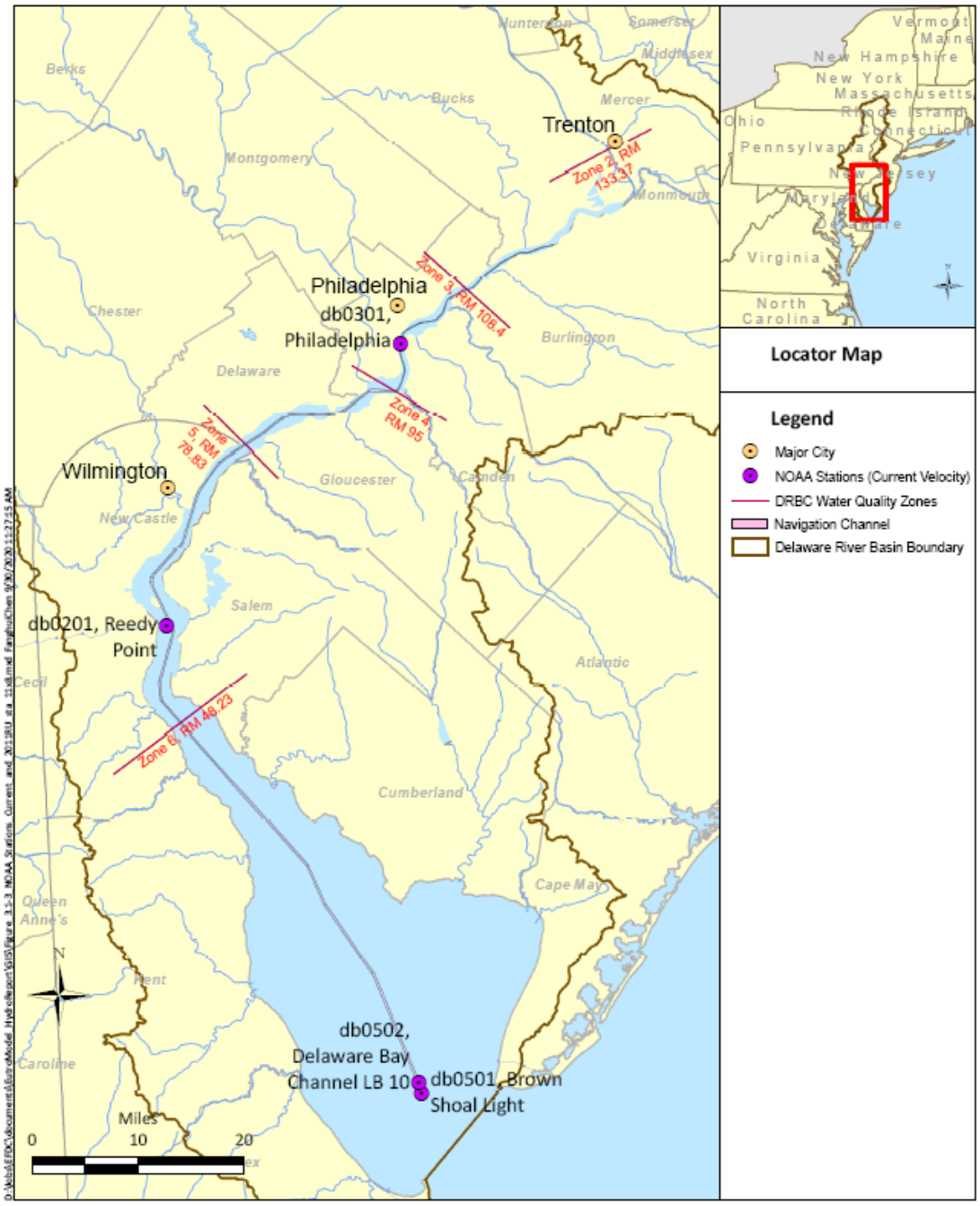

Figure 4.1-3 NOAA Stations that Collect Current Velocity Data in Delaware Estuary

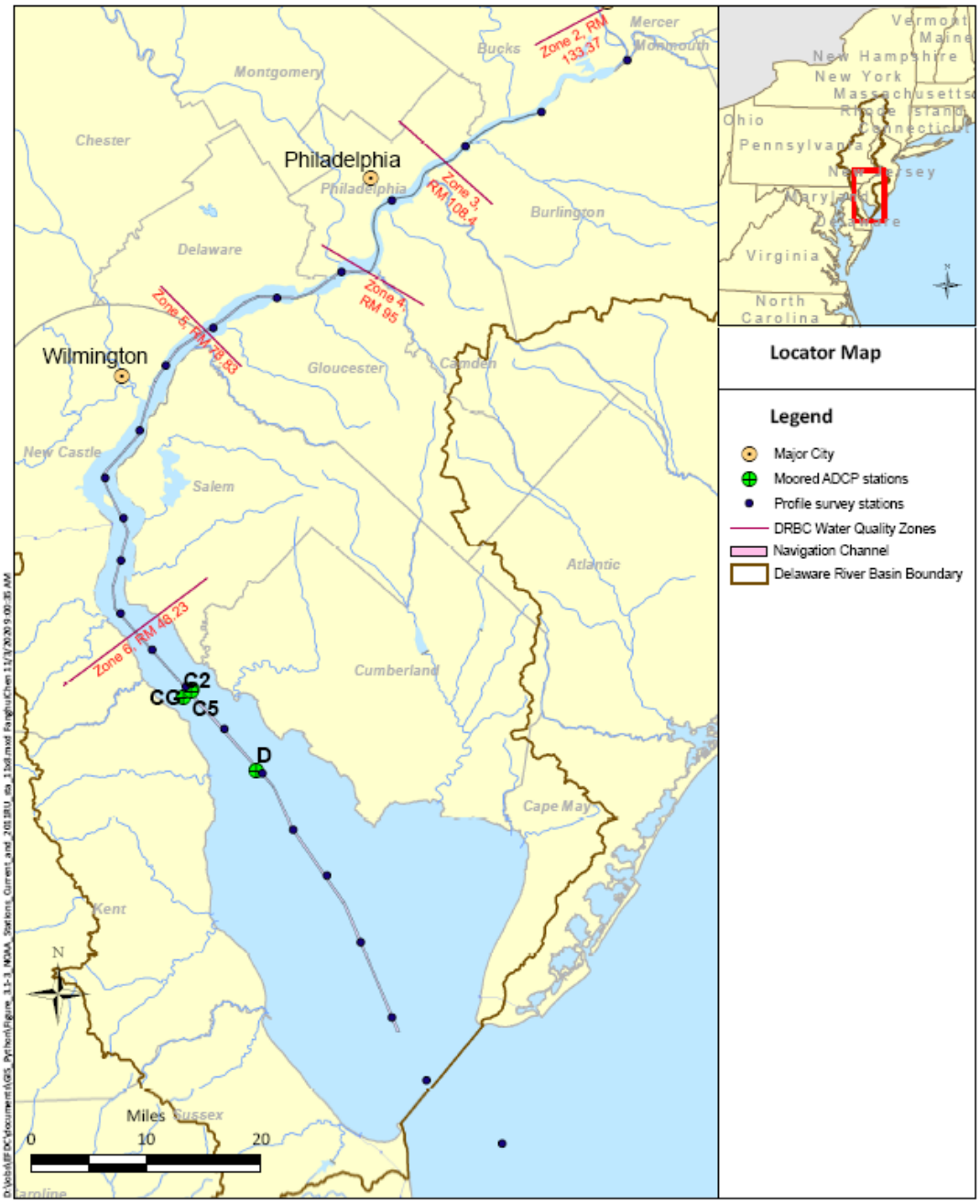

Figure 4.1-4 Rutgers University 2011 Survey Stations

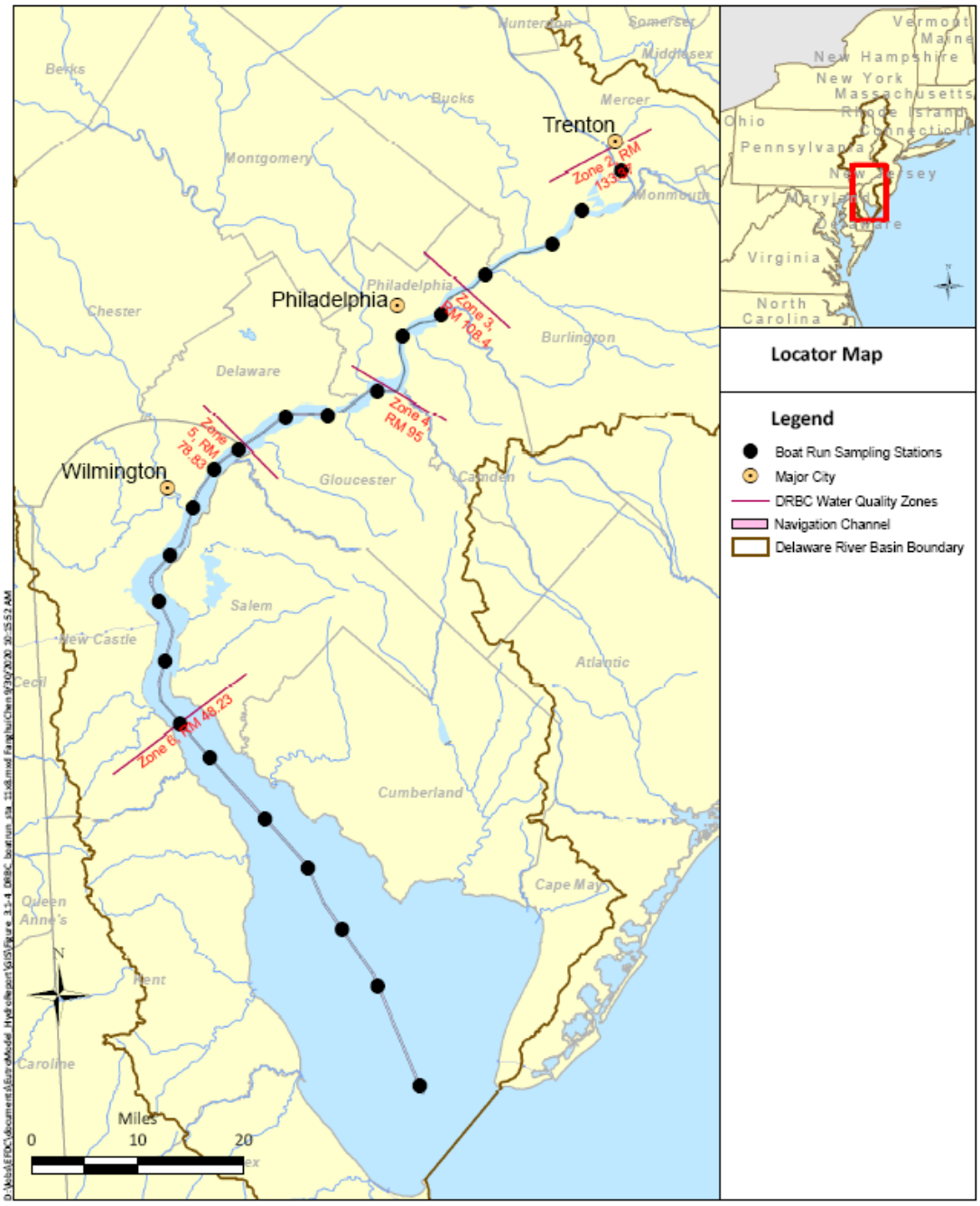

Figure 4.1-5 DRBC Boat Run Water Quality Sampling Locations in Delaware Estuary

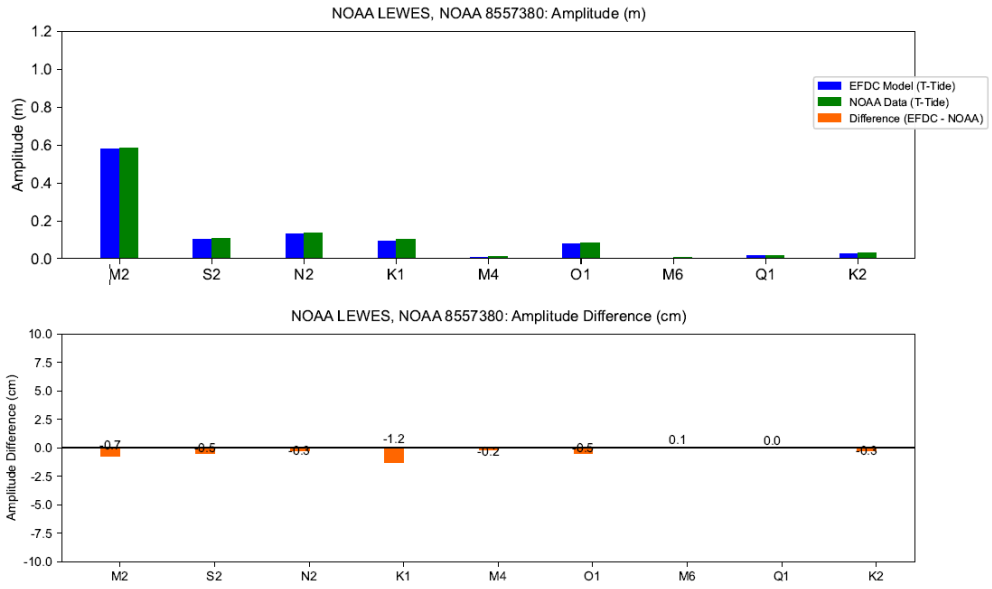

Figure 4.3-1 (1) Predicted and Observed Amplitude of Nine Tidal Harmonic Constituents based on Predicted Water Surface Elevation at NOAA Station 8557380, Lewes

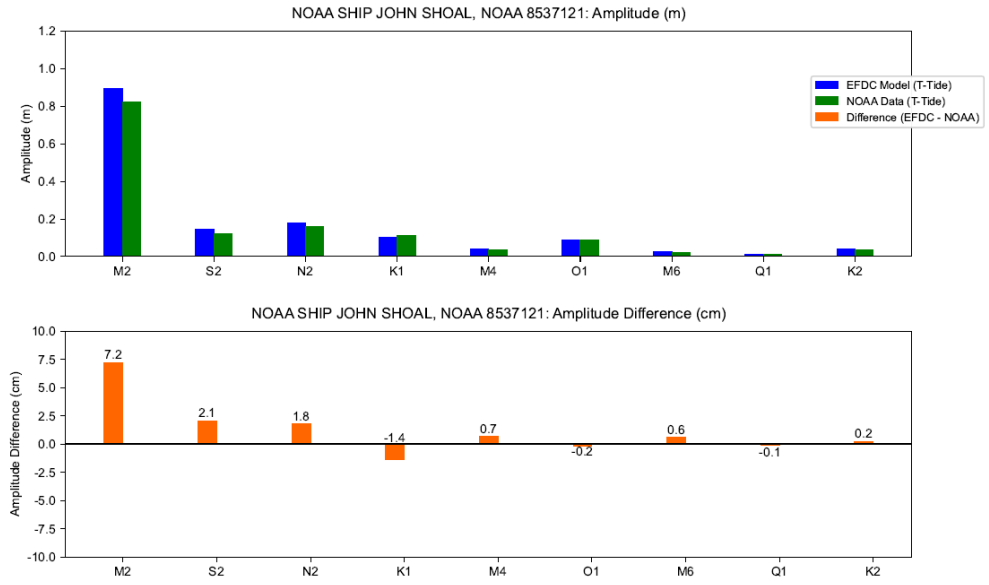

Figure 4.3-1 (2) Predicted and Observed Amplitude of Nine Tidal Harmonic Constituents based on Predicted Water Surface Elevation at NOAA Station 8537121, Ship John Shoal

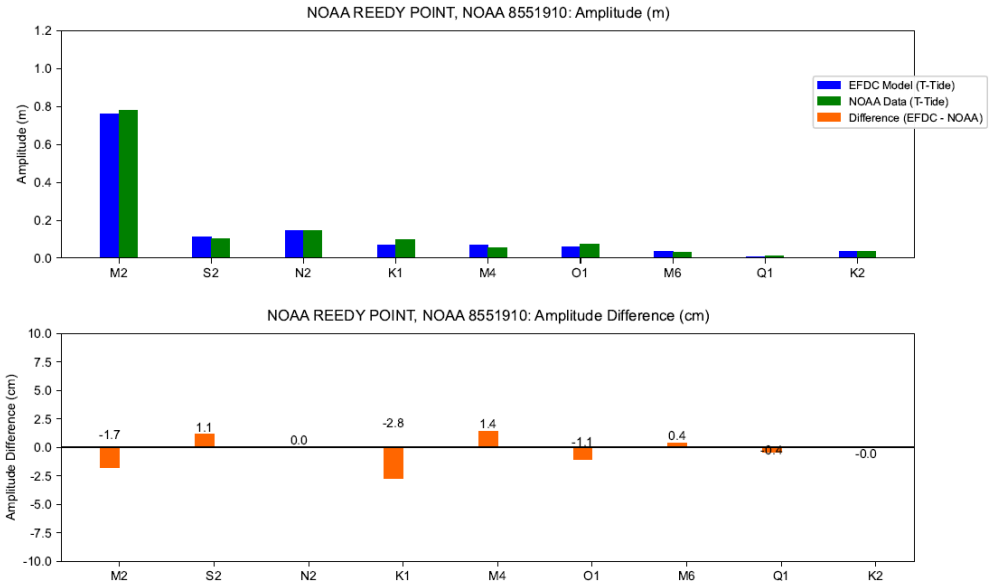

Figure 4.3-1 (3) Predicted and Observed Amplitude of Nine Tidal Harmonic Constituents based on Predicted Water Surface Elevation at NOAA Station 8551910, Reedy Point

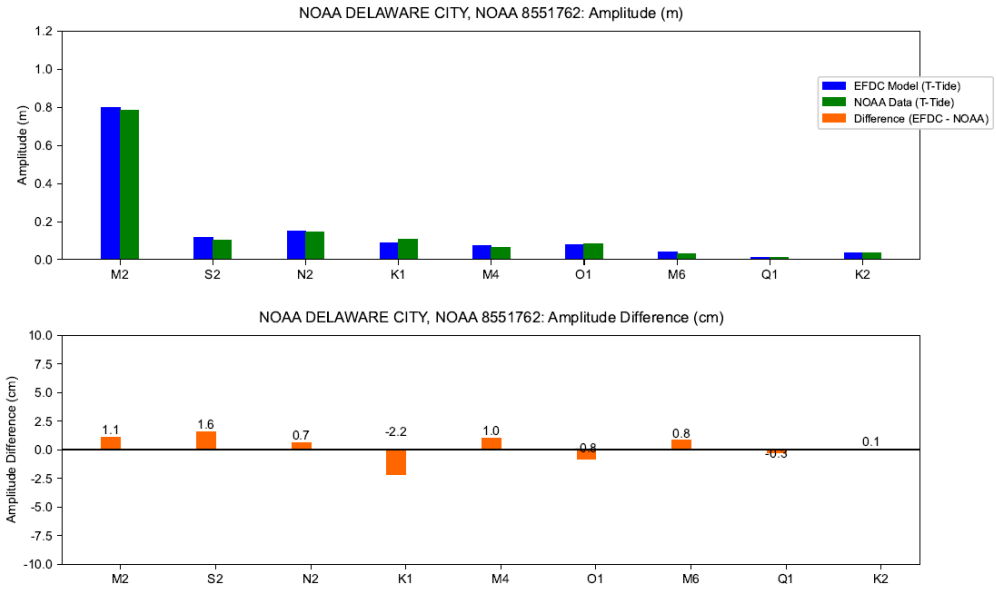

Figure 4.3-1 (4) Predicted and Observed Amplitude of Nine Tidal Harmonic Constituents based on Predicted Water Surface Elevation at NOAA Station 8551762, Delaware City

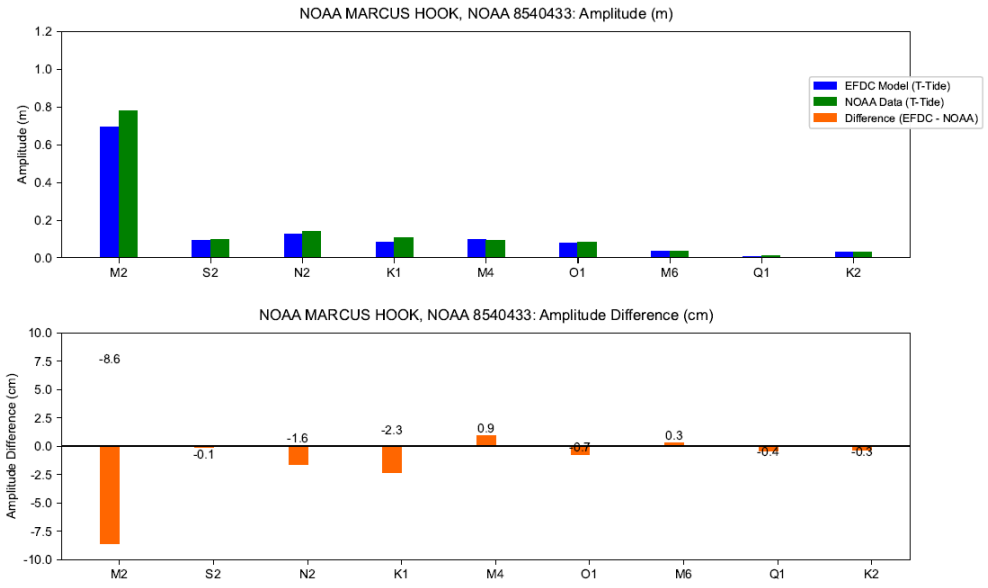

Figure 4.3-1 (5) Predicted and Observed Amplitude of Nine Tidal Harmonic Constituents based on Predicted Water Surface Elevation at NOAA Station 8540433, Marcus Hook

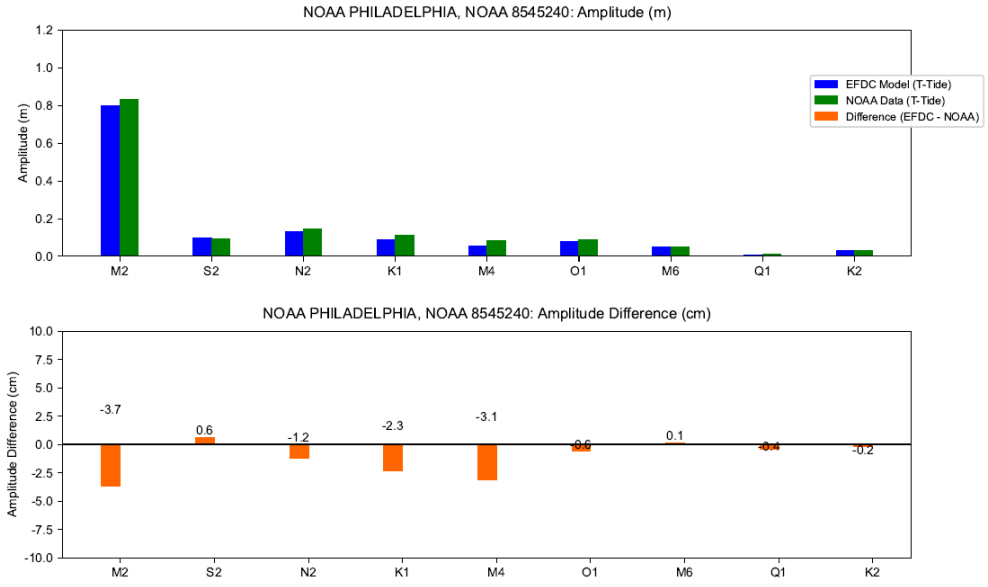

Figure 4.3-1 (6) Predicted and Observed Amplitude of Nine Tidal Harmonic Constituents based on Predicted Water Surface Elevation at NOAA Station 8545240, Philadelphia

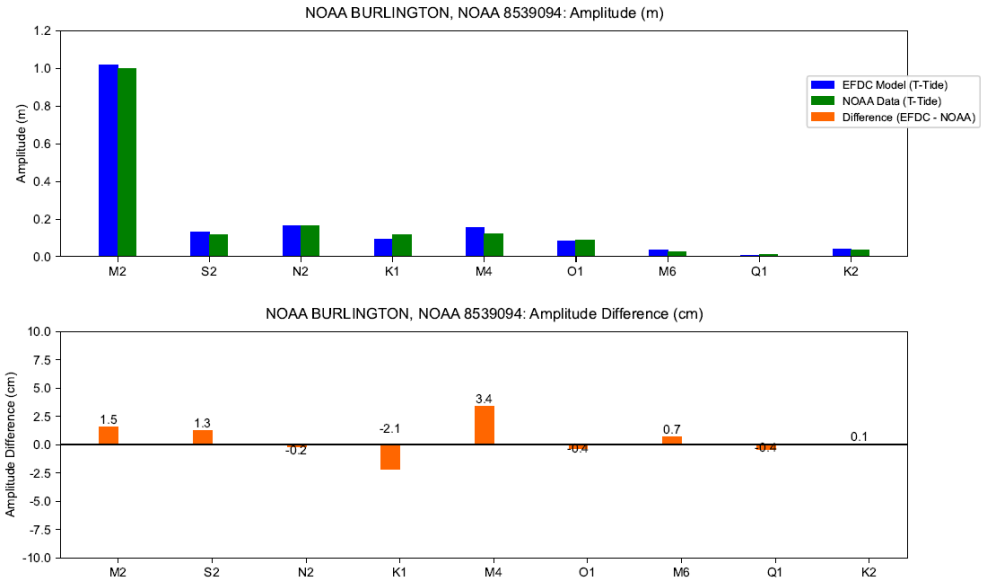

Figure 4.3-1 (7) Predicted and Observed Amplitude of Nine Tidal Harmonic Constituents based on Predicted Water Surface Elevation at NOAA Station 8539094, Burlington

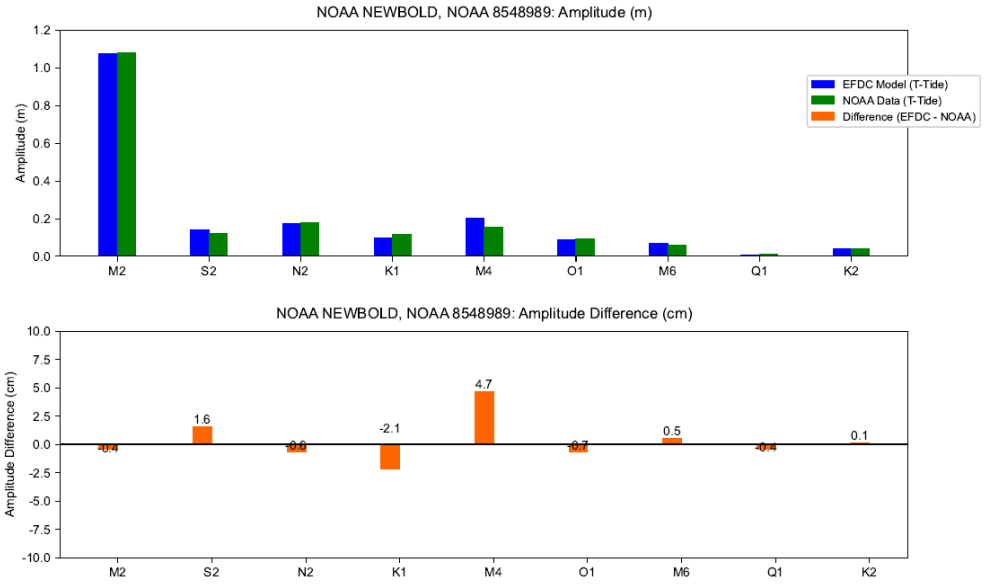

Figure 4.3-1 (8) Predicted and Observed Amplitude of Nine Tidal Harmonic Constituents based on Predicted Water Surface Elevation at NOAA Station 8548989, Newbold

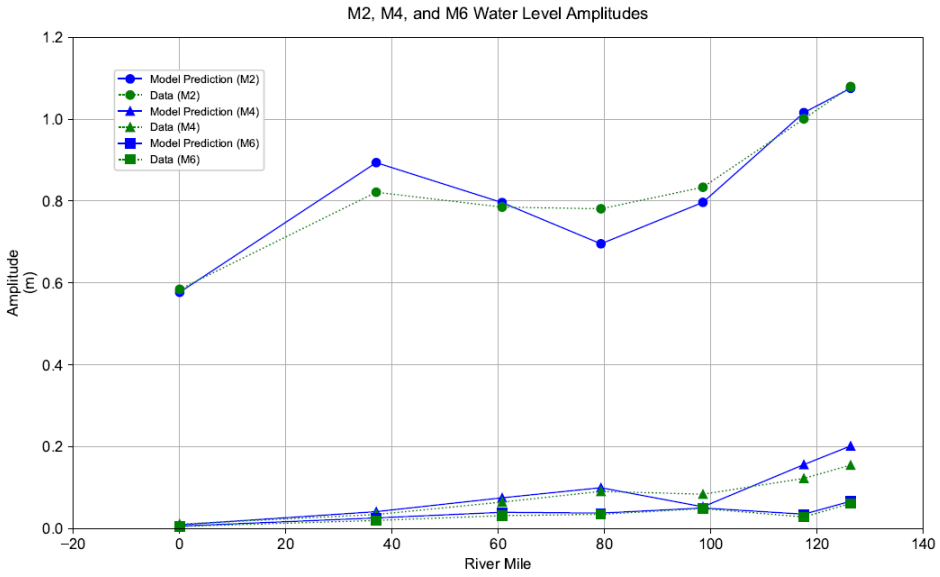

Model results from 2019 simulations were used for tidal harmonic analysis.

Figure 4.3-2 Observed and Predicted Distribution of M2, M4, and M6 Water Level Amplitudes

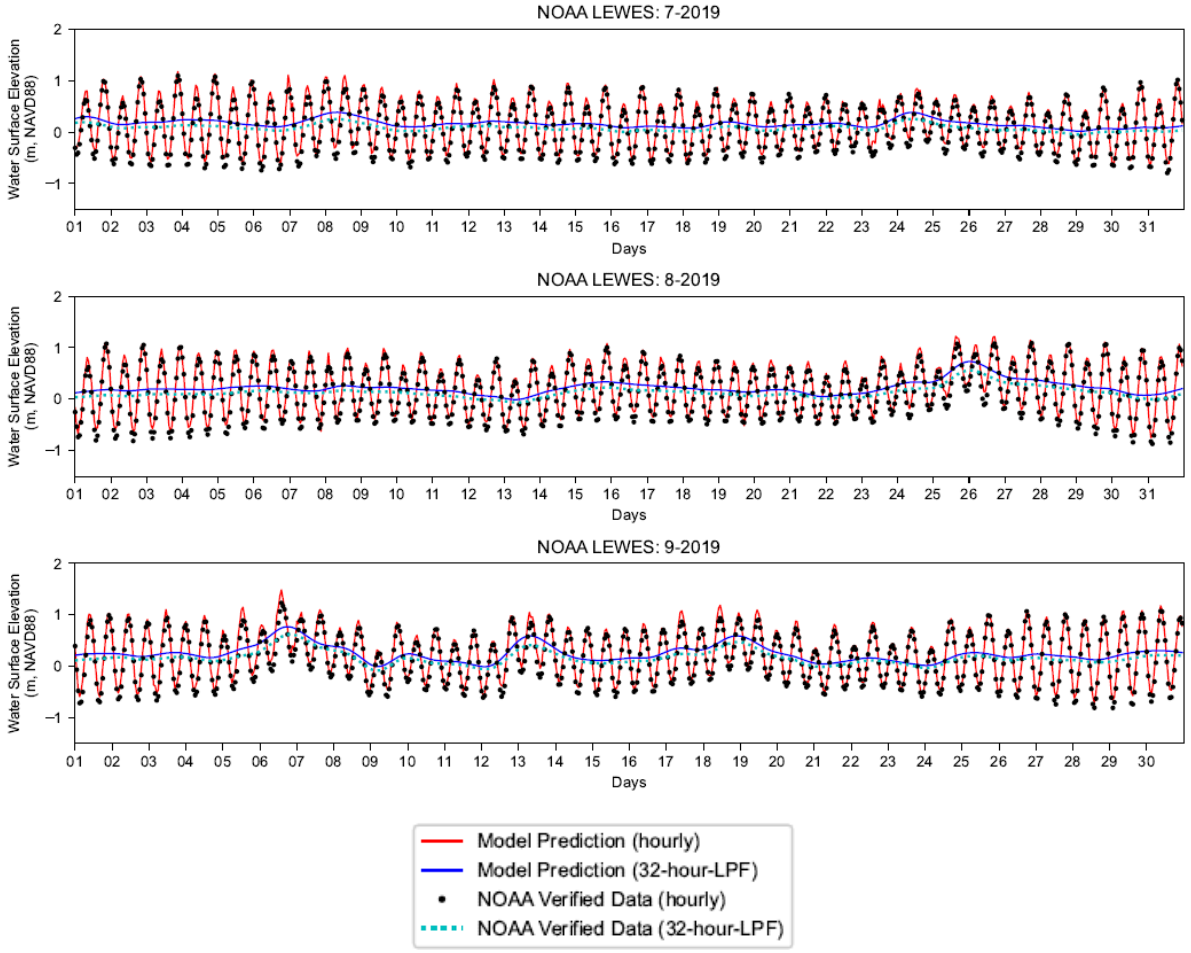

Figure 4.3-3 (1) Observed and Predicted Water Surface Elevation at NOAA Station 8557380, Lewes

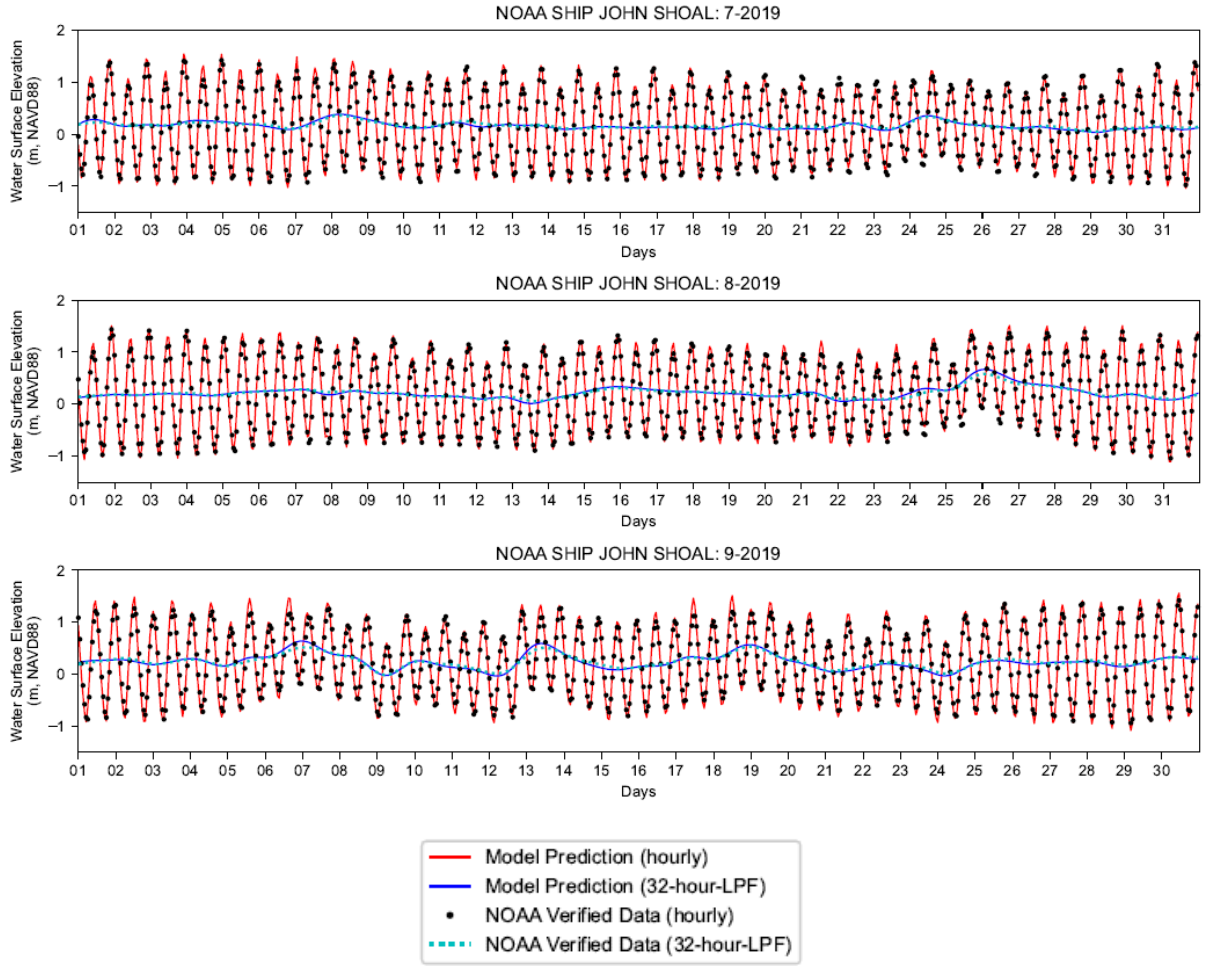

Figure 4.3-3 (2) Observed and Predicted Water Surface Elevation at NOAA Station 8537121, Ship John Shoal

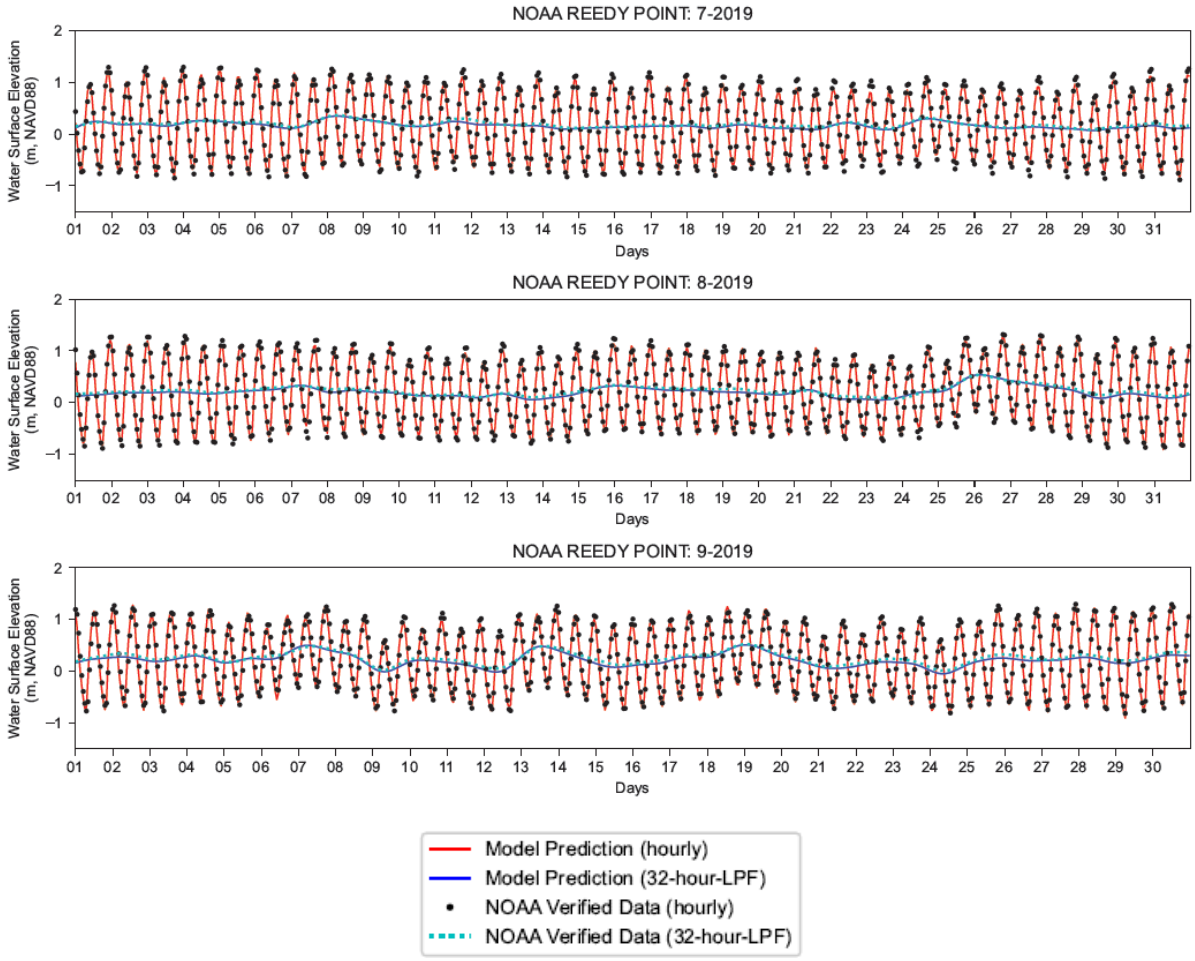

Figure 4.3-3 (3) Observed and Predicted Water Surface Elevation at NOAA Station 8551910, Reedy Point

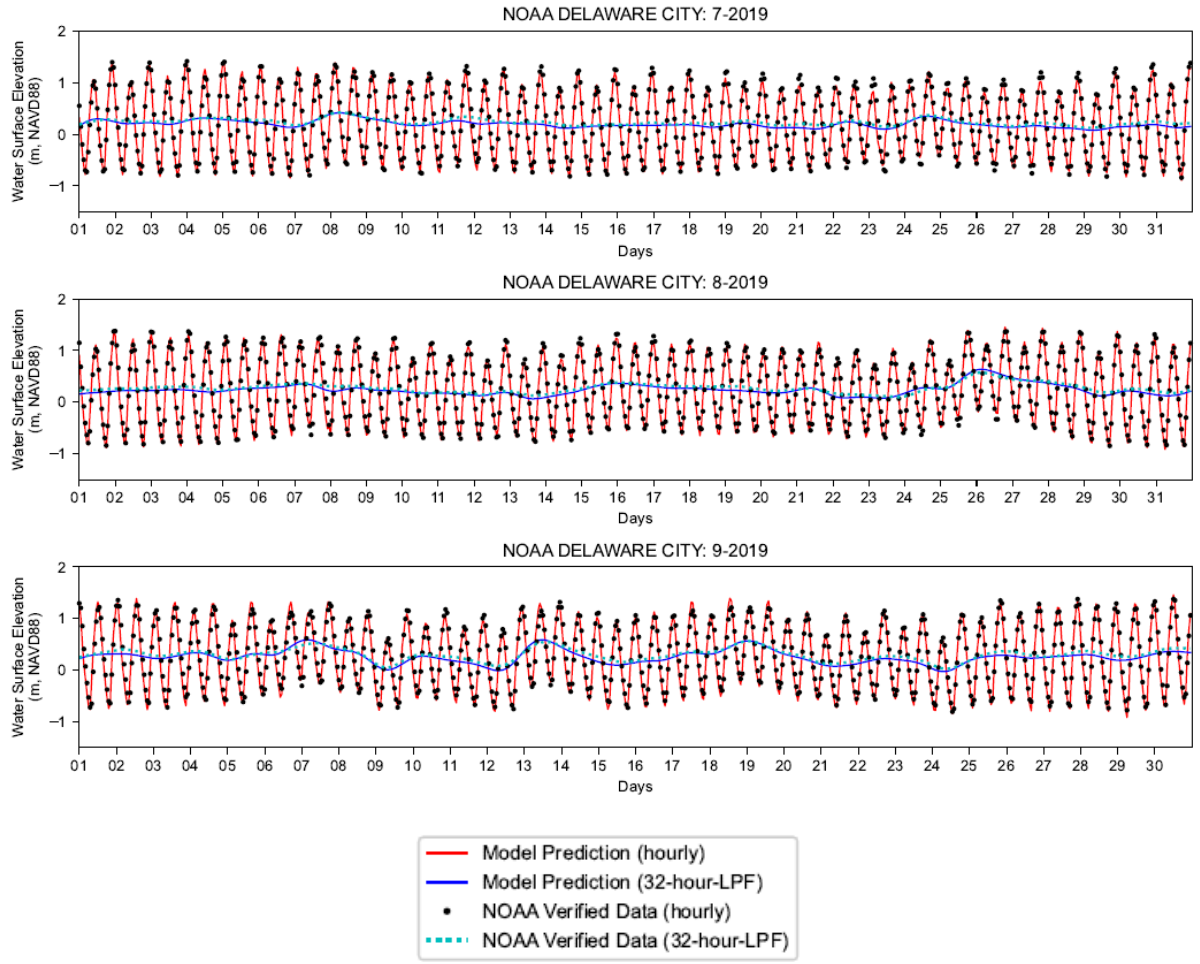

Figure 4.3-3 (4) Observed and Predicted Water Surface Elevation at NOAA Station 8551762, Delaware City

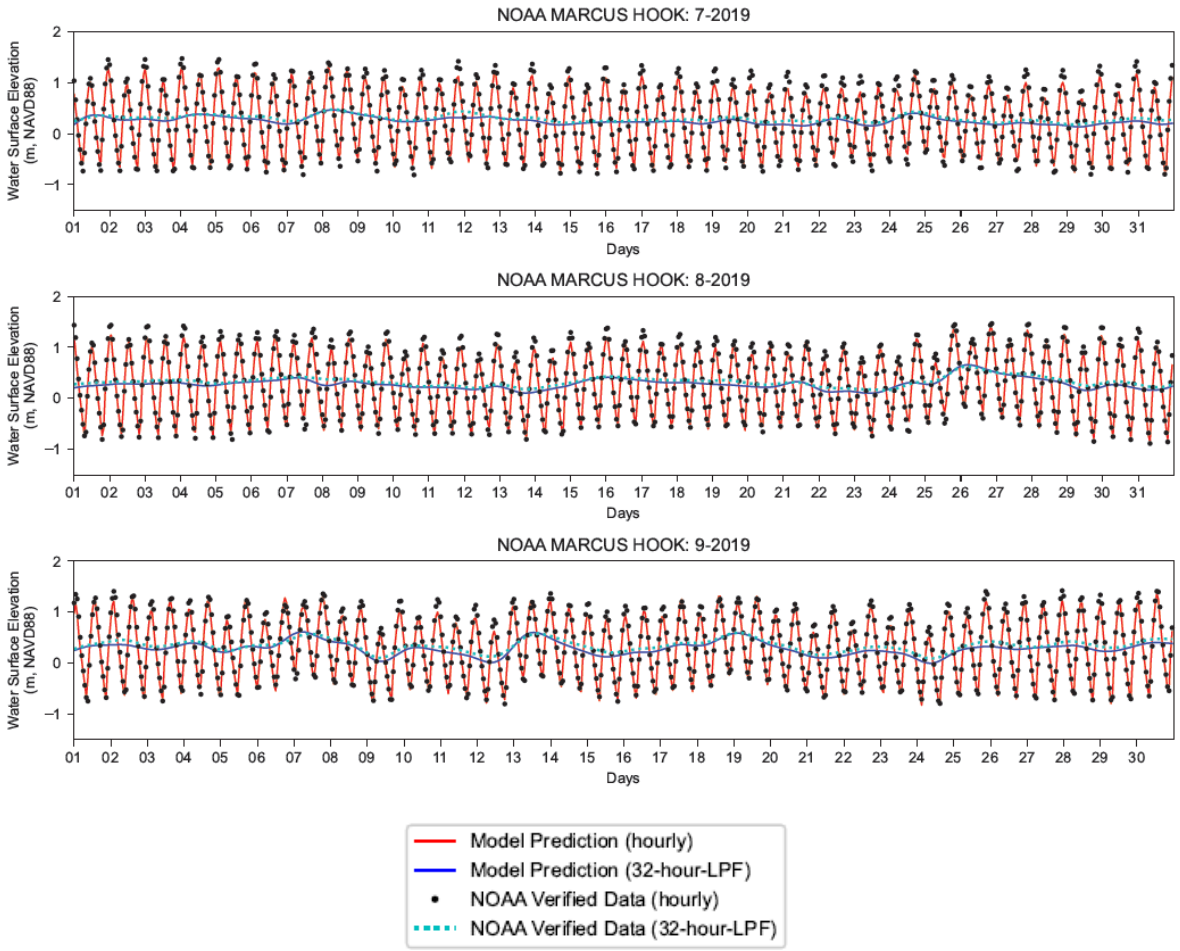

Figure 4.3-3 (5) Observed and Predicted Water Surface Elevation at NOAA Station 8540433, Marcus Hook

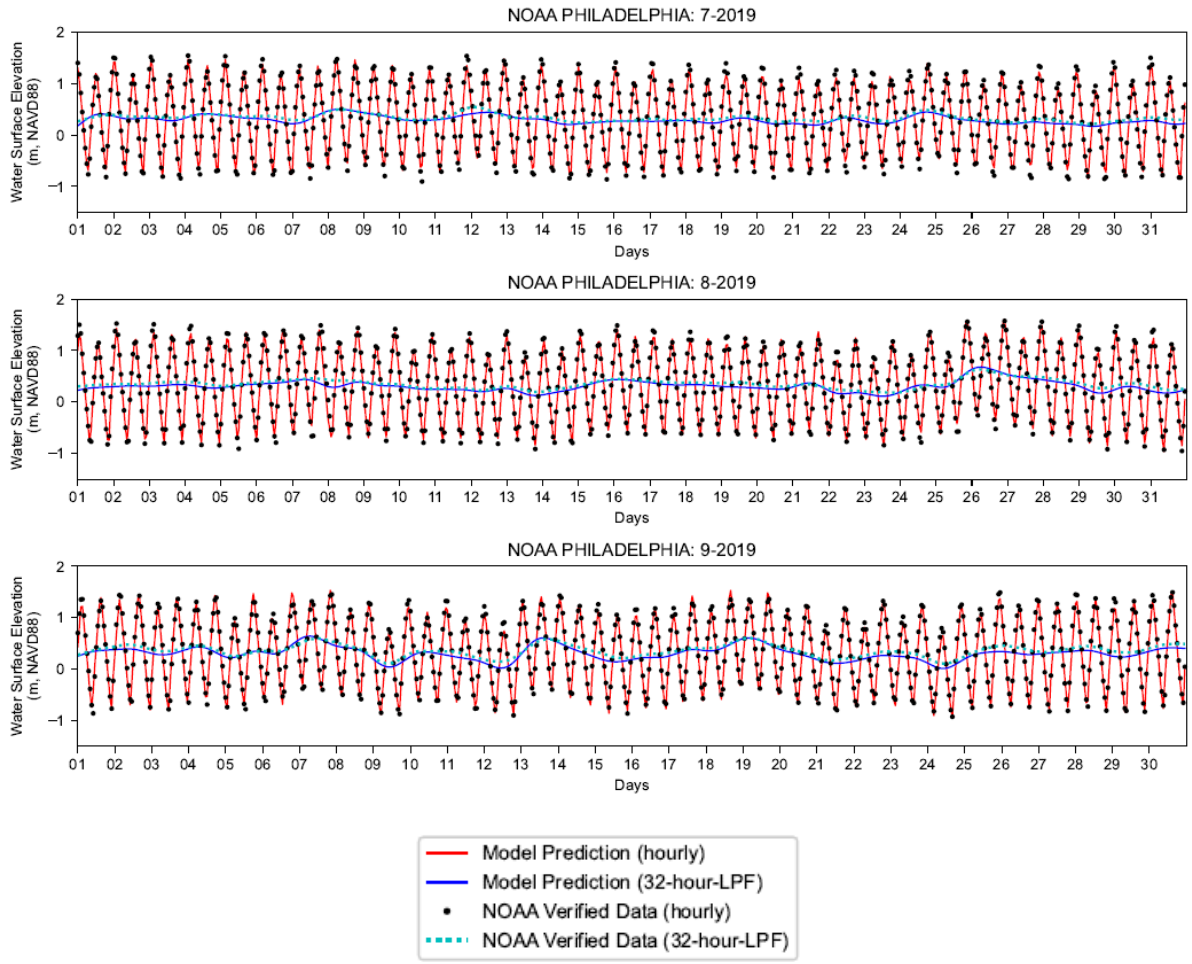

Figure 4.3-3 (6) Observed and Predicted Water Surface Elevation at NOAA Station 8545240, Philadelphia

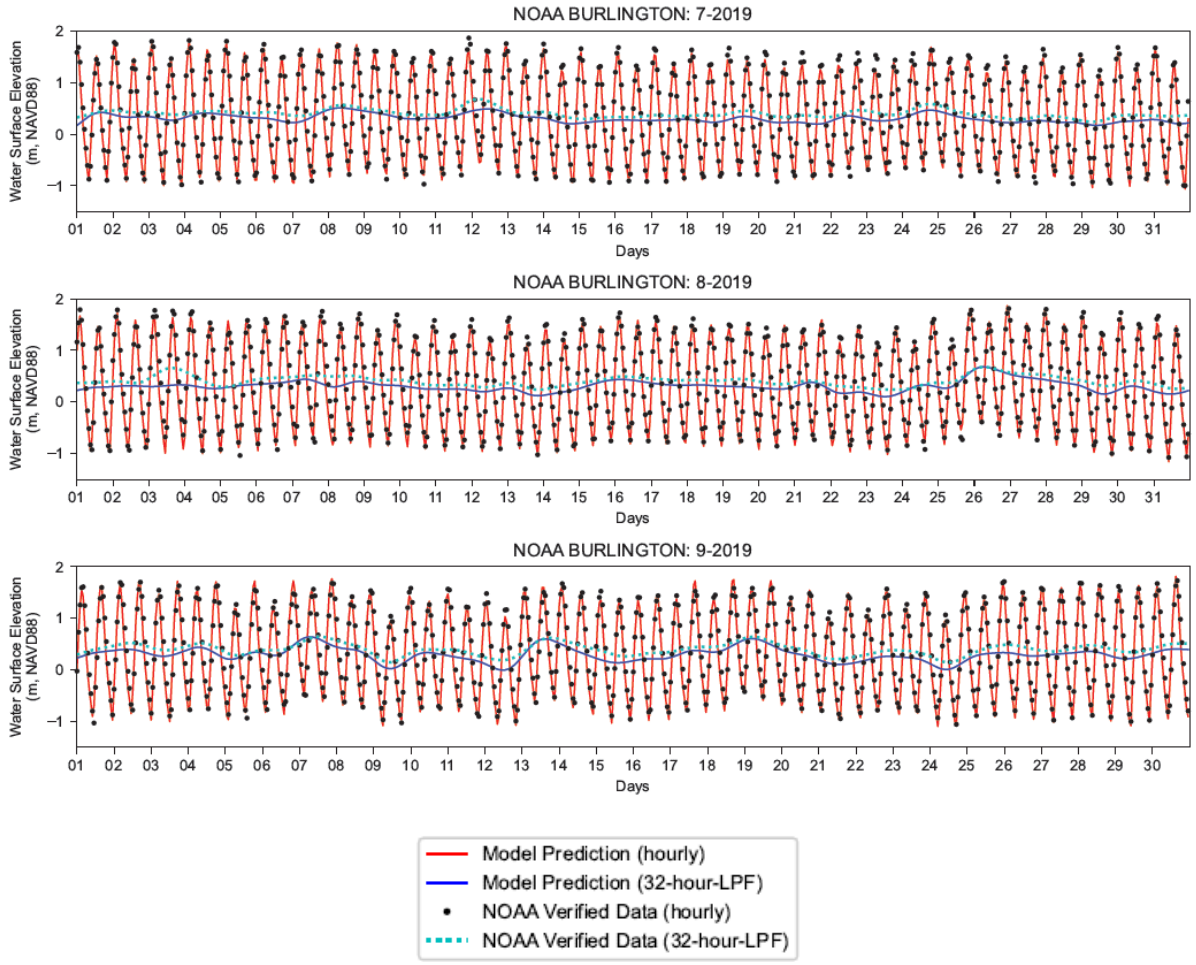

Figure 4.3-3 (7) Observed and Predicted Water Surface Elevation at NOAA Station 8539094, Burlington

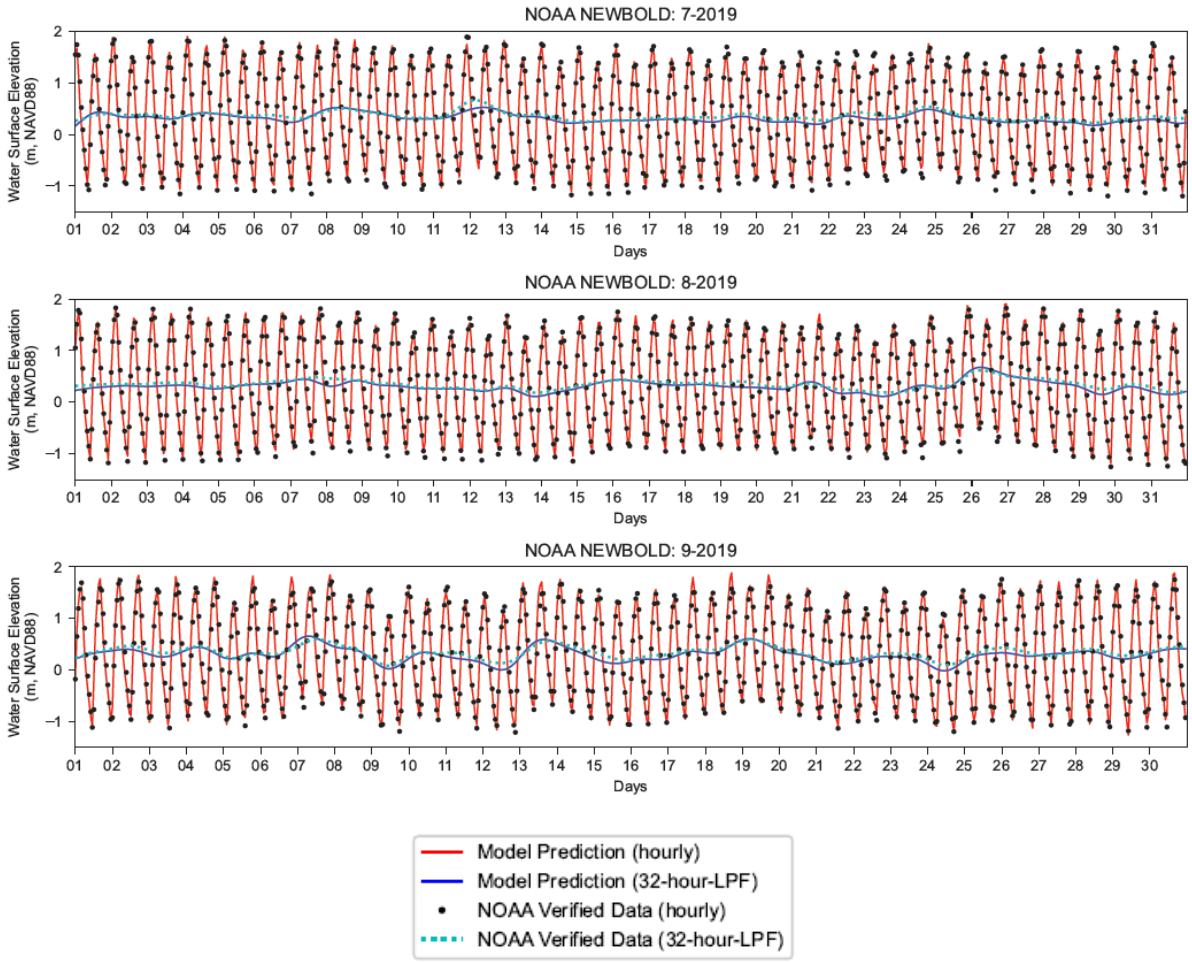

Figure 4.3-3 (8) Observed and Predicted Water Surface Elevation at NOAA Station 8548989, Newbold

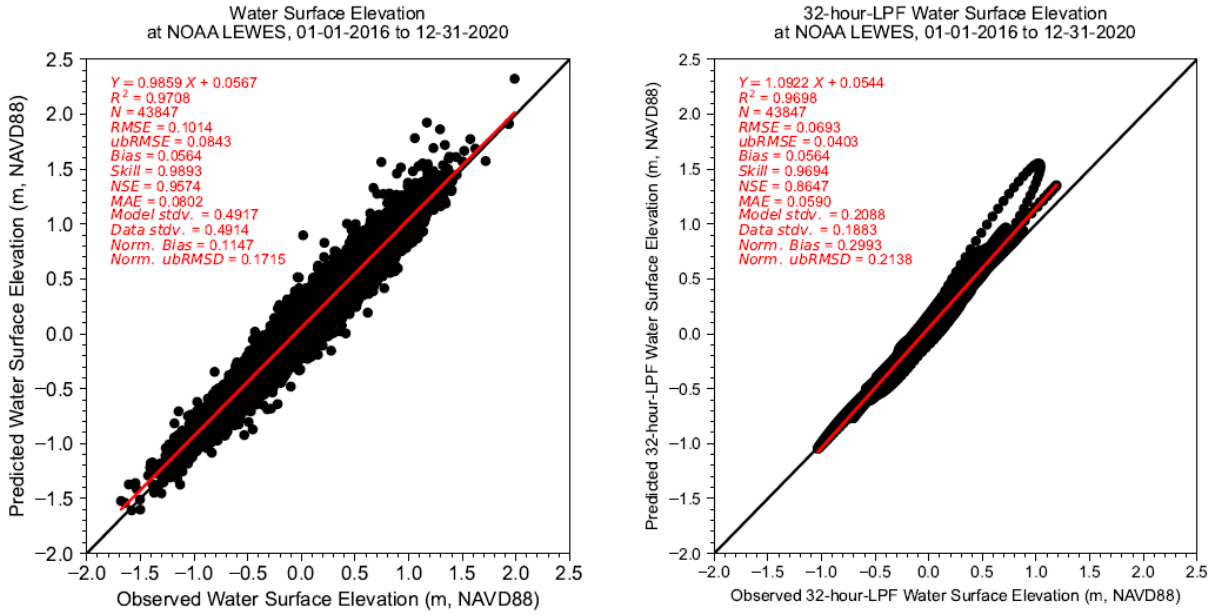

Figure 4.3-4 (1) Model-to-Data Comparison of Water Surface Elevation at NOAA Station 8557380, Lewes

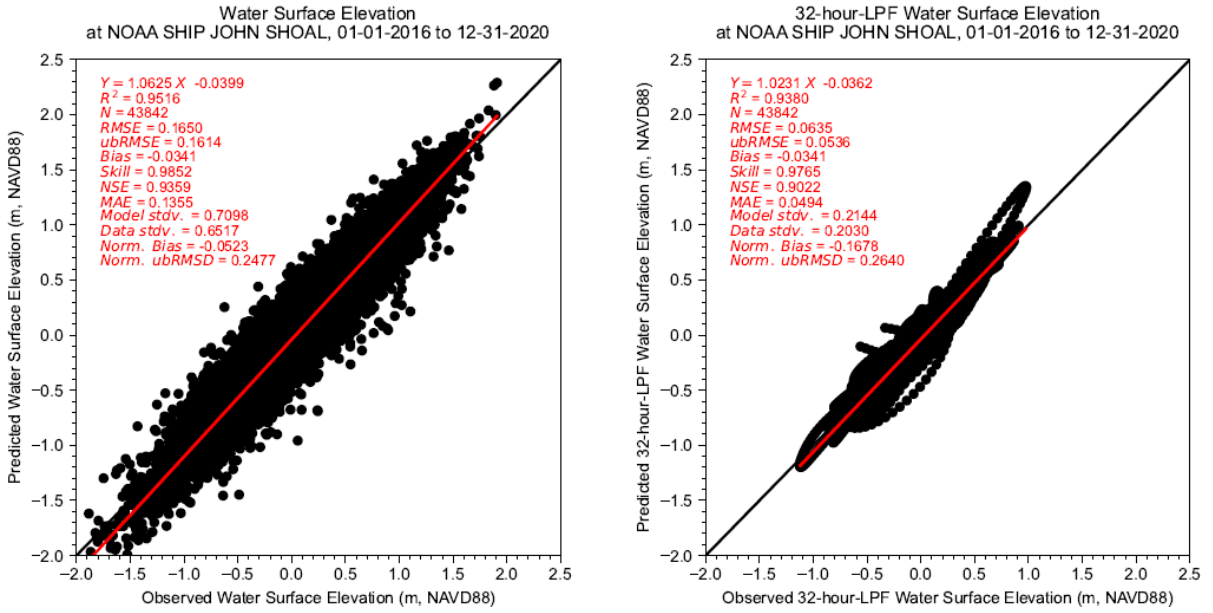

Figure 4.3-4 (2) Model-to-Data Comparison of Water Surface Elevation at NOAA Station 8537121, Ship John Shoal

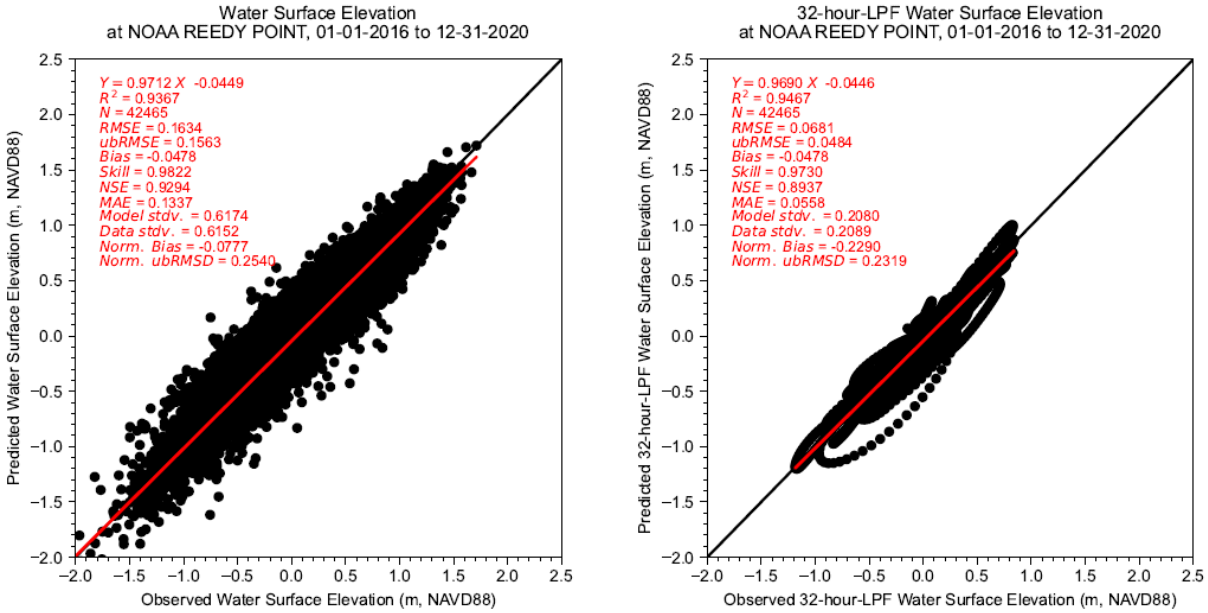

Figure 4.3-4 (3) Model-to-Data Comparison of Water Surface Elevation at NOAA Station 8551910, Reedy Point

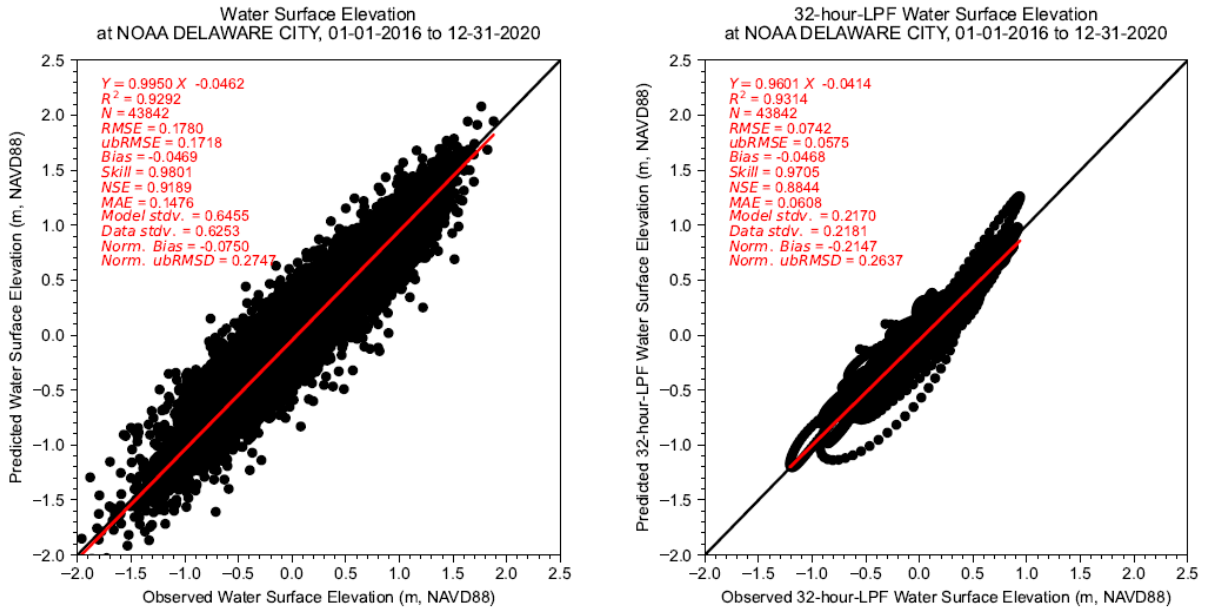

Figure 4.3-4 (4) Model-to-Data Comparison of Water Surface Elevation at NOAA Station 8551762, Delaware City

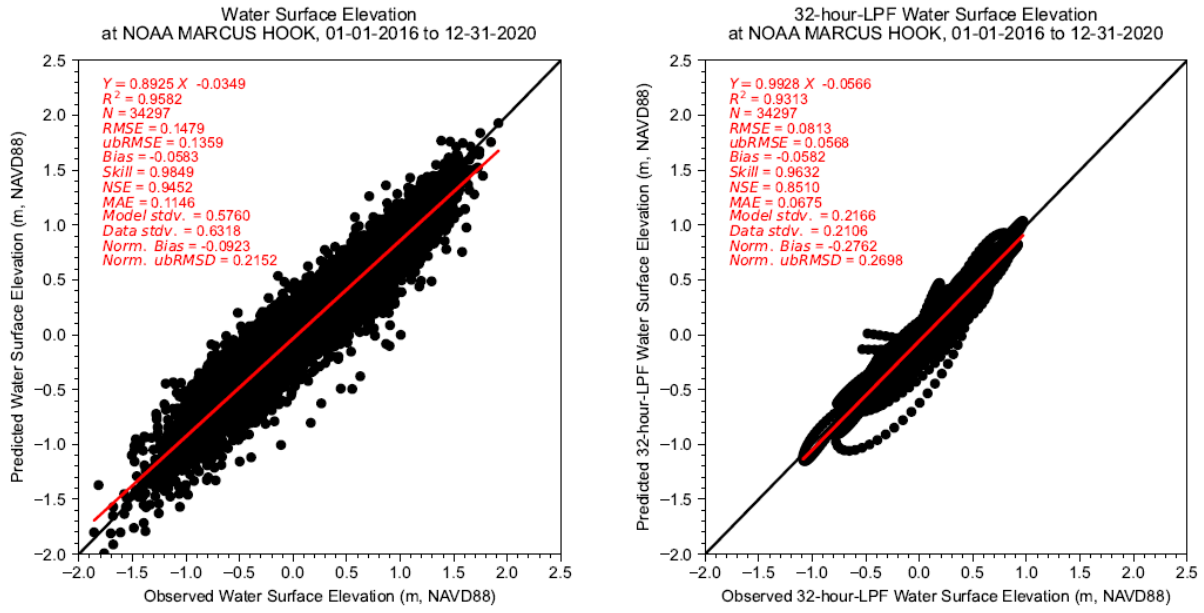

Figure 4.3-4 (5) Model-to-Data Comparison of Water Surface Elevation at NOAA Station 8540433, Marcus Hook

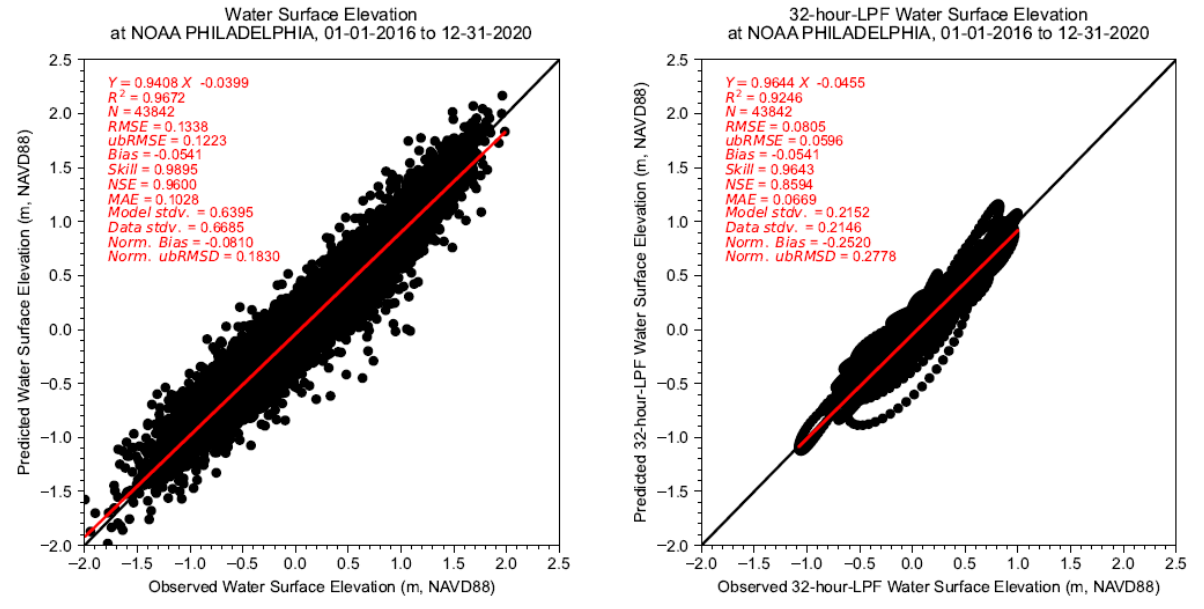

Figure 4.3-4 (6) Model-to-Data Comparison of Water Surface Elevation at NOAA Station 8545240, Philadelphia

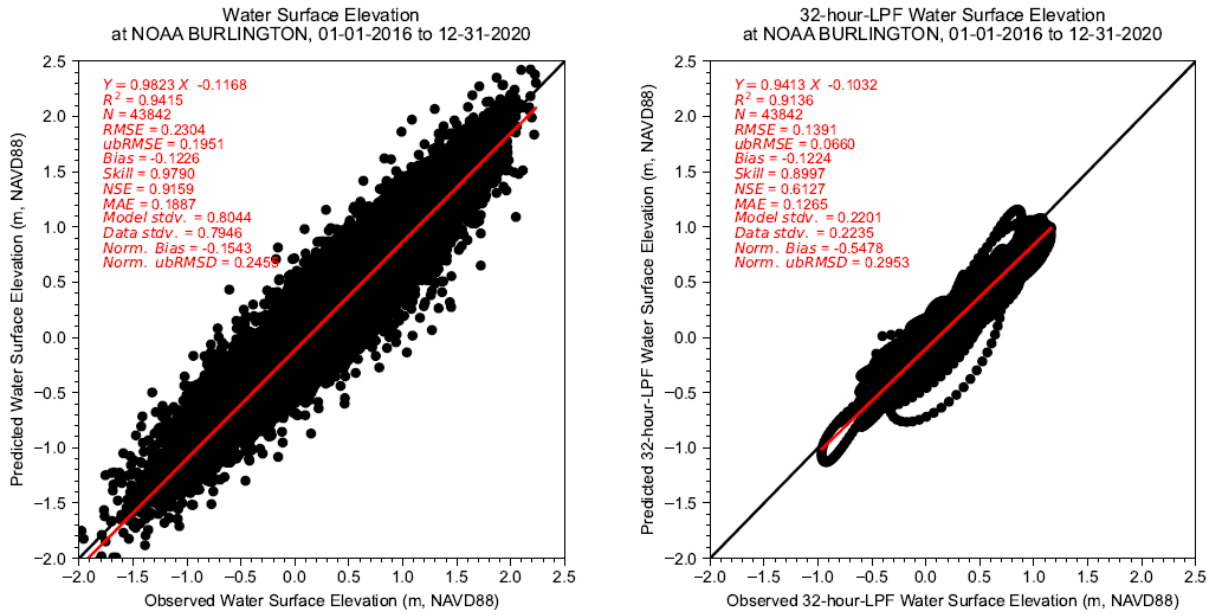

Figure 4.3-4 (7) Model-to-Data Comparison of Water Surface Elevation at NOAA Station 8539094, Burlington

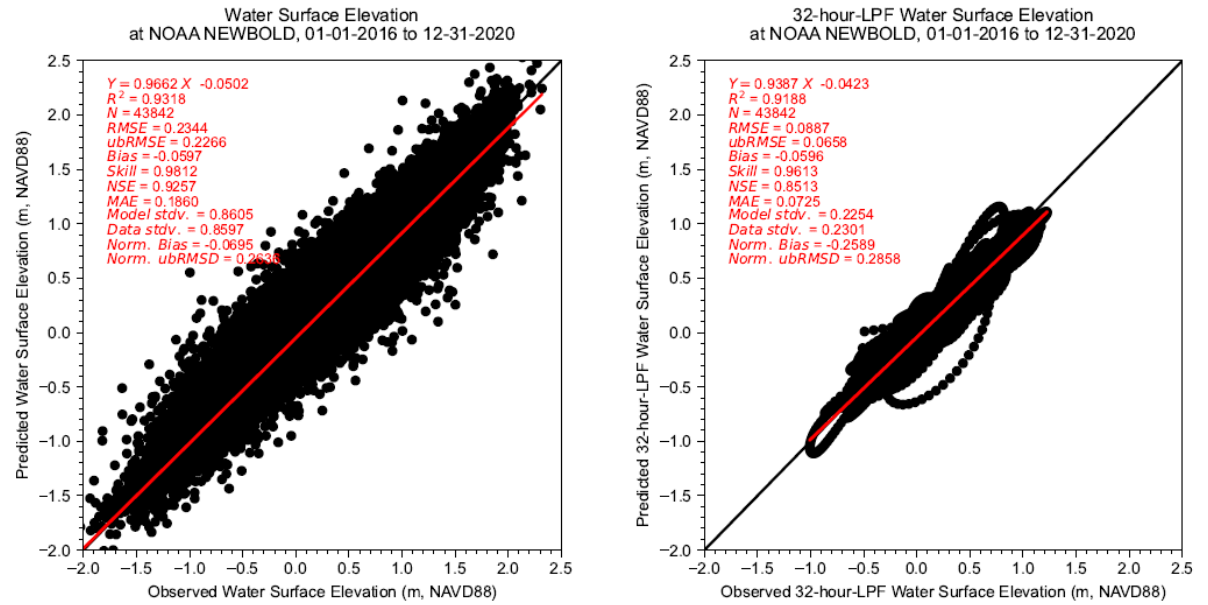

Figure 4.3-4 (8) Model-to-Data Comparison of Water Surface Elevation at NOAA Station 8548989, Newbold

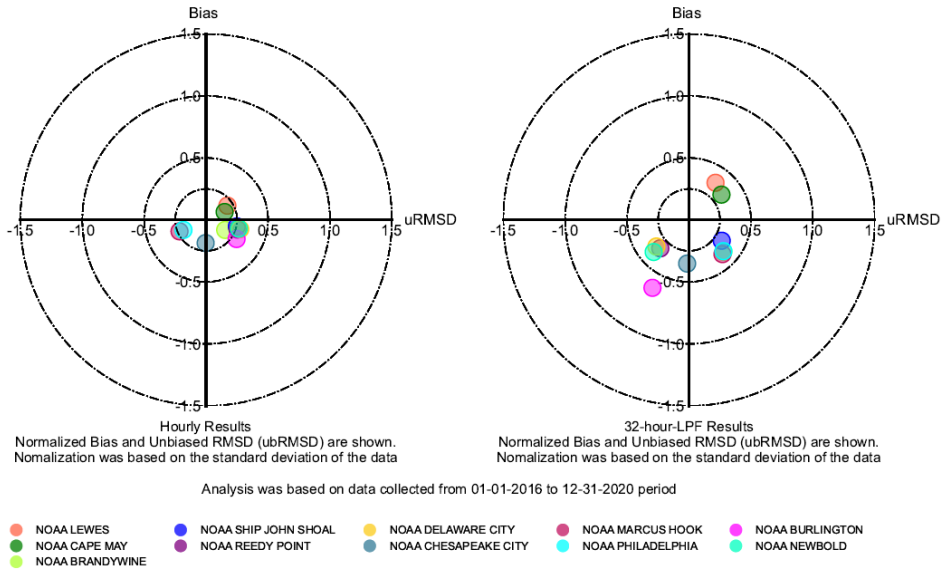

Figure 4.3-5 Target Diagram for the Observed and Predicted Hourly and 32-hour-LPF Water Surface Elevation for 2016 to 2020 Period

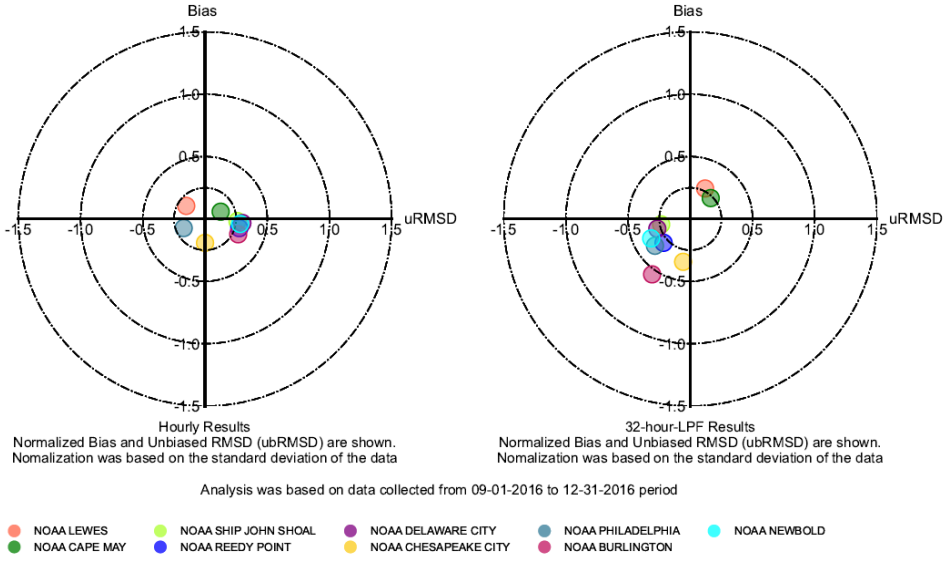

Figure 4.3-6 Target Diagram for the Observed and Predicted Hourly and 32-hour-LPF Water Surface Elevation for September through December 2016 Period

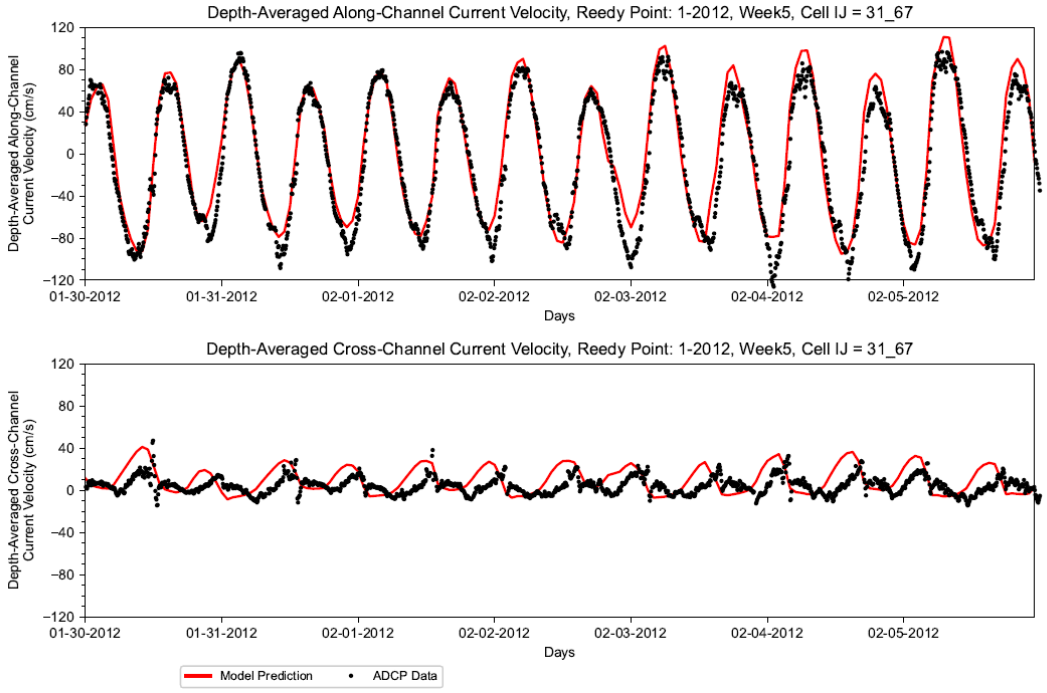

Figure 4.3-7 Observed and Predicted Depth-Averaged Along and Cross-Channel Current Velocity at Reedy Point, NOAA Station DB0201

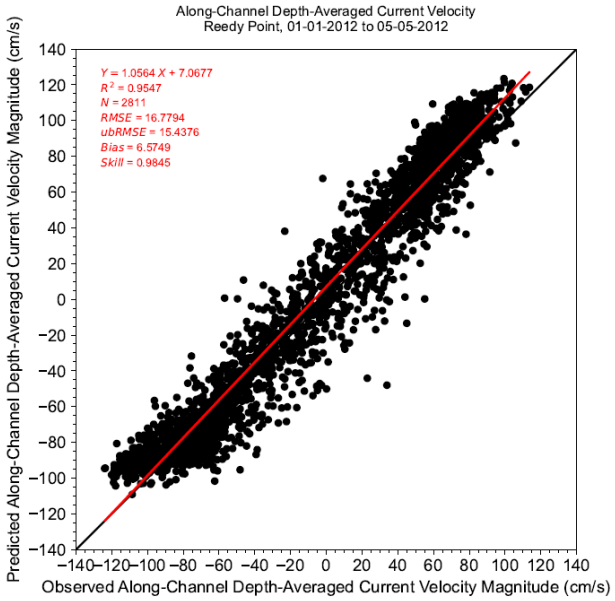

Figure 4.3-8 Comparison of Observed and Predicted Along-Channel Depth-Averaged Current Velocity Magnitude at Reedy Point during 01-01-2012 to 05-05-2012 period.

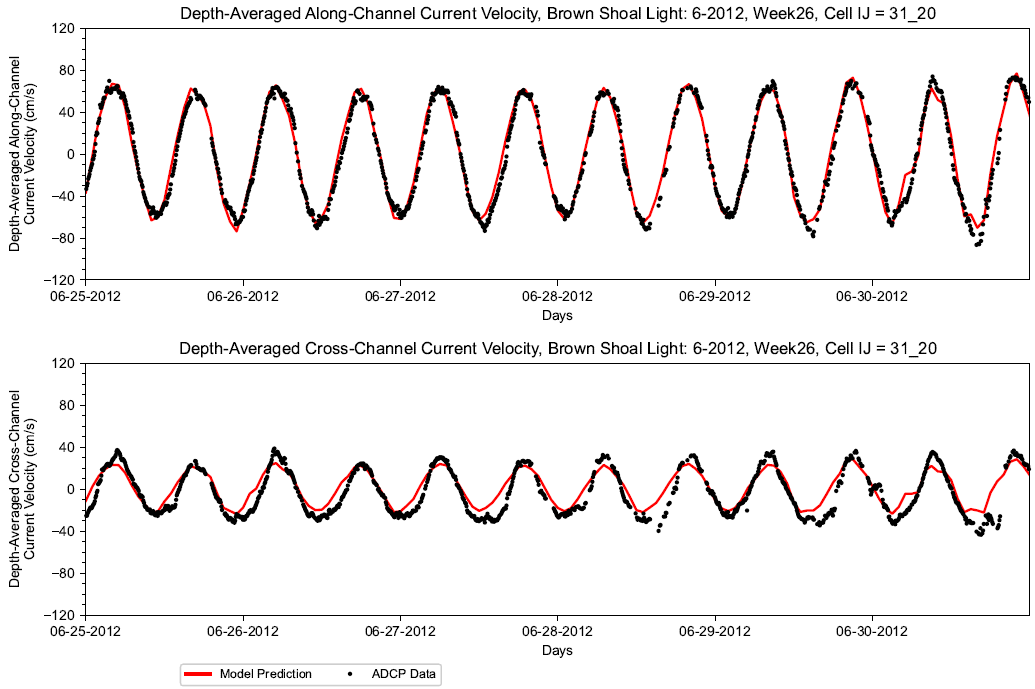

Figure 4.3-9 Observed and Predicted Depth-Averaged Along and Cross-Channel Current Velocity at Brown Shoal Light, NOAA Station db0501

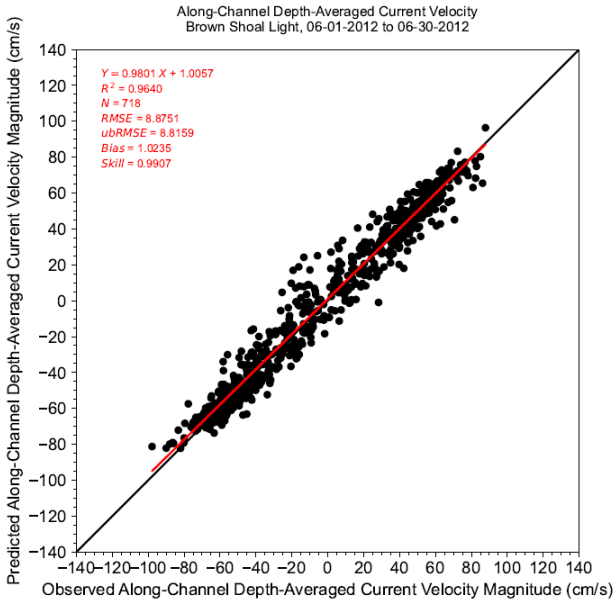

Figure 4.3-10 Comparison of Observed and Predicted Along-Channel Depth-Averaged Current Velocity Magnitude at Brown Shoal Light during 06-01-2012 to 06-30-2012 period, NOAA Station db0501.

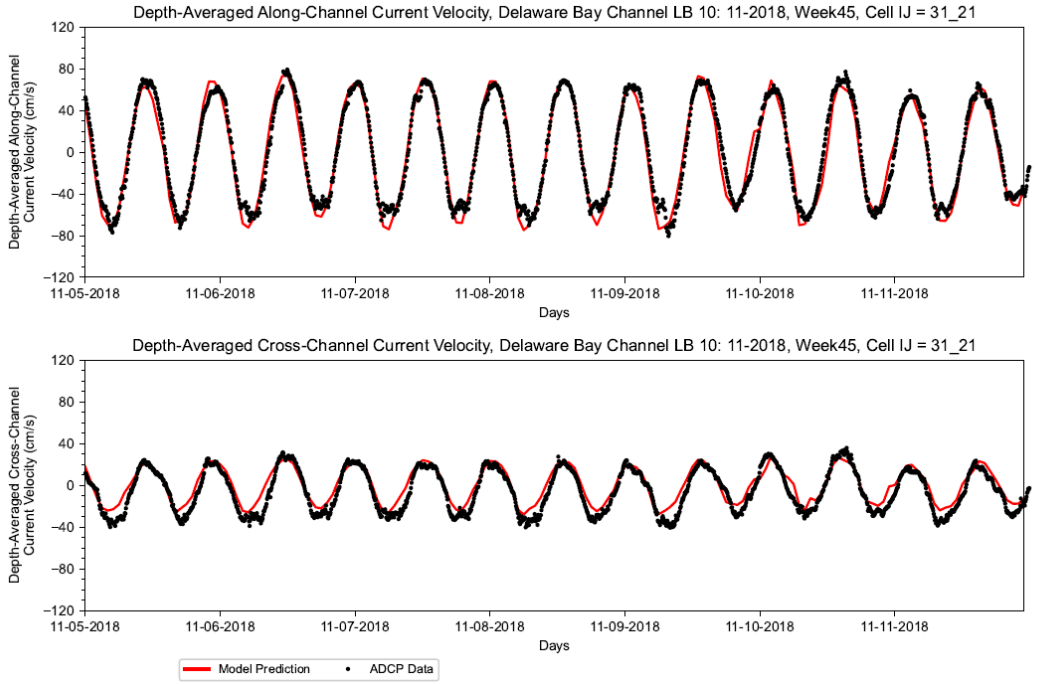

Figure 4.3-11 Observed and Predicted Depth-Averaged Along and Cross-Channel Current Velocity at NOAA station db0502 Delaware Bay Channel LB 10

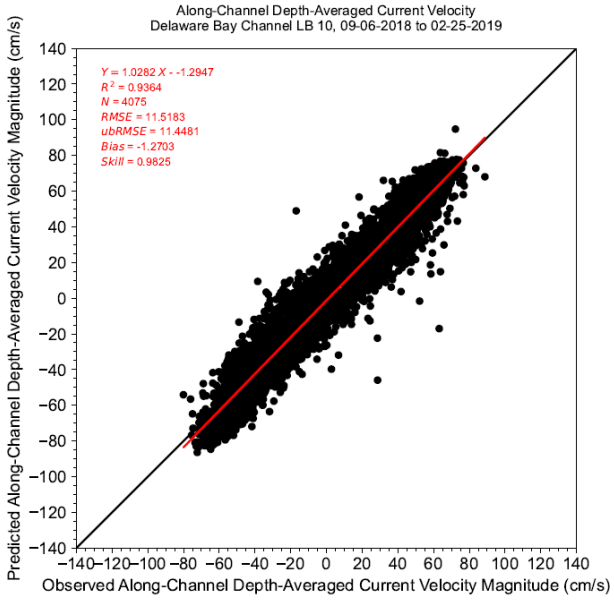

Figure 4.3-12 Comparison of Observed and Predicted Along-Channel Depth-Averaged Current Velocity Magnitude at Brown Shoal Light during 09-06-2018 to 02-25-2019 period at NOAA station db0502 Delaware Bay Channel LB 10

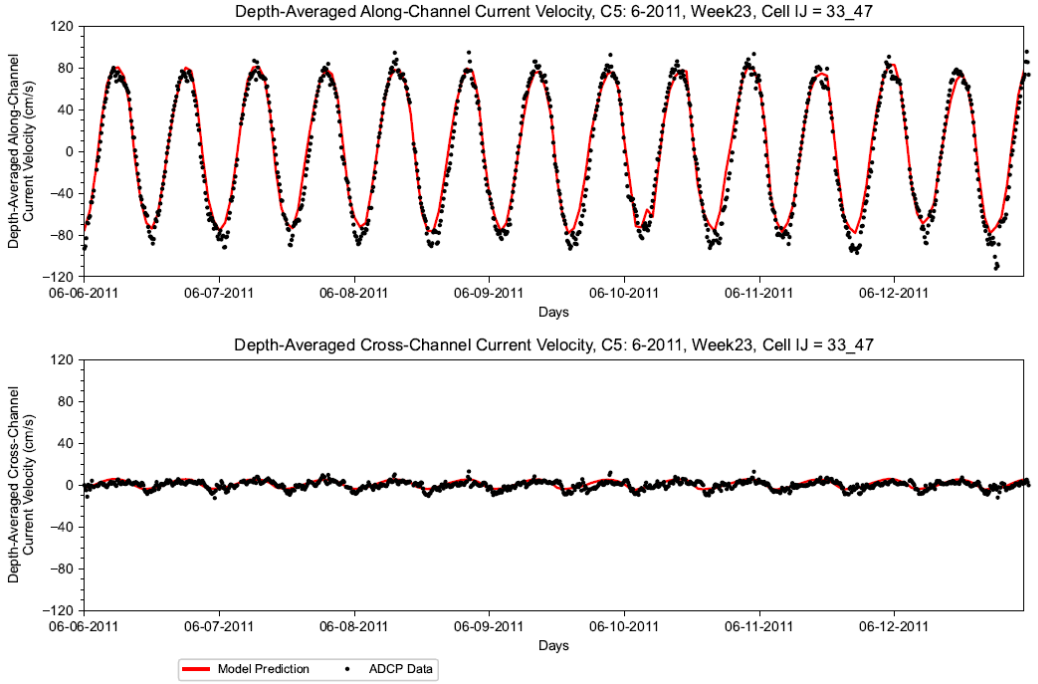

Figure 4.3-13 Observed and Predicted Depth-Averaged Along and Cross-Channel Current Velocity at Rutgers University 2011 Survey Station C5

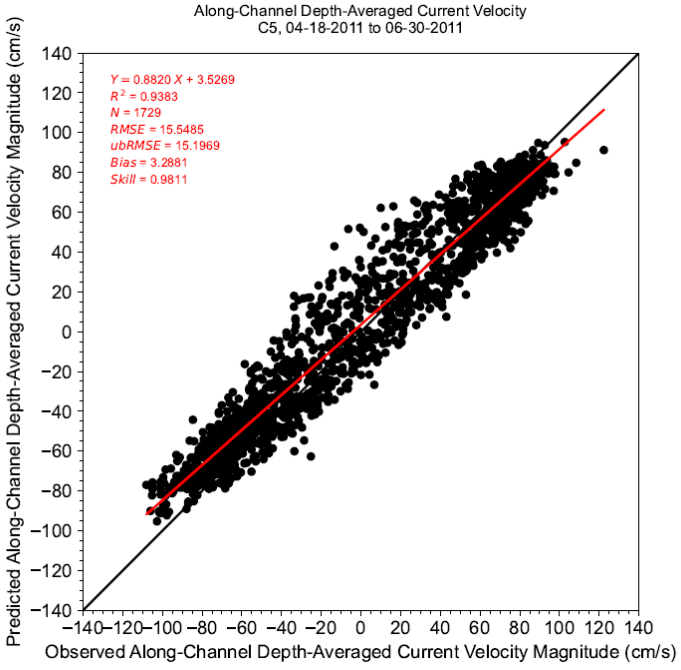

Figure 4.3-14 Comparison of Observed and Predicted Along-Channel Depth-Averaged Current Velocity Magnitude at C5 during 04-18-2011 to 06-30-2011 period.

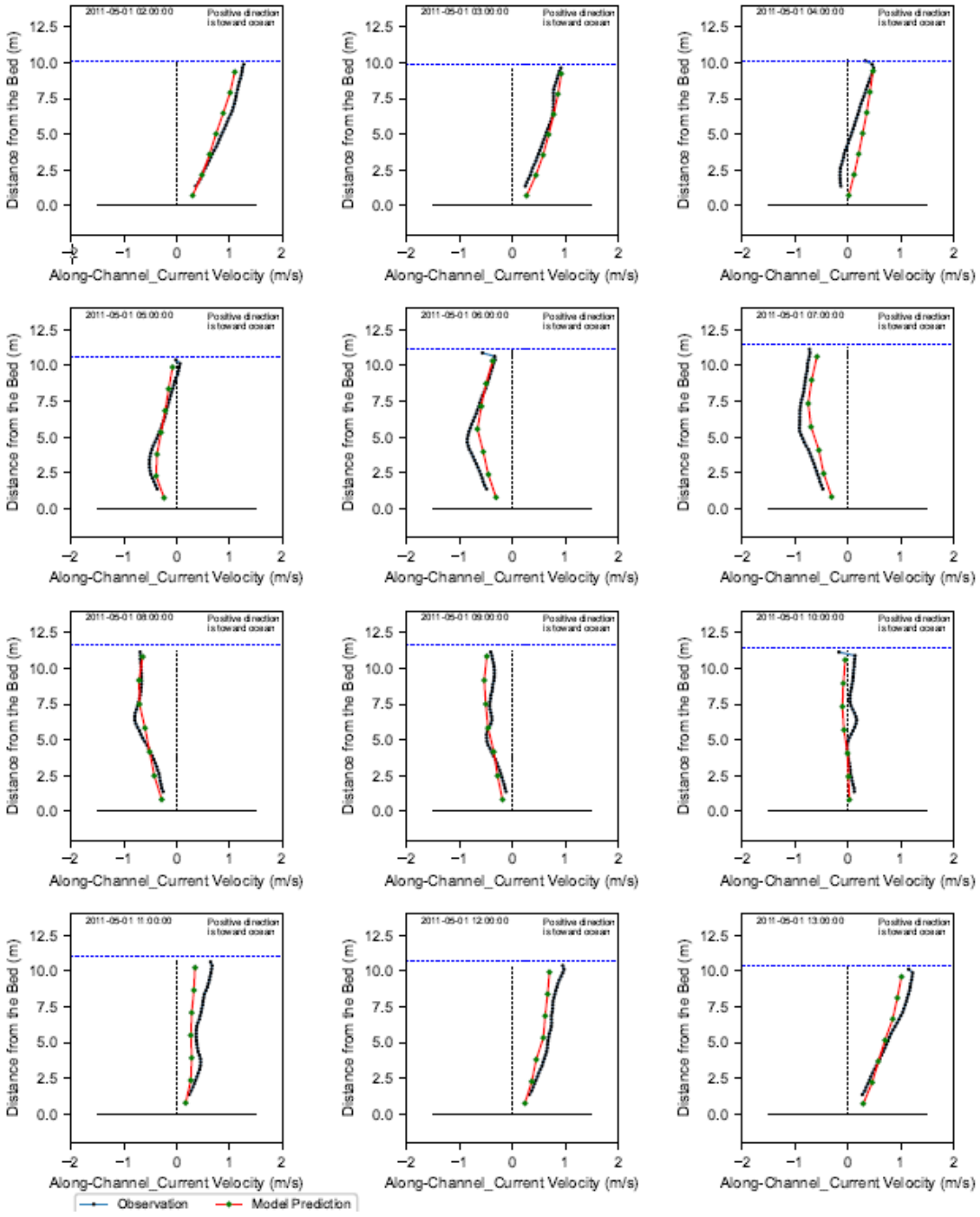

Note: 10-min ADCP current velocity measurements were averaged into an hourly window and compared to hourly average model outputs. ADCP survey data collected in 2011 were provided by Rutgers University.

Figure 4.3-15 Vertical Profile of Observed and Predicted Along-Channel Current Velocity at C5 during 2011-05-01 02:00:00 to 2011-05-01 13:00:00 period.

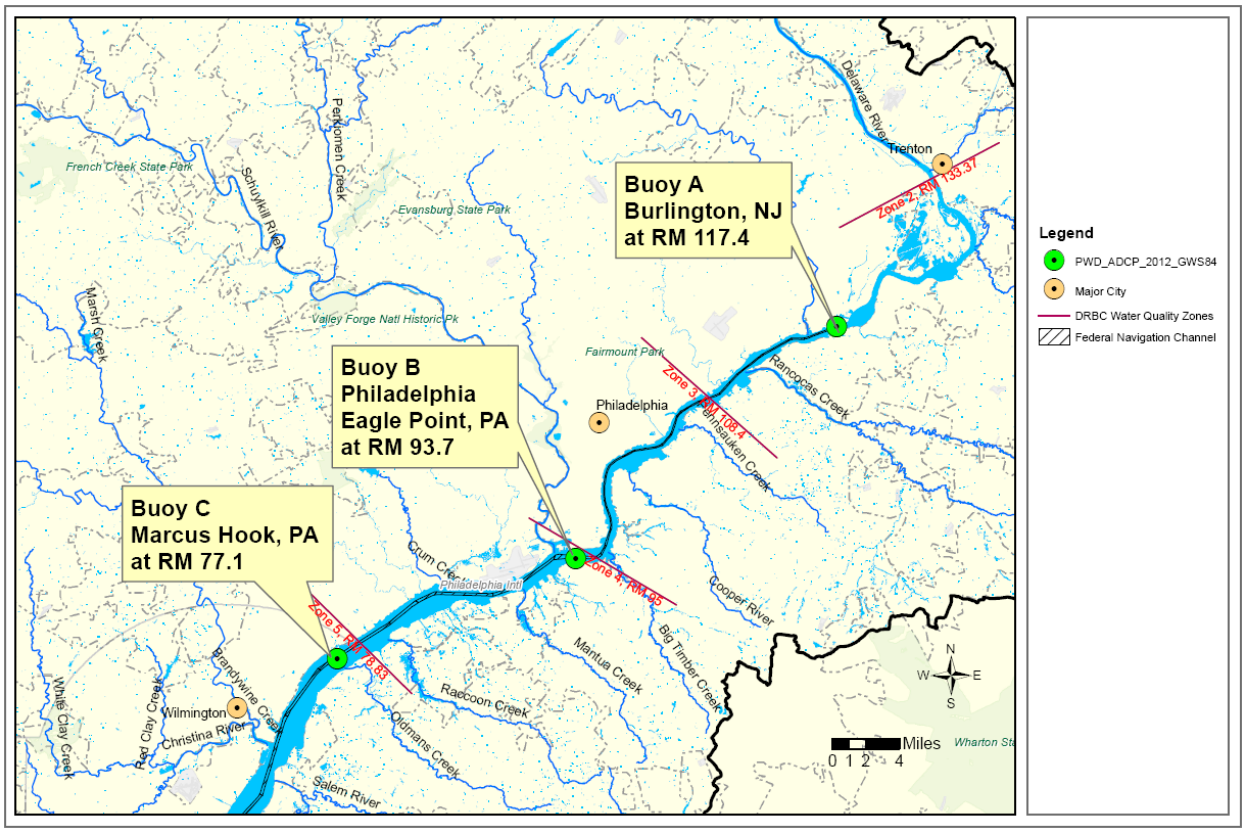

Figure 4.3-16. PWD ADCP Current Velocity Survey Locations

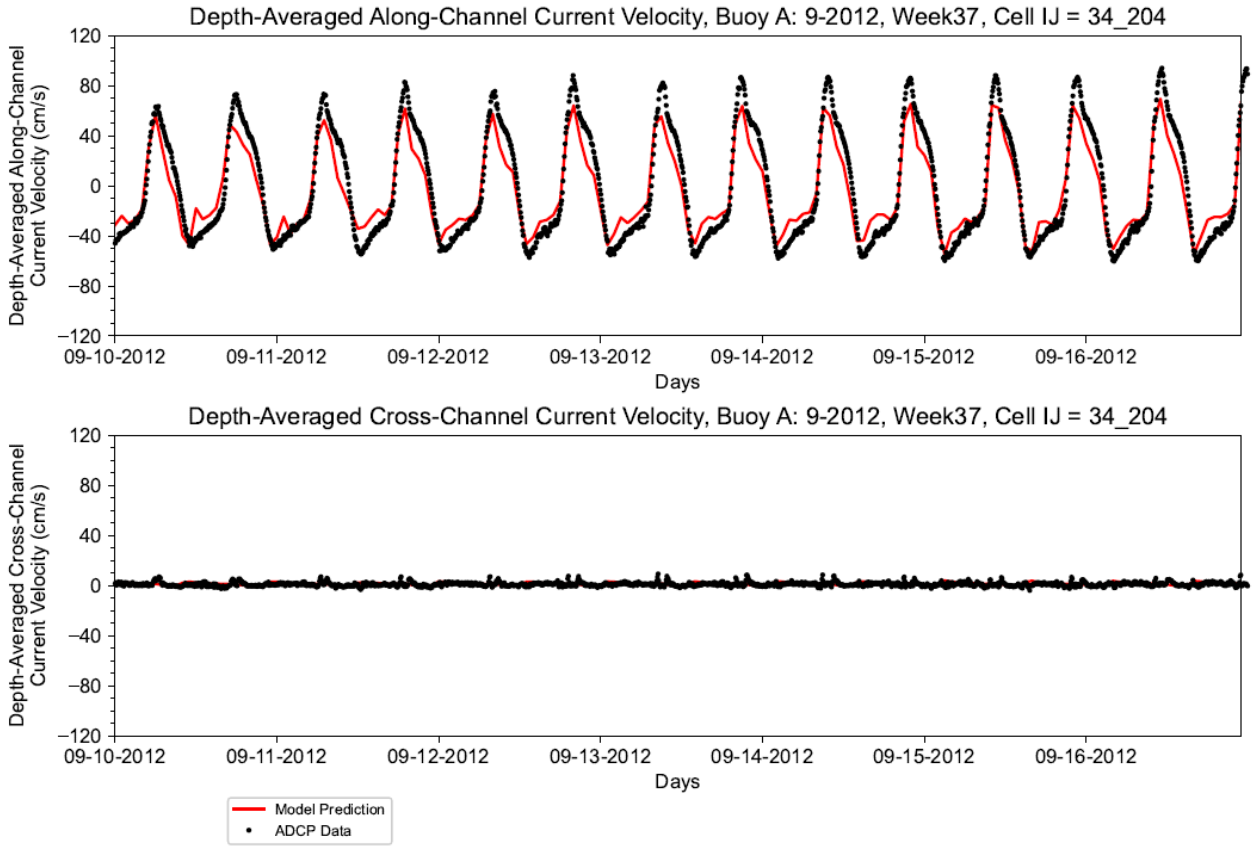

Figure 4.3-17. Observed and Predicted Depth-Averaged Along and Cross-Channel Current Velocity at Buoy A, September 10–16, 2012.

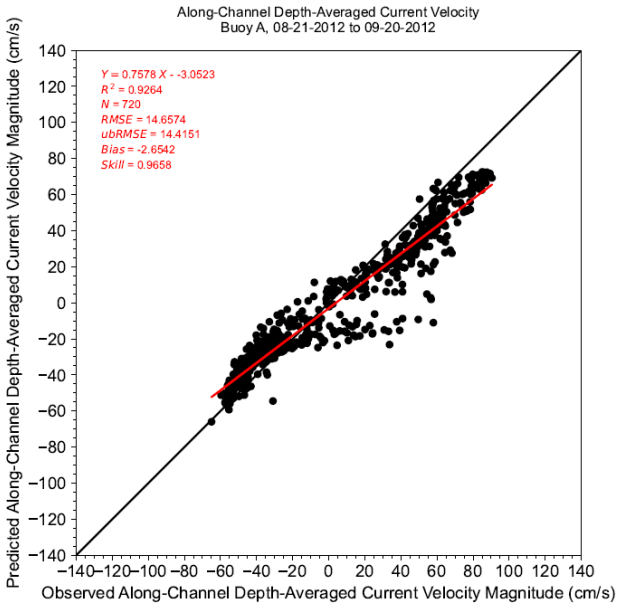

(a) 1-to-1 Plot

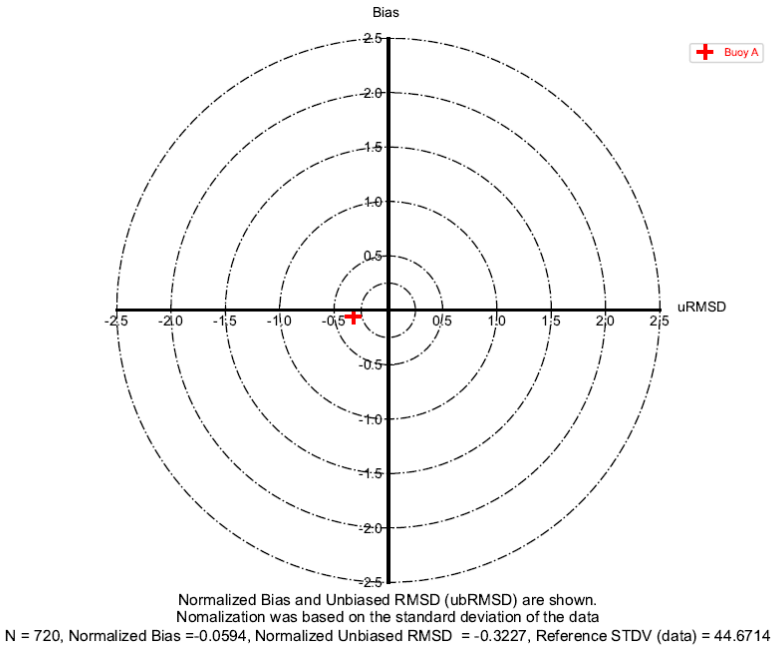

(b) Target Diagram

Figure 4.3-18. Comparison of Observed and Predicted Along-Channel Depth-Averaged Current Velocity Magnitude at Buoy A, August 21 to September 20, 2012.

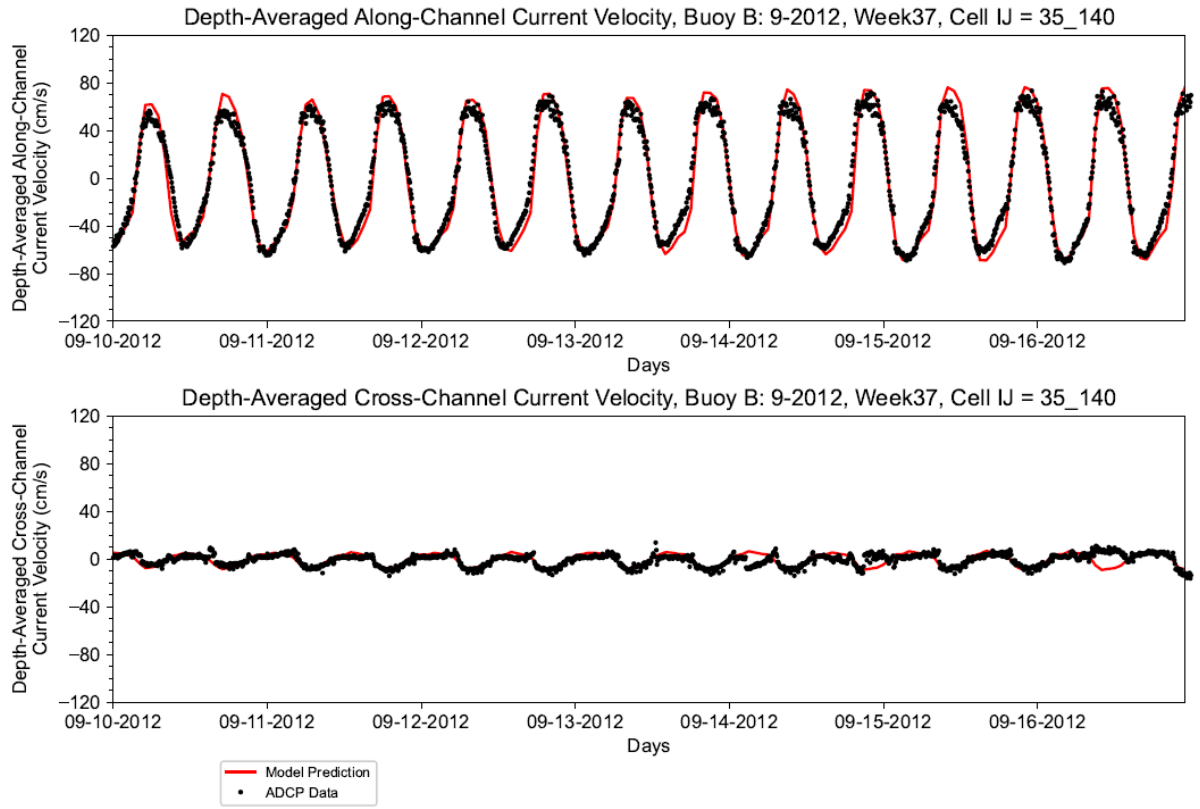

Figure 4.3-19. Observed and Predicted Depth-Averaged Along and Cross-Channel Current Velocity at Buoy B, September 10–16, 2012.

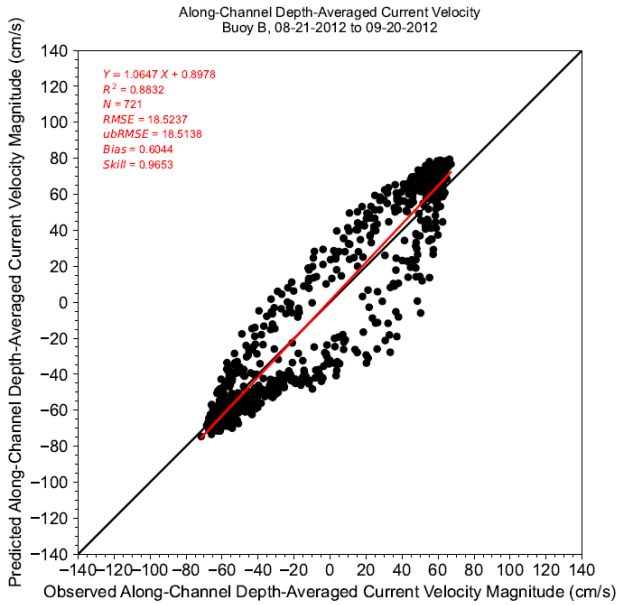

(a) 1-to-1 Plot

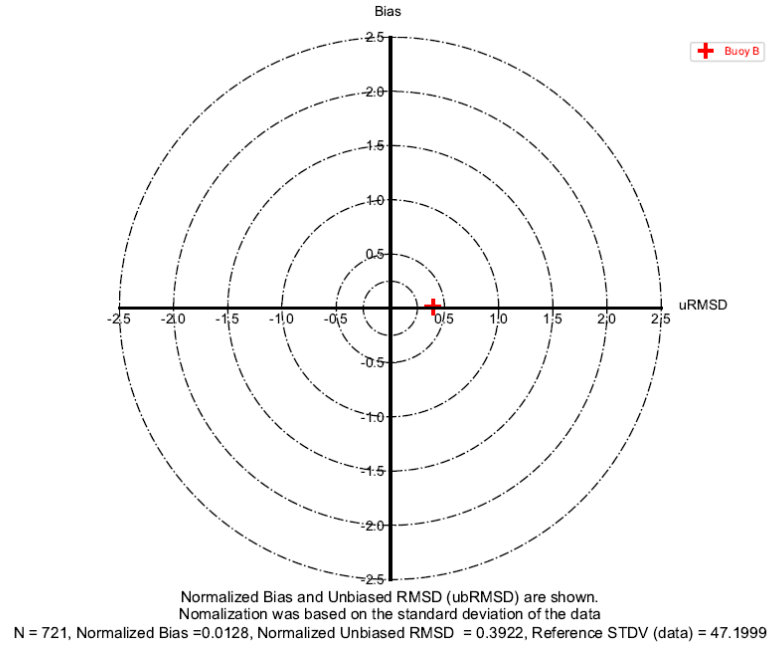

(b) Target Diagram

Figure 4.3-20. Comparison of Observed and Predicted Along-Channel Depth-Averaged Current Velocity Magnitude at Buoy B, August 21 to September 20, 2012.

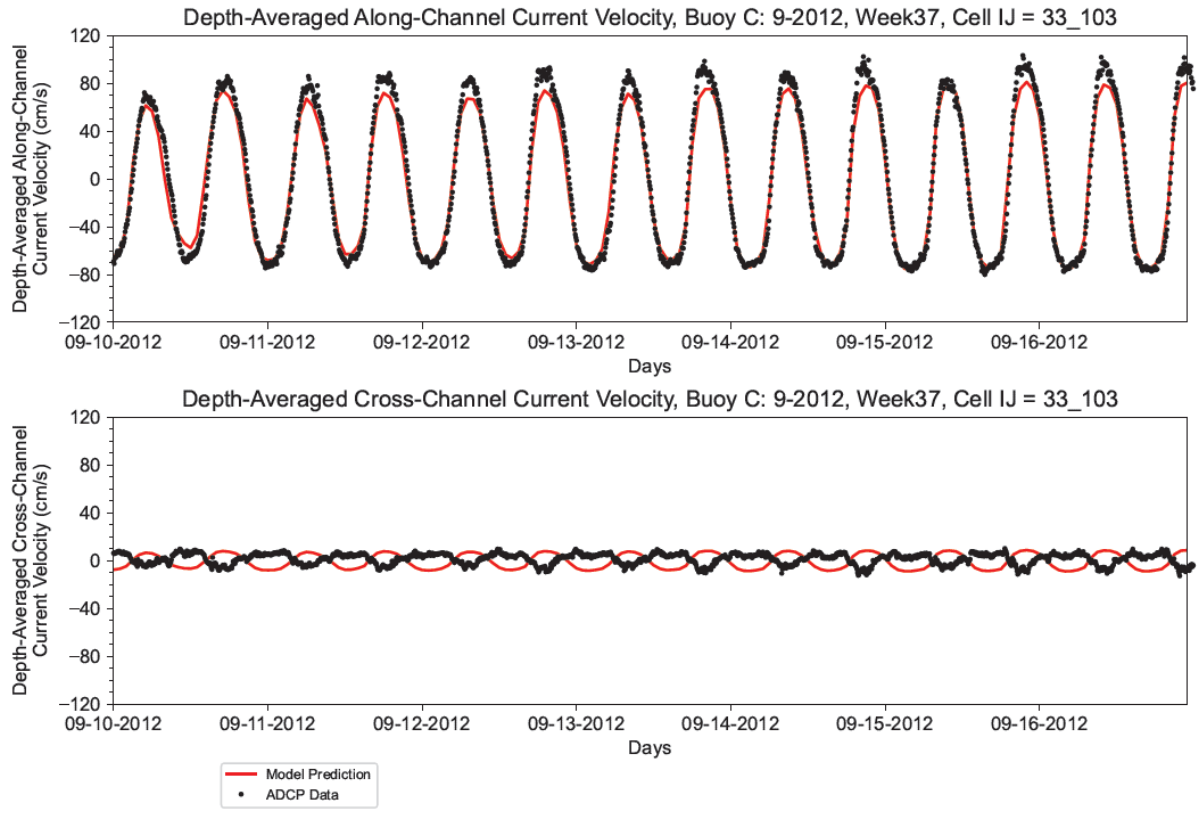

Figure 4.3-21. Observed and Predicted Depth-Averaged Along and Cross-Channel Current Velocity at Buoy C, September 10–16, 2012.

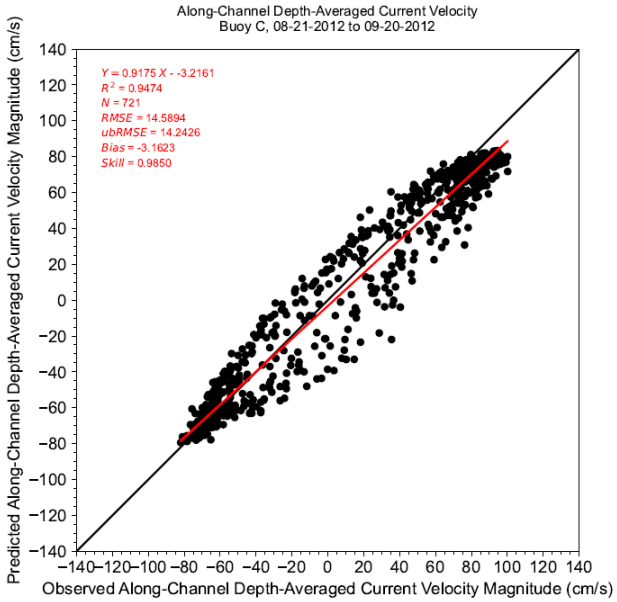

(a) 1-to-1 Plot

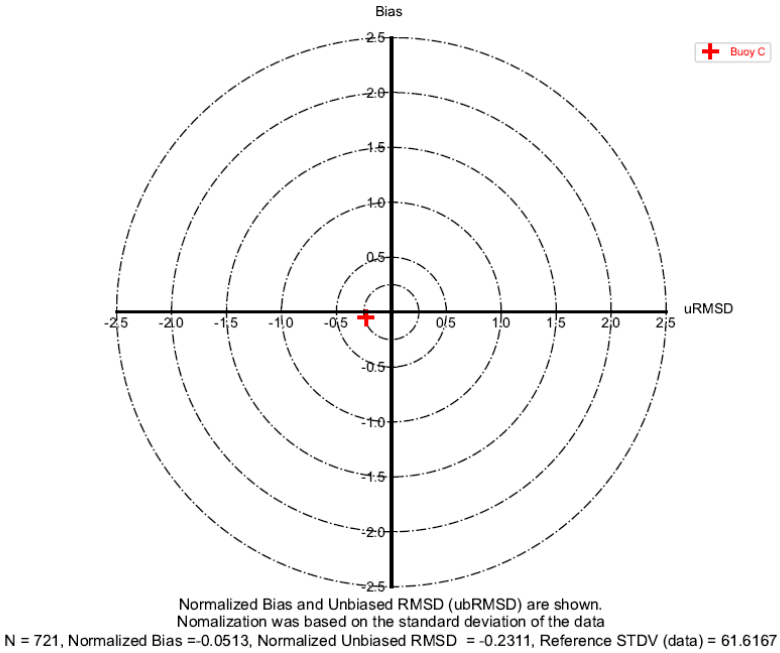

(b) Target Diagram

Figure 4.3-22. Comparison of Observed and Predicted Along-Channel Depth-Averaged Current Velocity Magnitude at Buoy C, August 21 to September 20, 2012.

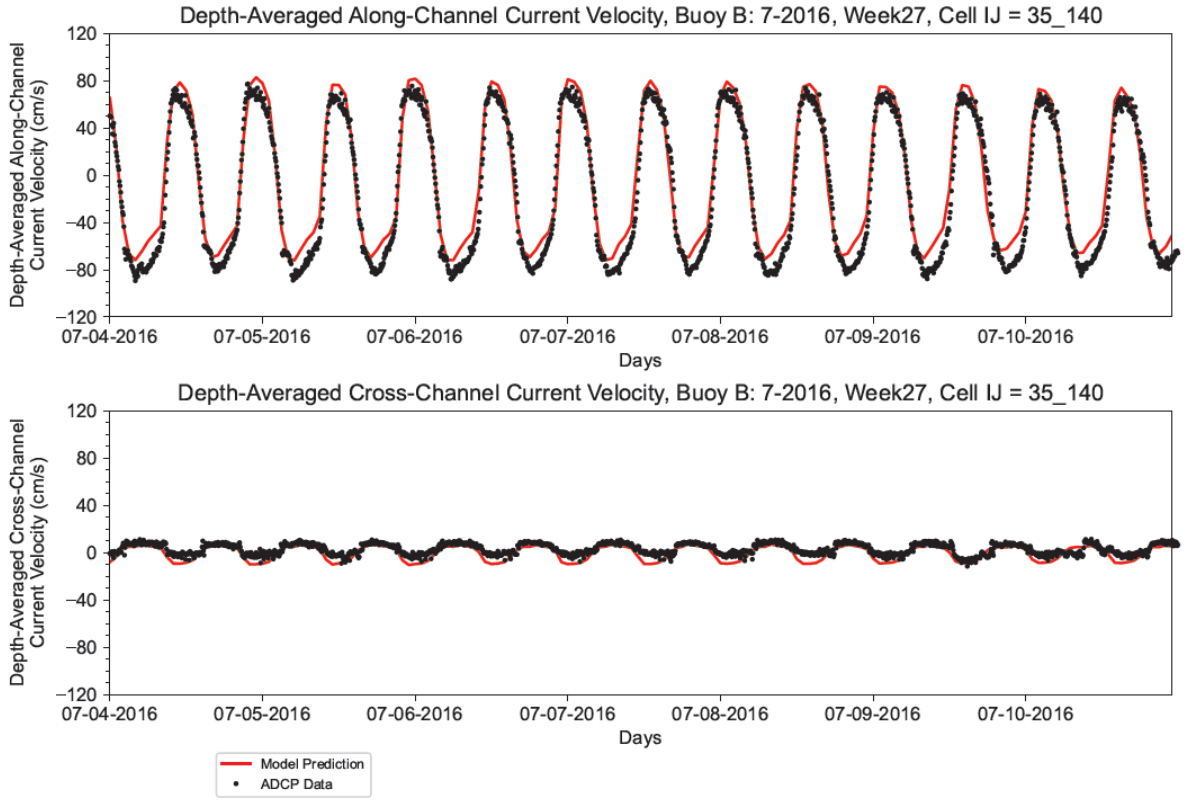

Figure 4.3-23. Observed and Predicted Depth-Averaged Along and Cross-Channel Current Velocity at Buoy B, July 4–10, 2016.

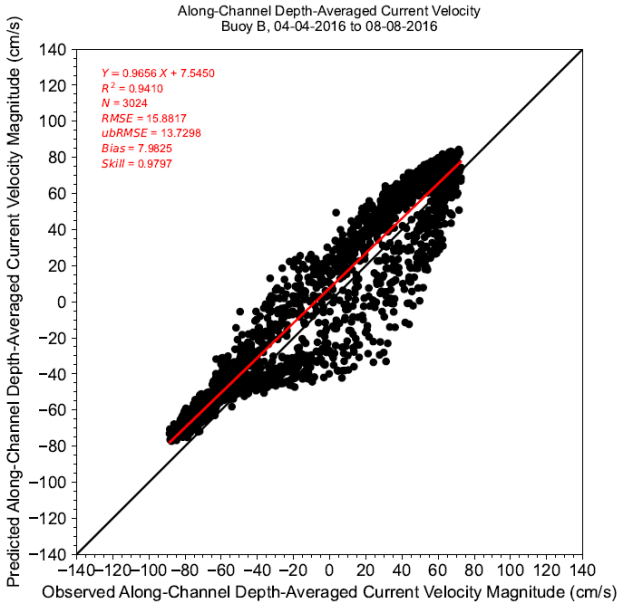

(a) 1-to-1 Plot

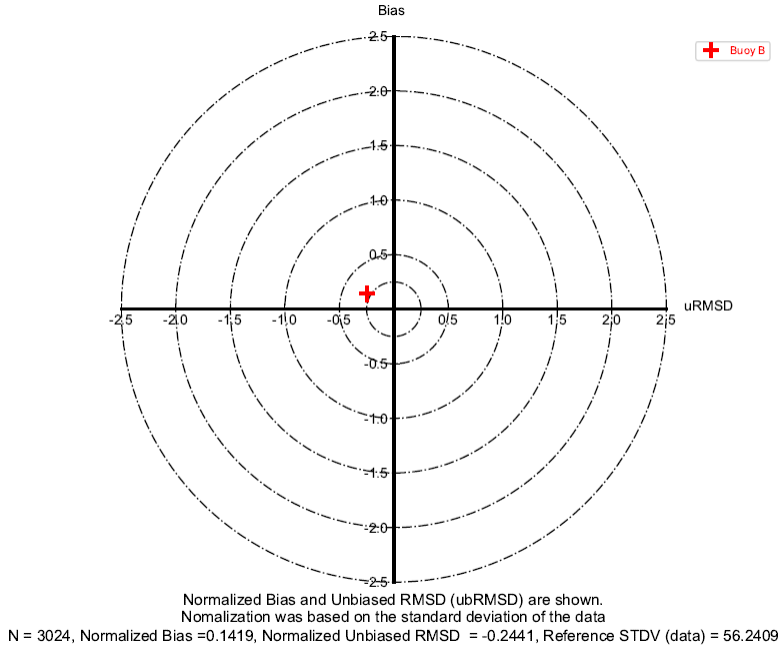

(b) Target Diagram

Figure 4.3-24. Comparison of Observed and Predicted Along-Channel Depth-Averaged Current Velocity Magnitude at Buoy B April 4 to August 8, 2016.

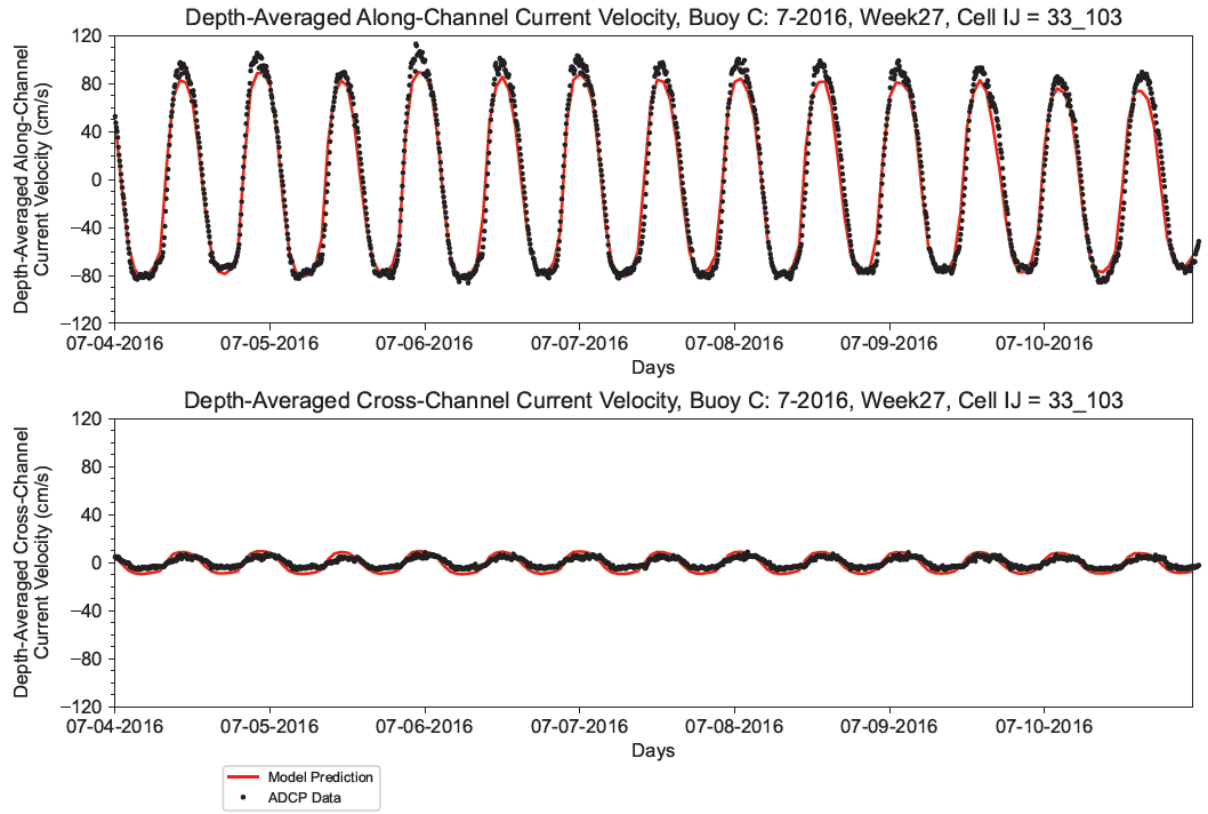

Figure 4.3-25 Observed and Predicted Depth-Averaged Along and Cross-Channel Current Velocity at Buoy C, July 4–10, 2016.

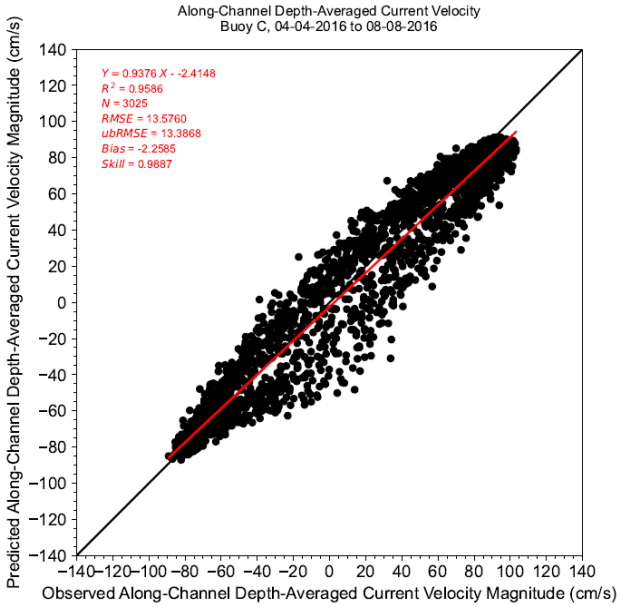

(a) 1-to-1 Plot

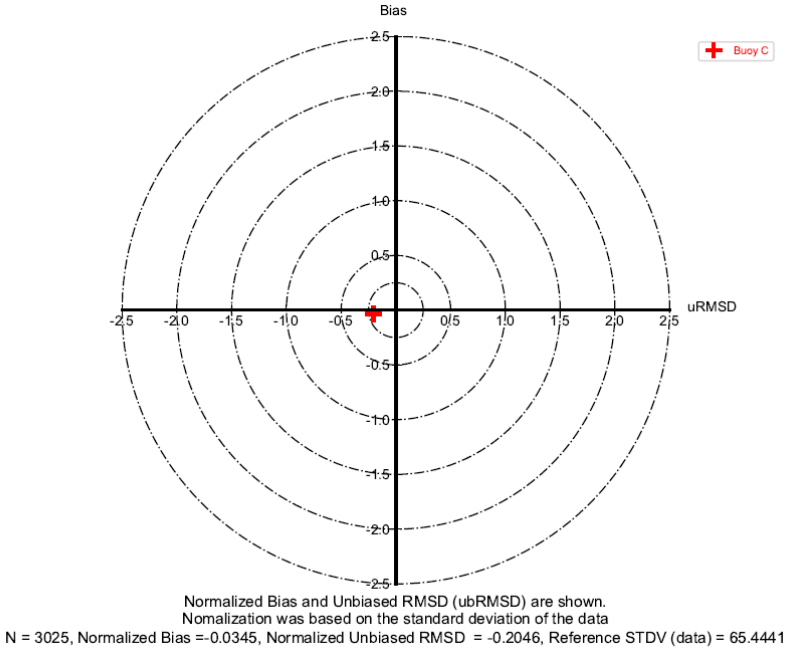

(b) Target Diagram

Figure 4.3-26. Comparison of Observed and Predicted Along-Channel Depth-Averaged Current Velocity Magnitude at Buoy C, April 4 to August 8, 2016.

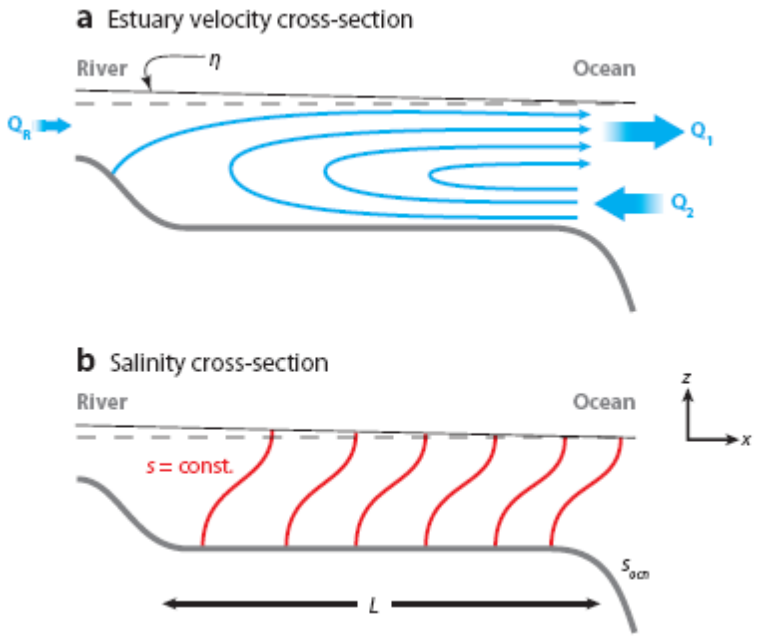

Figure 4.3-27 Definition sketch of an idealized partially mixed estuary, showing (a) the tidally-averaged circulation highlighting the exchange flow and (b) isoahalines. Figure from MacCready and Geyer 2010

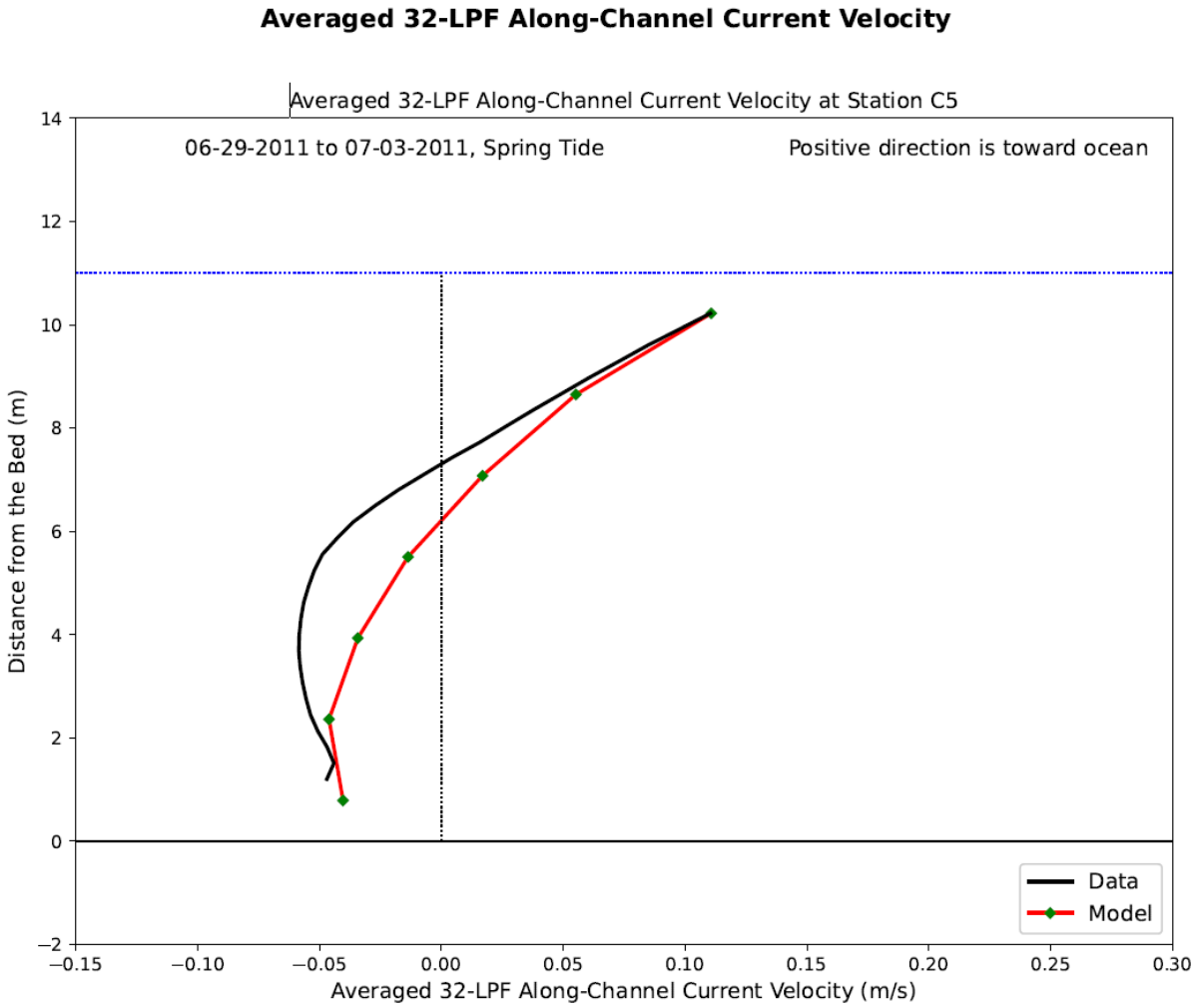

Figure 4.3-28 Comparison of Averaged Vertical Profile of 32-Low-pass-filtered Along-channel Current Velocity at C5 Station during June 29 to July 3, 2011 in a Spring Tide Period

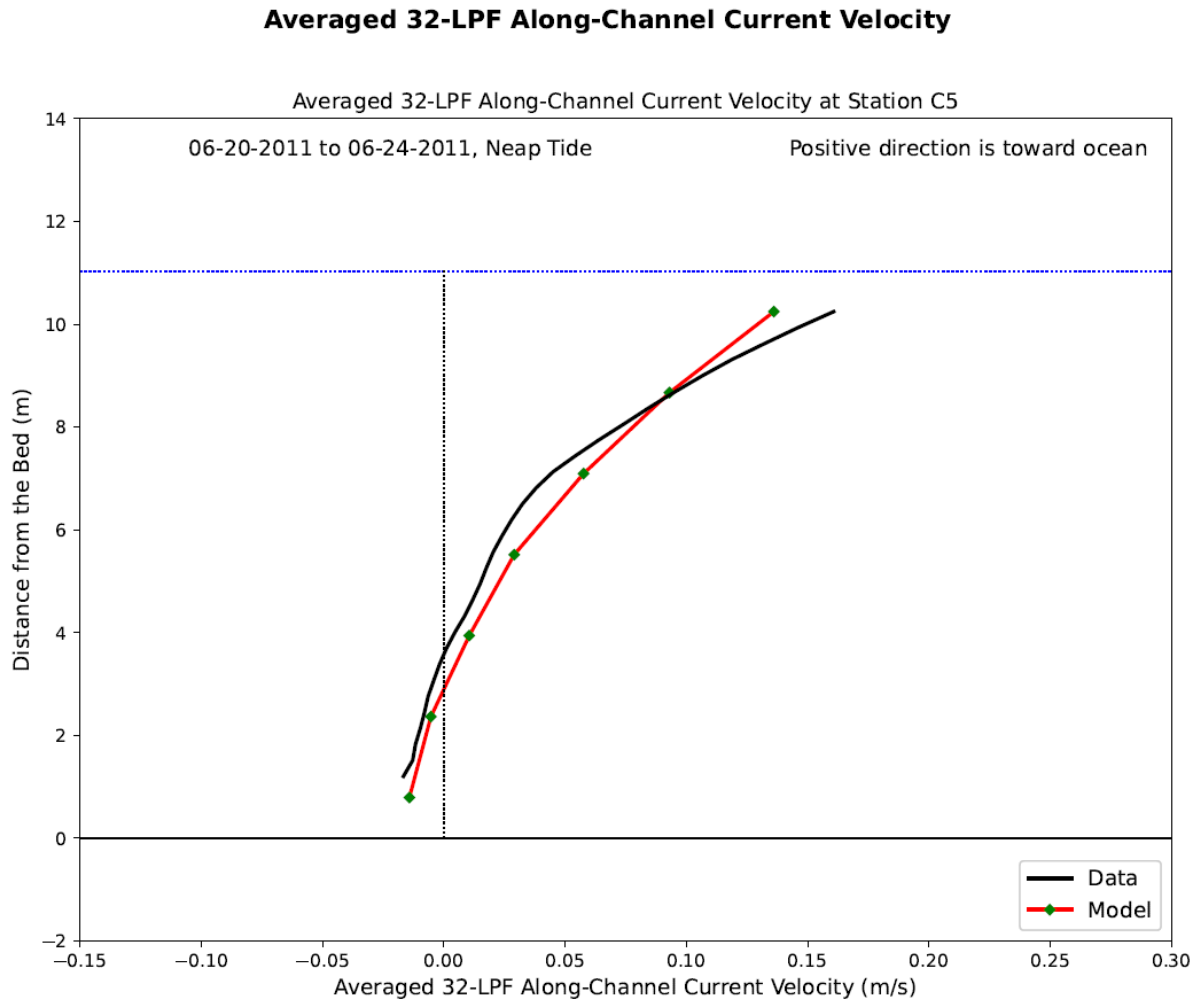

Figure 4.3-29 Comparison of Averaged Vertical Profile of 32-Low-pass-filtered Along-channel Current Velocity at C5 Station during June 20 to 24, 2011 in a Neap Tide Period

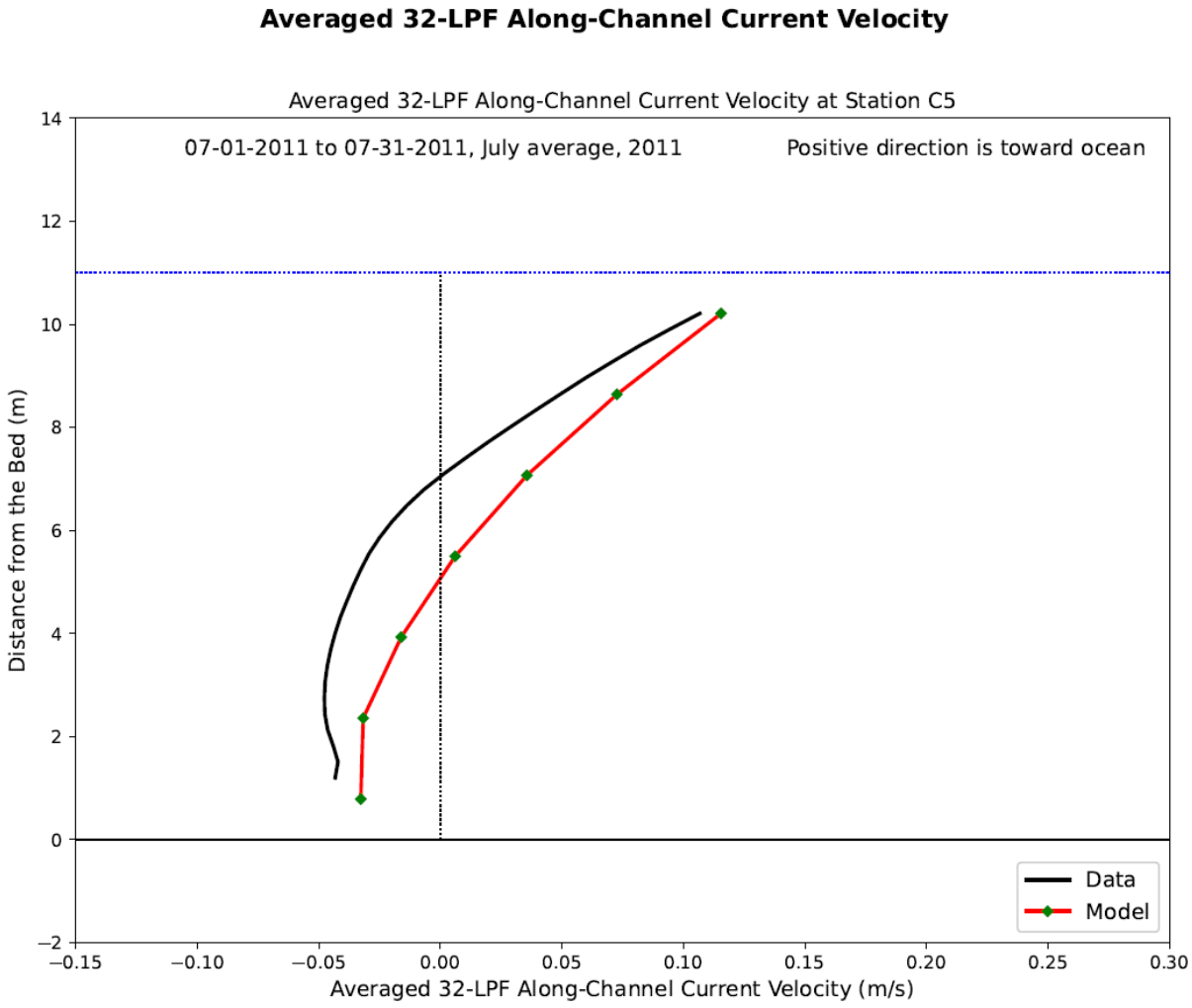

Figure 4.3-30 Comparison of Vertical Profile of 32-Low-pass-filtered Along-channel Current Velocity at C5 Station during one-month Period of July 2011

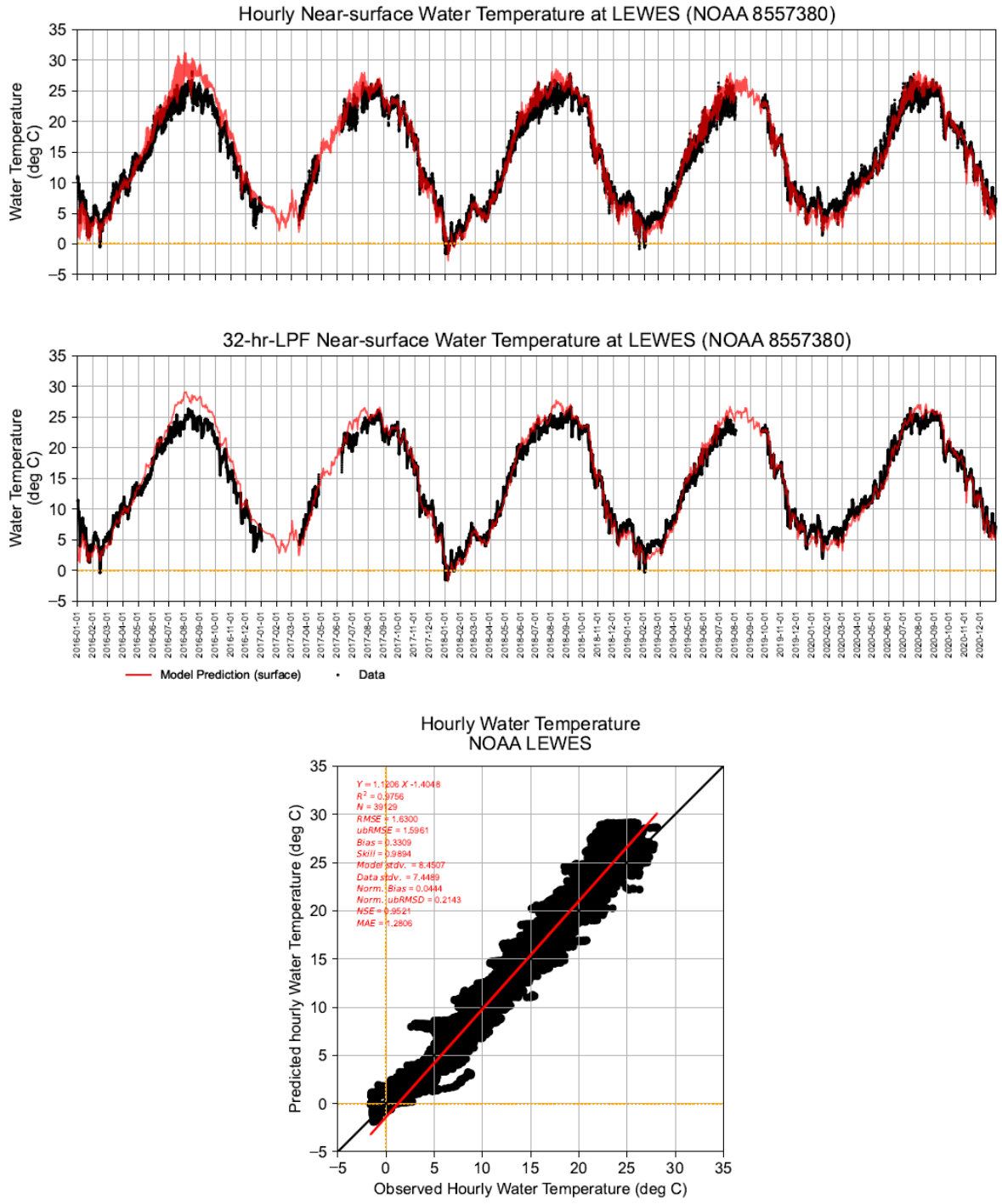

Note: data were collected near the surface

Figure 4.3-31 (1) Observed and Predicted Water Temperature at NOAA Station 8557380 Lewes during 2016-2020 Period

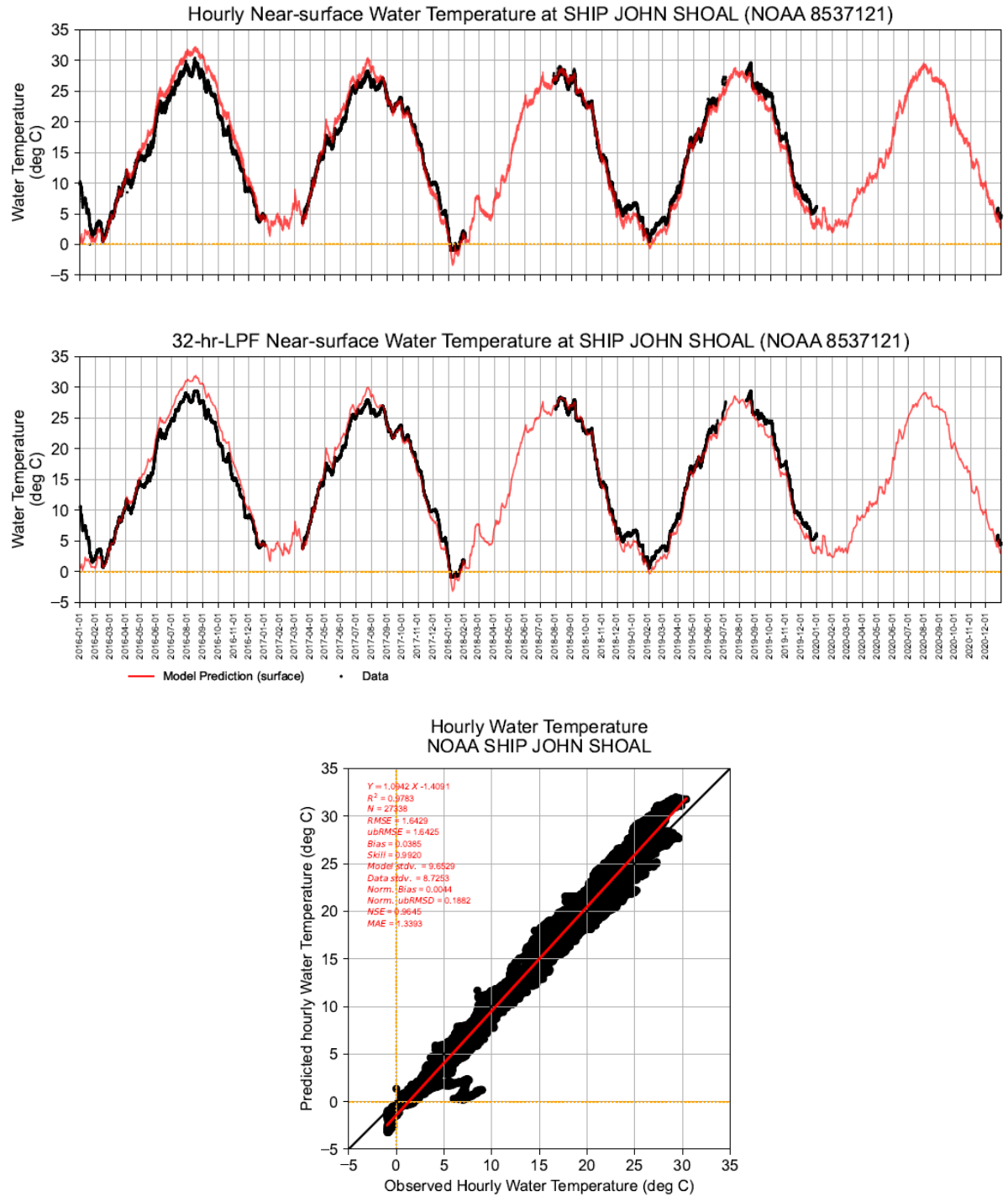

Note: data were collected near the surface

Figure 4.3-31 (2) Observed and Predicted Water Temperature at NOAA Station 8537121 Ship John Shoal during 2016-2020 Period

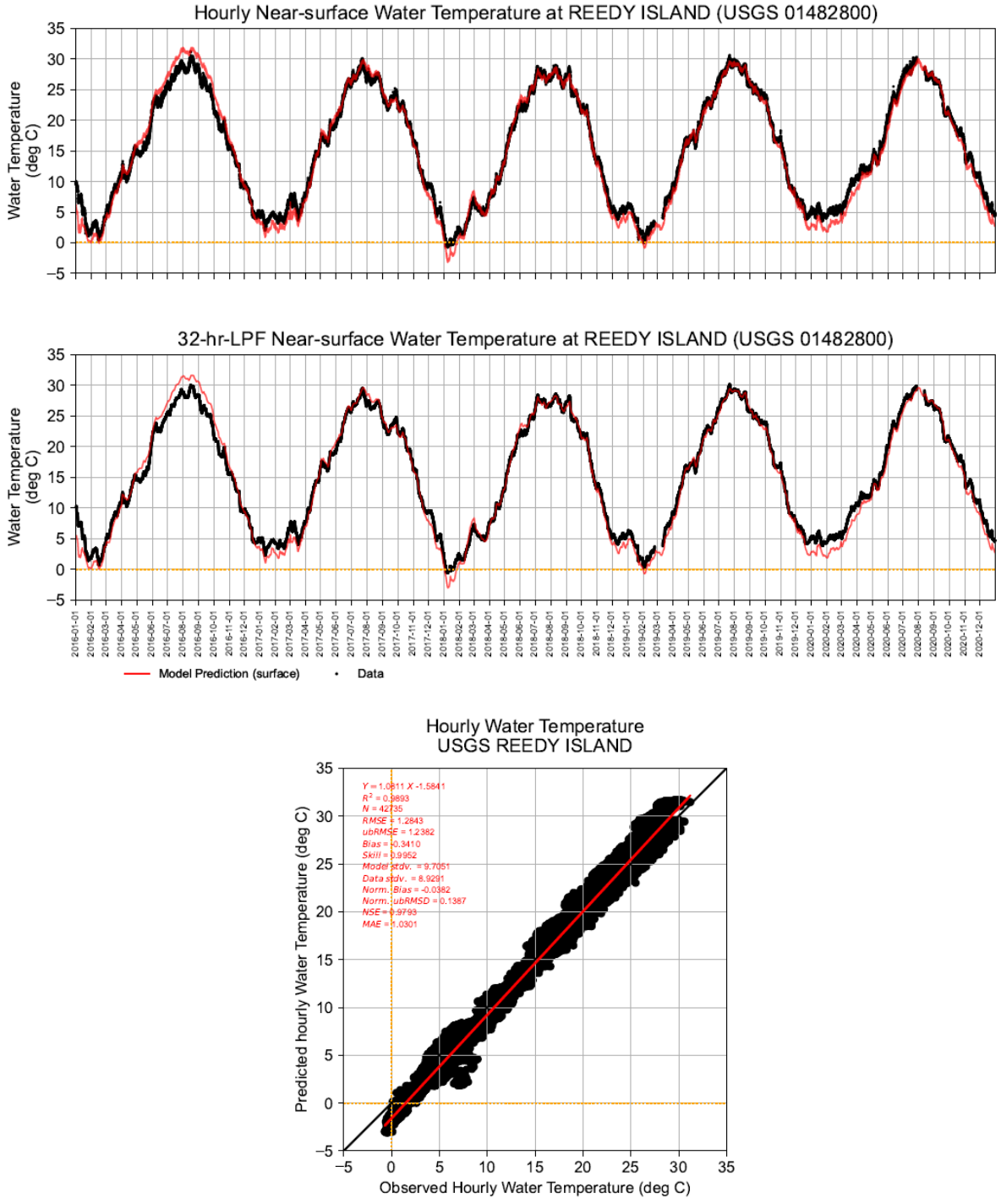

Note: data were collected near the surface

Figure 4.3-31 (3) Observed and Predicted Water Temperature at USGS Station 01482800 Reedy Island during 2016-2020 Period

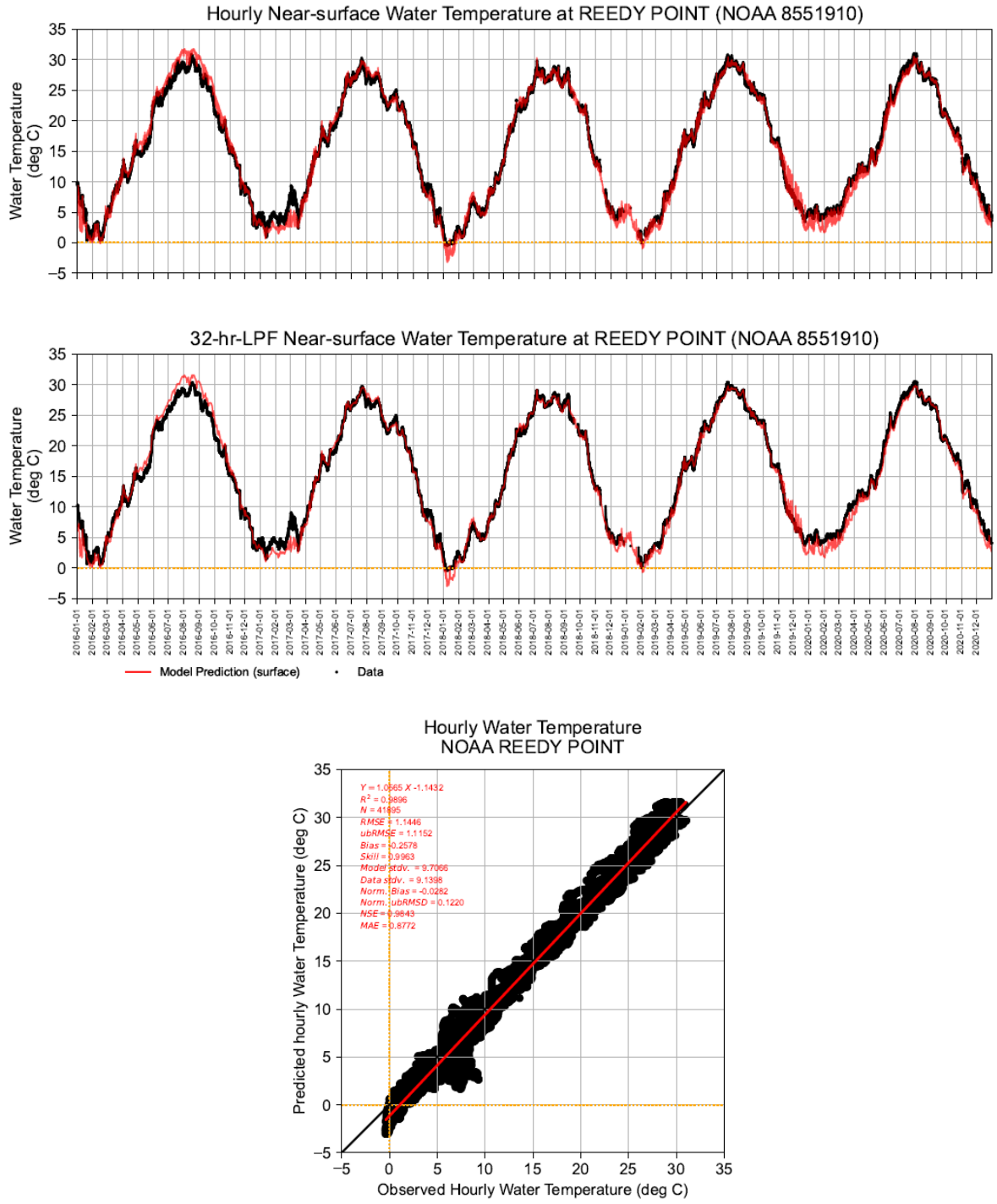

Note: data were collected near the surface

Figure 4.3-31 (4) Observed and Predicted Water Temperature at NOAA Station 8551910 Reedy Point during 2016-2020 Period

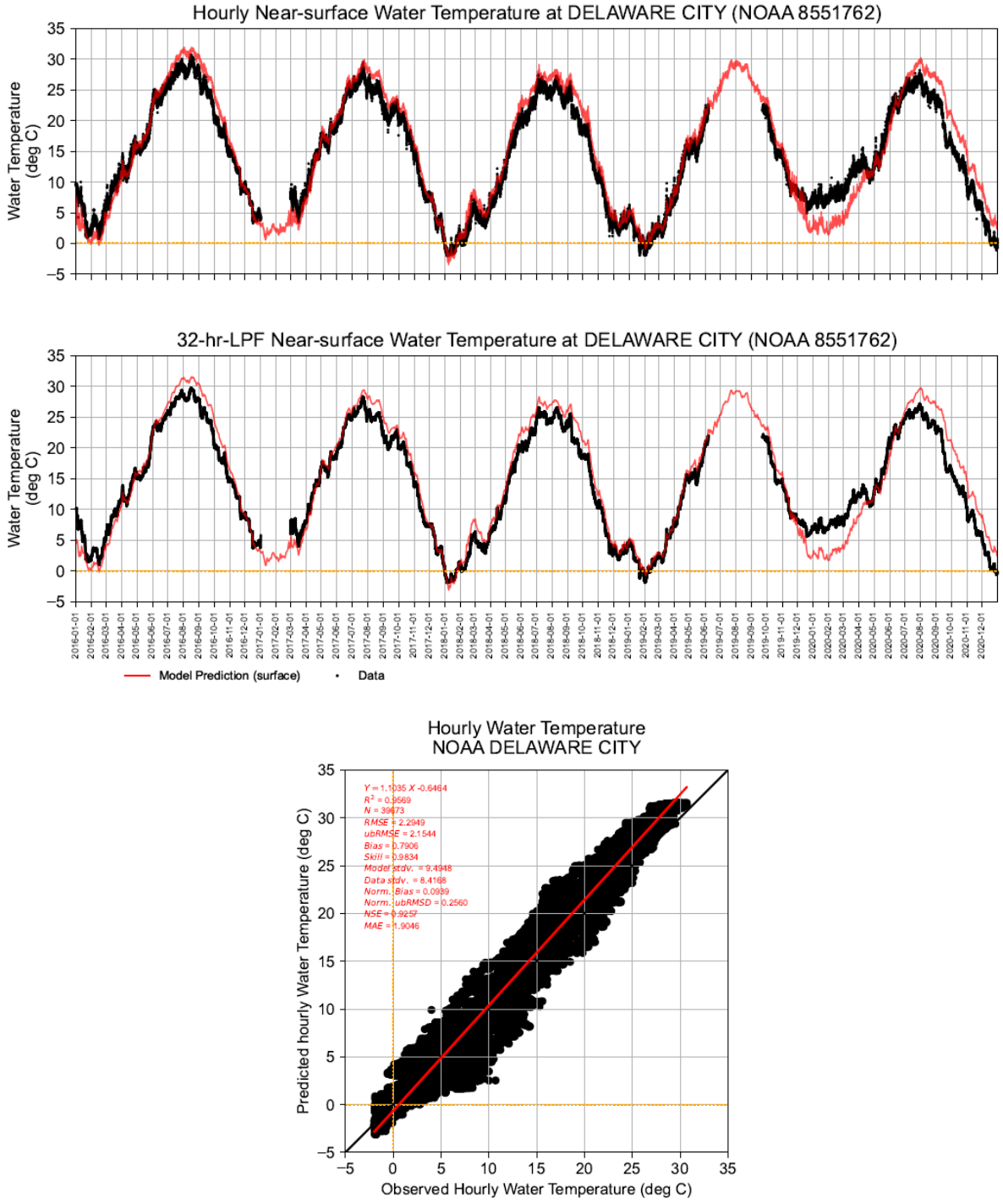

Note: data were collected near the surface

Figure 4.3-31 (5) Observed and Predicted Water Temperature at NOAA Station 8551762 Delaware City during 2016-2020 Period

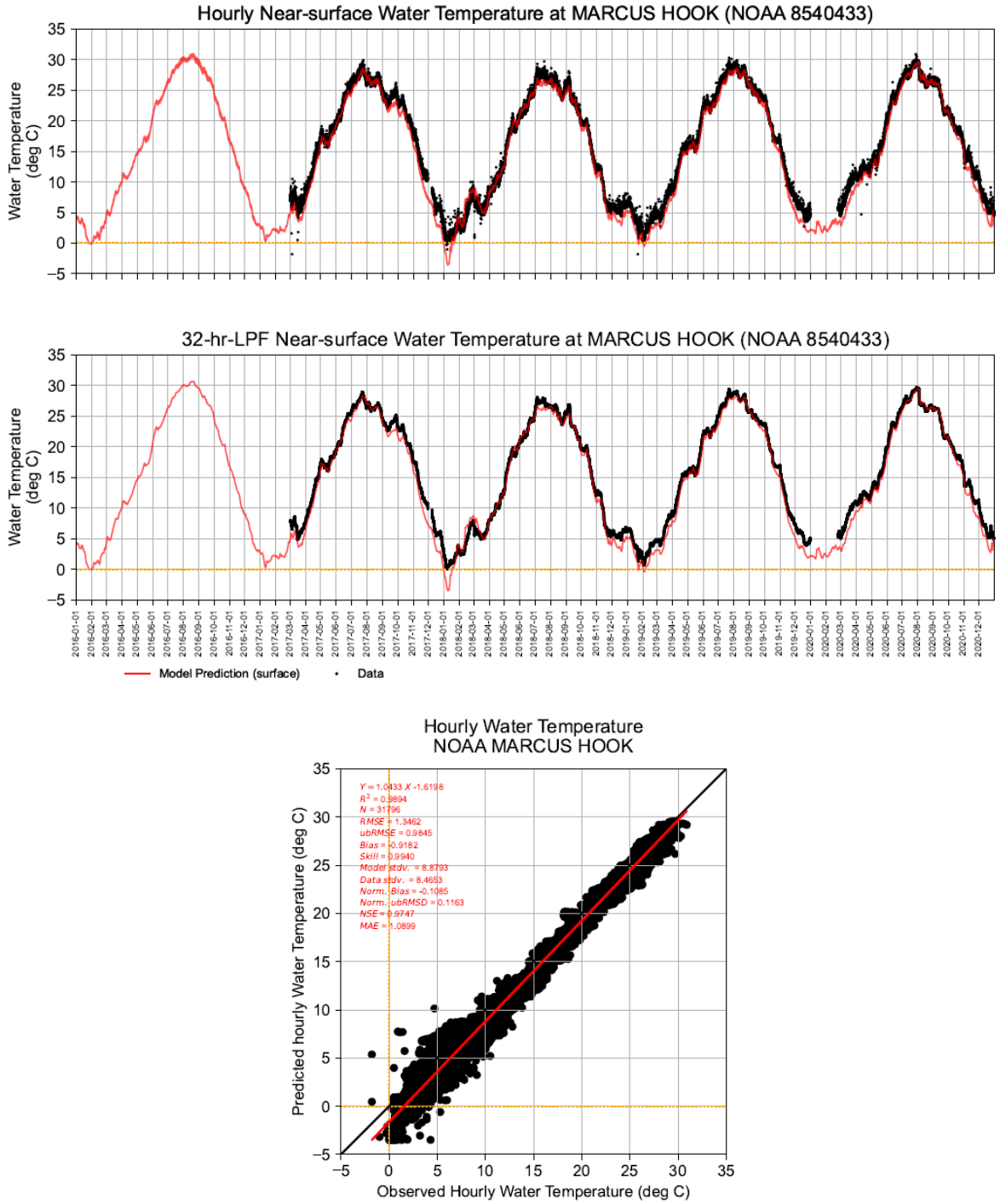

Note: data were collected near the surface

Figure 4.3-31 (6) Observed and Predicted Water Temperature at NOAA Station 8540433 Marcus Hook during 2016-2020 Period

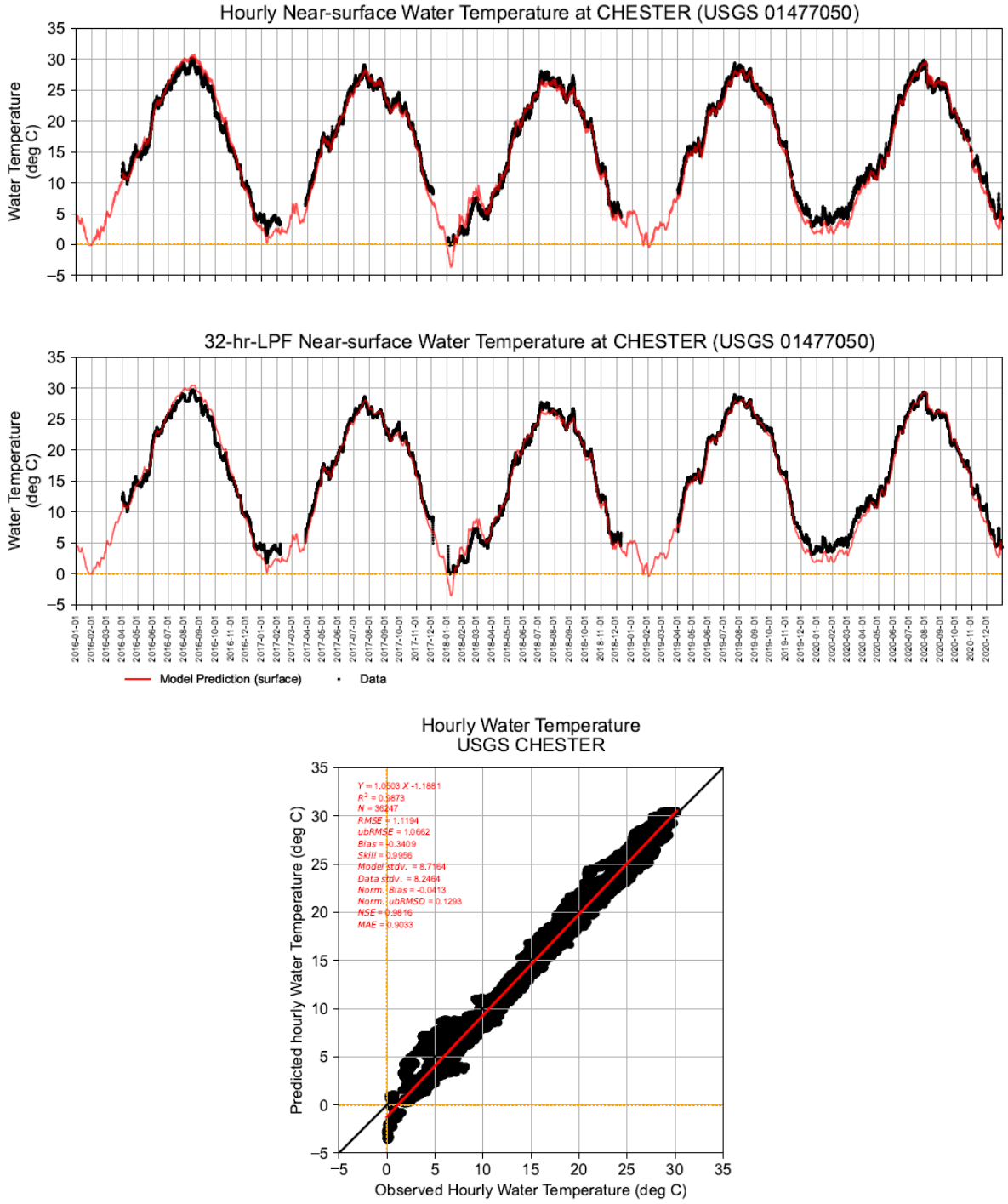

Note: data were collected near the surface

Figure 4.3-31 (7) Observed and Predicted Water Temperature at USGS Station 01477050 Chester during 2016-2020 Period

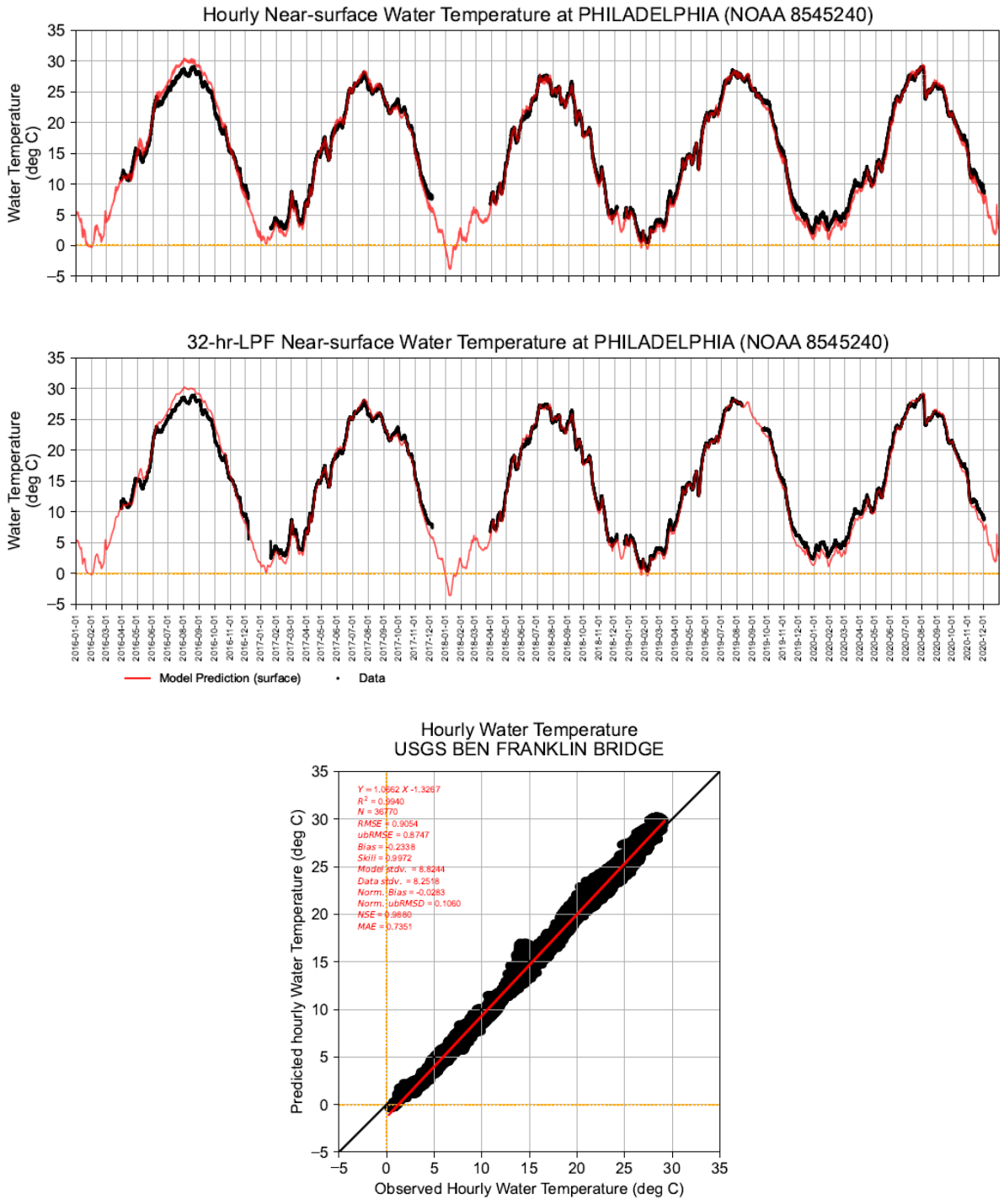

Note: data were collected near the surface

Figure 4.3-31 (8) Observed and Predicted Water Temperature at USGS Station 01467200 Ben Franklin Bridge during 2016-2020 Period

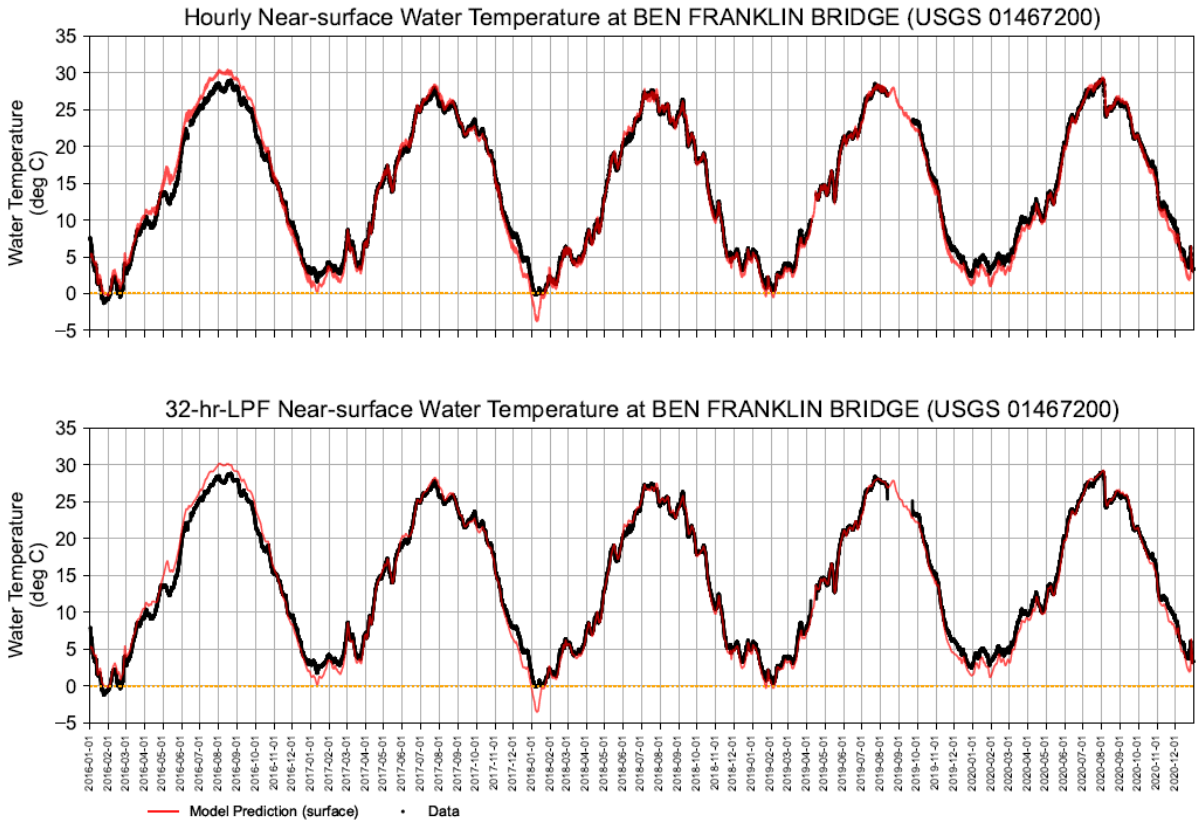

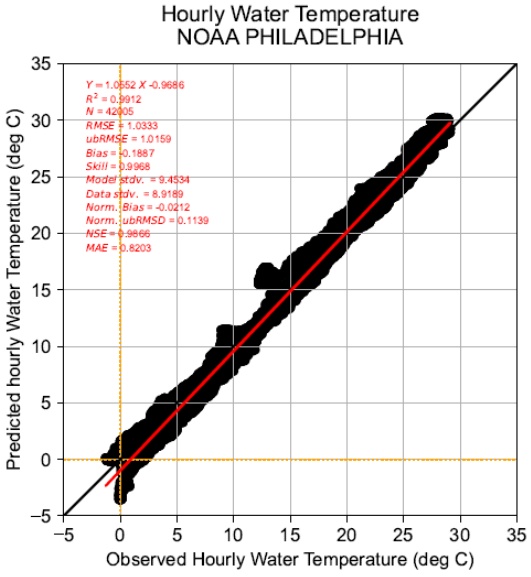

Note: data were collected near the surface

Figure 4.3-31 (9) Observed and Predicted Water Temperature at NOAA Station 8545240 Philadelphia during 2016-2020 Period

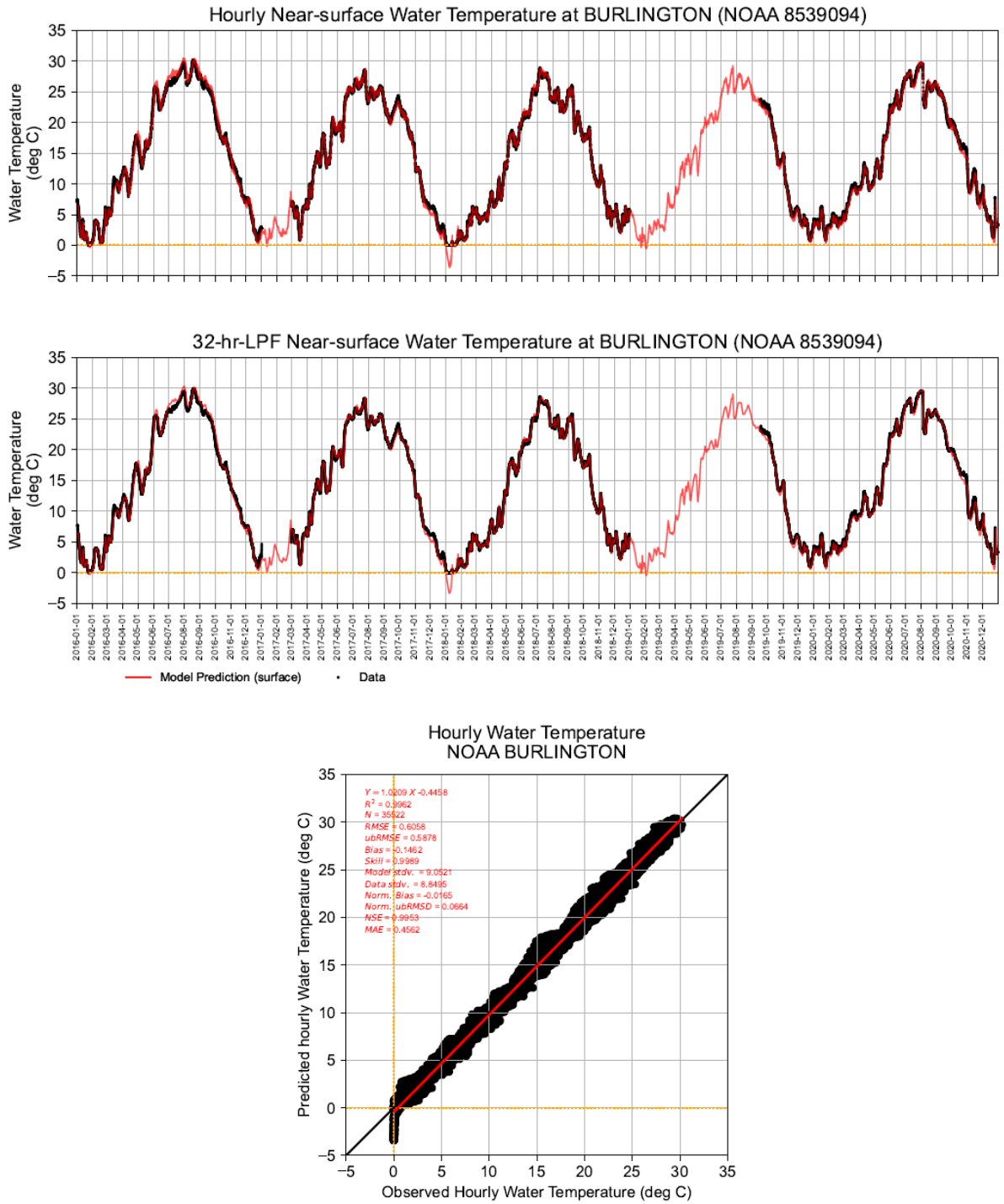

Note: data were collected near the surface

Figure 4.3-31 (10) Observed and Predicted Water Temperature at NOAA Station 8539094 Burlington during 2016-2020 Period

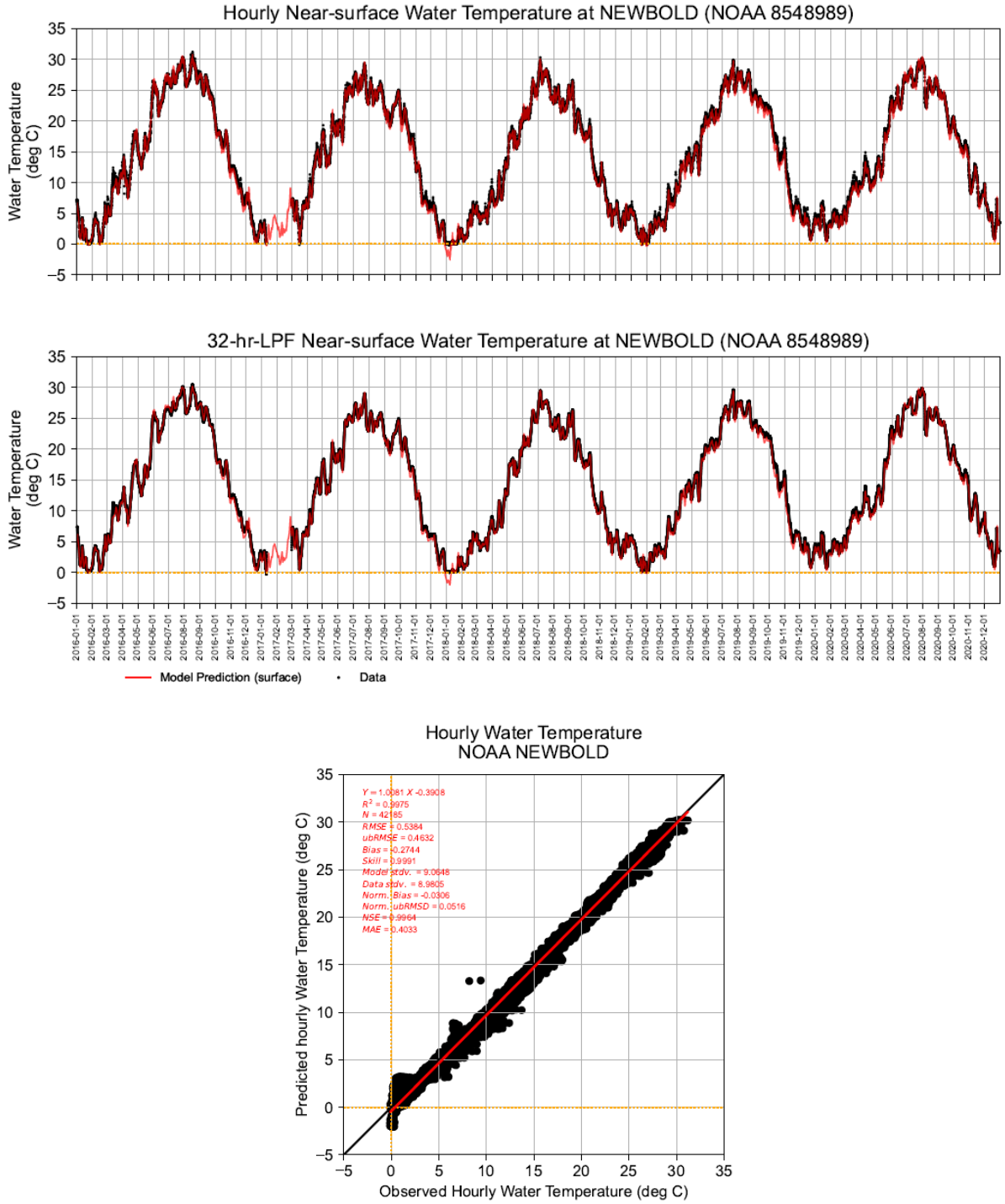

Note: data were collected near the surface

Figure 4.3-31 (11) Observed and Predicted Water Temperature at NOAA Station 8548989 Newbold during 2018 Period

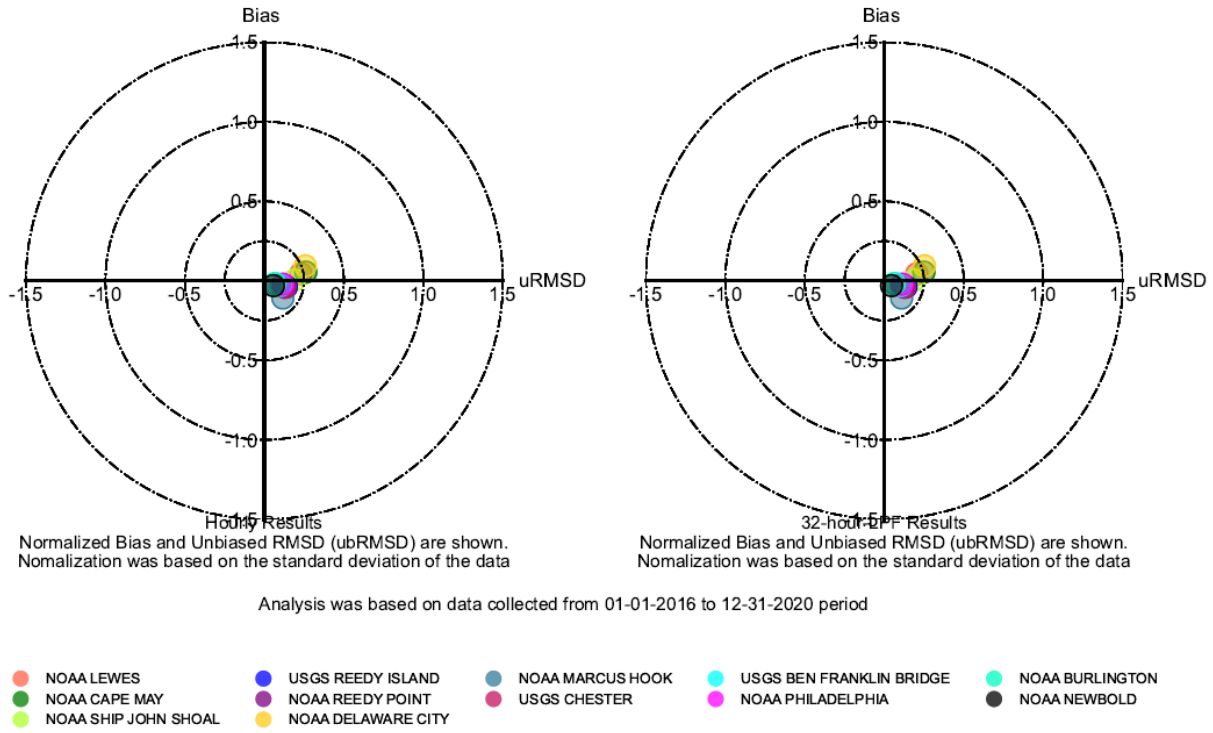

Figure 4.3-32 Target Diagram for the Observed and Predicted Hourly and 32-hour-LPF Near-Surface Water Temperature during 2016 to 2020 Period

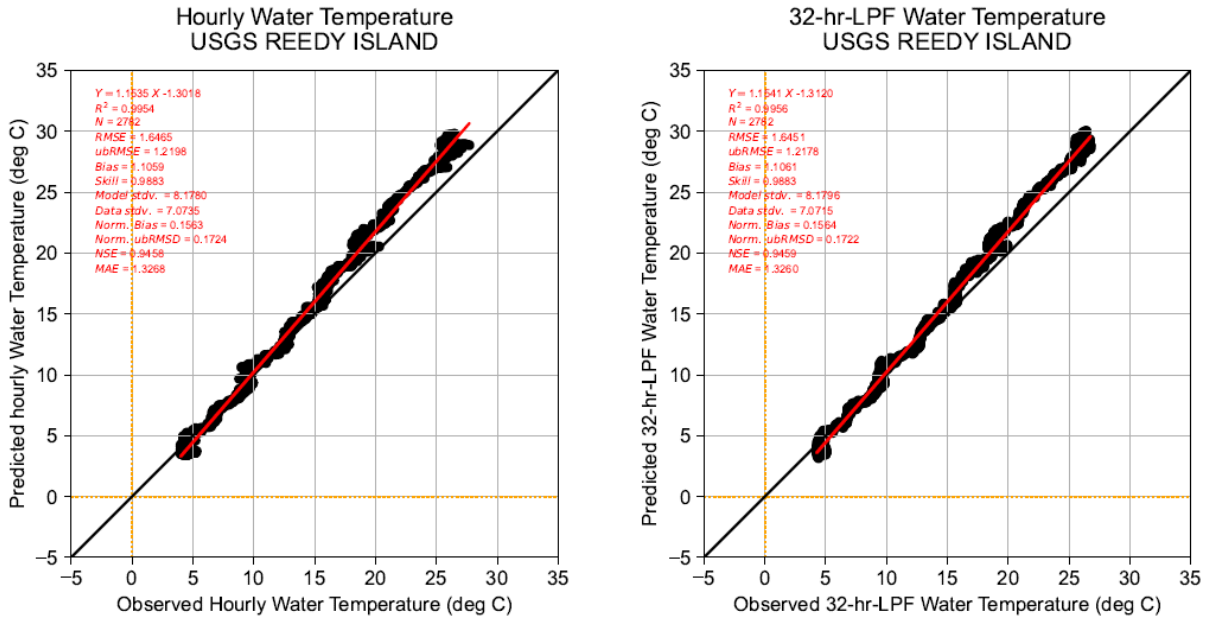

Figure 4.3-33 (1) Observed and Predicted Water Temperature at USGS Station 01482800 Reedy Island during Critical Season from September to December 2016

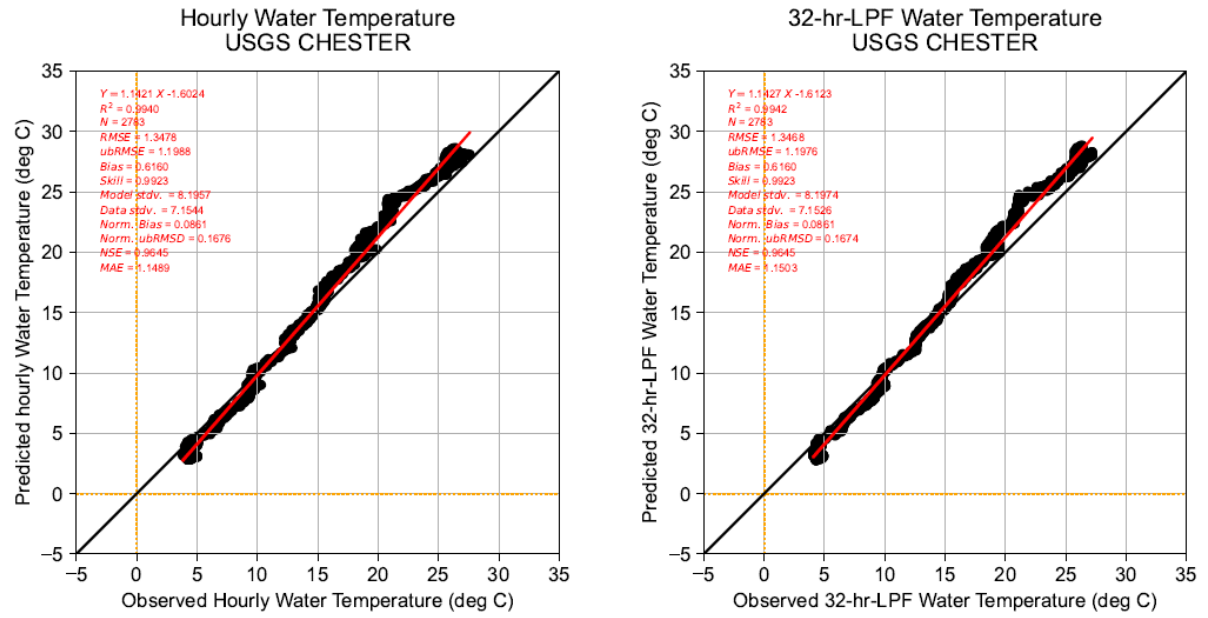

Figure 4.3-33 (2) Observed and Predicted Water Temperature at USGS Station 01477050 Chester during Critical Season from September to December 2016

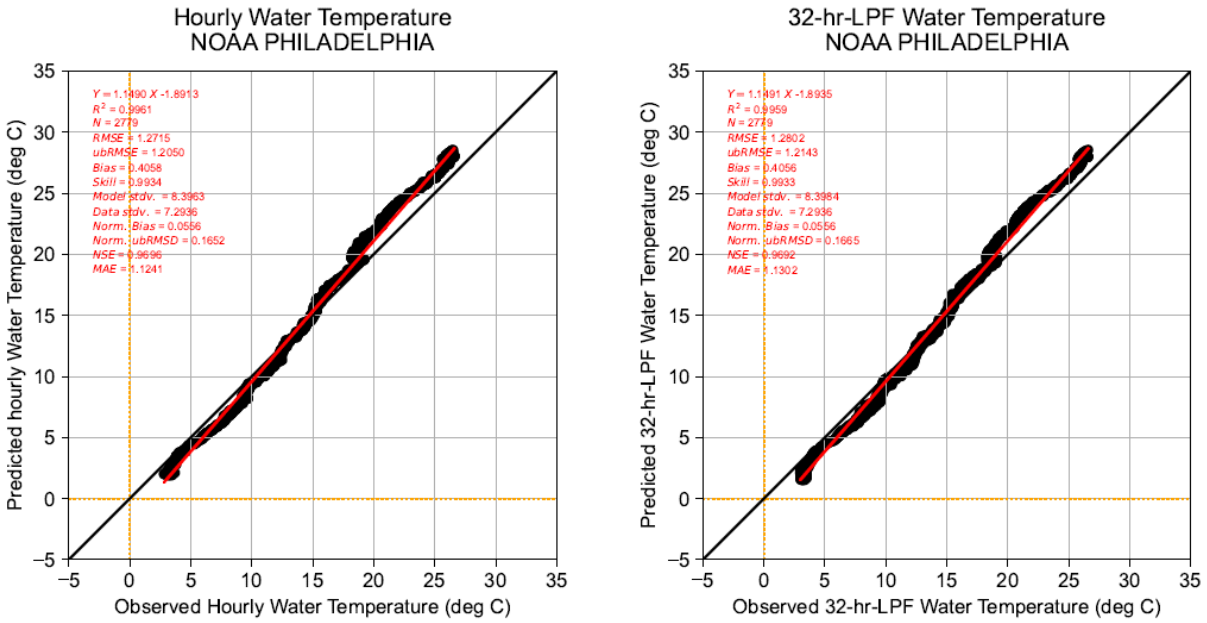

Figure 4.3-33 (3) Observed and Predicted Water Temperature at NOAA Station 8545240 Philadelphia during Critical Season from September to December 2016

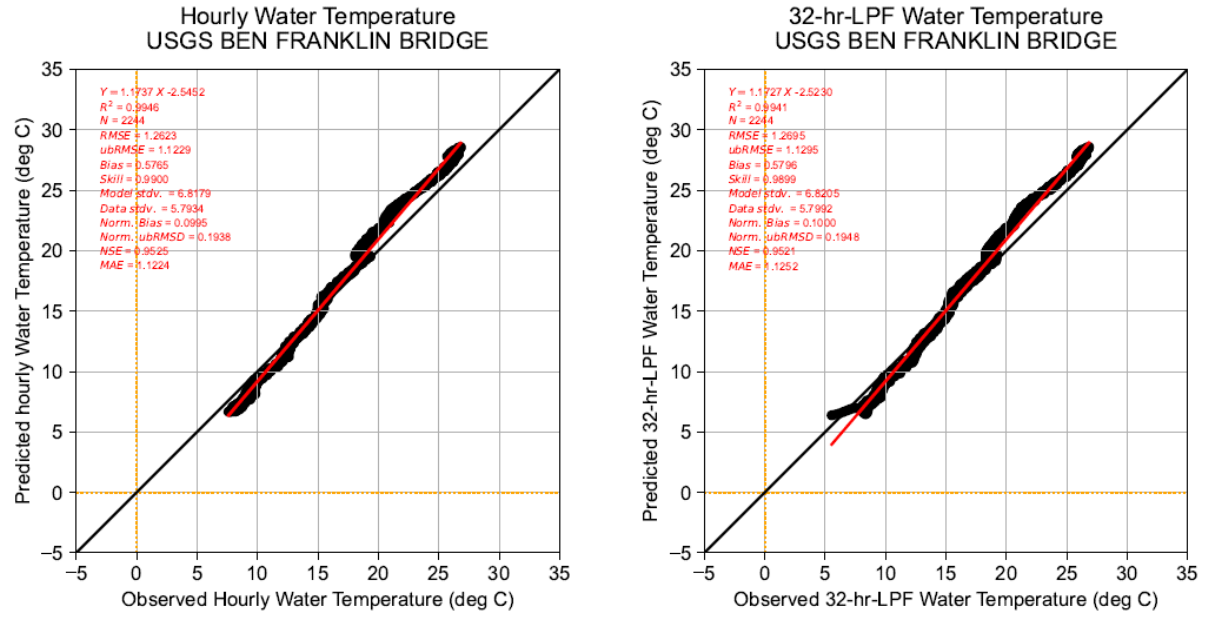

Figure 4.3-33 (4) Observed and Predicted Water Temperature at USGS Station 01467200 Ben Franklin Bridge during Critical Season from September to December 2016

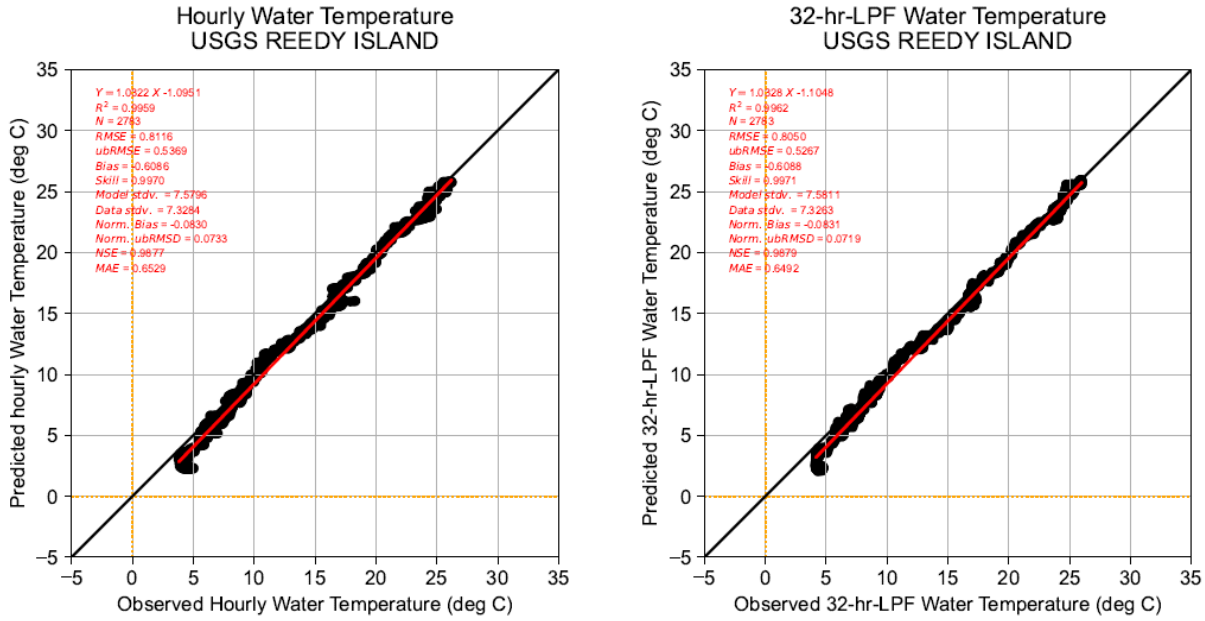

Figure 4.3-34 (1) Observed and Predicted Water Temperature at USGS Station 01482800 Reedy Island during Critical Season from September to December 2019

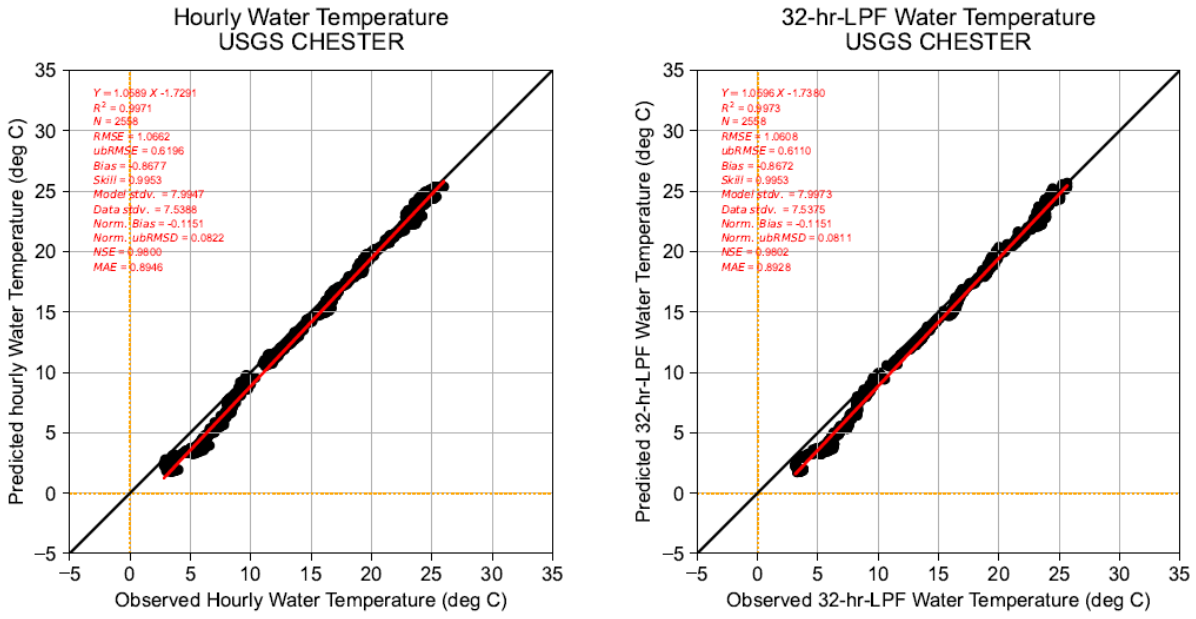

Figure 4.3-34 (2) Observed and Predicted Water Temperature at USGS Station 01477050 Chester during Critical Season from September to December 2019

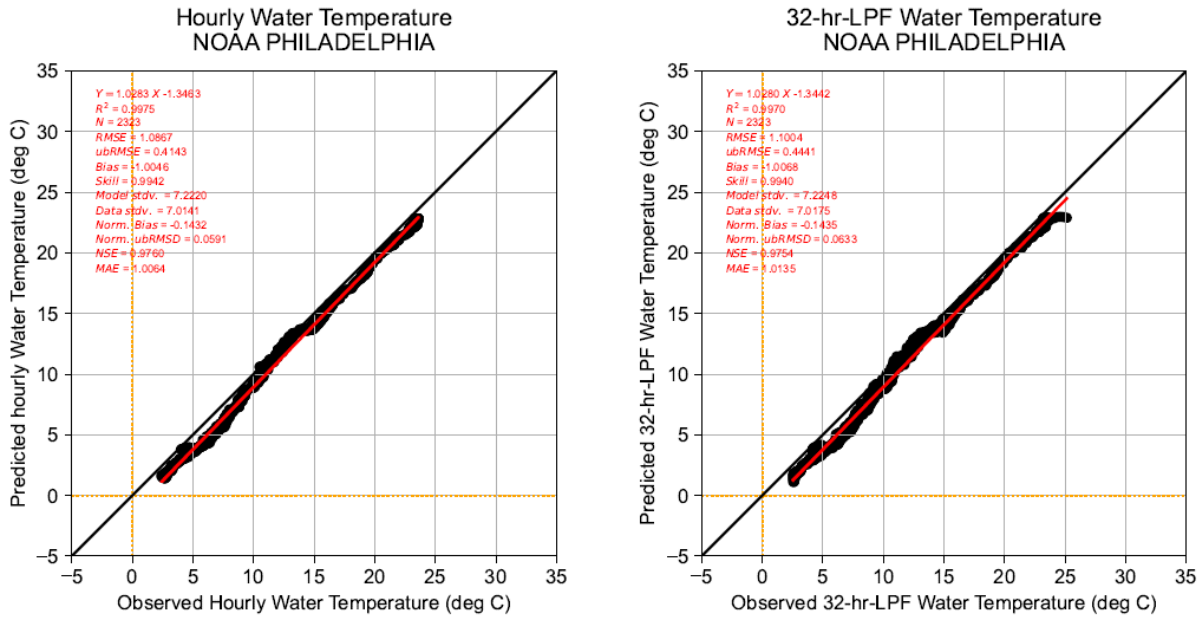

Figure 4.3-34 (3) Observed and Predicted Water Temperature at NOAA Station 8545240 Philadelphia during Critical Season from September to December 2019

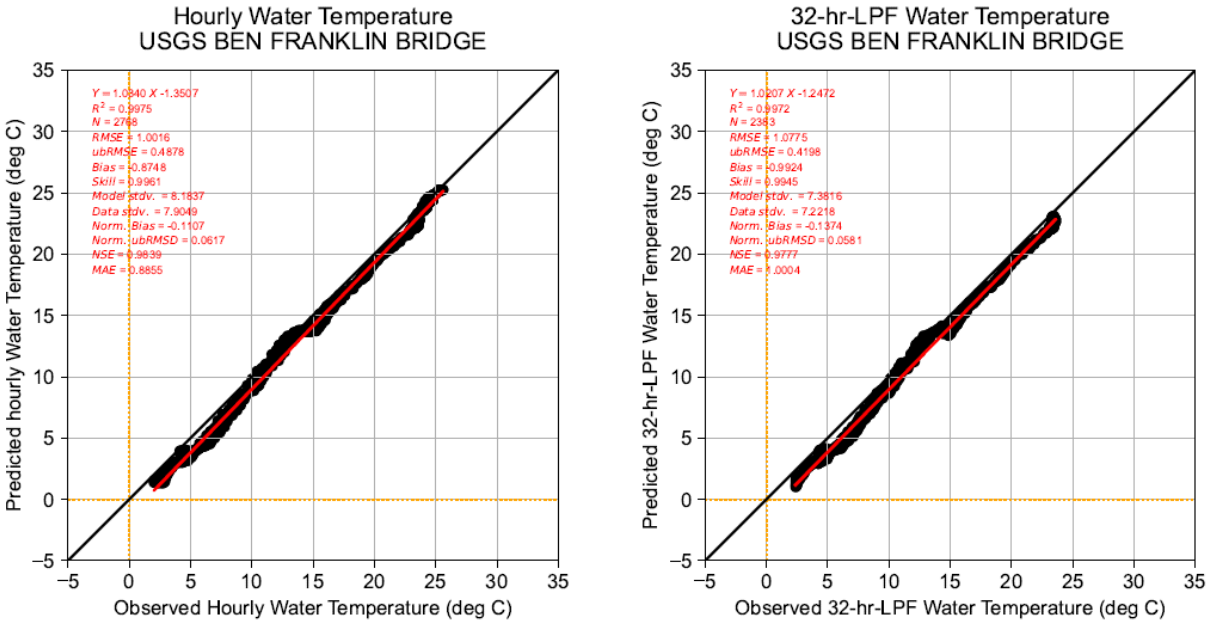

Figure 4.3-34 (4) Observed and Predicted Water Temperature at USGS Station 01467200 Ben Franklin Bridge during Critical Season from September to December 2019

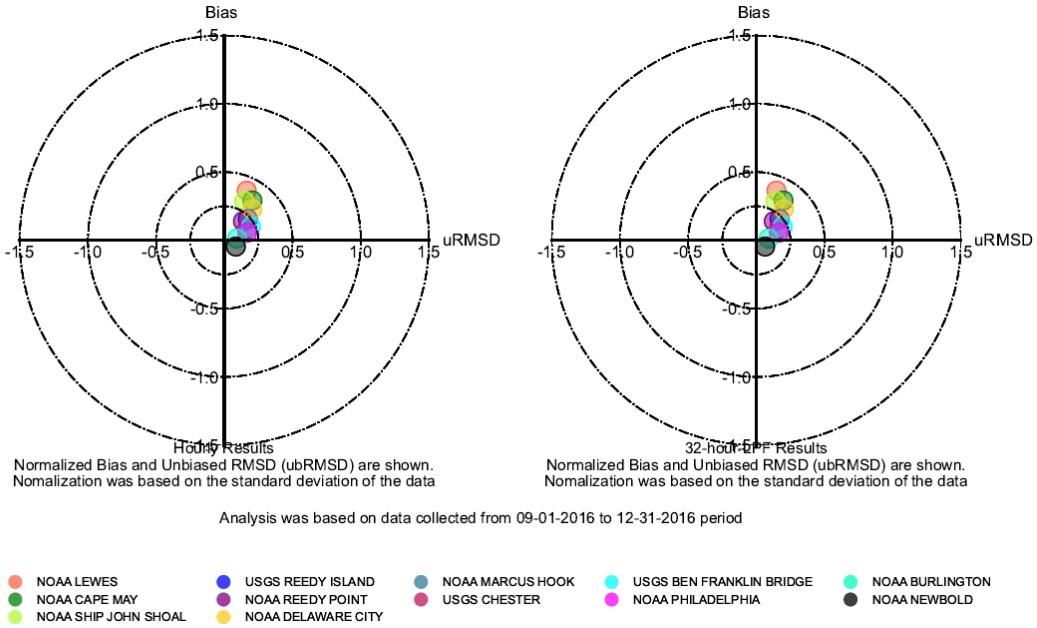

Figure 4.3-35 Target Diagram for the Observed and Predicted Hourly and 32-hour-LPF Near-Surface Water Temperature during Critical Season from September to December 2016

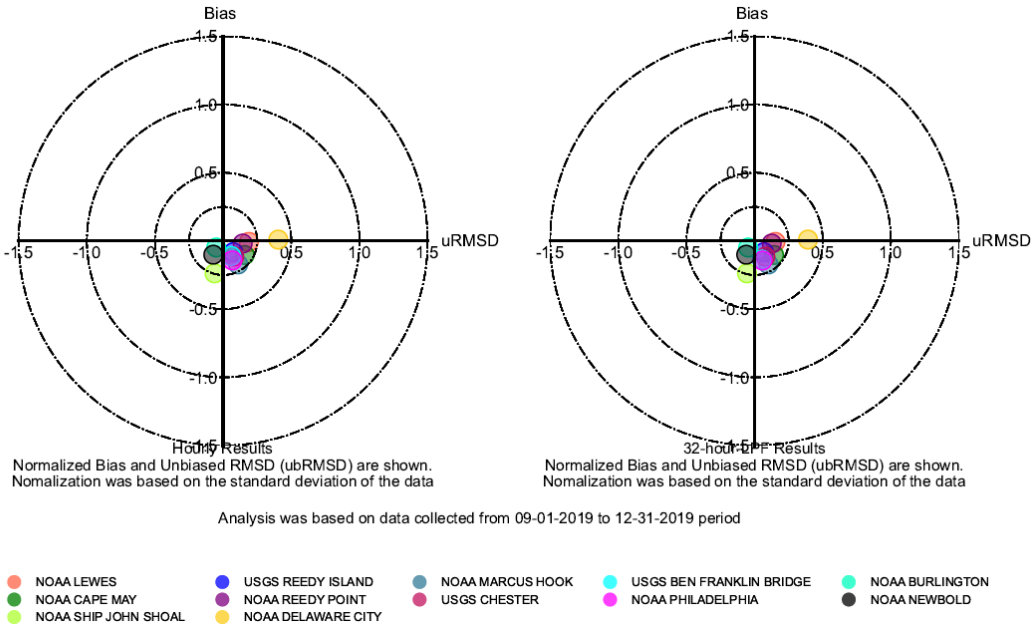

Figure 4.3-36 Target Diagram for the Observed and Predicted Hourly and 32-hour-LPF Near-Surface Water Temperature during Critical Season from September to December 2019

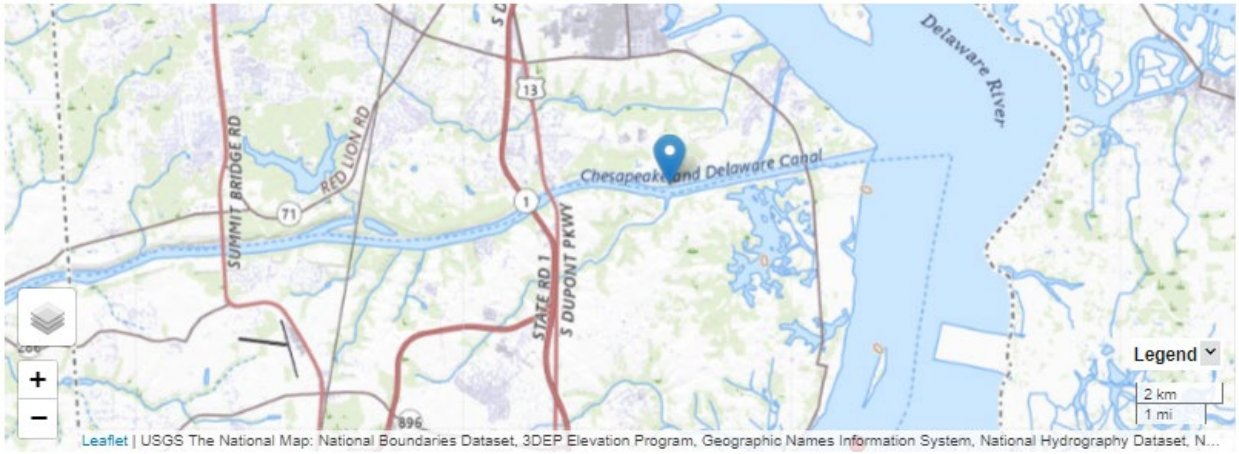

https://waterdata.usgs.gov/monitoring-location/01482695/#parameterCode=72137&ts_id=310374&period=P7D&showMedian=true

Figure 4.3-37 Location of USGS Gage (01482695) at C And D Canal NR Delaware City, DE

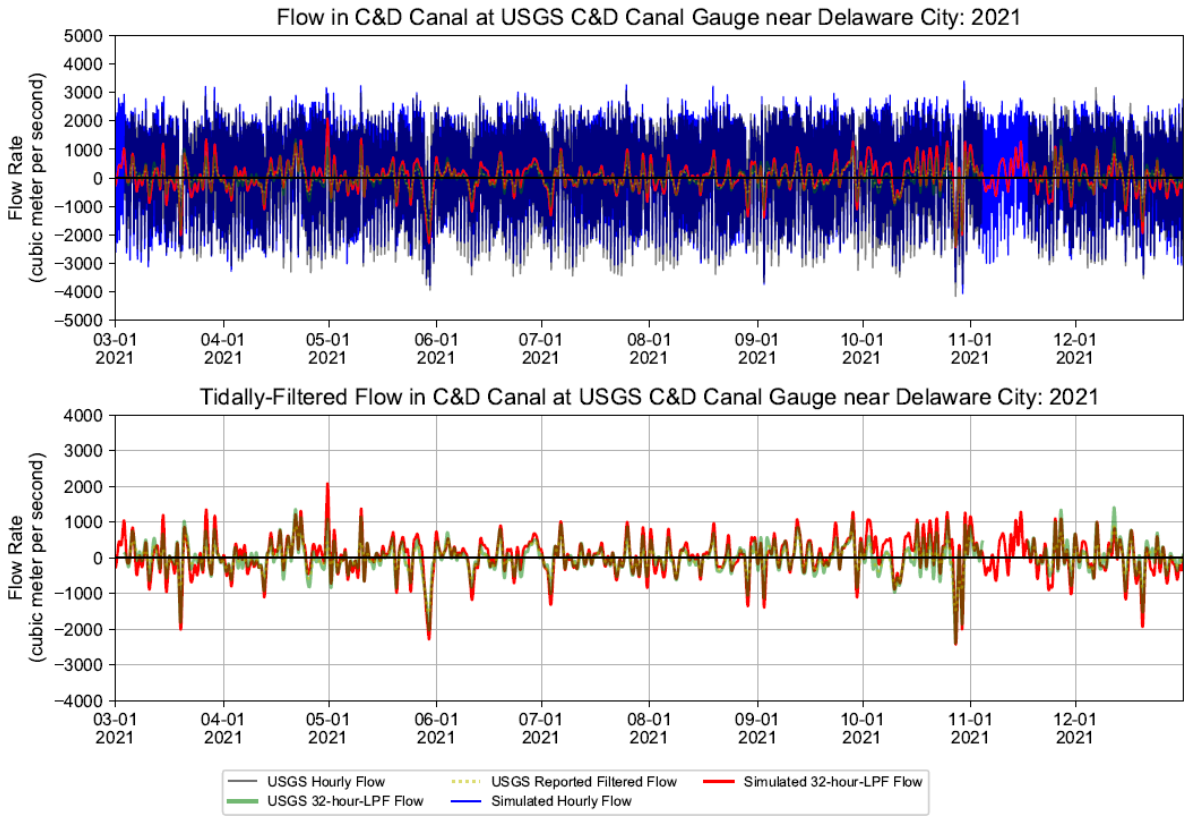

Figure 4.3-38 Simulated and Observed Hourly and Tidally filtered Flow in C&D Canal at USGS C&D Canal Gauge during March through December 2021

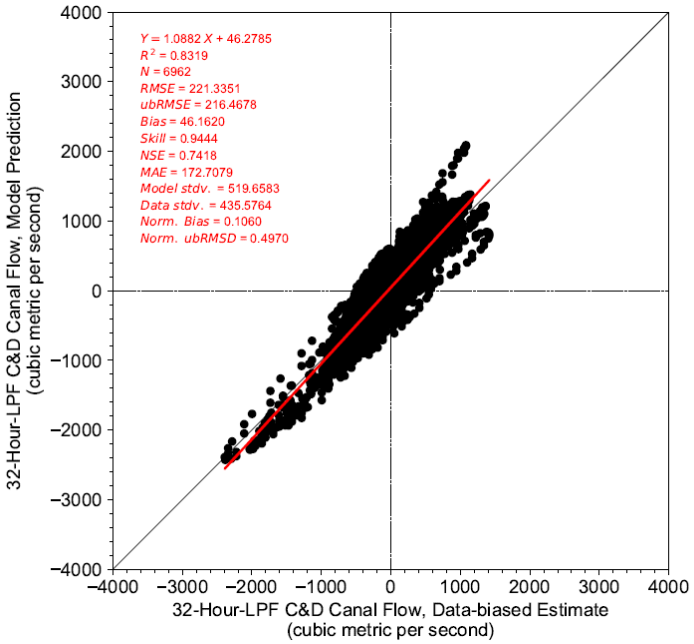

Figure 4.3-39 Comparison of Simulated and Observed 32-hour-Low-Pass filtered Flow at USGS C&D Canal Gauge during March through December 2021

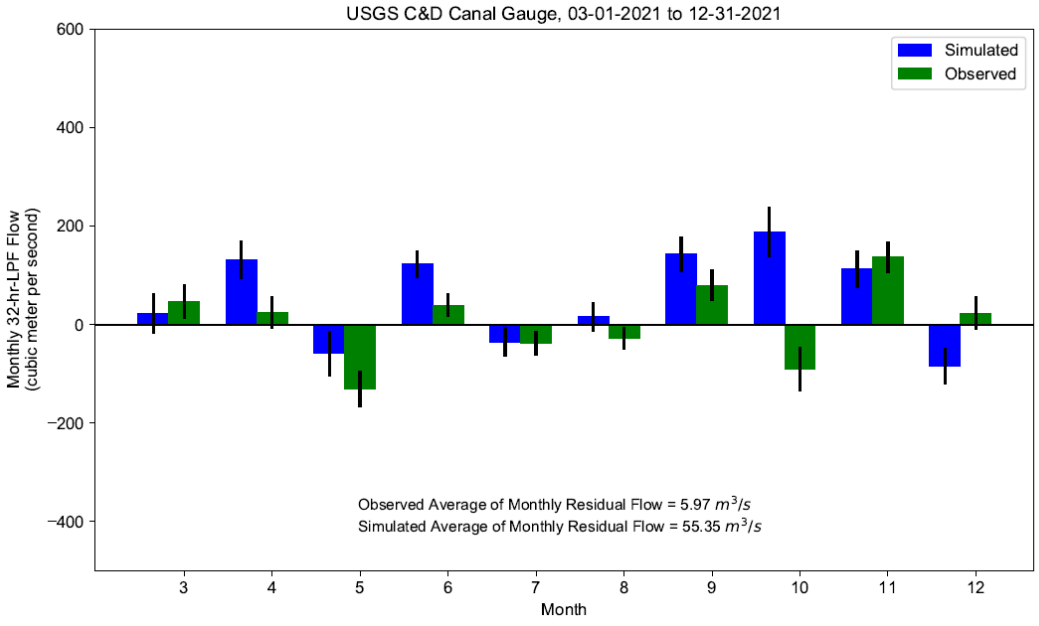

Figure 4.3-40 Simulated and Observed Monthly Residual Flow ("Net Flow") in C&D Canal at USGS C&D Canal Gauge during March through December 2021

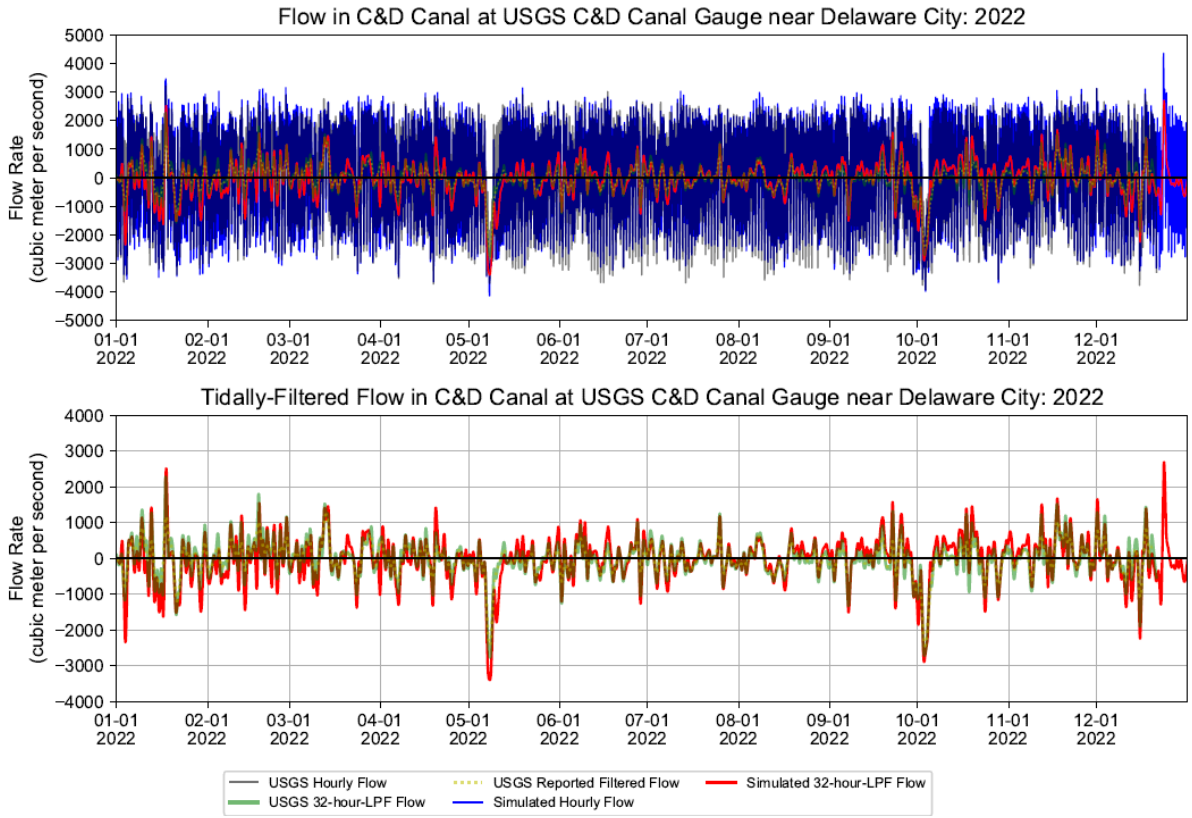

Figure 4.3-41 Simulated and Observed Hourly and Tidally filtered Flow in C&D Canal at USGS C&D Canal Gauge during March through December 2022

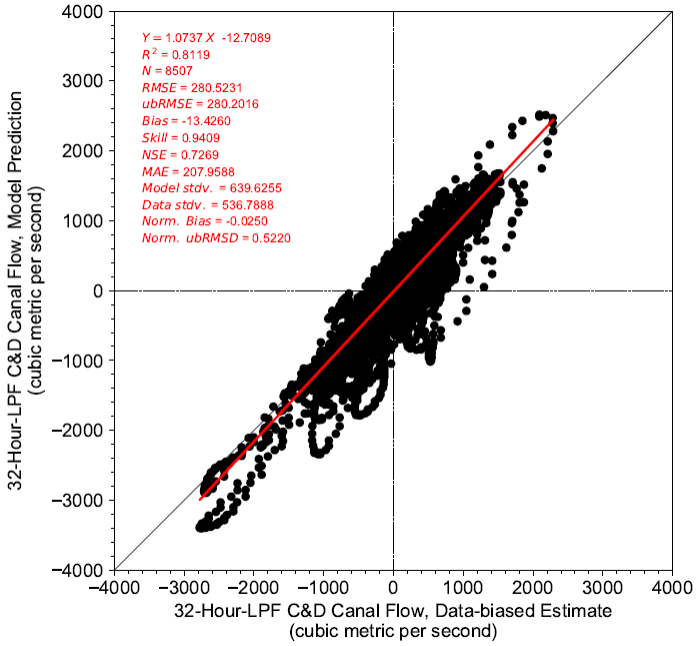

Figure 4.3-42 Comparison of Simulated and Observed 32-hour-Low-Pass filtered Flow at USGS C&D Canal Gauge during March through December 2022

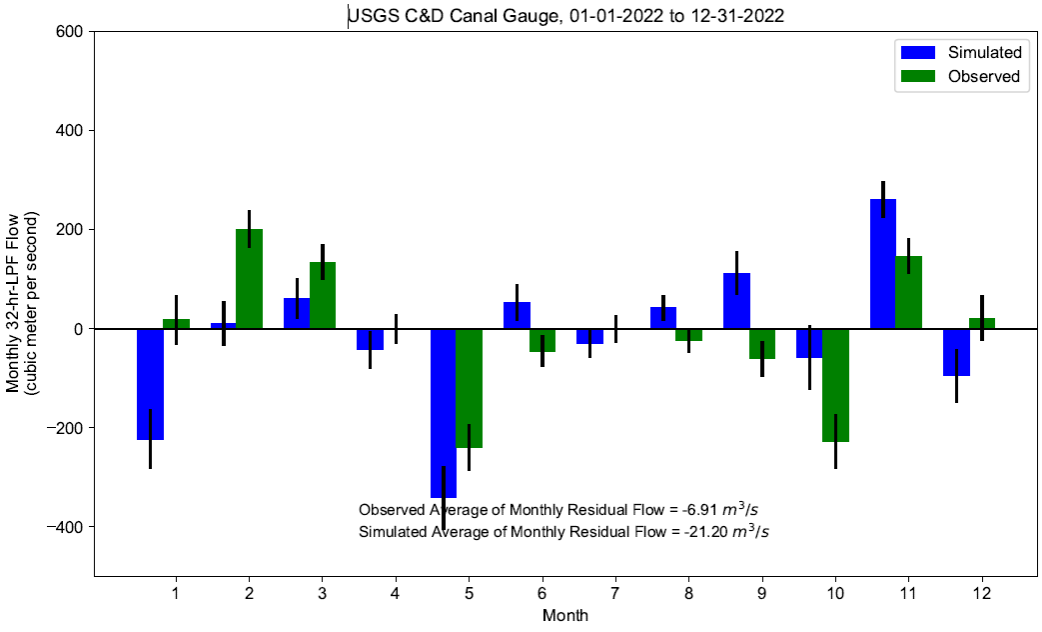

Figure 4.3-43 Simulated and Observed Monthly Residual Flow ("Net Flow") in C&D Canal at USGS C&D Canal Gauge during March through December 2022

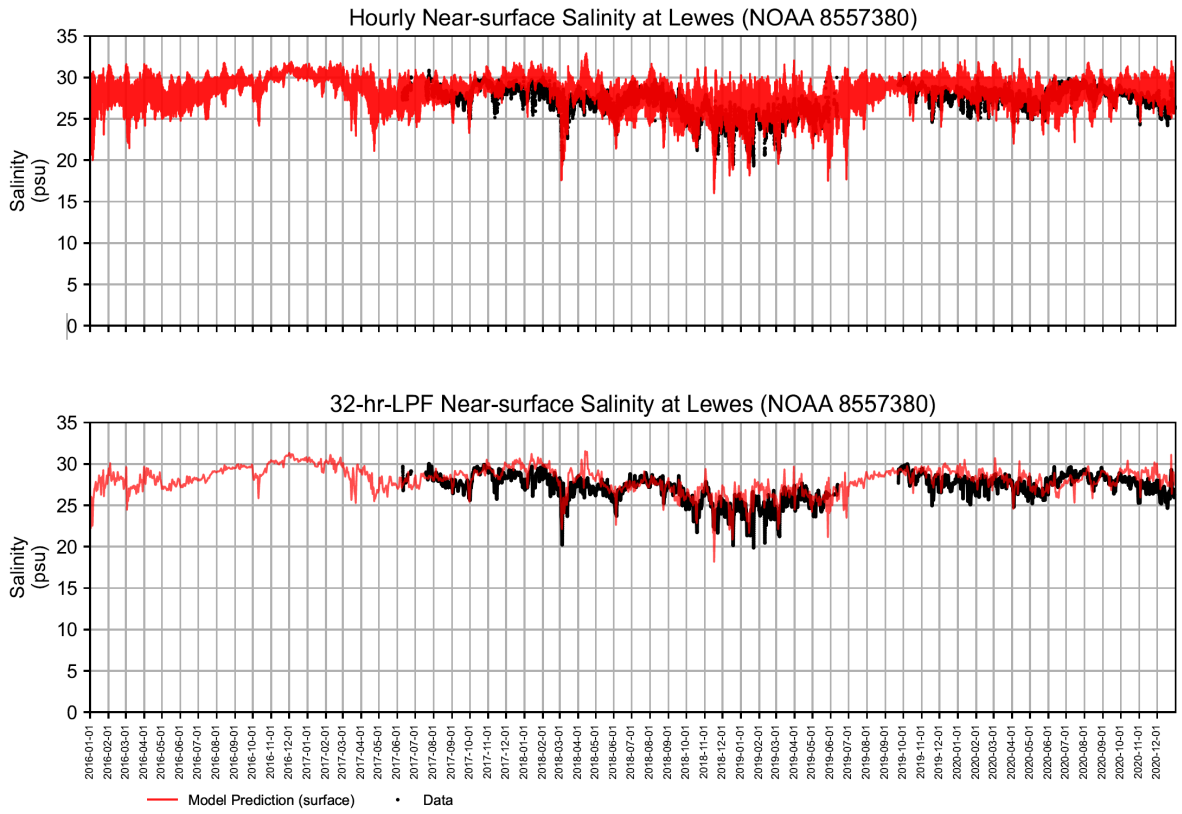

Notes: Salinity data was derived from conductivity and water temperature based on Standard Methods for the Examination of Water and Wastewater, 19th Ed. 1995.

Figure 4.3-44 (1) Time History of Observed and Simulated Near-surface Hourly and 32-HR-LPFSalinity during 2016 to 2020 Period at NOAA 8557380 at Lewes, DE.

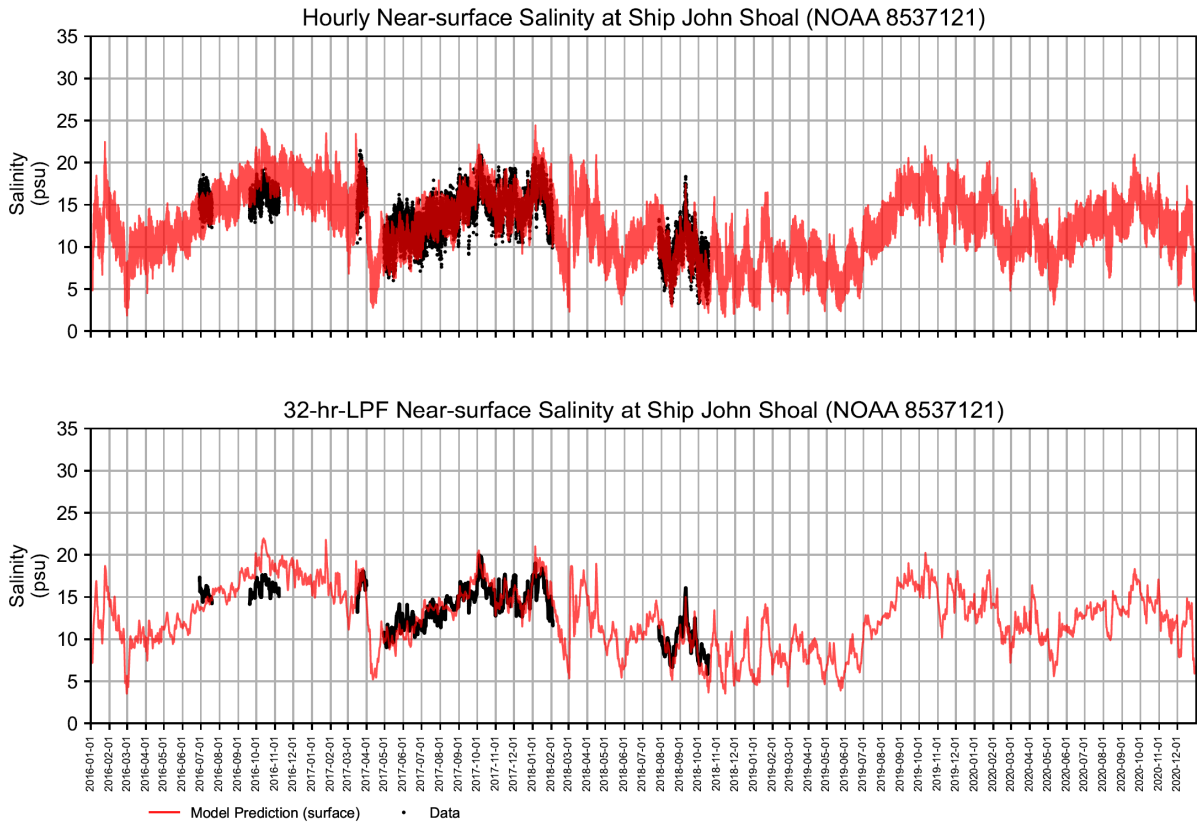

Notes: Salinity data was derived from conductivity and water temperature based on Standard Methods for the Examination of Water and Wastewater, 19th Ed. 1995.

Figure 4.3-44 (2) Time History of Observed and Simulated Near-surface Hourly and 32-HR-LPFSalinity during 2016 to 2020 Period at NOAA 8537121 at Ship John Shoal.

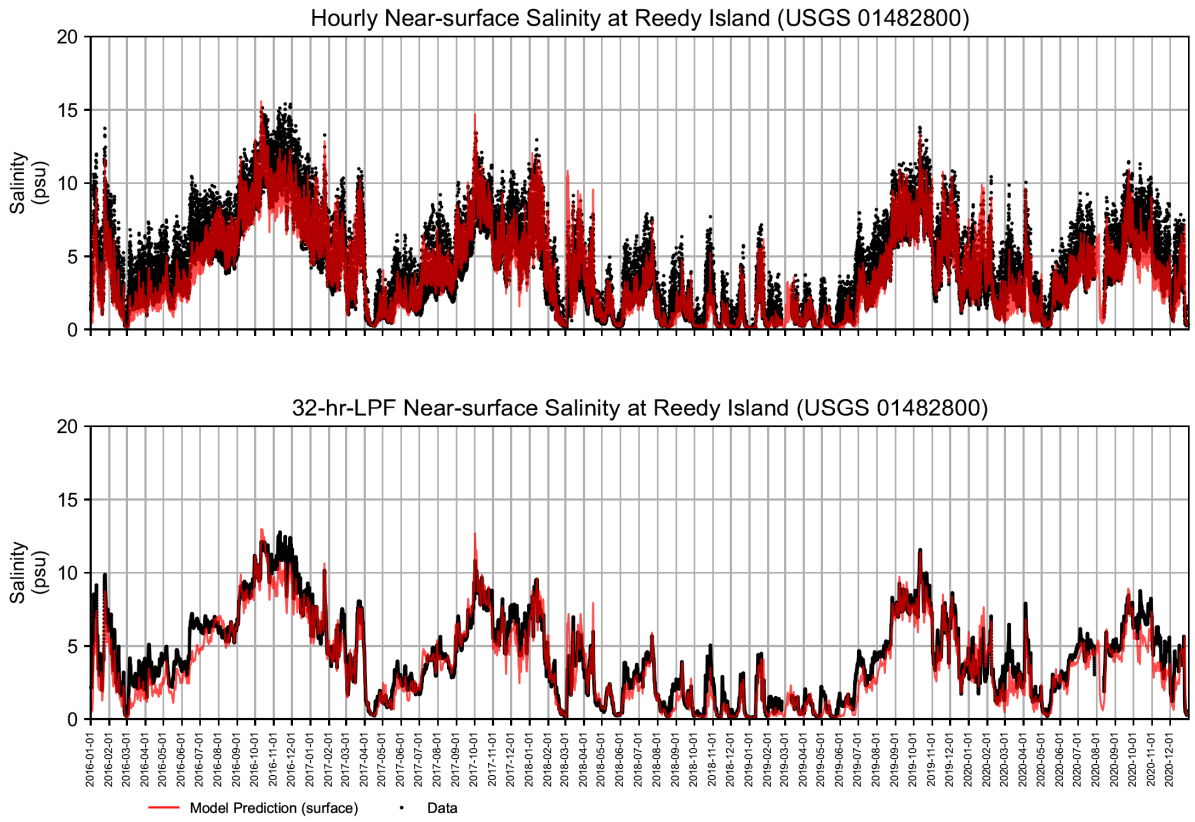

Notes: Salinity data was derived from specific conductance and water temperature based on Standard Methods for the Examination of Water and Wastewater, 19th Ed. 1995.

Figure 4.3-44 (3) Time History of Observed and Simulated Near-surface Hourly and 32-HR-LPF Salinity during 2016 to 2020 Period at USGS 01482800 at Reedy Island Jetty, DE.

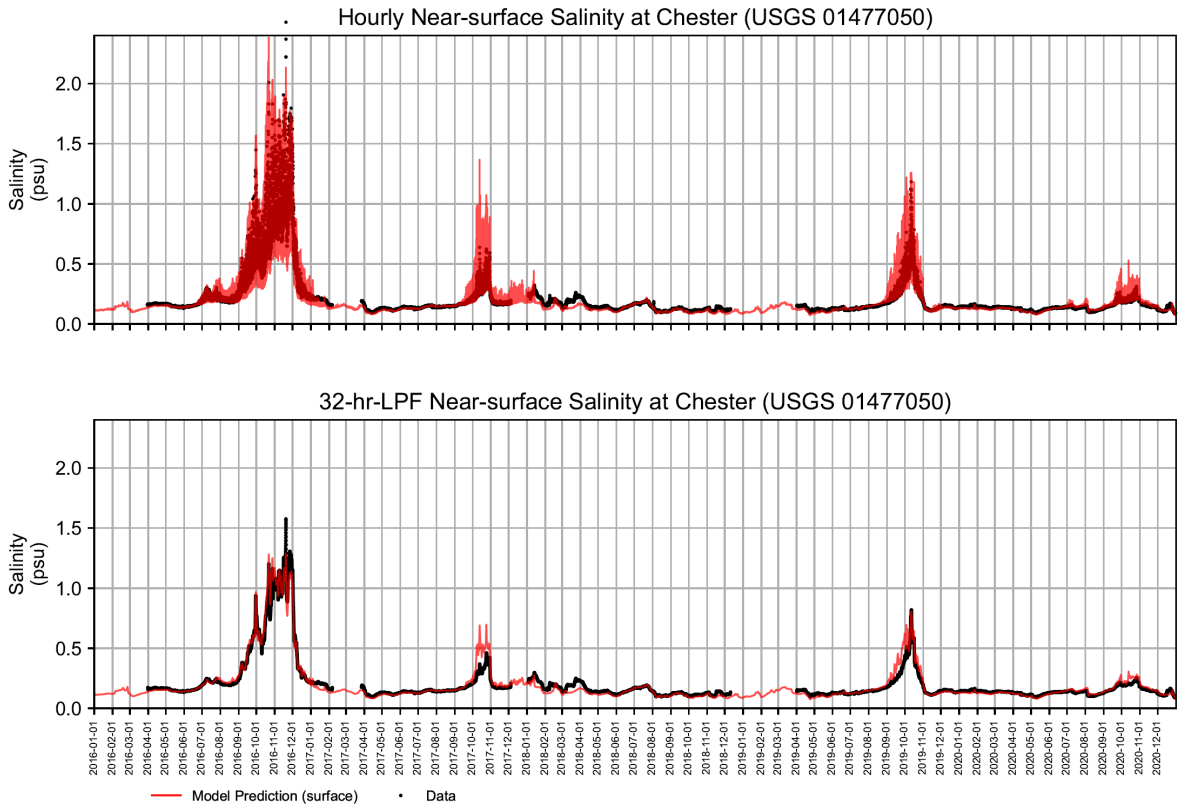

Notes: Salinity data was derived from specific conductance and water temperature based on Standard Methods for the Examination of Water and Wastewater, 19th Ed. 1995.

Figure 4.3-44 (4) Time History of Observed and Simulated Near-surface Hourly and 32-HR-LPF Salinity during 2016 to 2020 Period at USGS 01477050 at Chester, PA.

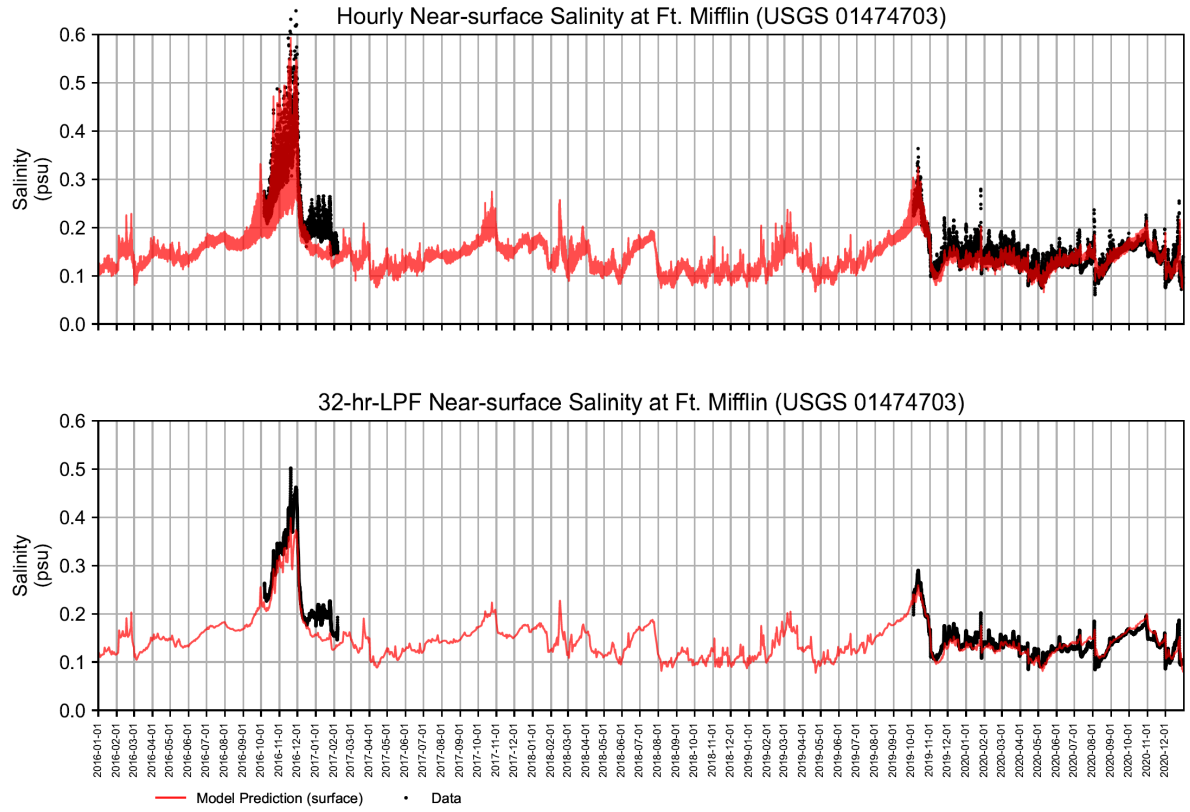

Notes: Salinity data was derived from specific conductance and water temperature based on Standard Methods for the Examination of Water and Wastewater, 19th Ed. 1995.

Figure 4.3-44 (5) Time History of Observed and Simulated Near-surface Hourly and 32-HR-LPF Salinity during 2016 to 2020 Period at USGS 01474703 at Fort Mifflin at Philadelphia, PA.

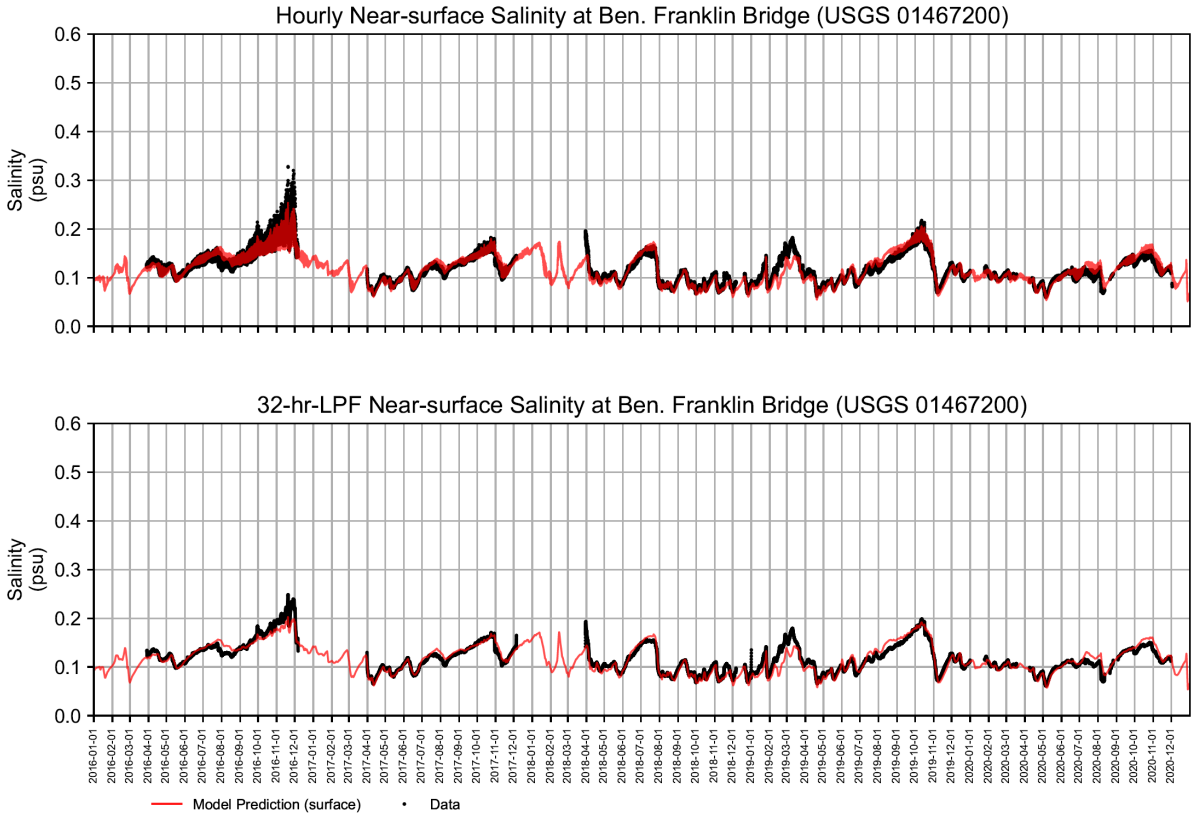

Notes: Salinity data was derived from specific conductance and water temperature based on Standard Methods for the Examination of Water and Wastewater, 19th Ed. 1995.

Figure 4.3-44 (6) Time History of Observed and Simulated Near-surface Hourly and 32-HR-LPF Salinity during 2016 to 2020 Period at USGS 01467200 Ben Franklin Bridge (now at Delaware River at Penn's Landing), Philadelphia, PA.

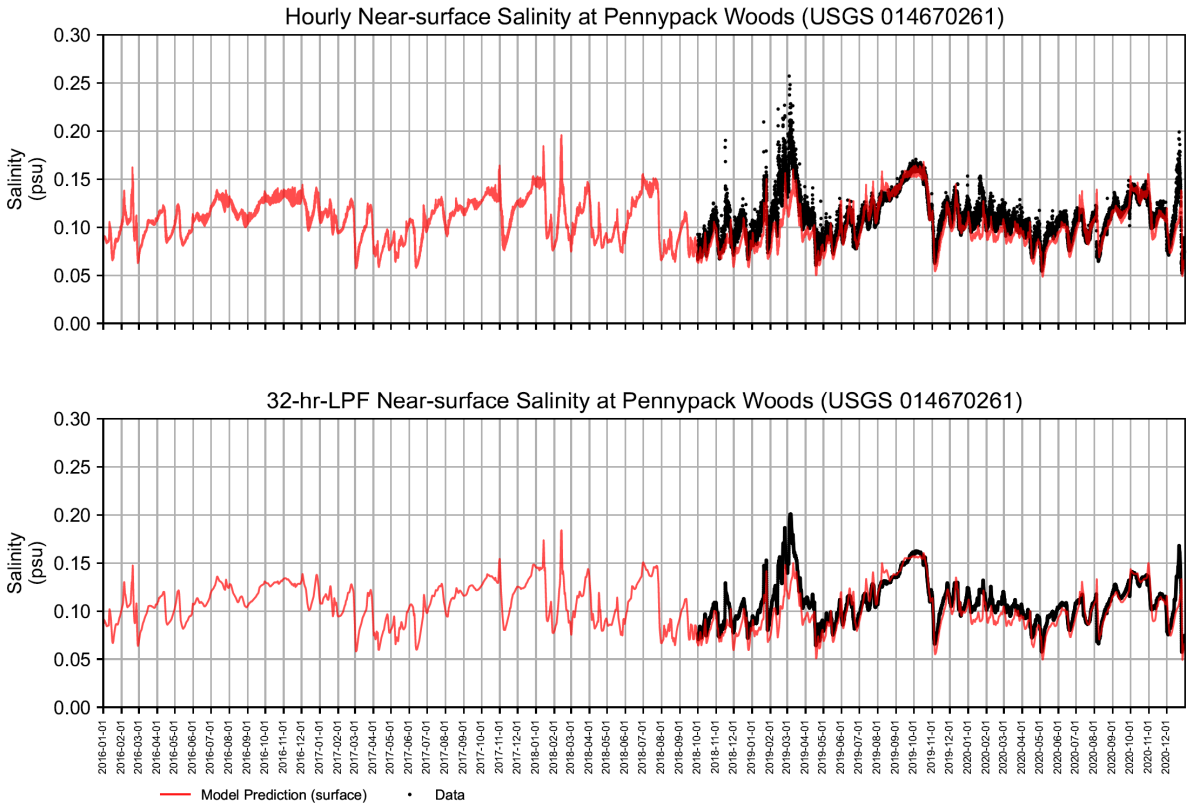

Notes: Salinity data was derived from specific conductance and water temperature based on Standard Methods for the Examination of Water and Wastewater, 19th Ed. 1995.

Figure 4.3-44 (7) Time History of Observed and Simulated Near-surface Hourly and 32-HR-LPF Salinity during 2016 to 2020 Period at USGS 014670261 Pennypack Woods, PA.

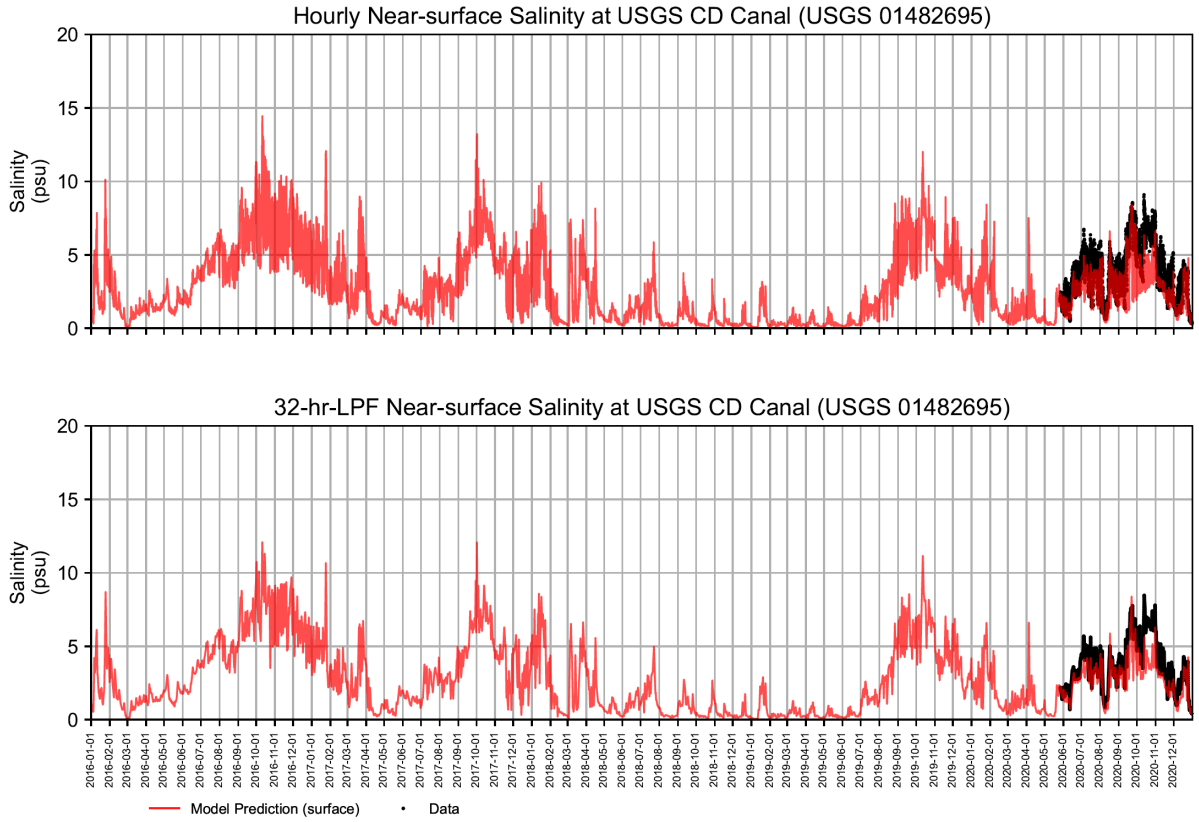

Notes: Salinity data was derived from specific conductance and water temperature based on Standard Methods for the Examination of Water and Wastewater, 19th Ed. 1995.

Figure 4.3-44 (8) Time History of Observed and Simulated Near-surface Hourly and 32-HR-LPF Salinity during 2016 to 2020 Period at USGS 01482695 C&D Canal near Delaware City, DE.

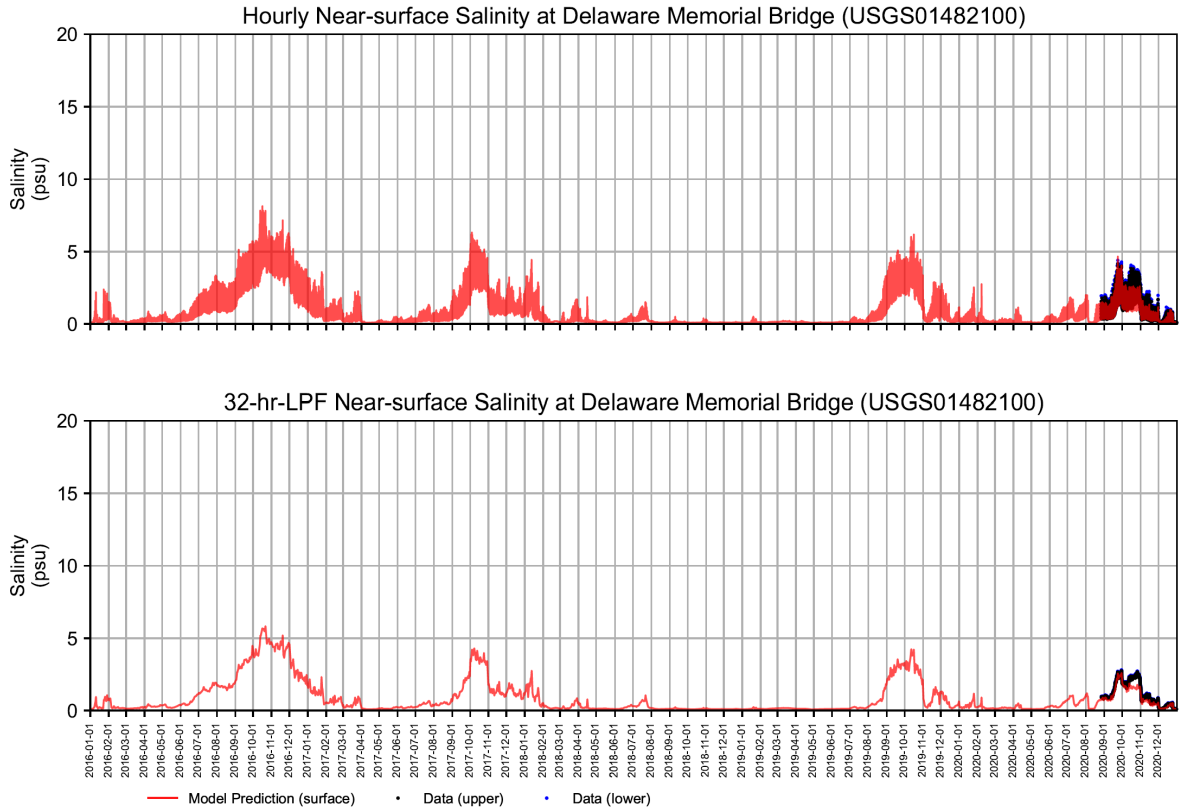

Notes: Salinity data was derived from specific conductance and water temperature based on Standard Methods for the Examination of Water and Wastewater, 19th Ed. 1995.

Figure 4.3-44 (9) Time History of Observed and Simulated Near-surface Hourly and 32-HR-LPF Salinity during 2016 to 2020 Period at USGS 01482100 Delaware River at Delaware Memorial Bridge at Wilmington DE.

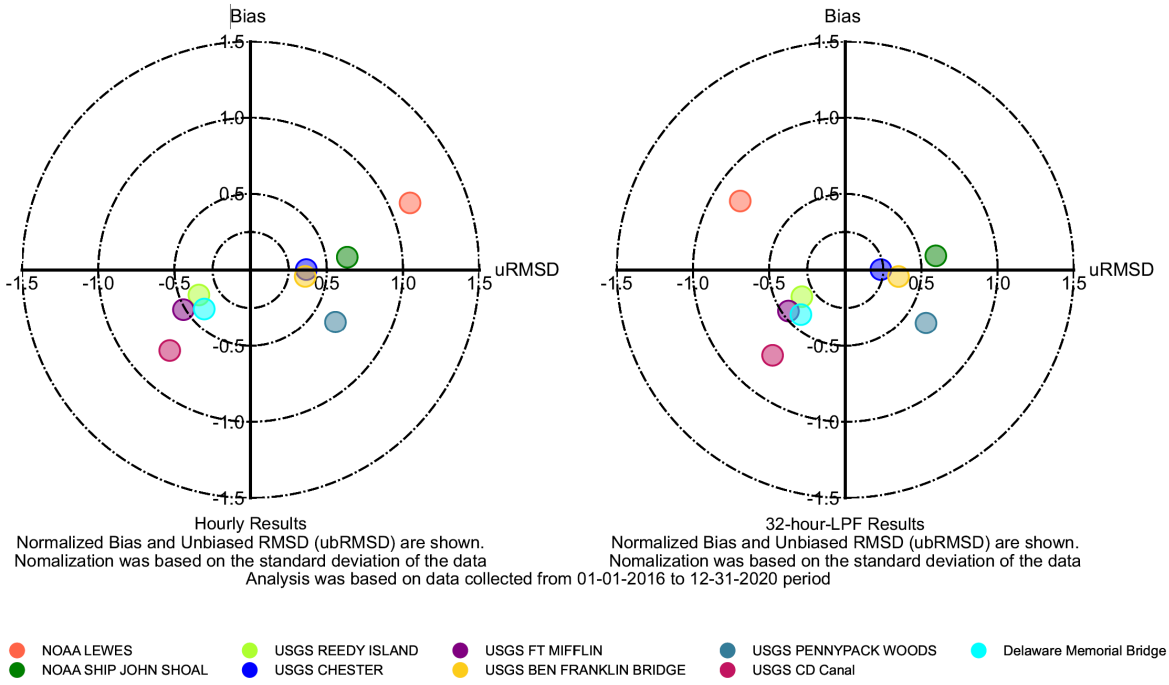

Figure 4.3-45 Target Diagram for the Observed and Predicted Hourly and 32-hour-LPF Near-Surface Salinity during 2016 to 2020 Period

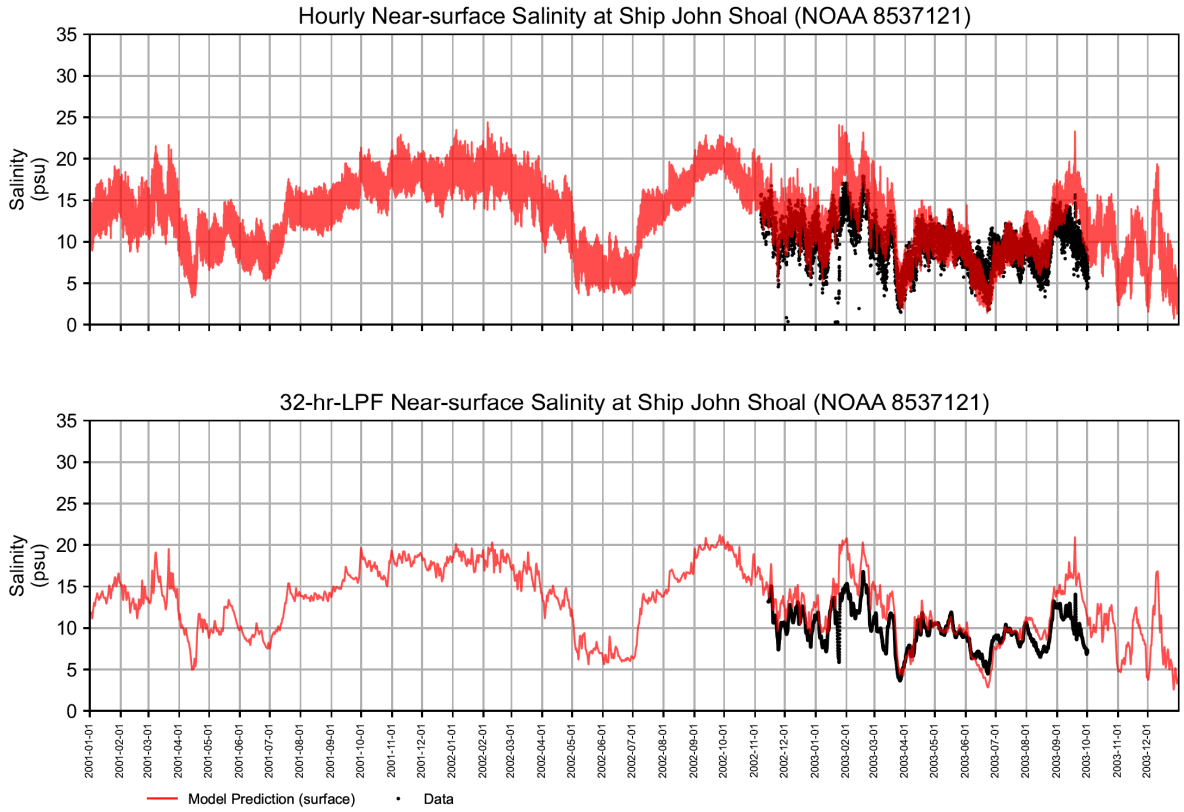

Notes: Salinity data was derived from conductivity and water temperature based on Standard Methods for the Examination of Water and Wastewater, 19th Ed. 1995.

Figure 4.3-46 (1) Time History of Observed and Simulated Near-surface Hourly and 32-HR-LPF Salinity during 2001 to 2003 Period at NOAA 8537121 at Ship John Shoal.

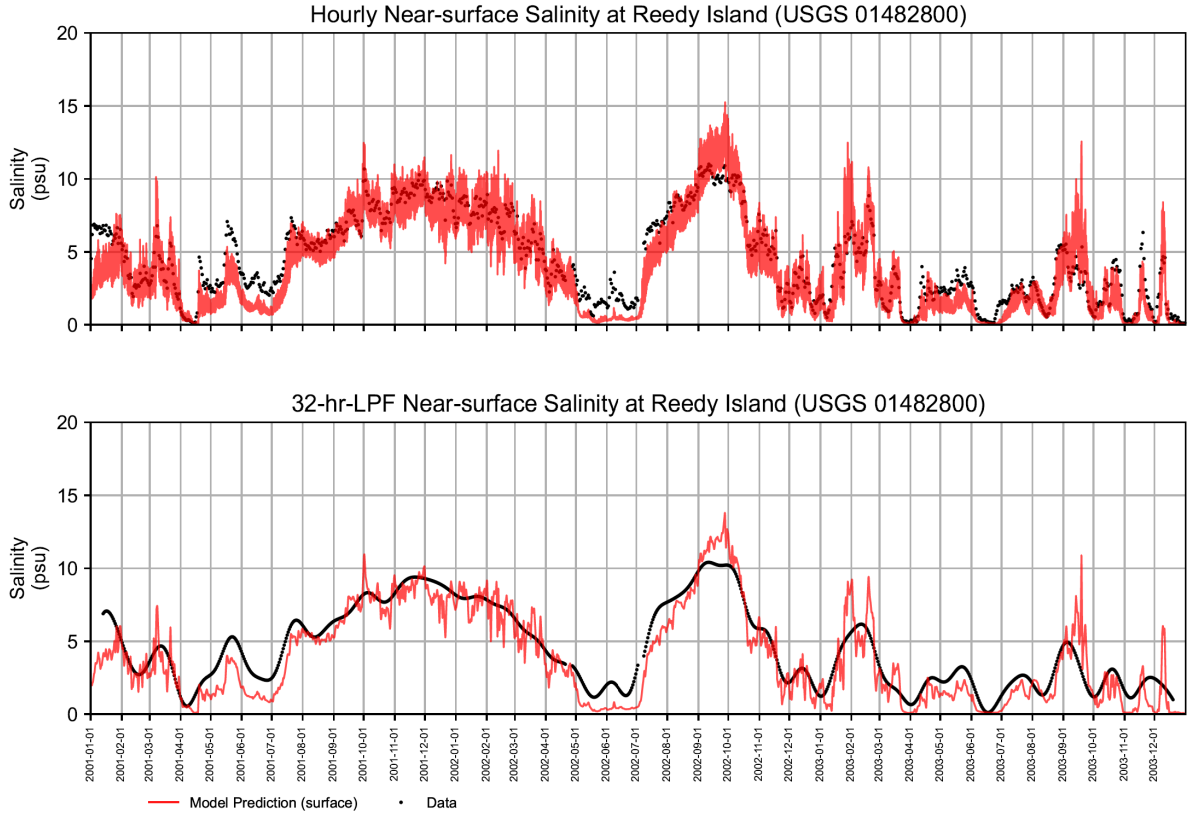

Notes: Salinity data was derived from specific conductance and water temperature based on Standard Methods for the Examination of Water and Wastewater, 19th Ed. 1995.

Figure 4.3-46 (2) Time History of Observed and Simulated Near-surface Hourly and 32-HR-LPF Salinity during 2001 to 2003 Period at USGS 01482800 at Reedy Island Jetty, DE.

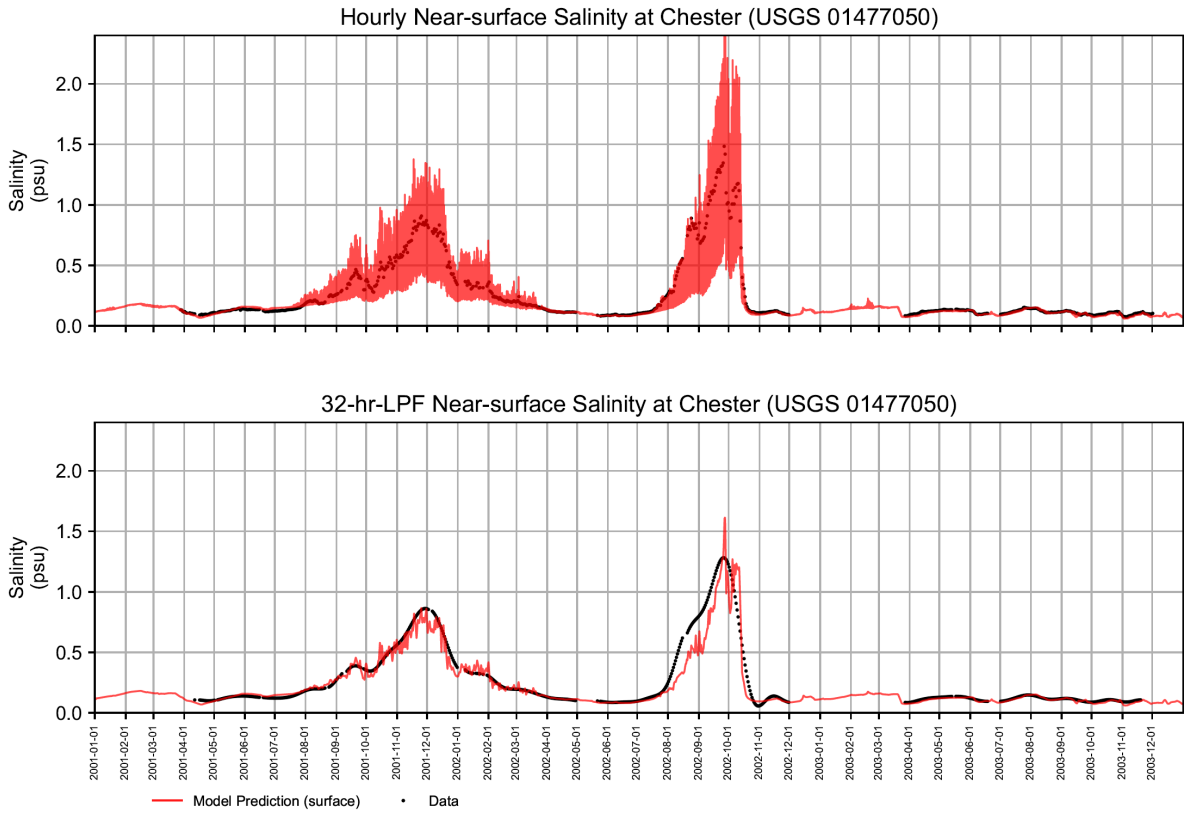

Notes: Salinity data was derived from specific conductance and water temperature based on Standard Methods for the Examination of Water and Wastewater, 19th Ed. 1995.

Figure 4.3-46 (3) Time History of Observed and Simulated Near-surface Hourly and 32-HR-LPF Salinity during 2001 to 2003 Period at USGS 01477050 at Chester, PA.

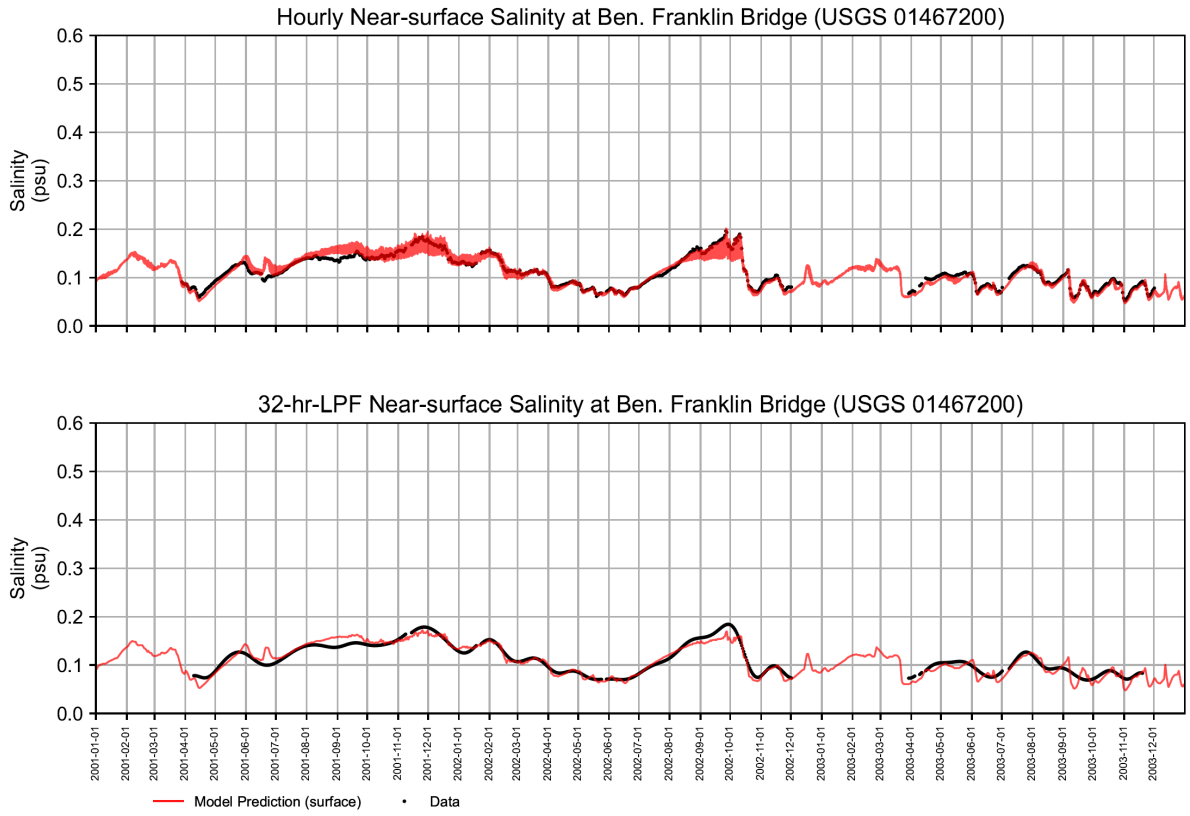

Notes: Salinity data was derived from specific conductance and water temperature based on Standard Methods for the Examination of Water and Wastewater, 19th Ed. 1995.

Figure 4.3-46 (4) Time History of Observed and Simulated Near-surface Hourly and 32-HR-LPF Salinity during 2001 to 2003 Period at USGS 01467200 Ben Franklin Bridge (now at Delaware River at Penn's Landing), Philadelphia, PA.

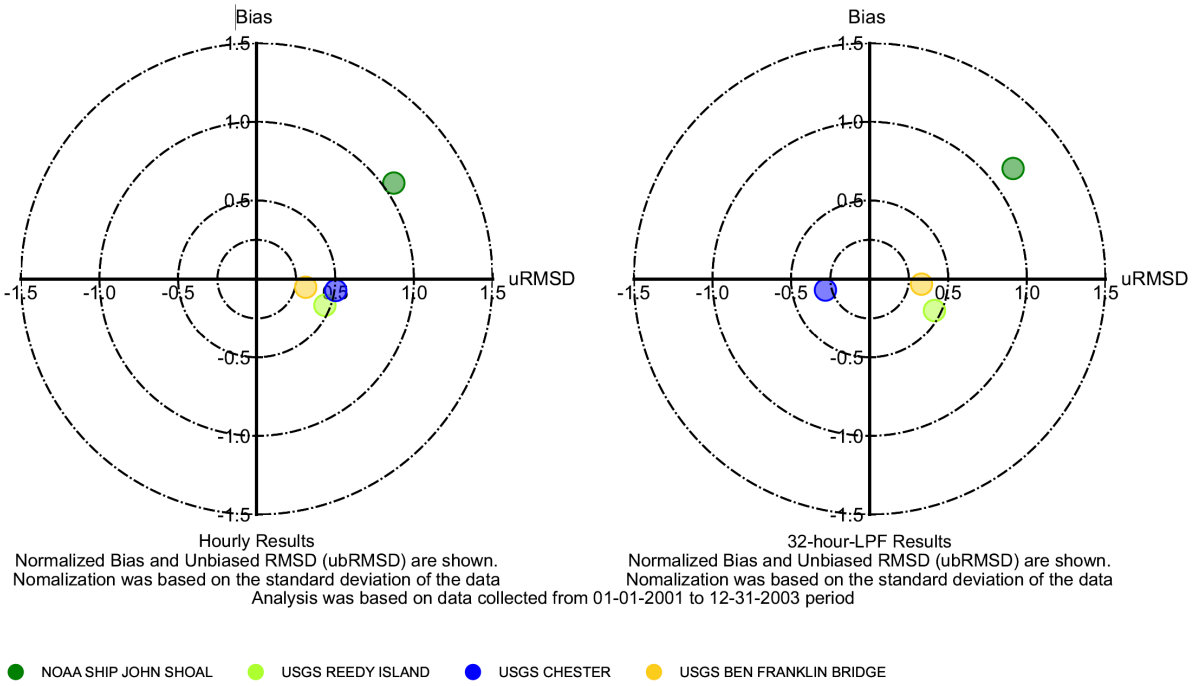

Figure 4.3-47 Target Diagram for the Observed and Predicted Hourly and 32-hour-LPF Near-Surface Salinity during 2001 to 2003 Period

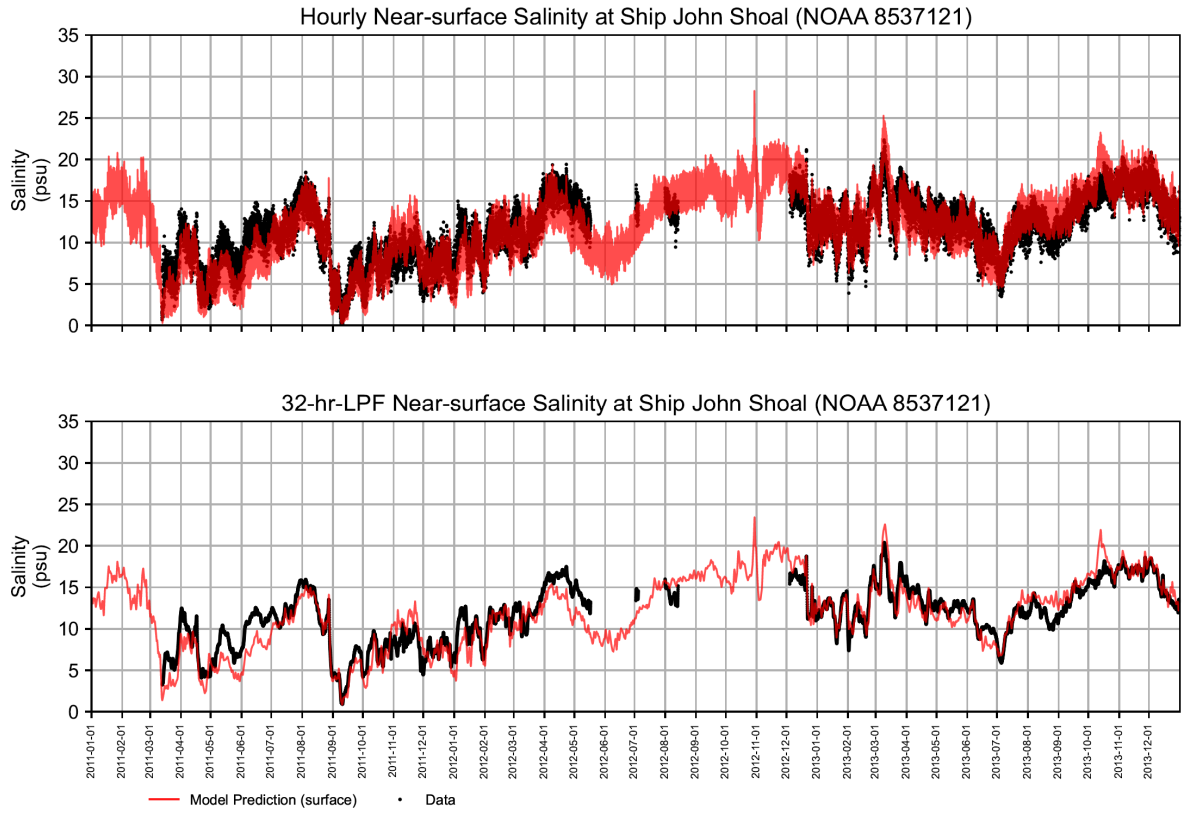

Notes: Salinity data was derived from conductivity and water temperature based on Standard Methods for the Examination of Water and Wastewater, 19th Ed. 1995.

Figure 4.3-48 (1) Time History of Observed and Simulated Near-surface Hourly and 32-HR-LPF Salinity during 2011 to 2013 Period at NOAA 8537121 at Ship John Shoal.

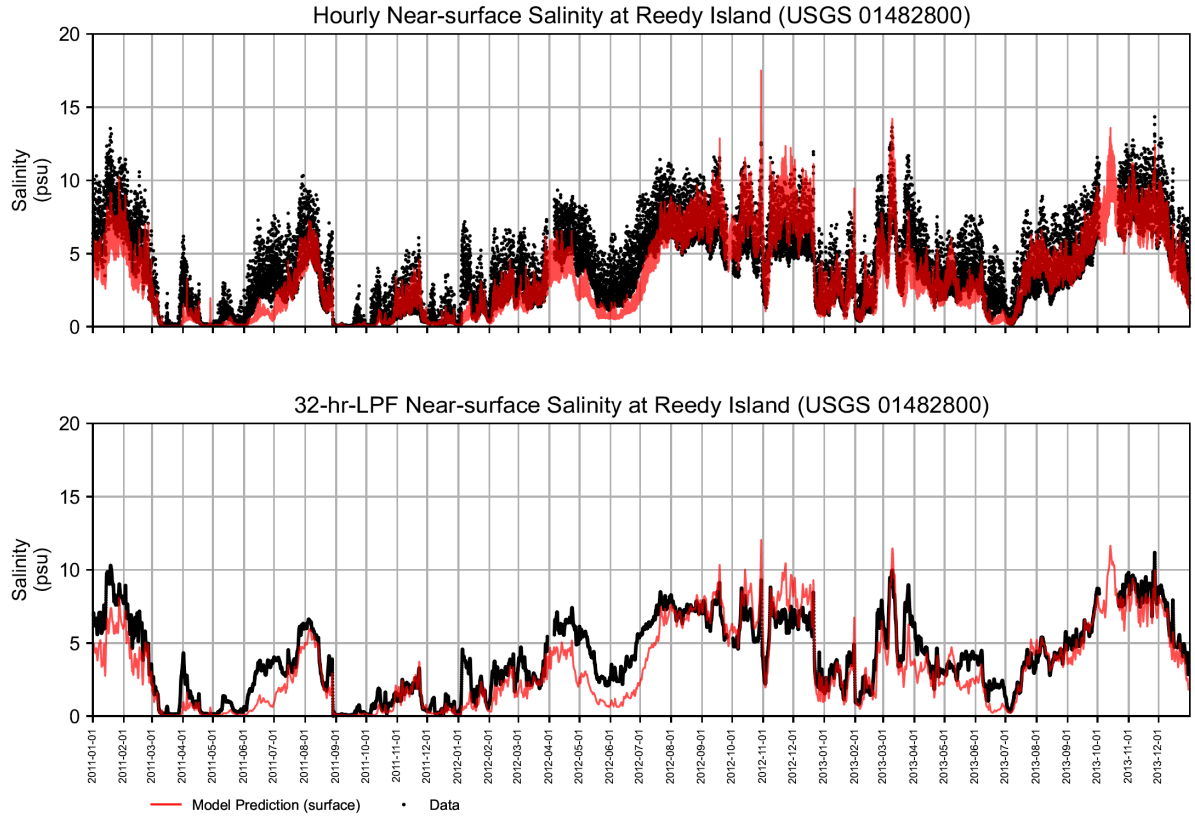

Notes: Salinity data was derived from specific conductance and water temperature based on Standard Methods for the Examination of Water and Wastewater, 19th Ed. 1995.

Figure 4.3-48 (2) Time History of Observed and Simulated Near-surface Hourly and 32-HR-LPFSalinity during 2011 to 2013 Period at USGS 01482800 at Reedy Island Jetty, DE.

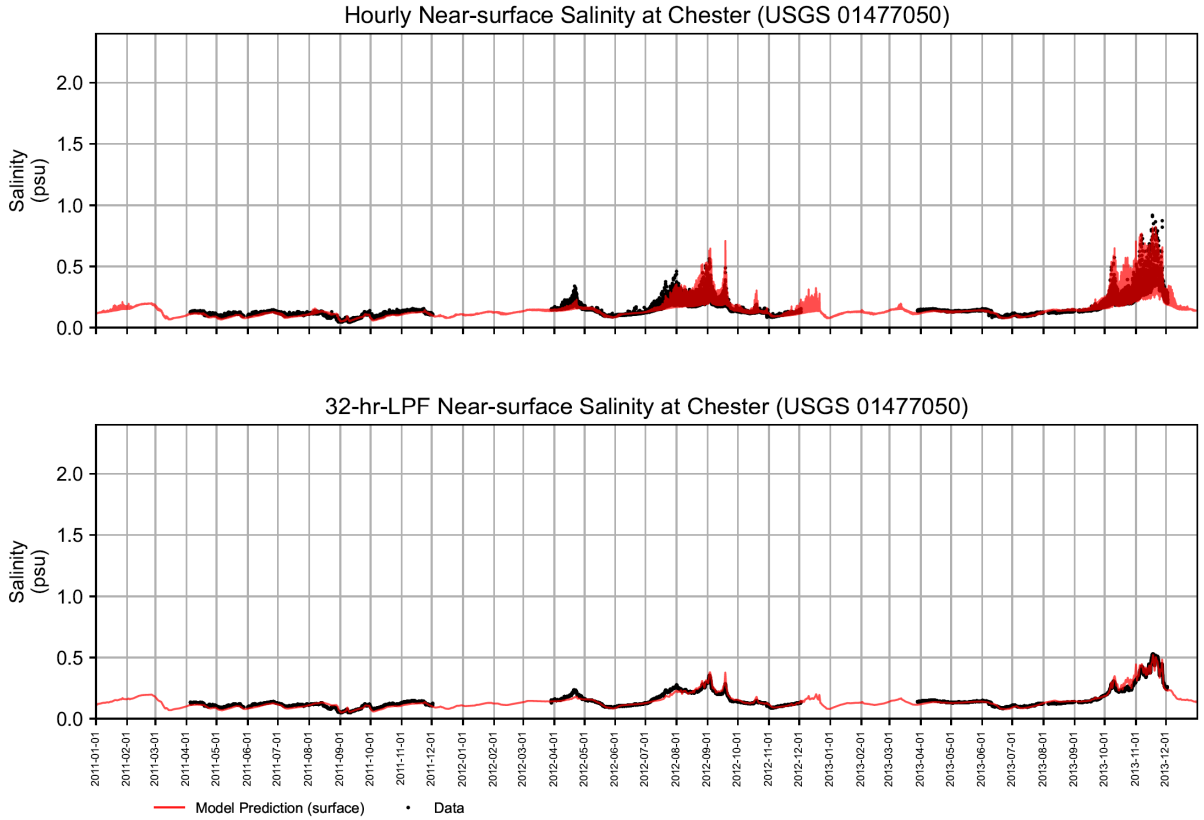

Notes: Salinity data was derived from specific conductance and water temperature based on Standard Methods for the Examination of Water and Wastewater, 19th Ed. 1995.

Figure 4.3-48 (3) Time History of Observed and Simulated Near-surface Hourly and 32-HR-LPFSalinity during 2011 to 2013 Period at USGS 01477050 at Chester, PA.

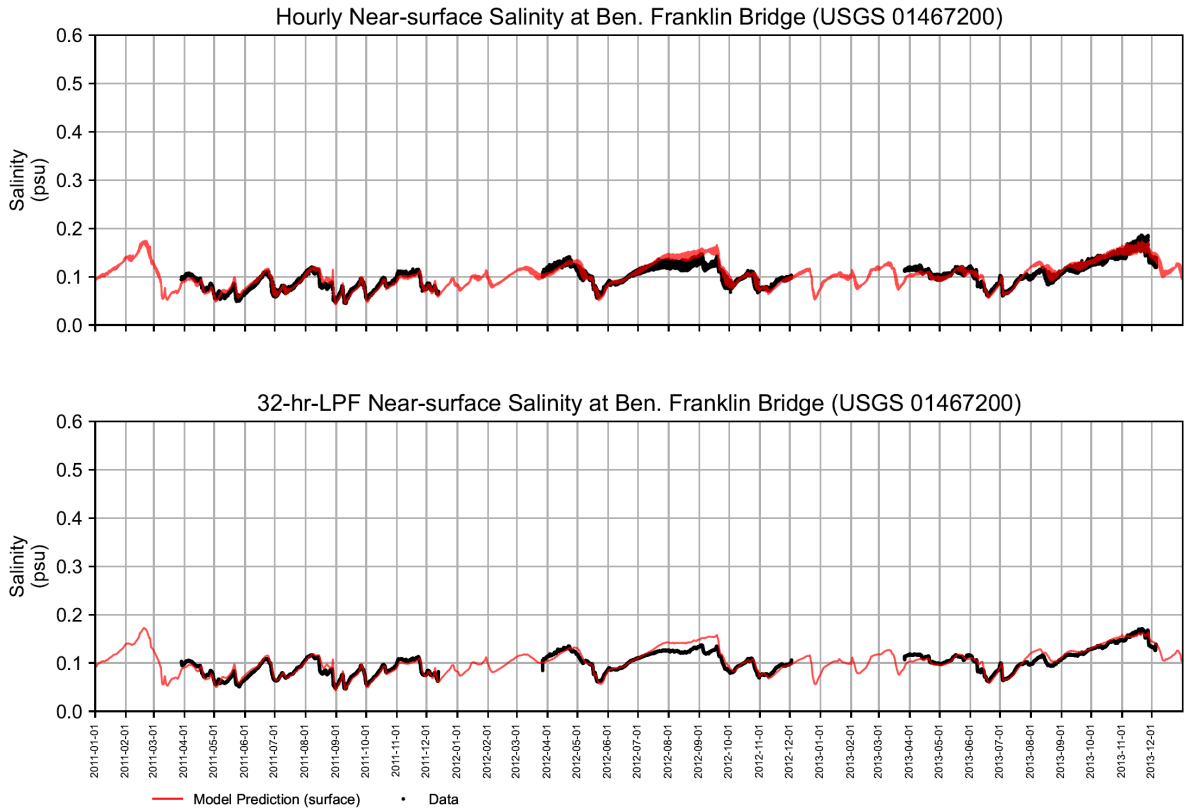

Notes: Salinity data was derived from specific conductance and water temperature based on Standard Methods for the Examination of Water and Wastewater, 19th Ed. 1995.

Figure 4.3-48 (4) Time History of Observed and Simulated Near-surface Hourly and 32-HR-LPF Salinity during 2011 to 2013 Period at USGS 01467200 Ben Franklin Bridge (now at Delaware River at Penn's Landing), Philadelphia, PA.

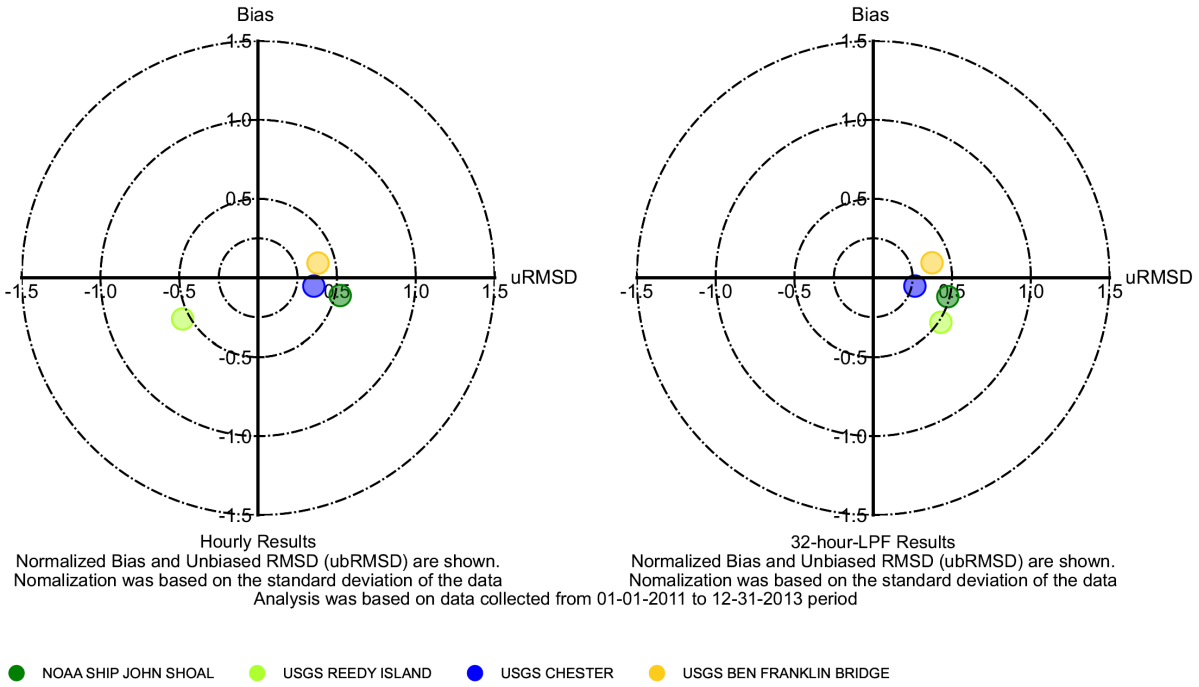

Figure 4.3-49 Target Diagram for the Observed and Predicted Hourly and 32-hour-LPF Near-Surface Salinity during 2011 to 2013 Period

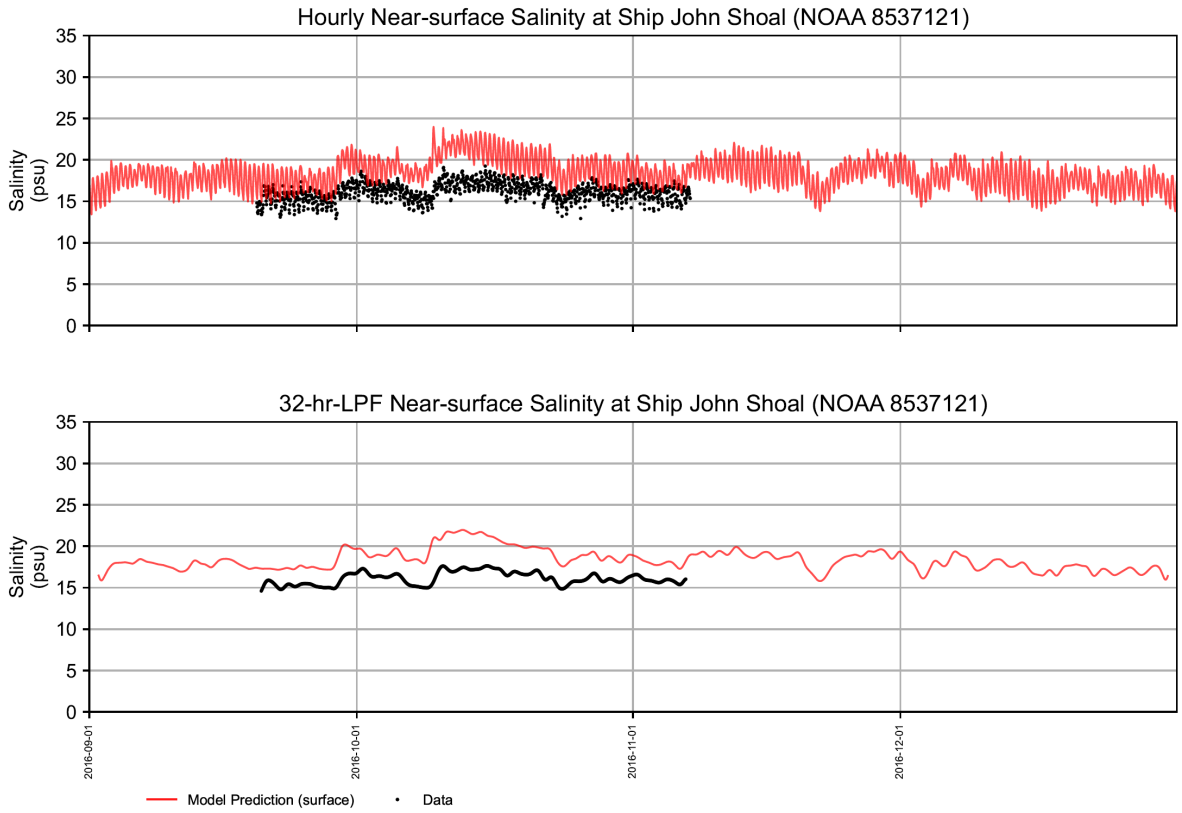

Notes: Salinity data was derived from conductivity and water temperature based on Standard Methods for the Examination of Water and Wastewater, 19th Ed. 1995.

Figure 4.3-50 (1) Time History of Observed and Simulated Near-surface Hourly and 32-HR-LPF Salinity during Critical Season 2016 at NOAA 8537121 at Ship John Shoal.

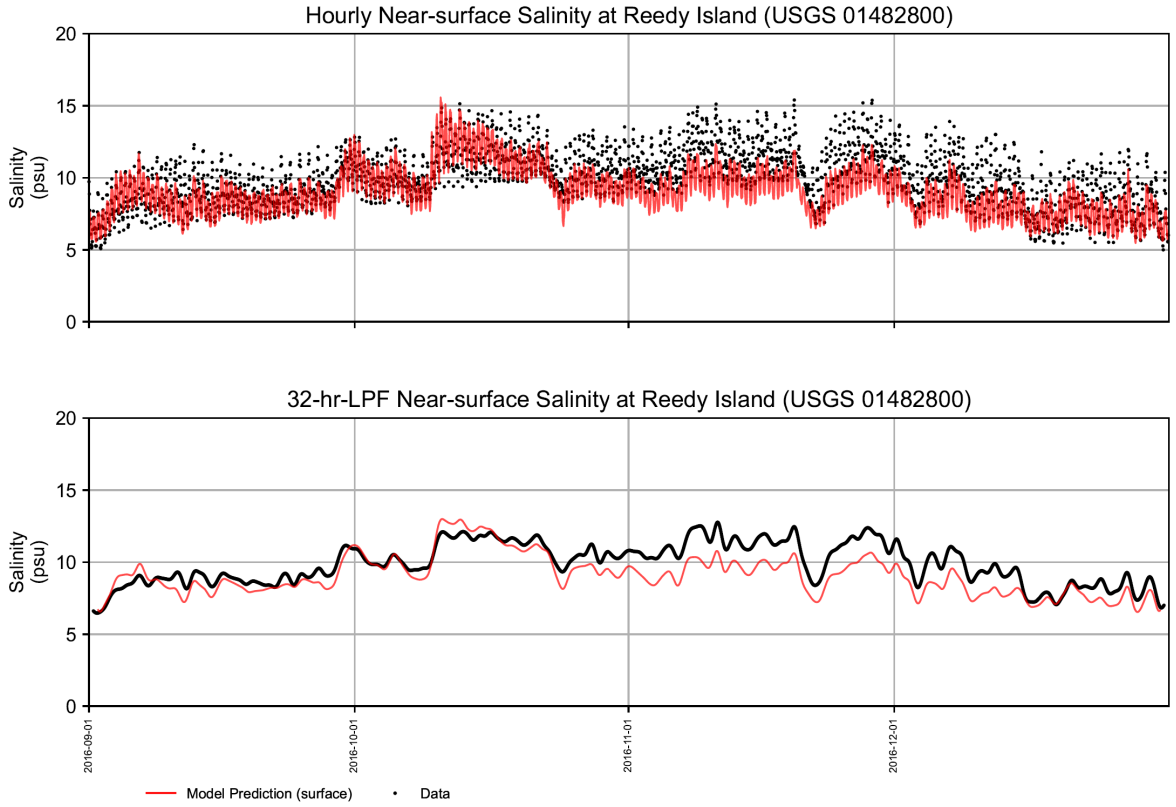

Notes: Salinity data was derived from specific conductance and water temperature based on Standard Methods for the Examination of Water and Wastewater, 19th Ed. 1995.

Figure 4.3-50 (2) Time History of Observed and Simulated Near-surface Hourly and 32-HR-LPFSalinity during Critical Season 2016 at USGS 01482800 at Reedy Island Jetty, DE.

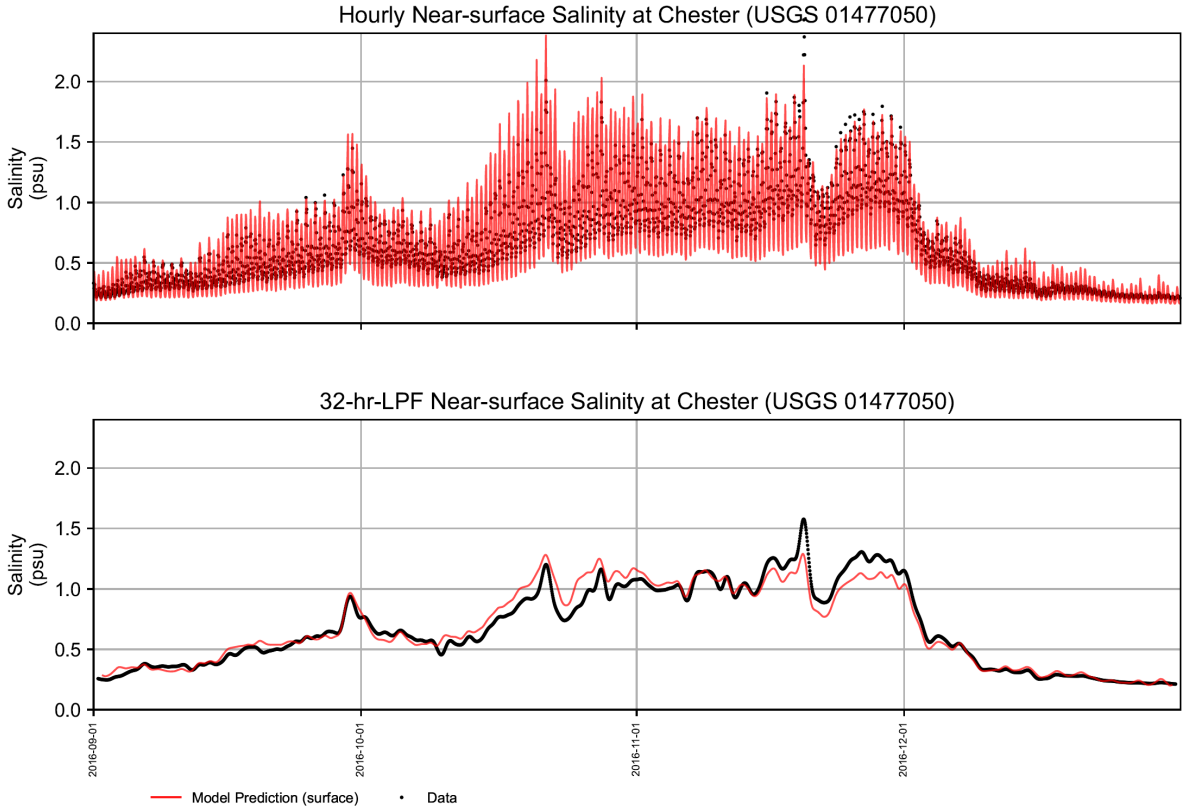

Notes: Salinity data was derived from specific conductance and water temperature based on Standard Methods for the Examination of Water and Wastewater, 19th Ed. 1995.

Figure 4.3-50 (3) Time History of Observed and Simulated Near-surface Hourly and 32-HR-LPFSalinity during Critical Season 2016 Period at USGS 01477050 at Chester, PA.

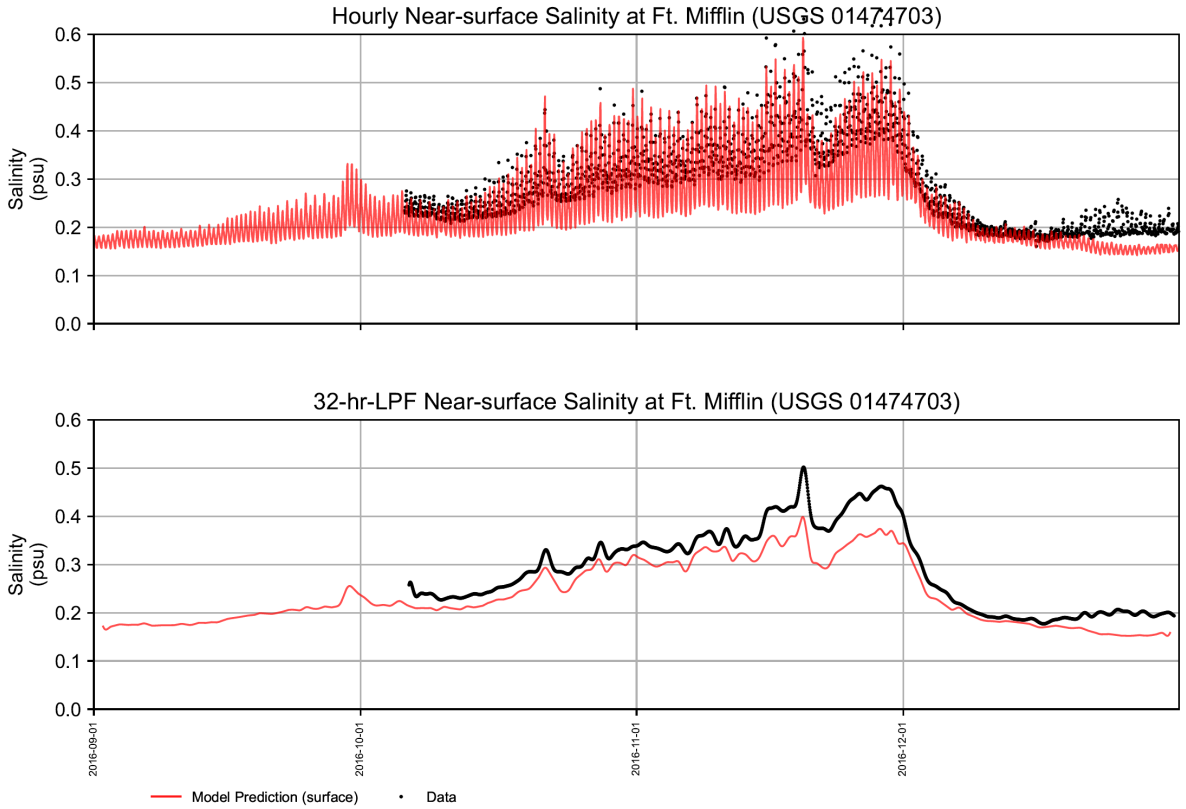

Notes: Salinity data was derived from specific conductance and water temperature based on Standard Methods for the Examination of Water and Wastewater, 19th Ed. 1995.

Figure 4.3-50 (4) Time History of Observed and Simulated Near-surface Hourly and 32-HR-LPF Salinity during Critical Season 2016 at USGS 01474703 at Fort Mifflin at Philadelphia, PA.

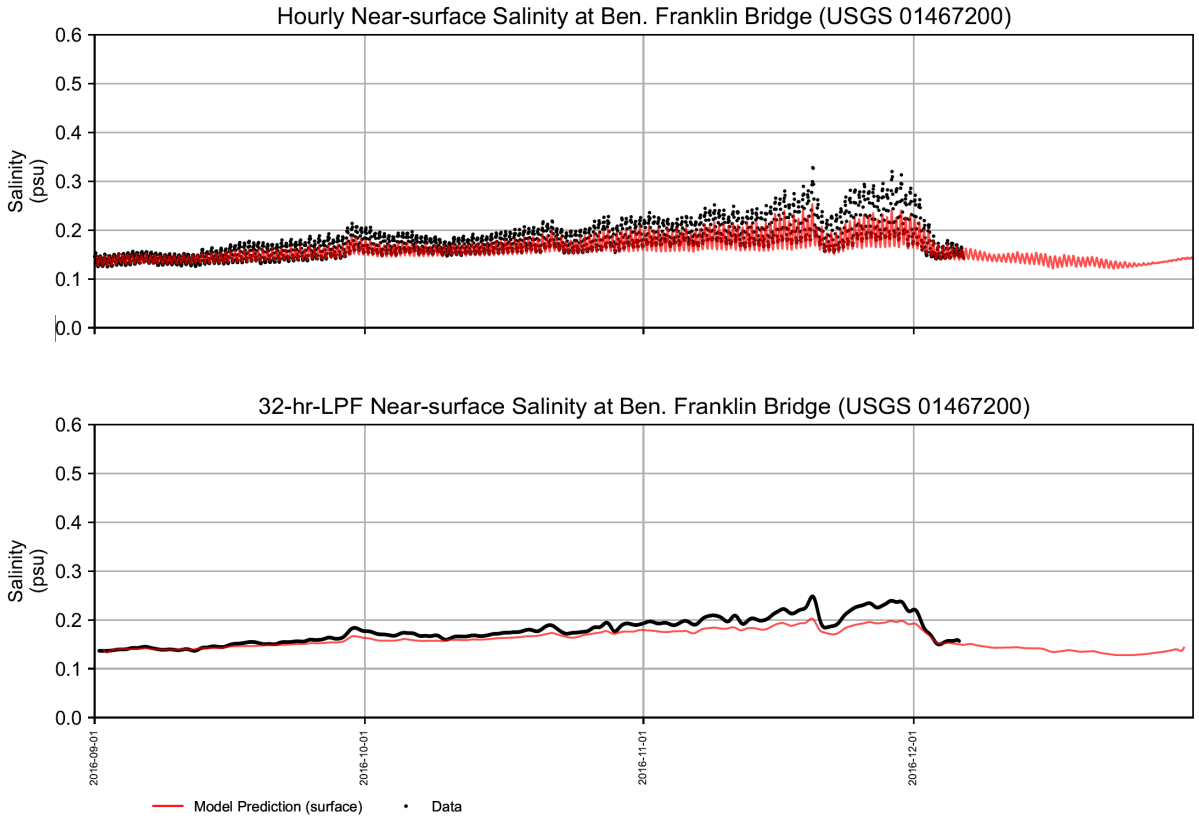

Notes: Salinity data was derived from specific conductance and water temperature based on Standard Methods for the Examination of Water and Wastewater, 19th Ed. 1995.

Figure 4.3-50 (5) Time History of Observed and Simulated Near-surface Hourly and 32-HR-LPF Salinity during Critical Season 2016 at USGS 01467200 Ben Franklin Bridge (now at Delaware River at Penn's Landing), Philadelphia, PA.

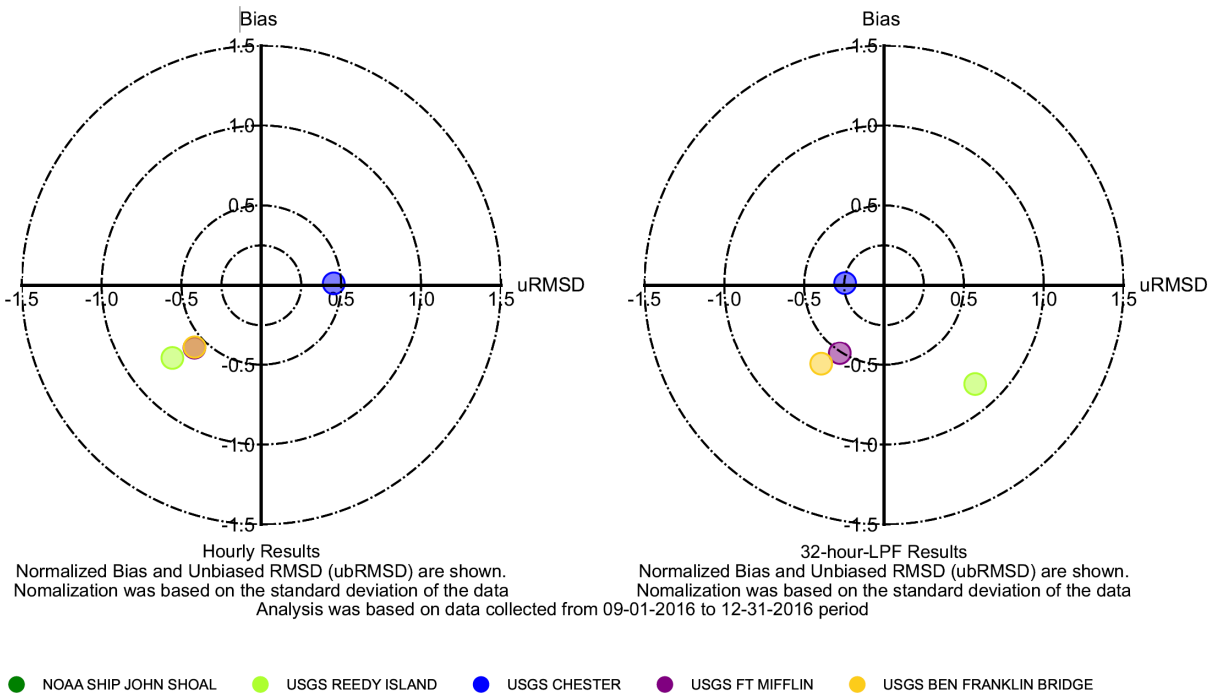

Figure 4.3-51 Target Diagram for the Observed and Predicted Hourly and 32-hour-LPF Near-Surface Salinity during Critical Season 2016

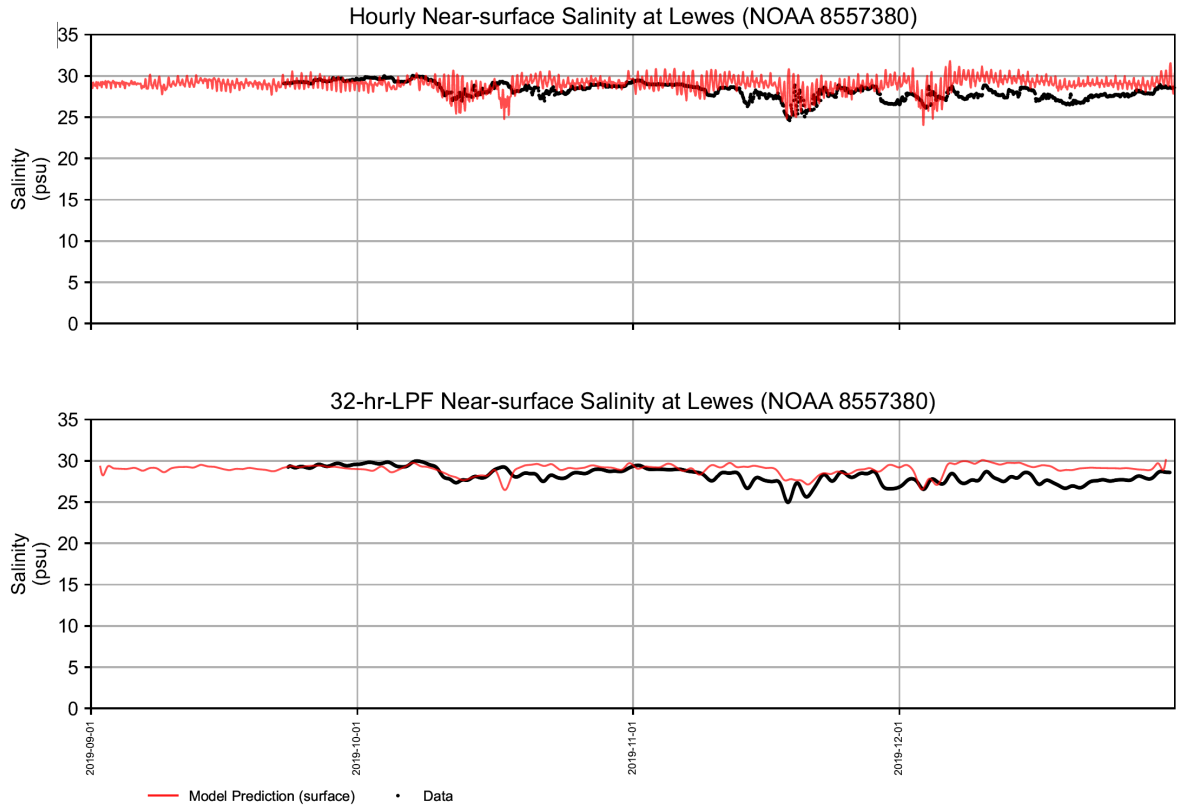

Notes: Salinity data was derived from conductivity and water temperature based on Standard Methods for the Examination of Water and Wastewater, 19th Ed. 1995.

Figure 4.3-52 (1) Time History of Observed and Simulated Near-surface Hourly and 32-HR-LPF Salinity during Critical Season 2019 at NOAA 8557380 at Lewes, DE.

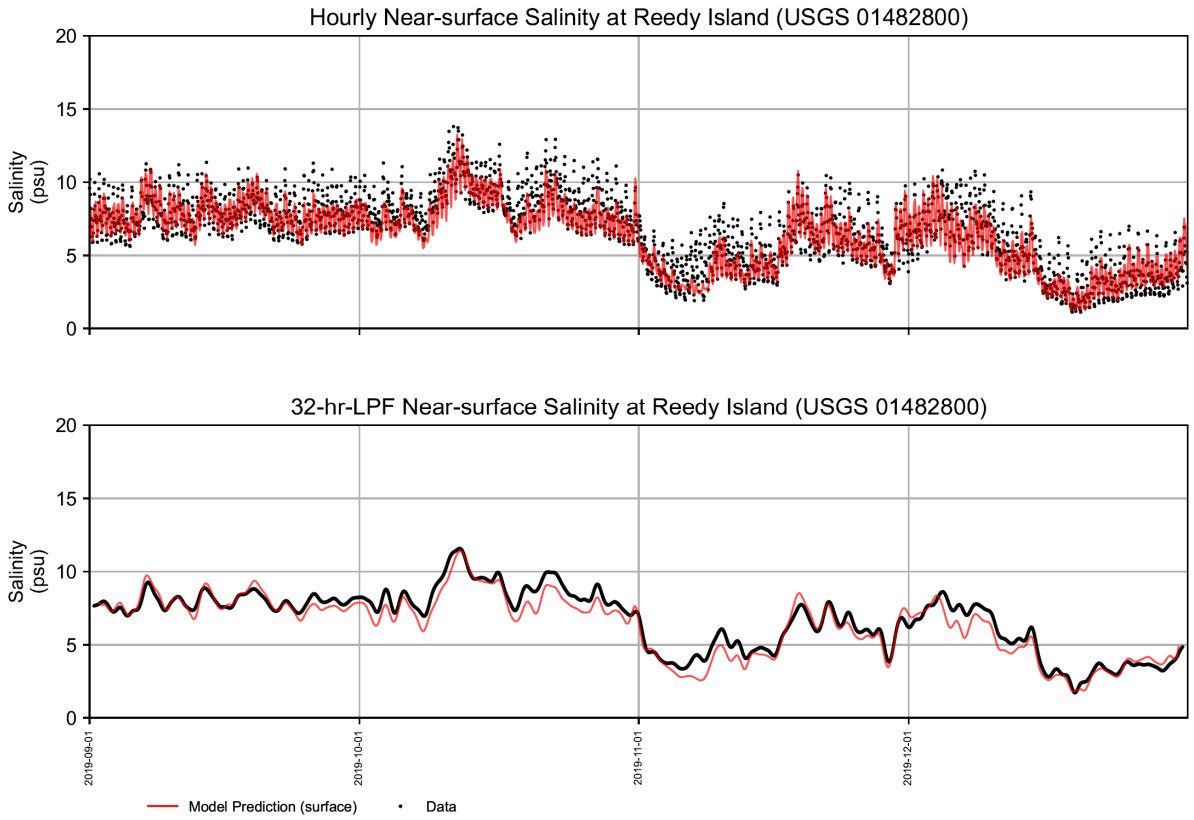

Notes: Salinity data was derived from specific conductance and water temperature based on Standard Methods for the Examination of Water and Wastewater, 19th Ed. 1995.

Figure 4.3-52 (2) Time History of Observed and Simulated Near-surface Hourly and 32-HR-LPFSalinity during Critical Season 2019 at USGS 01482800 at Reedy Island Jetty, DE.

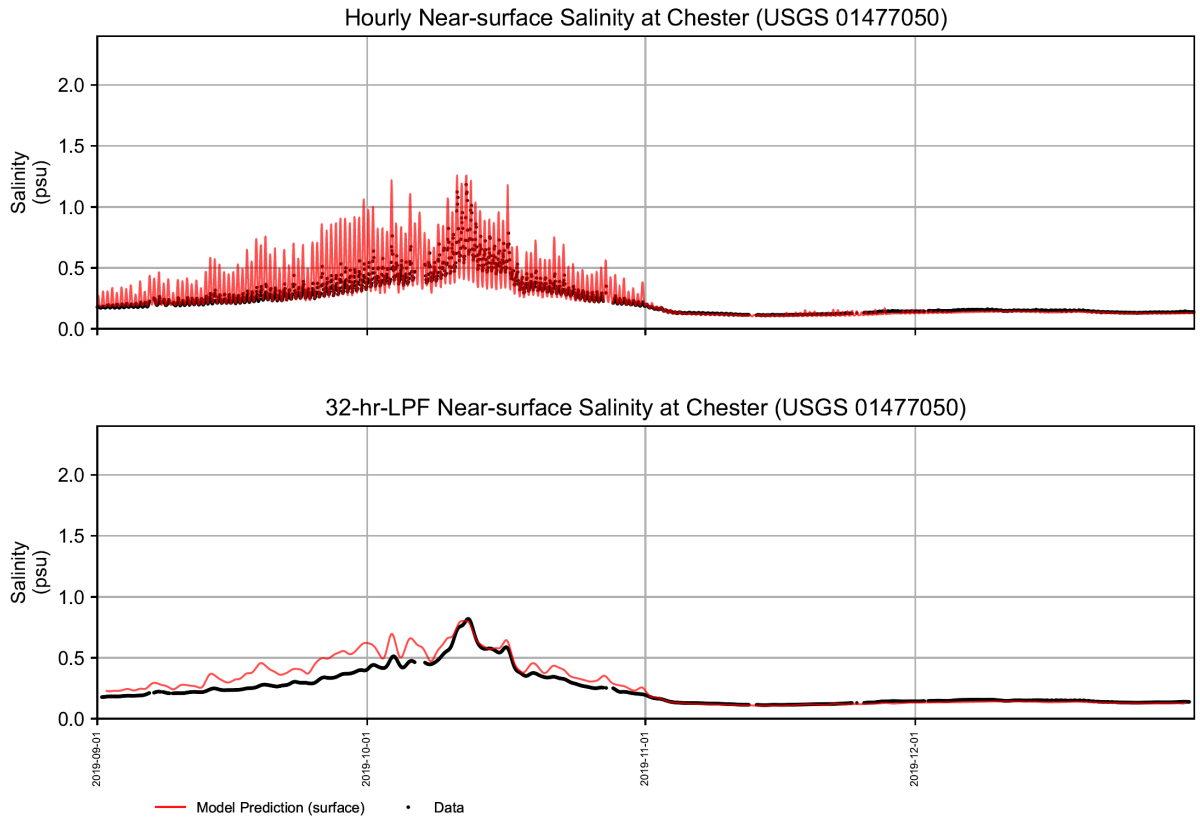

Notes: Salinity data was derived from specific conductance and water temperature based on Standard Methods for the Examination of Water and Wastewater, 19th Ed. 1995.

Figure 4.3-52 (3) Time History of Observed and Simulated Near-surface Hourly and 32-HR-LPFSalinity during Critical Season 2019 Period at USGS 01477050 at Chester, PA.

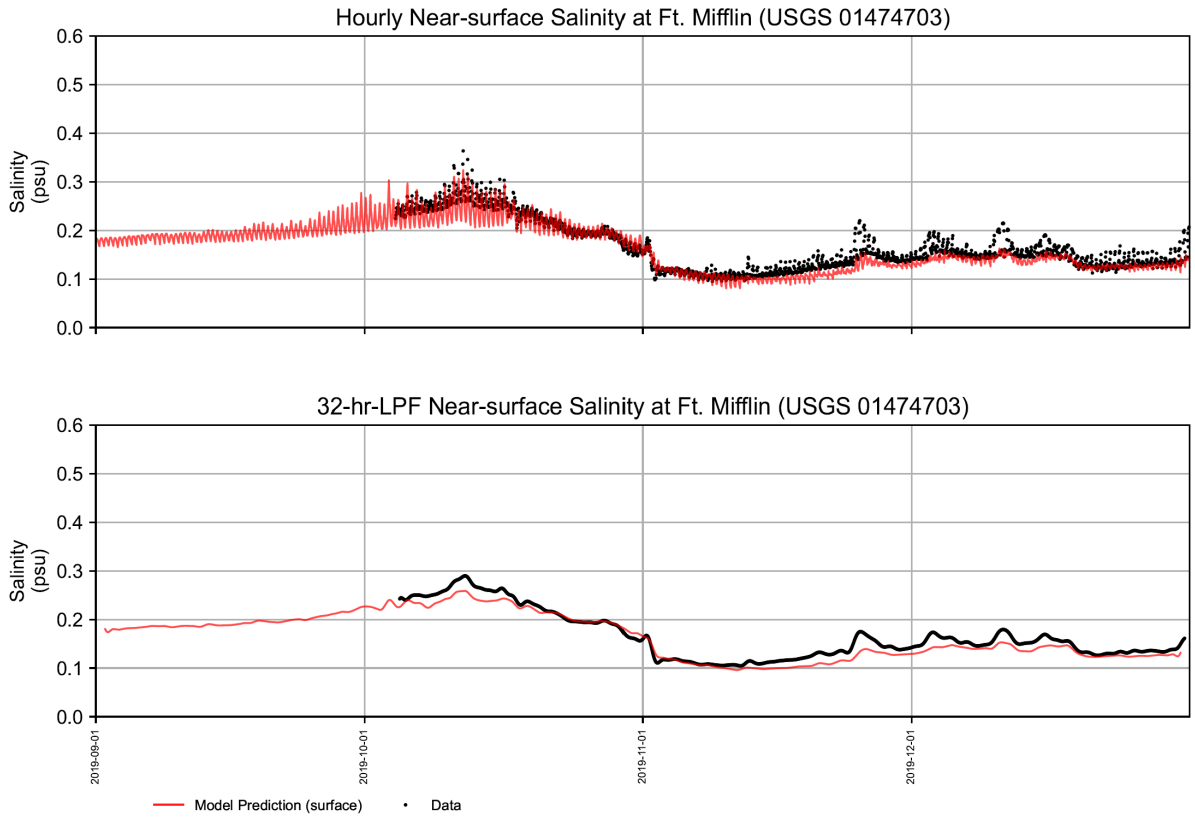

Notes: Salinity data was derived from specific conductance and water temperature based on Standard Methods for the Examination of Water and Wastewater, 19th Ed. 1995.

Figure 4.3-52 (5) Time History of Observed and Simulated Near-surface Hourly and 32-HR-LPF Salinity during 2016 to 2020 Period at USGS 01474703 at Fort Mifflin at Philadelphia, PA.

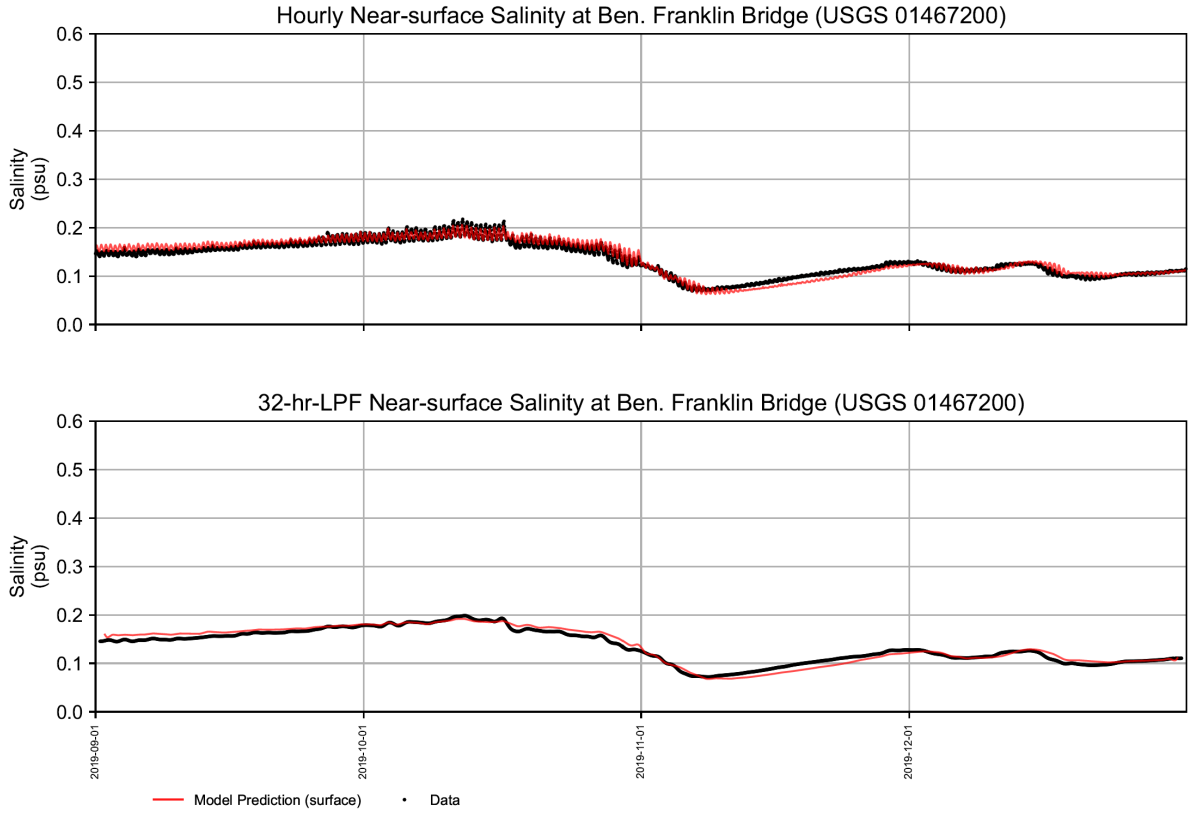

Notes: Salinity data was derived from specific conductance and water temperature based on Standard Methods for the Examination of Water and Wastewater, 19th Ed. 1995.

Figure 4.3-52 (5) Time History of Observed and Simulated Near-surface Hourly and 32-HR-LPF Salinity during Critical Season 2019 at USGS 01467200 Ben Franklin Bridge (now at Delaware River at Penn's Landing), Philadelphia, PA.

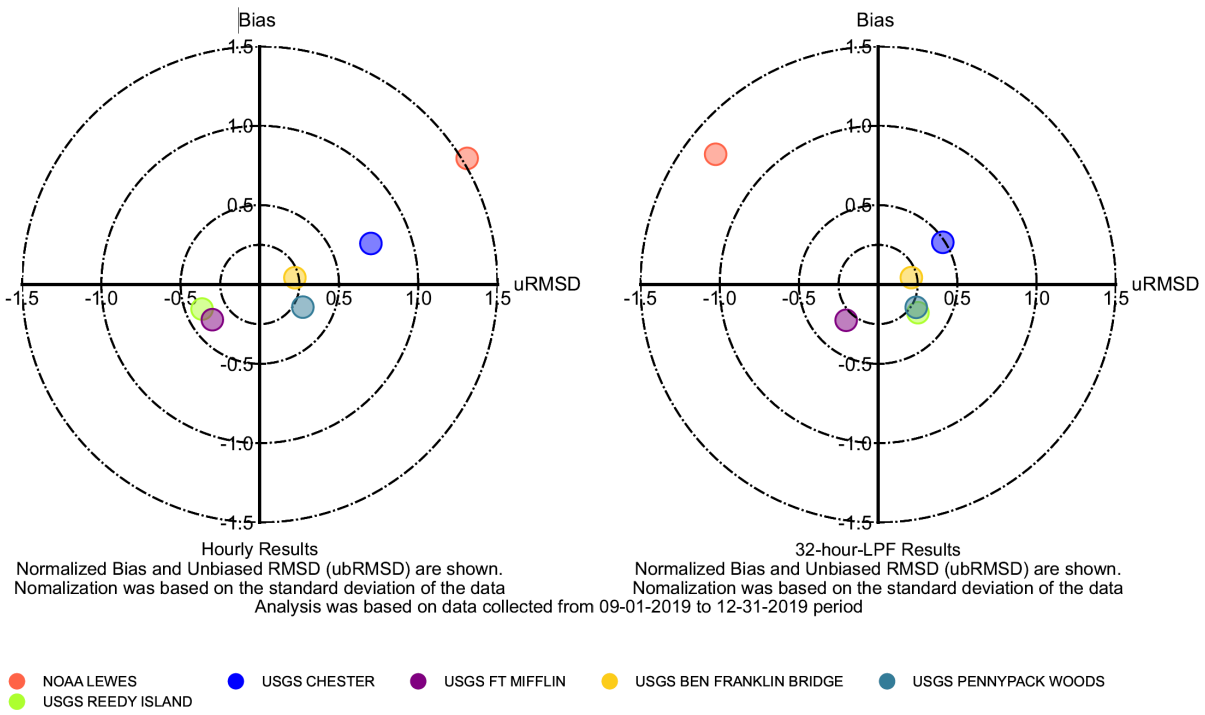

Figure 4.3-53 Target Diagram for the Observed and Predicted Hourly and 32-hour-LPF Near-Surface Salinity during Critical Season 2019

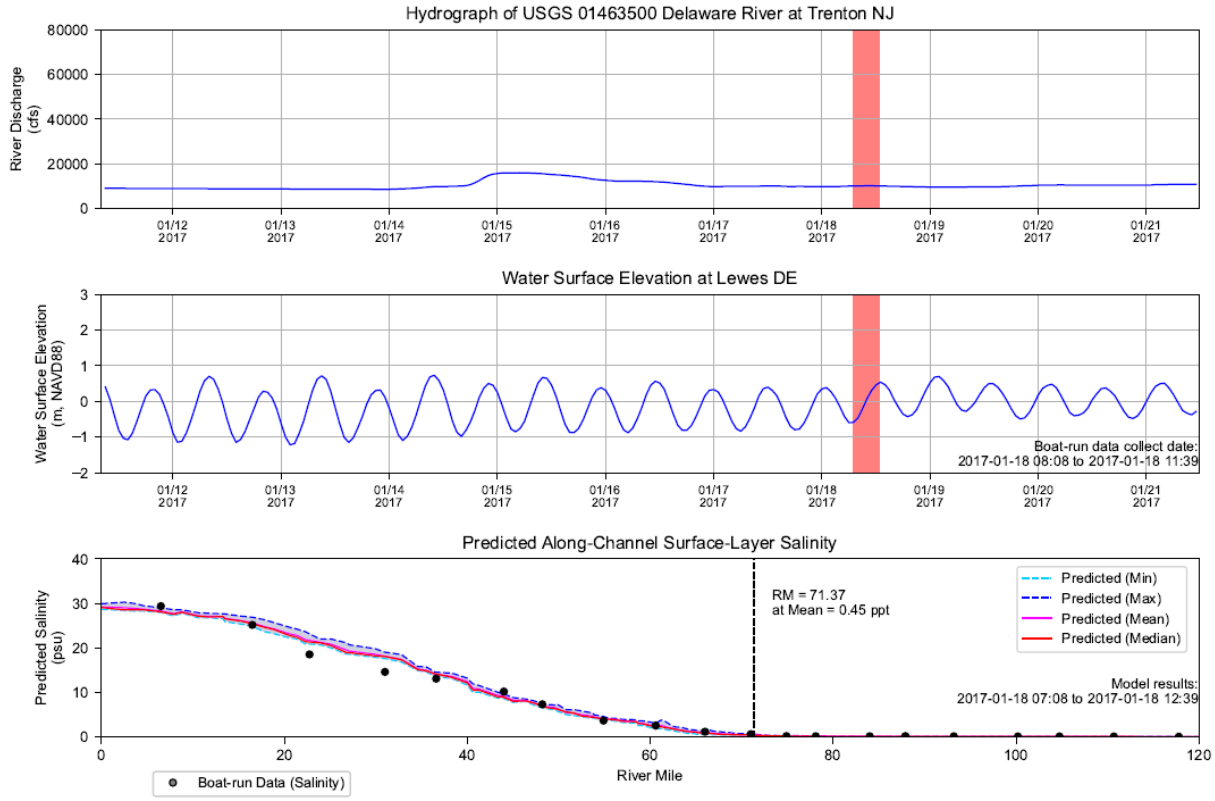

Notes: Salinity and Chloride data collected by Boat Run survey were used. Date that under detection limit were set to half of the detection limit. Red shaded area indicates the Boat Run survey time period: 2017-01-18 08:08 to 2017-01-18 11:39. Model results along the navigation channel during period of 2017-01-18 07:08 to 2017-01-18 12:39 were used in this analysis.

Figure 4.3-54 (1) Predicted Salinity Longitudinal Profile and DRBC Boat Run Data, January 18, 2017

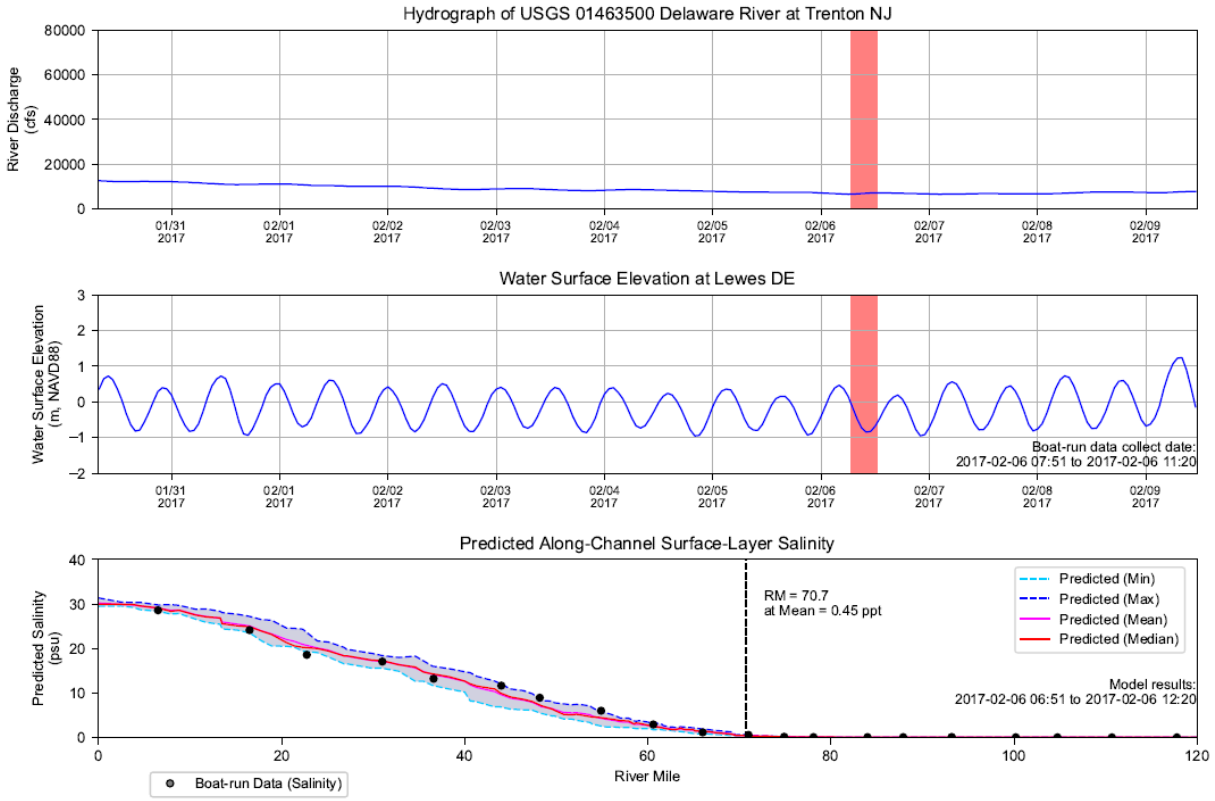

Notes: Salinity and Chloride data collected by Boat Run survey were used. Date that under detection limit were set to half of the detection limit. Red shaded area indicates the Boat Run survey time period: 2017-02-06 07:51 to 2017-02-06 11:20. Model results along the navigation channel during the period of 2017-02-06 06:51 to 2017-02-06 12:20 were used in this analysis.

Figure 4.3-54 (2) Predicted Salinity Longitudinal Profile and DRBC Boat Run Data, February 6, 2017

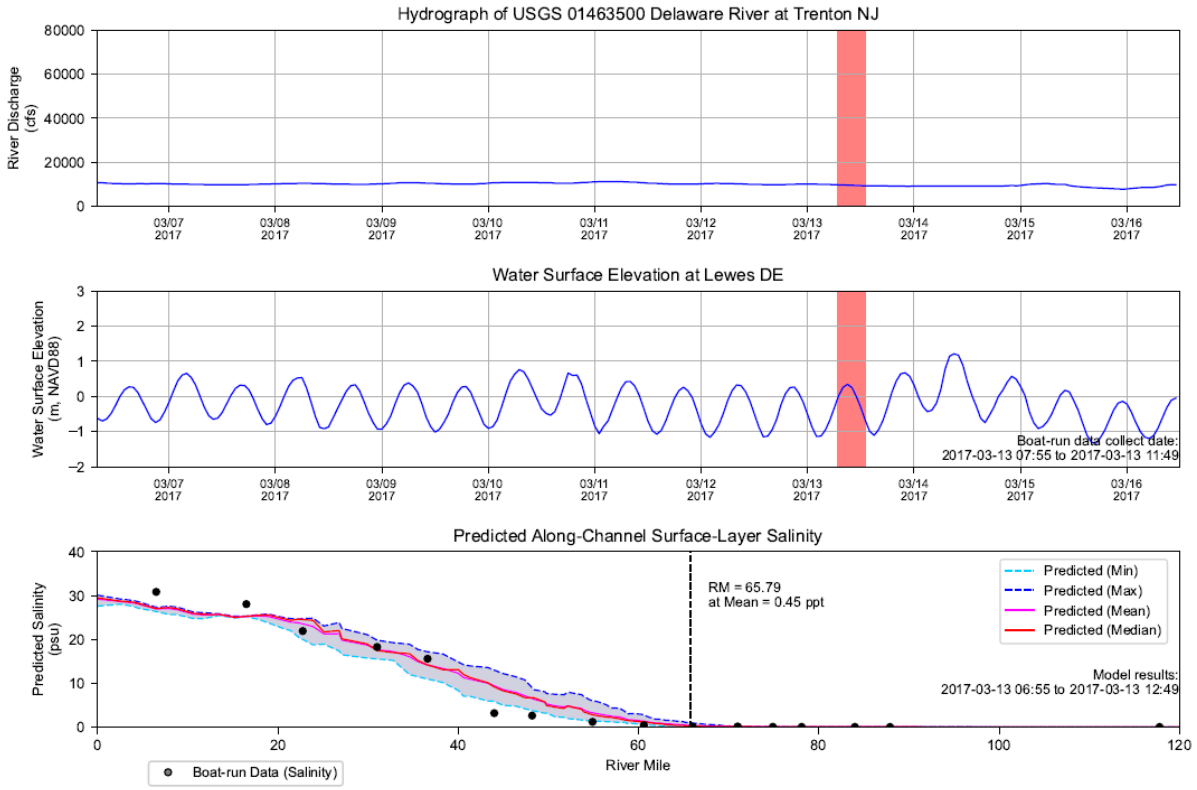

Notes: Salinity and Chloride data collected by Boat Run survey were used. Date that under detection limit were set to half of the detection limit. Red shaded area indicates the Boat Run survey time period: 2017-03-13 07:55 to 2017-03-13 11:49. Model results along the navigation channel during period of 2017-03-13 06:55 to 2017-03-13 12:49 were used in this analysis.

Figure 4.3-54 (3) Predicted Salinity Longitudinal Profile and DRBC Boat Run Data, March 13, 2017

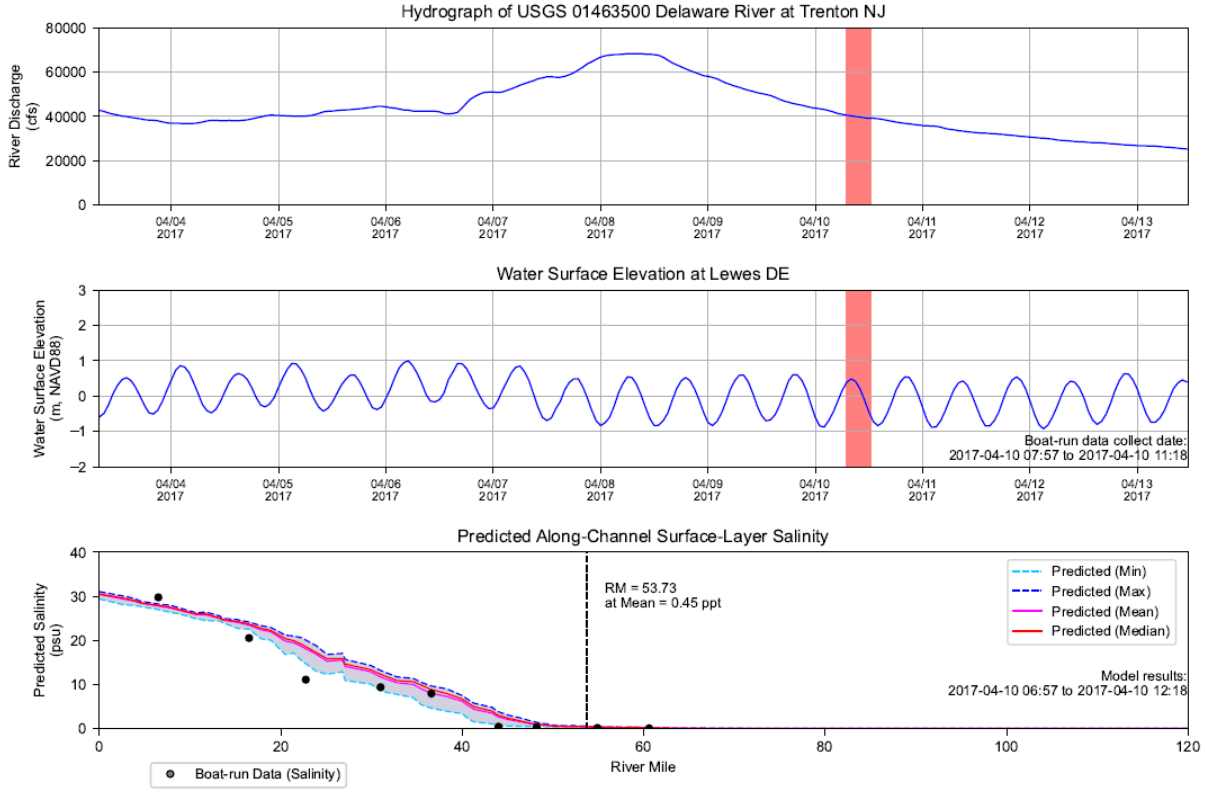

Notes: Salinity and Chloride data collected by Boat Run survey were used. Date that under detection limit were set to half of the detection limit. Red shaded area indicates the Boat Run survey time period: 2017-04-10 07:57 to 2017-04-10 11:18. Model results along the navigation channel during the period of 2017-04-10 06:57 to 2017-04-10 12:18 were used in this analysis.

Figure 4.3-54 (4) Predicted Salinity Longitudinal Profile and DRBC Boat Run Data, April 10, 2017

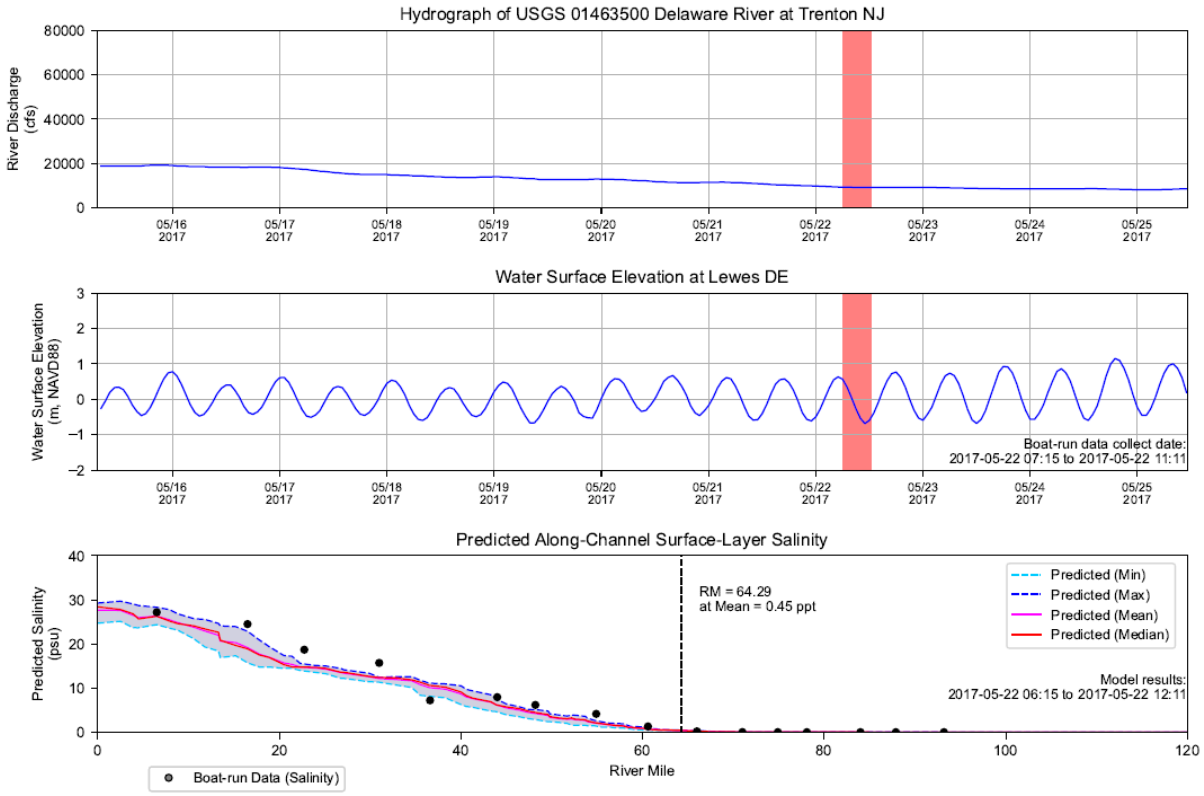

Notes: Salinity and Chloride data collected by Boat Run survey were used. Date that under detection limit were set to half of the detection limit. Red shaded area indicates the Boat Run survey time period: 2017-05-22 07:15 to 2017-05-22. Model results along the navigation channel during period of 2017-05-22 06:15 to 2017-05-22 12:11 were used in this analysis.

Figure 4.3-54 (5) Predicted Salinity Longitudinal Profile and DRBC Boat Run Data, May 22, 2017

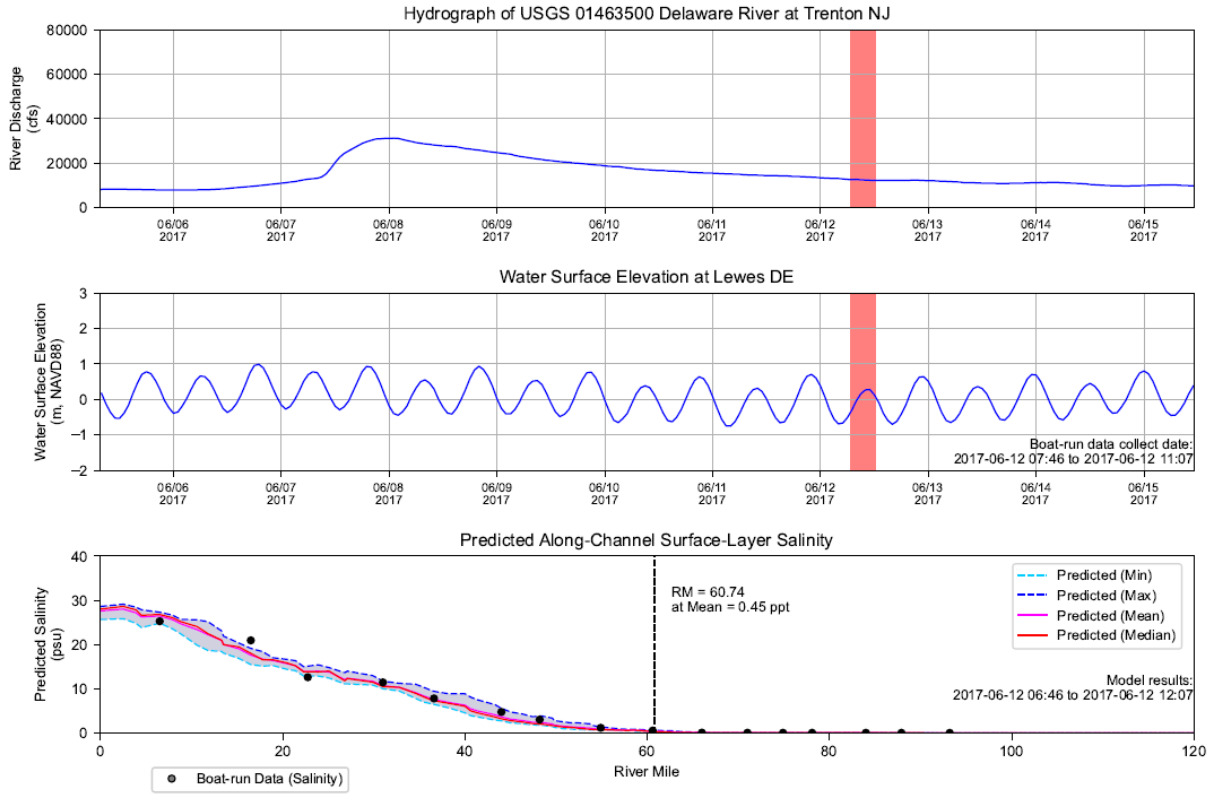

Notes: Salinity and Chloride data collected by Boat Run survey were used. Date that under detection limit were set to half of the detection limit. Red shaded area indicates the Boat Run survey time period: 2017-06-12 07:46 to 2017-06-12 11:07. Model results along the navigation channel during period of 2017-06-12 06:46 to 2017-06-12 12:07 were used in this analysis.

Figure 4.3-54 (6) Predicted Salinity Longitudinal Profile and DRBC Boat Run Data, June 12, 2017

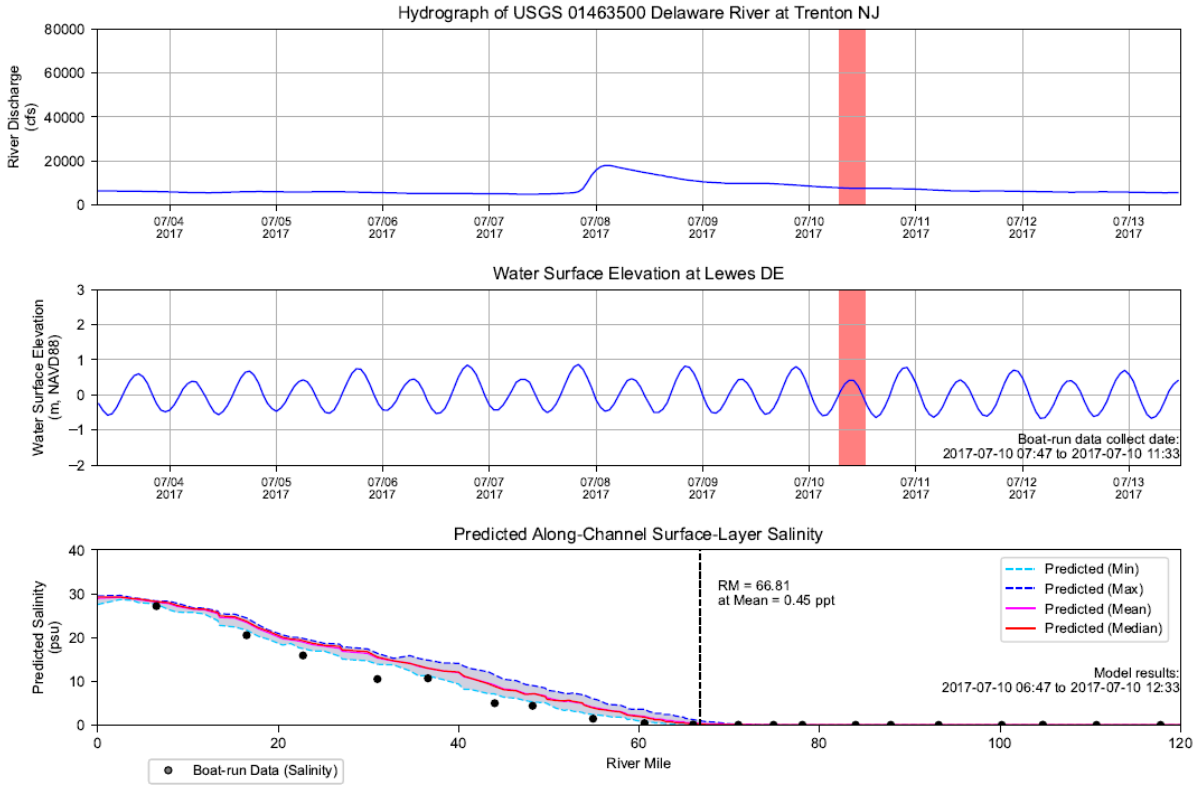

Notes: Salinity and Chloride data collected by Boat Run survey were used. Date that under detection limit were set to half of the detection limit. Red shaded area indicates the Boat Run survey time period: 2017-07-10 07:47 to 2017-07-10 11:33. Model results along the navigation channel during period of 2017-07-10 06:47 to 2017-07-10 12:33were used in this analysis.

Figure 4.3-54 (7) Predicted Salinity Longitudinal Profile and DRBC Boat Run Data, July 10, 2017

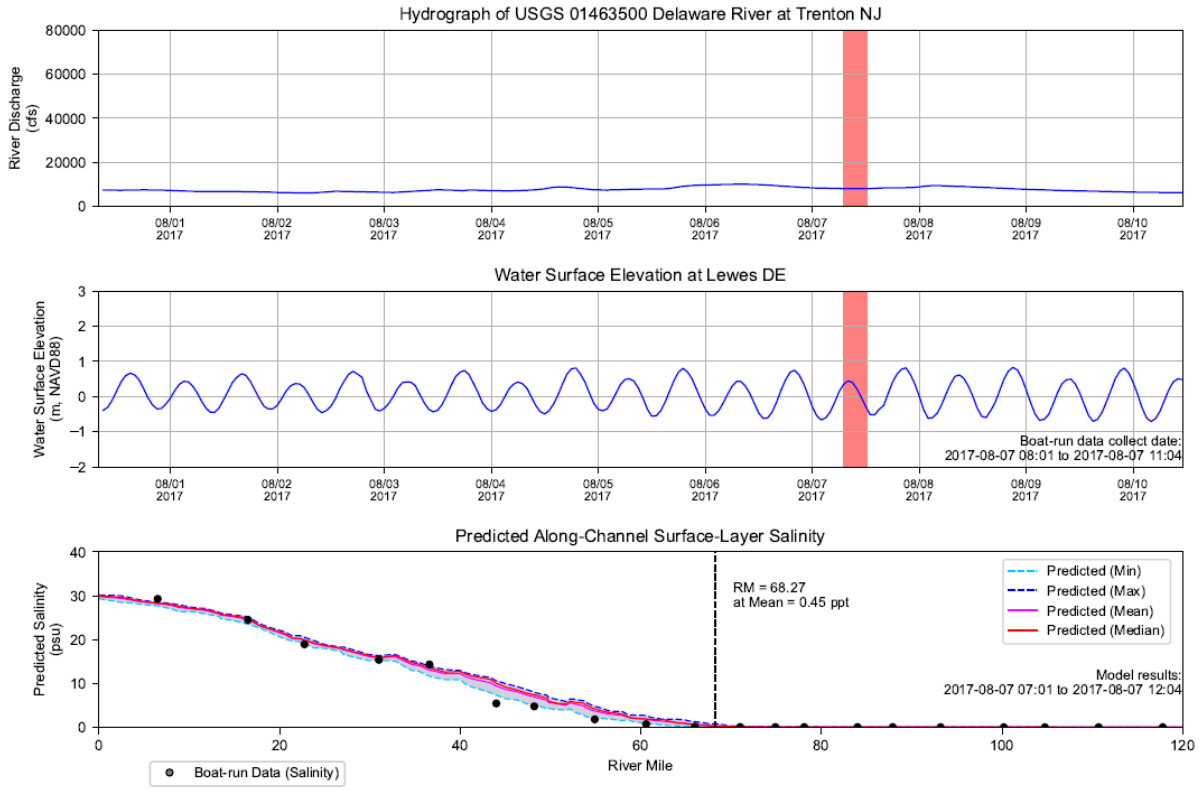

Notes: Salinity and Chloride data collected by Boat Run survey were used. Date that under detection limit were set to half of the detection limit. Red shaded area indicates the Boat Run survey time period: 2017-08-07 08:01 to 2017-08-07 11:04. Model results along the navigation channel during the period of 2017-08-07 07:01 to 2017-08-07 12:04 were used in this analysis.

Figure 4.3-54 (8) Predicted Salinity Longitudinal Profile and DRBC Boat Run Data, August 7, 2017

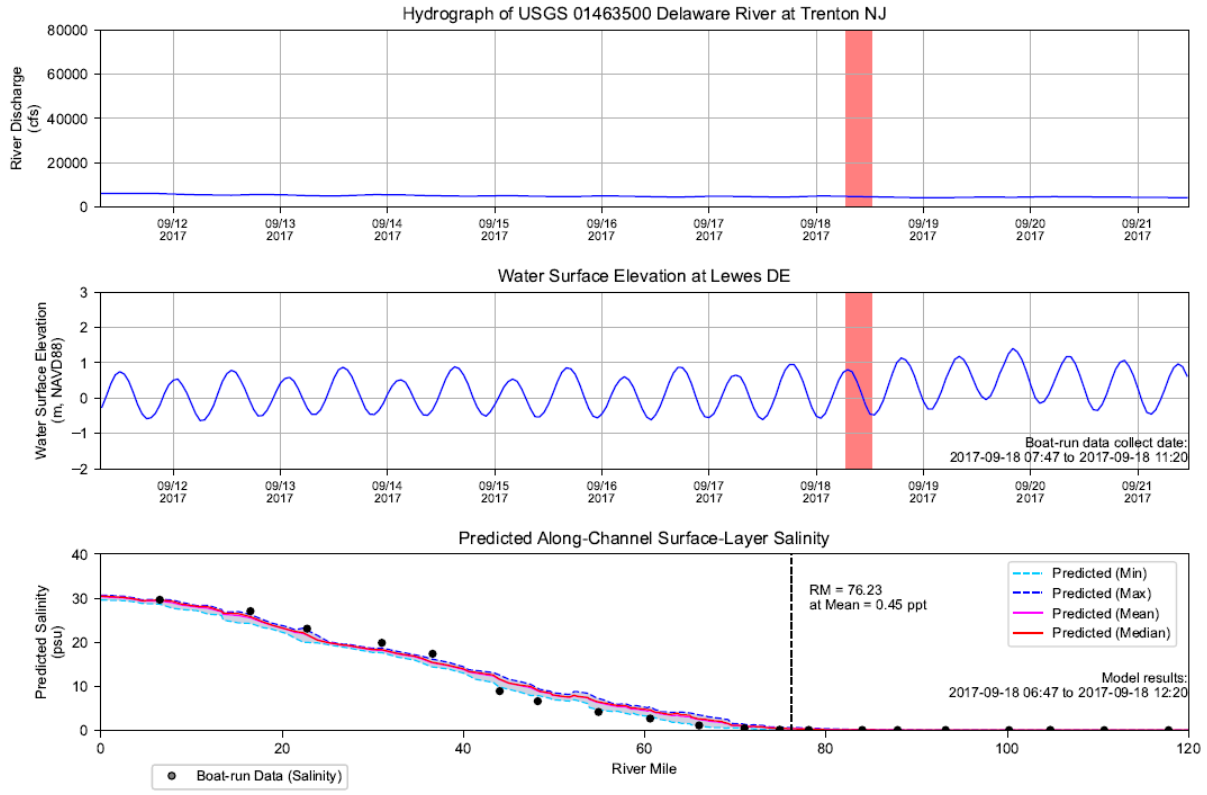

Notes: Salinity and Chloride data collected by Boat Run survey were used. Date that under detection limit were set to half of the detection limit. Red shaded area indicates the Boat Run survey time period: 2017-09-18 07:47 to 2017-09-18 11:20. Model results along the navigation channel during period of 2017-09-18 06:47 to 2017-09-18 12:20 were used in this analysis.

Figure 4.3-54 (9) Predicted Salinity Longitudinal Profile and DRBC Boat Run Data, September 18, 2017

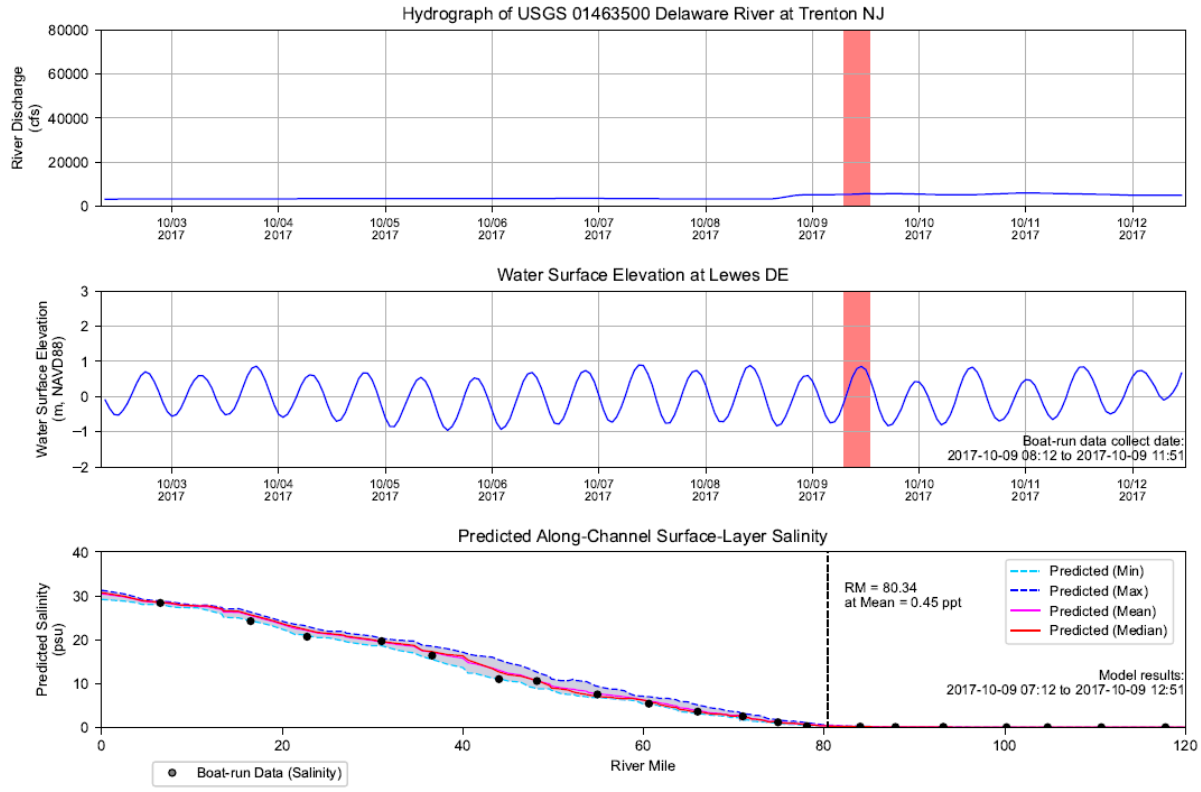

Notes: Salinity and Chloride data collected by Boat Run survey were used. Date that under detection limit were set to half of the detection limit. Red shaded area indicates the Boat Run survey time period: 2017-10-09 08:12 to 2017-10-09 11:51. Model results along the navigation channel during period of 2017-10-09 07:12 to 2017-10-09 12:51 were used in this analysis.

Figure 4.3-54 (10) Predicted Salinity Longitudinal Profile and DRBC Boat Run Data, October 9, 2017

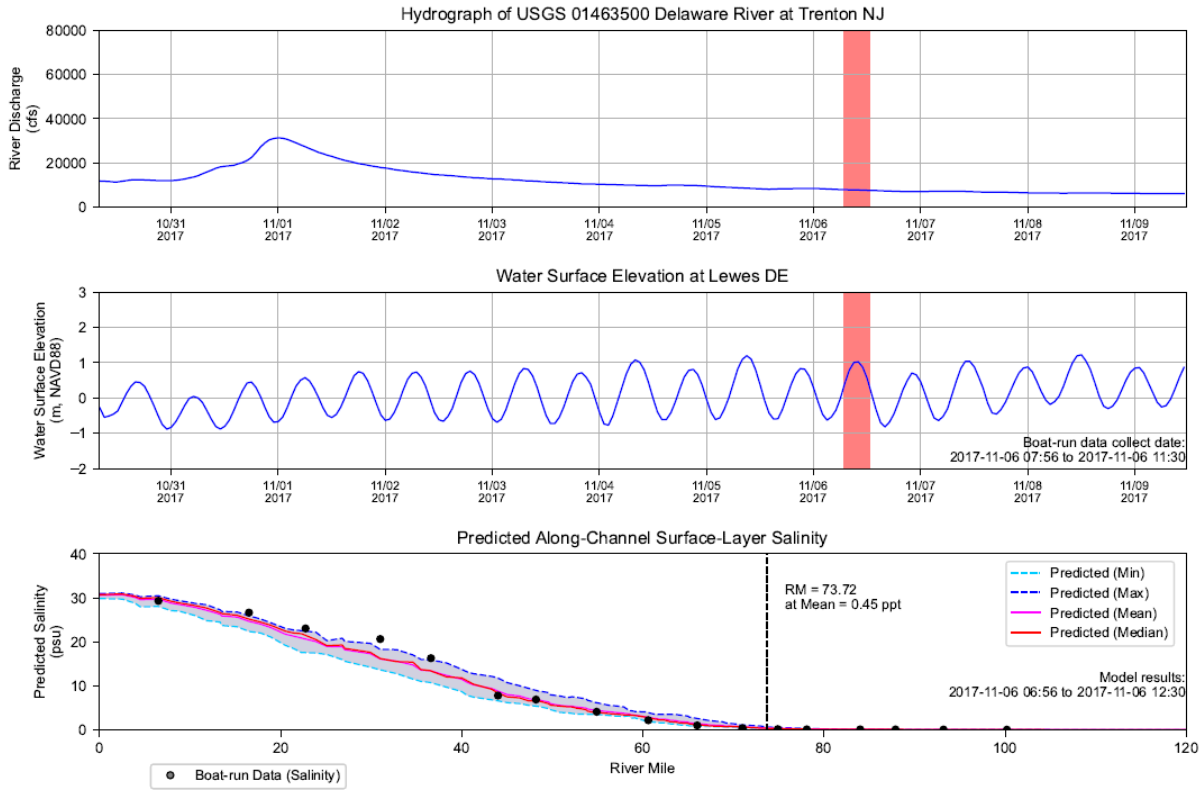

Notes: Salinity and Chloride data collected by Boat Run survey were used. Date that under detection limit were set to half of the detection limit. Red shaded area indicates the Boat Run survey time period: 2017-11-06 07:56 to 2017-11-06 11:30. Model results along the navigation channel during the period of 2017-11-06 06:56 to 2017-11-06 12:30 were used in this analysis.

Figure 4.3-54 (11) Predicted Salinity Longitudinal Profile and DRBC Boat Run Data, November 6, 2017

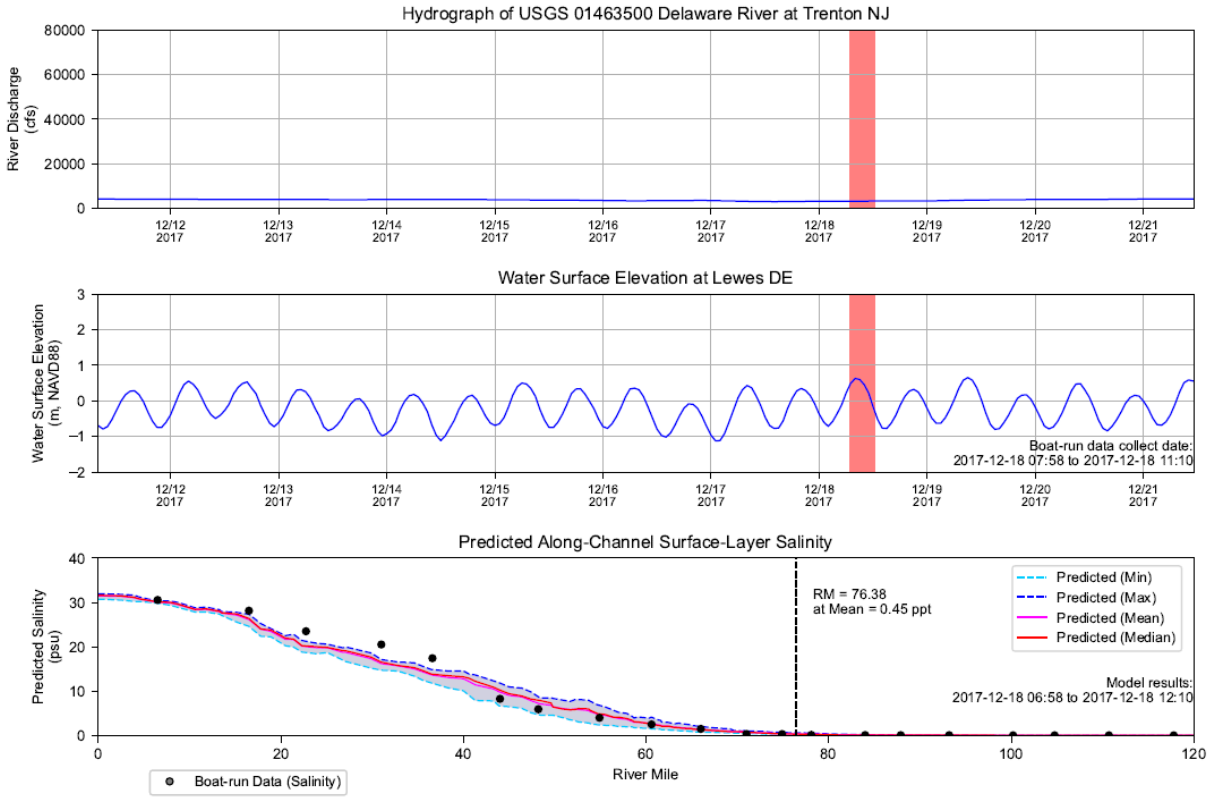

Notes: Salinity and Chloride data collected by Boat Run survey were used. Date that under detection limit were set to half of the detection limit. Red shaded area indicates the Boat Run survey time period: 2017-12-18 07:58 to 2017-12-18 11:10. Model results along the navigation channel during period of 2017-12-18 06:58 to 2017-12-18 12:10 were used in this analysis.

Figure 4.3-54 (12) Predicted Salinity Longitudinal Profile and DRBC Boat Run Data, December 18, 2017

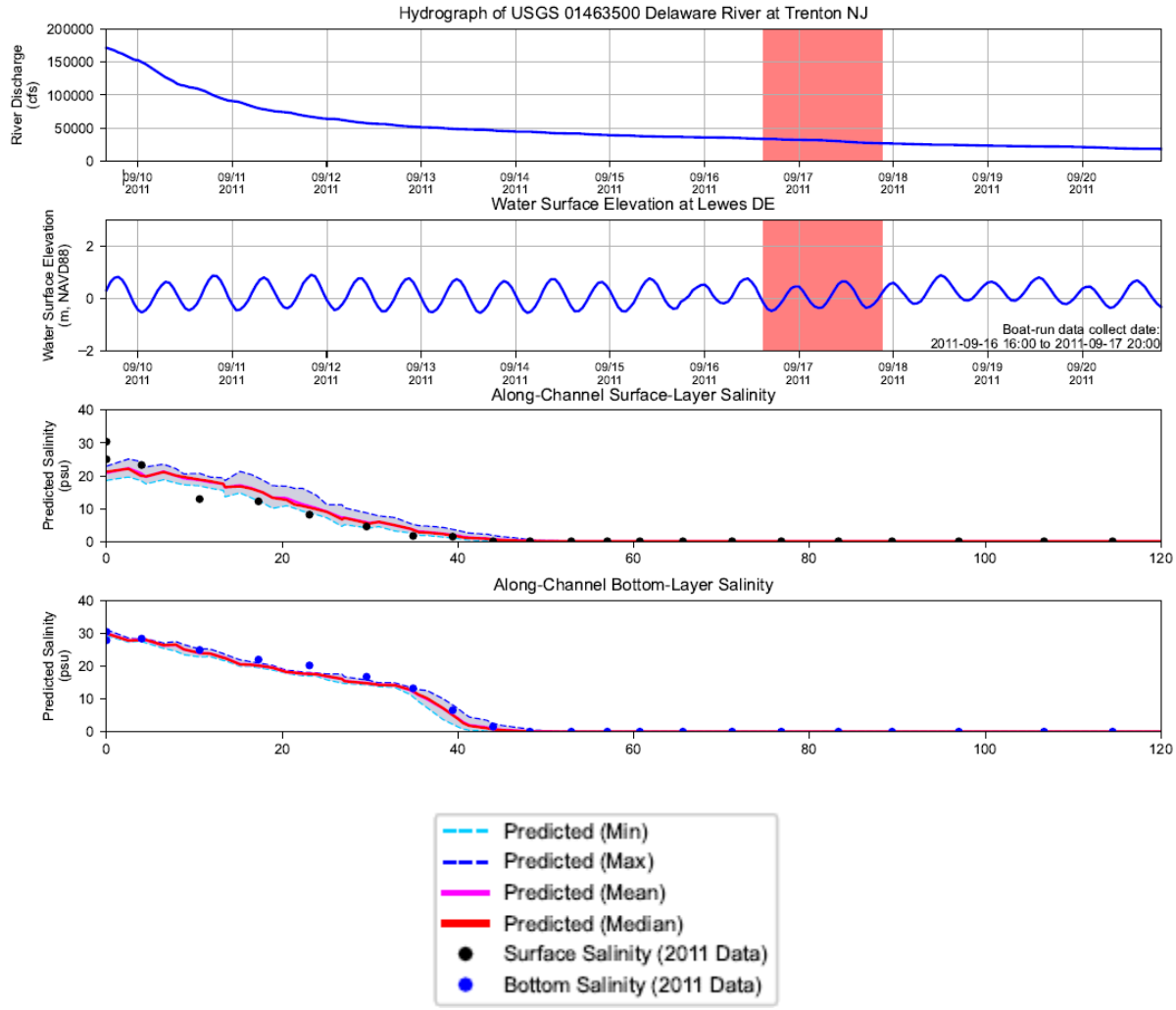

Notes: 2011 Survey data were provided by Rutgers University to DRBC on June 4th, 2019.

Red shaded area indicates the survey time period: 2011-09-16 16:00 to 2011-09-17 20:00

Model results along the navigation channel during the period of 2011-09-16 15:00 to 2011-09-17 21:00 were used in this analysis.

Figure 4.3-55 Predicted Longitudinal Profile of Salinity and 2011 Survey Data

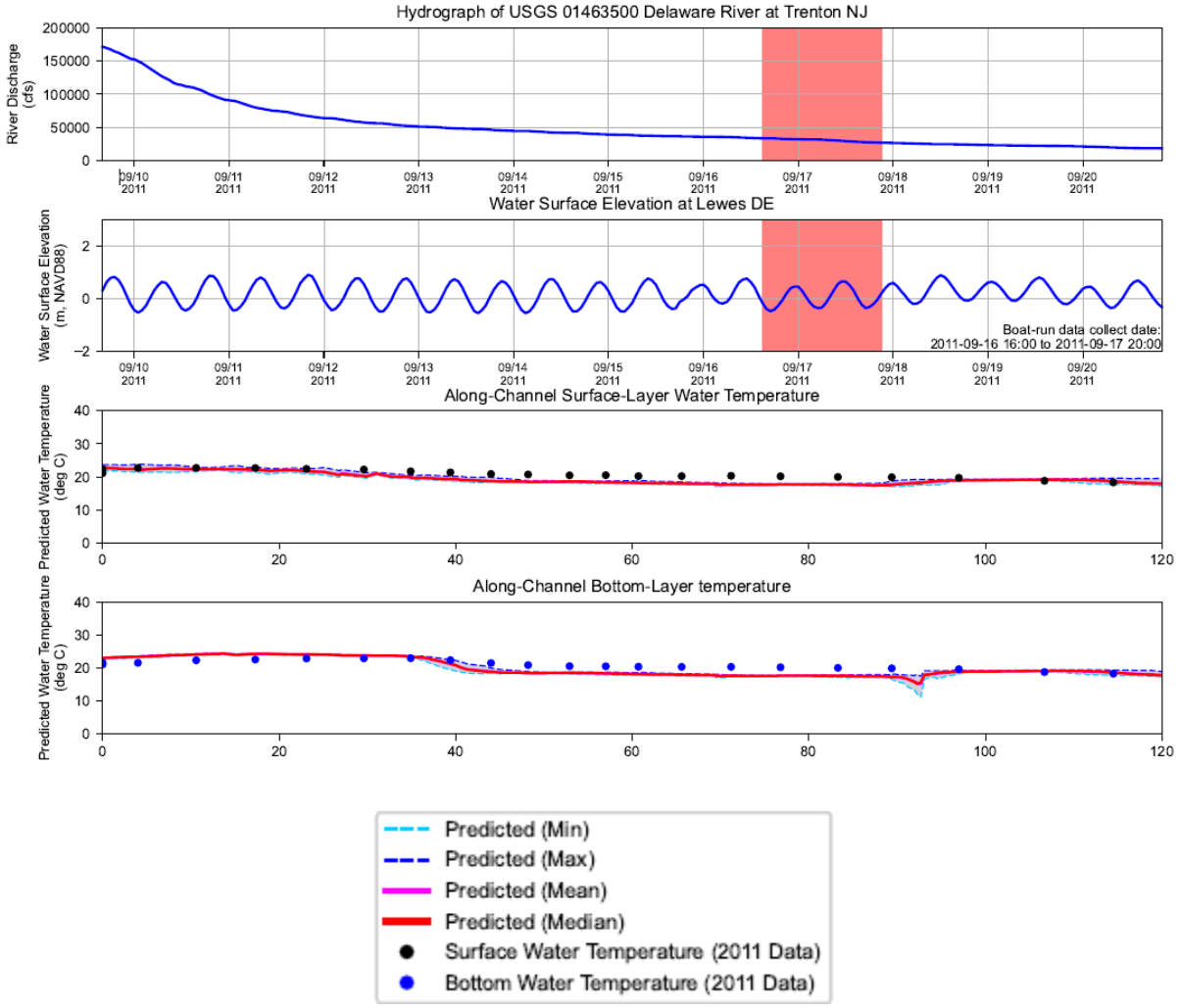

Notes: 2011 Survey data were provided by Rutgers University to DRBC on June 4th, 2019. Red shaded area indicates the survey time period: 2011-09-16 16:00 to 2011-09-17 20:00. Model results along the navigation channel during the period of 2011-09-16 15:00 to 2011-09-17 21:00 were used in this analysis.

Figure 4.3-56 Predicted Longitudinal Profile of Water Temperature and 2011 Survey Data

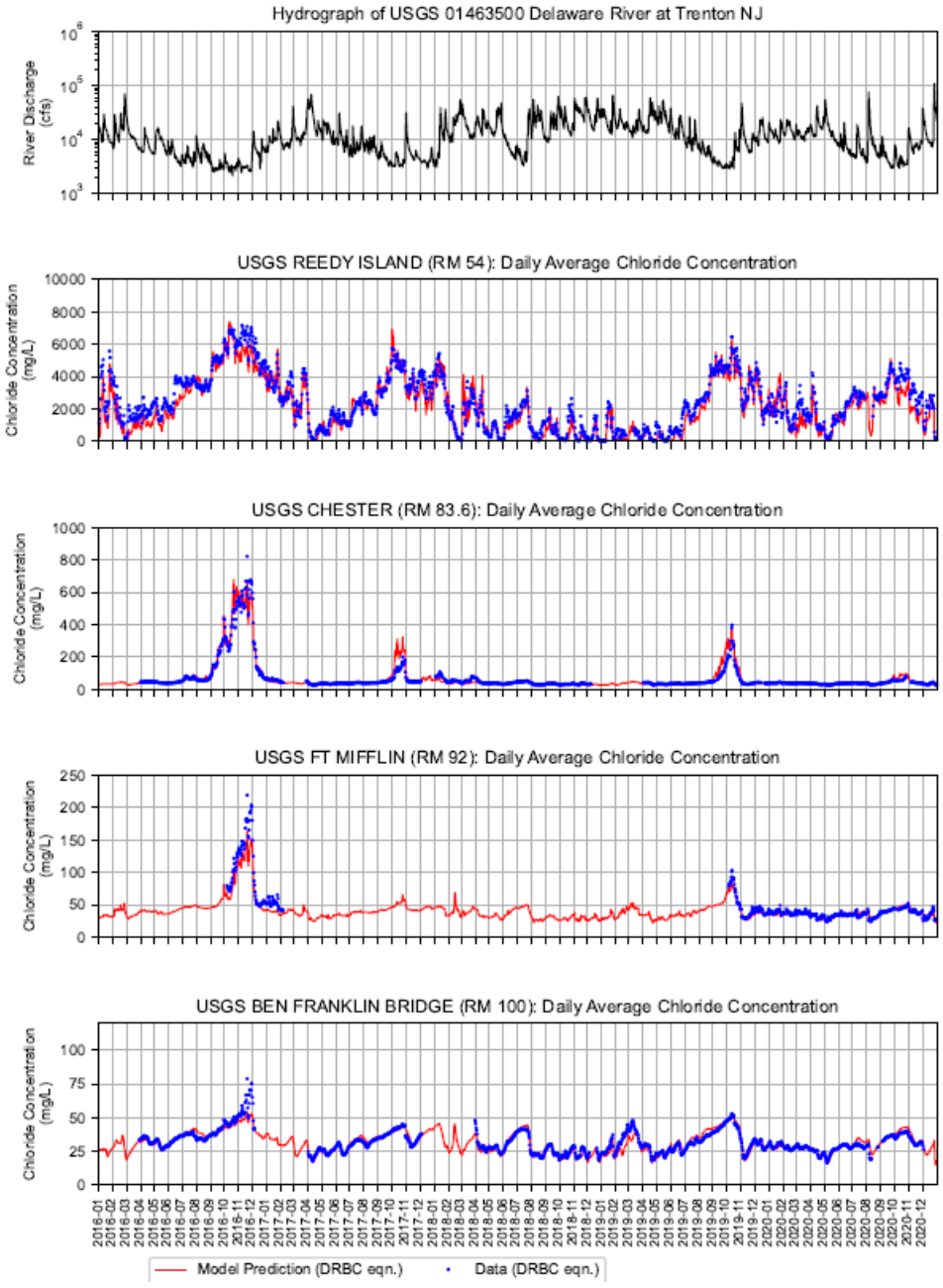

Notes: Observed Chlorinity was converted from observed salinity, which was derived from specific conductance (SC) and water temperature using the standard method. The predicted Chlorinity (red) was converted from model simulated salinity using a relationship developed by DRBC based on Boat Run data collected from 2000 to 2018 in the Delaware Estuary.

Figure 4.4-1 Observed and Predicted Daily Average Chlorinity at USGS Stations during 2016 to 2020. Observed-Salinity-Derived Chlorinity are Shown as Data.

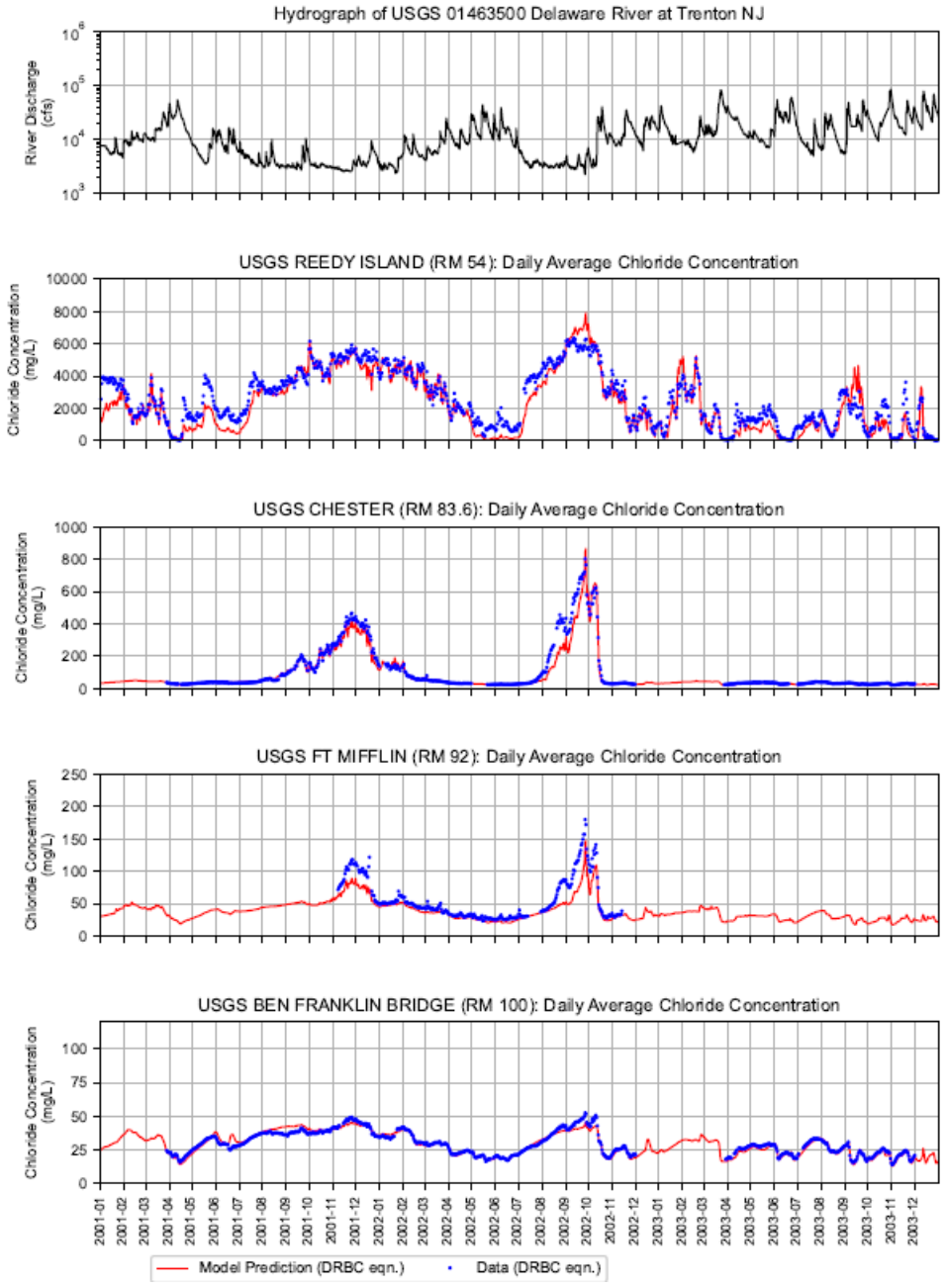

Notes: Observed Chlorinity was converted from observed salinity, which was derived from specific conductance (SC) and water temperature using the standard method. The predicted Chlorinity (red) was converted from model simulated salinity using a relationship developed by DRBC based on Boat Run data collected from 2000 to 2018 in the Delaware Estuary.

Figure 4.4-2 Observed and Predicted Daily Average Chlorinity at USGS Stations during 2001 to 2003. Observed-Salinity-Derived Chlorinity are Shown as Data.

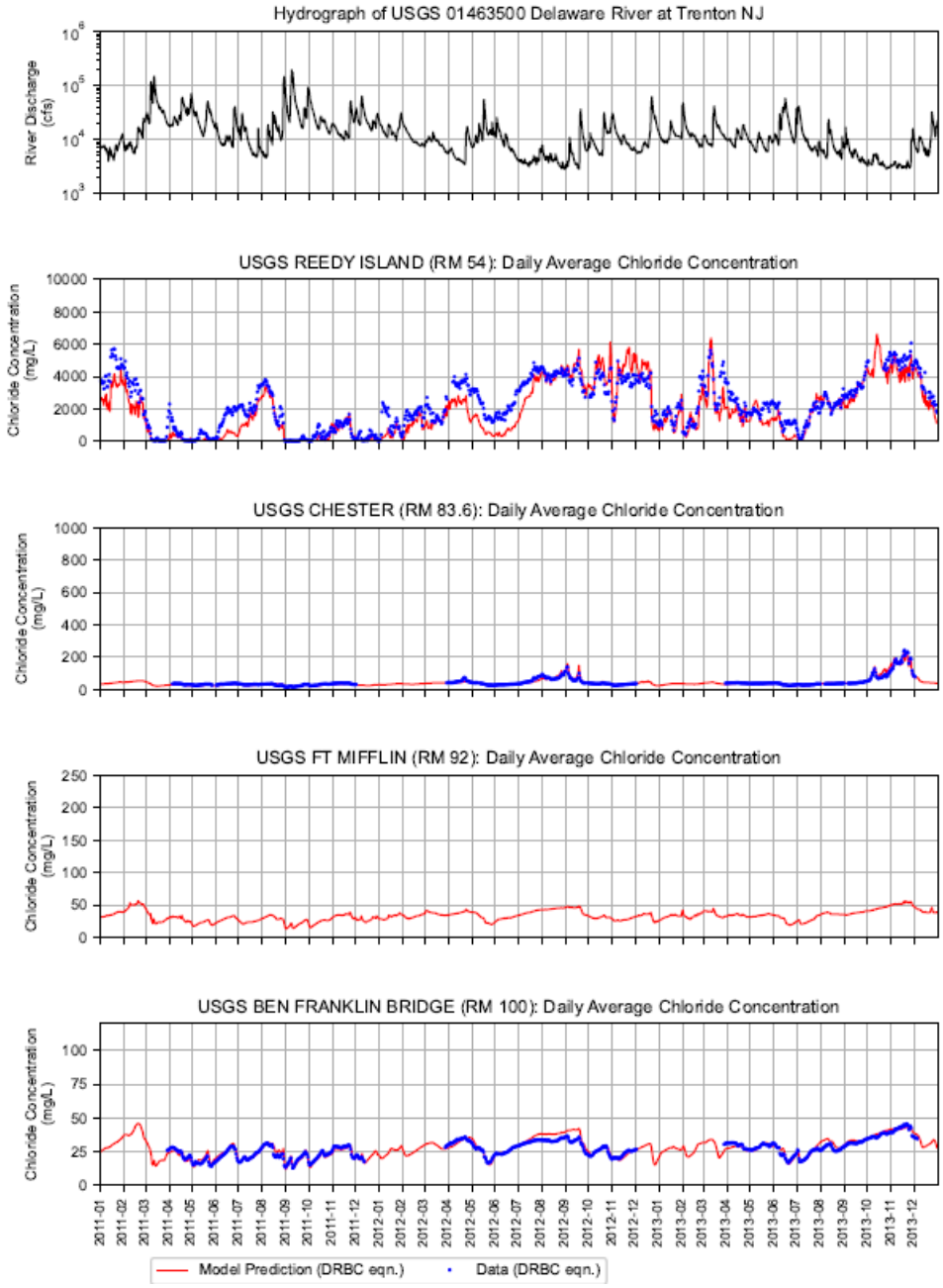

Notes: Observed Chlorinity was converted from observed salinity, which was derived from specific conductance (SC) and water temperature using the standard method. The predicted Chlorinity (red) was converted from model simulated salinity using a relationship developed by DRBC based on Boat Run data collected from 2000 to 2018 in the Delaware Estuary.

Figure 4.4-3 Observed and Predicted Daily Average Chlorinity at USGS Stations during 2001 to 2003. Observed-Salinity-Derived Chlorinity are Shown as Data.

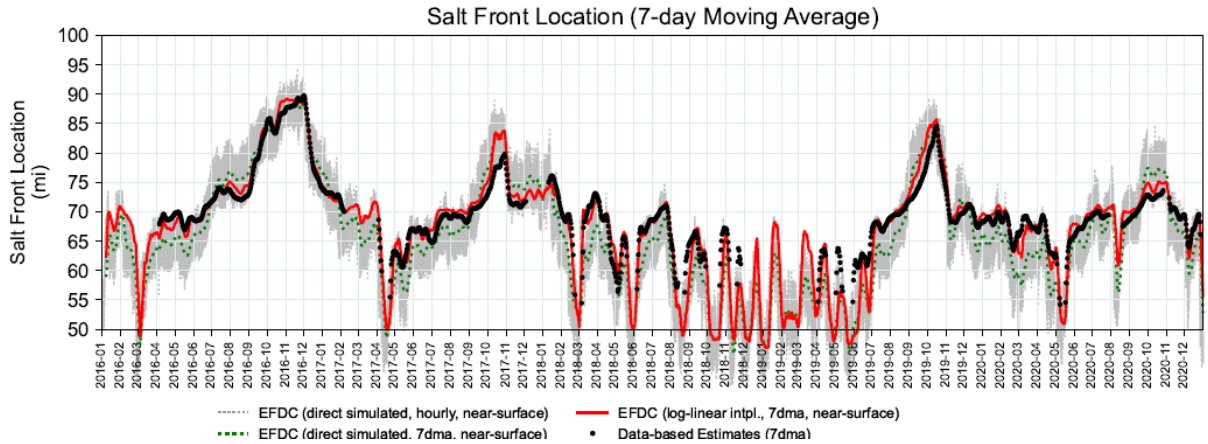

Note: EFDC Simulated Salt Front was based on the near-surface salinity. Data-based SF from optimal station pairs (OSP) were used.

Figure 4.4-4 (1) Time History of Predicted Salt Front during 2016 to 2020 Period

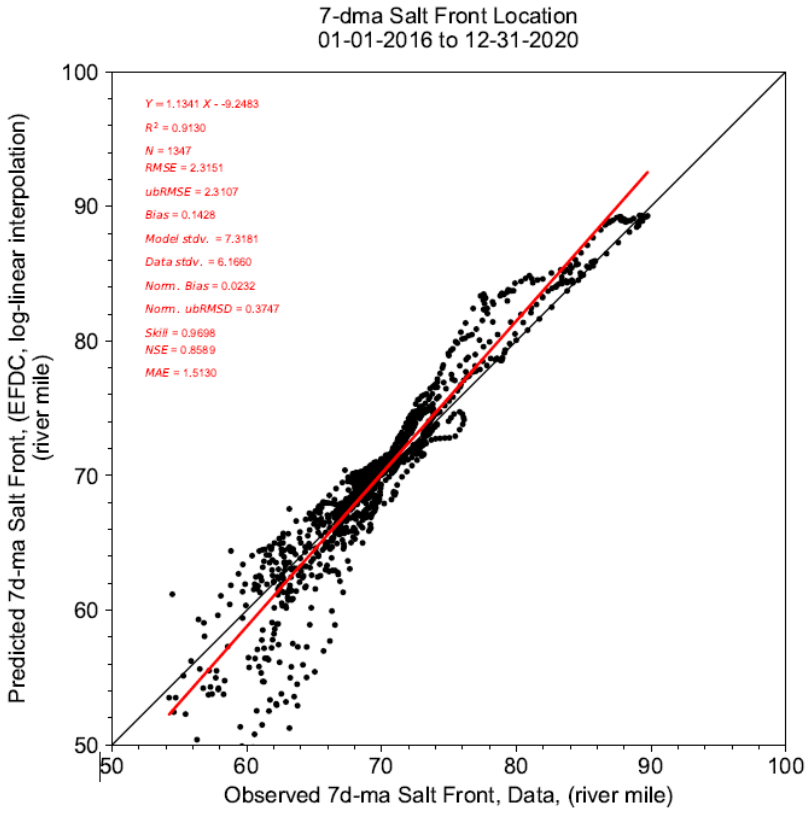

Figure 4.4-4 (2) Comparison of Observed and Simulated Salt Front during 2016 to 2020 Period

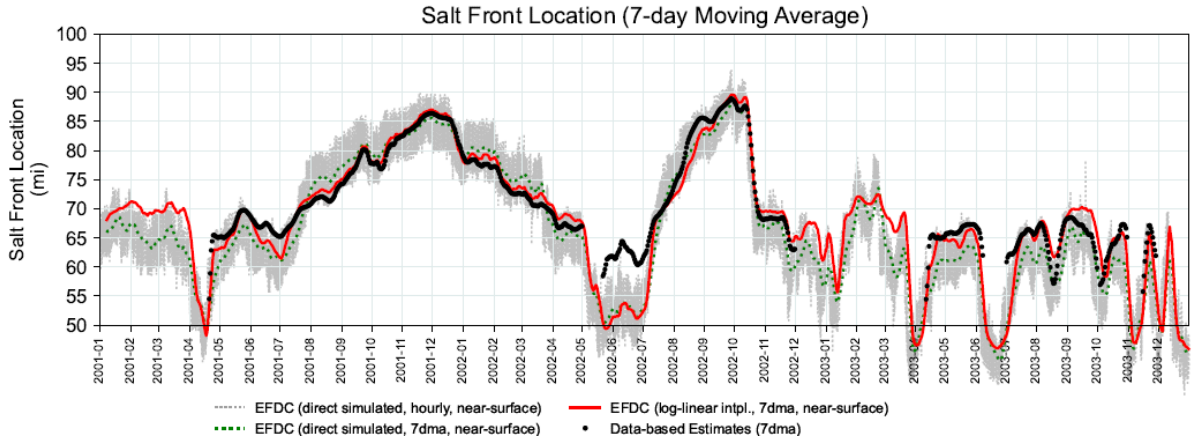

Note: EFDC Simulated Salt Front was based on the near-surface salinity. Data-based SF from optimal station pairs (OSP) were used.

Figure 4.4-5 (1) Time History of Predicted Salt Front during 2001 to 2003 Period

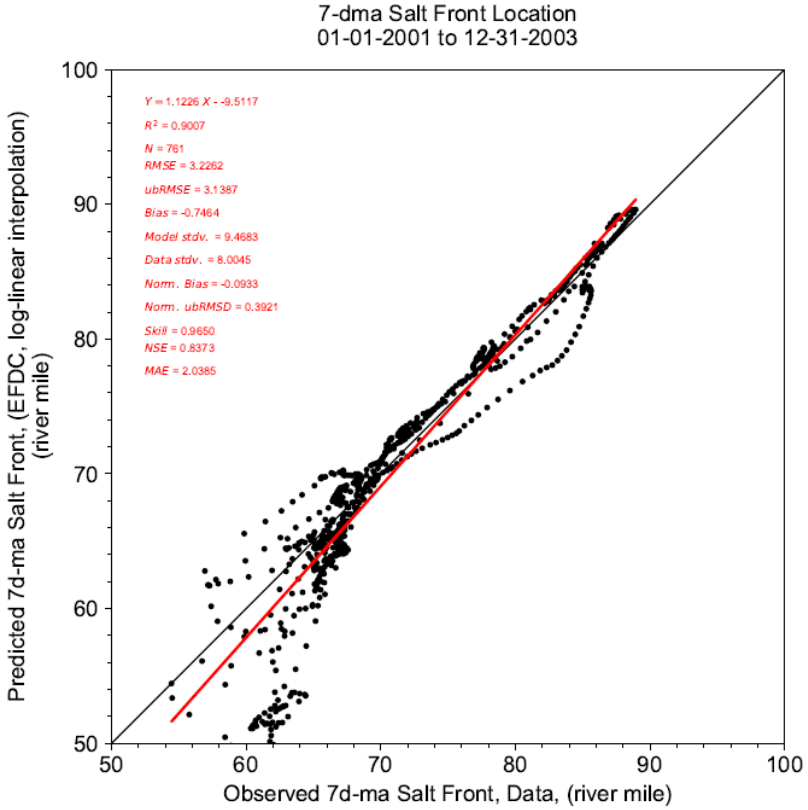

Figure 4.4-5 (2) Comparison of Observed and Simulated Salt Front during 2001 to 2003 Period

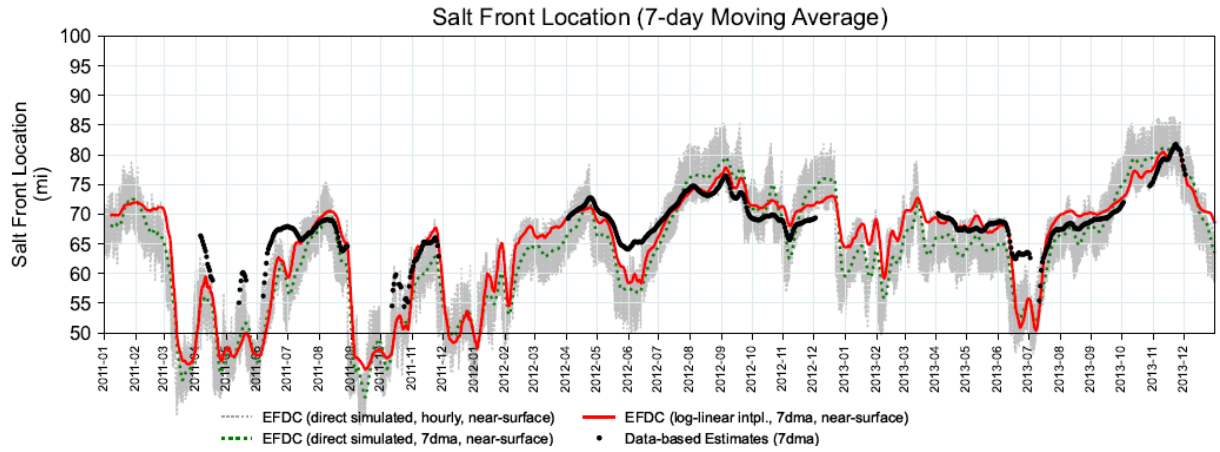

Note: EFDC Simulated Salt Front was based on the near-surface salinity. Data-based SF from optimal station pairs (OSP) were used.

Figure 4.4-6 (1) Time History of Predicted Salt Front during 2011 to 2013 Period

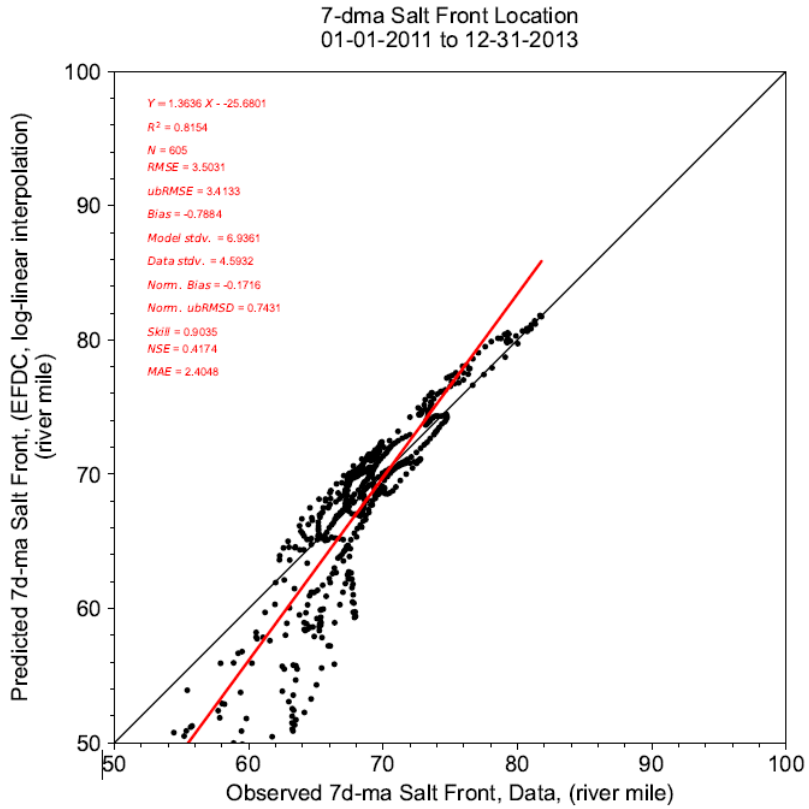

Figure 4.4-6 (2) Comparison of Observed and Simulated Salt Front during 2011 to 2013 Period

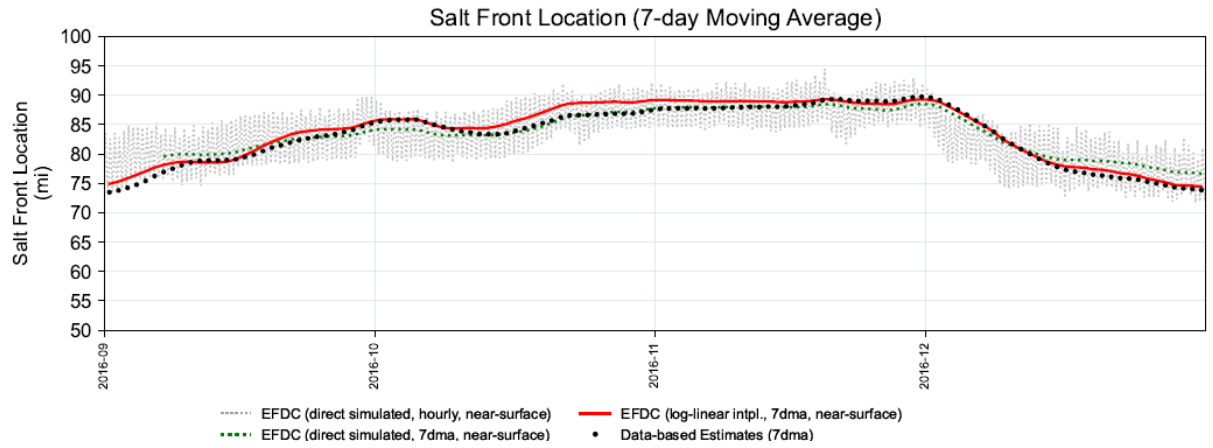

Note: EFDC Simulated Salt Front was based on the near-surface salinity. Data-based SF from optimal station pairs (OSP) were used.

Figure 4.4-7 (1) Time History of Predicted Salt Front during September through December 2016

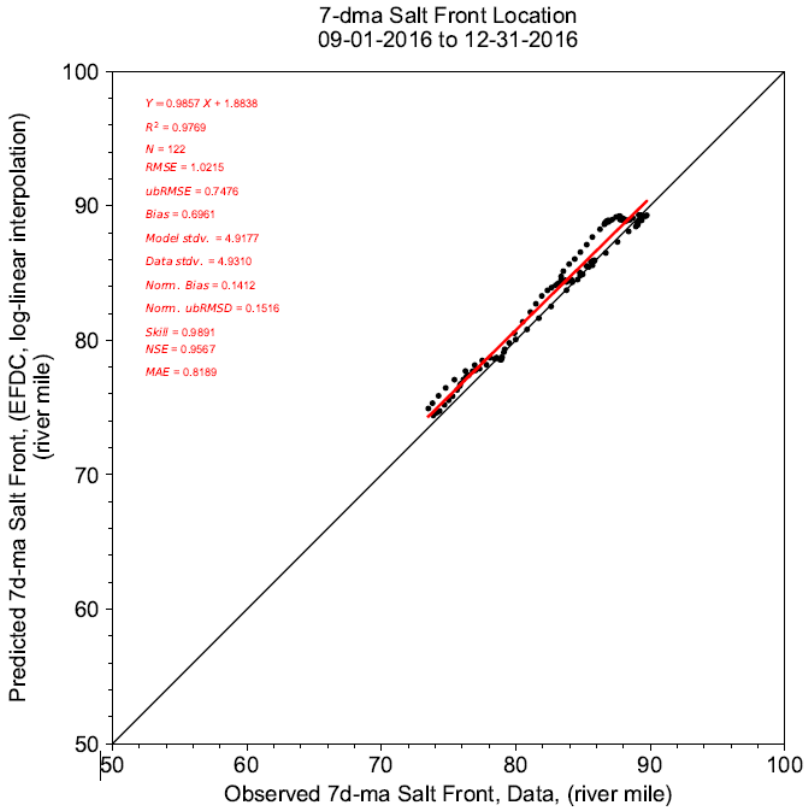

Figure 4.4-7 (2) Comparison of Observed and Simulated Salt Front during September through December 2016

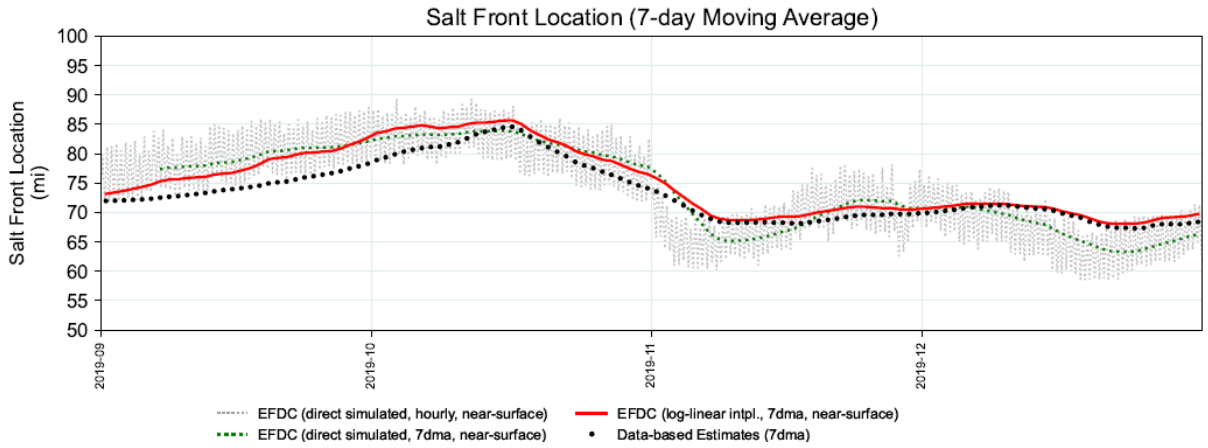

Note: EFDC Simulated Salt Front was based on the near-surface salinity. Data-based SF from optimal station pairs (OSP) were used.

Figure 4.4-8 (1) Time History of Predicted Salt Front during September through December 2019

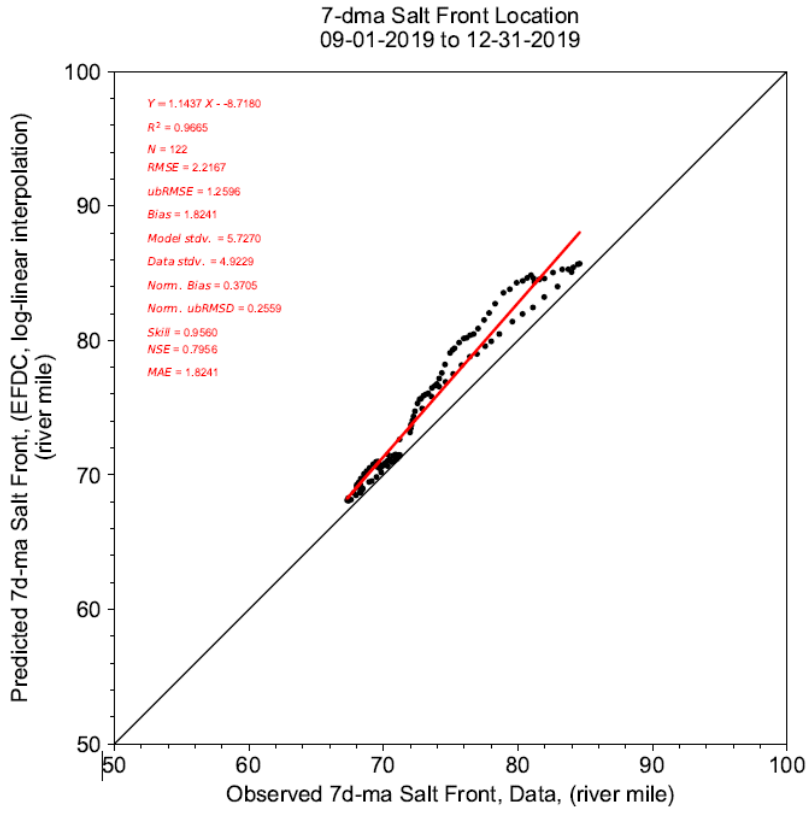

Figure 4.4-8 (2) Comparison of Observed and Simulated Salt Front during September through December 2019

REFERENCES

American Public Health Association. 1995. Standard Methods for the Examination of Water and Wastewater. APHA, Washington, DC.

Antonov J.I., Locarnini R.A., Boyer T.P., Mishonov A.V., Garcia H.E. and Levitus S. 2006. World Ocean Atlas 2005 Volume 2: Salinity, in: Jolley D.W. and Bell B.R. (Eds.) 2002. The North Atlantic Igneous Province: Stratigraphy, tectonic, volcanic, and magmatic processes. Geological Society Special Publication, 197: 253–269. NOAA Atlas NESDIS, 62(2). NOAA[S.l.]. 182 pp. https://doi.org/10.1144/GSL.SP.2002.197.

Aristizábal M. and R. Chant. 2013. A Numerical Study of Salt Fluxes in Delaware Bay Estuary. Journal of Physical Oceanography, American Meteorological Society, Volume 43, 1572–1588.

Aristizábal M. and R. Chant. 2014. Mechanisns driving stratification in Delaware Bay estuary, Ocean Dynamics 64: 1615–1629. https://doi.org/10.1007/s10236-014-0770-1.

Aristizábal M.F. and R.J. Chant. 2015. An Observational Study of Salt Fluxes in Delaware Bay. Journal of Geophysical Research: Oceans, American Geophysical Union, Volume 120 2751–2768.

Beven K. and Wood E.F. 1992. Flow routing and the hydrologic response of channel networks, in: Channel Networks Hydrology, Beven K. and Kirkby J.M. (Eds), John Wiley and Sons.

Bever A.J. and MacWilliams M.L. 2013. Simulating sediment transport processes in San Pablo Bay using coupled hydrodynamic, wave, and sediment transport models. Marine Geology. 345:235–253. https://doi.org/10.1016/j.margeo.2013.06.012.

Blumberg A.F. and Mellor G.L. 1987. A description of a three-dimensional coastal ocean circulation model in: Three-Dimensional Coastal Ocean Models, Coastal and Estuarine Science, Vol. 4. Heaps N.S. (Ed.) American Geophysical Union, 1–19.

Blumberg A.F., Khan L.A., and St. John J.P. 1999. Three-dimensional hydrodynamic model of New York Harbor region. Journal of Hydraulic Engineering, 125(8), 799–816.

Blumberg, A.F. and Pritchard D.W. (1997): Estimates of the Transport through the East River, New York. J. of Geophysical Research, Vol. 102, No. C3, 5685–5703.

Burchard, H. (2001): On the q2l Equation by Mellor and Yamada (1982). American Meteorological Society. May 2001. Page 1377.

Chen, F., Shallcross, A., and Nicholson, R. (2025). The Impact of Sea Level Rise on Salinity Intrusion in the Delaware River Estuary. (DRBC Report No: 2025-6). West Trenton, New Jersey. Delaware River Basin Commission. https://www.nj.gov/drbc/library/documents/SLR_WaterResourceImpactsDec2025.pdf

Chen, J.-L., Ralston, D. K., Geyer, W. R., Sommerfield, C. K., & Chant, R. J. (2018). Wave Generation, Dissipation, and Disequilibrium in an Embayment with Complex Bathymetry. Journal of Geophysical Research: Oceans, 123. doi: doi:10.1029/2018JC014381

Christine Szpilka, Kendra Dresback, Randall Kolar, Jesse Feyen and Jindong Wang. (2016). Improvements for the Western North Atlantic, Caribbean and Gulf of Mexico ADCIRC Tidal Database (EC2015). J. Mar. Sci. Eng. 2016, 4(4), 72; https://doi.org/10.3390/jmse4040072

Cook, Salme E., John C. Warner, Kendra L. Russell. A numerical investigation of the mechanisms controlling salt intrusion in the Delaware Bay estuary. Estuarine, Coastal and Shelf Science 283(2023)108257. https://doi.org/10.1016/j.ecss.2023.108257

Jones, Craig; Chang, Grace; and Roberts, Jesse, "Session 1 Presentation - Wave Energy Converter effects on wave, current, and sediment circulation: A coupled wave and hydrodynamic model of Santa Cruz, Monterey Bay, CA" (2015). Ocean Waves Workshop. 1. https://scholarworks.uno.edu/oceanwaves/2015/Session1/1

Dolgopolova, E. N. (2014). Sediment Transport and Saltwater Intrusion into the Weakly Stratified Estuary of the Delaware River. WATER RESOURCES Vol. 41 No. 2 2014.

DRBC, (2003). DYNHYD5 Hydrodynamic Model (version 2.0) and Chloride Water Qaulity Model for the Delaware Estuary. Delaware River Basin Commission, West Trenton, New Jersey, December 2003.

DRBC, (2017). DRBC resolution (2017-4): https://www.state.nj.us/drbc/library/documents/Res2017-04_EstuaryExistingUse.pdf

DRBC. October 2019. Modeling Eutrophication Processes in the Delaware Estuary: Quality Assurance Project Plan. Delaware River Basin Commission. West Trenton, New Jersey.

FEMA, 2011. FEMA Region III Storm Surge Study, “Coastal Storm Surge Analysis System Digital Elevation Model, Report 1: Intermediate Submission No. 1.1”. Prepared by USACE ERDC in March 2011.

Galperin B., L. H. Kantha, S. Hassid, and A. Rosati, (1988). A Quasi-equilibrium Turbulent Energy Model for Geophysical Flows. Journal of the Atmospheric Sciences, American Meteorological Society, Volume 45, No. 1 55-62.

Gardener, G.B. and Pritchard, D. W. (1974). Technical Report 87: Hydrographic and Ecological Effects of Enlargement of the Chesapeake and Delaware Canal: Appendix XV. Verification and Use of a Numerical Model of the C & D Canal. Final Report to The Philadelphia District, U.S. Army Corps of Engineers.

Castellano, P.J. and Kirby, J.T. (2011): Validation of a Hydrodynamic Model of Delaware Bay and the Adjacent Coastal Region. Research report NO. CACR-11-03, Ocean Engineering Laboratory, University of Delaware, Newark, Delaware 19716, June 2011.

Georgas, Nickitas (2010): Establishing Confidence in Marine Forecast Systems: The Design of a High-Fidelity Marine Forecast Model for the NY/NJ Harbor Estuary and Its Adjoining Coastal Waters. A Dissertation for Doctor of Philosophy, Steven Institute of Technology, NJ. Castle Joint on Hudson, Hoboken, NJ 07030, 2010.

Hamrick, J.M., (1992). A Three-Dimensional Environmental Fluid Dynamics Code: Theoretical and Computational Aspects. Special Report 317 in Applied Marine Science and Ocean Engineering, Virginia Institute of Marine Science, VA.

Hamrick, J.M. (2007a.) “The Environmental Fluid Dynamics Code User Manual: US EPA Version 1.01,” Tetra Tech, Inc., Fairfax, VA.

Hamrick, J.M. (2007b.) “The Environmental Fluid Dynamics Code Theory and Computation. Volume 1: Hydrodynamics and Mass Transport,” Tetra Tech, Inc., Fairfax, VA.

Hamrick, J.M. (2007c.) “The Environmental Fluid Dynamics Code Theory and Computation. Volume 2: Sediment and Contaminant Transport and Fate,” Tetra Tech, Inc., Fairfax, VA.

Hess, K.W., Gross T.F., Schmalz R.A., Kelley J.G.W., Aikman F. III, and Wei E., 2003. NOS Standards for Evaluating Operational Nowcast and Forecast Hydrodynamic Model Systems. NOAA Technical Report NOS CS 17. NOAA/NOS/CSDL. Silver Spring, Maryland. October 2003. 47p.

Ji, Z.-G., M.R. Morton, and J.M. Hamrick. (2001). “Wetting and drying simulation of estuarine processes,” Estuarine, Coastal and Shelf Science, 53:683-700.

Ji, Z.-G., G. Hu, J. Shen, and Y. Wan. (2007). “Three-dimensional modeling of hydrodynamic processes in the St. Lucie Estuary,” Estuarine, Coastal and Shelf Science, 73:188-200.

Johnson, B. H., Heath, R. E., Hsieh, B. B., Kim, K. W., and Martin, B. L. 1999. Assessment of Channel Deepening in the Chesapeake and Delaware Canal and Approach Channels in Upper Chesapeake Bay: Three-Dimensional Numerical Model Study. Draft Report. Waterways Experiment Station. Prepared for U.S. Army Engineer District, Philadelphia.

Johnson, B.H., K.W. Kim, R.E. Heath, B.B. Hsieh, and H.L. Butler, (1993): Validation of three-dimensional hydrodynamic model of Chesapeake Bay. J. Hyd. Eng., 119, 2-20.

Kim, S.-Cn (2013), Evaluation of a Three-Dimensional Hydrodynamic Model Applied to Chesapeake Bay Through Long-term Simulation of Transport Processes, JAWRA, Vol.49, No.5.

Kim, K.W. and Johnson, B.H. (2007): Salinity Re-validation of the Delaware Bay and River 3D Hydrodynamic Model with Applications to Assess the Impact of Channel Deepening, Consumptive Water Use, and Sea Level Change. Final report, April 2007, prepared for U.S. Army Engineer District, Philadelphia.

Leonard B. P., A. P. Lock, and M. K. MacVean, (1996). Conservative Explicit Unrestricted-Time-Step Multidimensional Constancy-Preserving Advection Schemes. Monthly Weather Review, American Meteorological Society, Volume 124, 2588-2606.

Locarnini, R. A., A. V. Mishonov, J. I. Antonov, T. P. Boyer, H. E. Garcia, O. K. Baranova, M. M. Zweng, C. R. Paver, J. R. Reagan, D. R. Johnson, M. Hamilton, D. Seidov, (2013). World Ocean Atlas 2013, Volume 1: Temperature. S. Levitus, Ed.; A. Mishonov, Technical Ed.; NOAA Atlas NESDIS 73, 40 pp. This document is available online at http://www.nodc.noaa.gov/OC5/indprod.html

MacCready and Geyer (2010): Advances in Estuarine Physics, Annu. Rev. Mar. Sci. 2010. 2:35–58. doi: 10.1146/annurev-marine-120308-081015

MacWilliams, Michael L., Bever, Aaron J., Gross, Edward S., Gerard S. Ketefian2, and Wim J. Kimmerer3 (2015). Three-Dimensional Modeling of Hydrodynamics and Salinity in the San Francisco Estuary: An Evaluation of Model Accuracy, X2, and the Low–Salinity Zone. San Francisco Estuary and Watershed Science, 13(1).

Mellor G. L. and T. Yamada, 1982. Development of a Turbulence Closure Model for Geophysical Fluid Problems. Reviews of Geophysics and Space Physics, Volume 20, No. 4, 851-875.

Mellor, G.L. and T. Ezer (1995): “Sea level variations induced by heating and cooling: An evaluation of the Boussinesq approximation in ocean models.” Journal of Geophysical Research. 100(C10): 20565-20577.

NOAA (2003): “NOS Standards for Evaluating Operational Nowcast and Forecast Hydrodynamic Model Systems.” NOAA Technical Report NOS CS 17. NOAA/NOS/CSDL. Silver Spring, Maryland. October 2003. 47p.

Pareja-Roman, L. F., Chant, R. J., and Ralston, D. K. (2019). Effects of locally generated wind waves on the momentum budget and subtidal exchange in a coastal plain estuary. Journal of Geophysical Research: Oceans, 124, 1005–1028. https://doi.org/10.1029/2018JC014585

Patchen, R., 2007. Establishment of a Delaware Bay Model Evaluation Environment. Proceedings of the 10th International Conference in Estuarine and Coastal Modeling (ECM10). Malcolm L. Spaulding, editor. 5-7 November 2007. Newport, RI. 783-818.

Paulson, R.W. A graphical summary of specific conductance data for the Delaware River Estuary correlated with Delaware River flow at Trenton, New Jersey, 1970. 10.3133/ofr70260, USGS Publications Warehouse, http://pubs.er.usgs.gov/publication/ofr70260

Pritchard, D. W., Gardner, G. B. 1974. Technical Report 85: Hydrography of the Chesapeake and Delaware Canal. Chesapeake Bay Institute, The Johns Hopkins University. U.S. Army Corps of Engineers Contract No. DACW 67-71-C-0062. Philadelphia, PA February 1974.

PWD (May, 2020), Delaware Estuary Salinity Model Validation, Philadelphia Water Department, Watershed Protection Program. https://water.phila.gov/wp-content/uploads/files/salinity-model-validation-report-2020-05.pdf

Salehi, M. (2017), Thermal Recirculation Modeling for Power Plants in an Estuarine Environment, J. of Marine Science and Engineering, 2017, Vol.5, No.5, doi: 10.3390/jmse5010005

Schmalz, R.A. (2011), Three-dimensional Hydrodynamic Model Developments for a Delaware River and Bay Nowcast/Forecast System. NOAA Technical Report NOS CS 28, January 2011. Office of Coast Survey, Coast Survey Development Laboratory, Silver Spring, MD

Schopp, R.D., and Firda, G.D., (2008), Flood magnitude and frequency of the Delaware River in New Jersey, New York, and Pennsylvania: U.S. Geological Survey Open-File Report 2008–1203, 7 p

St. Johns River Water Management District (SJRWMD). 2012. “St. Johns River Water Supply Impact Study,” Technical Publication SJ2012-1. St. Johns River Water Management District, Palatka, FL.

Saint-Venant, AJC (1871) “Theory of the non-permanent movement of water, with application to the flooding of rivers and the introduction of tides in their beds”. Minutes of the Sessions of the Academy of Sciences, 73, 147, 237.

Sharp, J. H., K. Yoshiyama, A. E. Parker, M. C. Schwartz, S. E. Curless, A. Y. Beauregard, J. E., Ossolinski, and A. R. Davis, (2009). A biogeochemical view of estuarine eutrophication: seasonal and spatial trends and correlations in the Delaware Estuary. Estuaries and Coasts, 32: 1023-1043.

Smagorinsky, J. (1963) General Circulation Experiments with the Primitive Equations, Part 1, Basic Experiments. Monthly Weather Review, 91, 99-164.

Sucsy, P.V., and F.W. Morris. (2002). "Calibration of a Three-dimensional Circulation and Mixing Model of the Lower St. Johns River," Technical Memorandum, St. Johns River Water Management District, Palatka, FL.

Sverdurp, H.U., Martin W. Johnson, Richard H. Fleming. (1942): The Oceans Their Physics, Chemistry, and General Biology. Prentice-Hall, Inc. New York. https://publishing.cdlib.org/ucpressebooks/view?docId=kt167nb66r

Tetra Tech, Inc. (2002). User's Manual for Environmental Fluid Dynamics Code. Hydro Version 1.00 for U.S. Environmental Protection Agency, Region 4, Atlanta, GA. August 1, 2002.

Tetra Tech, Inc. (2006). EFDC Technical Memorandum: Theoretical and Computational Aspects of the Generalized Vertical Coordinate Option in the EFDC MoDE Prepared for US Environmental Protection Agency, Region 4, Atlanta, GA. March 2006

Tetra Tech, Inc. (2015): Hydrodynamic and Water Quality Modeling Report for the Savannah Harbor, Georgia. Final Report V3, prepared for Army Corp Engineering, Savannah District, Corps of Engineers, 100 W Oglethorpe Avenue, Savannah, Georgia 31401-3640. Contract: 100-ATL-T32468

Thatcher, L. M., Najarian, T. O. 1981. Comparison of Salt Intrusion in the Delaware Estuary Under the Influence of Pre- and Post- Enlargement Flows in C & D Canal. U.S. Army Corps of Engineers Contract No. DACW 61-80-C-0080. Najarian, Thatcher & Associates Inc. Closter, NJ. March 1981. 51pp.

USACE (2014): Final Study Report, Influence of Open-Lake Placement of Dredged Material on Western Lake Erie Basin Harmful Algal Blooms. Prepared for USACE by Ecology and Environment Inc. and LimnoTech. Contract No. W912P4-10-D-0002. August 2014. http://wwwapp.ePAstate.oh.us/dsw/USACE/1-R-WLEB-Final-Report.pdf

Valle-Levinson, A. (2009). Definition and classification of estuaries. Cambridge University Press, 978-0-521-89967-3 – Contemporary Issues in Estuarine Physics, Edited by A. Valle-Levinson.

Wang, H. V. and Johnson, B. H. (2002). Validation and Application of the Second Generation Three-Dimensional Hydrodynamic Model of Chesapeake Bay. Water Quality and Ecosystem Modeling.

Ward, N.D., Gebert J.A, Weggel JR. 2009. Hydraulic Study of the Chesapeake and Delaware Canal. Journal of Waterway, Port, Coastal, and Ocean Engineering. ASCE. 135(1) Technical Note. https://doi.org/10.1061/(ASCE)0733-950X(2009)135:1(24)

Warner, B. A., Ruoying He, and Joseph B. Zambon1 (2010), Development of a Coupled Ocean-Atmosphere-Wave-Sediment Transport (COAWST) Modeling System, Ocean Modelling, 35(2010)230–244

Wei, X., Schramkowski, G.P., and Schuttelaars, H.M., (2016): Salt Dynamics in Well-Mixed Estuaries: Importance of Advection by Tides. AMS, J. of Physical Oceanography, Vol 46, pp1457-1475. DOI: 10.1175/JPO-D-15-0045.1

Willmott CJ. 1981. On the Validation of Models. Physical Geography. 2(2):184-194. https://doi.org/10.1080/02723646.1981.10642213

Wool, T.A., S.R. Davie, and H.N. Rodriguez. (2003). "Development of Three-Dimensional Hydrodynamic and Water Quality Models to Support Total Maximum Daily Load Decision Process for the Neuse River Estuary, North Carolina," Journal of Water Resources Planning and Management, 129(4), 295–306.

Xu, Long (2006): Numerical study in Delaware Inland Bays. Master's thesis, University of Delaware, Department of Civil and Environmental Engineering.

Xu, J., Long, W., Wiggert, J.D. et al. Climate Forcing and Salinity Variability in Chesapeake Bay, USA. Estuaries and Coasts 35, 237–261 (2012). https://doi.org/10.1007/s12237-011-9423-5.

Zhang, A. 2006. Implementation of Model Skill Assessment Software for Water Level and Current in Tidal Regions, U.S. Department of Commerce, National Oceanic and Atmospheric Administration, National Ocean Service, Office of Coast Survey, Coast Survey Development Laboratory.

Zhang, Q., Tan, F., Han, T., Wang, X., Hou, Z., & Yang, H. (2011). Simulation of Sorting Sedimentation in the Channel of Huanghua Harbor by Using 3D Multi-sized sediment Transport Model of EFDC. Coastal Engineering Proceedings, 1(32), sediment.22. https://doi.org/10.9753/icce.v32.sediment.22

Zhang, A., Hess, K.W., Wei, E., and Myers, E., 2006. Implementation of Model Skill Assessment Software for Water Level and Current in Tidal Regions, U.S. Department of Commerce, National Oceanic and Atmospheric Administration, National Ocean Service, Office of Coast Survey, Coast Survey Development Laboratory

Zheng, L., Chen, F., Bransky, J., Panuccio, E., Beganskas, S., Amidon, T., Yagecic, J., Suk, N., & Kavanagh, K.B. (2024). Modeling Eutrophication Processes in the Delaware River Estuary: Three-Dimensional Water Quality Model. (DRBC Report No. 2024-5). Delaware River Basin Commission. https://www.nj.gov/drbc/library/documents/ALDU_RestorationPathway/WQCalibration_FinalRpt_aug2024.pdf

Zweng, M. M, J. R. Reagan, J. I. Antonov, R. A. Locarnini, A. V. Mishonov, T. P. Boyer, H. E. Garcia, O.K. Baranova, D.R. Johnson, D. Seidov, M.M. Biddle, (2013). World Ocean Atlas 2013, Volume 2: Salinity. S. Levitus, Ed.; A. Mishonov, Technical Ed.; NOAA Atlas NESDIS 74, 39 pp. This document is available online at http://www.nodc.noaa.gov/OC5/indprod.html

APPENDIX A. COMPARISON OF TWO 3D HYDRODYNAMICS MODELS

Table A.1-1. Differences between the 3D Hydrodynamic Salinity Model (SM3D) and 3D-Hydrodynamic Model for the Eutrophication Study

	Aspect	SM3D	3D model for Eutrophication Modeling Study
1	Application	Evaluations of salinity-related questions (Impact of SLR on salinity intrusion; Drought Management, Water resource planning for future climate change	Eutrophication modeling study; part of eutrophication model framework
2	Link to water quality model (WASP)	No	Yes
3	Domain	From the head of tide at Trenton (RM 133) into the Atlantic Ocean. The eastern ocean open boundary includes the Atlantic Ocean 68 km (42 mi) from shore on the continental shelf along the 60 m isobath. The northern and Southern Ocean boundaries of the coastal zone are located 96 and 100 km (60 and 62 mi) from the mouth of Delaware Bay, respectively. Includes the C&D Canal.	From the head of tide at Trenton (RM 133) to the mouth of the Bay (RM 0). Includes the C&D Canal.
4	Grid resolution	Maximum of 20 vertical layers in the ocean; 8 to 9 layers in the federal navigation channel (FNC)	Maximum of 12 vertical layers; 10 layers in the federal navigation channel (FNC). Upstream of Philadelphia, the navigation channel may have 8 or fewer layers.
5	Reason for location where downstream boundary is set	The ocean boundary was used to minimize the uncertainty in salinity boundary conditions. Ocean salinity is relatively stable, whereas salinity at the mouth of the bay is highly variable. A large portion of the offshore coastal area was included to provide a more realistic representation of hydrodynamics and transport processes in the vicinity of the mouth of the Bay (e.g., fresher water transported into the Atlantic Ocean during ebb tide and saltwater transported into the Delaware Bay during a subsequent flood tide).	The downstream open boundary was set at the mouth of the bay, allowing for the utilization of nutrient data collected at the mouth of the Bay. Using observed data reduces uncertainty in the estimation and calibration of numerous model parameters for the simulation of the multiple bio-chemical processes in the linked EFDC–WASP modeling suite.

	Aspect	SM3D	3D model for Eutrophication Modeling Study
6	Wetting/Drying and Marsh inundation	Grid v2.2 (SM3D) was confined by the existing shoreline, which excludes marsh areas that are less frequently inundated. This more compact grid was used to manage computational efficiency. Grid v4.2 (SM3D+M) includes more of the low-lying marsh area. The impact of the additional marsh area on estuary hydrodynamics and salinity intrusion were investigated.	Not simulated
7	Inflow Boundaries	Flow from Trenton, 32 tributaries, 8 withdrawals, 71 point sources. Note: CSOs carry a high BOD load, affecting dissolved oxygen, but do not need to be modeled for salinity	Flow from Trenton, 32 tributaries, and 11 withdrawals, 71 point sources, 14 consolidated CSOs, 66 MS4s, and 37 non-point sources
8	Nutrient Loads	Not needed for salinity.	Yes, simulated in WASP
9	Numerical scheme for solving transport equation	Upwind	COSMIC
10	Turbulent Diffusion	Both horizontal and vertical diffusion are included	Vertical diffusion only
11	Primary Calibration Period	2017–2018 (later extended to 2016–2020)	2018–2019
12	Additional simulated period(s)	1964–1965, 2001–2003, 2011–2013, results for C&D Canal flow simulated for 2021-2022 period are also included in this report.	2012
13	Salinity and salt front location	Yes	Salinity was not of concern for this study. of salinity was considered.

APPENDIX B. SM3D SENSITIVITY TO VERTICAL GRID RESOLUTION

Downstream of RM 79, vertical stratification of salinity is typically observed, with fresher, less dense water from freshwater inflow moved seaward over the surface layer, and saltier, denser ocean water pushed landward in the bottom layer (see Section 1.2.1). To ensure that the model captures the vertical structure correctly, a sensitivity analysis was performed to determine adequate vertical grid resolution before setting up the model boundary conditions and carrying out model calibration. The main objective was to determine the number of vertical layers (KC parameter in EFDC) required to adequately simulate physical processes in the estuary while also maintaining model efficiency.

Three test models were developed with 5, 10, and 15 vertical layers in the navigation channel to determine an appropriate number. The downstream ocean open boundary was set at the mouth of the Delaware Bay, and tidal forcing was specified with the NOAA tide data at Lewes, DE. Sensitivity simulations were performed for August 2012, a relatively calm and dry period with average flow from the Delaware River at Trenton between 4,200 and 4,800 cfs. Current velocity, water surface elevation [WSE], water temperature, and salinity were analyzed for a spring tide (August 19, 2012, at 16:00 to August 21, 2012, at 16:00) and a neap tide (August 10, 2012, at 10:00 to August 12, 2012, at 10:00). Simulation conditions for flow and tide are shown in Figure B-1. Model results from the navigational channel as well as from three cross-sections (shown in Figure B-2, at RM 37, 42, and 69) were used to assess model performance.

As the number of vertical layers increases, the predicted velocity and salinity structures converge. With 5, 10, and 15 layers, the model produced WSE results with little difference at the three selected locations (Figure B-3). The longitudinal distribution of predicted tidally-averaged 32-HR-LPF salinity along the FNC during a spring tide and a neap tide are presented in Figure B-4. Comparisons of the predicted 32-HR-LPF depth-averaged salinity longitudinal profiles are shown in Figure B-5 for the same spring and neap tides. The higher vertical resolution grid tends to predict lower salinity along the longitudinal profile. The tidally-averaged longitudinal residual salinity profiles deviate upstream of RM 25, and the difference in predicted salinity is largest between RM 40 and 60, where the 5-layer model predicts salinities 2 to 3 psu higher than the 15-layer model.

Predicted current and salinity structures were compared among the three models by normalizing results from these test models. Each model result was divided by the maximum value of the cross-section to represent the intensity of salinity intrusion, with values ranging from 0 to 1. A similar approach was applied to normalize current velocity results, with normalized values ranging from -1 to 1. This approach focused on the gradient and shape of the vertical and longitudinal profiles rather than absolute values.

The predicted cross-sectional distribution of the 'raw' and normalized tidally-averaged 32-HR-LPF salinity are presented in Figures B-6 through B-8. At RM 69, as expected, the river was well-mixed with a near-uniform vertical salinity profile. Stronger vertical salinity stratification occurred at RM 37 and RM 42, with saltier water at the bottom. At these two locations, the vertical stratification was stronger during neap tide than spring tide. At RM 42, the water near the Delaware side of the bay was fresher than the water closer to the New Jersey side. The normalized salinity distribution produced by the three models were consistent, with the 10-layer model results being closer to the 15-layer model than the 5-layer model.

The predicted cross-sectional distribution of the 'raw' and normalized tidally-averaged 32-HR-LPF along-channel current velocity are presented in Figures B-9 through B-11. A clear typical estuary exchange flow structure was predicted at RM 37 and 42, with the fresher water moving seaward at the surface and the saltier water moving landward from the ocean near the bottom. At RM 69, the velocity profile became the typical logarithmic profile with unidirectional seaward flow. During neap tide, the model predicted a net landward movement of water near the New Jersey side and a net seaward movement of water near the Delaware side in the mid and upper bay; during spring tide, by contrast, the model predicted net seaward moving water on the top from shore to shore. The 10-layer model and 15-layer model produced similar normalized results.

Vertical profiles of tidally-averaged 32-HR-LPF current velocity, salinity, and water temperature in the FNC from the three cross-sections are presented in Figures B-12 through B-20 without normalization; the shape and gradient of the vertical profiles were evaluated. The 10-layer model and 15-layer model produced similar results, though the 10-layer model was considered more desirable because of its faster run time and efficiency in storing and processing data.

Sensitivity tests to vertical layer resolution indicated that: a) a model of 10-layers in the navigational channel adequately captures the vertical structures of salinity and current; b) a 5-layer model performed well but may not adequately capture all gradients; and c) it is likely that more than five layers but less than ten would also perform adequately. Based on this analysis, a model with 8 vertical layers in the FNC was chosen to ensure efficiency without compromising model predictability and accuracy. Two versions of the numerical model grid, Grid v2.2 (without low-lying marshes) and Grid v4.2 (with low-lying marshes) were constructed.

Figures for Appendix B

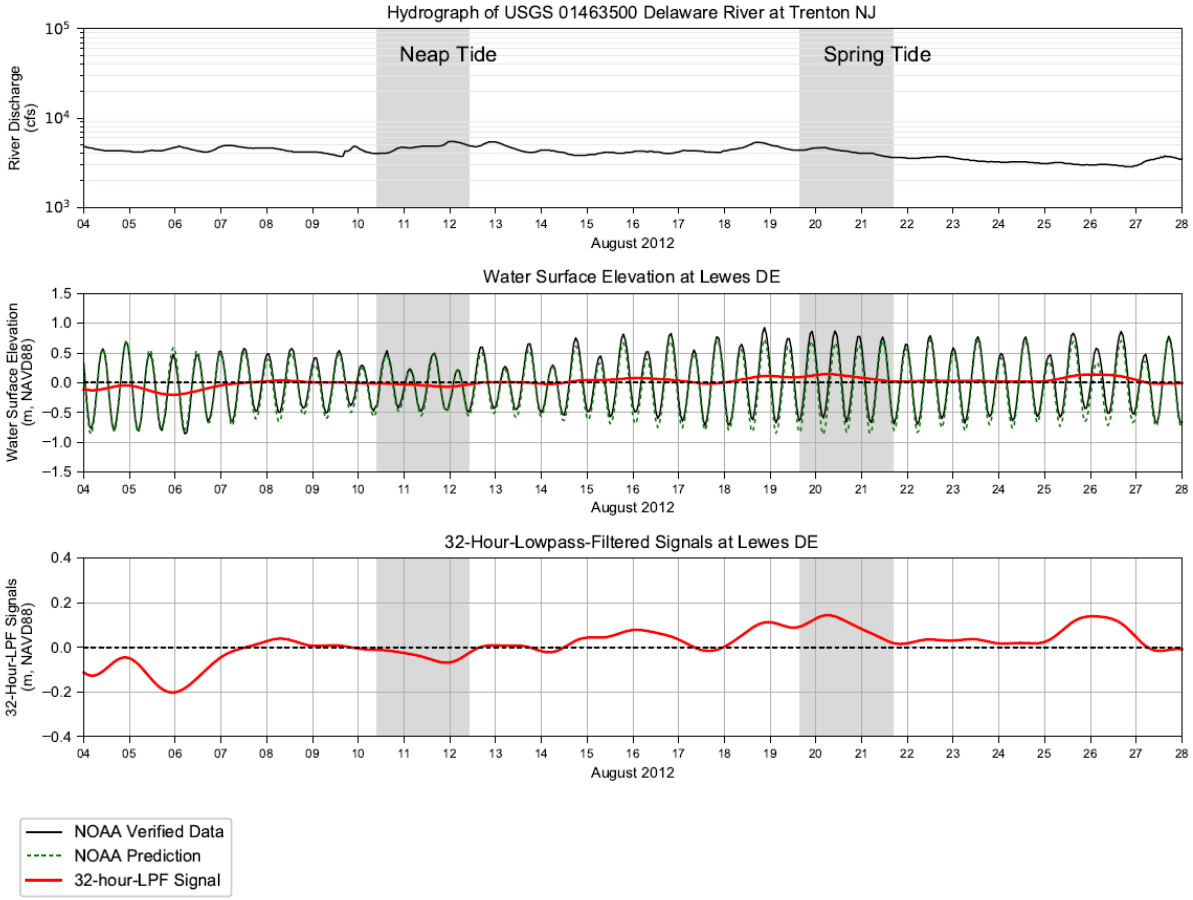

Selected time window for neap tide: 08-10-2012 10:00 to 08-12-2012 10:00
Selected time window for spring tide: 08-19-2012 16:00 to 08-21-2012 16:00

Figure B. 1 River Flow at Trenton and Observed Tide at Lewes during August 2012 Period

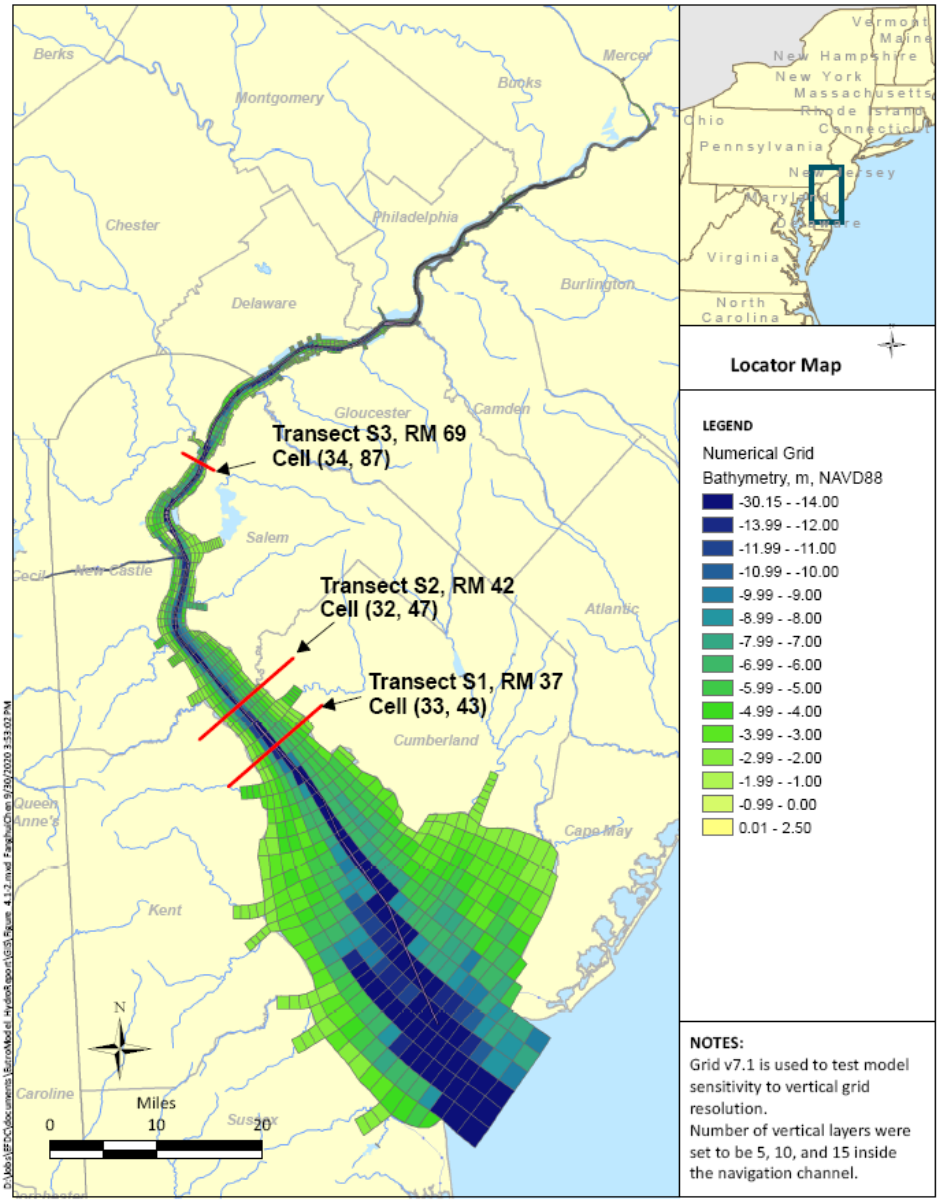

Note: This is a separate simplified grid that was used for sensitivity analysis

Figure B.2 Numerical Grid with Selected Cells and Transect Locations for Vertical Grid Resolution Sensitivity Analysis

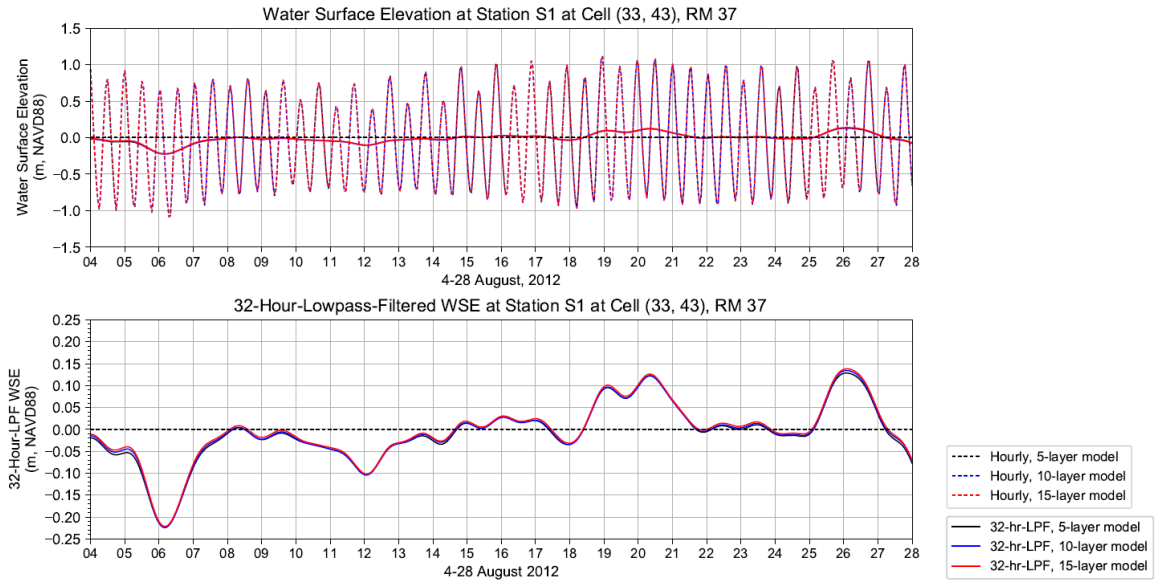

Figure B.3 (1) Simulated Hourly and 32-HR-LPF water Surface Elevation during 08-04-2012 to 08-28-2012 at Station S1 at Cell (33, 43), RM 37. The solid line in the top panel indicates the 32-LPF water levels.

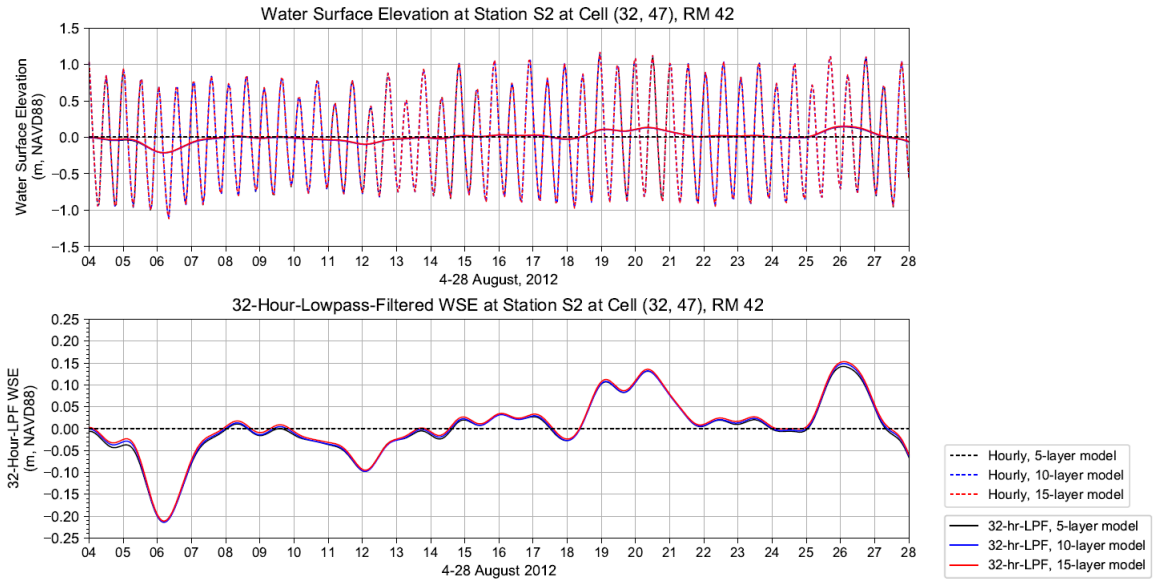

Figure B.3 (2) Simulated Hourly and 32-HR-LPF water Surface Elevation during 08-04-2012 to 08-28-2012 at Station S2 at Cell (32, 47), RM 42. The solid line in the top panel indicates the 32-LPF water levels.

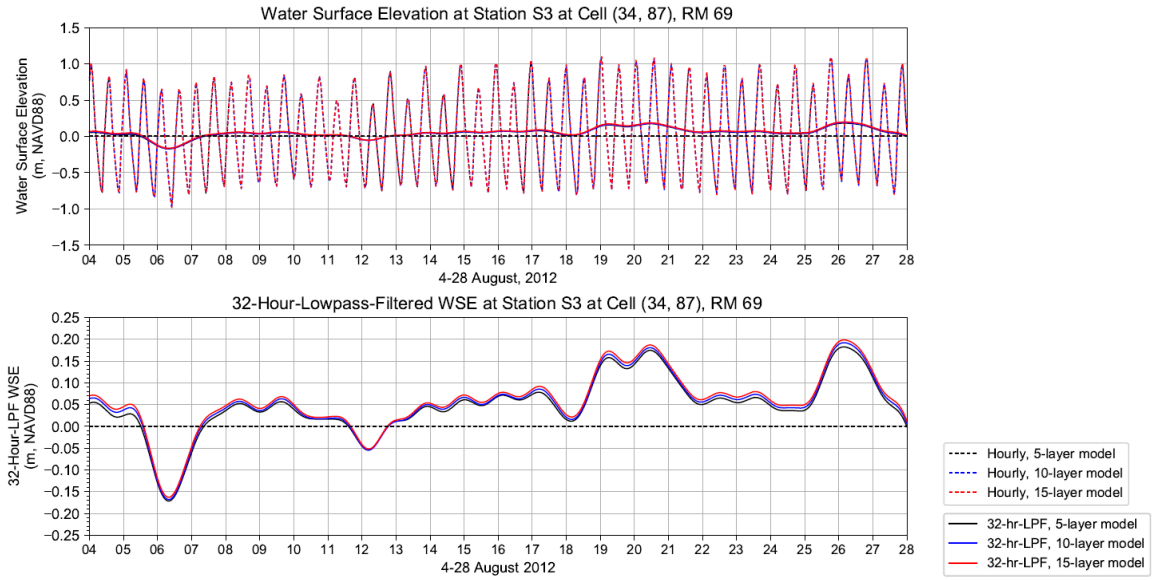

Figure B.3 (3) Simulated Hourly and 32-HR-LPF water Surface Elevation during 08-04-2012 to 08-28-2012 at Station S1 at Cell (33, 43), RM 37. The solid line in the top panel indicates the 32-LPF water levels.

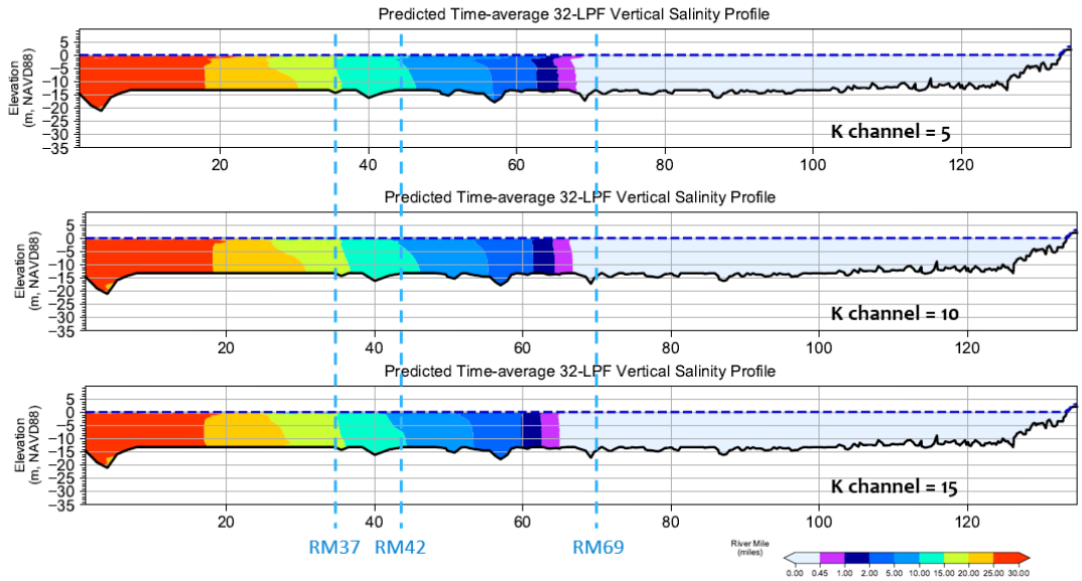

Figure B.4 (1) Longitudinal and Vertical Distribution of Tidally-averaged of Salinity (32-Lowpass-Filtered Results) - Spring Tide, Time period: 08-19-2012 16:00 to 08-21-2012 16:00

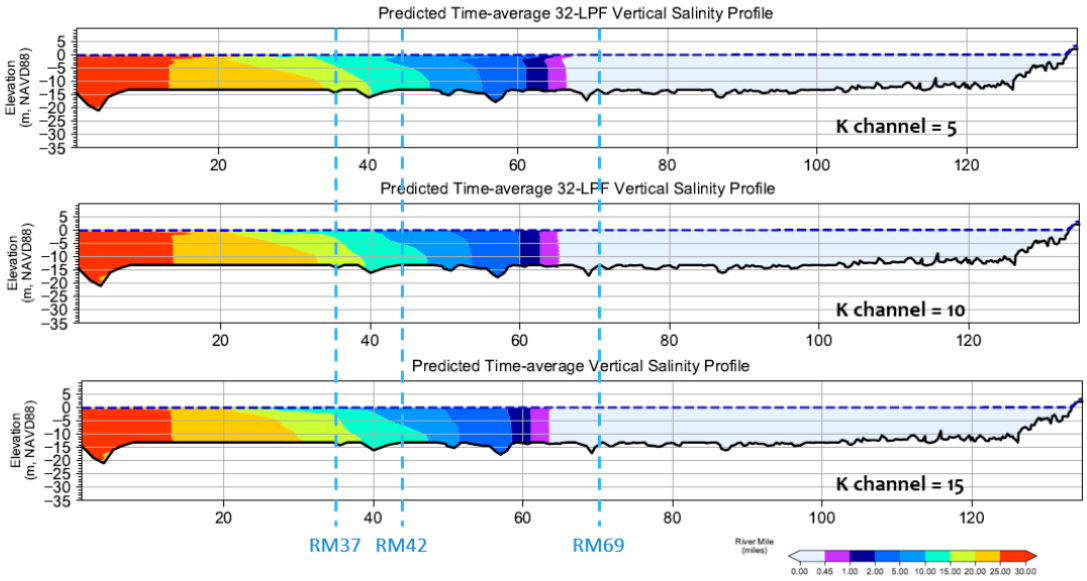

Figure B.4 (2) Longitudinal and Vertical Distribution of Tidally-averaged of Salinity (32-Lowpass-Filtered Results) - Neap Tide, Time period: 08-10-2012 10:00 to 08-12-2012 10:00

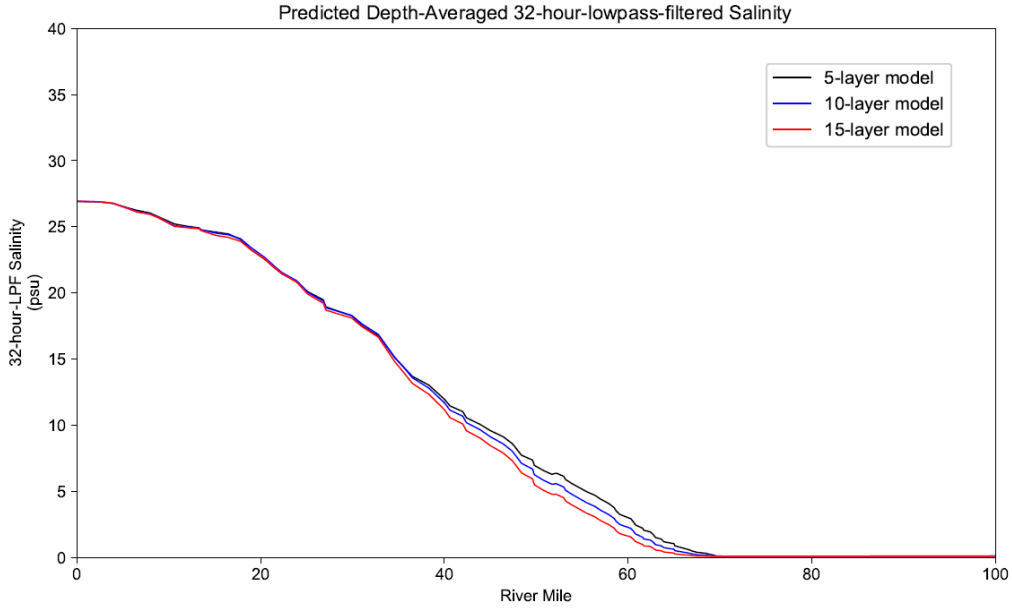

Figure B.5 (1) Comparison of Predicted Depth-Averaged 32-HR-LPFSalinity. Time-Averaged Values during Period of 08-19-2012 to 08-21-2012 are Shown, Spring Tide

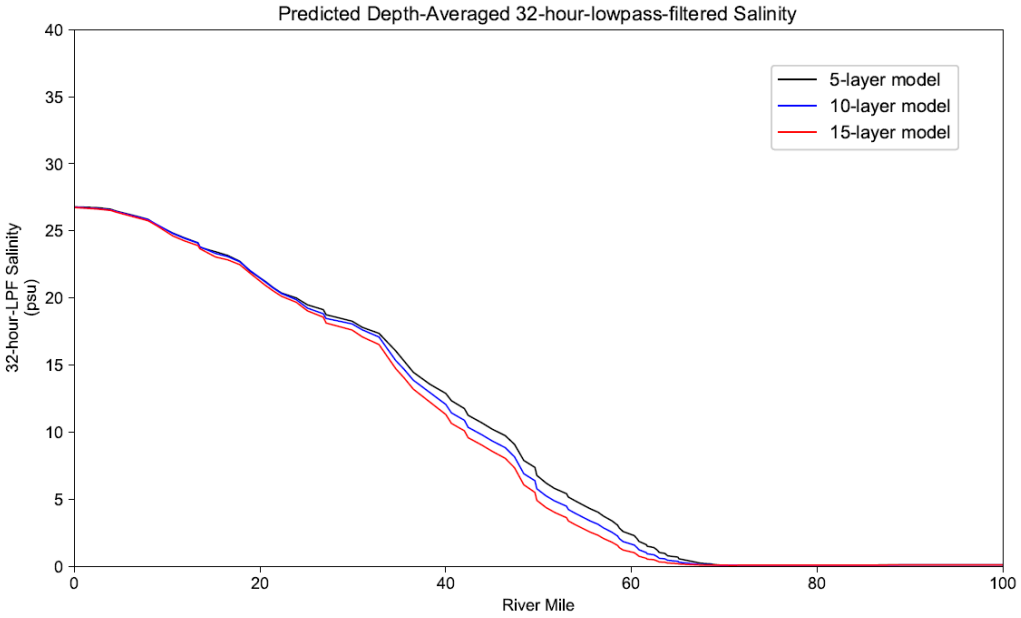

Figure B.5 (2) Comparison of Predicted Depth-Averaged 32-HR-LPFSalinity. Time-Averaged Values during Period of 08-10-2012 to 08-12-2012 are Shown, Neap Tide

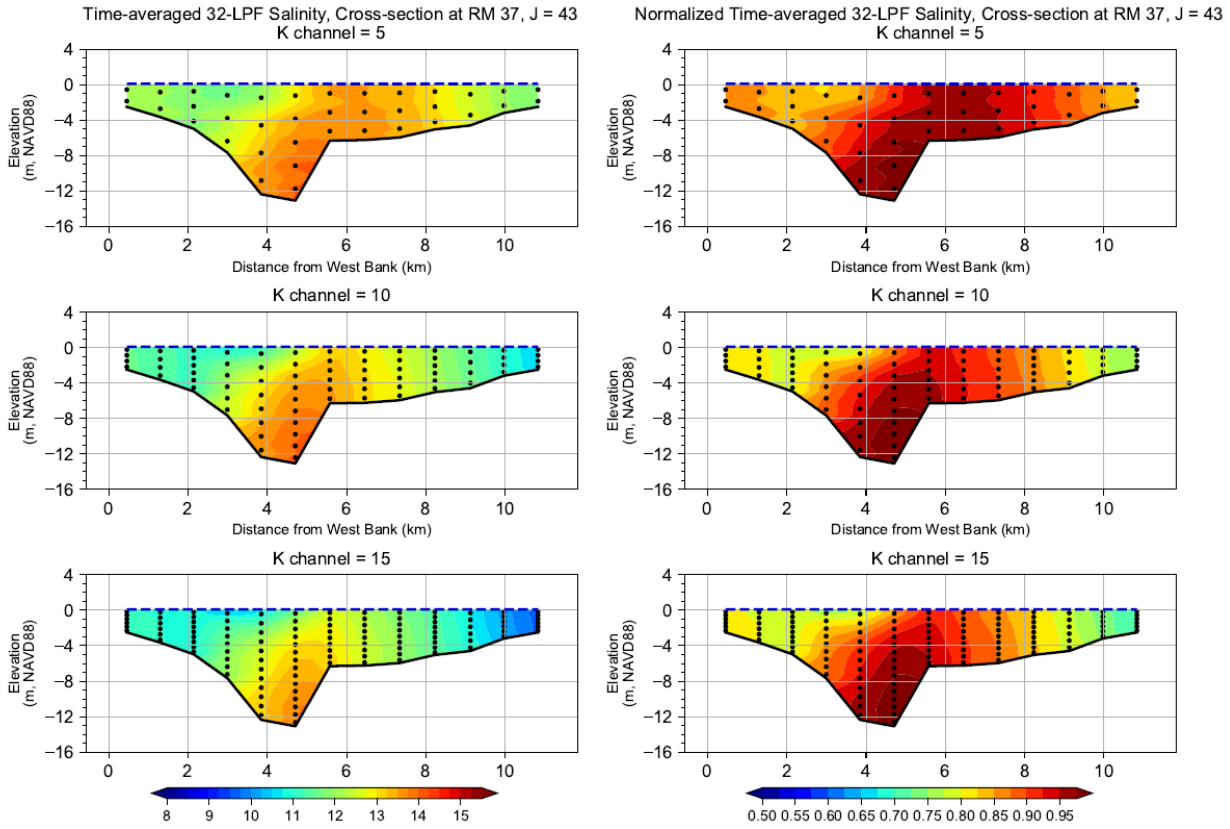

Notes: Salinity was normalized against the maximum salinity of the cross-section

Figure B.6 (1) Vertical Slide of Normalized Time-averaged 32-LPF Salinity at Cross-section at RM 37, J = 43 during 08-19-2012 to 08-21-2012 Period, Spring Tide

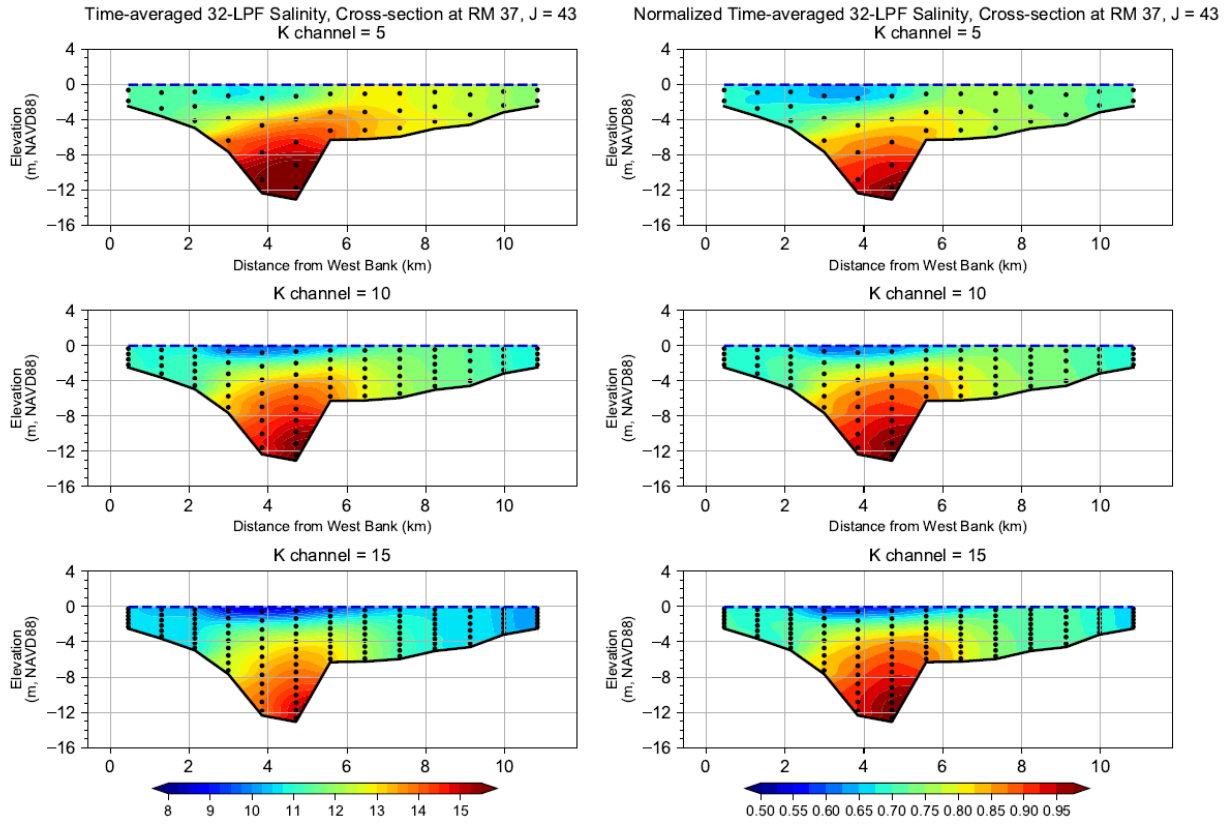

Notes: Salinity was normalized against the maximum salinity of the cross-section

Figure B.6 (2) Vertical Slide of Normalized Time-averaged 32-LPF Salinity at Cross-section at RM 37, J = 43 during 08-10-2012 to 08-12-2012 Period, Neap Tide

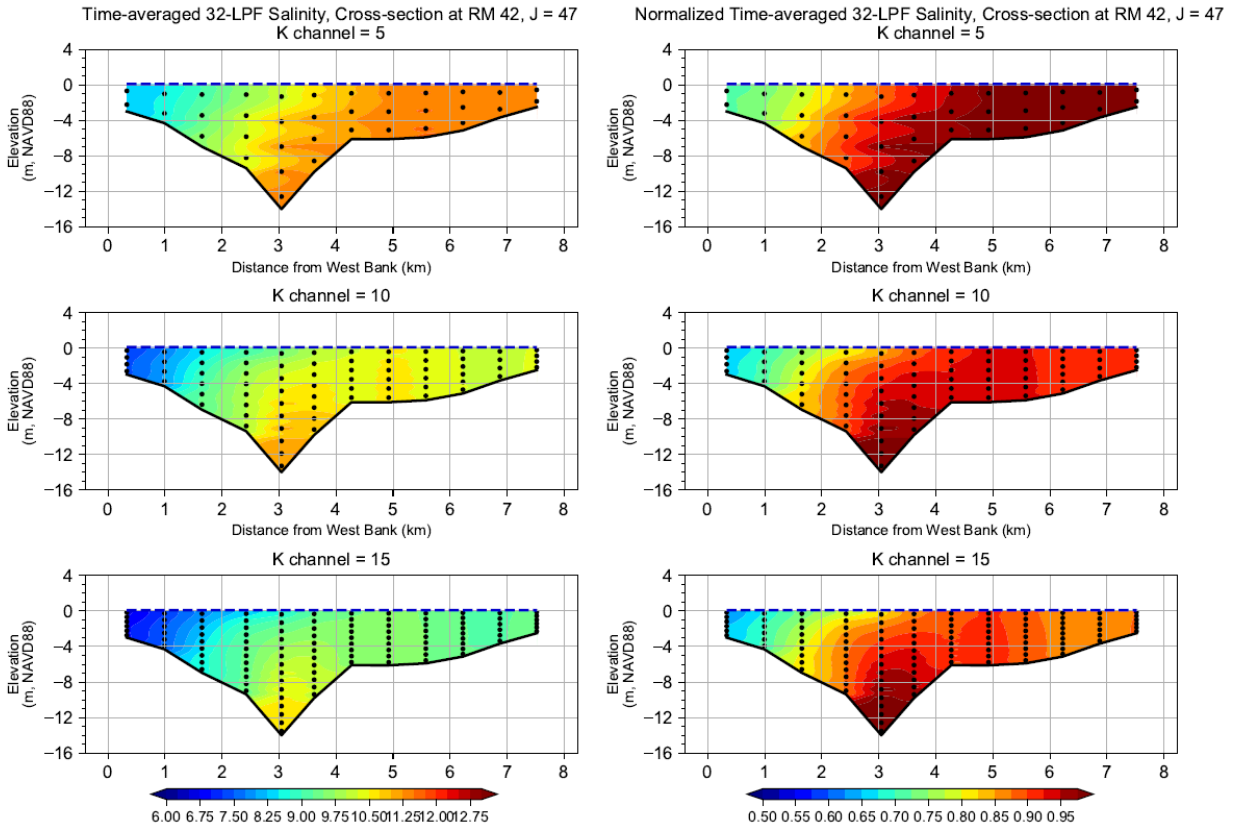

Notes: Salinity was normalized against the maximum salinity of the cross-section

Figure B.7 (1) Vertical Slide of Normalized Time-averaged 32-LPF Salinity at Cross-section at RM 42, J = 47 during 08-19-2012 to 08-21-2012 Period, Spring Tide

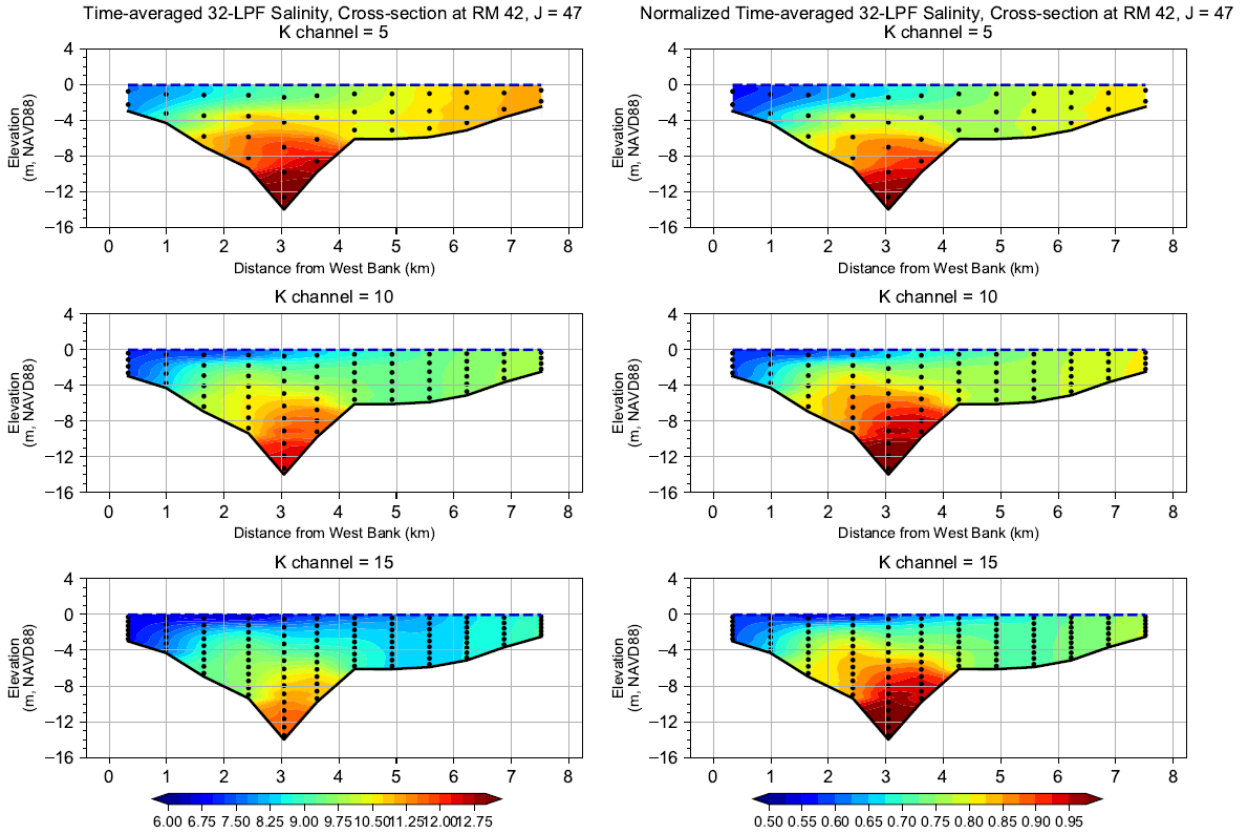

Notes: Salinity was normalized against the maximum salinity of the cross-section

Figure B.7 (2) Vertical Slide of Normalized Time-averaged 32-LPF Salinity at Cross-section at RM 42, J = 47 during 08-10-2012 to 08-12-2012 Period, Neap Tide

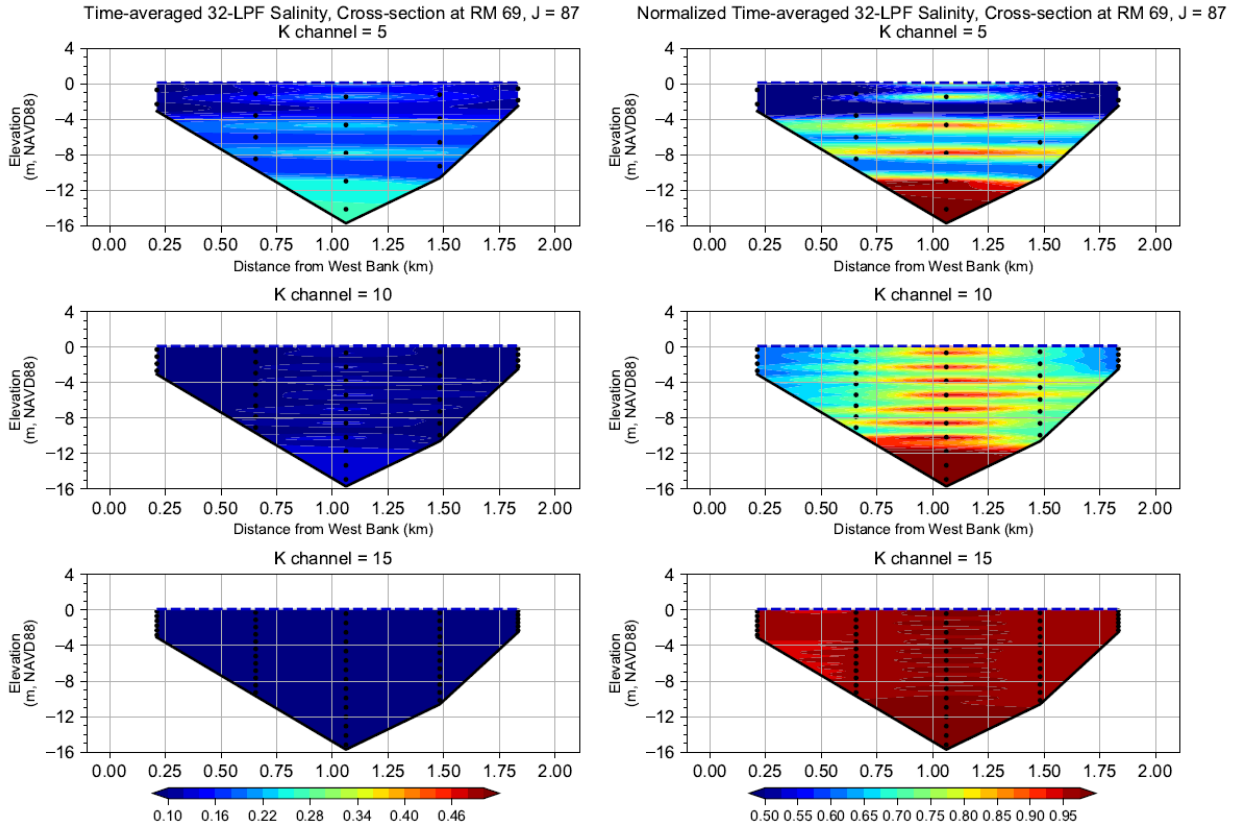

Notes: Salinity was normalized against the maximum salinity of the cross-section

Figure B.8 (1) Vertical Slide of Normalized Time-averaged 32-LPF Salinity at Cross-section at RM 69, J = 87 during 08-19-2012 to 08-21-2012 Period, Spring Tide

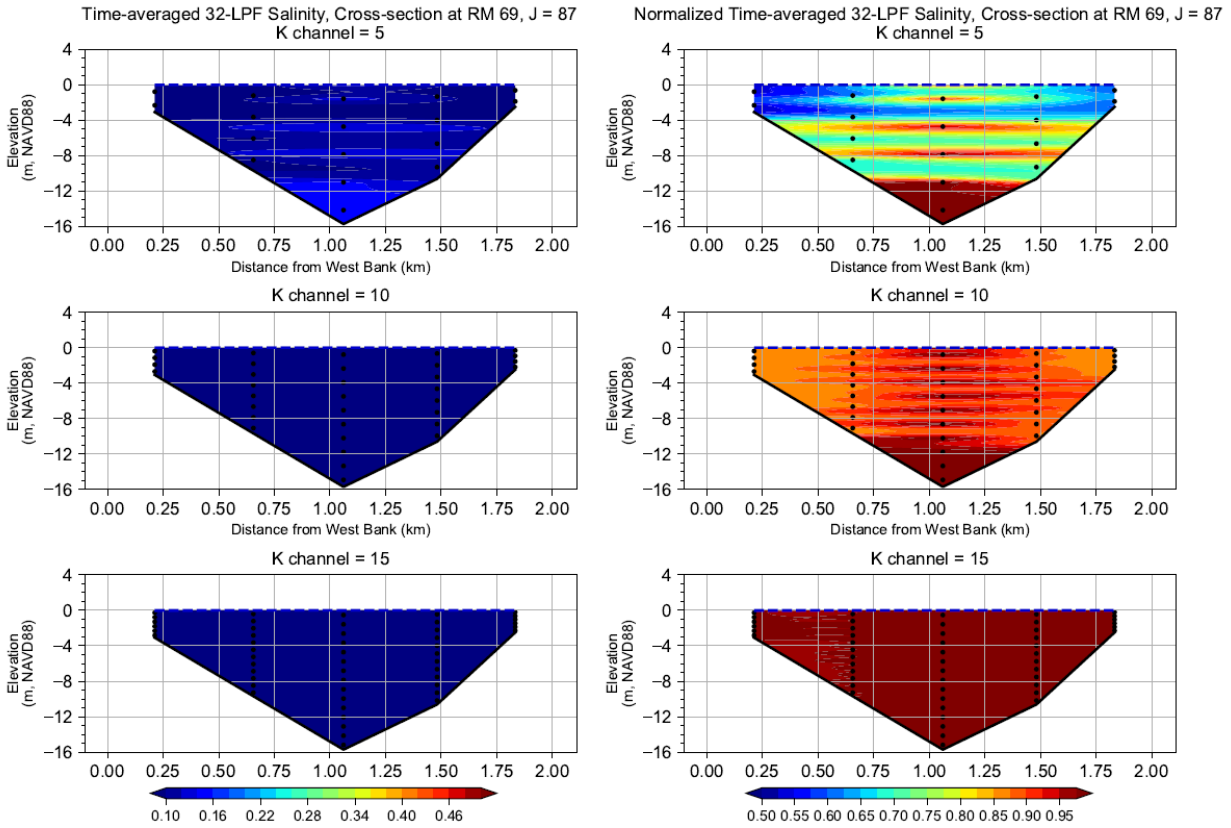

Notes: Salinity was normalized against the maximum salinity of the cross-section

Figure B.8 (2) Vertical Slide of Normalized Time-averaged 32-LPF Salinity at Cross-section at RM 69, J = 87 during 08-10-2012 to 08-12-2012 Period, Neap Tide

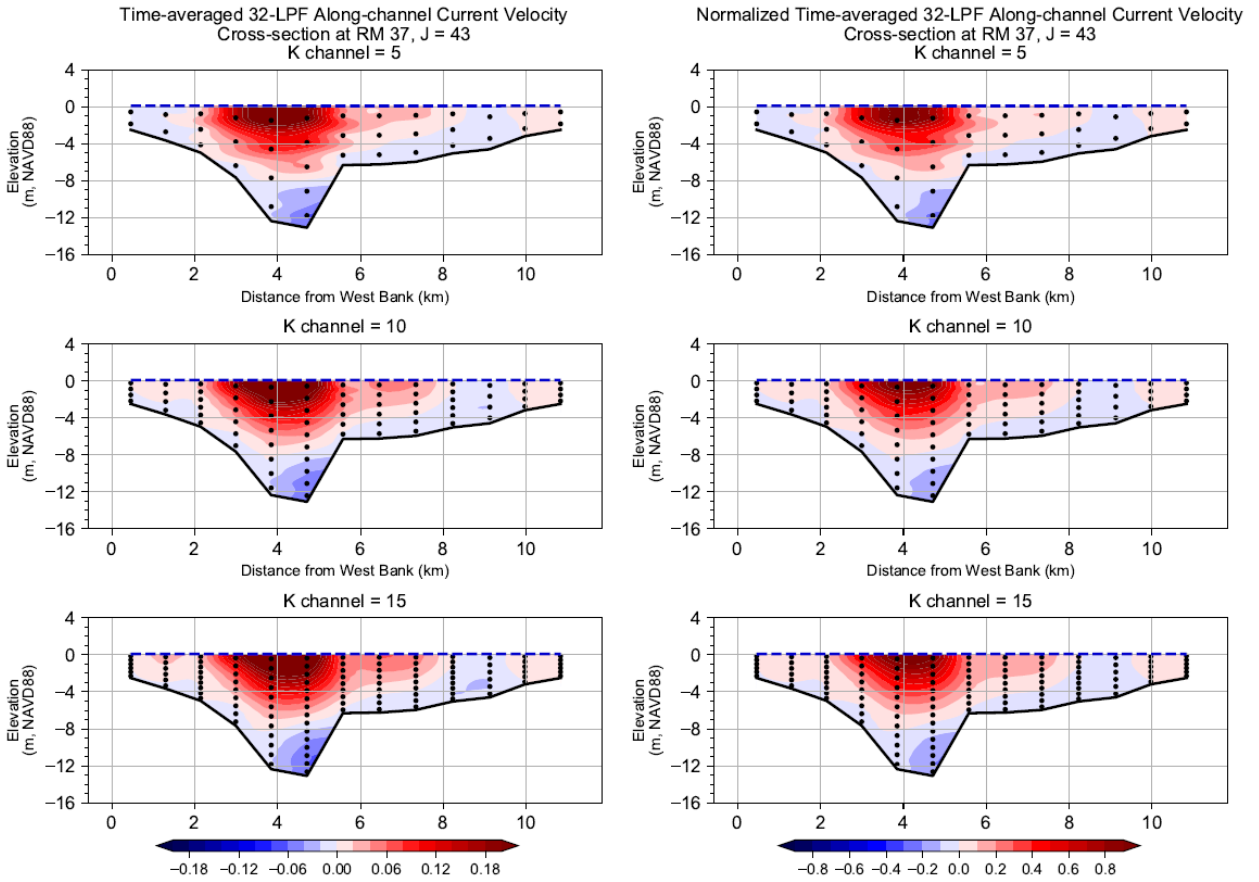

Notes: Positive is moving seaward. Velocity was normalized against the maximum velocity of the cross-section.

Figure B.9 (1) Vertical Slide of Normalized Time-averaged 32-LPF Along-channel Current Velocity at Cross-section at RM 37, J = 43 during 08-19-2012 to 08-21-2012 Period, Spring Tide

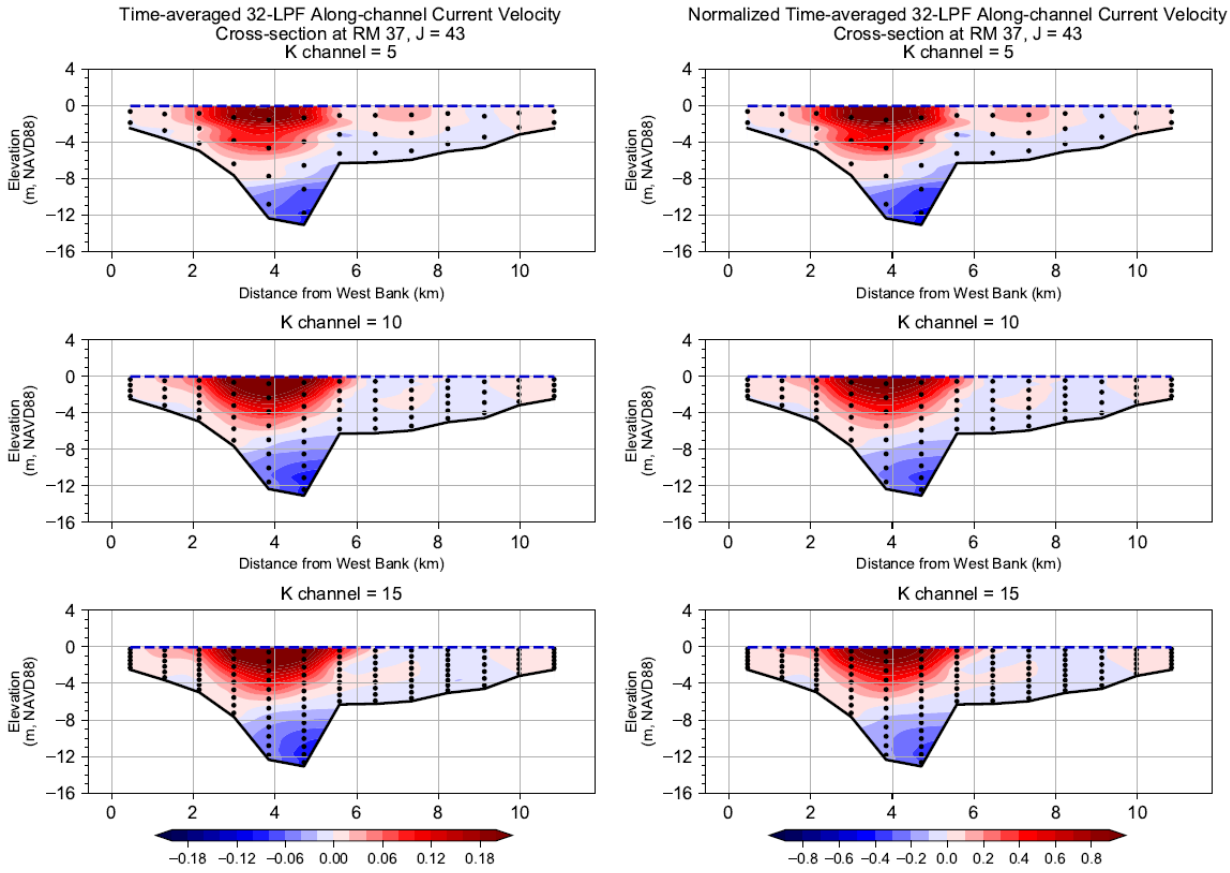

Notes: Positive is moving seaward. Velocity was normalized against the maximum velocity of the cross-section.

Figure B.9 (2) Vertical Slide of Normalized Time-averaged 32-LPF Along-channel Current Velocity at Cross-section at RM 37, J = 43 during 08-10-2012 to 08-12-2012 Period, Neap Tide

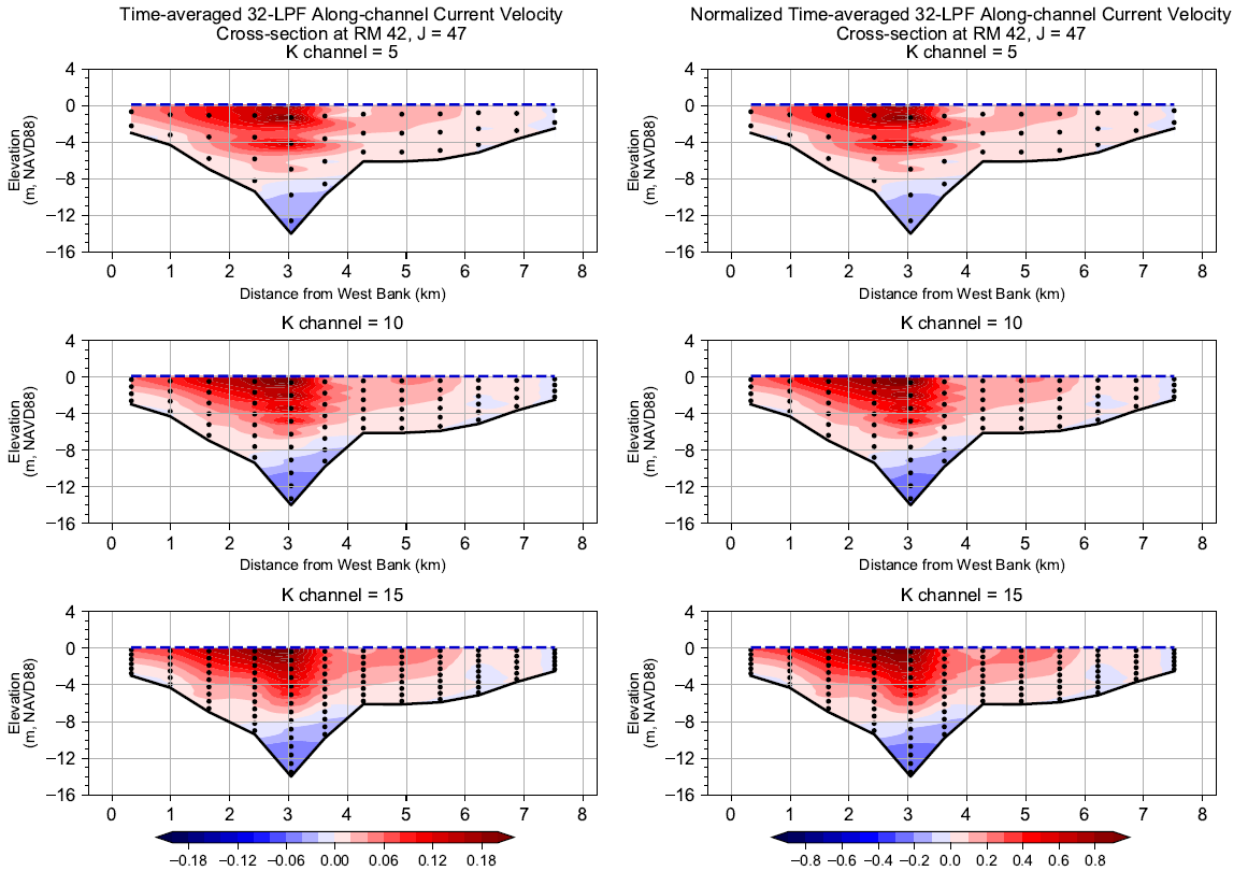

Notes: Positive is moving seaward. Velocity was normalized against the maximum velocity of the cross-section.

Figure B.10 (1) Vertical Slide of Normalized Time-averaged 32-LPF Along-channel Current Velocity at Cross-section at RM 42, J = 47 during 08-19-2012 to 08-21-2012 Period, Spring Tide

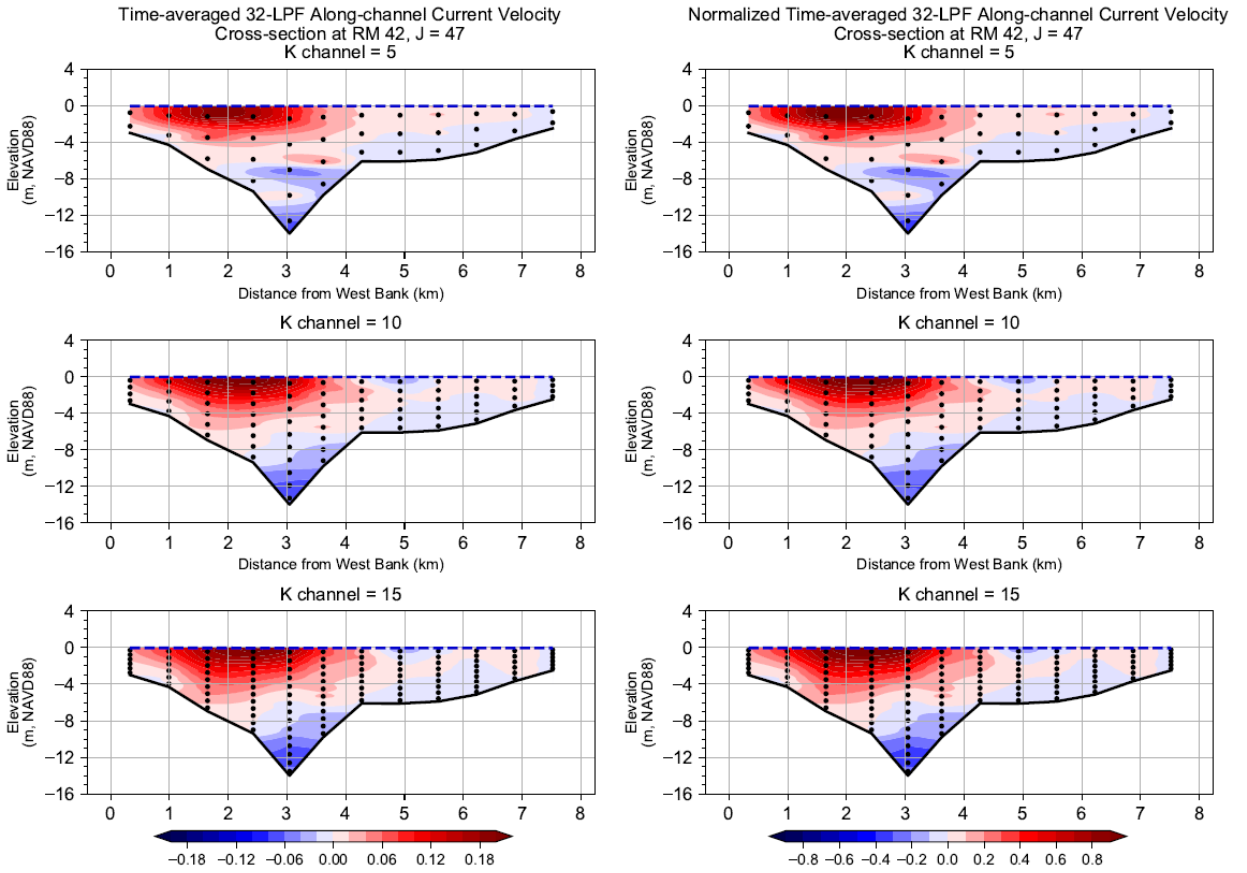

Notes: Positive is moving seaward. Velocity was normalized against the maximum velocity of the cross-section.

Figure B.10 (2) Vertical Slide of Normalized Time-averaged 32-LPF Along-channel Current Velocity at Cross-section at RM 42, J = 47 during 08-10-2012 to 08-12-2012 Period, Neap Tide

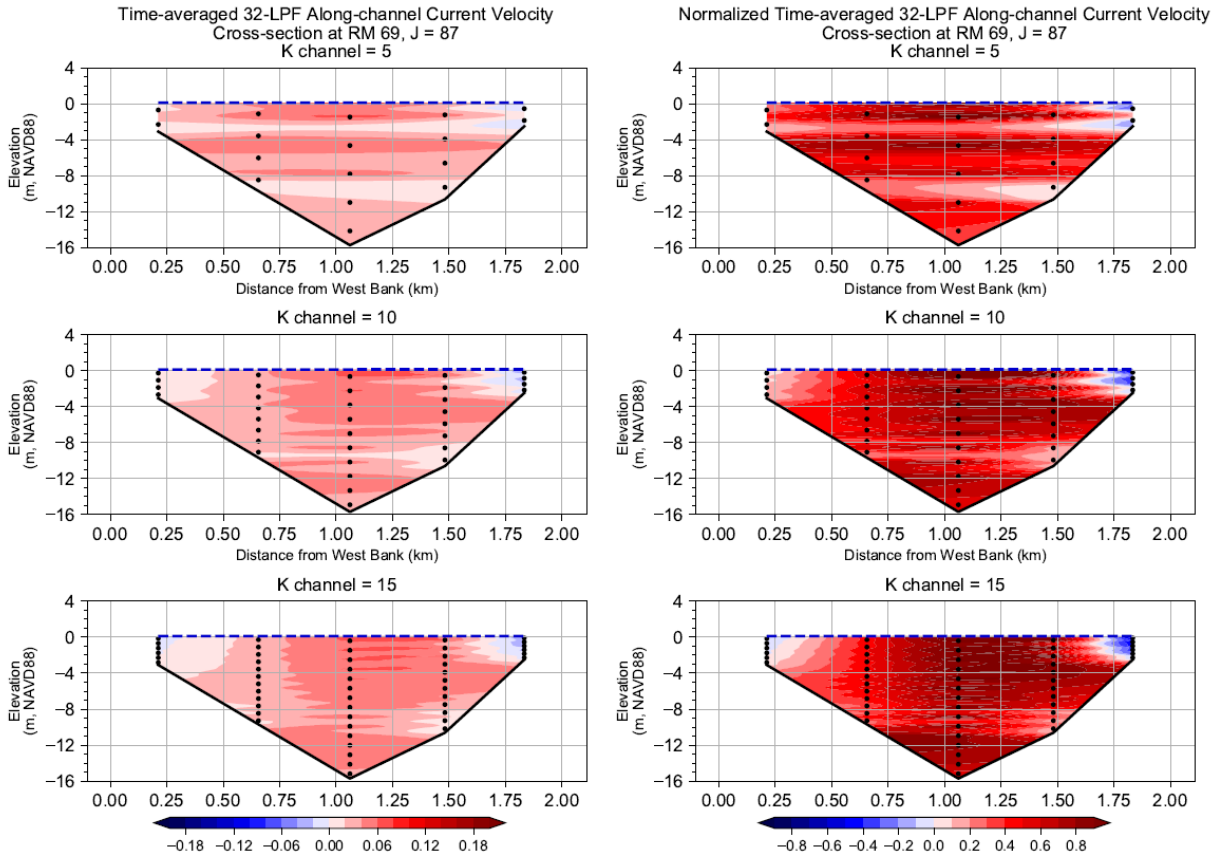

Notes: Positive is moving seaward. Velocity was normalized against the maximum velocity of the cross-section.

Figure B.11 (1) Vertical Slide of Normalized Time-averaged 32-LPF Along-channel Current Velocity at Cross-section at RM 69, J = 87 during 08-19-2012 to 08-21-2012 Period, Spring Tide

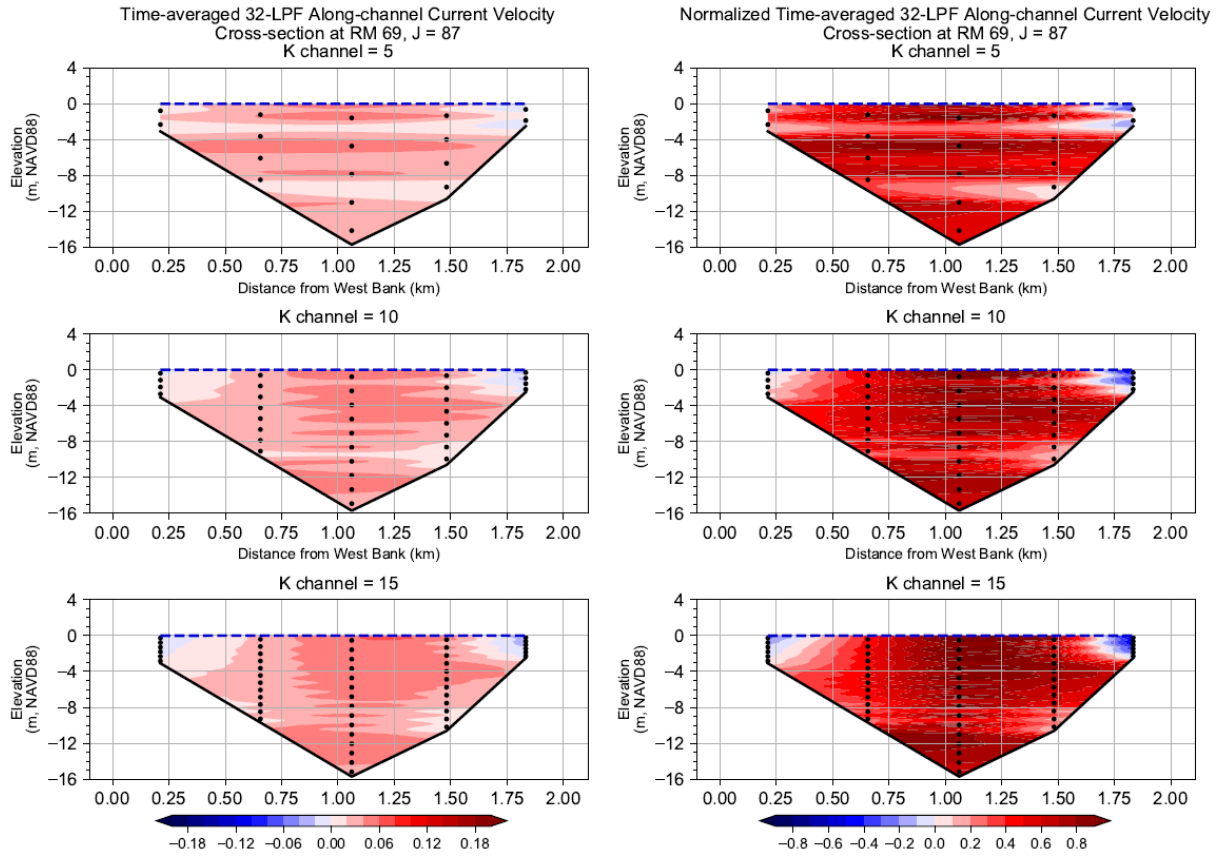

Notes: Positive is moving seaward. Velocity was normalized against the maximum velocity of the cross-section.

Figure B.11 (2) Vertical Slide of Normalized Time-averaged 32-LPF Along-channel Current Velocity at Cross-section at RM 69, J = 87 during 08-10-2012 to 08-12-2012 Period, Neap Tide

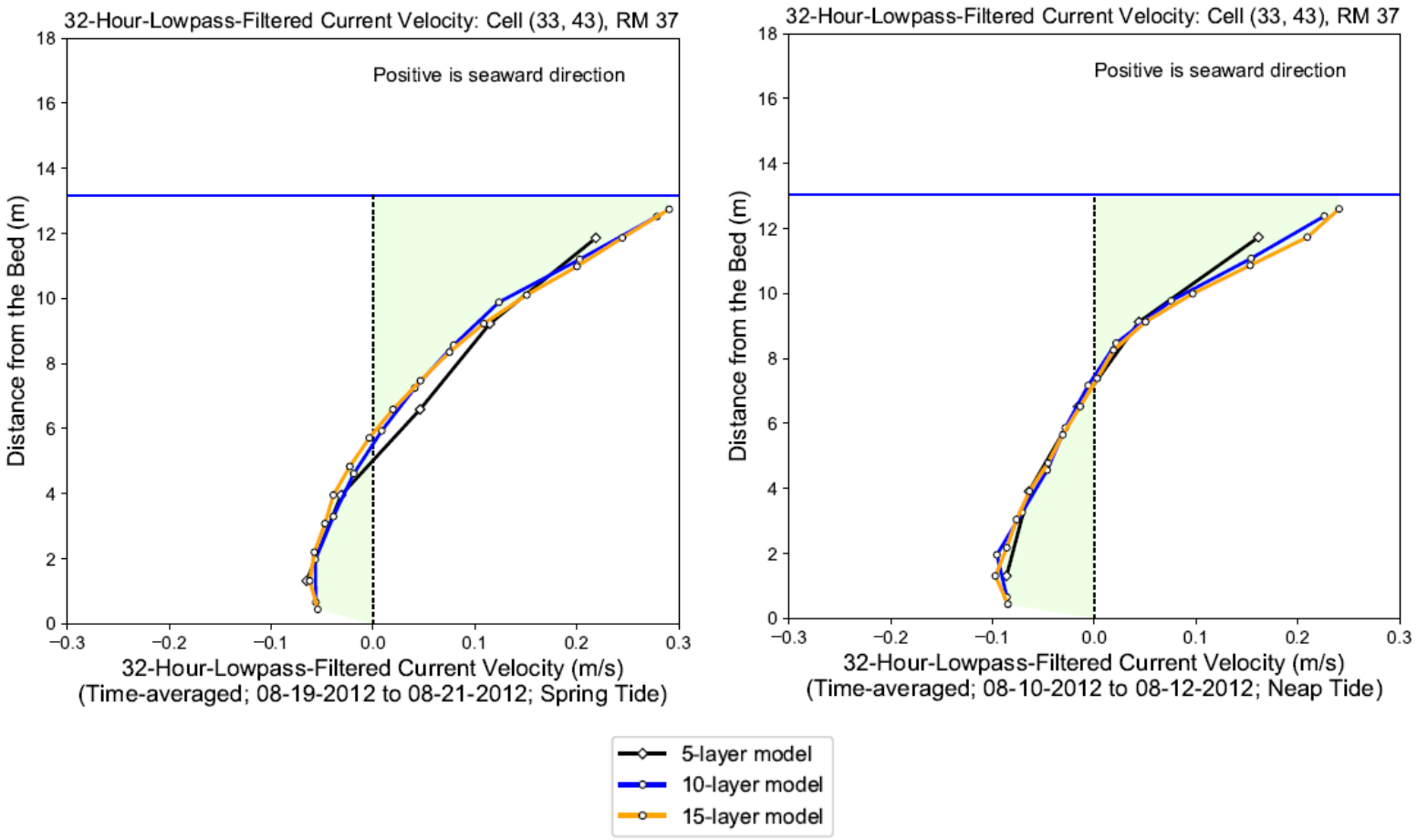

Notes: 32-hr LPF results were calculated first, and then averaged over the time period to represent the tidally-averaged vertical structure

Figure B.12 Simulated Tidally-averaged 32-HR-LPF Along-channel Current Velocity at Station S1 at Cell (33, 43), RM 37

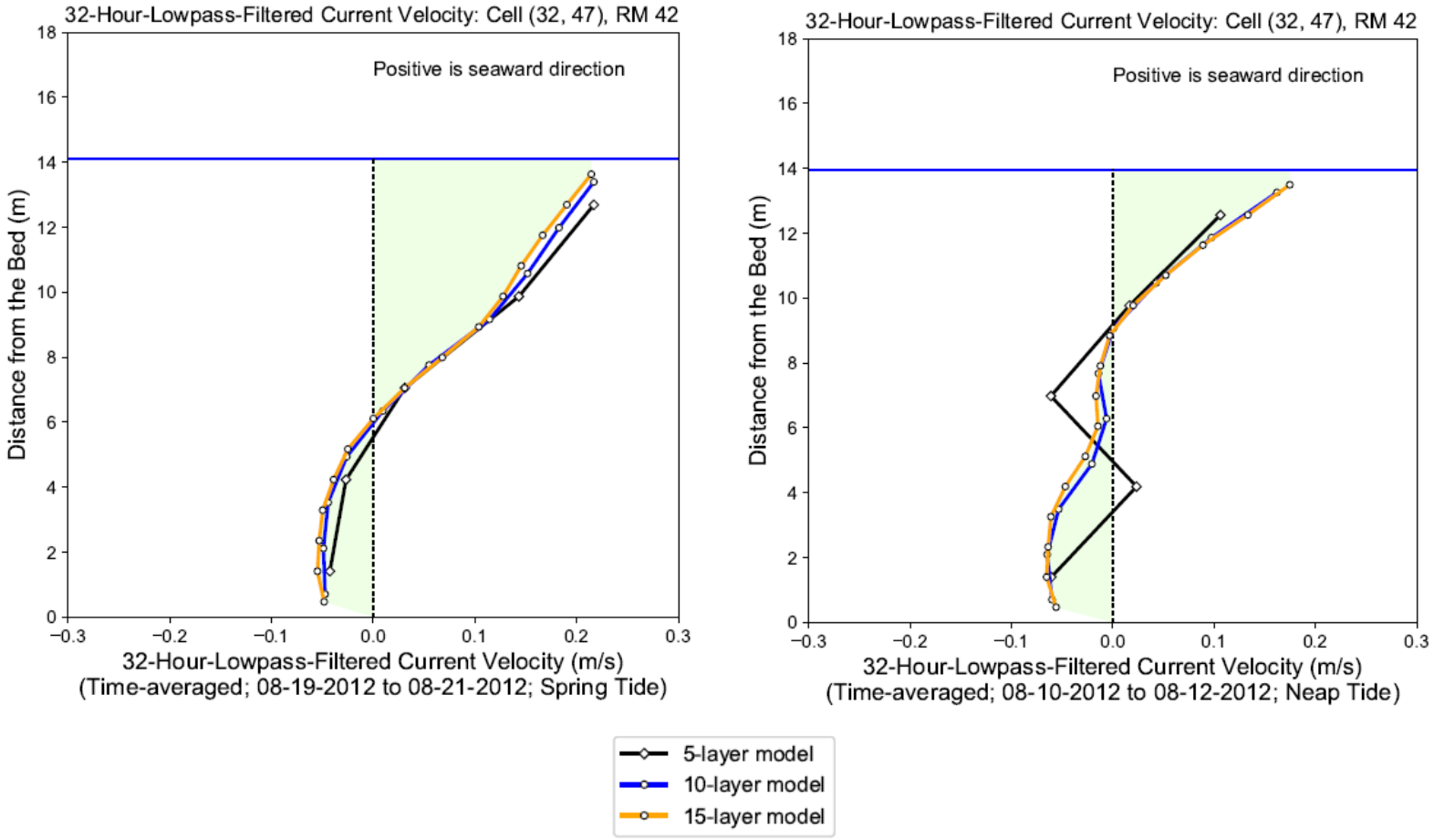

Notes: 32-hr LPF results were calculated first, and then averaged over the time period to represent the tidally-averaged vertical structure

Figure B.13 Simulated Tidally-averaged 32-HR-LPF Along-channel Current Velocity at Station S2 at Cell (32, 47), RM 42

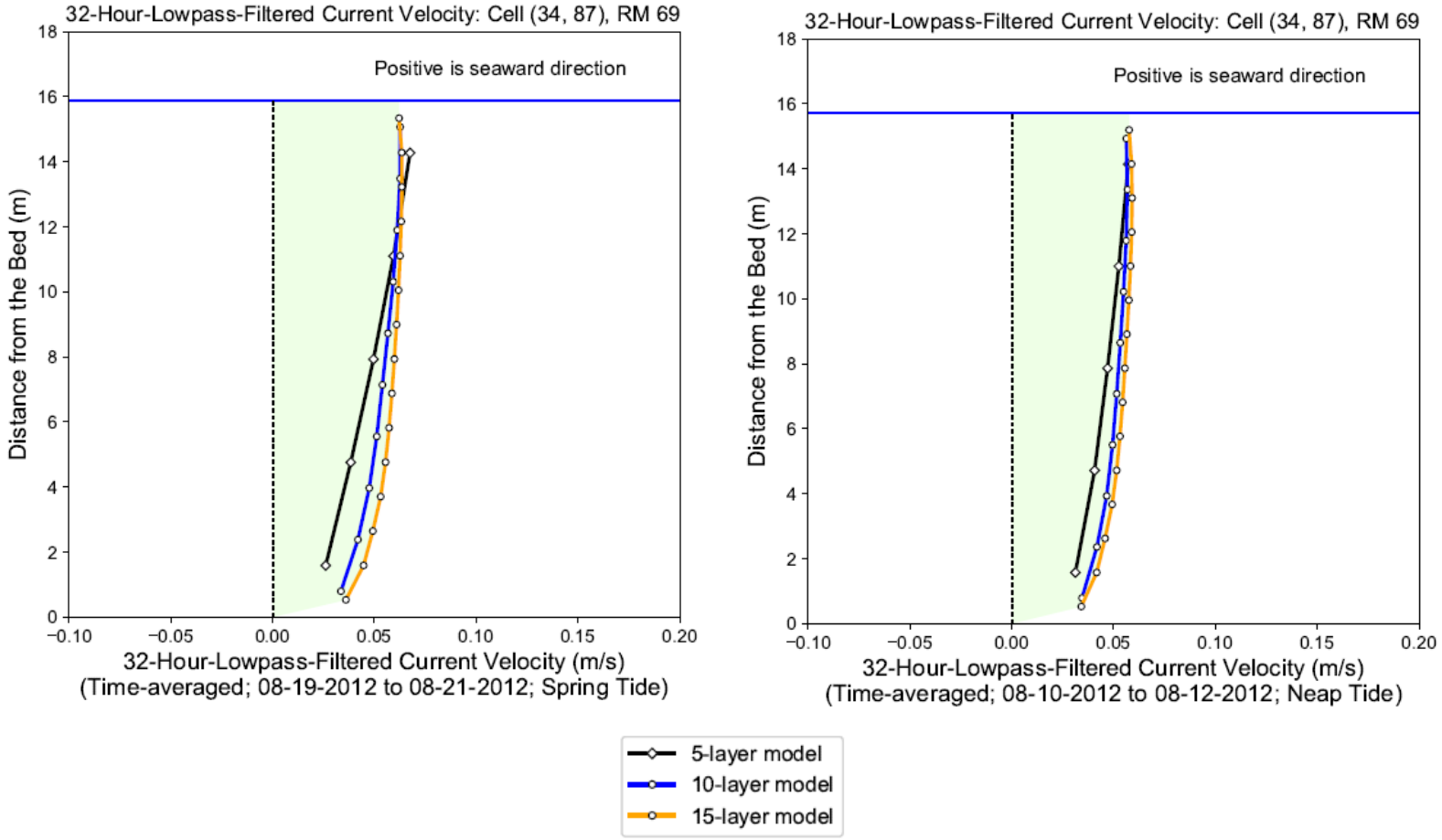

Notes: 32-hr LPF results were calculated first, and then averaged over the time period to represent the tidally-averaged vertical structure

Figure B.14 Simulated Tidally-averaged 32-HR-LPF Along-channel Current Velocity at Station S3 at Cell (34, 87), RM 69

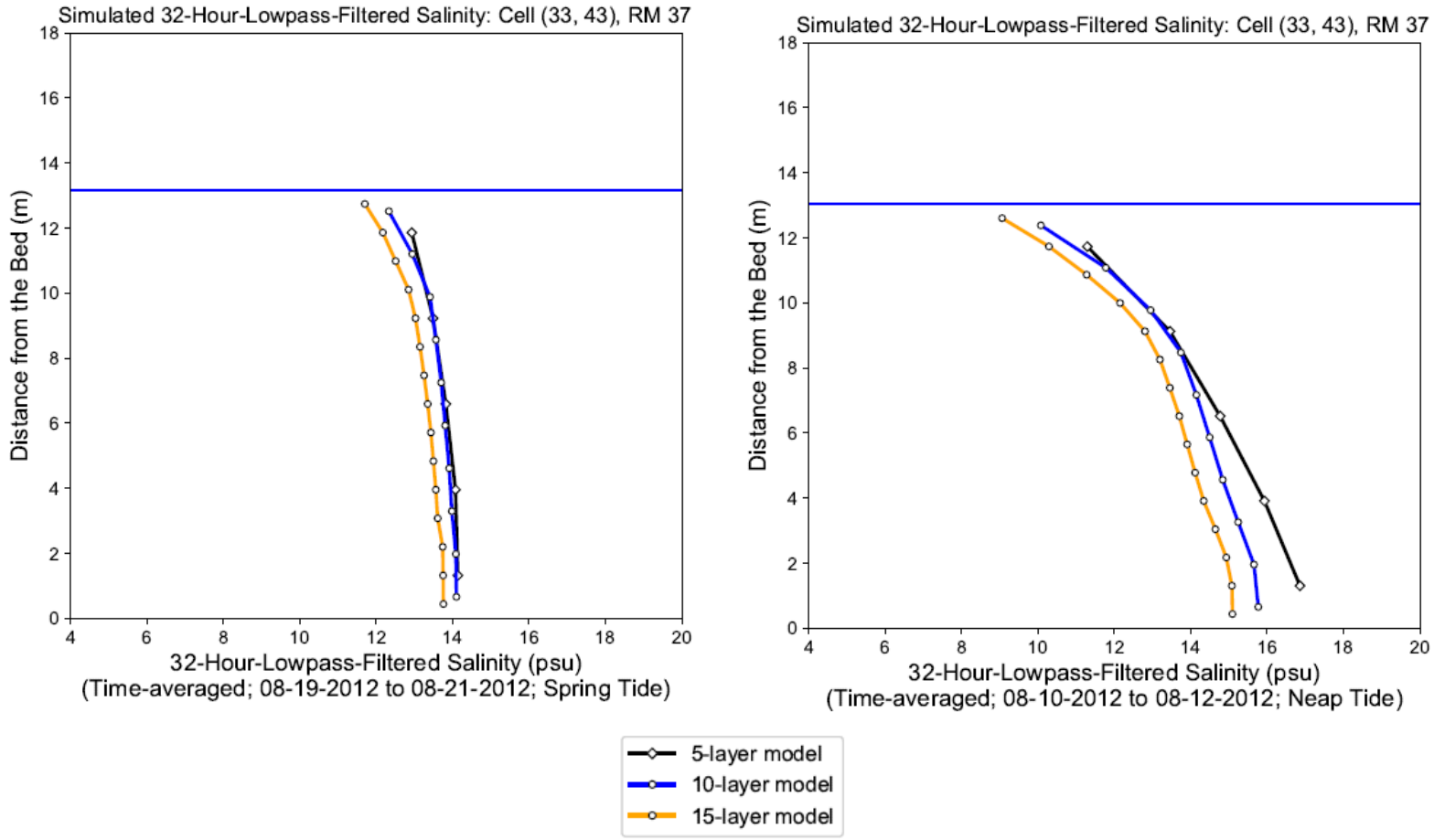

Notes: 32-hr LPF results were calculated first, and then averaged over the time period to represent the tidally-averaged vertical structure

Figure B.15 Simulated Tidally-averaged 32-HR-LPF Salinity at Station S3 at Cell (34, 87), RM 69

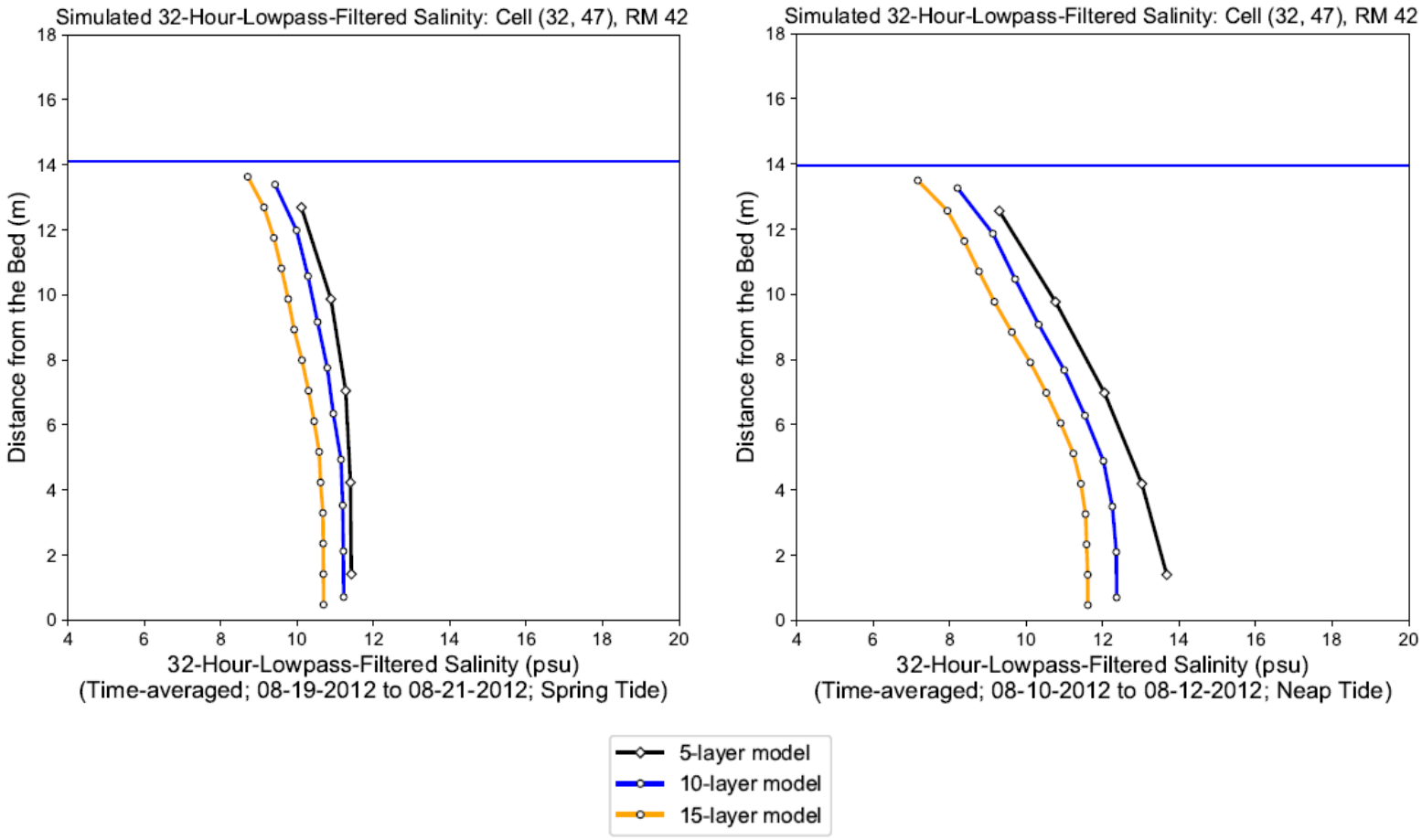

Notes: 32-hr LPF results were calculated first, and then averaged over the time period to represent the tidally-averaged vertical structure

Figure B.16 Simulated Tidally-averaged 32-HR-LPF Salinity at Station S3 at Cell (34, 87), RM 69

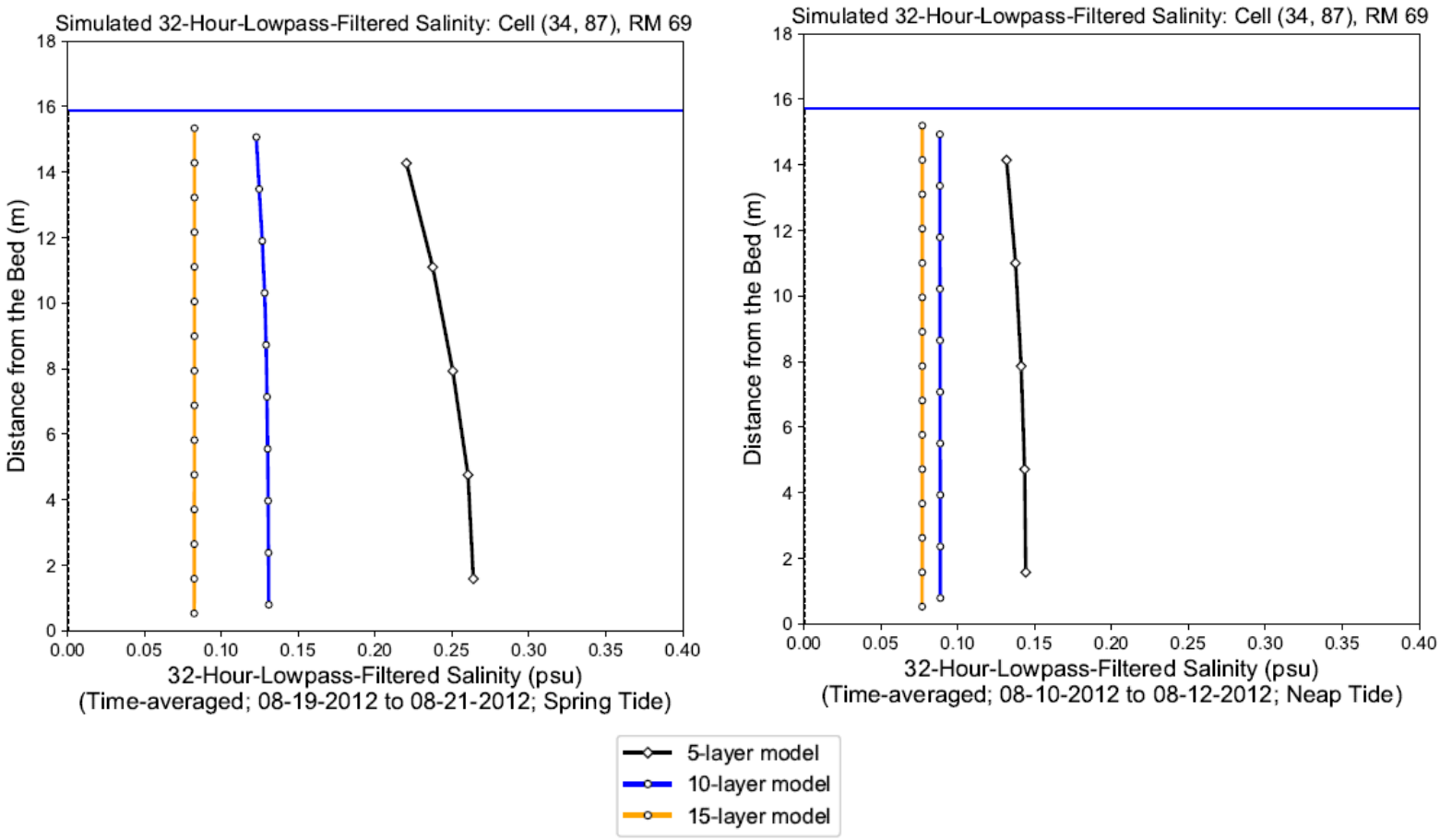

Notes: 32-hr LPF results were calculated first, and then averaged over the time period to represent the tidally-averaged vertical structure

Figure B.17 Simulated Tidally-averaged 32-HR-LPF Salinity at Station S3 at Cell (34, 87), RM 69

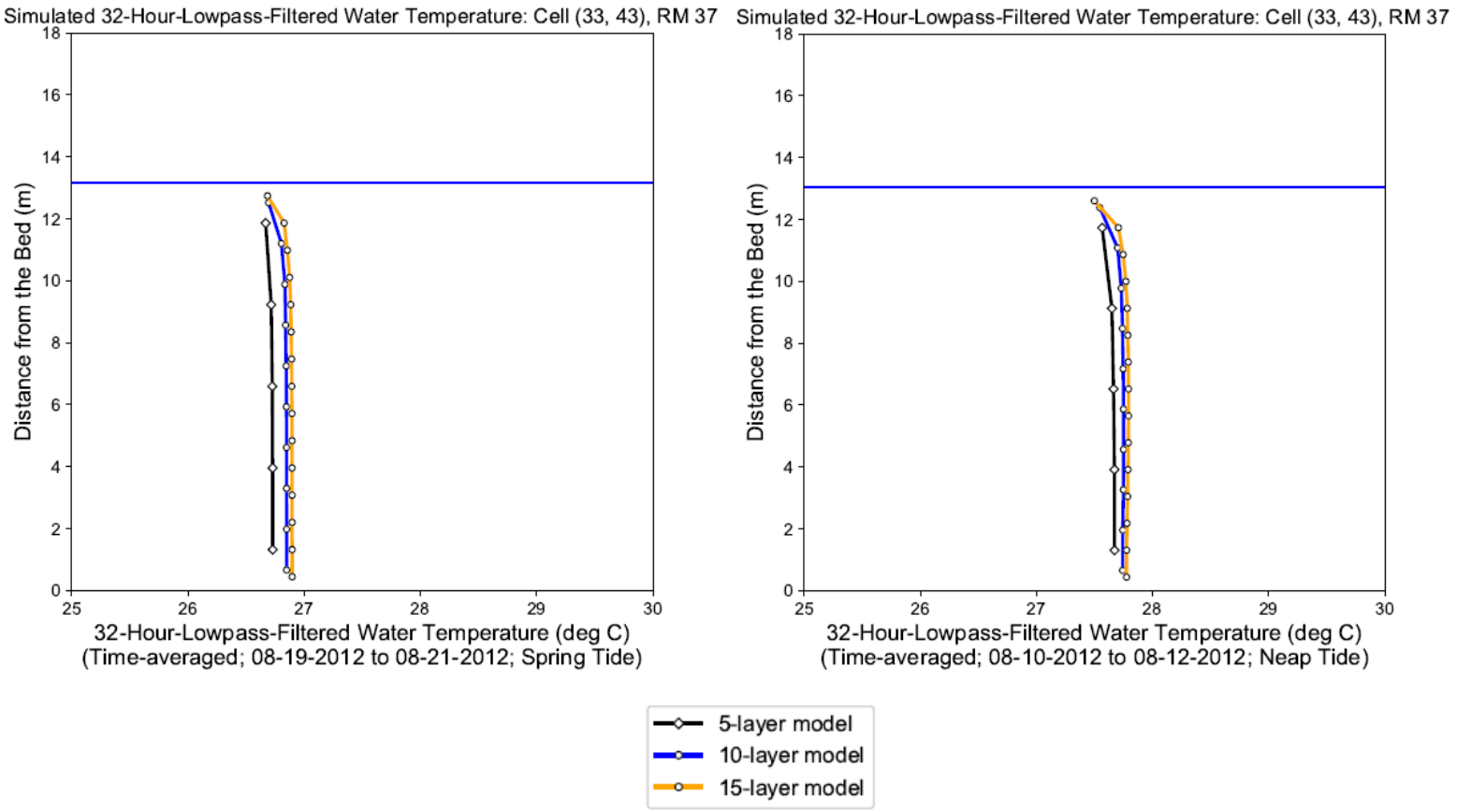

Notes: 32-hr LPF results were calculated first, and then averaged over the time period to represent the tidally-averaged vertical structure

Figure B.18 Simulated Tidally-averaged 32-HR-LPF Water Temperature at Station S3 at Cell (34, 87), RM 69

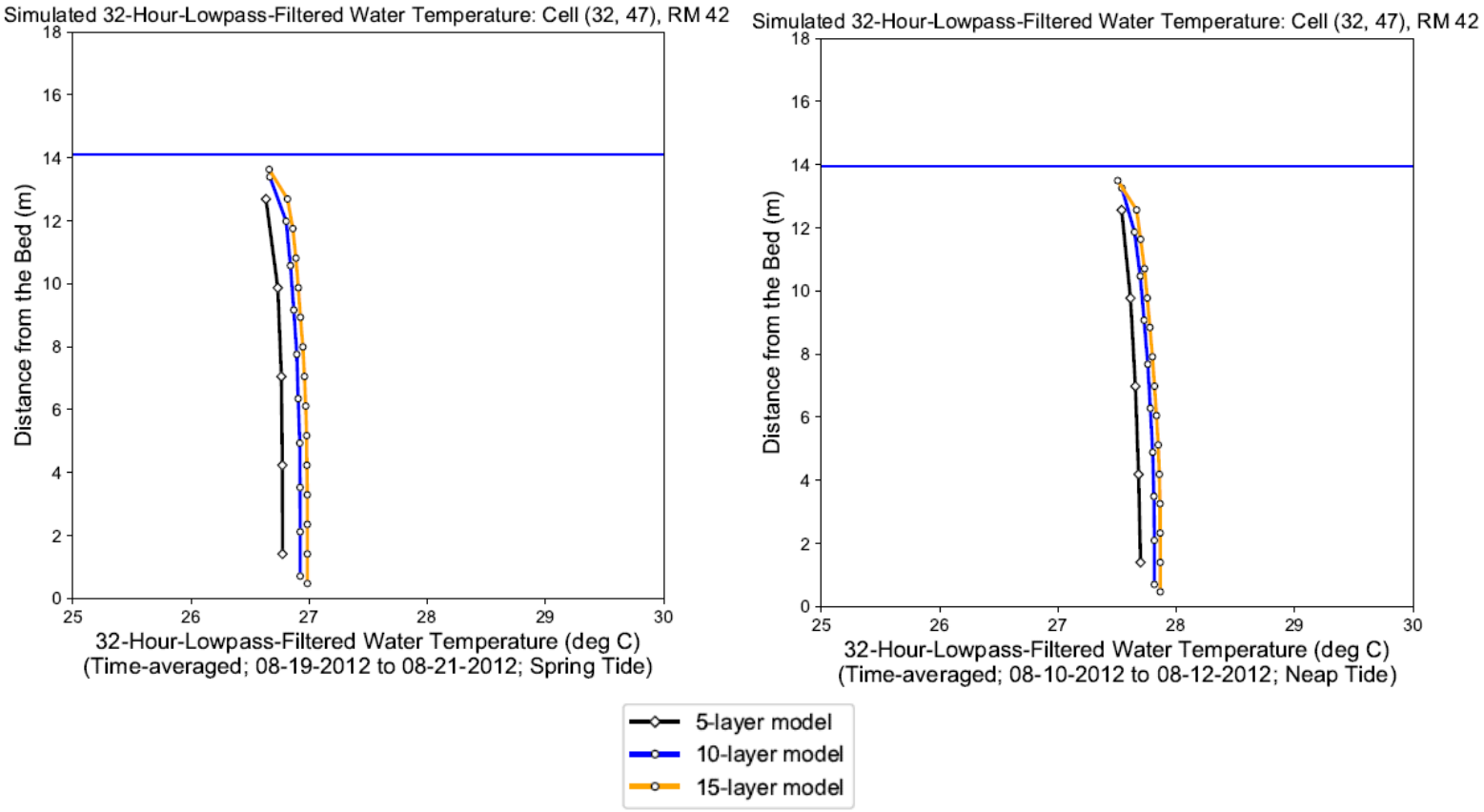

Notes: 32-hr LPF results were calculated first, and then averaged over the time period to represent the tidally-averaged vertical structure

Figure B.19 Simulated Tidally-averaged 32-HR-LPF Water Temperature at Station S3 at Cell (34, 87), RM 69

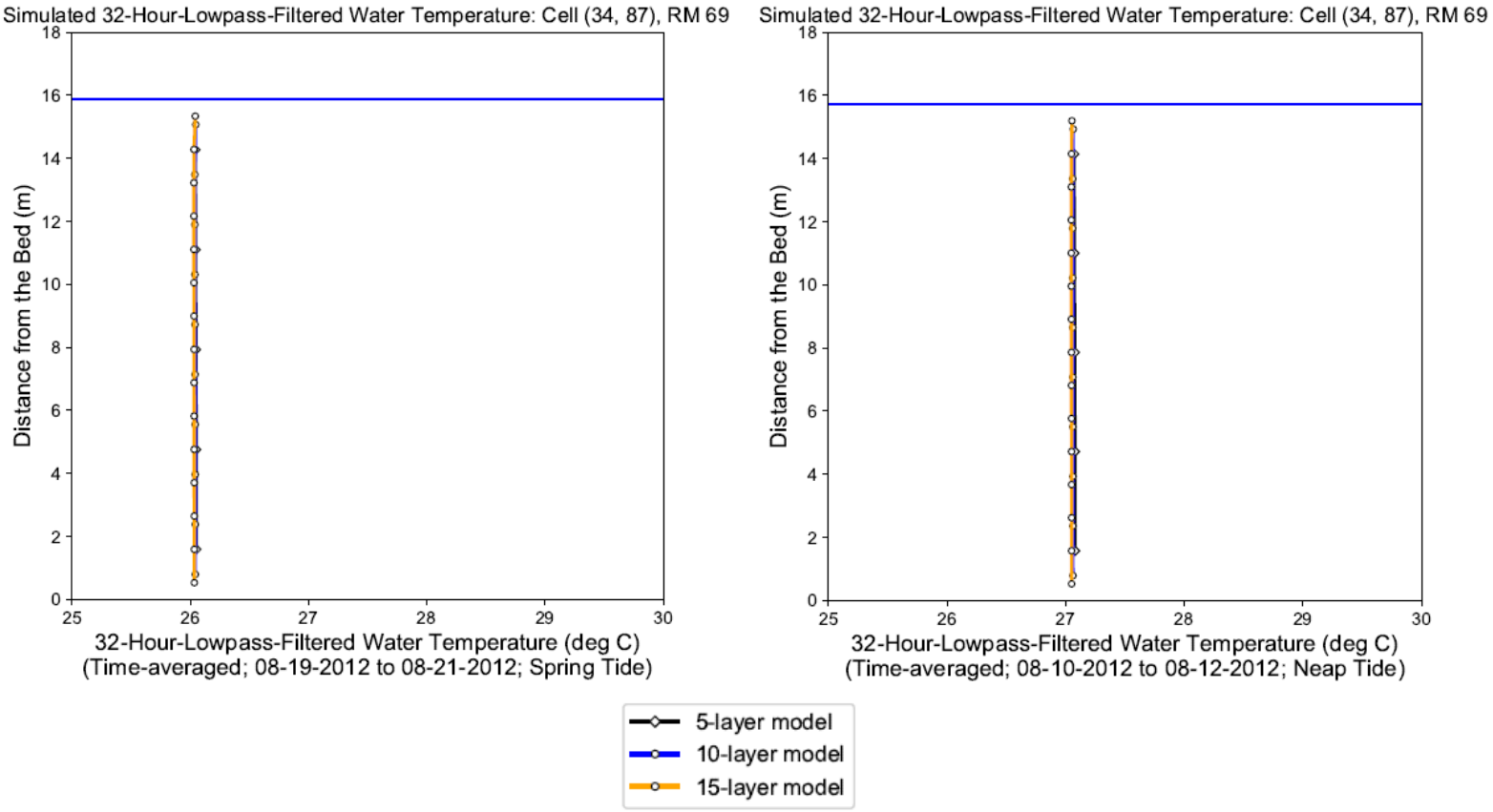

Notes: 32-hr LPF results were calculated first, and then averaged over the time period to represent the tidally-averaged vertical structure

Figure B.20 Simulated Tidally-averaged 32-HR-LPF Water Temperature at Station S3 at Cell (34, 87), RM 69

APPENDIX C. SENSITIVITY OF THE SM3D MODEL

Data to define model parameters may be unavailable, incomplete, or have inherent irreducible error. Sensitivity analyses of assumptions made to specify boundary conditions and model parameters are performed to understand how those assumptions may affect model results. This appendix documents sensitivity analyses related to flow from the C&D Canal and ocean salinity. Additional sensitivities analyses are documented in the companion report of use of SM3D for SLR analyses (Chen, F., et. al. 2025).

Table C.1-1 Summary of Sensitivity Simulations

Run	Boundary Condition Tested	Period	Descriptions
1	Net flow from C&D Canal (Adjusting tidal datum at the canal's western end)	2016	Set tidal datum adjustment as: base + 4 cm
2			Set tidal datum adjustment as: base + 2 cm
3			Set tidal datum adjustment as: base -2 cm
4			Set tidal datum adjustment as: base – 4 cm
5	Salinity at the C&D Canal western end	2016	Multiply the salinity at C&D boundary by 0.75
6			Multiply the salinity at C&D boundary by 1.25
7	Ocean salinity boundary	2017	The ocean salinity was reduced by 2 to 3 psu from the surface down to 10 m depth for four months (September–December)
8			The same change in ocean salinity was applied for seven months (June–December).

C.1 Net Flow from the C&D Canal

The C&D Canal provides a hydraulic linkage between Chesapeake Bay and the Delaware Estuary. Normally, the C&D Canal brings less saline water (fresher) from upper Chesapeake Bay eastward to the Delaware Estuary, though flow direction and magnitude varies. Varying the relative difference in water surface elevation at the western and eastern end of the canal effectively changes the net flow.

For each sensitivity test, a constant datum shift in the water surface elevation was made at the western end of the C&D Canal, adjusting flow through the canal. The tidal datum was adjusted over the entire simulation period and changes were within the tidal uncertainty range of +/- 10 cm

estimated by NOAA[46] The net (residual) flow was calculated by applying the 32-hr low-pass filter (32-HR-LPF) to the predicted time series.

Predicted cumulative net flow (i.e., 32-HR-LPF flow) over the course of 2016 is presented in Figure C.1-1 and Figure C.1-2. These figures show the total cumulative volume of water being transported from Chesapeake Bay into the Delaware Estuary throughout 2016. A negative value indicates the cumulative net flow was from the Delaware Estuary to Chesapeake Bay. The net cumulative flow for 2016 was approximately 0 billion m^3 for the base case. The total cumulative flow simulated at NOAA station Chesapeake City is roughly 2.5 and 5 billion m^3 when the water surface elevation is increased by 2 cm and 4 cm, respectively. The average of 12 monthly residual flows increased from the base case of 4 m^3/s to 79 and 157 m^3/s at NOAA Chesapeake City when the water surface elevation at the C&D Canal boundary was increased by 2 cm and 4 cm, respectively. The predicted net flow was always negative (i.e., moving towards Chesapeake Bay) when the water surface elevation was decreased by 4 cm.

Interannual variability can be assessed by sub-dividing the year into months, as in Figure C.1-3. For 2016, the net flow was smaller during wintertime and became negative during January. The highest net flow occurred in April. Predicted net flow in C&D Canal was also summarized by season for spring and neap tide periods (Figures C.1-4 and C.1-5). Wintertime has the lowest net flow compared to the other seasons, and net flow seems to be slightly higher during the neap tide period compared to the spring tide period.

Time series of simulated daily depth-averaged salinity from all five simulations at five locations in the Delaware Estuary are shown in Figure C.1-6 through C.1-10 during the course of one year with the 2016 hydrology. The statistical summary of the daily depth-averaged salinity is presented in Figure C.1-11 and C.1-12 for a total of eight locations and in Table C.1-2. The impact of the C&D Canal net flow, which varies due to the vertical datum adjustment applied at the western end of the canal, became more pronounced during the fall season, from September to December when the flow in the Delaware River was low. Generally, salinity increased when the datum adjustment was shifted downward, resulting in a reduced C&D net flow, while salinity decreased when the datum adjustment was shifted upward, leading to an increased C&D net flow. With a datum adjustment of -2cm, the maximum daily depth-averaged salinity at Chester (RM 83.6) increased by 30 percent from 1.34 to 1.74 psu and similarly increased by 31 percent from 0.39 to 0.51 psu at the mouth of the Schuylkill River (RM 92.5). On the other hand, with a datum adjustment of +2cm, the maximum daily depth-averaged salinity at Chester (RM 83.6) decreased by 23 percent from 1.34 to 1.03 psu and similarly decreased by 18 percent from 0.39 to 0.32 psu at the mouth of the Schuylkill River (RM 92.5). This suggests that a lower water level at the western end of the C&D Canal's open boundary, resulting from a negative datum adjustment, is more likely to cause a stronger salinity intrusion into the Delaware Estuary. In contrast, an increase in water level at the western end of the C&D Canal's open boundary, due to a positive datum adjustment, may allow more freshwater from Chesapeake Bay to flow into the Delaware

[46] Estimation of Vertical Uncertainties in Vdatum (NOAA): https://vdatum.noaa.gov/docs/est_uncertainties.html

Estuary, thereby hindering the upstream movement of saltwater. These results demonstrate that net flow through the C&D Canal has a significant impact on hydrodynamics and salinity transport in the Delaware Estuary. USGS established a new station in the canal near Delaware City and reports flow data since October 2021. The model is calibrated using the data collected in 2021 and 2022. When longer and sufficient data are available that cover multiple years with a variety of hydrologic conditions, the model may be further refined to more accurately represent tidal flows from C&D Canal.

Table C.1-2. Simulated Maximum Daily Depth-averaged Salinity during 2016: Sensitivity to C&D Canal Net Flow, which Varies with the Vertical Datum Adjustment Applied at the Western End of the C&D Canal

		Base + 4 cm			Base + 2 cm			Base -2 cm			Base – 4 cm		
	Base-line	Sensi.	Diff.	Percent Diff.	Sensi.	Diff.	Percent Diff.	Sensi.	Diff.	Percent Diff.	Sensi.	Diff.	Percent Diff.
Ship John Shoal (RM 37)	23.23	21.85	-1.38	-5.94	22.45	-0.78	-3.36	23.95	0.72	3.10	24.81	1.58	6.80
Reedy Island (RM 54)	13.48	11.46	-2.02	-14.99	12.40	-1.08	-8.01	14.71	1.23	9.12	16.02	2.54	18.84
Delaware Memorial Bridge (RM 69)	6.09	4.57	-1.52	-24.96	5.25	-0.84	-13.79	7.04	0.95	15.60	8.11	2.02	33.17
Chester (RM 83.6)	1.34	0.83	-0.51	-38.06	1.03	-0.31	-23.13	1.74	0.40	29.85	2.25	0.91	67.91
Schuylkill River (RM 92.5)	0.39	0.28	-0.11	-28.21	0.32	-0.07	-17.95	0.51	0.12	30.77	0.69	0.30	76.92
RM 98	0.22	0.19	-0.03	-13.64	0.20	-0.02	-9.09	0.26	0.04	18.18	0.32	0.10	45.45
Ben Fraklin Bridge (RM 100)	0.20	0.18	-0.02	-10.00	0.19	-0.01	-5.00	0.22	0.02	10.00	0.27	0.07	35.00
Drinking Water Intake (RM 110)	0.14	0.14	0.00	0.00	0.14	0.00	0.00	0.14	0.00	0.00	0.14	0.00	0.00

C.2 Salinity at the Western C&D Canal Boundary

Conductivity data were only available from NOAA since 2017 at the NOAA Station Chesapeake City in the C&D Canal. No historical conductivity data are available before 2017. A rating curve was used to specify the salinity at the C&D Canal boundary during periods when no conductivity measurements (see Section 3.3) were available. Multiple linear regression (MLR) analysis was

conducted using data from NOAA Station Chesapeake City, USGS Station at Reedy Island, and USGS Station (01576000) at Susquehanna River Flow at Marietta, PA from April 1, 2017, to May 31, 2019. The salinity was low when flows were high in the Susquehanna River, indicating an inverse relationship between the salinity at Chesapeake City and Susquehanna River Flow at Marietta, PA. The R squared score of 0.77 for this relationship indicates that about 20 to 30 percent of the variability is not explained by the independent variables in the rating curve. Usually, the salinity at the upper Chesapeake Bay near the western end of the C&D Canal is low (a few psu), and water is considered fresh. An uncertainty range of 25 percent in the C&D Canal salinity boundary was considered reasonable and was evaluated in this set of sensitivity tests. The salinity boundary condition for the Canal was varied for sensitivity runs 6 and 7 to examine the effect on computed salinity and chlorides in the Delaware Estuary. The variation was plus or minus 25 percent of the base case condition value. The same simulation period of 2016 was also used in this set of sensitivity analyses.

Time series of cumulative net flow in C&D Canal with the perturbation of C&D Canal salinity boundary conditions are shown in Figures C.2-1 and C.2-2 at the two NOAA stations, Chesapeake City and Reedy Point, respectively. Monthly residual flows are presented in Figure C.2-3. The legend label “sensitivity 1” and “sensitivity 2” in the figure refer to sensitivity run 5 and 6 listed in Table C.1-1. At Chesapeake City station, the average of the monthly residual flow for 2016 changed from 4 for the base case to -1 and to 8 m^3/s with the 25 percent decrease and increase in C&D Canal salinity boundary conditions, respectively. The total annual cumulative net flow increased by roughly 100 percent compared to the base case as the salinity at the C&D Canal boundary increased consistently by 25 percent through the course of the entire year 2016. The C&D Canal net flow decreased also by approximately 120 percent as the salinity at the C&D Canal boundary decreased consistently by 25 percent compared to the base case. It is important to note that the annual cumulative net flow for the base case is minimal for this particular dry year. Even with a 100 percent change, the absolute magnitude of the shift in the C&D salinity boundary condition can be regarded as insignificant.

Comparisons of simulated daily depth-averaged salinity at five locations along the Delaware River are presented in Figure C.2-4 through C.2-8. The ranges of simulated daily depth-averaged salinity for eight locations are presented in Figure C.2-9 and C.2-10. The simulated maximum daily depth-averaged salinity values are summarized in Table C.2-1. With a 25 percent increase or decrease in the salinity at the western end of the C&D Canal results in a slight increase or decrease in maximum daily depth-averaged salinity at Delaware Memorial Bridge (RM 69) from the baseline 6.09 psu to 6.26 psu (2.8 percent increase) or to 5.92 psu (2.8 percent decrease). The absolute change in the maximum daily depth-averaged salinity at Chester (RM 83.6) is 0.06 psu (or 4.5 percent). These results indicate that the simulated salinity in the Delaware Estuary, especially in the upper tidal river, is not sensitive to the salinity specified at the western end of the C&D Canal, and that may also imply that the model simulated salinity intrusion in the Delaware Estuary is not sensitive to the uncertainty of the salinity at the C&D Canal boundary.

Table C.2-1. Simulated Maximum Daily Depth-averaged Salinity during 2016: Sensitivity to C&D Canal Salinity Boundary Condition

		Base x 0.75			Base x 1.25		
	Base-line	Sensi.	Diff.	Percent Diff.	Sensi.	Diff.	Percent Diff.
Ship John Shoal (RM 37)	23.23	23.23	0.00	0.00	23.19	-0.04	-0.17
Reedy Island (RM 54)	13.48	13.45	-0.03	-0.22	13.55	0.07	0.52
Delaware Memorial Bridge (RM 69)	6.09	5.92	-0.17	-2.79	6.26	0.17	2.79
Chester (RM 83.6)	1.34	1.28	-0.06	-4.48	1.40	0.06	4.48
Schuylkill River (RM 92.5)	0.39	0.37	-0.02	-5.13	0.42	0.03	7.69
RM 98	0.22	0.22	0.00	0.00	0.23	0.01	4.55
Ben Fraklin Bridge (RM 100)	0.20	0.20	0.00	0.00	0.20	0.00	0.00
Drinking Water Intake (RM 110)	0.14	0.14	0.00	0.00	0.14	0.00	0.00

C.3 Sensitivity to Ocean Salinity Boundary

Salinity at the ocean boundary was specified based on statistical monthly mean values representing the relatively constant conditions. Short-term, extreme meteorological events or other phenomena may cause salinity at the boundary to deviate from the long-term mean values used for the boundary condition. The impact of the salinity specified at the open ocean boundary was tested with a simulation of the year 2017 because it was an extremely active Atlantic hurricane season. More intense storm events are likely to result in more mixing with freshwater in the top layer of the ocean, potentially causing greater stratification in salinity near the coast.

Two sensitivity runs (run 7 and 8 listed in Table C.1-1) were conducted, with different ocean salinities than the base case but using the methodology described in Section 3.3.3. For run 7, the ocean salinity was reduced by 2 to 3 psu from the surface down to 10 m depth for four months

(September–December). For run 8, the same change in ocean salinity was applied for seven months (June–December). Below 10-m depth, the salinity was not changed from the base case for either run. The reduction in salinity in the near surface layers produced a stronger vertical stratification at the ocean boundary compared to the base case.

The simulated cumulative C&D Canal net flow from the baseline and 2 sensitivity runs are presented in Figures C.3-1 and C.3-2. The monthly variation of the residual flow is presented in Figure C.3-3. The average monthly residual flow in the C&D Canal slightly increased from the base case 42 to 58 and 69 m^3/s. The increased vertical salinity stratification at the ocean open boundary reduces pressure and decreases ocean water density. This change also results in lower salinities and water density near the eastern side of the C&D Canal, but not significantly. The water in the upper Delaware Bay became less salty and as a result relatively fresher water moved into the Delaware Estuary from the Chesapeake Bay through the C&D Canal. The system responded to the change in the ocean salinity as expected, but the impact on the salinity intrusion to a 2 to 3 psu change at the model ocean open boundary seems to be small.

Time series of simulated daily depth-averaged salinity at selected locations are presented in Figure C.3-4 through C.3-8. The ranges of the simulated depth-averaged salinity at eight locations are presented in Figure C.3-9 and C.3-10. The maximum daily, depth-averaged salinity is summarized in Table C.3-1. These simulations demonstrate that the impact may be negligible if the 3 psu perturbation only occurs for a short period. A reduction of 3 psu in the top 10-m layer located 40 mi from the bay mouth for more than four months during a low flow season may result in an increase in C&D Canal net flow and decrease the salinity intrusion by only a small percentage.

Table C.3-1. Simulated Maximum Daily Depth-averaged Salinity during 2016: Sensitivity to Salinity at Ocean Boundary

		Base -2 to 3 psu for 4 months			Base -2 to 3 psu for 7 months		
	Base-line	Sensi.	Diff.	Percent Diff.	Sensi.	Diff.	Percent Diff.
Ship John Shoal (RM 37)	21.93	21.55	-0.38	-1.73	21.12	-0.81	-3.69
Reedy Island (RM 54)	12.61	12.17	-0.44	-3.49	11.75	-0.86	-6.82
Delaware Memorial Bridge (RM 69)	4.46	4.18	-0.28	-6.28	3.98	-0.48	-10.76
Chester (RM 83.6)	0.68	0.61	-0.07	-10.29	0.57	-0.11	-16.18
Schuylkill River (RM 92.5)	0.21	0.21	0.00	0.00	0.21	0.00	0.00
RM 98	0.17	0.17	0.00	0.00	0.17	0.00	0.00
Ben Fraklin Bridge (RM 100)	0.17	0.17	0.00	0.00	0.17	0.00	0.00
Drinking Water Intake (RM 110)	0.15	0.15	0.00	0.00	0.15	0.00	0.00

Figures for Appendix C

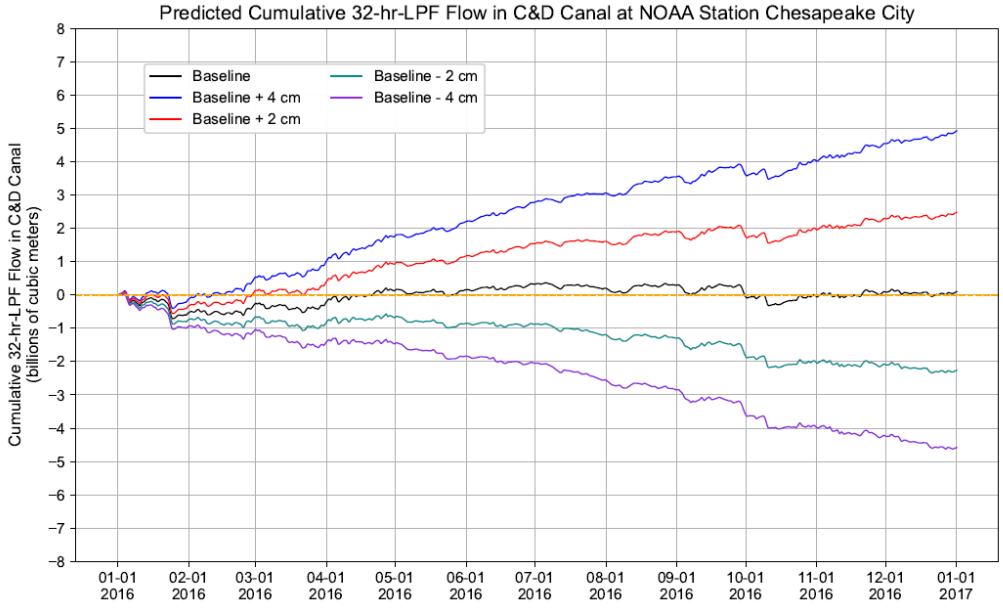

Figure C.1-1 Simulated Cumulative 32-HR-LPF Tidal Flow in C&D Canal at NOAA Station Chesapeake City during 2016

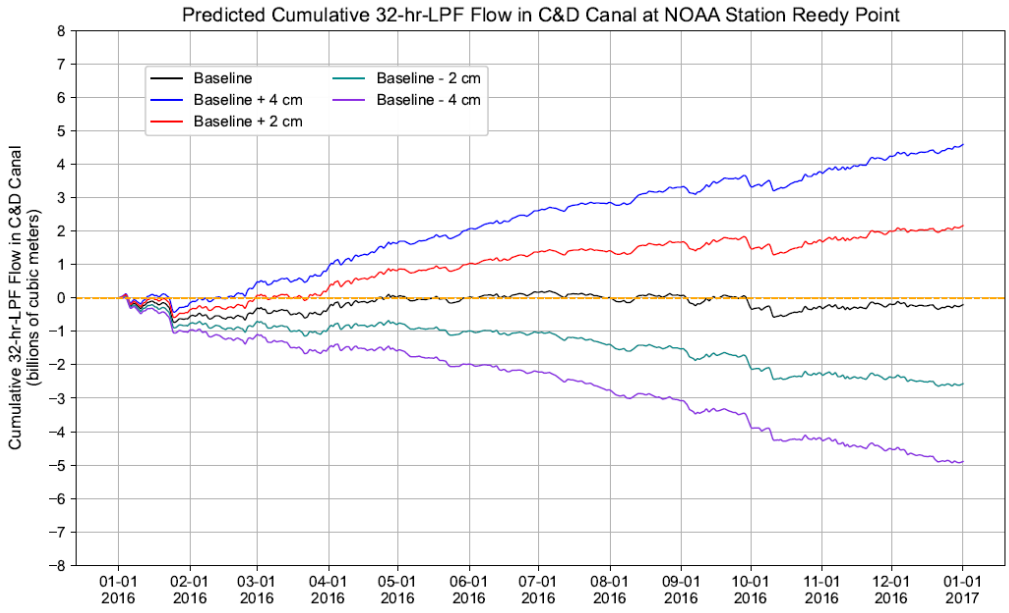

Figure C.1-2 Simulated Cumulative 32-HR-LPF Tidal Flow in C&D Canal at NOAA Station Reedy Point during 2016

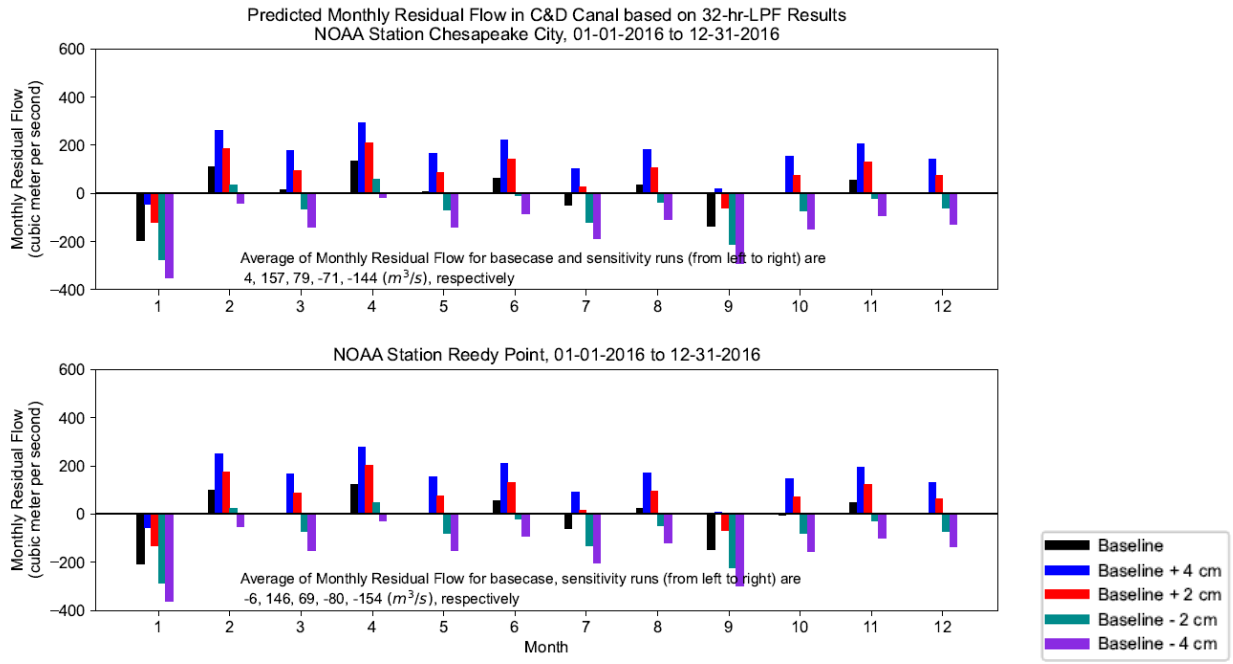

Figure C.1-3 C&D Canal Water Surface Elevation Sensitivity: Predicted Monthly Residual Flow in C&D Canal at NOAA Stations during 01-01-2016 to 12-31-2016 Period.

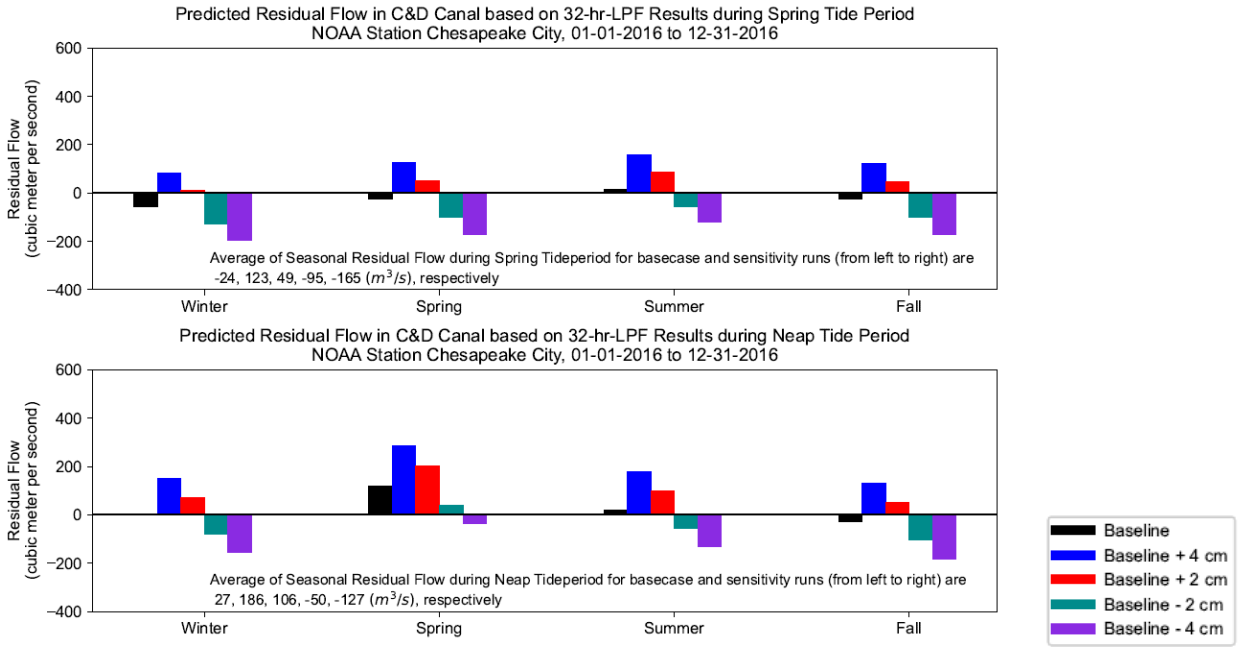

Figure C.1-4 C&D Canal Water Surface Elevation Sensitivity: Predicted Monthly Residual Flow in C&D Canal at NOAA Station Chesapeake City during 2016 Period Summarized by Season and Spring Tide and Neap Tide

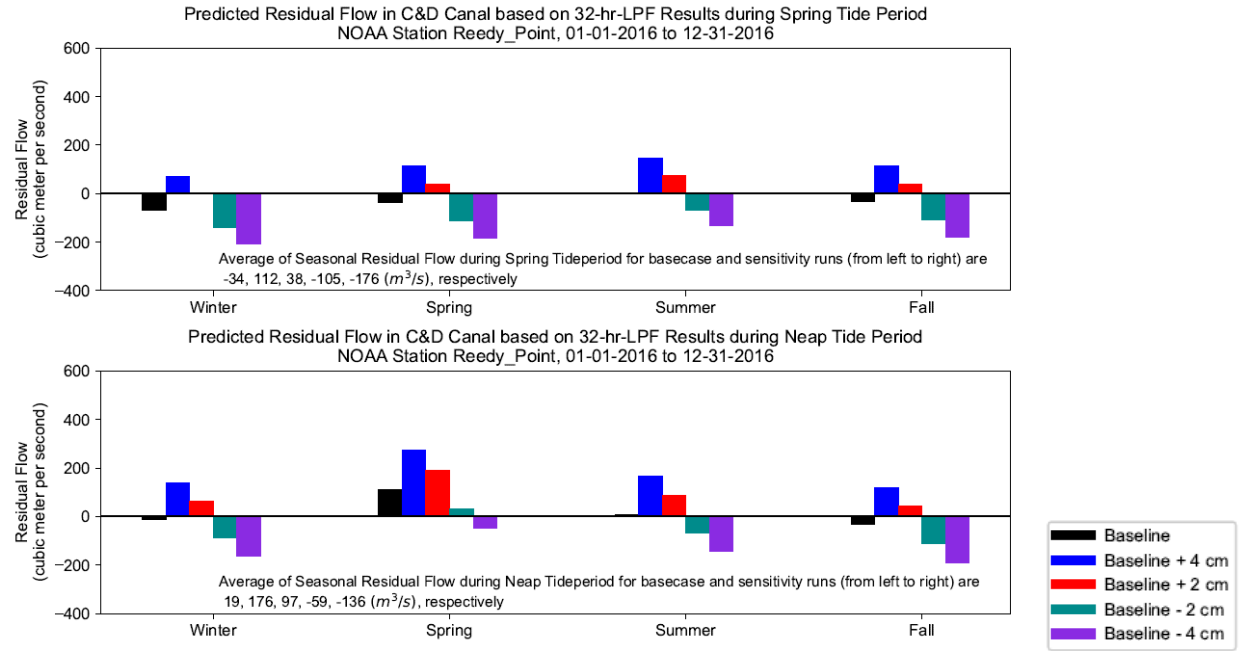

Figure C.1-5 C&D Canal Water Surface Elevation Sensitivity: Predicted Monthly Residual Flow in C&D Canal at NOAA Station Reedy Point during 2016 Period Summarized by Season and Spring Tide and Neap Tide

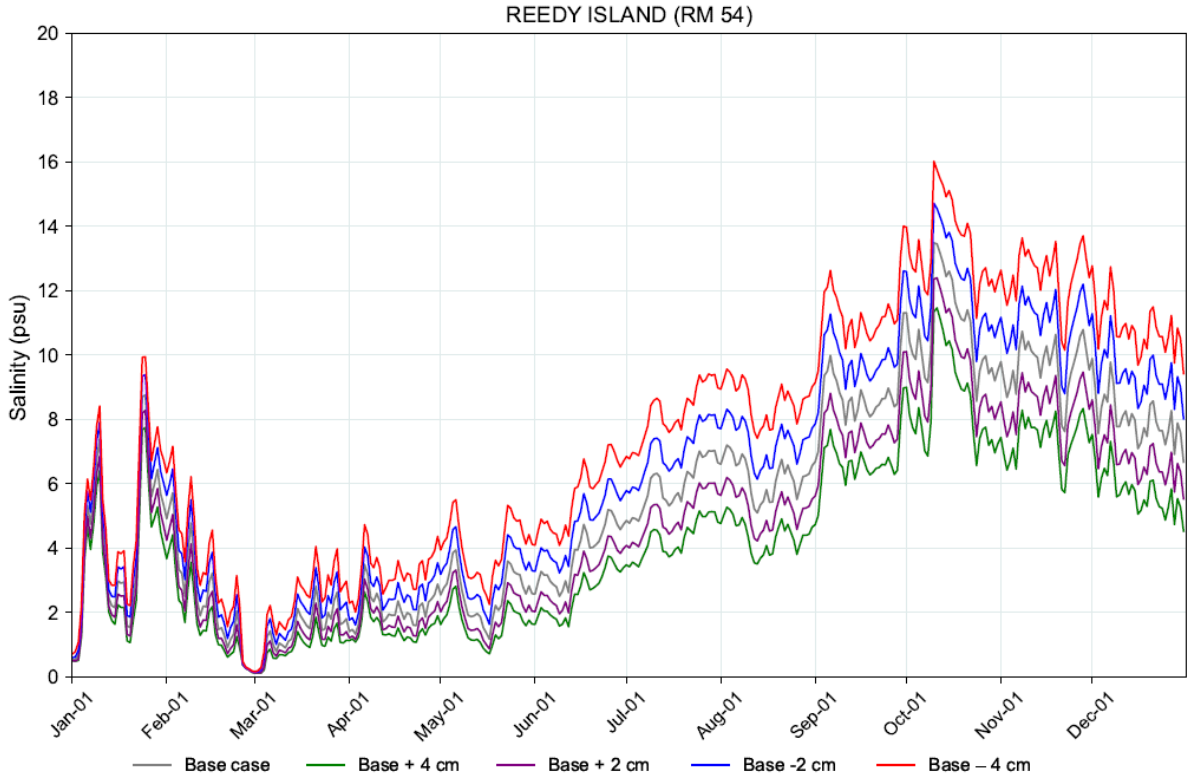

Figure C.1-6 Simulated Daily Depth-averaged Salinity at Reedy Island (RM 54): Sensitivity to C&D Canal Net Flow, which Varies with the Vertical Datum Adjustment Applied at the Western End of the C&D Canal

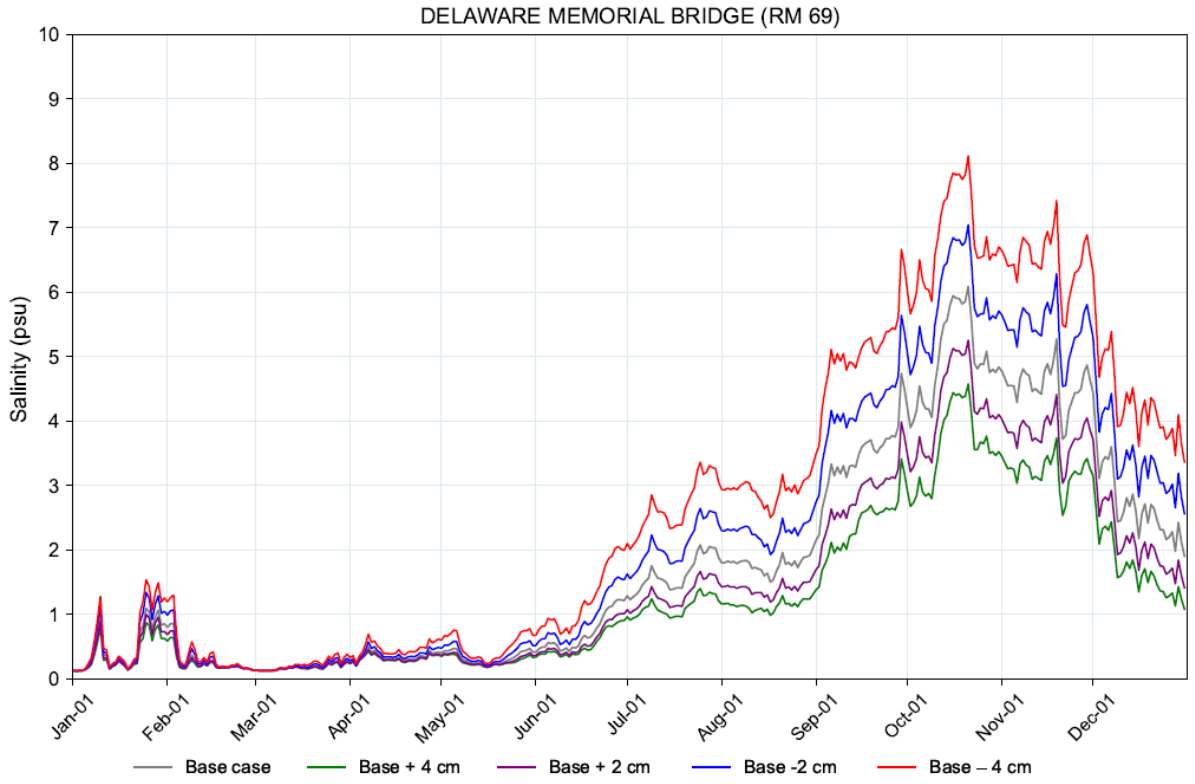

Figure C.1-7 Simulated Daily Depth-averaged Salinity at Delaware Memorial Bridge (RM 69): Sensitivity to C&D Canal Net Flow, which Varies with the Vertical Datum Adjustment Applied at the Western End of the C&D Canal

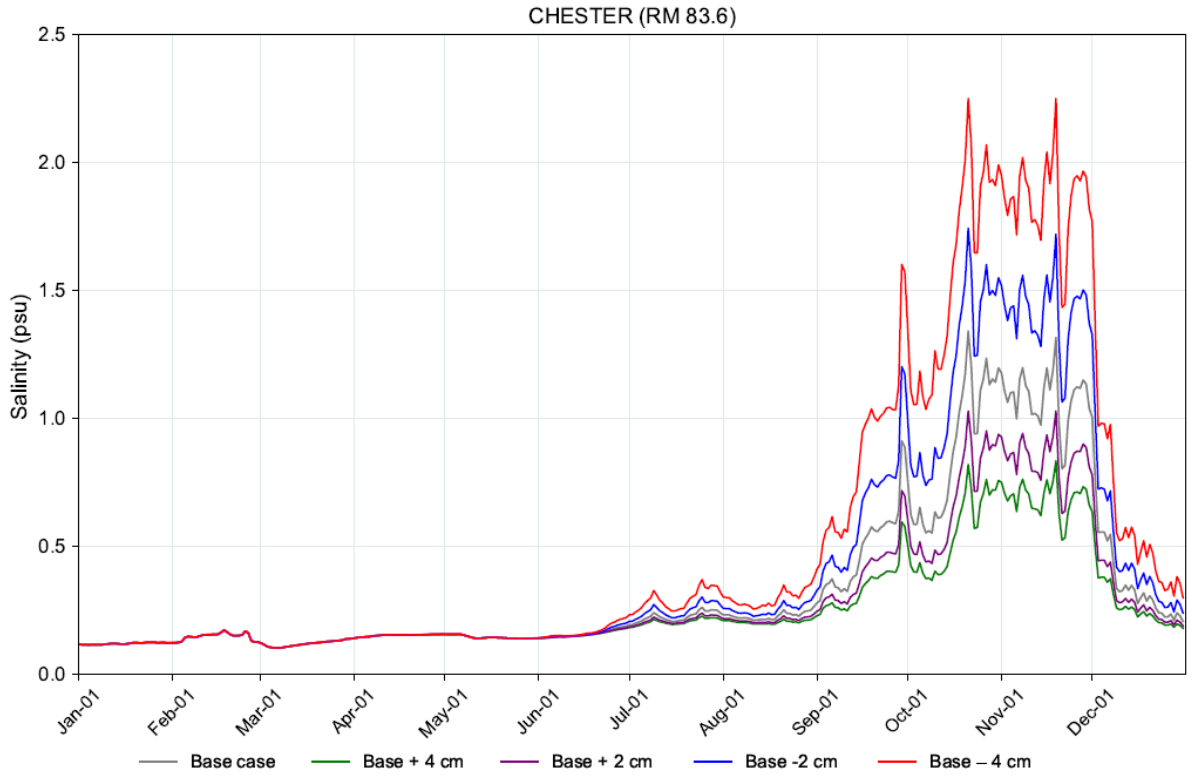

Figure C.1-8 Simulated Daily Depth-averaged Salinity at Chester (RM 83.6): Sensitivity to C&D Canal Net Flow, which Varies with the Vertical Datum Adjustment Applied at the Western End of the C&D Canal

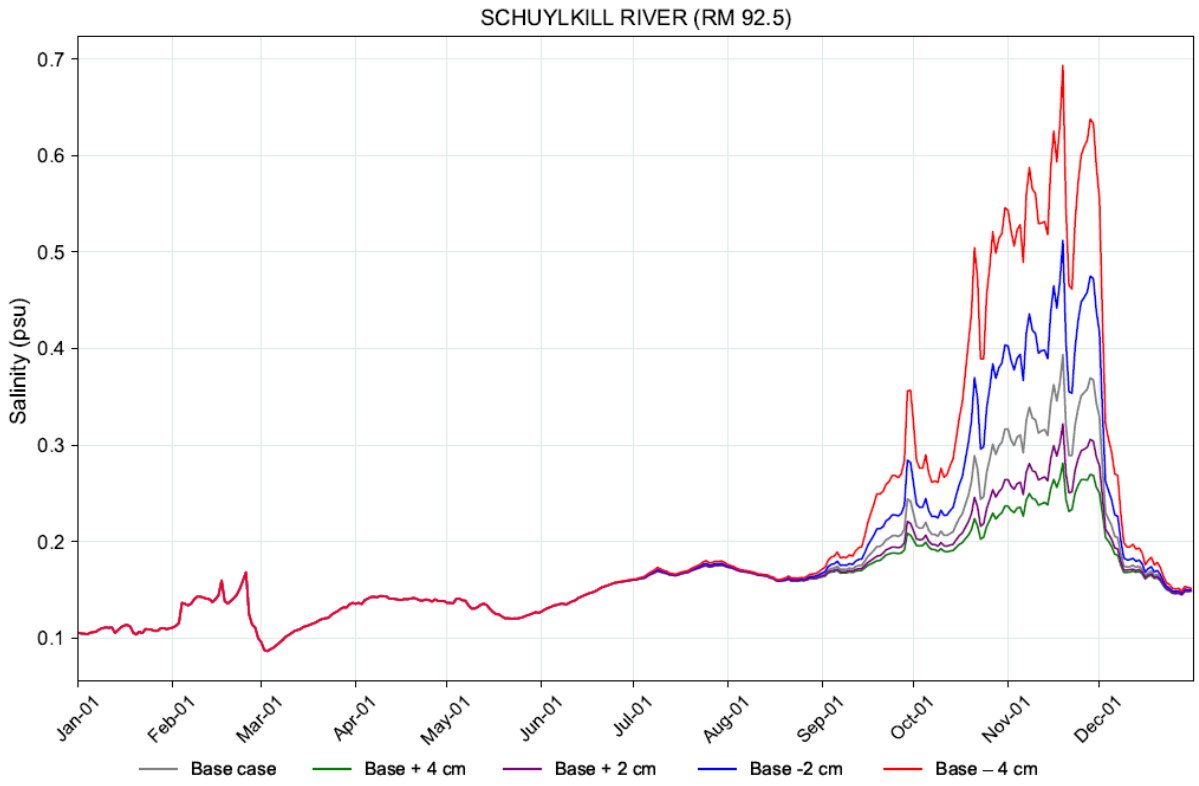

Figure C.1-9 Simulated Daily Depth-averaged Salinity at Schuylkill River confluence with the Delaware River (RM 92.5): Sensitivity to C&D Canal Net Flow, which Varies with the Vertical Datum Adjustment Applied at the Western End of the C&D Canal

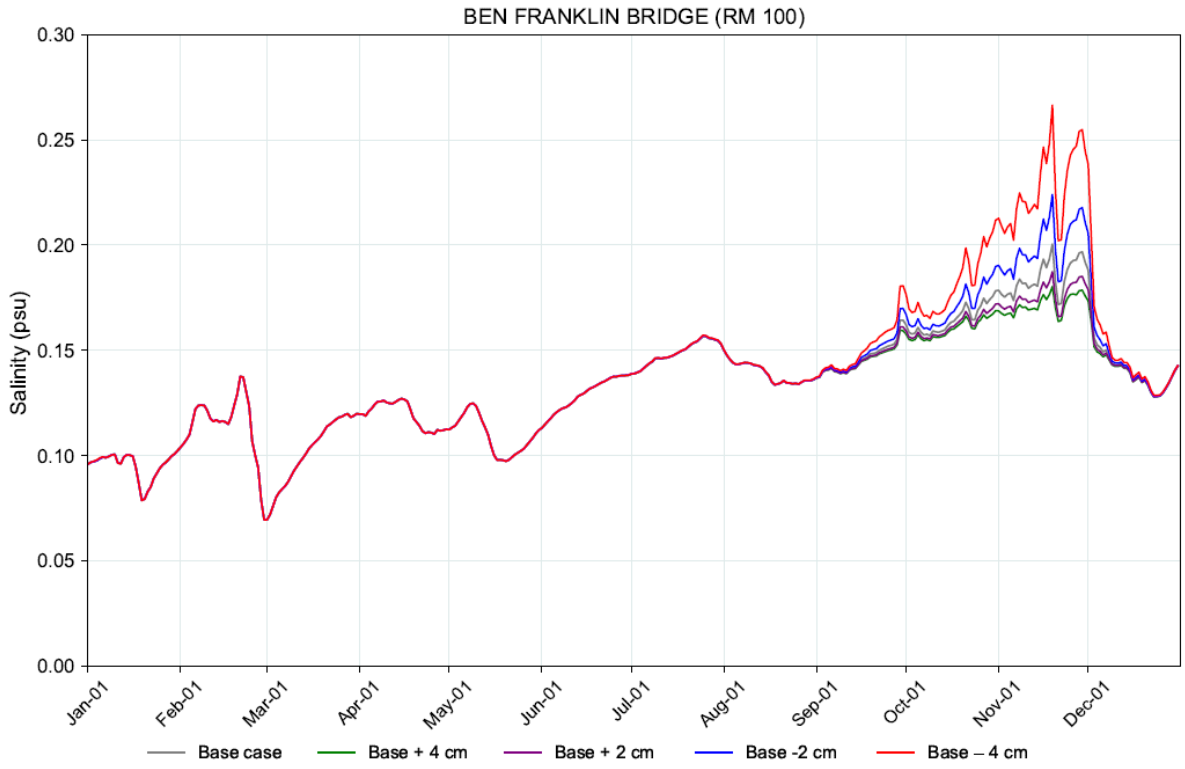

Figure C.1-10 Simulated Daily Depth-averaged Salinity at Ben Franklin Bridge (RM 100): Sensitivity to C&D Canal Net Flow, which Varies with the Vertical Datum Adjustment Applied at the Western End of the C&D Canal

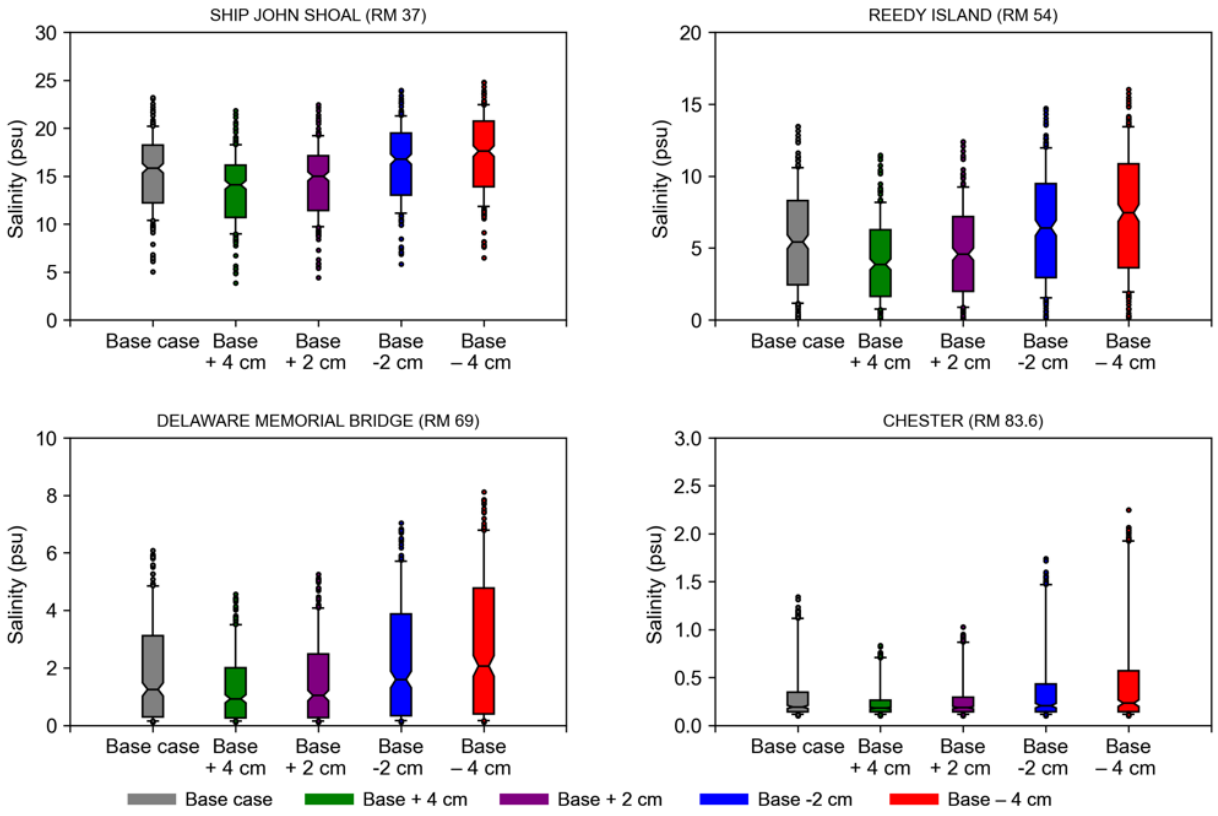

Notes: for box plot, middle line = median; Edge = 25, 75-th percentile; Whiskers = 5, 95-th percentile.

Figure C.1-11 Simulated Range of the Daily Depth-averaged Salinity between RM 37 and RM 83.6: Sensitivity to C&D Canal Net Flow, which Varies with the Vertical Datum Adjustment Applied at the Western End of the C&D Canal

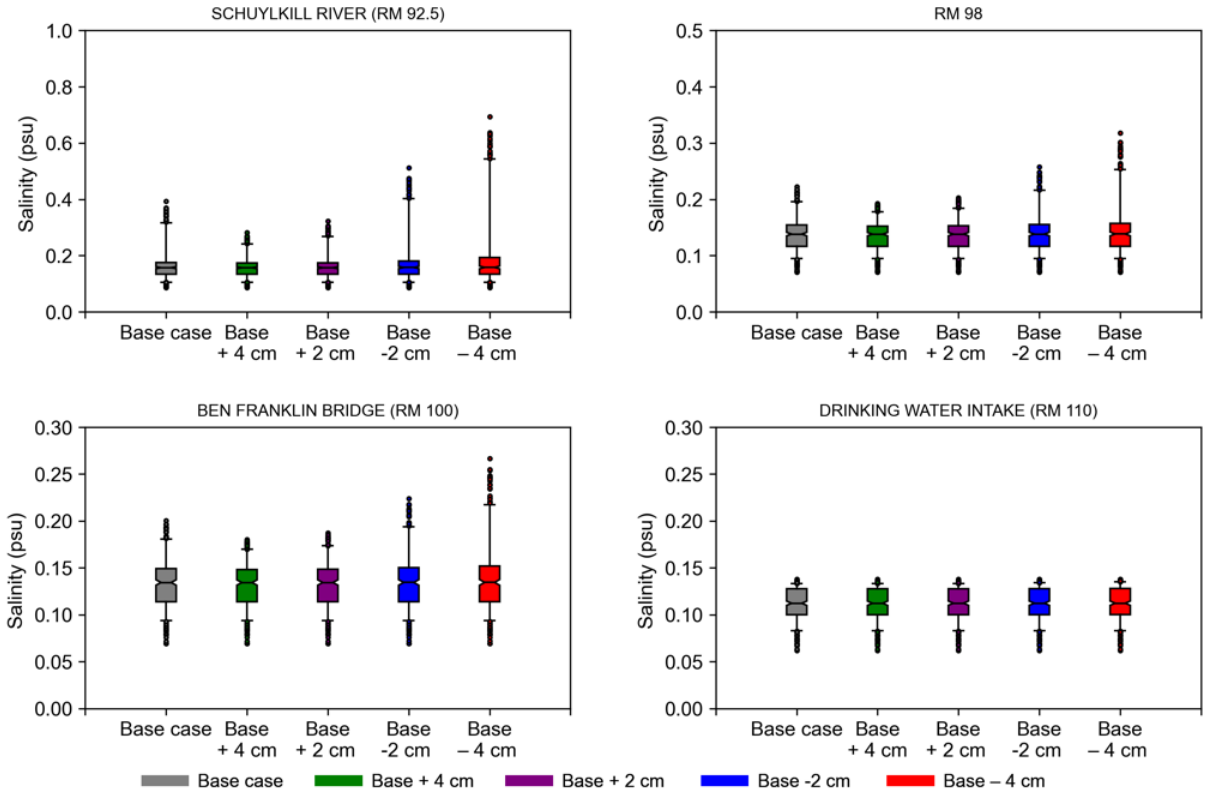

Notes: for box plot, middle line = median; Edge = 25, 75-th percentile; Whiskers = 5, 95-th percentile.

Figure C.1-12 Simulated Daily Depth-averaged Salinity between RM 92.5 and RM 110: Sensitivity to C&D Canal Net Flow, which Varies with the Vertical Datum Adjustment Applied at the Western End of the C&D Canal

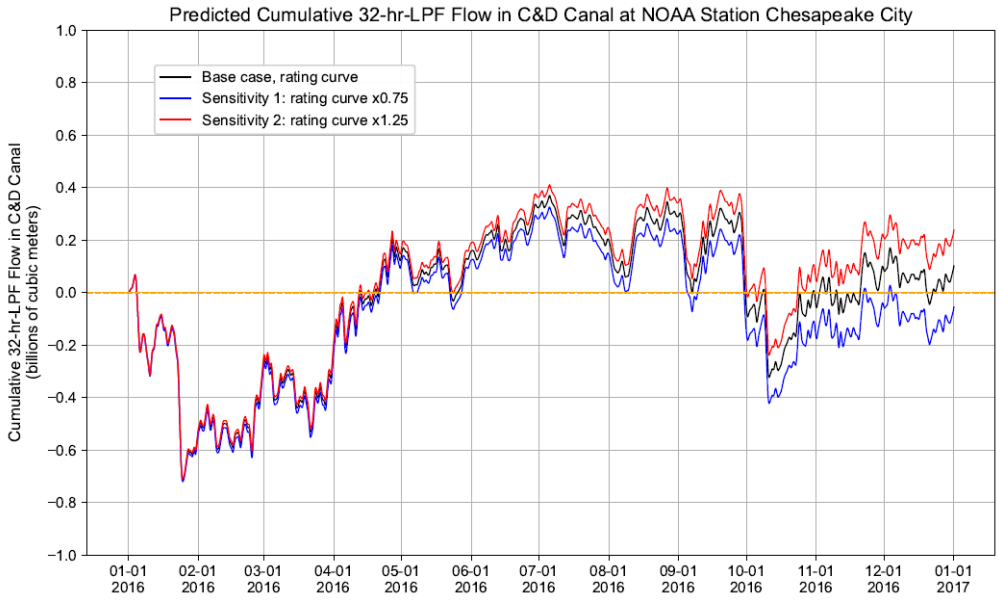

Note: The legend label "sensitivity 1" and "sensitivity 2" in the figure refer to sensitivity run 5 and 6 listed in Table C.1-1.

Figure C.2-1 Predicted Cumulative 32-HR-LPF Tidal Flow in C&D Canal at NOAA Station Chesapeake City during 2016: Sensitivity of Predicted Saltwater Intrusion to C&D Canal Salinity Boundary.

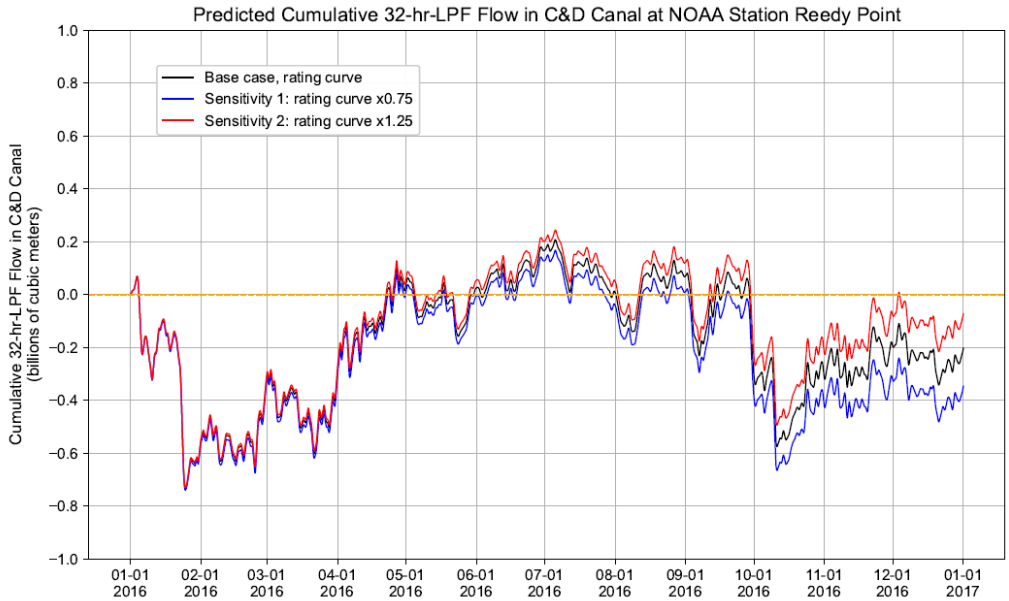

Note: The legend label "sensitivity 1" and "sensitivity 2" in the figure refer to sensitivity run 5 and 6 listed in Table C.1-1.

Figure C.2-2 Predicted Cumulative 32-HR-LPF Tidal Flow in C&D Canal at NOAA Station Reedy Point during 2016: Sensitivity of Predicted Saltwater Intrusion to C&D Canal Salinity Boundary.

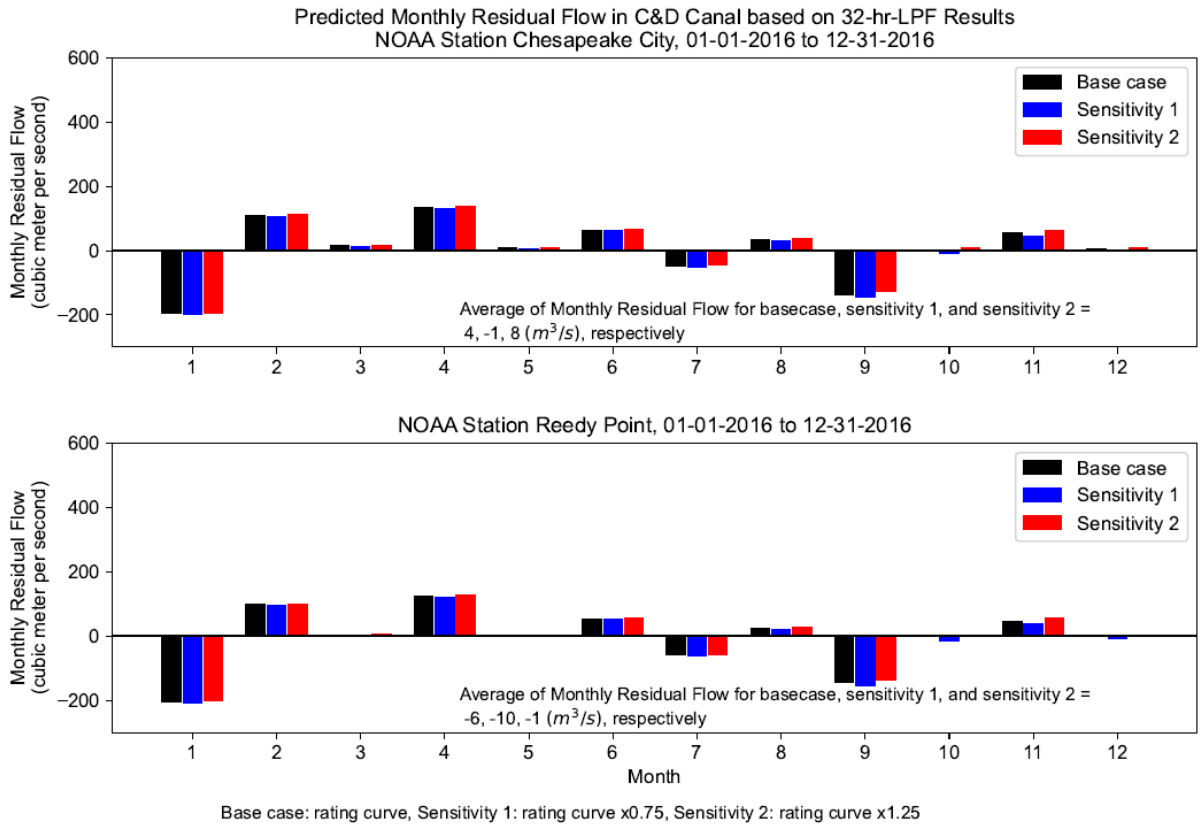

Note: The legend label “sensitivity 1” and “sensitivity 2” in the figure refer to sensitivity run 5 and 6 listed in Table C.1-1.

Figure C.2-3 Predicted Monthly Residual Flow in C&D Canal at NOAA Stations during 2016 Period: Sensitivity of Predicted Saltwater Intrusion to C&D Canal Salinity Boundary.

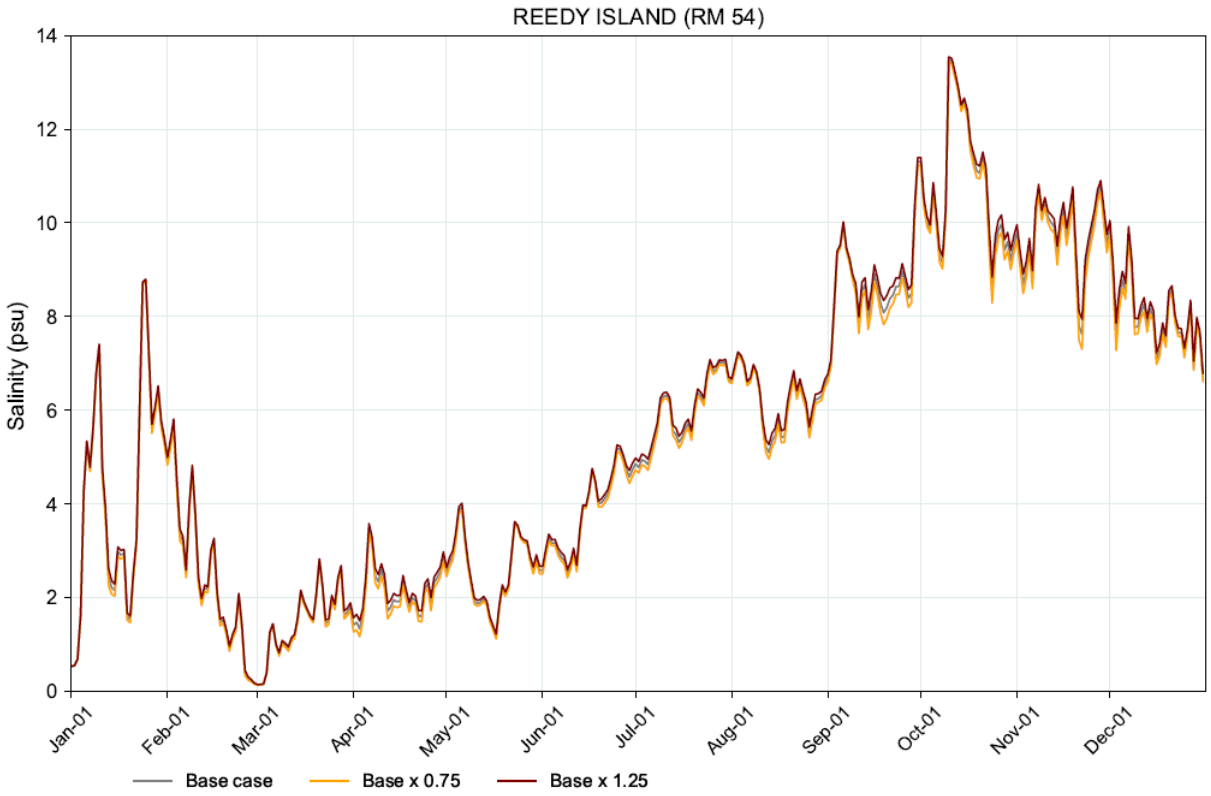

Figure C.2-4 Simulated Daily Depth-averaged Salinity at Reedy Island (RM 54): Sensitivity to C&D Canal Salinity Boundary Condition

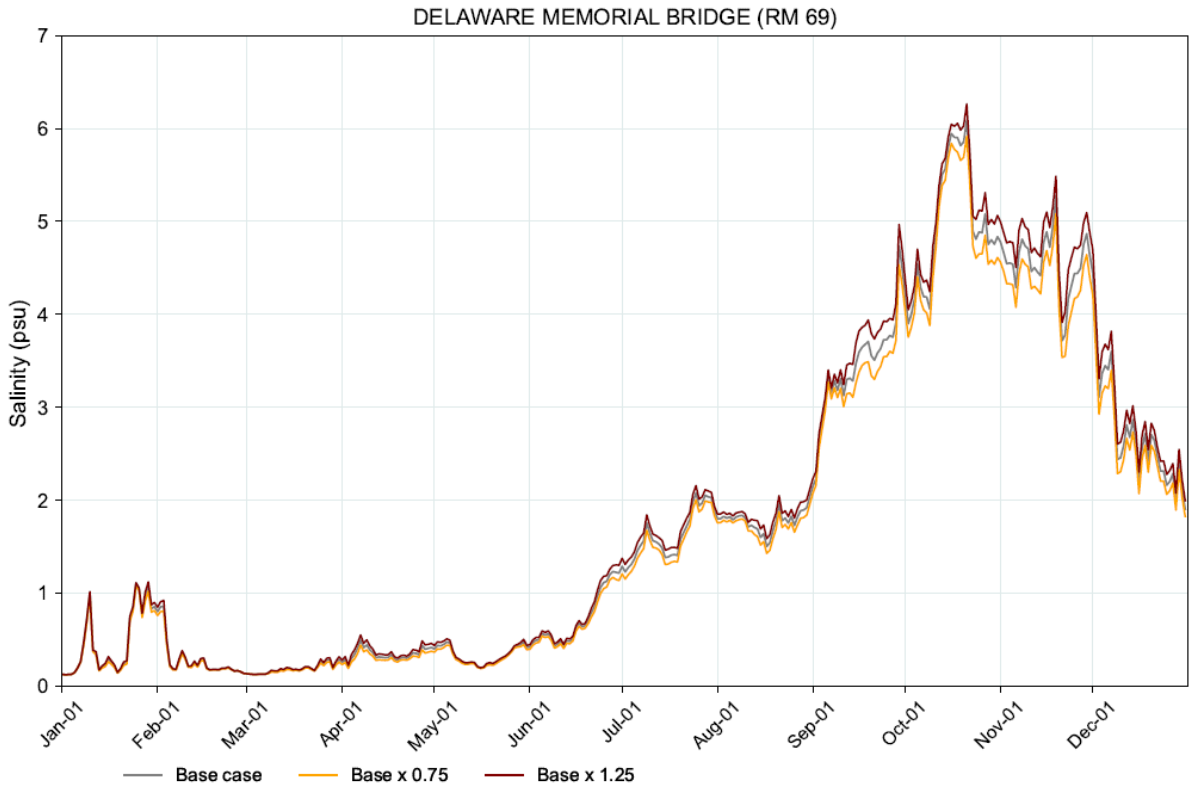

Figure C.2-5 Simulated Daily Depth-averaged Salinity at Delaware Memorial Bridge (RM 69): Sensitivity to C&D Canal Salinity Boundary Condition

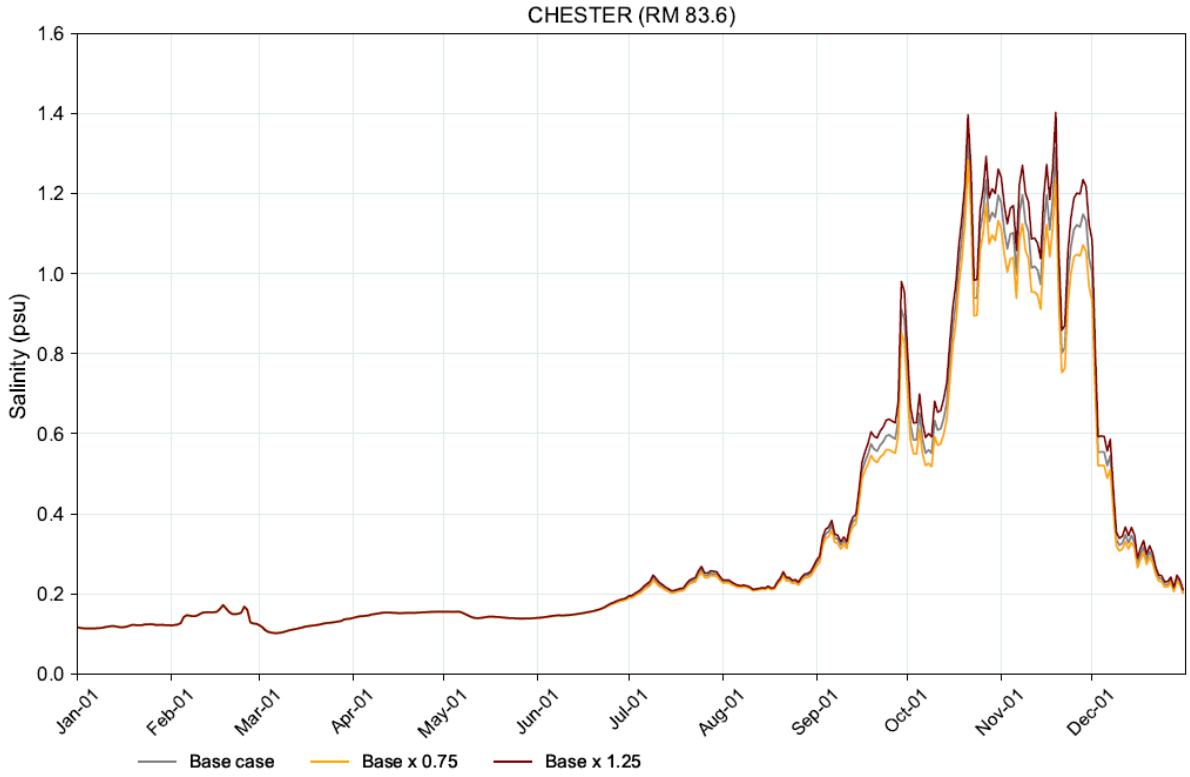

Figure C.2-6 Simulated Daily Depth-averaged Salinity at Chester (RM 83.6): Sensitivity to C&D Canal Salinity Boundary Condition

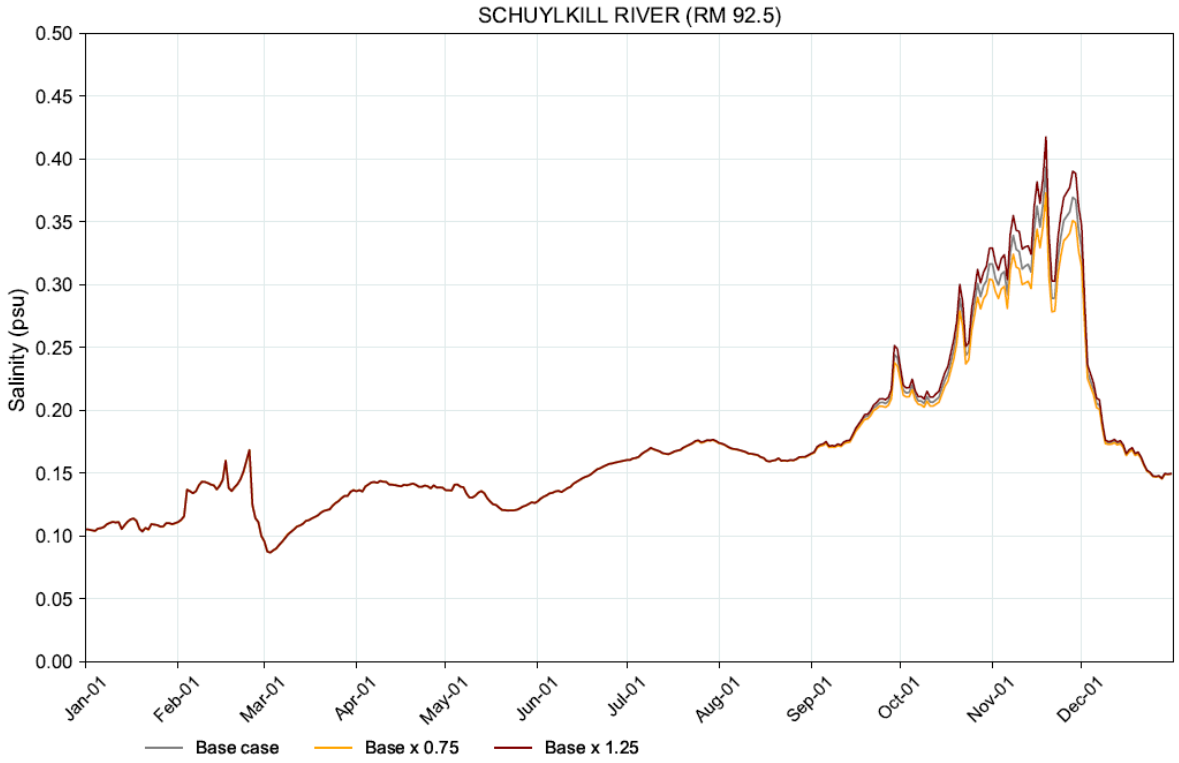

Figure C.2-7 Simulated Daily Depth-averaged Salinity at Schuylkill River confluence with the Delaware River (RM 92.5): Sensitivity to C&D Canal Salinity Boundary Condition

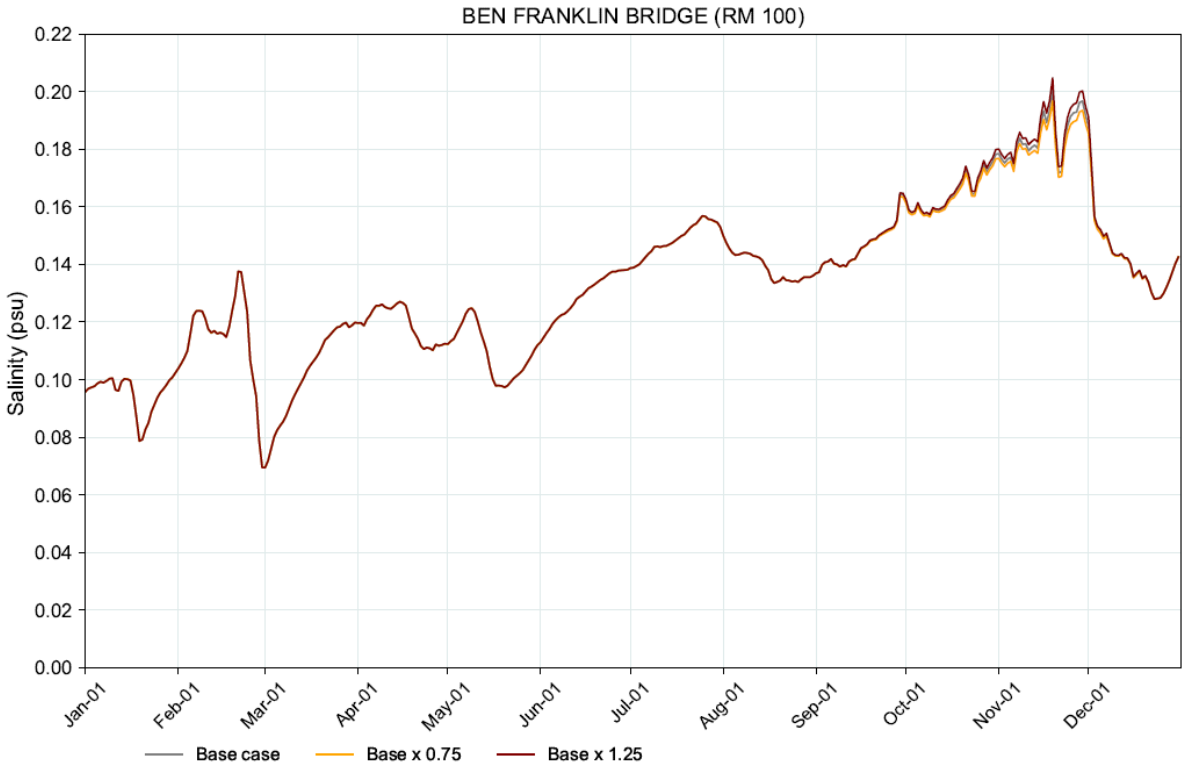

Figure C.2-8 Simulated Daily Depth-averaged Salinity at Ben Franklin Bridge (RM 100): Sensitivity to C&D Canal Salinity Boundary Condition

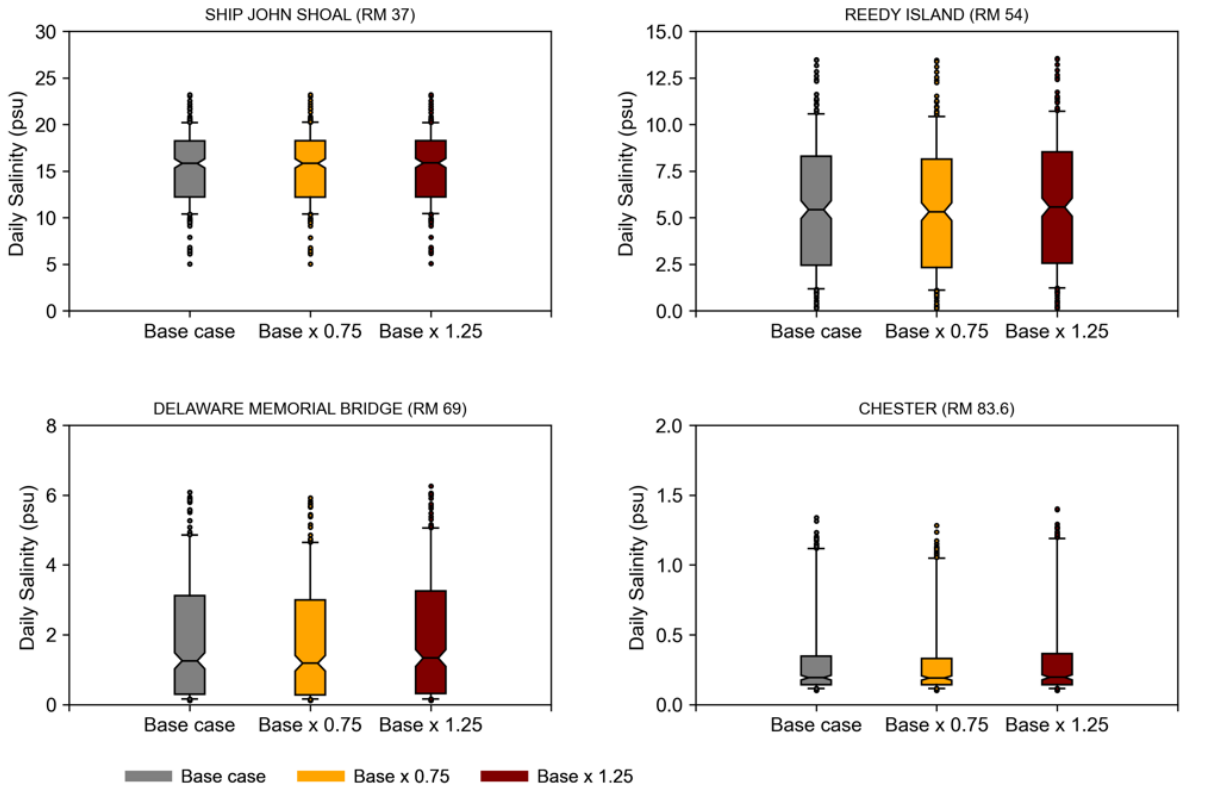

Notes: for box plot, middle line = median; Edge = 25, 75-th percentile; Whiskers = 5, 95-th percentile.

Figure C.2-9 Simulated Range of the Daily Depth-averaged Salinity between RM 37 and RM 83.6: Sensitivity to C&D Canal Salinity Boundary Condition

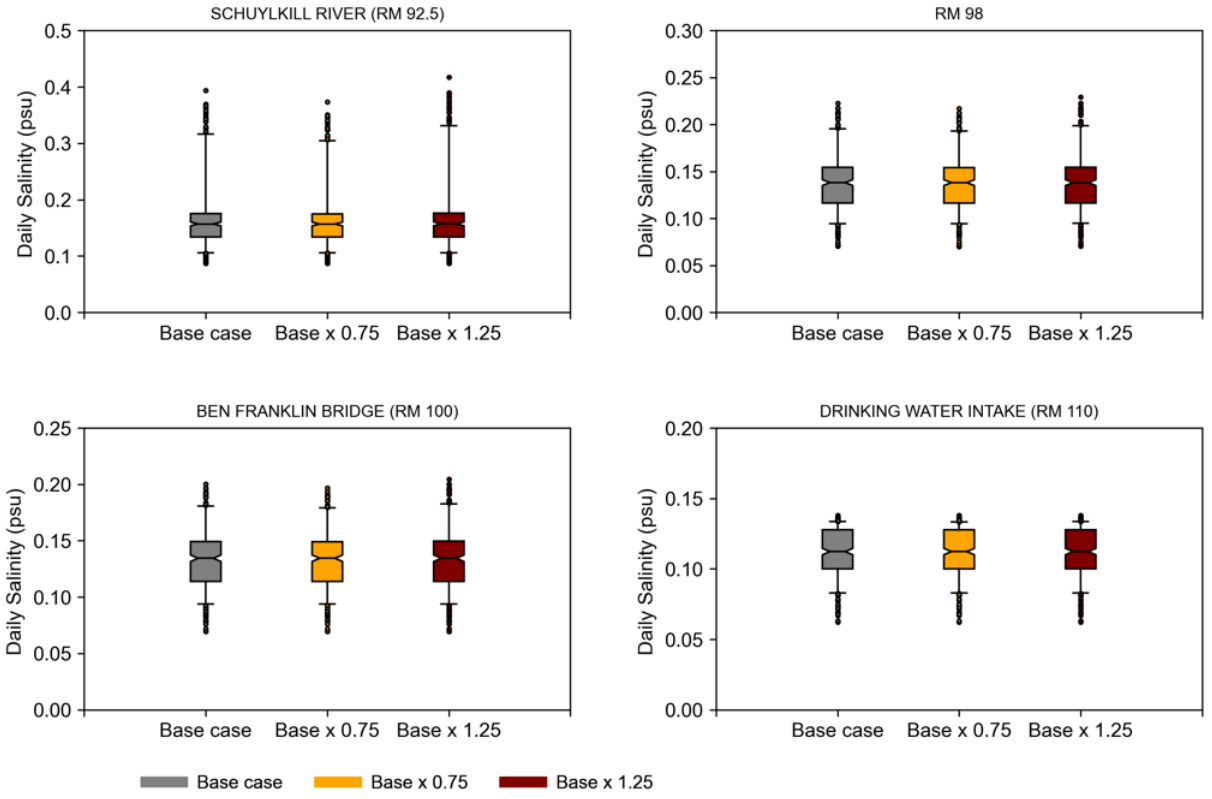

Notes: for box plot, middle line = median; Edge = 25, 75-th percentile; Whiskers = 5, 95-th percentile.

Figure C.2-10 Simulated Daily Depth-averaged Salinity between RM 92.5 and RM 110: Sensitivity to C&D Canal Salinity Boundary Condition

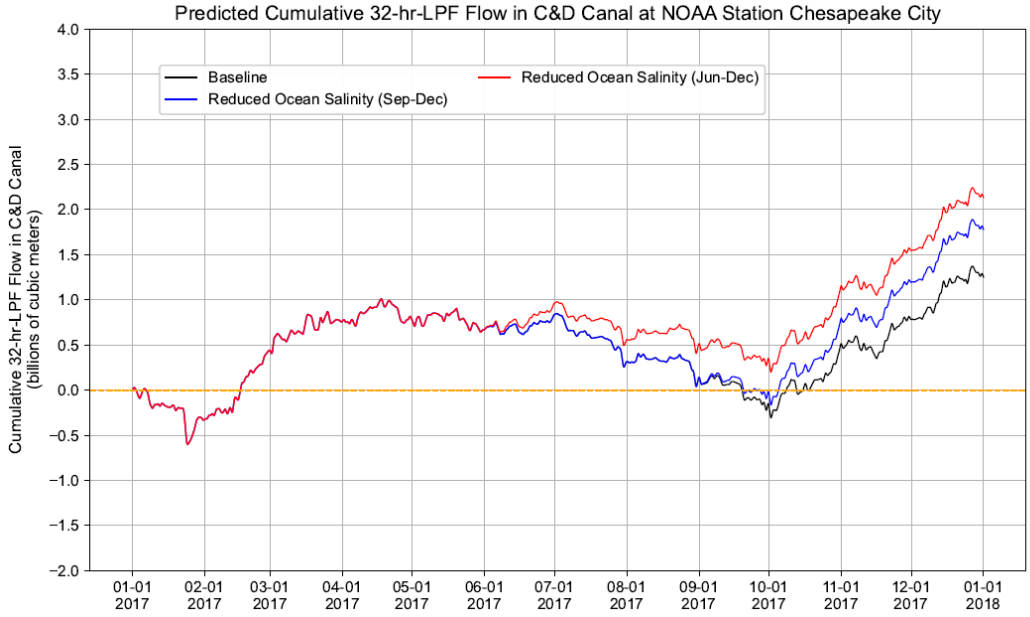

Figure C.3-1 Predicted Cumulative 32-HR-LPF Tidal Flow in C&D Canal at NOAA Station Chesapeake City during 2017 Period: Sensitivity of Predicted Saltwater Intrusion to Ocean Salinity Boundary.

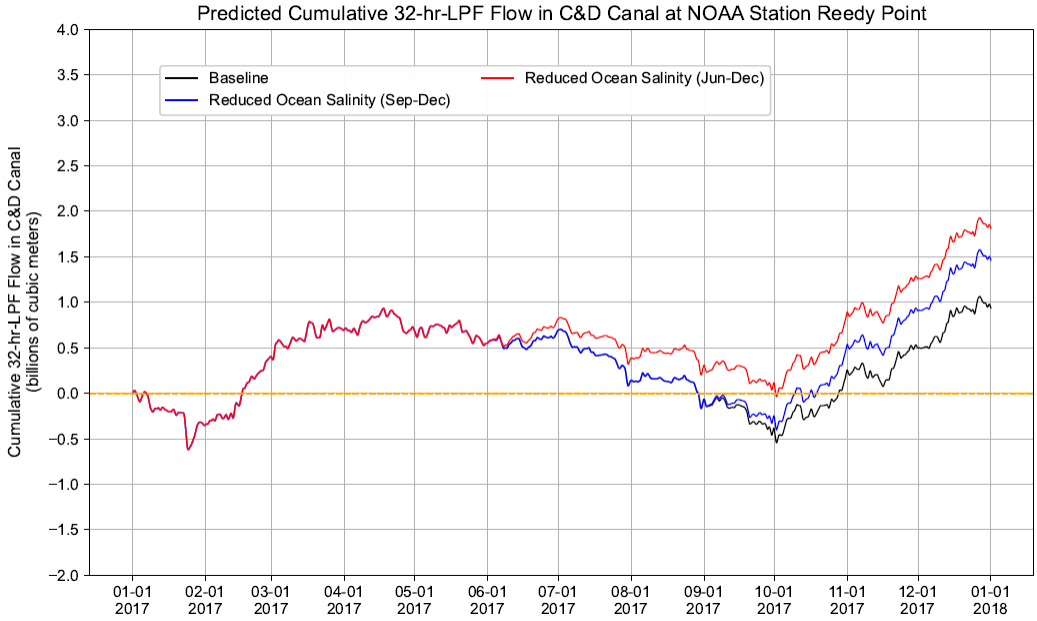

Figure C.3-2 Predicted Cumulative 32-HR-LPF Tidal Flow in C&D Canal at NOAA Station Reedy Point during 2017 Period: Sensitivity of Predicted Saltwater Intrusion to Ocean Salinity Boundary.

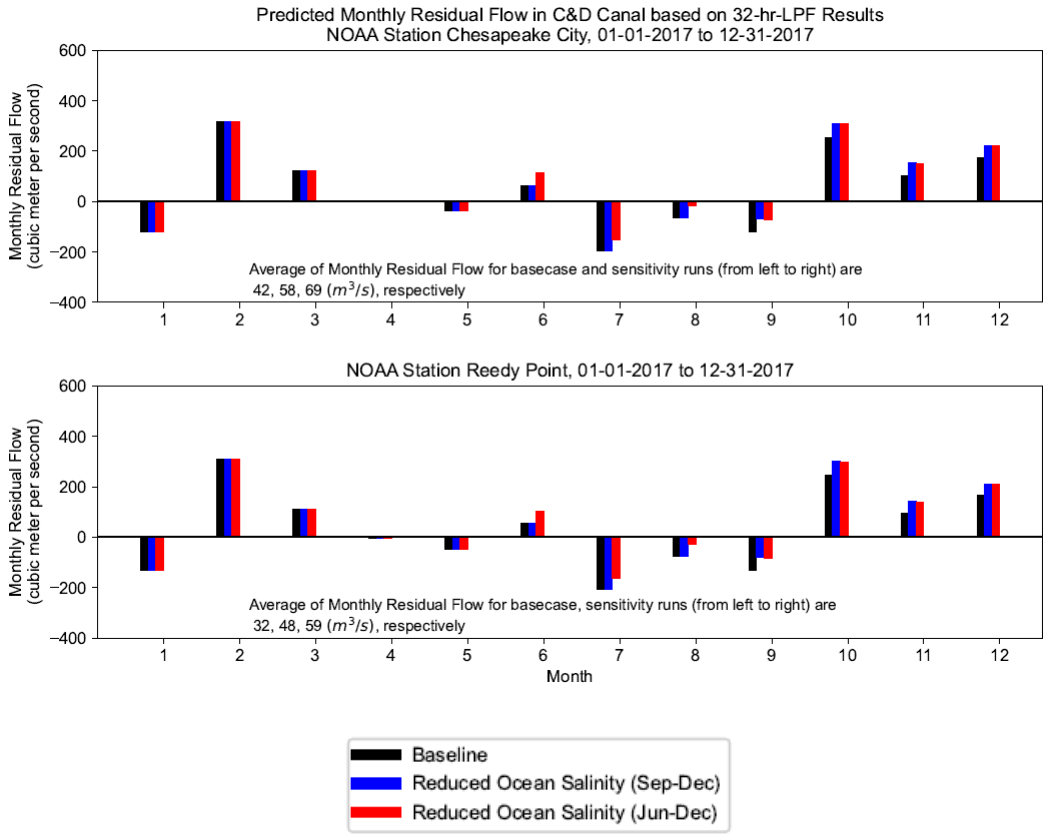

Figure C.3-3 Predicted Monthly Residual Flow in C&D Canal at NOAA Stations during 2017 Period: Sensitivity of Predicted Saltwater Intrusion to Ocean Salinity Boundary.

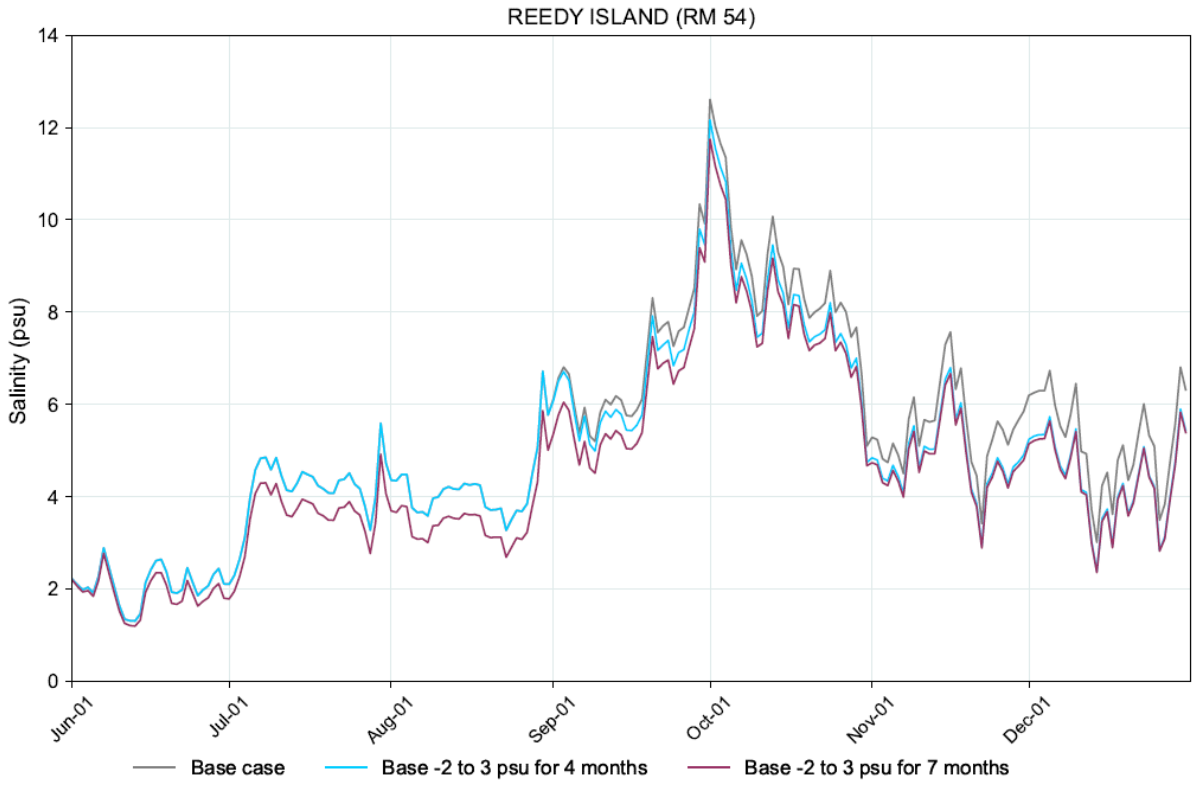

Figure C.3-4 Simulated Daily Depth-averaged Salinity at Reedy Island (RM 54) during June through December 2017: Sensitivity to Salinity at Ocean Boundary

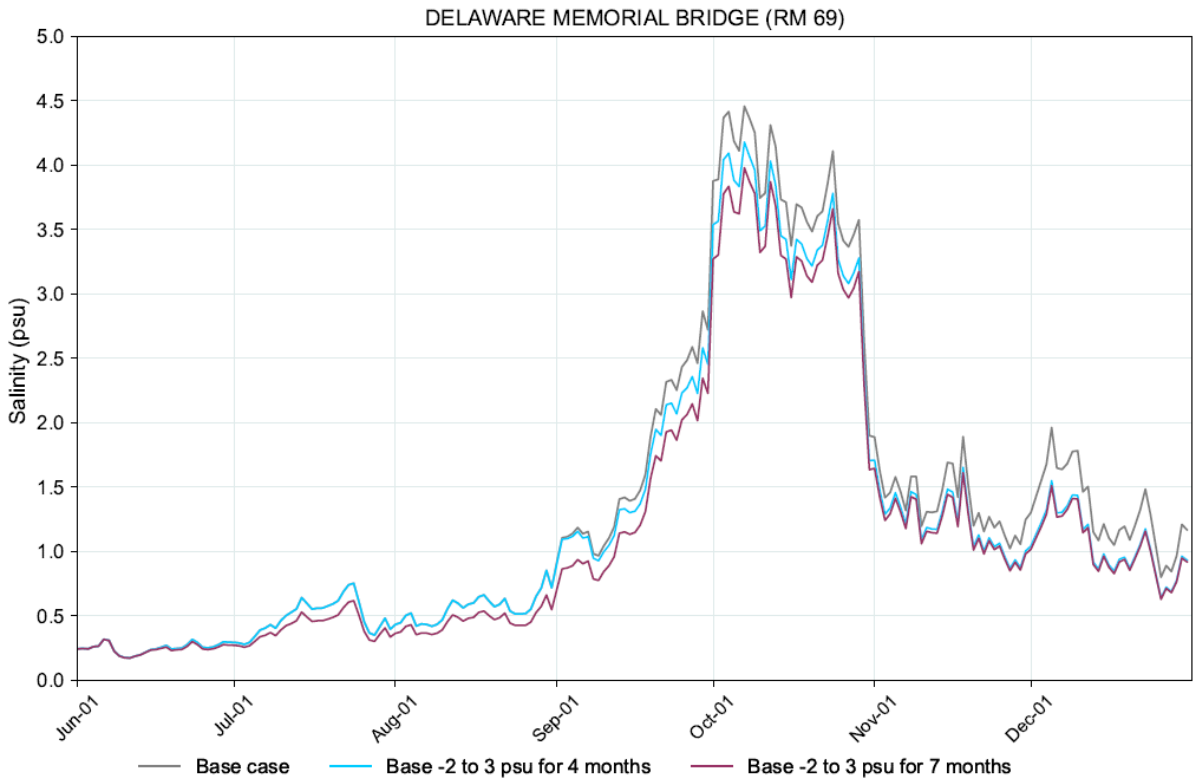

Figure C.3-5 Simulated Daily Depth-averaged Salinity at Delaware Memorial Bridge (RM 69) during June through December 2017: Sensitivity to Salinity at Ocean Boundary

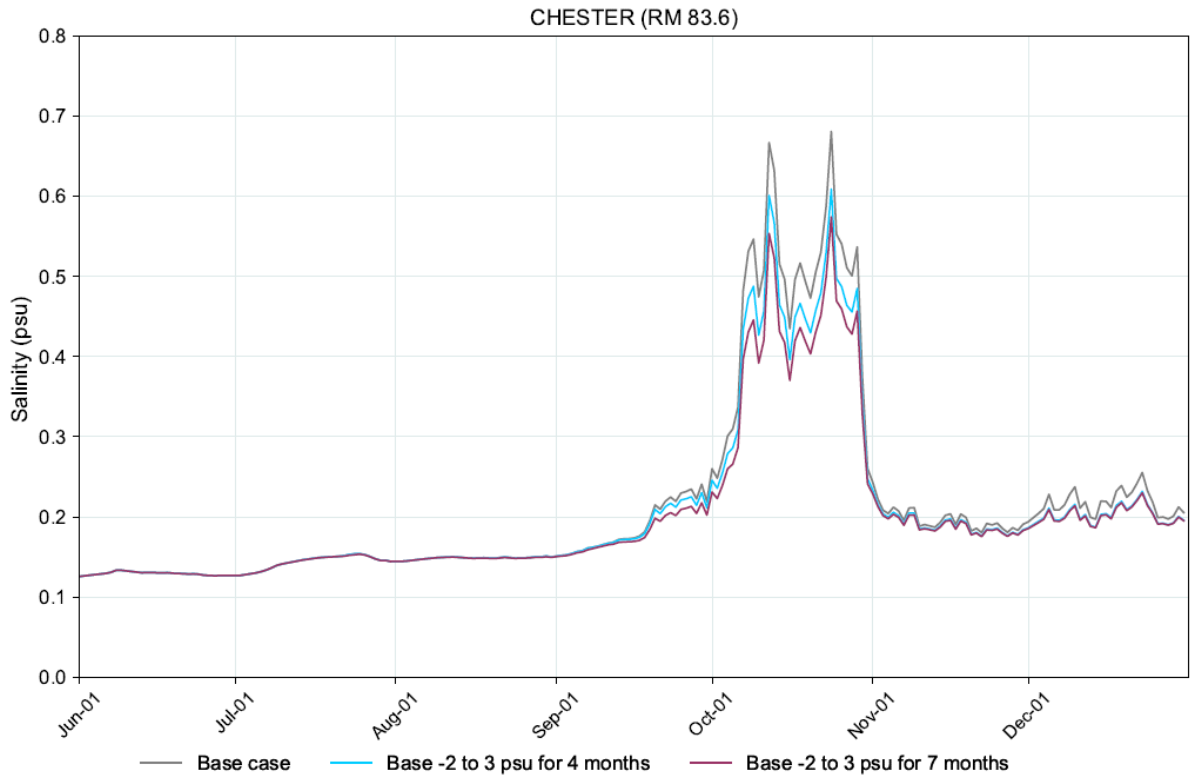

Figure C.3-6 Simulated Daily Depth-averaged Salinity at Chester (RM 83.6) during June through December 2017: Sensitivity to Salinity at Ocean Boundary

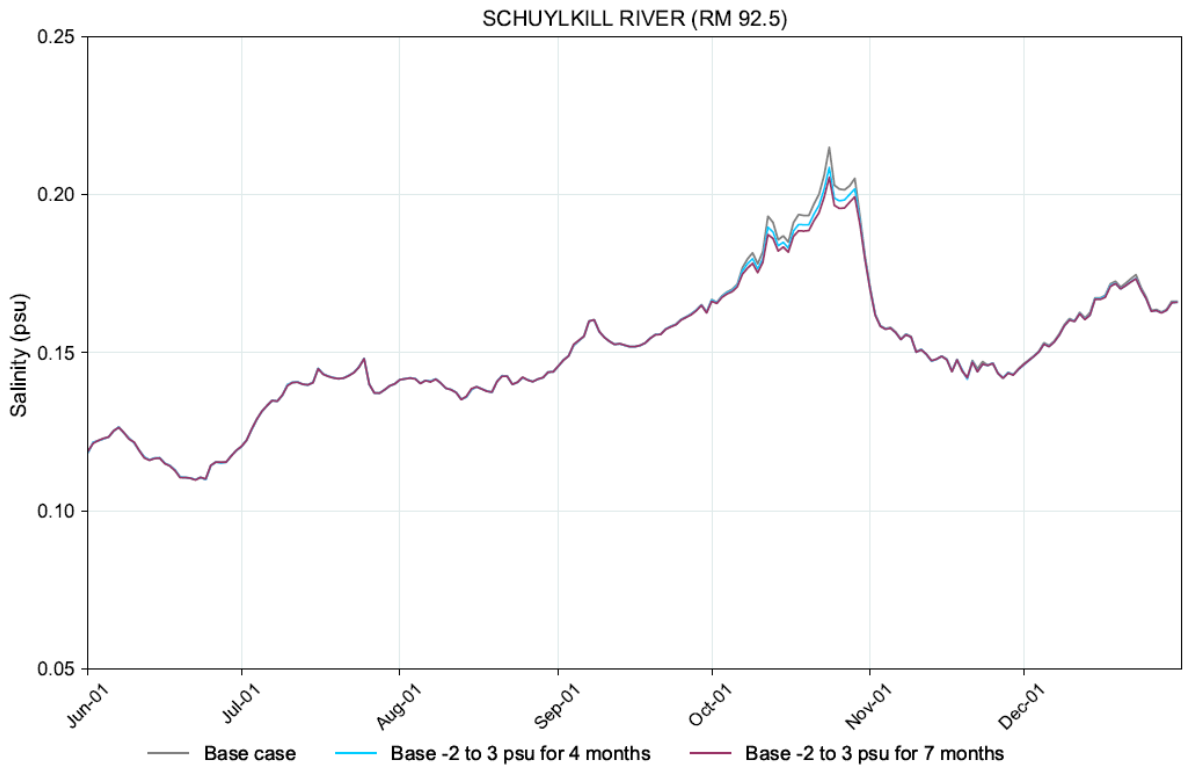

Figure C.3-7 Simulated Daily Depth-averaged Salinity at Schuylkill River confluence with the Delaware River (RM 92.5) during June through December 2017: Sensitivity to Salinity at Ocean Boundary

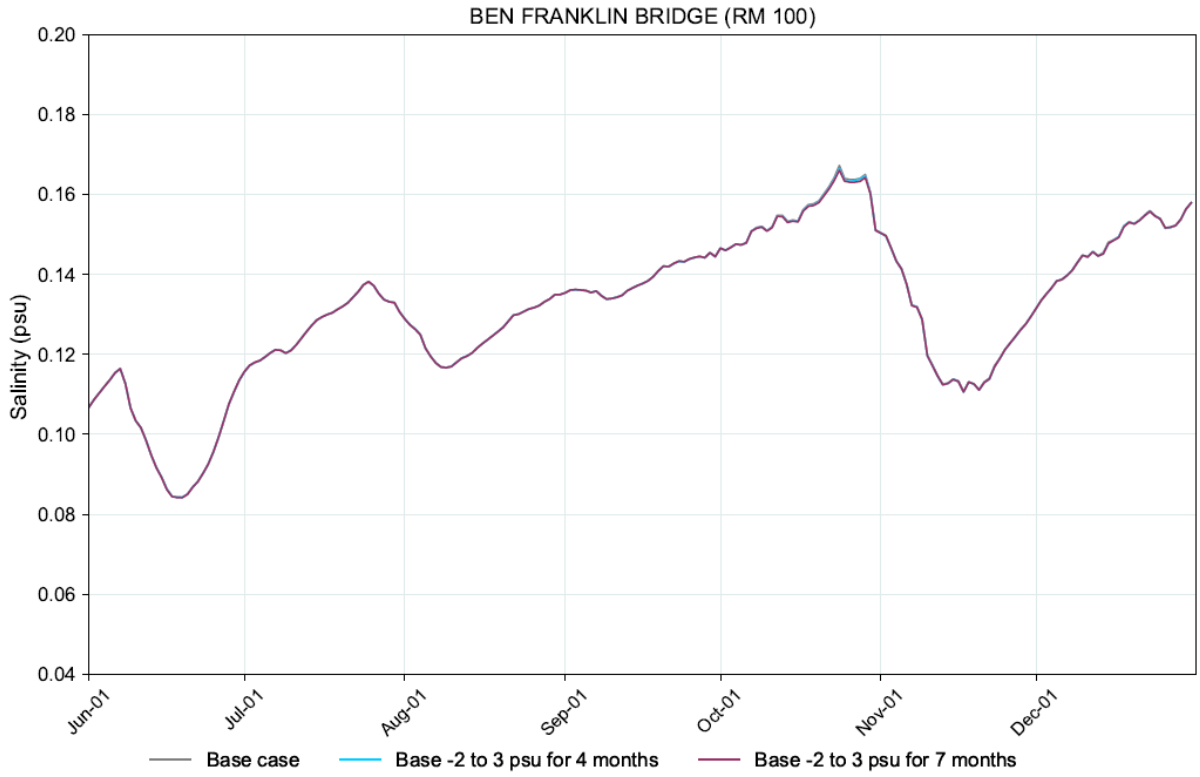

Figure C.3-8 Simulated Daily Depth-averaged Salinity at Ben Franklin Bridge (RM 100) during June through December 2017: Sensitivity to Salinity at Ocean Boundary

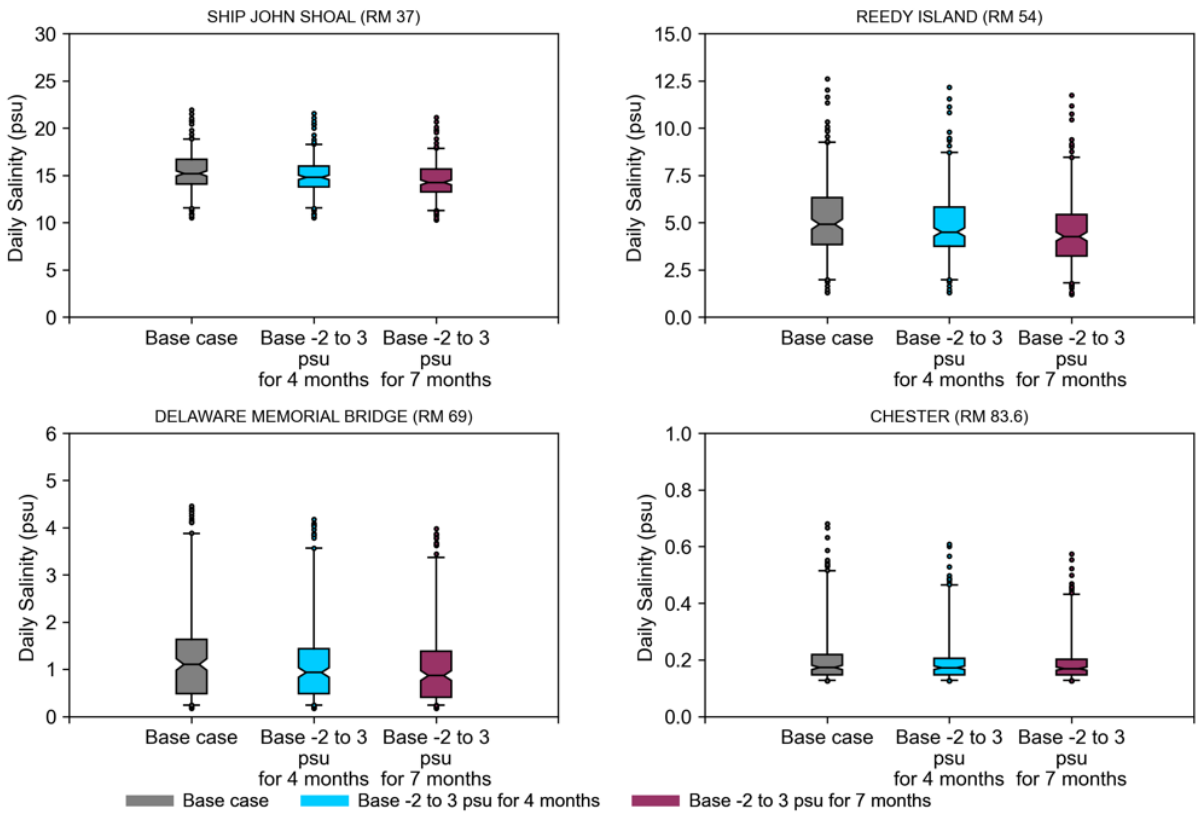

Notes: for box plot, middle line = median; Edge = 25, 75-th percentile; Whiskers = 5, 95-th percentile.

Figure C.3-9 Simulated Range of the Daily Depth-averaged Salinity between RM 37 and RM 83.6 during June through December 2017: Sensitivity to Salinity at Ocean Boundary

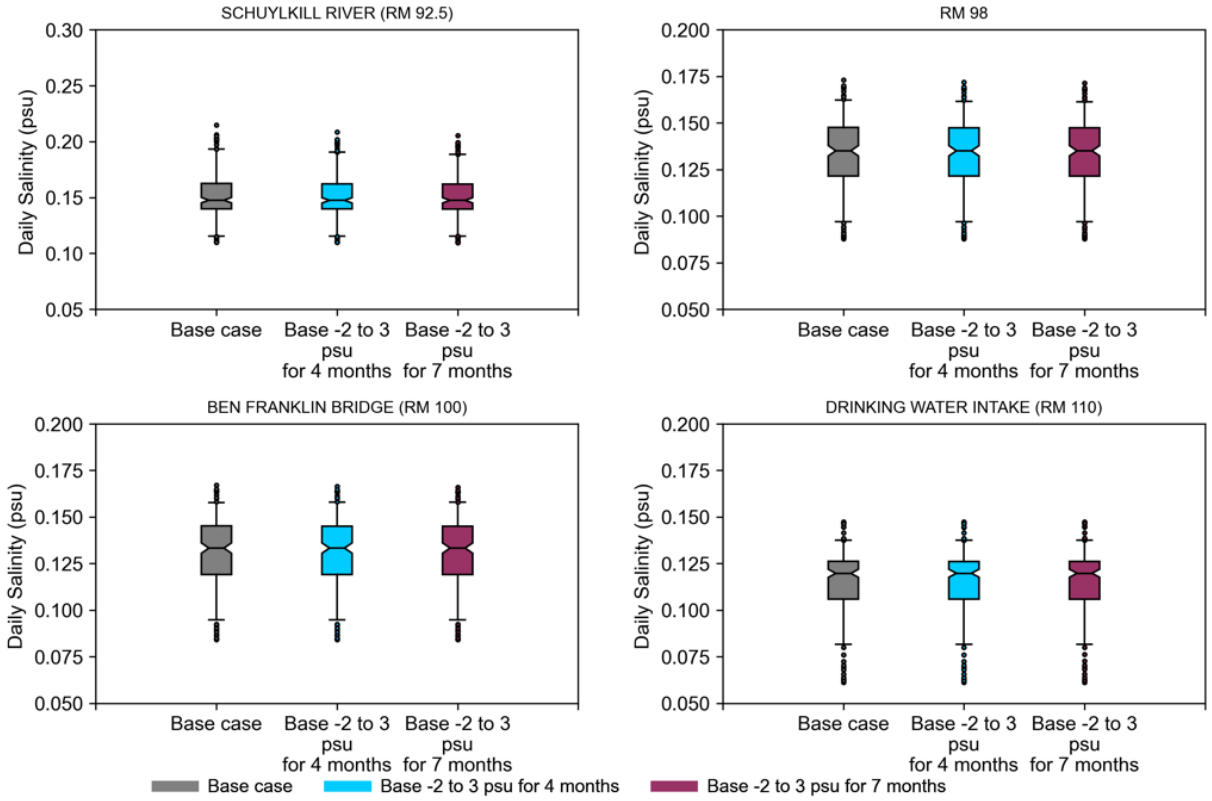

Notes: for box plot, middle line = median; Edge = 25, 75-th percentile; Whiskers = 5, 95-th percentile.

Figure C.3-10 Simulated Daily Depth-averaged Salinity between RM 92.5 and RM 110 during June through December 2017: Sensitivity to Salinity at Ocean Boundary